Key Features and Curriculum Model for Renewable Energy Master Programmes

Some Reflections

Michael Golba, Andreas Guenther

Institute of Physics, Carl von Ossietzky University of Oldenburg
Ammerländer Heerstr. 114-118, 26129 Oldenburg, Germany
michael.golba@uni-oldenburg.de
andreas.guenther@uni-oldenburg.de

Against the background of a globally fast developing and significantly changing higher education sector, and simultaneously a rapidly increasing demand for qualified personnel in the Renewable Energy sector this paper proposes some key features for Renewable Energy Master Programmes. In this context a curriculum model will be presented in some detail, suitable also for developing countries.

Keywords— Higher Education, Renewable Energy Master Programme, Internationalisation, Flexibility, Mobility, Curriculum Model

I. INTRODUCTION

The demand for qualified personnel in the renewable energy (RE) sector is still growing fast, driven by increasing RE implementations into the grid and for off-grid systems. The main driving forces for this development are the climate change mitigation, energy security and, for the developing countries, providing access to the society.

A. Global Trends in Higher Education

Since the late 1950s, starting in the industrialised countries enrolment rates in the national tertiary education sectors have already reached 70% and more (Figure 1). Higher education participation developed from an elite qualification to a mass phenomenon with major consequences for the national education systems and the individuals [1]. In parallel, the "number of female students in tertiary institutions has grown almost twice as fast as that of men since 1970" [2].

These tendencies have been accompanied by a significant internationalisation of higher education. Not only ever more students spend at least parts of their studies (master's and PhD in particular) abroad, even more important: The referential point for students, the national education systems including the individual universities is no longer a national but rather a global one. Even though, the dominant host countries for foreign students still remain the 'traditional' Anglo-Saxon countries USA, United Kingdom, Canada and Australia. The demand for highly qualified foreign students for national higher education institutions is further strengthened by the decreasing demographical development in all industrialised countries.

Consequently, universities particularly from Australia, the USA and Great Britain take on higher education as a business model to co-fund their universities. Financing schemes based on tuition fees seem to become even more promising, particular for international leading universities: One of the most recent studies of the British Councils still sees extremely fast growing tertiary market segments by the numbers, above all in India, China, Indonesia, Saudi-Arabia, Pakistan, and e.g. in Nigeria [3].

These higher education tendencies (see also [4]) lead to a certain matching of demand and supply, e.g. additional opportunities for individual careers for the middle classes of selected countries (including China, India, Brazil, Saudi Arabia, and Qatar). Obviously, this causes significant brain drain effects to the disadvantage of developing countries and corresponding brain gain effects for the industrialised countries "The African diaspora provides powerful intellectual input to the research achievements of other countries but returns less benefit to the countries of birth. That is at least in part because of a chronic lack of investment in facilities for research and teaching; a deficit that must be remedied" [5].

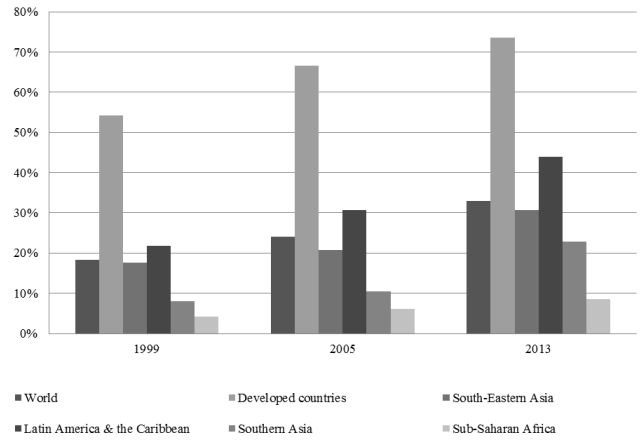

Figure 1: Gross Enrolment Ratio, based on [2]

II. KEY FEATURES OF A RENEWABLE ENERGY MASTER'S PROGRAMME

The following key features are considered to be essential for any further planning and improvement of renewable energy Master's programmes. For these aspects, a permanent and close communication process between the national higher education institutions and the international teaching and research community are considered as essential.

A. Mobility and flexibility requiring comparability and modularity

Two core aspects will play a major role for any future changes and improvements of higher education, largely independent of any particular field of teaching and research: Firstly, the increasing requirement for mobility, first and foremost for the students, but also for lecturers, technical and managerial staff at the universities. Secondly, flexibility of students regarding their selection of a particular major, specialisation, venue, and also teaching format and, for the university and the master's programme respectively.

The core structural prerequisites to achieve both maximum mobility and flexibility are the implementation of comparability and modularity of the teaching units (lectures). The European approach seeks to achieve this by means of clustering individual lectures to modules and, by establishing a normalised 'currency' (i.e. Credit Point, based on the content independent workload) to make all lectures comparable with each other [6]. Independently from the particular format any further higher education development has to address this issue.

B. Competence-oriented teaching, learning and examination

Increasing complexity, uncertainty and dynamics of societal changes place high demand on the individuals [7, 8]. These changing conditions require graduates with competences

to act in highly complex contexts and situations and to organise themselves adequately in different and fast changing environments. Against this background, a paradigm shift from input orientation towards outcome orientation has taken place in the education discourse in recent years. The main focus in education is no longer on the required knowledge alone but rather with the competencies students should develop.

Academic skills should enable students to apply scientific concepts to complex contexts, to analyse and reflect unknown and uncertain problem areas scientifically, and to develop innovative concepts and solutions [9]. The integration of renewable energy technologies into the energy system can be seen as one prominent example for a multidisciplinary approach, requiring technical and social knowledge, skills and competences.

The following aspects should be considered for a competence-oriented curriculum design and for teaching [10]:

- Curriculum development: The design of new programmes starts with the determination of the competence profile: This includes the definition and detailed description of learning outcomes for the whole course as well as for individual modules. In addition to the lecturers, students and other stakeholders should be involved in the process of formulating the objectives.
- Competence-based design of teaching and learning: Competences cannot be taught but must be developed by the students, accompanied by the lecturers. Especially suitable are activating teaching and learning methods such as research-based, problem-based and project-based learning. This leads to a change of the role of the lecturer from a purely expert towards a process facilitator.
- Competence-oriented examination: Exams should be designed to support the development of competences and give students feedback on their learning processes. This requires that examination formats are based on the content of the expected learning outcomes. Here, a case study comprising the simulation of the energy supply system of a village can serve as an example.
- Supervision and support: Students need support and advice to facilitate the development of their competences, e.g. to enable reflections about their progress. This may include mentoring programmes, self-assessments, coaching offers as well as activities to foster the development of key competences. A gender sensitive approach is required here, in order to ensure equal opportunities for male and female students.
- Competence-based evaluation: The acquisition of competences should be the focus of teaching evaluation. The evaluation criteria should relate to the expected subject-specific learning outcomes, but also consider the development of generic competences. This may include questionnaires for the self-assessment of competence development as well as objective competence tests.
- Training opportunities for lecturers: Competence-based teaching requires a high degree of motivation from the lecturers, but also the development of teaching skills that enable them to design innovative teaching-learning settings. Academic teaching training may facilitate the development of the necessary teaching skills and provides opportunities for exchange and networking among the lecturers, and should explicitly be open for young and female staff.

C. Key competencies

Instead of focusing on a wide range of highly specialised and fast changing knowledge and skills only, it is becoming ever more important to support the development of so called key competencies, renewable energy education being no exception. These competencies can be roughly grouped into three clusters:

i) Competencies fostering to manage tools, in order to communicate with others, such as new technologies and e.g. languages

ii) Competencies enhancing the ability to communicate with socially / culturally heterogeneous groups of people, and

iii) Competencies enabling the individual to take over full responsibility for their own lives.

All competencies require the ability to reflect one's own behaviour and thinking at almost all stages. In an environment with increasing uncertainties for the individual and the organisation in particular the sensitive and continuous monitoring, control and reflection is of particular importance. It can be looked upon as an unavoidable risk absorption mechanism for the individual and the organisation [11].

D. Close relation between research and teaching

Higher education, in particular at master's level, substantially has to rely and relate to research. Within the here proposed RE Curriculum Model (Figure 2) the components 'Tracks' and 'Master Thesis' will be related closely to the research groups and hence will be shaped by the individual research profile of each university. Whereas the 'Basics' and to a certain extent the 'Core' components can be covered by well-established lectures, with already standardised content and methods.

Regarding the particular energy requirements in some developing regions (e.g. Africa and Southern Asia) specific consideration should be given to the interdisciplinary field of 'access to modern form of energy'. It is therefore recommended that any renewable energy Master's Programme should address this issue as an applied research track.

E. Blurring of boundaries

With the following categories the actual tendencies in higher education to re-measure and re-define formerly well established and often unsurpassable boundaries come into the picture. The frequent process of re-measuring and redefining new boundaries will be required by the individual, in this case the student, and, by the organisation, in this case the university and the programme. As a consequence, the student as well as

the university/programme will themselves require additional consultancies for their decision making processes [12].

1) Internationalisation

One of the blurring boundaries comes as the internationalisation: Higher education programmes should facilitate the international mobility of students and staff. They should have close relations to international partners (universities, research institutes, private companies, international organisations etc.), should go along with international standards. The universities need to establish an internationalisation strategy for their individual university, defining their own priorities.

It is recommended to mandatorily adopt English language courses, in order to foster English proficiency and thus enabling students and staff to cooperate internationally.

2) Interdisciplinarity

The second blurring of boundaries applies to the strict distinction of academic disciplines. Higher education programmes should facilitate interdisciplinary approaches: Development of projects, comprising research and implementation with the students should become a vital part of any master's programme. Since any substantial change in the energy infrastructure will have far reaching consequences on its disciplinary environments sound knowledge from adjacent disciplines and interdisciplinary approaches are imperative.

3) Transdisciplinarity

Another blurring of boundaries applies to the borderline between the academia and organisations in its environment. Higher education programmes should provide access and hence have to establish close relations to institutions outside the university, in particular to the public and private sector. It is essential, that universities permanently observe possible changes or irritations in their environment in order to adapt accordingly and in due time. Furthermore, these relations can help students to do internships and conduct co-supervised master's theses. A transdisciplinary approach may include the involvement of external stakeholders in the curriculum development process, the participation of external representatives in the programme's advisory board or regular lectures and workshops with experts from outside the academia.

F. Quality Assurance

1) Evaluation

Continuous evaluation processes are required in order to assure the quality of the programme. It is necessary to implement international quality standards, in particular international accreditation. This issue comprises the qualification of staff, but also frequent tracer studies.

Institutionalised self and external reflection observation processes are required in order to prepare the organisation to adequately adapt to external changes. Therefore, quality assured processes should be installed and verified by accreditation agencies. The installation of an advisory board facilitates institutionalised external observation to assure the quality standard and to generate the legitimacy of the programme.

2) Selection process

Student's selection process for higher education programmes is crucial - for the programme and the students. Together with an intensive supervision and guidance of the students this is one of the key elements to control a successful process for the students and the programme. This holds all the more true when the programme opens up for a wider range of educational backgrounds. Indicators like drop-out rate or successful study completion within the specified time frame can serve as indicators for the quality of programme. Special attention should be given to equal opportunities of male and female applicants in order to reach a reasonable gender balance among students.

3) Supervision and networking

As already mentioned, mobility and flexibility will lead to an increasing demand for supervision and guidance by the students – and also from the university and the programme. The intensive supervision, counselling, advising and guidance of the candidates and students have to get highest priority (keyword: career coaching). Equal career prospects for male and female students and staff must be actively pursued. Graduates / alumni have to be integrated frequently into networking activities such as workshops or alumni seminars. Alumni networking activities provide more options for the actual students (see transdisciplinarity) but also facilitate the marketing of the study programmes by personal recommendations.

G. Further Options

In addition to the above features, long-term planning should also consider the following aspects:

- Involvement of distance education elements in order to overcome the shortage of lecturers
- Individually tailored model for the acknowledgement of existing qualification, especially for the basic knowledge in the first semester
- Provision of certificates for specific courses
- Extension of the target group by providing special further education

III. Concept and Recommendations for RE Master's Programme Development

A. Motivation

In many developing regions the training of academically qualified personnel is still deficient regarding several aspects – inter alia enrolment figures, scientific publications, number of patents [14] [15]. This also applies to the renewable energy master's training. This situation is accompanied, related and intertwined with the still weak development of national and regional renewable energy and corresponding job markets [16].

Since the job market for renewable energy is still limited, graduates have to be trained to become highly flexible and creative to give incentives to these markets (e.g. as entrepreneur or developing the political framework). Instead of focusing on highly specialised areas, higher education RE

master's programmes should rather be inter- and transdisciplinary oriented.

B. Introduction to the Renewable Energy Curriculum Model

Taking into account these considerations, a Renewable Energy Curriculum Model has been developed. It adjoins and incorporates experiences and conclusions predominantly drawn from the European higher education system, but also takes into account particularities of the developing regions. The model shall serve to minimise risk for any further planning in an age of increasing uncertainty and complexity [7].

Study programmes will have to deal with risk absorption strategies, addressing and reducing in particular the risk for candidates / students to embark on any particular career, and also to reduce the risk for the institution / organisation (here the university) to establish a particular master's programme. It sees the higher education sector positioned into an environment, where the planners increasingly do have to consider variations, irritations and impulses, and where the responsible politicians are challenged ever more to react to – often unforeseeable - changes. Another aspect is the still very low (but unknown) number and types of available jobs in the renewable energy sector - despite the huge potential. This applies also to the required skills and competencies. Thus, the master students need to acquire competencies to be able to react and reflect on fluctuating demands, including entrepreneurship qualifications and strategies to start their own business.

The Renewable Energy Curriculum Model presented here (Figure 2), provides a strategic approach for renewable energy master's programmes, based on theoretical considerations and empirical analyses. The model describes the frame for a four semester master's programme with an overall scope of 120 credit points (30 CP per semester; based on the European Credit Transfer System / ECTS), characterised by a modular and flexible structure. Nevertheless, this model allows the establishment of shorter master's programmes as well, but in this case the 'bridging entry structure' and / or the 'tracking / specialising procedure' has to be provided outside the actual programme structure.

As a conclusion from the experiences and the analyses of measures to enhance mobility and compatibility in the European higher education system it is strongly proposed to use highly flexible programme structures. Nevertheless, simultaneously the still existing restrictions and drawbacks of this system have to be considered. The Credit Points, commonly already named as the 'currency' for the model of a unified European higher education area come with two characteristic distinctions to an actual currency: Obviously, the credit points are strictly coupled to the person and hence, are not transferable from one student to the other. Secondly, they are coupled with the content: These results inter alia in a still rather limited student exchange between study programmes within the European higher education area. To overcome this bottleneck, the proposal here is to establish a largely uniform core semester at every university, in terms of subject-specific competencies.

Ideally, the master's programme should be accessible for students from different educational backgrounds. However, the range has to be defined by the individual university on the basis of its particular resources. Through several specialisation options (tracks), students will get the opportunity to qualify for a range of professions. Here again, the range of specialisations will depend on the decision of each university, closely related to its research profile. The model's intention therefore is not to harmonise the higher education systems, neither nationally nor regionally, but rather to encourage and enable comparability and mobility between the universities and strengthen each universities individual research and teaching profile. Of course, these efforts should be accompanied by the establishment of institutionalised evaluation schemes: In East Africa for example, the development of a homogeneous quality assurance system including a structured regional credit point system has already been started [17][18].

The master's graduates will then gain the competences to work both in the public and private sector as engineers, entrepreneurs, planners or politicians as well as in academia and education as teachers, professors and researchers. It is aspired to impart a minimum of technical and non-technical knowledge to all participants, essentially independent from their educational backgrounds (bachelor studies, working experiences). In spite of the interdisciplinary qualifications, it still can be expected that students with e.g. a bachelor in mechanical engineering will rather work as engineers afterwards, whereas the majority of graduates who decided for the political area may have a background in political science or jurisprudence.

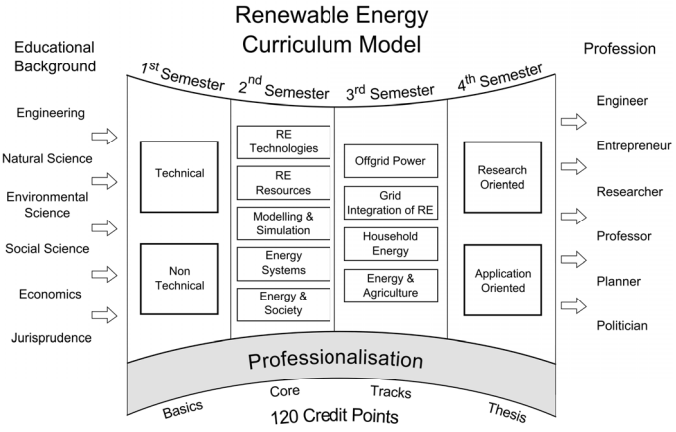

Figure 2: Renewable Energy Curiculum Model

In the following, the concept of the Renewable Energy Curriculum Model will be explained in more detail.

The first semester ("Basics") serves as a bridge between the already gained knowledge and competencies from previous studies and professional experiences on the one hand, and the requirements for the subsequent semesters on the other hand. The modules of this first semester should therefore include e.g. fundamentals of mathematics, material science, electronics, fluid mechanics, and biochemistry as well as the basics of economics and other social sciences. In order to motivate the students as much as possible, methods and content should be taught by way of using examples from the renewable energy

field, e.g. with exercises and exams applying practical examples. After completion of the first semester, students should have the basic understanding, both in technical and non-technical areas, to follow the core semester.

The second semester ("Core") is designed to provide a thorough understanding of renewable energy technologies, resources, systems, and simulation and modelling methods and tools, and not least, should address the interface and interrelation between the energy system (the technology) and the society (the social dimension). With the module 'RE Technologies' the focus should be on the renewable energy technologies with the highest potential in the respective region. The technical knowledge concerning particular energy conversion processes corresponding with different RE technologies and its components should be complemented by a module specifically addressing RE resources (RE Resources) including prediction approaches (Energy Meteorology), and of course a sound teaching of the RE system approach, including an introduction to energy systems (Module Energy Systems). Additionally, all students should receive a sound insight in modelling concepts and simulation tools. Complementary to these technical approaches, there should be lectures on economic and political aspects, e.g. regarding the complex relationship between the energy system and society (Module 'Energy and Society'), related to the use of energy and its impact on markets and groups of society, including women and the poor. Whether these lectures are mandatory or some will come as electives depends on the decision and the resourcing of each university.

With the third semester ("Tracks") several specialisation options should be provided. The track concept implies more than solely the specialisation. Actually, it comprises a number of by the university defined particular courses through the master's programme, with the specialisation and the final master's thesis at the centre. Each track is designed with a problem-centred approach, i.e. the topics will be discussed from different perspectives including technical, economic and political aspects. The specialisations shall be tailored according to the needs of the respective region / country in compliance with the specific scientific research profile at the providing university. The different tracks may widely overlap and also include specific foci, such as entrepreneurship, research or policy.

The tracks shown in Figure 2 serve as examples. "Off-grid Power" would focus on the electrification of rural areas, ranging from (Pico) Solar Home Systems to mini-grids powered by different renewable energy sources (e.g. including hybrid systems with Diesel generators). In addition to technical knowledge, students would also learn about social and economic aspects. "Grid Integration of Renewable Energy" focuses on the electrification through grid extension in general, and for urban as well as semi-urban areas in particular. This should include technical knowledge about grid specifications or economic and political aspects comprising financial support schemes for renewable energy, e.g. feed-in tariffs and auction models. The focus of the specialisation "Household Energy" would be on the utilisation of biomass for cooking (small-scale biogas digesters, improved cooking stoves, including also household electrification), covering technical, social as well as environmental aspects, e.g. deforestation and climate change. The track "Energy and Agriculture" deals with the "Water-Energy-Food Nexus" and refers to the actual debate: "Throughout developing countries, agriculture remains the most prominent source of livelihood for most households. […] Increasing the agricultural sector's access to clean energy technologies will enable farmers to mechanize their operations, add value to commodities through processing, and store fresh produce in refrigerated containers to extend its shelf-life. These advancements will lead to more food in the market, increased incomes for farmers and traders, and decreased dependency of the agriculture sector on fossil fuels" [19]. Similarly to the before mentioned specialisations, this track covers technical and non-technical topics and can be tailored to different professions.

During their fourth semester ("Thesis"), students will work on their master's thesis. They may choose between a "Research-Oriented" and an "Application-Oriented" approach. The first option is especially designated to future lecturer / researcher career and shall provide a basis to continue with a doctoral thesis. A research-oriented thesis will usually be pursued at a research institution and aims for a publication in a peer-reviewed journal. An application-oriented thesis should be conducted in close cooperation with an external public or private organisation, e.g. a company, a development organisation or a regulatory agency including research work on a real-life project.

Subject-specific knowledge (basic and specialisation) will be complemented by professionalisation modules throughout the whole programme in order to prepare the students for their professional career. As an additional core component of the curriculum, students will acquire key competencies as e.g. communication or (project) management skills. Practical experience will be gained during an internship for several months at an external organisation in the public or private sector. Also, the master's thesis can be written in cooperation with an external institution, to facilitate student's access to professional working environment. A coaching process should support the students during their thesis. Professionalisation skills and competences such as teamwork and language can be acquired in particular courses at the university or during internship or master's thesis in a professional working environment.

IV. CONCLUSIONS

When addressing the fast increasing demand for academic qualified personnel for renewable energy experts it is not enough to increase the supply. The fast transforming higher education sector also requires significant qualitative adjustments. With the here proposed key features and the developed curriculum model for RE Master Programmes some referential points are indicated, for universities in developing as well as in industrialised regions.

REFERENCES

[1] P. G. Altbach, International Handbook of Higher Education, Boston College: Springer , 2007.

[2] UNESCO Institute for Statistics, "UIS.Stat," 2014. [Online]. Available: http://data.uis.unesco.org/.

[3] British Council, “Postgraduate student mobility trends to 2024,” 2014. [Online]. Available: http://www.britishcouncil.org/sites/britishcouncil.uk2/files/postgraduate_mobility_trends_2024-october-14.pdf.

[4] M. Gibbons, C. Limoges, H. Nowotny, S. Schwartzmann, P. Scott and M. Trow, The New Production of Knowledge, London: Sage, 2005.

[5] J. Adams, C. King and D. Hook, “Global Research Report Africa,” 2010. [Online]. Available: http://researchanalytics.thomsonreuters.com/m/pdfs/globalresearchreport-africa.pdf.

[6] S. Kühl, Der Sudoku-Effekt. Hochschulen im Teufelskreis der Bürokratie. Eine Streitschrift, Bielefeld: transcript, 2012.

[7] R. Barnett, Realizing the University in an Age of Supercomplexity, SRHE & Open University Celtic Court, 2000.

[8] H. Nowotny, P. Scott and M. Gibbons, Re-Thinking Science. Knowledge and the Public in an Age of Uncertainty, Cambridge: Polity, 2001.

[9] N. Schaper, O. Reis, J. Wildt, E. Horvath and E. Bender, “Fachgutachten zur Kompetenzorientierung in Studium und Lehre,” 1 August 2012. [Online]. Available: http://www.hrk-nexus.de/fileadmin/redaktion/hrk-nexus/07-Downloads/07-02-Publikationen/fachgutachten_kompetenzorientierung.pdf.

[10] G. Michelsen and M. Rieckmann, “Kompetenzorientiertes Lehren und Lernen an Hochschulen – Veränderte Anforderungen und Bedingungen für Lehrende und Studierende,” in *Transformation. Education, Qualification & Digitalization*, Berlin, Logos Verlag, 2014, pp. 45-65.

[11] OECD, “The Definition and Selection of Key Competencies. Executive Summary.,” 2005. [Online]. Available: http://www.oecd.org/pisa/35070367.pdf.

[12] M. Golba and C. Vajna, “Entgrenzungsprozesse und deren Folgen bei Konzeption und Durchführung internationaler Studiengänge,” in *Offene Hochschulen*, Münster, Waxmann, 2013, pp. 168-178.

[13] M. Golba, P. Cattelaens and N. Hayek, “Scoping Mission for a Regional Trilateral Renewable Energy Master’s Programme Cooperation,” European Union Energy Initiative Partnership Dialogue Facility (EUEI PDF), Eschborn, 2014.

[14] D. E. Bloom, D. Canning and K. Chan, “Higher Education and Economic Development in Africa,” 2006. [Online]. Available: http://www.tfhe.net/resources/mastering_globalization.htm - _ftn1.

[15] IRENA, “Renewable Energy and Jobs: Annual Review 2014,” 2014. [Online]. Available: http://www.irena.org/publications/rejobs-annual-review-2014.pdf.

[16] IUCEA, “Inter-University Council for East Africa: Developing a Regional Qualifications Framework for Higher Education in East Africa,” 2015. [Online]. Available: http://www.iucea.org/index.php?option=com_content&view=article&id=317&Itemid=279. [Accessed 20 February 2015].

[17] R. Odongo, *Quality Assurance of Academic Programmes, Presentation at RECP Workshop in Kigali,* 2014.

[18] Powering Agriculture, “Powering Agriculture: An Energy Grand Challenge for Development,” 2015. [Online]. Available: http://poweringag.org/problem. [Accessed 15 January 2015].

[19] I. Warde, “Der Ausverkauf der Universität,” *Le Monde Diplomatique No. 6398,* pp. 22-23, 16 March 2001.

[20] A.-M. Sendegeya, *Southern African Sustainable Energy Initiative (SASEI), Presentation at RECP Workshop in Kigali,* 2014.

[21] P. Scott, “Cross-Border Higher Education and Internationalisation - Overview of Concepts, Trends and Challenges,” 15-16 November 2005. [Online]. Available: http://www.unesco.org/iau/conferences/alexandria/ic_papers/speech_Scott.rtf.

[22] U. Schneidewind, Nachhaltige Wissenschaft. Plädoyer für einen Klimawandel im deutschen Wissenschafts- und Hochschulsystem, Marburg: metropolis, 2009.

[23] G. Rees, R. Fevre, J. Furlong and S. Gorard, “History, Biography and Place in the Learning Society: Towards a Sociology of Life-Long Learning,” in *Education, Globalization and Social Change*, Oxford New York, Oxford University Press, 2006, pp. 927-935.

[24] B. Readings, University in Ruins, 4 ed., Cambridge/Mass. London: Harvard University Press, 1999.

[25] M. M. Kritz, “Globalization of Higher Education and International Student Mobility,” 2012. [Online]. Available: http://www.un.org/esa/population/meetings/EGM_MigrationTrends/KritzPresentationFinal.pdf.

[26] V. Kajibanga, “Ensino Superior e Dimensão Cultural de Desenvolvimento - Reflexões Sobre o Papel do Ensino Superior em África,” *Africana Studia – Revista Internacional de Estudos Africanos,* pp. 137-151, 2000.

[27] J. Enders and O. Fulton, Eds., Higher Education in a Globalising World, Dordrecht Boston London: Kluwer, 2002.

[28] U. Beck and B. Holzer, “Reflexivität und Reflexion,” in *Entgrenzung und Entscheidung: Was ist neu an der Theorie reflexiver Modernisierung?*, Frankfurt a.M. , Suhrkamp , 2004, pp. 165-192.

[29] M. W. Apple, J. Kenway and M. Singh, Eds., Globalizing Education, New York: Peter Lang, 2005.

[30] P. G. Altbach, Global Perspectives on Higher Education, Vol 27, The International Imperative in Higher Education, Boston: Sense Publishers, 2013.

[31] UNESCO, Unesco Science Report 2010, Paris , 2010.

[32] World Bank, “Education Statistics,” 2014. [Online]. Available: http://data.worldbank.org/data-catalog/ed-stats.

Designing of an Optimized Building Integrated Hybrid Energy Generation System

Md. Rayhan Sharif, Md. Nafeez Rahman,Md. Hafezur Rahman Chowdhury,Md. Asaduzzaman Shoeb
Department of Electrical and Electronic Engineering
American International University-Bangladesh
Dhaka, Bangladesh.
sharif.mdrayhan@gmail.com, nafeezrahman.du@gmail.com,
hafezurrahman@yahoo.com, shoeb_1064@yahoo.com

***Abstract*—This paper deals with designing a biomass and solar based hybrid power plant for residential building. The main focus of this work is to propose a hybrid energy system consists of biomass and solar PV. The system will produce enough electricity to power up an entire building just by collecting MSW and solar energy. As a part of this work, various research were done regarding different processes and techniques of biomass power plant which will be suitable for electricity production for a building. This work mainly includes designing of the hybrid power plant, estimating its cost and calculating different loads using Homer Pro software. Schematic diagram of the plant along with waste management are also within the scope of this paper. This proposed hybrid plant has a peak load of 115 KW. Average energy consumption of the building is estimated approximately 1399kwh/day and it will consume almost 1584 kg of biomass per day. The proposed system is designed to provide approximately 70-80% of energy from the biomass,20% from PV and the rest will be dependent on main grid line.**

Index Terms—Biomass, Municipal Solid Waste (MSW), Direct Combustion, Solar Power, Pv Design,Load Calculation, Energy Management, Flue Gas Cleaning, Building Electricity Production

I. INTRODUCTION

The system is all about renewable energy generation system. In the system biomass, solar, and grid electricity is connected in a synchronized way. The present generation of electricity in Bangladesh is not enough to prevent load shedding. There is a huge difference between the peak demand and the actual produced electricity. This problem can be somehow be minimized by establishing a plant based on renewable energy sources.

The concept of hybrid power plant is somewhat new in Bangladesh. Though developed countries are utilizing this energy for producing electricity for a long time but in Bangladesh it is far behind in this energy sector. Biomass energy offers substantial advantages over other renewable energy, it is abundant, renewable and clean energy, and it reduces dependency on fossil fuel. Since Bangladesh is an agrarian country, agricultural crop residues, animal manure and municipal solid waste which are the major sources of biomass energy system and the unlimited power of solar from sun are abundant in here also. So biomass and solar both will serve as the potential renewable energy sources in Bangladesh and there are huge prospect of these energies to minimize energy crisis in the country.

II. PROSPECT OF HYBRID GENERATION

Classification of hybrid system with renewable energy sources(HSRES) According to the presence of conventional energy sources: x Hybrid systems with conventional sources – mostly the systems, using conventional sources are more powerful and responsible; x Hybrid systems without conventional sources – as a general, that kind of systems are relatively low-power and/or tend to be more irresponsible. If the systems are correctly designed and if energy storage is provided, they would be able to generate sustainable energy. These systems are independent of energy sources, which make them especially preferred. Hence, comes the need to develop reliable optimization models. According to the number of the sources – The number of the energy sources is one of the factors that define the complexity of the HSRES as well as its sustainability and efficiency [1].

❖ Classification of HSRES[2]

According to the presence of conventional energy sources:

- Hybrid systems with conventional sources
- Hybrid systems without conventional sources

According to the type of the produced energy:

- Mechanical
- Electrical
- Thermal
- Mixed

According to the rated power:

- Low power (less than 1 kW)
- Middle power (more than 1 and less than 10 kW)
- High power (more than 10 kW)

According to the energy storage:

- Without storage
- With storage

According to the connection to the distribution grid:

- Grid connected
- Stand alone

Advantages of the System [19]:

- Fuel saving (up to 50%).
- Lower atmospheric contamination.
- Savings in maintenance.
- Silent system.
- Connection to other power supplies (Wind turbines, solar panels, etc.)

III. PROCESS DESCRIPTION

In process description it includes how electricity will produce from both biomass waste and solar photovoltaic panel. It also includes the grid purchase for the system.

A. Electricity Production from Biomass:

The system will use direct combustion process for biomass waste to energy production. In this process biomass wastes will be store in a storage tank and from this storage tank it will move to direct combustion boiler for combustion. Air is needed for combustion which will be provided by forced draft fan. After completion of combustion we will find steam and flue gas. Steam is required for power generation. It will pass through a steam turbine for mechanically power up the turbine. Then the turbine will mechanically couple to the generator. Generator will produce electrical power from mechanical rotation of turbine. In that case we will use steam turbine genset for electrical power production. Final Electrical power will be provided for powering up the building. Residual heat from the turbine will move to the condenser where it will be cooled by attaching a cooling tower with condenser. Cold water from condenser will be used as feed water that will be provided to the combustion boiler. Flue gas which will be produce as byproduct will be cleaned by using flue gas cleaning system. Clean gas will be moved to the environment through chimney.

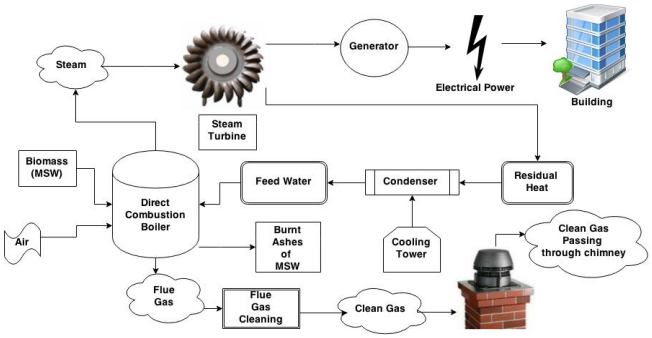

Fig. 1 Process of Biomass waste to Electrical Energy Production.

B. Electricity Production from solar:

Solar PVs will be used for solar energy production for the building. In this process solar photovoltaic panel converts the sunrays into electrical power by exciting electrons in silicon cells using the photons of light from sun.[22]Solar panel consumes sunlight and produce DC voltage which goes to the solar charge controller. A charge controller is used to maintain the proper charging voltage on the batteries. Since the brighter the sunlight, the more voltage the solar cells produce, the excessive voltage could damage the batteries. As the input voltage from the solar array rises, the charge controller regulates the charge to the batteries preventing any overcharging. [23]Lead acid battery is used for store DC voltage that comes from the charge controller. An inverter which is usually known as DC to AC converter is used to convert DC to AC. From Inverter the final electrical power goes to high rise building for powering up the building.

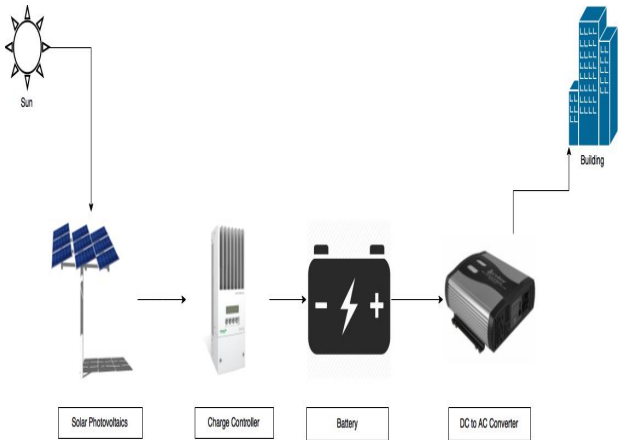

Fig. 2 Process of Solar PV to Electrical Energy production.

C. Grid Purchase:

Actually the grid acts as a backup protection medium in any hazardous situation like minimum production of biomass in rainy seasons. In addition, it'll also become an earning source of extra production to the grid if necessary.

IV. PROPOSED GENARATION MODEL

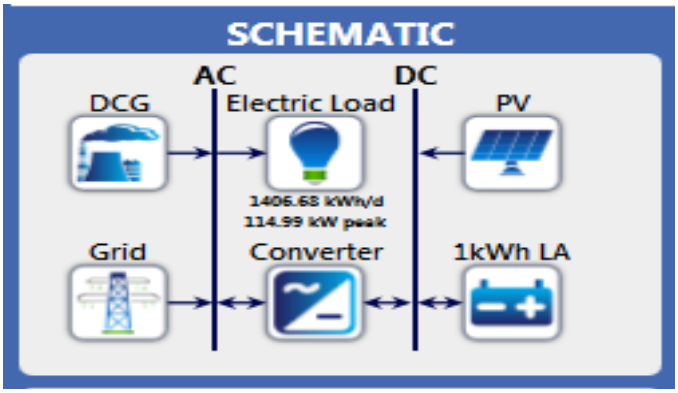

Fig. **3** HOMER Representation of the System

The schematic diagram simulated in the Homer software has been shown in
Fig. 3. Solar PV is connected with the DC system where a battery is also connected as storage device.

Fig. 4 shows the building section of proposed power plant model. Here, biomass reserve tank, boiler etc. are placed at the underground of the building. Switching station & rest of the equipment like generator & transformer are located at basement 2. Basement 1 & ground floor is provided for car parking & free space.

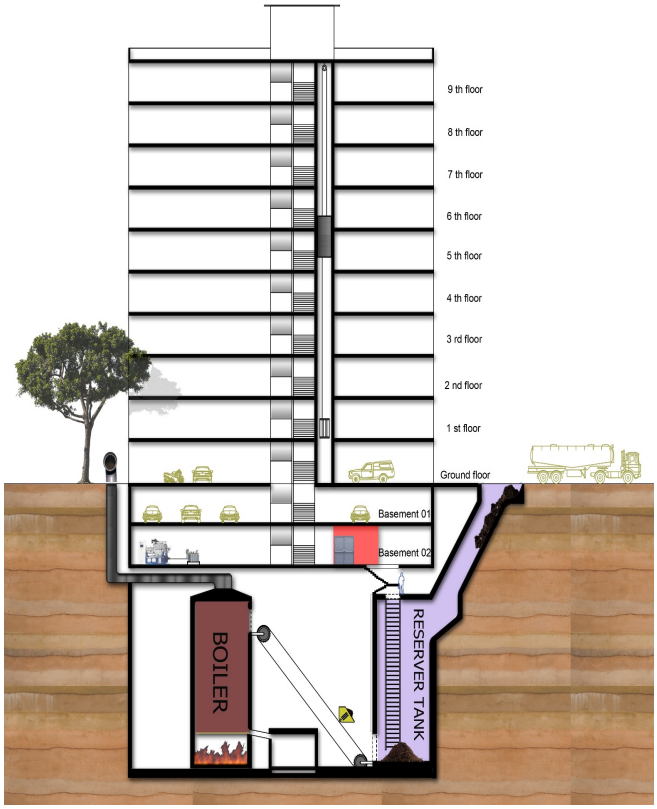

Fig. 4 Building Section.

Fig. 5 shows the zoom section of the proposed power plant where steps of waste to energy production also showing. In zoom section all the equipment's are labeled properly for recognizing the entire model.

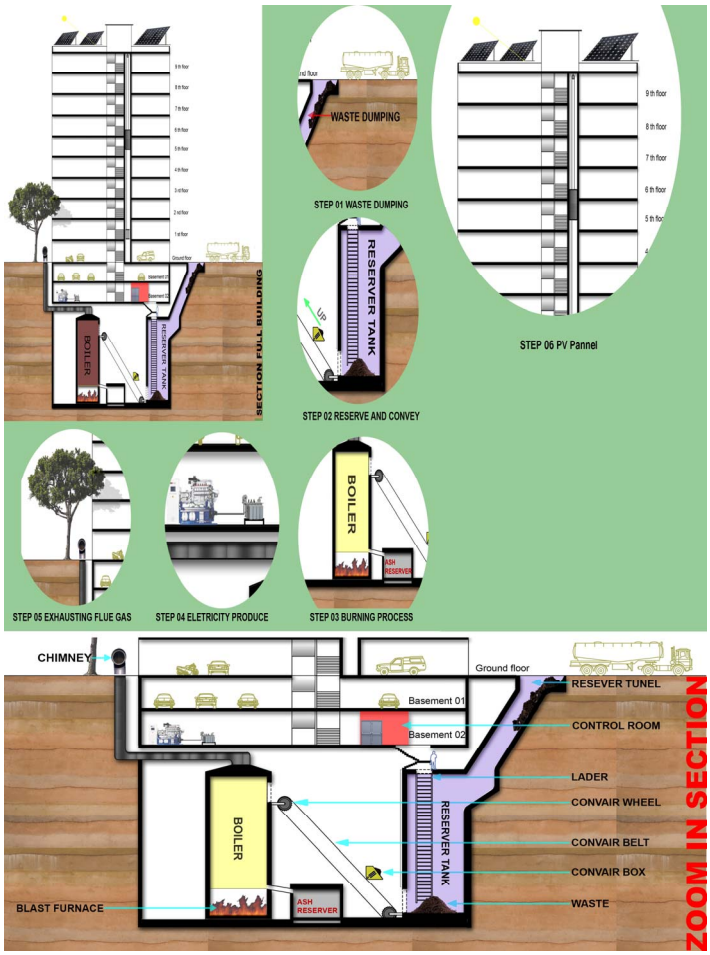

Fig. 5 Zoom in section.

In this proposed building there are two basements and under the second basement the main biomass plant is situated. In this work we have done load calculation of per flat along with full building common load. The calculation also includes proposed plant's supplementary loads as well. The calculation is conducted for summer and winter separately as the load varies along the seasons.

Table **1** represents the load calculation of the full building only for summer season stating from noon to mid night. The complete load calculation for both summer and winter has been used in the simulation [6].

Table 1 Load Calculation for the building (for 12 hours)

Time	Household Appliances	Single Flat Load, KW	Common load,KW	Total Load for Building (KW)
12:00 - 13:00	fridge, deep fridge,laptop-1,washing machine, exhaust fan, TV	1.53	29.6	60.05
13:00 - 14:00	fridge, deep fridge,laptop-1,tv,AC (1Ton)-1	2.48	30.3	79.8
14:00 - 15:00	fridge, deep fridge,laptop-1,tv,AC split (.75 ton)-1	1.7	29.6	63.45
15:00 - 16:00	fridge, deep fridge,laptop-1,AC split (.75 ton)-1	1.7	29.6	63.45
16:00 -17:00	fridge, deep fridge,laptop-1,oven	2.25	29.6	74.55
17:00 - 18:00	fridge, deep fridge,laptop-1,	2.25	26.3	71.325
18:00 - 19:00	fridge, deep fridge,laptop-2,tube-5,cfl-1,tv,oven	4.3	26.3	112.325
19:00 - 20:00	fridge, deep fridge,laptop-2,tube-5,cfl-1,tv,AC (1Ton),AC split (.75 ton)-2	4.3	26.3	112.325
20:00 - 21:00	fridge, deep fridge,laptop-2,tube-5,cfl-1,tv,AC (1Ton),AC split (.75 ton)-2	4.3	26.3	112.325
21:00 - 22:00	fridge, deep fridge,laptop-2,tube-5,cfl-1,tv,AC (1Ton),AC split (.75 ton)-2	4.3	26.3	112.325
22:00 - 23:00	fridge, deep fridge,laptop-2,tube-5,cfl-1,tv,AC (1Ton),AC split (.75 ton)-2	4.3	26.3	112.325
23:00 - 00:00	fridge, deep fridge,laptop-2,tube-5,cfl-1,tv,AC (1Ton),AC split (.75 ton)-2	4.3	26.3	112.325

Table 2 Demonstrates the common load of the building along with the utilities of the power station which is calculated.

Table 2 Common Loads of the Building.

Load	*Rating, W*	*Quantity*	*Total, W*
CFL Light	15	25 (For common spaces, ground floor and basements)	375
Tube	40	45(For Control room and basements)	1800
Computer	250	3 (for control room)	750
Air Conditioner	3000	3 (for control room)	9000

V. SIMULATION PROCESS

A. Primary Load Inputs:

For November to January hourly variation of loads are small because winter session remained in that time. On the other hand for February to October hourly variation of loads is more than the period of November-January. Since warm weatheris remained most of the time in a year in Bangladesh so in that time demand of electricity is higher than winter session. Here Primary Load type is AC.Forevery single hour of a day load data has been put in the data tables demand wise.

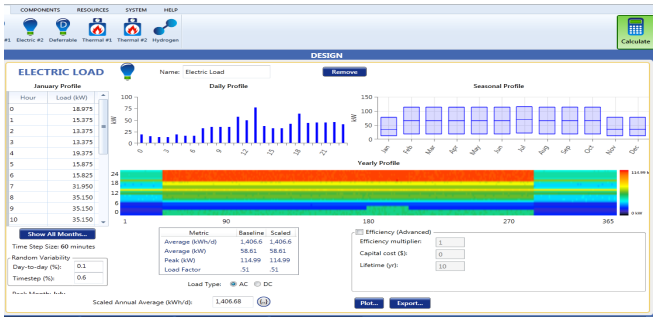

Fig. 6 Daily & Seasonal Profile of Electric Load.

Random variability factor consists of day to day which is 0.1% & time step to time step which is
0.6%. Scaled Annual Average is 1406.68 kwh/d. Figure (2) also shows some graphical pictures which are showing Daily Profile, DMap1 & Seasonal Profile.
A DMap (Data Map) is a type of graph showing one year of hourly data.

B. Electrical Power Production & Consumption:

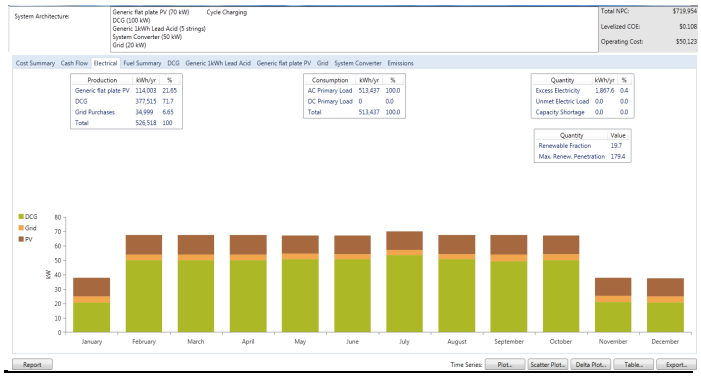

Fig. 7 Electrical Power Production & Consumption.

Fig. 7shows the electrical power production & consumption per year. For 20 kW grid & 100kw direct combustion generator (DCG) & 70 kW flat plate solar PV power system produces total power of 526,518
kwh/yr. where direct combustion generator produces 377,515 kwh/yr, grid power purchases is 34,999 kwh/yr& generic flat solar pv produces 114,003 kwh/yr. Electrical power consumption of AC primary load is 513,437 kwh/yr which shows 100% consumption of power production. Other quantity such as excess electricity is 1,867.6 kwh/yr,unmet electric load is 0 kwh/yr and capacity

shortage is0 kwh/yr. other quantity named renewable fraction is 19.7 &max renewable penetration is 179.4. Data plot shows the monthly average electric power production of generator, grid & solar photovoltaic.

C. Grid Used:

Fig. 8shows the monthly grid energy purchases, net energy purchases, peak demand, energy charge & demand charge for a whole year. Here, annual energy purchased is 34,999 kWh, net energy purchases is 34,999 kWh, annual peak demand is 17 kW, annual energy charge is $3,500& demand charge is$0.

Resources.ReportingService_GenerateInputsReport_Month	Energy Purchased (kWh)	Energy Sold (kWh)	Net Purchases (kWh)	Peak Demand (kW)	Energy Charge ($)	Demand Charge ($)
January	3,184	0	3,184	16	0	0
February	2,527	0	2,527	16	0	0
March	2,926	0	2,926	16	0	0
April	2,850	0	2,850	17	0	0
May	2,830	0	2,830	17	0	0
June	2,752	0	2,752	16	0	0
July	2,802	0	2,802	16	0	0
August	2,771	0	2,771	16	0	0
September	3,213	0	3,213	17	0	0
October	3,054	0	3,054	17	0	0
November	2,905	0	2,905	17	0	0
December	3,187	0	3,187	16	0	0
Annual	34,999	0	34,999	17	3,500	0

Fig. 8 Grid use data for whole year.

D. Time Series Plot:

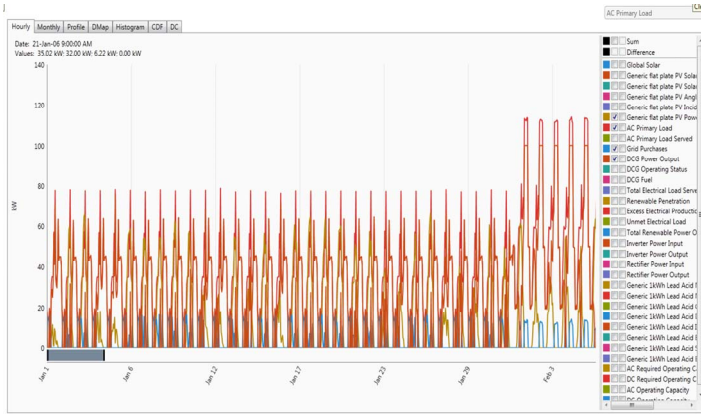

Fig. 9 Time series plot of power production and consumption.

Fig. 9shows the hourly variation of all the quantities regarding AC primary load, Direct Combustion Generator (DCG) power output, Grid purchases& solar photovoltaic power output for the month of January.

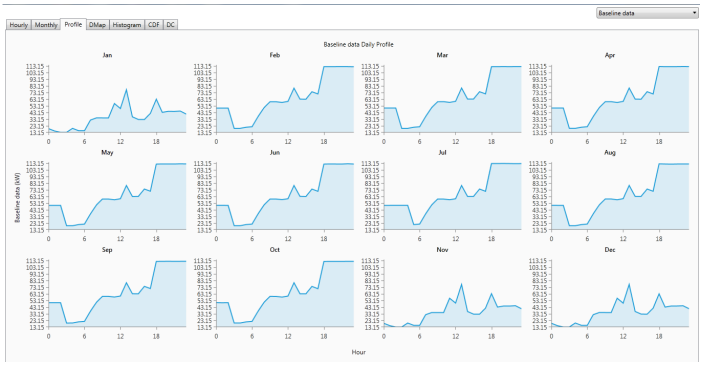

Fig. 10 Hourly variation of all quantities for 12 months.

Fig. 10shows the AC primary load monthly profile in respect of 24 hour time period.

VI. RESULT

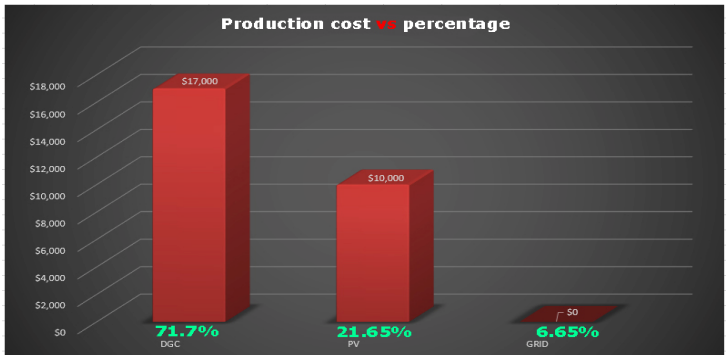

Fig. 11 Bar diagram of production cost vs percentage.

Fig. 11 this graph shows the percentage of different source generation with their respective cost of production. It's so clear that the PV/Photovoltaic will cost almost half of biomass production cost whereas grid production cost is not the concern anymore rather the negligible purchase cost of 6.65% of production. Moreover it also proves that Biomass and PV generation are enough to meet the maximum demand of the building in any typical situation.

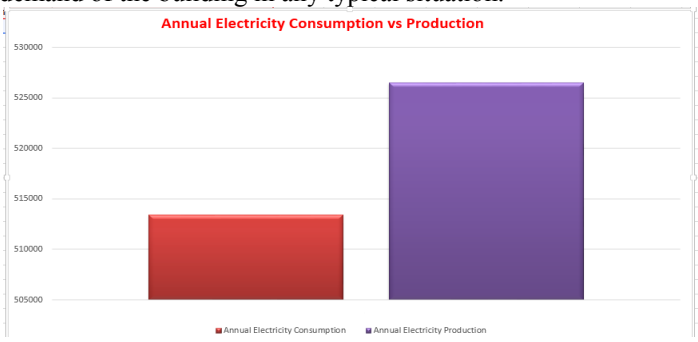

Fig. 12 Bar diagram of annual electricity consumption vs. production

Usually it's more convenient to expect the overall Electricity consumption and production will reach as high as possible with optimize annual cost. Luckily the graph shows

the best outcome in this case. So, according to the graph almost half of energy can be saved in the PV batteries after meeting the annual load demands. In such a way there will be an opportunity to ensure the safety measures in unwanted shutdown of any generation source.

VIII. CONCLUSIONS

Typical biomass based power generation system produces electricity about 90% and above by using only biomass resources (e.g municipal solid waste) [21]. On the other hand, hybrid generation system discussed in this paper is producing 70% from biomass, 20% from solar and rest of the power is from conventional grid system (e.g is case of backup). So, there is less dependency on a single source (e.g biomass or solar PV). Therefore, the generation diversity results in increased security of supply. Bangladesh is a developing country and load shedding is a severe phenomenon. Rapid increase of population makes the demand of electricity high in every consecutive year. Moreover, Bangladesh government purchases a healthy amount of electricity with the help of quick rental service which costs a lot. By establishing this kind of hybrid energy generation system may become most optimized solution to cut off conventional fossil fuel based power plant productions in our urban residential buildings. However, it also reveals the possibility to keep our environment green with zero emission. Though the system has designed for the high-rise buildings, it will ensure the use of annual power consumption in more economic and secure manner for the total electric load. In addition, near future there might be a scope that the system can be used for grid sell purposes to make money from extra generation. In contrast, the proposed hybrid system is now proved to be a unique pathway to solve the shortcomings of electricity problems not only for High rise buildings but also it can cost-effectively installed in rural electrification.

REFERENCES

[1] "Hybrid Renewable Energy System"[Online].Available :http://www.ripublication.com/irph/ijeee_spl/ijeeev7n5_15.pdf [Accessed: 2-june-2015]

[2] "Hybrid Power Systems with Renewable Energy Sources – Types, Structures, Trends for Research and Development"[Online]. Available:http://www.researchgate.net/publication/236012467_Hybrid_Power_Systems_with_Renewable_Energy_Sources__Types_Structures_Trends_for_Research_and_Development [Accessed: 3-june-2015]

[3] "Gasification". Available : http://bisyplan.bioenarea.eu/html-files-en/04-02.html [Accessed: 5-june-2015]

[4] (2014) Tensorcrete website [Online]. Available : http://tensorcrete.com/why-gasification [Accessed: 5-june-2015]

[5] (2014) Biomass technology, Direct combustion [Online]. Available :http://www.biomasstechnology.org/direct-combustion [Accessed: 15-june-2015]

[6] (2014) DESCO [Online]. Available : https://www.desco.org.bd/?page=bill-calculator [Accessed: june-2015]

[7] (2014) Biodegradable waste [Online] Available: http://ec.europa.eu/environment/waste/compost/ [Accessed: 18-june-2015]

[8] "What is non-biodegradable waste?" [Accessed: 18june-2015] Available: http://www.ask.com/science/non-biodegradable-waste-9154deccb3048454

[9] (2014) "Organic Disposal LLC friends of the earth: What is organic waste?" [online] Available : http://www.organicdisposal.net/Pages/organicwaste.aspx [Accessed: 01-june-2015]

[10] Sadaka, Samy, and Donald Mack Johnson. *Biomass Combustion*. Cooperative Extension Service, University of Arkansas, US Department of Agriculture and county governments cooperating, 2011.[Accessed: 01-june-2015]

[11] Works, Yakima County Public. "Review of Biomass Fuels and Technologies." (2003).Available: https://www.uaex.edu[Accessed : 06-june-2015]

[12] "Biomass Combined Heat and Power Catalog of Technologies". Available: http://www.epa.gov/chp/documents/biomass_chp_catalog.pdf [Accessed : 10-june-2015]

[13] (2014) DP clean tech website. Exeter (Flue gas cleaning) [Online]. Available : http://www.dpcleantech.com/china/biomass-projects/biomass-power-plant-project-case-studies/fluegas-cleaning [Accessed: 05-june-2015]

[14] A. Kumar, David D. Jones and Milford A. Hanna. "Thermochemical Biomass Gasification"[Online]. Available : www.mdpi.com/journal/energies

[15] "What is Gasification?"[Online]. Available : http://www.chamco.net/Gasification.htm [Accessed :02- june-2015]

[16] (2014) IEA clean coal centre. Co-firing biomass with coal [Online]. Available: http://www.iea-coal.org.uk/[Accessed: 13-july-2015]

[17] "Introduction of PHOTOVOLTAICS". [Online]. Available:http://ec.europa.eu/research/energy/eu/index_en.cfm?pg=research-photovoltaics[Accessed: 13-June-2015]

[18] "History of Photovoltaics" [Online]. Available:http://www.sunlightelectric.com/pvhistory.php[Accessed: 13-June-2015]

[19] "ADVANTAGES OF hybrid THE SYSTEM "[Online]. Available:http://www.inmesol.com/hybrid-system/advantages-of-the-hybrid-system.asp[Accessed: 13-June-2015]

[20] "How to store your solar generated electricity". [Online]. Available:http://www.yougen.co.uk/blog-entry/1668/How+to+store+your+solar+generated+electricity+to+use+in+the+evening+/[Accessed: 14-June-2015]

[21] Hafezur Rahman, Md. Rayhan Sharif, Rifayat Ahmed, Tamzid Nijam, Md. Asaduzzaman Shoeb, "Designing of Biomass Based Power Plant for Residential Building EnergySystem", Proceedings of 2nd International Conference on Electrical Engineering and Information & Communication Technology, May 21-23, 2015, Dhaka, Bangladesh

[22] "how do solar systems produce energy". [Online]. Available:http://www.nwwindandsolar.com/solar-power-in-seattle-and-the-northwest/how-do-solar-systems-produce-energy/[Accessed: 15-June-2015]

[23] "Modern multi-stage charge controllers".[Online]. Available:http://www.freesunpower.com/chargecontrollers.php[Accessed: 15-June-2015]

Impacts of Fixed Speed Wind Generators on Static Voltage Stability of Distribution Systems

M. H. Haque

School of Engineering
University of South Australia
Mawson Lakes, Australia
Mohammed.Haque@unisa.edu.au

***Abstract*— Small-scale wind generators are increasingly being integrated into distribution systems. The increased penetration of wind generators can significantly change many operating characteristics of the system including voltage profile and hence voltage stability. This paper proposes a simple method of evaluating voltage stability index of a radial distribution system with fixed-speed wind generators. Time varying system demand and measured wind data over a period of one year are considered. The proposed method of evaluating voltage stability index is then tested on a 12.66-kV, 32-bus radial distribution system and the results found are systematically described.**

***Keywords*—Distributed generation, fixed speed wind generators, integration of renewable sources, static voltage stability.**

I. INTRODUCTION

Integration of distributed generation (DG) into power systems affects several operating characteristics of the systems including voltage profile and hence voltage stability [1-3]. However, present trend is to integrate more and more DGs or renewable energy sources into distribution networks and the driving force behind that is environmental concern and recent development of technologies for small-scale power generation. Wind and solar are the fastest growing renewable energy technologies in the world [4, 5] and a large number of small-scale solar photovoltaic systems and wind generating systems has recently been integrated into distribution networks.

There are mainly two types of wind generating systems: fixed speed and variable speed [6, 7]. A fixed speed wind generating system employs a squirrel-cage induction generator (SCIG) which is directly connected to a power network through a step-up transformer. On the other hand, a variable speed wind generating system employs a doubly-fed induction generator (DFIG) with partial size power converters or a permanent magnet synchronous generator with full-size power converters. Most of the large size modern wind farms employ variable speed wind generators. However, fixed speed wind generators are very common for small power application in distribution systems because of some advantages such as brushless and rugged construction, low cost, maintenance free, and operational simplicity [8].

Integration of wind generators (or DGs) into a distribution system has many benefits such as improvement of voltage profile, loss reduction, reliability improvement, capacity release, etc. Voltage stability is associated with voltage profile of the system. Despite time varying system demand and stochastic nature of wind power, maintaining a suitable voltage profile and hence voltage stability is very essential for secure and reliable operation of the system. There are two approaches of analysing voltage stability of a system: static and dynamic [9]. The static approach determines the ability of the network to support a specific demand and the dynamic approach tries to determine the mechanism of voltage collapse. The traditional *P-V* curve is commonly used as a tool to assess static voltage stability of a system and it requires the results of repetitive power flow solutions [9, 10]. Other methods of determining static voltage stability are also described in a number of articles but are mainly applicable for high voltage transmission systems [11-13]. However, only a few articles described the voltage stability assessment of distribution systems with distributed generation [14-16].

This paper proposes a simple method of evaluating static voltage stability of a radial distribution system integrated with fixed speed wind generators. Both time varying system demand and intermittent nature of wind power are considered. For a given wind speed, the turbine power is first determined from manufacturer's supplied data and then carefully incorporated into the generator model. The effectiveness of the proposed method is then evaluated on a 12.66-kV, 32-bus radial distribution system.

II. VOLTAGE STABILITY INDEX

Consider a simple 2-bus system as shown in Fig. 1 where the generator supplies power to a load through a line having an impedance of (R + jX). The power flow at the receiving-end of the line is (P + jQ). The magnitude of sending-end and receiving-end voltage is considered as V_S and V_R, respectively. The relationship between V_S and V_R can be written as

$$\overline{V}_S = \overline{V}_R + \frac{(P - jQ)}{\overline{V}_R^*}(R + jX) \quad (1)$$

The above phasor equation can be re-written in the following scalar form

$$V_R^4 + [2(RP + XQ) - V_S^2]V_R^2 + (P^2 + Q^2)(R^2 + X^2) = 0 \quad (2)$$

For a given sending-end voltage V_S, eqn. (2) provides two positive real solutions of V_R when the load is within the voltage stability limit [17]. The higher solution is called stable solution and the lower solution is called unstable solution. Variation of stable and unstable solutions against load power is known as *P-V* curve and is commonly used as a tool to

assess voltage stability of the system [10]. In order to guarantee two positive real solutions of (2), the following condition must be satisfied [17].

$$[2(RP+XQ)-V_S^2]^2-4(P^2+Q^2)(R^2+X^2)>0 \quad (3)$$

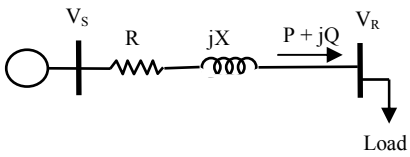

Fig. 1 Single line diagram of a simple 2-bus system

When the load approaches to the voltage collapse point, the stable solution coalesces with the unstable solution and for such a case eqn. (3) becomes zero. Beyond the voltage collapse point, eqn. (3) becomes negative and that cease to provide any positive real solution of (2). Thus, the value of eqn. (3) is an indicator of the distance to voltage collapse. In this study, the value of eqn. (3) is considered as the voltage stability index (*VSI*) at the receiving-end bus [15]. Thus,

$$VSI=[2(RP+XQ)-V_S^2]^2-4(P^2+Q^2)(R^2+X^2) \quad (4)$$

Note that a similar *VSI* is also proposed in [14] but that requires phase difference between sending- and receiving-end voltages. However, no such calculation is required in (4). For V_S = 1 pu, *VSI* of (4) becomes unity at no-load ($P = Q = 0$). In other words, *VSI* varies between unity (at no-load) and zero (at voltage collapse point). Evaluation of *VSI* at the receiving-end bus requires the voltage magnitude at the sending-end bus and the complex power flow at the receiving-end of the branch. The above information can easily be obtained from power flow solutions. By knowing the power flow results, the *VSI* of all buses of a system can be evaluated through (4) and the minimum value of *VSI* can be considered as the overall *VSI* of the system. The bus having the lowest value of *VSI* can be considered as the weakest bus in the system.

III. Model of Wind Generating Systems

A wind generating system consists of a wind turbine (WT) and a generator. The WT converts the kinetic energy of moving air into mechanical energy and the generator converts the mechanical energy into electrical energy. This Section describes the model of a fixed speed wind generating system.

A. Wind Turbine Model

The mechanical power (P_m) captured by a WT can be written as [18]

$$P_m=\frac{1}{2}\rho A V_w^3 C_p(\lambda,\beta) \quad (5)$$

Here ρ is air density (kg/m^3), A is turbine blade swept area (m^2), V_w is wind speed (m/sec), and C_p is performance coefficient which depends on tip-speed-ratio λ and blade pitch angle β. Fortunately, most of the turbine manufacturers provide the power curve (or data) of the turbine [19-21].

In this study, GWL 225-kW WT is used. The power data of the WT obtained from manufacturer's website [21] is given in Table-I. The cut-in (V_{in}) and cut-out (V_{out}) wind speeds of the turbine are specified as 4 m/s and 25 m/s, respectively. Note that the turbine power is zero when the wind blows below the cut-in speed V_{in} or above the cut-out speed V_{out} [22].

Table-I Power data of a 225-kW WT (V_w in m/s and P_m in kW)

V_w	P_m	V_w	P_m	V_w	P_m
4	9	12	189.3	19	225
5	19.5	13	206	20	215
6	32.8	14	217	21	212
7	58.8	15	230	22	210
8	87.6	16	234	23	210
9	118.7	17	230	24	210
10	149.6	18	229	25	210
11	171.4				

B. Generator Model

As mentioned, a squirrel-cage induction generator (SCIG) is commonly used in a fixed-speed wind generating system. The per-phase equivalent circuit of a SCIG is shown in Fig. 2 where R_1, R_2, X_1, X_2, R_c and X_m represent stator resistance, rotor resistance, stator leakage reactance, rotor leakage reactance, core loss resistance and magnetizing reactance, respectively. For generator operation, slip s is negative and thus the rightmost resistance $R_2(1\text{-}s)/s$ of Fig. 2 is also negative. For such an operation, the resistance delivers power instead of absorbing power [23]. The power of this resistance represents the mechanical power P_m supplied by the WT and is also indicated in the figure.

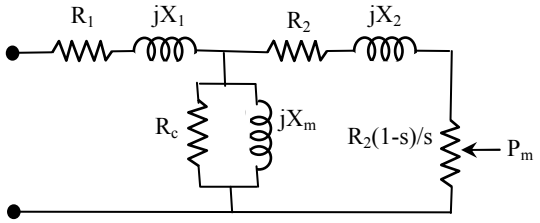

Fig. 2 Per-phase equivalent circuit of a SCIG

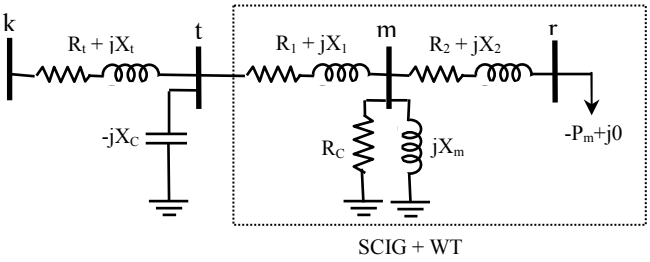

Fig. 3 Representation of a SCIG including a shunt capacitor and a transformer

A SCIG absorbs reactive power and that may deteriorate the voltage profile and hence voltage stability index. A shunt capacitor is usually used to compensate a part of reactive power demand of the generator. The overall equivalent circuit of the SCIG including a shunt capacitor and a step-up transformer is shown in Fig. 3 where X_c is the reactance of the shunt capacitor and (R_t+jX_t) is the leakage impedance of the transformer. Note that the rightmost resistance of Fig. 2 is represented by a load of (-P_m + j0) in Fig. 3. Thus, integration of a wind generator into a power network simply involves the addition of the circuit of Fig. 3 at the interfacing bus k.

IV. Results and Discussions

The effect of fixed speed wind generating systems on voltage stability is investigated on a 12.66-kV, 32-bus radial distribution system having a main feeder and three sub-feeders. The single line diagram of the modified system (with two wind generating systems at buses 17 and 32) is shown in Fig. 4. The system has a base load of (4715 + j2300) kVA and its data is given in [24]. Because of the lack of time varying load data, it is assumed that the hourly load variation of all buses of the system follows the same pattern as described in [25] while keeping the mean value the same as the base load.

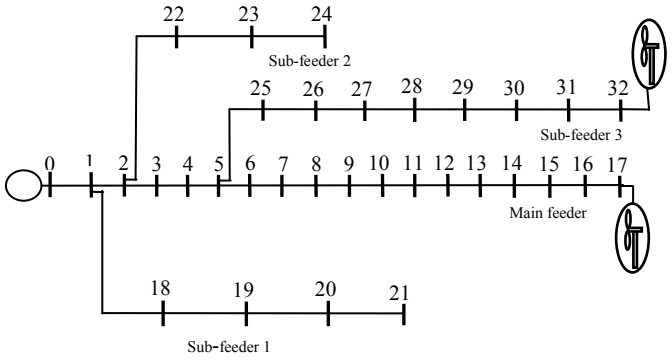

Fig. 4 Single line diagram of the 32-bus system with wind generators

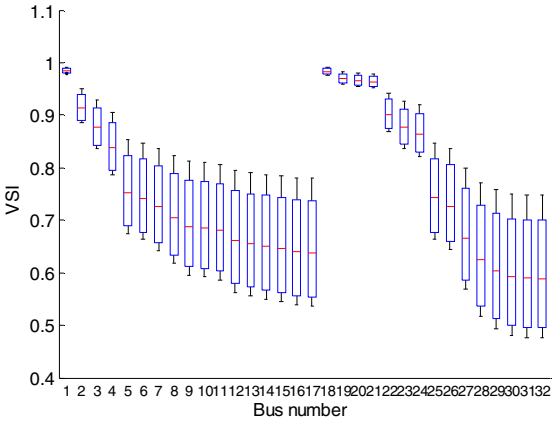

Fig. 5 VSI of the original system (without wind generators)

First, the *VSI* of all buses of the original system (without wind generators) is evaluated for 24-hour periods and the results found are shown in Fig. 5. The load flow results required for this purpose are obtained using the technique described in [26]. The boxplot of Fig. 5 shows the median value (central mark), and the 25th and 75th percentiles at the box edges. The whiskers extend to the most extreme values of *VSI*. It can be noticed in Fig. 5 that bus 32 (end of sub-feeder 3) has the lowest median value of *VSI*. Lower median value of *VSI* can also be observed at the end of the main feeder (bus 17). Thus, the end of sub-feeder 3 and the main feeder can be considered as the weakest part of the network.

To improve voltage stability of the system, three identical GWL 225-kW wind turbines are installed at buses 17 and 32. Thus, the total capacity of wind power is 1,350 kW (= 6x225 kW) and is 28.6% of base load of 4715 kW. The rating of each SCIG is considered as 690-V, 250-kVA, 0.9 lagging power factor. The parameters of the generator are given in [23].

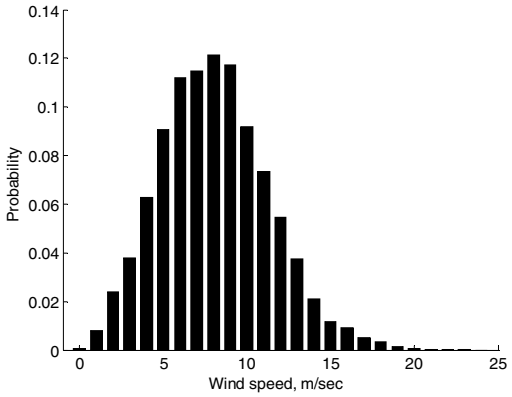

Fig. 6 Discrete probability density of measured wind data

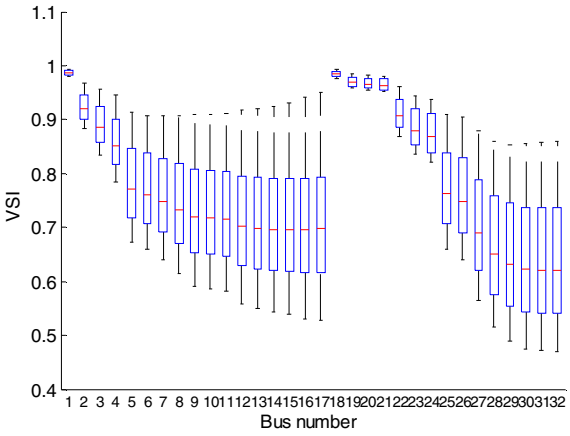

Fig. 7 VSI of the 32-bus system with wind generators

The hourly wind speed of all WTs is considered to be the same as the measured data at a particular site in South Australia and is obtained from [27]. The discrete probability density of measured wind data is shown in Fig. 6. The annual average wind speed is found as 8.16 m/s. The *VSI* of all buses of the system is then evaluated at every hour of the year (365x24 = 8760 hours) using the measured wind data and time varying system demand. The load flow results of the system with wind generators are obtained using the technique described in [23]. It is assumed that 50-kVAr of shunt capacitor (20% of generator rating of 250 kVA) is installed at the terminal of each wind generator. The boxplot of *VSI* of the system with wind generators is shown in Fig. 7. By comparing Figs. 5 and 7, one can observe that the WTs cause a wide variation of *VSI* because of intermittent nature of wind power. However, the WTs increase the mean value of *VSI* of all buses of the system as can be seen in Fig. 8. The improvement is significant in the weakest parts of the network. It may be mentioned here that the *VSI* depends on the value of the shunt capacitor used. Fig. 9 shows the variation of mean *VSI* of all buses of the system for different values of shunt capacitor (% of generator rating) and it can be noticed that the *VSI* increases with the increase in shunt capacitor size, as expected.

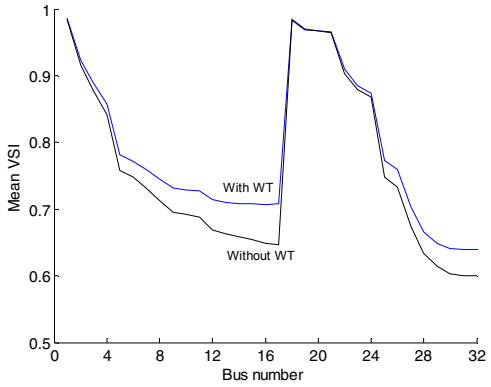

Fig. 8 Mean value of VSI with and without wind generators

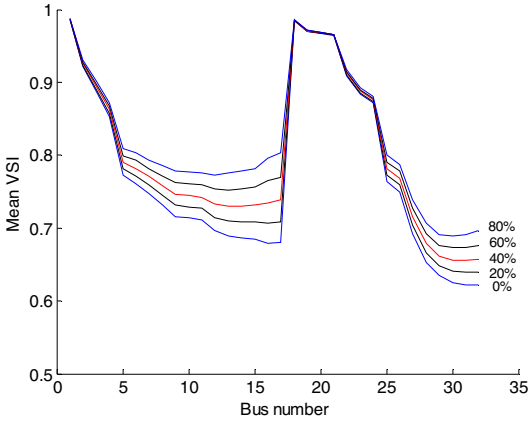

Fig. 9 Variation of mean VSI for different values of shunt capacitors.

V. Conclusions

Integration of wind generators into distribution systems can significantly change the system voltage profile and hence voltage stability index. This paper investigated the effects of fixed speed wind generators on voltage stability of a radial distribution system with time varying demand and measured wind data. A simple method of evaluating voltage stability index (*VSI*) is also discussed. For a given wind speed, the turbine power is first determined through manufacturer's supplied data and then carefully incorporated into the generator model. The proposed technique of evaluating voltage stability is then tested on a 12.66-kV, 32-bus radial distribution system. It has been found that the *VSI* of the system, with wind generators, can vary widely because of intermittent nature of wind power. However, the mean value of *VSI* is significantly improved, especially in the weakest parts of the network, when the wind generators are placed at appropriate locations. The degree of improvement of *VSI* depends on reactive power support and hence the size of the shunt capacitors used at the generator terminals.

References

[1] P. P. Barker and R. W. de Mello, 'Determining the impact of distributed generation on power systems: I. Radial distribution systems", IEEE PES Summer Meeting, Vol. 3, pp. 1645-1656, 2000.

[2] J. P. Lopes, N. Hatziargyriou, J. Mutale, P. Djapic and N. Jenkins, "Integrating distributed generation into electric power systems: A review of drivers, challenges and opportunities", Electric Power Systems Research, Vol. 77, No. 9, pp. 1189-1203, 2007.

[3] Working Group on Distributed Generation Integration, "Summary of distributed resources impact on power delivery systems", IEEE Trans. on Power Delivery, Vol. 23, No. 3, pp. 1636-1644, 2008.

[4] http://www.thewindpower.net/.

[5] Photovoltaic Power Systems Programme - Annual Report 2013, International Energy Agency.

[6] IEEE PES Wind Plant Collector System Design Working Group, "Characteristics of wind turbine generators for wind power plants", Proc. 2009 IEEE Power and Energy Society General Meeting, Calgary, Canada, 2009.

[7] H. Li and Z. Chen, "Overview of different wind generator systems and their comparisons", IET Renewable Power Generation, Vol. 2, No. 2, 2008, pp. 123-138.

[8] J. H. Liu and C. C. Chu, "Long-term voltage instability detections of multiple fixed-speed induction generators in distribution networks using synchrophasors", Accepted for publication in the IEEE Trans. on Smart Grid.

[9] T. V. Cutsem and C. Vournas, "Voltage stability of electric power systems", Kluwer Academic Press, Massachusetts, USA, 1998.

[10] C. W. Taylor, "Power system voltage stability", McGraw-Hill, NY, USA, 1994.

[11] M. H. Haque, "Use of V-I characteristic as a tool to assess static voltage stability limit of a power system", IEE Proc. – Gener. Transm. Distrib., Vol. 151, No. 1, pp. 1-7, 2004.

[12] K. Vu, M. M. Begovic, Novosel, D. and M. M. Saha, "Use of local measurements to estimate voltage stability margin", IEEE Trans on Power Systems, Vol. 14, No. 3, pp. 1029-1034, 1999.

[13] M. H. Haque, "On-line monitoring of maximum permissible loading of a power system within voltage stability limit", IEE Proc. – Gener. Transm. Distrib., Vol. 150, No. 1, pp. 107-112, 2003.

[14] P. Raja, M. P. Selvan and N. Kumaresan, "Enhancement of voltage stability margin in radial distribution system with squirrel-cage induction generator based distributed generators", IET Generation, Transmission and Distribution, Vol. 7, No. 8, pp. 898-906, 2013.

[15] M. H. Haque, "Voltage stability assessment of distribution systems with fixed speed wind generating systems", Proc. of the IEEE ISGT-ASIA conference, Bangkok, 2015.

[16] R. S. Al-Abri, E. F. El-Saadany and Y. M. Atwa, "Optimal placement and sizing methods to improve the voltage stability margin in a distribution systems using distributed generation", IEEE Trans. on Power Systems, Vol. 28, No. 1, pp. 326-334, 2013.

[17] M. H. Haque, "A fast method of determining the voltage stability limit of a power system" Electric Power Systems Research, Vol. 32, No. 1, pp. 35-43, 1995.

[18] S. Heier, "Grid integration of wind energy conversion systems", 2nd Edition, John Wiley, Chichester, West Sussex, UK, 2006.

[19] Vestas: http://www.vestas.com/en/media/brochures.aspx#!

[20] Siemens: http://www.energy.siemens.com/mx/en/renewable-energy/wind-power/platforms/

[21] Freebreeze: http://www.freebreeze.com/wind-turbines/gwl-225kw-wind-turbine.html.

[22] G. M. Masters, "Renewable and efficient electric power systems", Second Edition, IEEE Press, 2013.

[23] M. H. Haque, "Incorporation of fixed speed wind turbine generators in load flow analysis of distribution systems", International Journal on Renewable Energy Technology, Vol. 6, No. 4, pp. 317-333, 2015.

[24] M. E. Baran and F. F. Wu, 'Network reconfiguration in distribution systems for loss reduction and load balancing", IEEE Trans. on Power Delivery, Vol. 4, No. 2, pp. 1401-1407, 1989.

[25] J. R. Aguero, "Distribution system planning in smart grid era", IEEE Power and Energy Magazine, Vol. 9, No. 5, 2011, pp. 82-93.

[26] M. H. Haque, "Efficient load flow method for distribution systems with radial or mesh configuration", IEE Proc. - Gener. Transm. Distrib., Vol. 143, No. 1, pp. 33-38, 1996.

[27] Bureau of Meteorology (BoM), Commonwealth of Australia: http://www.bom.gov.au/.

Development and Testing of a Two-axis Tracking Spherical Solar Cooker

Md. Rafsunjani[1], Erina Baynojir Joyee[2], A. N. M. Mizanur Rahman[3,*]

[1,2]UG Student, [3]Professor
Department of Mechanical Engineering,
Khulna University of Engineering & Technology, Khulna 9203, Bangladesh
drmizan84@gmail.com; rafsunjanihemel@yahoo.com

Abstract: **Solar energy, the clean and non-polluting energy source, has a great potential to supply world's energy needs. It is one of the largest renewable energy resources which is available almost everywhere. There are many fields where solar energy is used such as water & air heating, drying, distillation, cooking etc. But the efficiency of solar systems is less than conventional systems. It might be because of lack of proper technology and high cost to develop efficient system. Solar cooker is a device which is used for cooking food. It is simple, safe and convenient to cook food without consuming conventional fuel. In the previous year a parabolic type spherical solar cooker was designed and constructed. In that cooker, single axis manual tracking was used. In order to improve the efficiency of the cooker, a two axis tracking mechanism was designed and constructed and the cooker was installed on it. But, the motors that were needed for two axis tracking were expensive. So, an alternative manual tracking system was developed that could serve the purpose of facing the collector towards the sun every half an hour. Performance of the cooker has been measured. The maximum temperature inside the cooking pot was found to be 97°C, with a load of 300 g rice and 100 g dal, within 40 minutes at a radiation level of 260-394 W/m^2.**

Keywords: ***Solar cooking, spherical cooker, tracking system, two axis tracking, performance test.***

I. INTRODUCTION

In developing country like Bangladesh, energy crisis is very serious. Natural energy resources such as fossil fuel, oil, natural gas etc. will be finished within very short time until new sources are explored. So, energy conservation by developing efficient energy systems and developing energy alternatives has become important consideration. This led to considerable research and significant progress has been made in this sector [1]. In some cases renewable energy is the most suitable solution for the growing energy demand. Among these energy sources, solar energy is the most widely available one. Solar energy has been utilized by human being since the dawn of civilization. Solar technology can be classified according to capture, conversion and distribution. Solar energy is cheap, abundantly available almost everywhere and can be used for various domestic as well as industrial applications like cooking, dehydration, drying, heating of water or air, power generation etc. Solar energy can be directly used for cooking. There are different types of solar cooking methods. For example, in box type solar cooker green house effect is used for cooking, in panel cookers transparent glass bowl along with a reflective panel is used, in parabolic dish cookers concentration of sunlight is used for cooking.

In developing countries like Bangladesh energy consumption for cooking is a lion share of the total energy consumption. In the rural areas cooking is mainly made by fuel wood but in the urban areas this is served either by gaseous or liquid fuels. But, in most of the areas mainly fuel woods are used for cooking purpose which is a major cause of deforestation [2].

The sun moves from east to west across the sky within the day. Also, position of the sun varies in different seasons. If the payload can be moved with the movement of the sun, it gets more solar radiation. To get maximum solar radiation solar trackers are used. Solar tracking system is a device for orienting a solar collector or panel towards the sun all the time. Reflectors are devices to deflect the solar radiation towards a specified direction to increase the radiation intensity. Solar trackers are used to collect more solar energy. So, if a solar tracker is used in a solar cooker or any other device that uses solar energy, its efficiency will increase as the payload will get more radiation. In the previous year, a parabolic dish type solar cooker was constructed and tested [3]. In that cooker, a single axis manual east-west tracking system was used and after every 15 minutes interval the cooker was manually tracked. To overcome these limitations, attempts have been made to develop a two axis tracking system in the present work. Four LDR sensors were used for tracking the sun. Depending on the variation of light intensity, the sensors send signal to the control unit about the right position of the sun. The control unit sends signal to two motors (one is fixed with the vertical axis and the other fixed with the horizontal axis) for getting the most likely position i.e. perpendicular to the sun. The two motors would rotate the cooker until all the four sensors read equal resistance due to incident sunlight.

II. THEORETICAL ASPECTS AND LITERATURE REVIEW

The sun is the star of our planetary system and one of the largest stars in our galaxy. The source of energy in the sun is at its core where hydrogen is converted to helium in a thermonuclear reaction. This energy travels from core of the sun to its surface and then to the earth in two main forms, heat and light. Every hour enough sunlight reaches the earth to meet the world's energy demand for the whole year. The

amount of energy from the sun that reaches the earth annually is 4×10^{18} Joules. The amount of energy consumed annually by the world's population is about 3×10^{14} Joules. The earth is the third planet from the sun at a distance of about 1.495×10^{8} km. On the other hand, for light it takes only 8.5 minutes to reach the earth from the surface of the sun travelling at the speed of 2.993×10^{5} km /sec [4, 5]. The solar energy received per unit time per unit area of the surface perpendicular to the direction of propagation when the sun is at its mean distance from the earth is known as solar constant and its accepted value is 1353 W/m^2 with an estimated error of ±1.5%. The World Radiation Center (WRC) has adopted a value of 1367 W/m^2, with an uncertainty of the order 1% [6]. But the radiation available on earth surface is much less than this value. In fact, solar energy available on a location depends on several parameters like, time of day, season of year, latitude, clearness index of the sun.

Fortunately the location of Bangladesh is in a favourable position in respect of availability of solar energy. The daily amount of solar radiation varies from 1575 - 4320 Wh/m^2 which is 50 – 100% higher than that in Europe [7, 8]. It has variety of uses like water and air heating, cooking, distillation, drying etc. In developing countries like Bangladesh energy consumption for cooking is a major share of the total energy consumption. In rural areas, cooking is mostly made by fuel wood. In urban areas, this is served either by fuel wood or gaseous or liquid fuels. Using fuel wood increases deforestation and gaseous and liquid fuels are mostly imported. So, there is lot of scope of using solar energy for cooking purposes.

Solar cooker is a device which cooks food without using any conventional cooking fuel such as fuel-wood, straw, kerosene etc. Solar cooker works by collecting solar energy and delivering it into cooking element. Solar cooker ensures an economically beneficial and environmental friendly cooking method. There are various types of solar cooker. In box type cooker a greenhouse effect is used for cooking, whereas in panel cookers transparent glass bowl along with a reflective panel is used, in the parabolic dish cookers concentration of sunlight is used for cooking and so on.

III. DESIGN AND CONSTRUCTION

The sun moves across the sky throughout the day and also the position of the sun changes seasonally. To get maximum radiation the payload must be at normal to the sun. Tracking is a system for orienting a solar collector towards the sun so that the radiation is mostly perpendicular to the receiving surface. In panel cooker or parabolic dish cooker tracking is necessary to get optimum power from the system. There are several ways of tracking for any solar collector. Two axis tracking system will maximize the radiation on the solar cooker.

A. Design Basics

Tracking of the sun was carried out by using four LDR sensors which using the differences in radiation detect the position of the sun. The microcontroller sends signal to the driving motors for getting the most likely position i.e. perpendicular to the sun. The two motors (connected to the vertical and horizontal axis shaft) would rotate the cooker until all the four sensors experience equal resistance due to incident sunlight. Since the motors consume energy, one would want use them only when necessary. So, instead of a continuous motion, trackers may be moved in discrete steps. Also, if the radiation is below some threshold level there would not be any need for reorientation. Consideration must be made to keep the tracker from wasting energy.

B. Electronic Circuit Design

The overall circuit layout of the LDR is shown in Fig. 1. An Ardino UNO embedded with ATmega 328P micro-controller is used in the circuit.

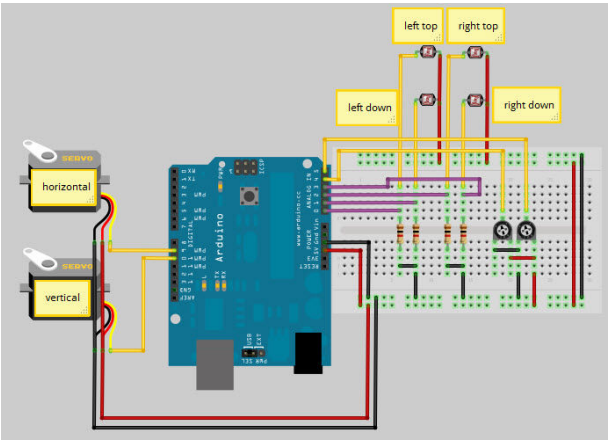

Fig.1 Overall circuit layout

C. Microcontroller Code

A computer program in C language is used for the microcontroller operation.

D. Construction of Experimental Setup

For good stability and flexibility in the movement of the tracking system two considerations made were. They are- (i) the diameter of the base of the structure must be equal to or greater than the diameter of the spherical reflector so that it doesn't tilt over while tracking and (ii) the distance between two supporting points of the horizontal shaft must be equal to or greater than the radius of the spherical solar cooker for better stability.

Fig. 2 shows the schematic arrangement of the frame of the tracking system of the said cooker. The materials were chosen on the basis of the structural stability and also the weight of the tracking system. The dimensions of the frame were chosen on the basis of the design considerations described to obtain better stability and flexibility. In fact the reflector and the cooking location were made in the previous year. Therefore, the dimensions were fixed previously; only the bottom supporting system is constructed in the present work.

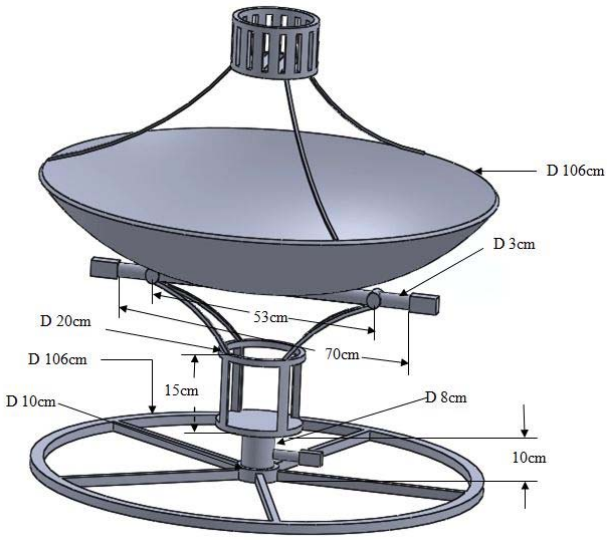

Fig. 2 Schematic of proposed Spherical solar cooker

IV. PERFORMANCE TEST

In order to compare the performance of the present two axis tracking solar cooker with that of the single axis tracking one, the experiments were conducted with the same loading as it was made earlier (i.e., same quantity of rice, dal and water). According to the measurement water was taken into the cooking pot and the cooker was positioned at the proper direction toward the sun. Thermocouple wire with display was placed inside the cooking pot to observe the temperature. The temperatures were recorded after every 10 minutes interval. At the same time solar intensity was also recorded from the solarimeter. When sufficient temperature was raised, the loading of rice and dal of different quantities were made to the cooking pot. Because of financial constraint in actual experiments, the motors which control the vertical and horizontal movements were not used. Rather a manual two axis tracking system was developed that track in a discrete manner. After every 10 minutes the cooker was manually tracked. The experiments were conducted during the month of April – May for several days and 18 observations were made. Some of the typical data are presented in Table I to Table IV.

TABLE I
Data for different loads on 29-04-15

No. of Obs	Cooking item & quantity	Watch Time	Intensity W/m^2	Energy Wh/ m^2	Temperature ˚C
Observation No. 1					
1	250 g rice, 50 g dal & 600 ml water	10.10	331	00	33
2		10.20	343	113	72
3		10.30	357	208	84
4		10.40	378	323	97
5		10.50	385	354	97
Started at: 10.10 AM End at: 10.50 AM Remarks: 250 g rice and 50 g dal boiled properly in 40 mins. Maximum Temperature: 97˚C					
Observation No. 2					
1	300 g rice, 50 g dal & 700 ml water	11.05	308	00	33
2		11.15	325	154	74
3		11.25	347	283	85
4		11.35	382	348	97
5		11.45	394	368	97
Started at: 11.05 AM End at: 11.45 AM Remarks: 300 g rice and 50 g dal boiled properly in 40 mins. Maximum Temperature: 97˚C					

TABLE II
Data for different loads on 1-05-15

No. of Obs	Cooking item & quantity	Watch Time	Intensity W/m^2	Energy Wh/ m^2	Temperature ˚C
Observation No. 3					
1	300 g rice, 100 g dal & 800 ml water	9.50	280	00	33
2		10.00	289	118	62
3		10.10	297	209	74
4		10.20	309	323	92
5		10.30	316	354	96
Started at: 9.50 AM End at: 10.35 AM Remarks: 300 g rice and 100 g dal boiled properly in 45 mins. Maximum Temperature: 96˚C					
Observation No. 4					
1	300 g rice, 50 g dal & 700 ml water	10.55	288	00	33
2		11.05	308	125	77
3		11.15	329	283	89
4		11.25	357	318	96
5		11.35	372	368	96
Started at: 10.55 AM End at: 11.35 AM Remarks: 300 g rice and 50 g dal boiled properly in 40 mins. Maximum Temperature: 96˚C					

TABLE III
Data for different load on 3-05-15

No. of Obs	Cooking item & quantity	Watch Time	Intensity (W/m^2)	Energy (Wh/ m^2)	Temperature (˚C)
Observation No. 5					
1	300 g rice, 50 g dal & 700 ml water	9.50	315	00	33
2		10.00	323	95	62
3		10.10	349	178	83
4		10.20	358	289	91
5		10.30	377	365	97
6		10.35	384	410	97
Started at: 9.50 AM End at: 10.35 AM Remarks: 300 g rice and 50 g dal boiled properly in 45 mins. Maximum Temperature: 97˚C					

TABLE IV
Data for different load on 8-05-15

No. of Obs.	Cooking item & quantity	Watch Time	Intensity (W/m^2)	Energy (Wh/ m^2)	Temperature (˚C)
Observation No. 6					
1	250 g rice, 50 g dal & 600 ml water	9.50	290	00	33
2		10.00	317	63	62
3		10.10	355	191	83
4		10.20	372	223	96
5		10.30	389	254	97
Started at: 9.50 AM				End at: 10.30 AM	
Remarks: 250 g rice and 50 g dal boiled properly in 40 mins. Maximum Temperature: 97˚C					

V. RESULT AND DISCUSSION

A. Result

The variations in the temperatures inside the cooking pot with various cooking elements were recorded and are plotted. They are shown in Figs. 3 to 12. The time required for good cooking was noted. It is to be noted that only visual observation of rice cooking was compared. For comparison the time required with the previous single axis tracking are also presented with the present one under same loading conditions.

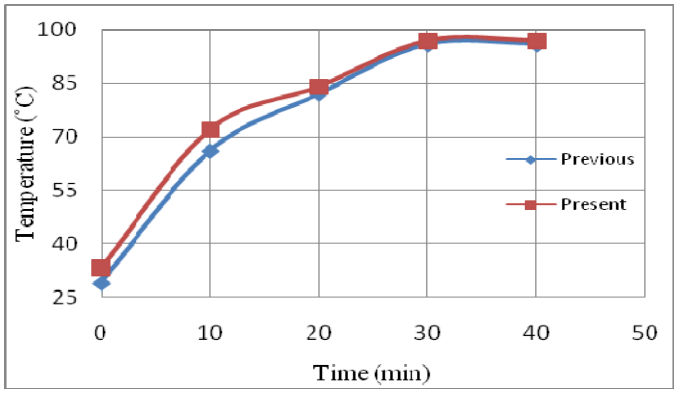

Fig. 3: Temperature Vs time curve for 300g load on 29-04-15

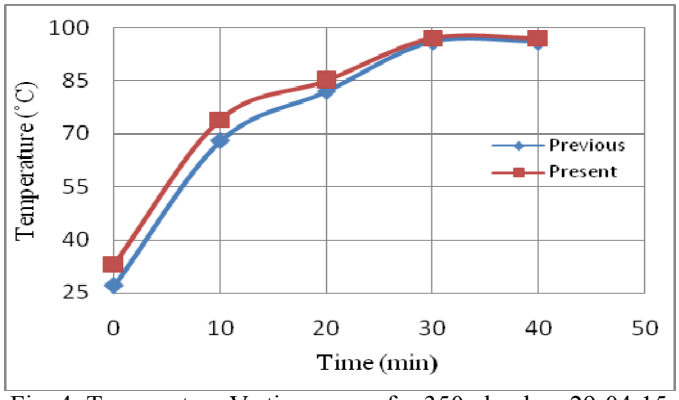

Fig. 4: Temperature Vs time curve for 350g load on 29-04-15

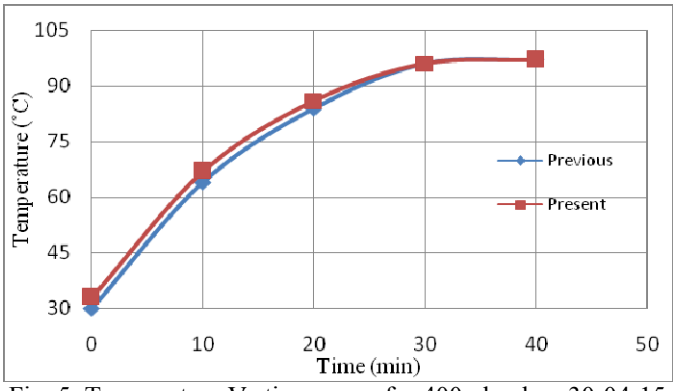

Fig. 5: Temperature Vs time curve for 400g load on 30-04-15

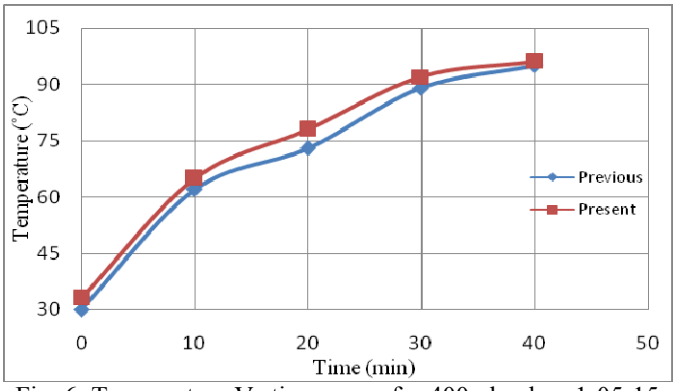

Fig. 6: Temperature Vs time curve for 400g load on 1-05-15

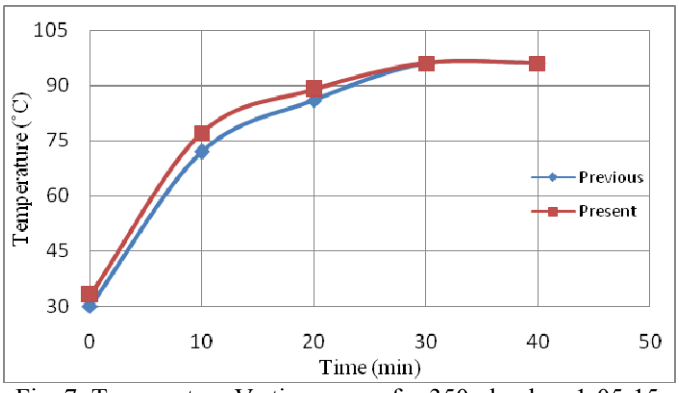

Fig. 7: Temperature Vs time curve for 350g load on 1-05-15

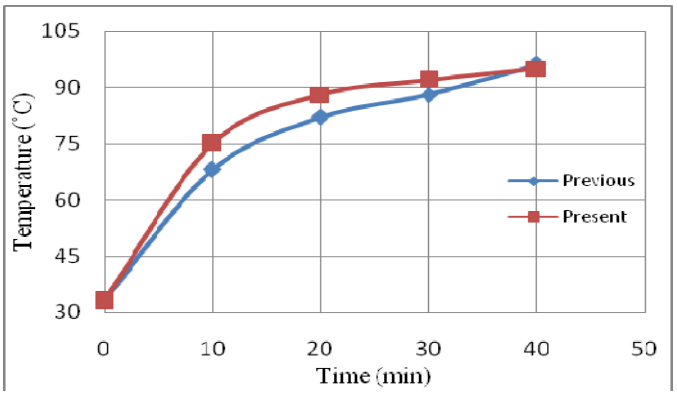

Fig. 8: Temperature Vs time curve for 400g load on 2-05-15

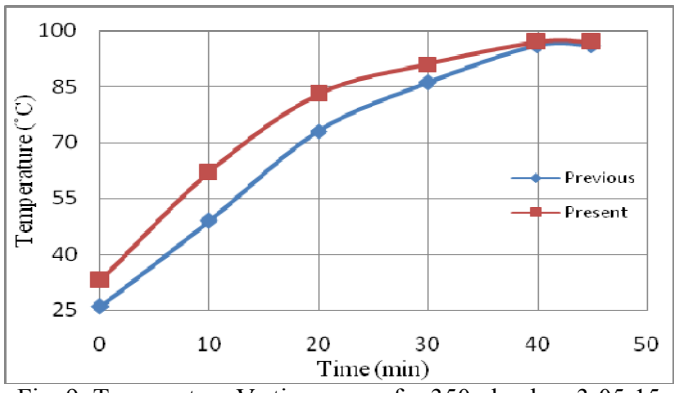

Fig. 9: Temperature Vs time curve for 350g load on 3-05-15

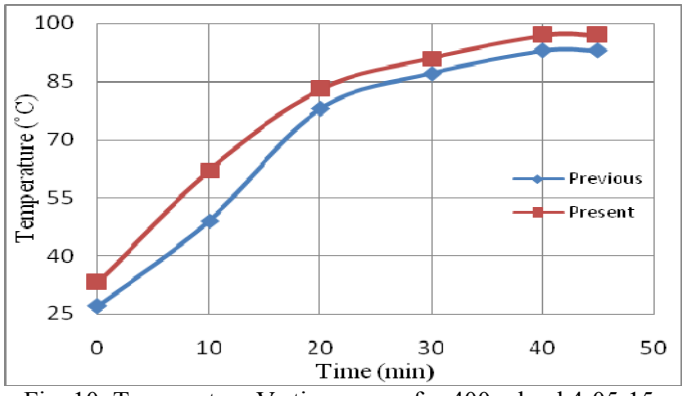

Fig. 10: Temperature Vs time curve for 400 g load 4-05-15

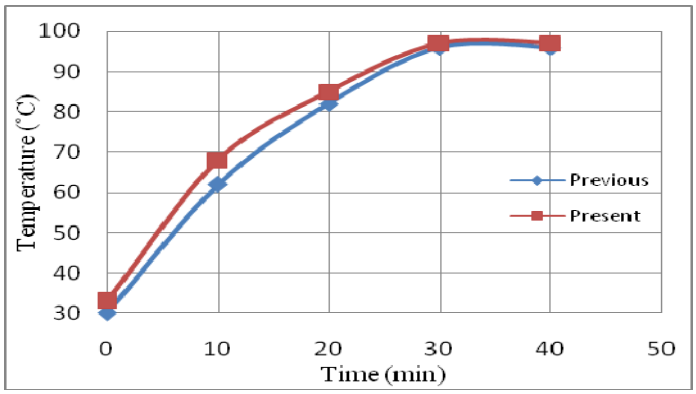

Fig. 11: Temperature Vs time curve for 350g load on 6-05-15

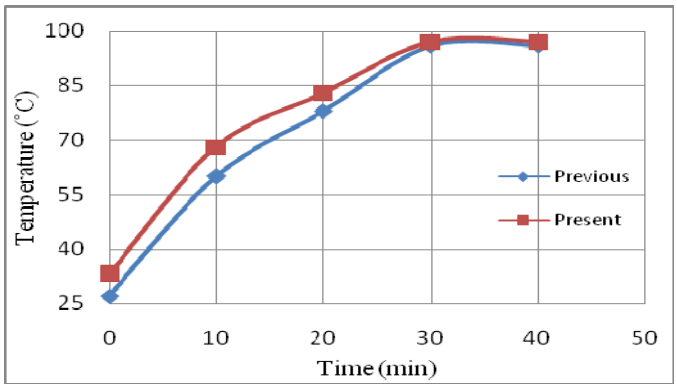

Fig. 12: Temperature Vs time curve for 300g load on 8-05-15

B. Discussion

Figs. 3 to 12 show the temperature inside the cooking pot vs time for both the present and previous cooker [3] for same loading at different days. From the figures it is clear that the temperature inside the cooking pot increases as the time increases but the rate of increase is more with two axis tracking. There is no significant improvement in the quality of cooking. The graphs show almost similar pattern because the time for cooking is not too long and also only the loading varies on different days.

From Figs 3, 4, 11 and 12 it is clear that the maximum temperature inside the cooking pot was found to be 97˚C with different loadings within 40 minutes at an available radiation level of 260-394 W/m^2. From Fig 9 it is evident that the maximum temperature obtained inside the cooking pot was also 97˚C with a load of 350g in 40 minutes but the cooking was completed in 45 minutes at a radiation level of 260-388 W/m^2. In Figs 5 and 10 it is seen that the maximum temperature raised inside the cooking pot was 97˚C with different loads in 50 minutes at a radiation level of 260-384 W/m^2. So, it is clear that as radiation level decreases, the time taken is more for cooking.

Figs. 3 to 12 also depicts that temperature inside the cooking pot at any time is higher for two axis tracking than single axis tracking. But as cooking continues, the differences decrease. This is because that cooking temperature is fixed. But the cooking time was less in almost all observations although they were not very significant. But with single axis tracking the diurnal variation of the sun is difficult to accommodate. Although continuous tracking could not be adapted but from the comparison of single axis tracking and two axis tracking, it may be concluded that continuous tracking will not provide significant improvement in the performance. Rather provision of two axis tracking (manual) is enough to get optimum benefit from the solar cooker.

Box type solar cooker is not efficient to cook food quickly compared to conventional cooking but a concentrating solar cooker may compete with the conventional cooking. The initial construction cost of such solar cooker is bit high but it does not require any fuel for cooking. So, in the long run it is comparable with the conventional cooking. In a cloudy day, a concentrating solar cooker is not effective as the radiation does not make sharp shadows so reflection is less. In addition a certain threshold value of radiation level is necessary for good cooking. The radiation value will not remain exactly same on other day, so for comparison a radiation range was considered for the present one and previous one.

VI. CONCLUSION

The solar cooker with tracking system represents a potential subsidiary to cooking compared to conventional ways. The following points can be drawn to depict the conclusion:

- Performance of the two axis manual tracking cooker showed that similar maximum temperature inside the cooking pot reached with similar loading in less time with similar radiation level compared to single axis tracking.
- Although the radiation level was not exactly same for same loading on two different cases still there is considerable saving in time with a two axis tracking.
- The instantaneous temperature rise with two axis tracking is more under similar radiation intensity. But it gives significant improvement in the quality of cooking.

Acknowledgment: The authors acknowledge the financial support granted for the project by the KUET authority. Also the permission of using the laboratory facilities of Mechanical Engineering department is acknowledged.

References

[1] http://research.brac.net/reports/altenergy.pdf
[2] http://en.wikipedia.org/wiki/Renewable_energy_policy_of Bangladesh.
[3] Erina Baynojir Joyee, "Design and Construction of a Parabolic Dish Type Solar Cooker", UG Project report. Department of Mechanical Engineering, KUET, 2014
[4] http://solarenergy.wikia.com/wiki/about solar energy
[5] Wikipedia, the free encyclopaedia, http:// en.wikipedia.org/wiki/solar energy.
[6] John A. Duffie and William A. Beckman, "Solar Engineering of Thermal Processes", Second Edition, John Wiley & Sons, Inc. New York, 1991,
[7] Nasima Akter. "Alternative Energy Situation in Bangladesh: A Country Review", Paper presented at the Regional Training Orientation Course on Alternative Energy Technologies, organized by APPROTEC ASIA Philippines Social Development Centre, Philippines at July 1997.
[8] http://en.wikipedia.org/wiki/Solar_tracker
[9] H. P. Garg and J. Prakash, "Solar Energy", First Edition, Tata McGraw Hill, New Delhi, 2000,
[10] Ferdinand P. Beer, E. Russell Johnston, Jr., John T. Dewolf and David F. Mazurek, "Mechanics of Materials", McGraw-Hill Book Company, 2012.

Development and Performance Test of an Evacuated Tube Solar Water Heater

Nafiz Ahmed Badhan[1], Farzana Mollick Ela[2], Dr. A. N. M. Mizanur Rahman [3]

[1,2]UG Student, [3]Professor
Department of Mechanical Engineering
Khulna University of Engineering & Technology, Khulna-9203, Bangladesh
drmizan84@gmail.com; nafiz-kuet@hotmail.com

Abstract: ***The climate change because of global warming and worldwide energy scarcity are prompting almost all the countries of the world to look for alternate energy sources like nuclear and renewable. Because of infrastructure and other reasons, developed countries can tap into nuclear energy but developing country like Bangladesh is not fortunate enough to have that option. Consequently, the only option that is left open to developing countries is renewable energy. Among renewable energy solar, wind, hydro, geo-thermal and wave energies are most reliable, which do not cause carbon emission. Solar energy can be used in many purposes like water heating, air heating etc. Among the various types of solar collector, evacuated tube solar collector is one of the most effective water heating device.***

An evacuated tube solar water heater was constructed from locally available materials and investigated in the department of Mechanical Engineering of KUET. In the first attempt, the highest storage tank temperature obtained was only 47°C. In the present attempt, cylindrical parabolic reflectors were placed under each evacuated tube. Consequently, the maximum water temperature obtained at outlet to collector was 81°C and 76°C in the storage tank in the month of April-May.

Keywords: Renewable energy, solar energy, evacuated tube, solar water heater, collector performance.

I. INTRODUCTION

Now-a-days, the most important subject in each part of the world is to produce energy with low cost and less pollution. On the other hand, extensive efforts to decrease global warming, which are the result of CO_2 emission to the atmosphere, enforced governments of those countries to look for new and alternative energy sources. Burning of fossil fuels is the main cause of emission of huge amount of various polluting gases. One possible solution to this situation may be use of nuclear energy and/or adaptation of renewable energy with sustainable technologies. Use of nuclear energy is not straight forward for all countries because of its illegal use to nuclear weapons and also electricity produced from this needs well developed grid-connections for fast transfer of huge amounts of power. At the same time this technology is not with all developing countries and therefore they must be purchased by using huge amounts of foreign currencies. Even the risk of accidents of nuclear power is devastating. So, because of infrastructure facilities, financial constraints and other reasons, developed countries can tap into nuclear energy but developing countries are not fortunate enough to have this option. Consequently, the only option left open for developing countries is renewable energy. Among renewable energy sources solar, wind, hydro, geo-thermal and wave energies are most reliable, that do not cause carbon emission.

Solar energy has a great potential in energy crisis. To some extent it is an economically feasible, environment friendly energy source and can be used in a variety of thermal applications like water or air heating, drying of crops, distillation of water, cooking, refrigeration and many more. Another way of using solar energy is by using photovoltaic cells where direct electrical energy is obtained.

Solar collector is basically a heat exchanger, which transfers the radiant heat energy of the sun to sensible heat to a working fluid. In general, a solar water heater is nothing but a solar collector with water as the heat transferring fluid. There are two types of solar collectors based on concentration ratio. One is flat plate collector (FPC) and another is concentrating collector (CC). In FPC, concentration ratio is one, whereas in CC, the concentration ratio is more than one. It increases the radiation intensity on the absorber resulting in higher thermal efficiency and higher temperatures [1]. FPC is suitable for both direct and diffuse radiation but concentrating collector is suitable for direct radiation.

Evacuated tube solar collector is neither a FPC nor a CC. Its main objective is to reduce the heat loss from the absorber surface and thereby increase the useful heat. It performs better for achieving high temperature than FPC. But it is bit complicated to construct an evacuated tube solar collector because of maintaining the metal-to-glass junction vacuum seal. The vacuum is created to reduce heat loss from the absorber tube. An evacuated tube solar water heater was constructed in the previous year but the performance was not satisfactory. The tubes were not evacuated properly. As a result the desired temperature could not be achieved [2]. To rectify the problem, a concept is proposed in the new design. Since all the radiation falling on the collector area is not falling on the absorber surface, so an idea of reflecting back the radiation energy to the absorber was conceived. As a result, in the new

design it is thought that cylindrical parabolic reflector would be placed under each evacuated tube to increase its aperture area. At the same time, care should be made during construction to ensure the sealing of the annular space.

II. Construction of Proposed Collector

The world market for solar water heaters expanded significantly during 1990's and as a result there has been a substantial increase in range and quality of products now available. Solar water heater production is now a major industry in China, Australia, Greece, Israel and the USA [3]. Solar water heaters are generally composed of a collector, a storage tank, connecting pipes and a fluid system to move the heat from the collector to the tank. The type and complexity of a solar water heater is mostly determined by: (i) the changes in ambient temperature during the day-night cycle, (ii) changes in ambient temperature and solar radiation between summer and winter and (iii) the temperature of water required from the system [4].

Conventional FPCs were developed for use in sunny and warm climates. Their benefits however are greatly reduced when conditions become unfavorable in cold, cloudy and windy climates. Furthermore, weathering influences, such as, condensation and moisture will cause early deterioration of internal materials resulting in reduced performance and system life. Concentrating collectors are only suitable for direct radiations. Evacuated tube collectors are one of the most innovative forms of solar collector. Evacuated tube technology was first developed by Quing Hua University in Beijing, China in the early 1980s. Manufacturing of these new solar collectors began in 1985. Evacuated tube collectors operate differently than other collectors. These collectors consist of a heat pipe working as absorber inside a vacuum tube. The vacuum envelope reduces convection and conduction losses, so the collectors can operate at higher temperatures than FPC. Like FPC, they collect both direct and diffuse radiation. However, their efficiency is higher at low incidence angles. This effect tends to give evacuated tube collector an advantage over FPC in day-long performance [5].

III. Design and Development

On the basis of the limitations as described earlier, a new concept was conceived to increase the performance. The schematic diagram of the collector is shown in Fig. 1. The collector consists of glass tubes, copper tubes, storage tank, connecting pipes, reflectors, insulation and a suitable stand for mounting. There are four copper tubes with black coating at the outer surface which absorbs heat energy from the sun and heats the inside flowing water. These absorber tubes are surrounded by glass tubes with vacuum in between the two tubes to reduce the heat loss. The ends of each glass tubes were sealed with a non-porous sealing material. The cylindrical parabolic reflector is set under each tube in such a way that the focal points (in this case a line) of each reflector will lie on glass tube's centre. Solar radiation falls on the glass tube and transmits through the glass and finally fall on to the absorber tube. The reflector is used to collect more energy from the sun and after reflection it also reflected back to the glass tube and thereby to the absorber tube. The concentration ratio of the collector was thus increased. After connecting the tubes with each other, they were mounted on a structure which when put under the sun makes an angle of 15° while facing south. The headers were connected to the storage tank. Thermometers were placed at inlet and outlet of the storage tank. Another thermocouple was placed inside the storage tank. The absorber tubes were interconnected with each other by PPR pipes. Water was circulated through the tubes by thermo-siphon principle. The process was continuing throughout the day.

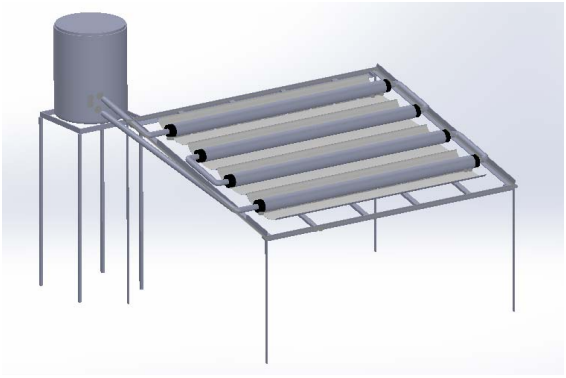

Fig. 1: Schematic of Proposed Evacuated tube solar collector

IV. Construction of Proposed Collector

At first, four parabolic shape structures were made for supporting and giving proper shape of the reflector and at the same time to give the structural rigidity of the reflector. The structure was made from 5 mm diameter GI wire. The exact parabolic shape was first drawn on paper and then the GI wires were made alike to give the exact shape. Each reflector was 90 cm long. Then 0.4 mm thick stainless steel sheet with proper size was taken and it was bent to form the shape as desired by a bending machine. The sheet was fixed tightly with the reflector structure. The reflectors were then put under the evacuated tubes and were fixed to the collector stand. The size of the collector stand was 106.5 cm by 88.5 cm and it was inclined to an angle of 15° with the horizontal. The whole system was commissioned facing towards south. Absorber tubes enclosed by glass tubes were sealed by non-porous rubber on both sides. From one end high pressure hose pipe was fitted to each annular space of glass and absorber tubes and the other end was connected to the vacuum pump to create a vacuum in the annular spaces. A gate valve was used in the middle of this hose pipe. After making vacuum, the gate valve was closed and then the pressure pipe was detached from the pump. The four copper tubes were connected tightly with the PPR pipes and sealing was ensured. The total collector area was 0.612 m^2.

V. Experimental Data

When the experimental setup was ready, experiments were conducted for 10 days under different operating conditions.

6.5 liters of water was stored in the storage tank for testing. Two thermometers and one thermocouple were installed to measure the inlet, outlet and storage tank water temperatures. The instantaneous solar radiation during the experimental period was also measured by a solarimeter. The collector was tested during the month of April – May. The required data were collected and only typical 2 days data are presented in Table I to Table II.

TABLE I. RADIATION INTENSITY, WATER TEMPERATURE AT INLET & OUTLET AND INSTANTANEOUS EFFICIENCY ON 27-04-15

Time am/pm	Radiation Intensity W/m^2	Collector inlet temp. °C	Collector outlet temp. °C	Storage tank temp. °C	Instantaneous efficiency (%)
10.00	270	38	53	36	69.66
11.00	320	51	66	52	69.83
12.00	350	60	72	64	71.65
1.00	420	69	79	70	77.62
2.00	390	70	78	72	73.66
3.00	310	65	73	70	67.66
4.00	220	52	63	65	62.18

TABLE II. RADIATION INTENSITY, WATER TEMPERATURE AT INLET & OUTLET AND INSTANTANEOUS EFFICIENCY ON 01-05-15

Time am/pm	Radiation Intensity W/m^2	Collector inlet temp. °C	Collector outlet temp. °C	Storage tank temp. °C	Instantaneous efficiency (%)
10.00	270	38	53	36	69.60
11.00	320	54	67	50	74.1
12.00	350	60	70	62	74.91
1.00	435	69	81	72	76.35
2.00	400	71	80	74	71.82
3.00	305	66	74	70	68.77
4.00	210	53	62	65	68.47

As reported in [6], the instantaneous efficiency of the collector was calculated from the following expression:

$$\eta_c = \frac{q_u}{I_T \times A_c} = \frac{mC_p \times (T_2 - T_1)}{I_T \times A_c} \qquad (1)$$

where, η_c is instantaneous collector efficiency, q_u is useful heat, I_T is radiation intensity over tilted surface, A_c is collector area, m is mass flow rate, C_p is specific heat of water, T_1 & T_2 are temperatures of water at collector inlet and outlet.

VI. RESULTS AND DISCUSSION

The experimental data were analyzed and are plotted in Figs. 2 to 7. The performance of the evacuated tube solar collector is dependent on solar radiation, ambient temperature, design parameters like properties of reflector material, properties of absorber tube material, concentration ratio, insulation etc. From Table I to Table II, it was observed that highest collector outlet temperature was obtained at highest radiation intensity but the storage tank temperature need not be the highest at the same time. The highest storage tank temperature was bit latter. Similar nature was observed on the other days. Fig. 2 to 7 show the graphical representation of temperatures recorded at various time of the day.

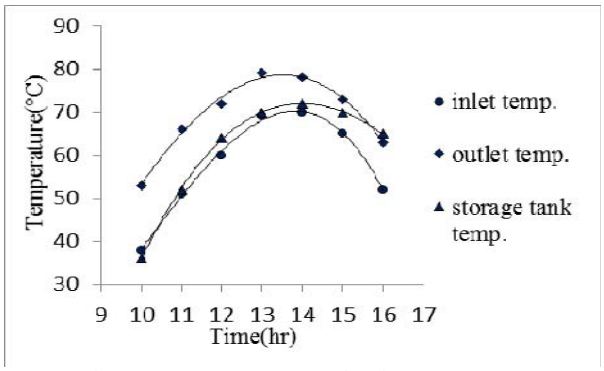

Fig. 2: Water temperature vs. day-time on 27-04-15

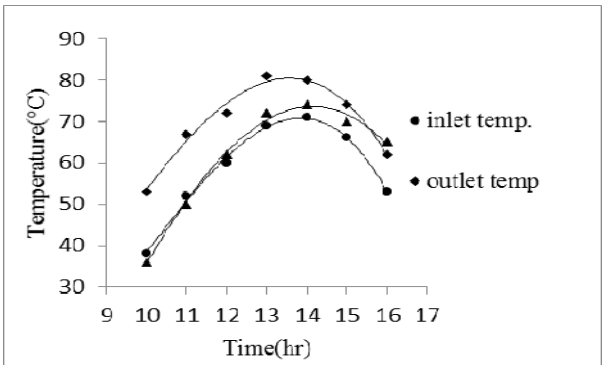

Fig. 3: Water temperature vs. day- time on 01-05-15

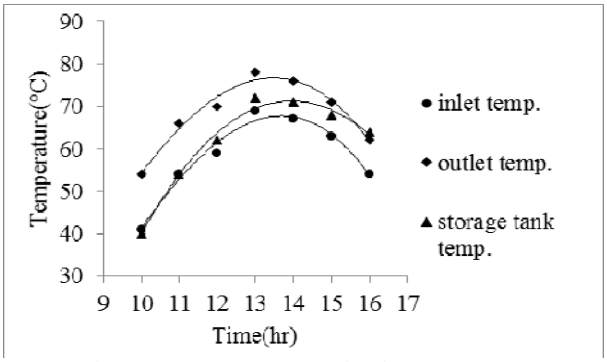

Fig. 4: Water temperature vs. day-time on 03-05-15

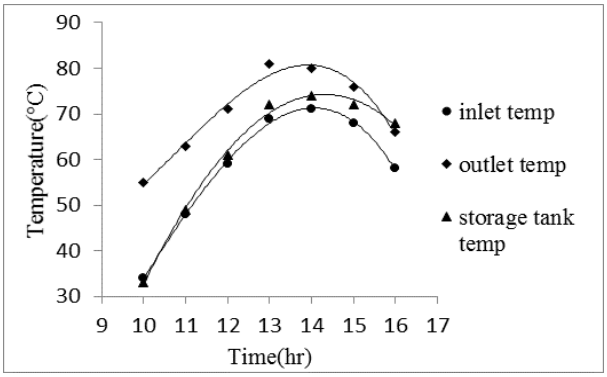

Fig. 5: Water temperature vs. day-time on 06-05-15

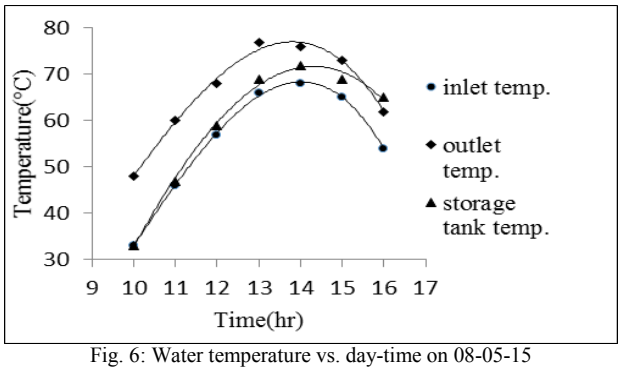

Fig. 6: Water temperature vs. day-time on 08-05-15

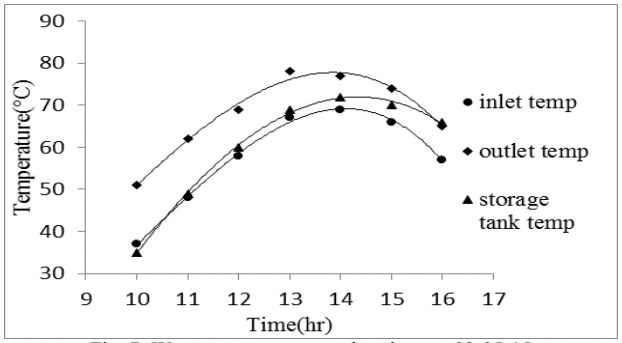

Fig. 7: Water temperature vs. day-time on 09-05-15

As mentioned the variations of inlet, outlet and storage tank temperatures with respect to time for six days are plotted on Fig. 2 to 7. From the graphs, it is seen that the rise of water temperature depends on the radiation intensity. As radiation increases, the water temperature increases. The highest outlet temperature was 81°C obtained at 1 pm and the highest storage tank water temperature was 74°C obtained at 2 pm. Again from Fig. 2 to 7, it is noticed that sometimes outlet water temperature was lower than storage tank water temperature. It could happen because storage tank has insulation and it helps to reduce heat loss from water. But at around 3 or 4 pm. the ambient temperature was decreased and heat loss occurred in PPR pipes. This heat loss decreased the inlet water temperature as well as outlet water temperature. But for the insulation, storage tank water temperature did not decrease abruptly.

Fig. 8 and 9 shows the instantaneous efficiency vs. time for six days. From the two graphs it is evident that the instantaneous efficiency increases as radiation increases. The highest instantaneous efficiency obtained was 78.20% and the highest overall efficiency for a day was 74.91% on 27-04-15.

VII. Conclusion

The evacuated tube solar water heater with the cylindrical parabolic reflector is more effective than the normal flat plate collector. In this case only four evacuated tubes were used. But the number of tubes can be increased within the same collector area and it could be expected that the system would be more effective when more number of tubes and proper insulation of the piping are used.

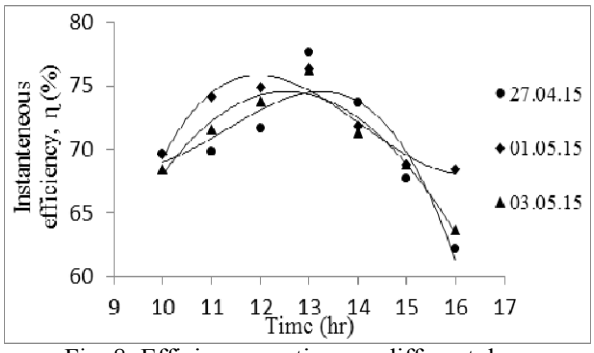

Fig. 8: Efficiency vs. time on different days

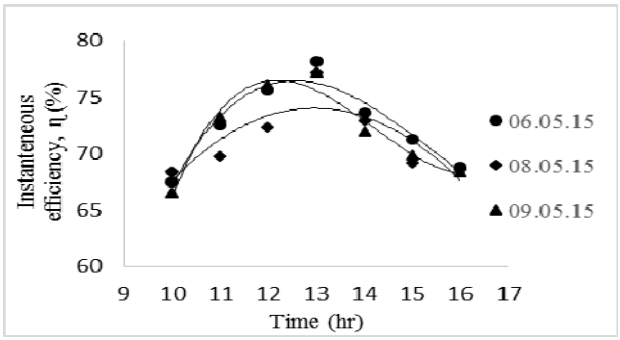

Fig. 9: Efficiency vs. time on different days

References

[1] Marian Jacobs Fisk, "Introduction to Solar Technology", Anderson-Wesley Publishing Company, printed in USA, 1982.

[2] Farzana Mollick Ela, "Design, Construction and Performance Test of an Evacuated Tube Solar Collector", UG project report, Department of Mechanical Engineering, KUET, Bangladesh, 2014.

[3] G. L. Morrison, B. D. Wood, Packaged Solar Water Heating Technology - Twenty Years of Progress; School of Mechanical and Manufacturing Engineering, The University of New South Wales, Sydney, Australia.

[4] http://en.wikipedia.org/wiki/Solar_energy.

[5] Soteris A. Kalogirou, "Solar Thermal Collectors and Applications", Journal of Progress in Energy and Combustion Science, pp. 240-247.

[6] Grag, H. P. and Prakash, J. "Solar Energy, Fundamentals and Applications", First revised edition, Tata McGraw-Hill company limited, New Delhi, 2002.

Performance of droop based load controller in interconnected micro hydro power plants.

Rojesh Dahal, Shailendra Kumar Jha, Brijesh Adhikary
Dept. of Electrical and Electronics Engineering
Kathmandu University
Dhulikhel, Kavre, Nepal
rojeshdahal@ku.edu.np, shailendra@ku.edu.np,brijesh@ku.edu.np

Abstract— **Droop based controller ensures the parallel operation of power plants in power system. Such controller is also required for Micro hydro power plants to work in interconnected micro hydro power plants. The approach with frequency droop to make a Mini-Grid model has been studied. Model of such frequency droop based controller has been successfully designed. Various real time cases were designed and simulated using the controller. This paper describes performance of simulated droop based electronic load controller for interconnected micro hydro power plants or Mini-Grid.**

.Keywords— Droop, Electronic Load Controller (ELC), Standalone system, Mini-grid, Micro-hydro plants (MHPs),

I. INTRODUCTION

Institutional development of micro-hydro sector dates back to 1960s through few private institutions supported by Swiss foundations and United Mission to Nepal (UMN).This took a new turn with the announcement of subsidy for rural electrification in 1985 AD [1]. Since then, Nepalese MHP sector has been progressively electrifying various parts of rural Nepal. Currently, 44,645 KW (including Micro Hydro-24,604 KW, Mini- Hydro- 16,338 kW, and Pico- 3,703 kW) are being generated at an average rate of 1500 kW annually and providing electricity to 350,000 rural households [2].

MHPs in Nepal range from 10kW to 100kW in capacity, and use Synchronous Generator (SG) and Electronic Load Controller (ELC) for fulfilling their load demand [3]. These plants generally operate in close vicinity of and provide power to their respective Load Centers (LCs). If MHPs in these areas could be connected together, there would be ample possibilities of power sharing and saving for entire network or Mini-Grid. Mini-grid is a "network for the electrification with its own generating capacity (one or several generators) and ability to serve the local demand"[4]. This will help in maintaining voltage and frequency stability of the system [5]. But, to ensure the income for each plant connected in Mini-Grid, load sharing technology is required [6]. Load sharing ensures equal proportion of load for all distributed load controllers keeping the balance between production and consumption optimums. This can be achieved with the Droop Controlled Mechanism. The controllers while utilizing the droop help the ballast to share power generated proportionally to the load required. This will help MHPs to operate efficiently and also generate better revenue for each MHPs owner. There is a great need of technology for interconnecting the generating units.

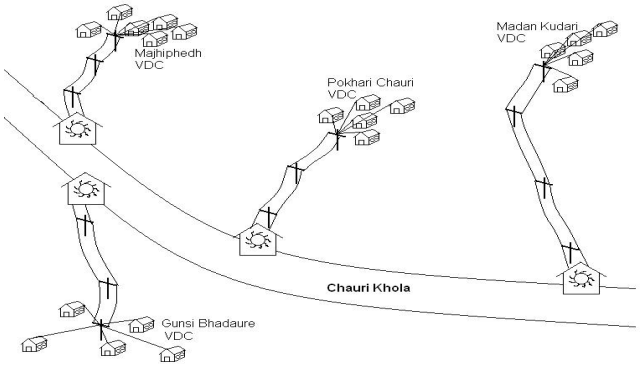

Fig 1: Present Scenario- Isolated MHPs

Fig1 shows present scenario of MHP of Nepal. The MHP plants are in stand-alone mode and are serving their own Load Centers.

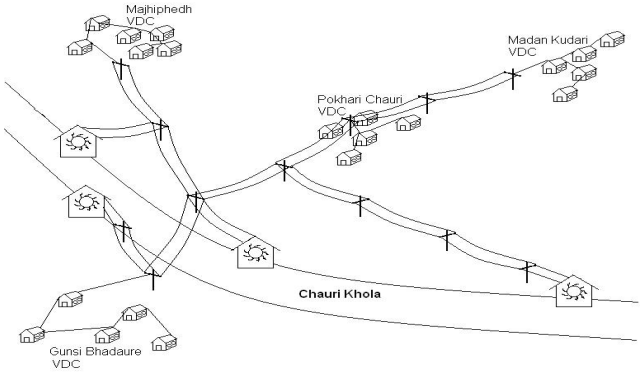

Fig 2: Future Proposed Mini-grid systems of MHPs

If these MHPs are interconnected as shown in Fig 2, they can share power produced in each MHP in Mini-Grid among the connected loads. So Power deficit in one load center can be compensated by other MHPs with excess power. Later if the utility - grid enters the area, Micro Hydro Power Stations (MHPs) will be self-sufficient to connect them to the utility-

grid. Networks of these independent MHPs can form Mini-grid and finally this Mini-grid can also be connected to the utility grid as well.

II. MODELS DESCRIPTION

MATLAB has been used for the Modelling and Simulation of Mini-Grids in this paper. In the First phase, Load Controller has been designed with varying droop. 5th order model of the Synchronous Generator and Automatic Voltage Controller (AVR) are used for the simulation. After tuning the parameters to required values, MHP model was constructed combining Synchronous Generator and Electronics Load Controller and AVR. Mini-Grid was formed after the MHP model was capable of working, followed by the replication of MHP models.

A. Electronic Load Controller

Binary Ballast based system has been used to Model the ELC [8]. This system uses discrete values of ballast to ensure the optimum ballast consumption. The schematic of the Load Controller is presented in Fig 3.

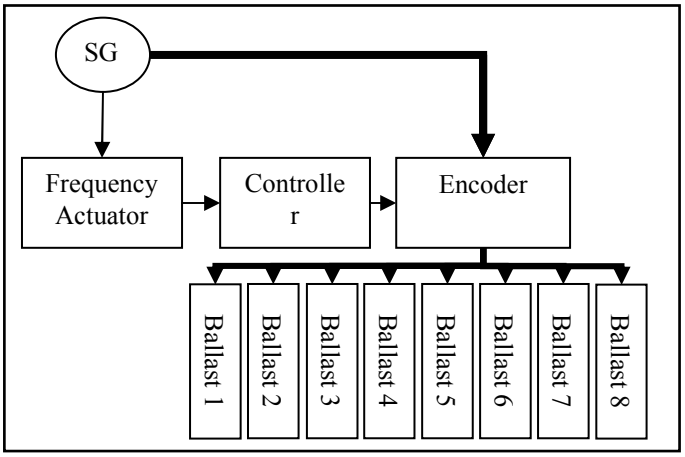

Fig 3: Block Diagram of ELC

The ELC controller comprises of three parts viz. Actuator, Controller and Encoder. The Actuator senses the frequency from the voltage waveform, and sends to the Controller. The Controller used is a P type controller for this paper. The two main parts in P controller are reference value (which determines the frequency of system i.e. 50 Hz) and Proportional Value (which determines droop in the system). These two parameters help the whole system to keep in limits of frequency and droop for MHPs. Finally, the encoder interprets the value from controller and closes the number of ballasts as required by the system to maintain the frequency. Reference [6] gives the details about the working principle of the unit mentioned above.

The basic principle of Load Controller is given by equation

$$P_g = P_{consumer} + P_{dump} \quad \text{---------- (i)}$$

Where,

P_g = *Generated power*

$P_{consumer}$ = *Power consumed by the consumer load*

P_{dump} = *Power fed to the ballast load*

Thus, ELC balances Power balance between Load and Ballast by sensing frequency of generator.

B. MHP plant

5th order model of synchronous generator is used along with AVR for MHP model. The Main load is modelled as continuously increasing load in fixed time interval. Modelling of ELC is shown in previous section. Complete model of MHP was created by combining the three block along with measurement blocks.

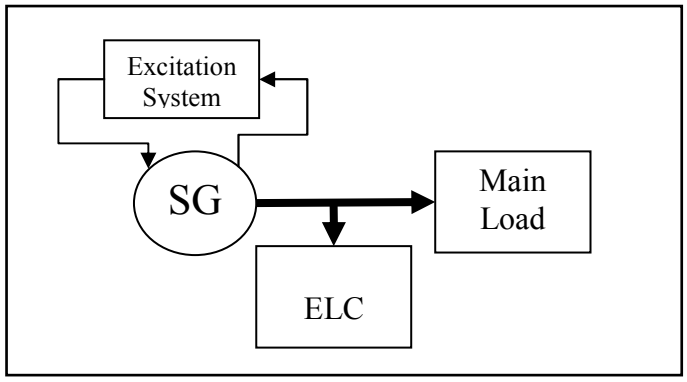

Fig 4: Block Diagram of MHP

The controller has been tuned to 50 Hz and 2.5% droop as per standards for Mini-Grid in Nepal [9].

C. Mini-Gird

Two different MHP (MHP1 and MHP2) plants are taken for developing Mini-Gird Model. Two MHPs were connected with each other via transmission line, which was connected to the Main Load via breaker. The transmission line model was designed for short transmission line (0-85km). The distance and voltage level of transmission could also be changed as per need of simulation. To check complete performance of ELC, Main Load was always equal to total generation.

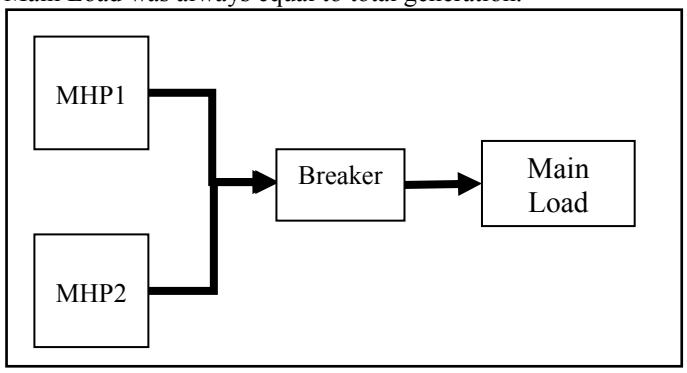

Fig 5: Block Diagram of Mini-Grid

III. TESTING OF MHP MODEL

Synchronous Generator of 8.1KVA, 400V, 50 Hz was used from Pre-defined model in MATLAB. The ELC basic parameters to be tuned were P value and Reference value. The Reference was taken to be 1 (1 represents 50 Hz) and P value was taken to be 30 (P 30 give 2.5% droop). The breaker

connecting generators to the main load closed at 0.25sec. Main Load for this simulation was of 7.2 kW given in 8 steps in interval of 0.25 seconds starting from 0.5sec. Responses of MHP model after simulation are shown below.

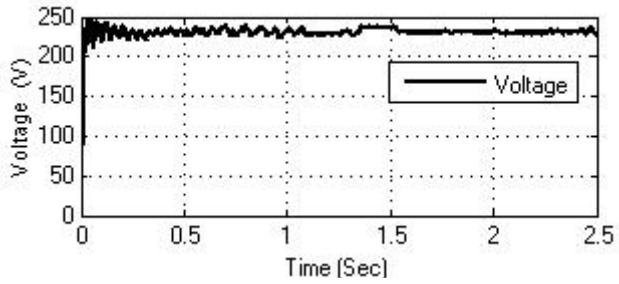

Fig 6: Voltage Profile in Standalone MHP System

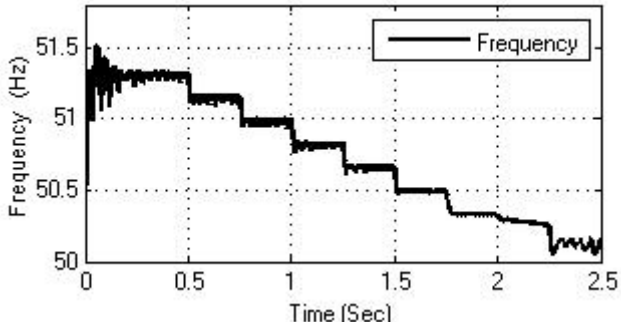

Fig 7: Frequency profile in MHP System

From Fig 6 and 7, it can be inferred that the Voltage and Frequency of the MHP System are in limit. The Voltage level is controlled by the AVR. The frequency was changed from 51.25 to 50 Hz which is 2.5% droop is maintained.

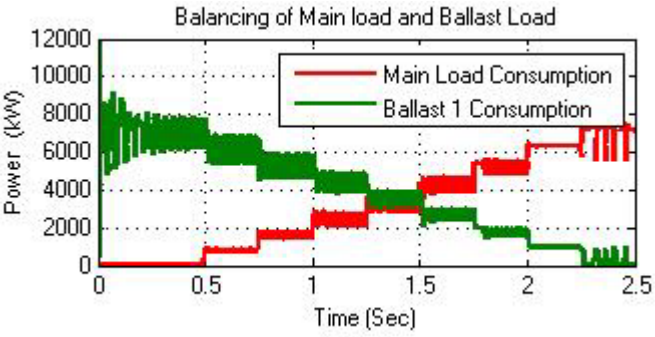

Fig 8: Performance of ELC

The Load and Ballast waveform Fig 8 shows typical curve of Load Controller. The beginning (till 0.5 sec), all of the power was consumed in Ballast. As Main load was increased there was equal decrease in power dumped in Ballast. Finally, when the full power was used in the main load, there was no power being sent to the ballast. This response describes balancing of power between main load and ballast in MHPs..

IV. CASES

Once the Model of MHP's simulation was complete, it was used to create the Mini-Grid model. To test the Mini-Grid Model, simulation of real-time scenarios were created. Three different cases were chosen and simulations were run for them. Simulations were completed and the main parameters of the Mini-Grid were analyzed.

A. Two Identical MHP forming Mini-Grid

In Case A, two independent and identical system or MHP were tied together. Each generators of 8.1 KVA, 400V and 50Hz were used. So Ballast sized were of 8kW was used for each MHP. Main Load for this model was upgraded to 15kW (As the total generation was 8+8).

Both of the generations were at full torque, and had identical excitation system. Load was started at 0.5sec with increase of nearly 2kW every 0.25sec. Simulation was run and main parameters voltage and frequency were analyzed.

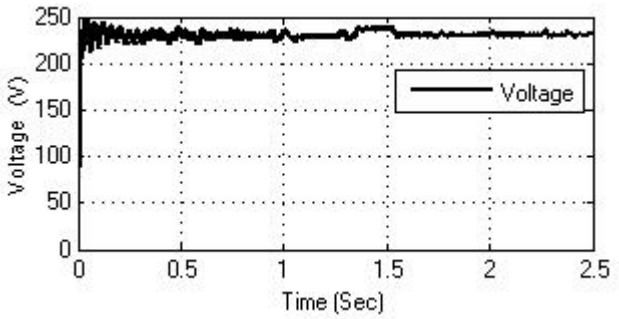

Fig 9: Voltage Profile in Mini-Grid System (identical generators)

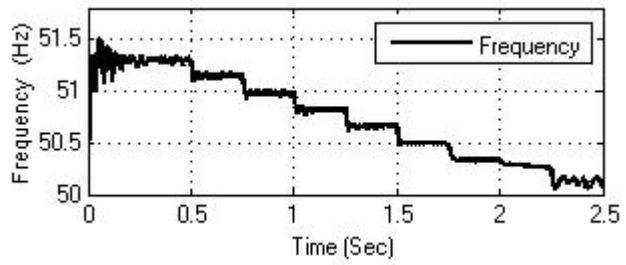

Fig 10: Frequency of Mini-Grid (identical generators)

Fig 9 and Fig 10 shows that voltage and frequency are in limit according to the standard. The droop is also maintained in Mini-Grid mode during the simulation. Thus we can say 2.5 % droop tuned to the MHP model also works for Mini-Grid model.

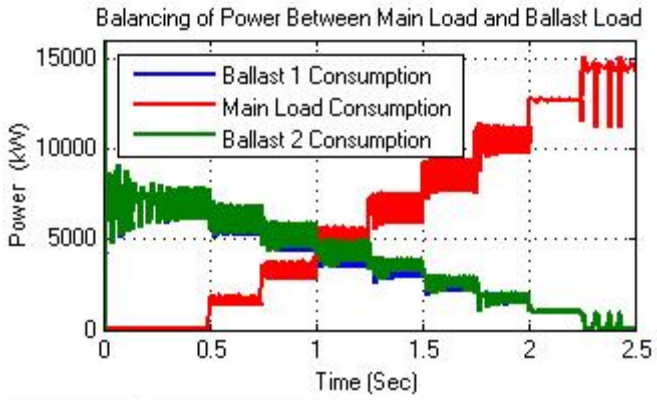

Fig 11: Performance of ELC (identical Generators)

Since both system were identical, both the ballast graphs are completely overlapped as seen in Fig 11. In the beginning MHPs are disconnected with main load till 0.25 sec. and no power is needed till 0.5secs, so both ballasts consumed the power generated till 0.5 seconds. 7.2 kW power in each ballast reached 14.4 kW which was nearly equal to the total generation. As the main load was increased, there was equal decrease in power consumed in sum of ballast. Finally the ballast didn't consume any power when main load was full. This signifies that the controller is working as per need of Mini-Grid being under limits of voltage and frequency.

B. Two different sized MHP forming Mini-Grid

For Case B, different size of MHP were chase from predefined model. Size of MHP1 of 8.1 kVA and MHP2 was of 16kVA were chose. The ballast loads were also upgraded to 8kW and 16 kW respectively. Since the total generation was increased, main load was increased to 23kW. Remaining parts were kept as same.

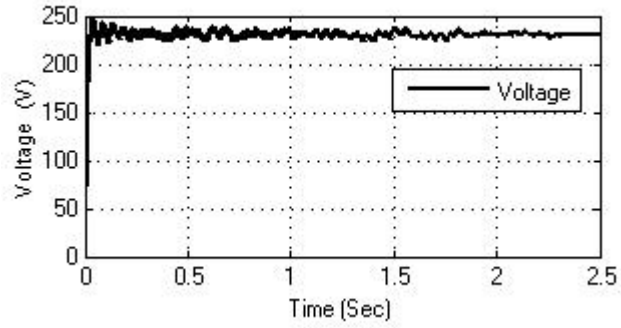

Fig 12: Voltage Profile in Mini-Grid System (different sized generators)

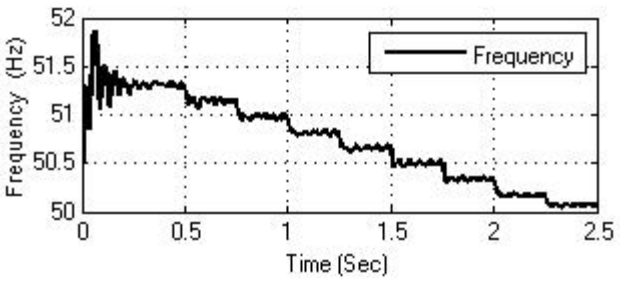

Fig 13: Frequency of Mini-Grid (Non identical System)

Fig 12 and Fig 13 shows that voltage and frequency are in limit for Case B. The droop of 2.5% is also maintained in the simulation.

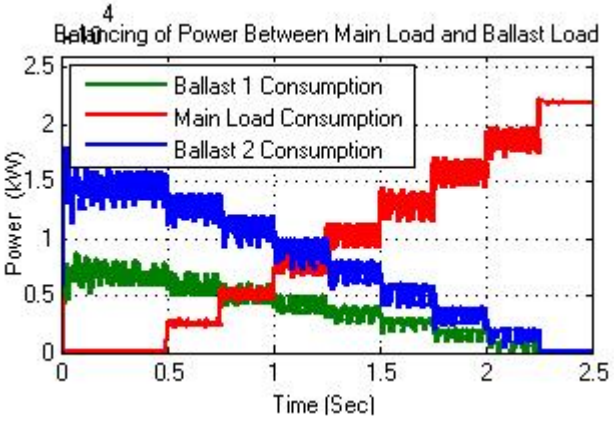

Fig 14: Performance of ELCs (Non identical System)

From Fig 14, the two ballasts consumed nearly 22 kW till 0.5 sec. When the Main load starts drawing power, power consumption from ballasts decreases. However, decrease in power from ballasts at different rate are seen in Fig 14. When observed in many simulations, the rate seemed to be directly proportional to their KVA rating. Finally, when the full power is drawn by the Main Load, the Ballasts did not dump any power. This means that the controller is working as per need of Mini-Grid being under limits of voltage and frequency for different rating of MHPs. Sharing the load is controlled by the controller with the voltage and frequecny in the given limit.

C. Two same sized MHP with transmission line in between them

In this case the MHP2 was generating and feeding Main Load. MHP 1 is kept at arbitrary distance of 10km from MHP2. It is connected by transmission line with MHP2. Since power cannot flow at 400V even for 1 km, therefore transmission line voltage is boosted next level with transformer to 11 kV [8]. Short transmission line model using Dog conductor has been selected for the simulation.

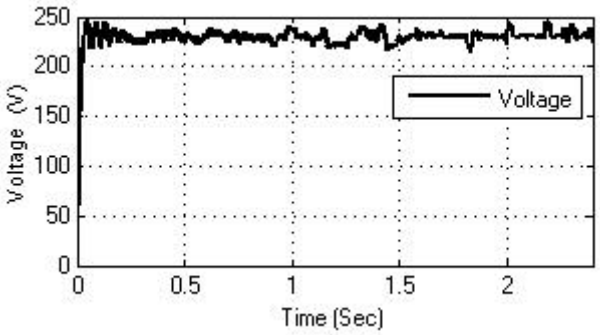

Fig 15: Voltage Profile in Mini-Grid System (Using transmission line)

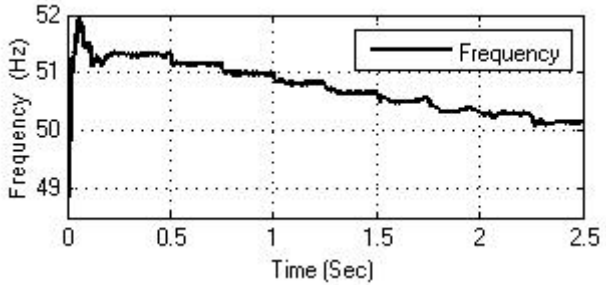

Fig 16: Frequency in Mini-Grid (Using Transmission Line)

From Fig 15 and Fig 16 it is seen that voltage and frequency are maintained within limits. The droo p of 2.5% is also maintained in the simulation irrespective of the distance.

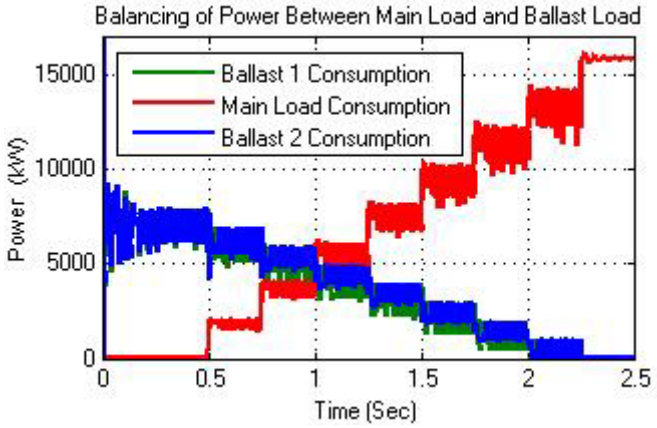

Fig 17: Performance of ELCs (Using Transmission Line)

The Fig 17 resembles with the Fig 11 from Case A. Since two MHPs are identical, the overlapping of two Ballast curves has been expected (as of Case A). From close observation it is seen that as power is drawn from Main Load, there is small difference in the two Ballast curve. It is result of transmission line losses. Thus the controller seems to be working even with the transmission line in Mini-Grid system.

V. CONCLUSION

From the simulation results it is seen that, P type controller can maintain the voltage and frequency deviation in limit, maintain required droop and create a balanced power in system (generation and demand). Controller also ensures that each MHP is producing full power and ballasts are consuming according to their KVA rating which again ensures that MHP owner will be repaid fairly. The system is operational for all sizes of MHP with or without transmission line. Hence this type of controller can be utilized for making of Mini-Grid systems.

VI. BIBLIOGRAPHY

[1] R. K. Maskey and K. Kandel, "Nepalese Engineering Consultants' Presepective For Promoting Micro/Mini Hydropower Projects In Developing Countries," in *International Workshop on the Role of Microhydel for Developing*, Kathmandu, 2013.

[2] "Micro Hydro in Nepal: At a glance," *Jalshakti,* vol. 13, pp. 9-10, 2014.

[3] Rural Infrastructure and Management Consultant (RIMC) Pvt. Ltd, "Baseline for Rural Renewable Energy Related NDIs and Other Indicators Related to NRREP Output," National Rural and Renewable Energy Programme (NRREP),Alternative Energy Promotion Center (AEPC), Kathmandu, 2013.

[4] V. Bhandari, R. Dahal, B. Adhikary, R. K. Maskey and N. Shrestha, "Establishment of Mini-Grid Laboratory in Kathmandu University□," in *National Seminar for Power and Communication Sector Development (PCSD)*, Dhulikhel, Dec.2010.

[5] V. Bhandari, R. Dahal, B. Adhikary, R. K. Maskey and N. Shrestha, "Performance Evaluation of laboratory fabricated test-kit for mini-grid systems," in *International Conference in Quality, Reliability and Information Technology (ICQRIT),*, Kathmandu, Dec,2011.

[6] V. Bhandari, R. Dahal, B. Adhikary, R. K. Maskey and N. Shrestha, "Prospects for Small-Hydro power-plants-Based Mini-Grid Power Systems in Nepal," in *IEEE*, Dhaka, 2012.

[7] P. Karki, R. Dahal, B. Adhikary and R. K. Maskey, "Improved electronic load controller and synchronizer unit for mini gird connection," in *IEEE*, Kathmandu, 2013.

[8] B. L. Theraja and A. K. Theraja, "AC Transmission and Distribution," in *A Textbook of Electrical technology vol III*, New Delhi, S. CHAND & COMPANY LTD, 2005, p. 1604.

[9] "MHP Interconnection Equipment Standards & Specification," Alternative Energy Promotion Centre (AEPC), National Rural and Renewable Energy Program (NRREP), Community Electricity Sub Component (CESC), Kathmandu, 2013.

Design and Economic Feasibility Analysis of Autonomous Hybrid Energy System For Rural Bangladesh

H.M. Rafeed Leon
Electrical and Electronic Engineering
American International University Bangladesh
Dhaka, Bangladesh
leon.rafeed@gmail.com

Md. Asaduzzaman Shoeb
Electrical and Electronic Engineering
American International University Bangladesh
Dhaka, Bangladesh
shoeb@aiub.edu

Md. Saifur Rahman
Electrical and Electronic Engineering
American International University Bangladesh
Dhaka, Bangladesh

Muaser Uddin Ahmed
Electrical and Electronic Engineering
American International University Bangladesh
Dhaka, Bangladesh

Md. Sadiqul Islam
Electrical and Electronic Engineering
American International University Bangladesh
Dhaka, Bangladesh

***Abstract*— The main perspective of the work is to represent the design and economic feasibility analysis of an autonomous hybrid energy system for rural Bangladesh. To overcome the many of the environmental problems our country faces today result from our fossil fuel dependency. These impacts include global warming, air quality deterioration, oil spills, or acid rain. In view of this, the hybrid energy systems are becoming popular in remote area power generation applications due to advancements in renewable energy technologies and substantial rise in prices of petroleum products. A rural village in Narayangonj (Araihazar), Dhaka, Bangladesh ($23^0$36.9'N, $90^0$30.2'E), has been taken as the case study. The proposed hybrid system consists of photovoltaic array and biogas accompanied by battery and diesel generator for emergency backup. This research also highlights the future developments, which have the potential to increase the economic attractiveness of such systems and their acceptance by the user.**

Keywords—— Hybrid System, Solar, Biogas, Survey, Homer & Retscreen Software, Diesel Generator.

I. INTRODUCTION (*HEADING 1*)

Energy plays a crucial factor in technological and economic development of present society. It has always been the key to man's greatest dream of a better world. Throughout the history of human their race, major advances in civilization have been accompanied by increased consumption of energy. There is a positive relation between per capita energy consumption and per capita income. Therefore, adequate supply of energy at a reasonable cost is a key factor in the advancement of a country in almost all sectors. Bangladesh is a country with numerically dominant rural population, where its village inhabits about 70 percent of its human resources. Hence, the development of country as a whole is intimately related with the rural development [1]. In Bangladesh, highest generation of electricity in 2015 is 7817.00 MW; however, demand is 10,283 MW and only 62% of the population has access to electricity [2]. In general, rapid industrialization and urbanization has propelled the increase in demand for energy by more than 8% per year [2].

It has become seriously important to look for energy solutions outside the conventional sources like domestic Natural Gas, Coals, Hydroelectricity and Imported Fuels. The natural oil and gas are rapidly decreasing due to excessive consumption. Extreme competition and instability of fuel price in the global energy market is continuously hammering the small players like Bangladesh. . Global warming and the subsequent increase of the sea level and natural calamities due to excessive carbon emission from fossil fuels are causing severe environmental and ecological havoc for low-lying countries like Bangladesh. The most feasible way out of this multi-dimensional crisis is to increase our reliance on renewable energy [3].

This paper emphasizes the renewable energy based hybrid generation system to obtain a reliable autonomous system with the optimization of the components size and the improvement of the capital cost. This hybrid energy system consists of photovoltaic array and biomass plant accompanied with battery

and diesel generator for emergency backup considering uncertain availability of these weather dependent sources. A rural village in Narayangonj (Araihazar), Dhaka, Bangladesh (23036.9'N, 90030.2'E), has been taken as the case study. As a first step, an operational scheme has been organized for measuring the electrical load profile, renewable sources availability, demography of the habitants and specifications like solar irradiation with the help of a field survey. Then, the whole system is simulated in HOMER and RETScreen software. Finally, results are presented for the proposed hybrid energy system.

II. HYBRID RENEWABLE ENERGY SYSTEM

Isolated grid renewable energy technologies satisfy energy demand directly and avoid the need for long distribution infrastructures. A combination of different but complementary energy generation systems based on renewable energies or mixed (Renewable energy source - with a backup of Liquefied Petroleum Gas / diesel/gasoline genset), is known as a hybrid power system ("hybrid system"). Hybrid systems can provide a steady community-level electricity service, such as village electrification, offering also the possibility to be upgraded through grid connection in the future. Furthermore, due to their high levels of efficiency, reliability and long term performance, these systems can also be used as an effective backup solution to the public grid in case of blackouts or weak grids, and for professional energy solutions, such as telecommunication stations or emergency rooms at hospitals [4].

A typical hybrid system combines two or more energy sources, from renewable energy technologies, such as photovoltaic panels, wind, biomass or small hydro turbines; and from conventional technologies, usually diesel or LPG gensets. In addition, it includes power electronics and electricity storage batteries. The hybrid system can be designed following different configurations to effectively use the locally available renewable energy sources and to serve all power appliances (requiring DC or AC electricity) [5].

III. SURVEY

An effective survey must be carefully planned and maintain the legal obligations. A survey has done to find information on energy consumption, present energy cost, life style, available source etc.; all the data was collected from all 95 houses from the proposed community. The entire survey outcome is discussed in brief here.

A. Survey Outcome

Location Profile:

Name: Narayangonj (Araihazar), Dhaka, Bangladesh

Latitude and Longitude: 23036.9'N, 90030.2'

No. of houses considered: 95

Average family size: 5

Population: 630

Bio-gas resource:

- Cattle: 150 (Average weight of waste from per cattle is 10kg/day)
- Poultry Farm: 4 (Average weight of waste from per farm is 10kg/day)
- Municipal Bio-waste: 5kg from 95 houses per day.

Solar resource:

The graphical representation of solar resources data for the Proposed Zone is shown in **Figure: 1**

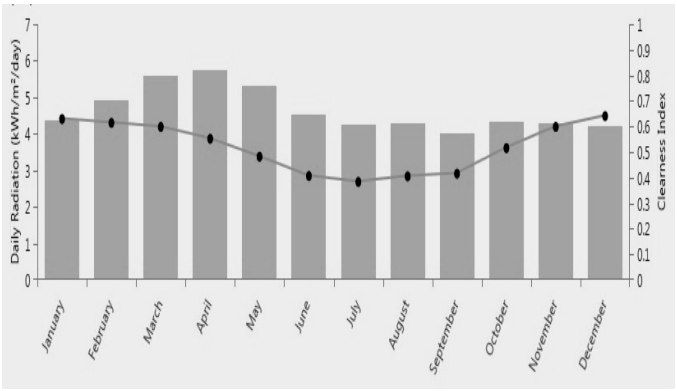

Figure 1: Daily solar radiation at Proposed Zone Using Homer

B. Electrical Load:

Connected load: 98.78 kW

Average energy: 680.33 kWh/ day

Electrical Cost: $14688 (or BDT 11, 40,000)/year

IV. SYSTEM DESIGN

A. Load Estimation:

This system is designed for a community of a rural village in Narayangonj (Araihazar), Dhaka, Bangladesh and considering ninety five houses. According to the survey total load connected in this community is 98.78 KW and detail calculation given below:

Maximum Demand=Connected Load ×h

=98.78 ×8765 =865.81 MWh/year grammar:

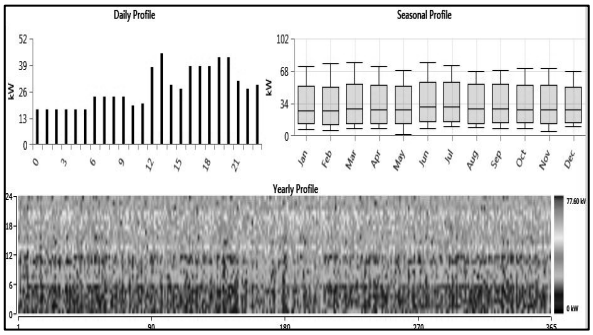

Figure 2: Electrical load inputs using HOMER

B. Source Selection

According to the survey the selected renewable sources based on their potential are Solar PV & Biogas.

1) Solar PV: This data is necessary for solar PV. NASA Research center provides the annual solar radiation (KW/m2/day),air temperature, relative humidity, atmospheric pressure, wind speed, earth temperature etc. to the RETScreen software. The detail value is presented in **Table I**

Table 1:
ANNUAL SOLAR RADIATION (KW/M2/DAY), AIR TEMPERATURE, RELATIVE HUMIDITY, ATMOSPHERIC PRESSURE, WIND SPEED, EARTH TEMPERATURE

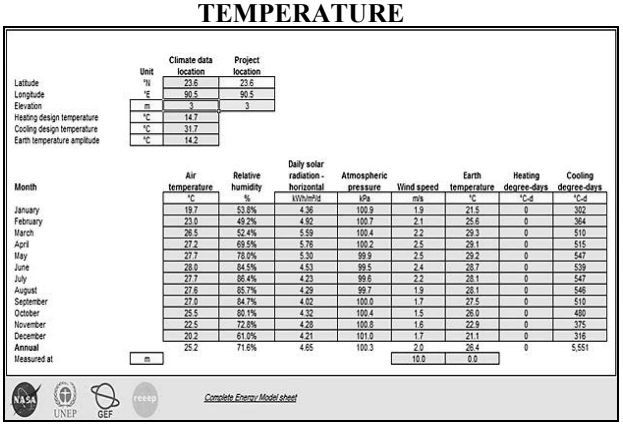

	Unit	Climate data location	Project location
Latitude	°N	23.6	23.6
Longitude	°E	90.5	90.5
Elevation	m	3	3
Heating design temperature	°C	14.7	
Cooling design temperature	°C	31.7	
Earth temperature amplitude	°C	14.2	

Month	Air temperature °C	Relative humidity %	Daily solar radiation - horizontal kWh/m²/d	Atmospheric pressure kPa	Wind speed m/s	Earth temperature °C	Heating degree-days °C-d	Cooling degree-days °C-d
January	19.7	53.8%	4.36	100.9	1.9	21.5	0	302
February	23.0	49.2%	4.92	100.7	2.1	25.6	0	364
March	26.5	52.4%	5.59	100.4	2.2	29.3	0	510
April	27.2	69.5%	5.76	100.2	2.5	29.1	0	515
May	27.7	78.0%	5.30	99.9	2.5	29.2	0	547
June	28.0	84.5%	4.53	99.5	2.4	28.7	0	539
July	27.7	86.4%	4.23	99.6	2.2	28.1	0	547
August	27.6	85.7%	4.29	99.7	1.9	28.1	0	546
September	27.0	84.7%	4.02	100.0	1.7	27.5	0	510
October	25.5	80.1%	4.32	100.4	1.5	26.0	0	480
November	22.5	72.8%	4.28	100.8	1.6	22.9	0	375
December	20.2	61.0%	4.21	101.0	1.7	21.1	0	316
Annual	25.2	71.6%	4.65	100.3	2.0	26.4	0	5,551
Measured at	m				10.0	0.0		

Complete Energy Model sheet

2) Biogas Resources: The biomass data was collect from the survey which has been discussed detail in previous chapter. So all the data we have, put in to the RETScreen software. The detail software simulation is presented in **Table II**

Table 2:
BIOGAS PRODUCTION CALCULATION USING RETSCREEN

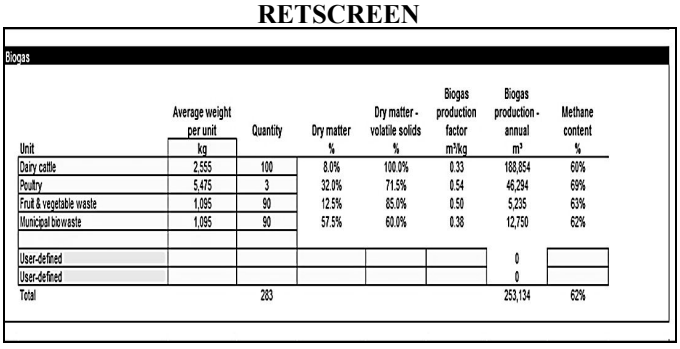

Biogas

Unit	Average weight per unit kg	Quantity	Dry matter %	Dry matter - volatile solids %	Biogas production factor m³/kg	Biogas production - annual m³	Methane content %
Dairy cattle	2,555	100	8.0%	100.0%	0.33	188,854	60%
Poultry	5,475	3	32.0%	71.5%	0.54	46,294	69%
Fruit & vegetable waste	1,095	90	12.5%	85.0%	0.50	5,235	63%
Municipal biowaste	1,095	90	57.5%	60.0%	0.38	12,750	62%
User-defined						0	
User-defined						0	
Total		283				253,134	62%

C. Energy Model

An autonomous hybrid renewable energy system is designed using Solar and Biogas resources. **Figure: 3** shows the HOMER implementation of the designed model which shows the implementation of the proposed model. PV indicates photovoltaic cell which is connected to the DC grid and Biomass resources are connected to AC grid. The Generator on the figure is the biogas generator and its run using biogas as fuel. A bidirectional converter is used which can be used both as rectifier and inverter. The battery used as storage system of the system connected to DC grid which can store extra energy produced from grid and PV.

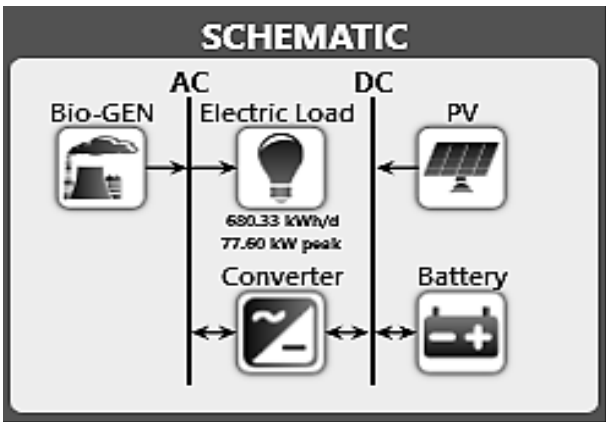

Figure 3: HOMER implementation of the autonomous hybrid energy system

D. Software Simulation

The implemented model with proper data shows the two types of results. One is equipment sizing & another is production analysis of the system. **Figure: 4** shows the optimized output of electricity production analysis. The combination shown in figure is analyzed as the paper focuses mainly on maximization of power production rather than optimization. The results show the total fuel consumption, electricity produced and excess electricity production.

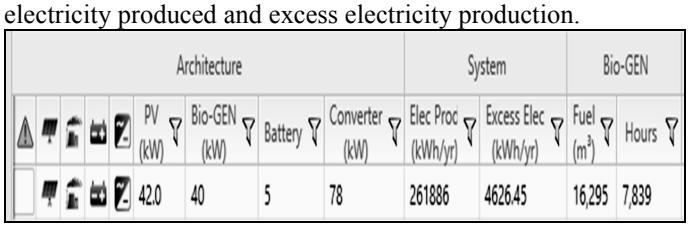

Architecture				System		Bio-GEN	
PV (kW)	Bio-GEN (kW)	Battery	Converter (kW)	Elec Proc (kWh/yr)	Excess Elec (kWh/yr)	Fuel (m^3)	Hours
42.0	40	5	78	261886	4626.45	16,295	7,839

Figure 4: Optimization of result using HOMER

1) Biogas Generator: The output power of the biogas generator in a day showed below in **Figure: 5**

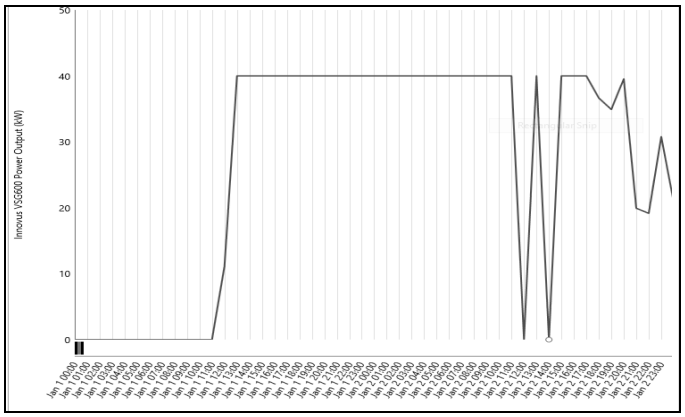

Figure 5: Generator output power using RETScreen

*2) Solar Output:*Yearly solar irradiance of the site is shown in **Figure: 6**

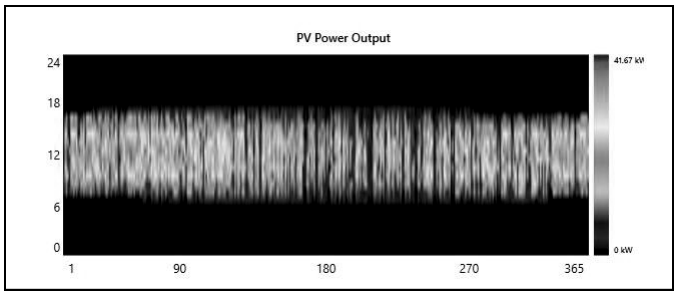

Figure 6: Solar Output Using HOMER

3) Converter: The converter output as inverter and rectifier is presented in **Figure: 7** and **Figure: 8**

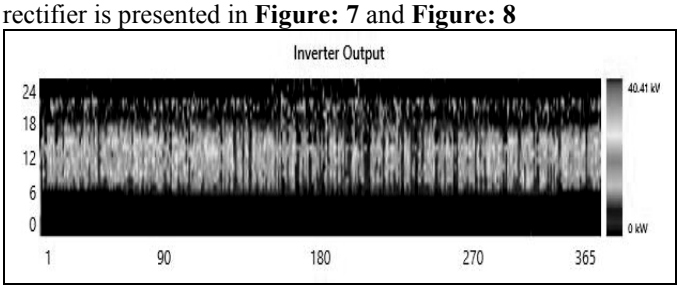

Figure 7: Converter Output as an Inverter Using HOMER

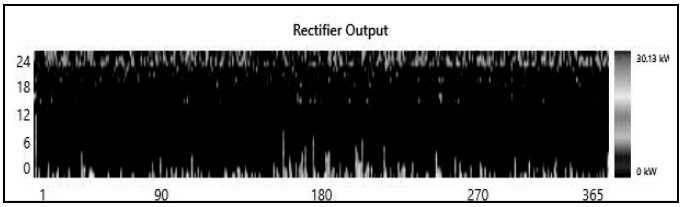

Figure 8: Converter output as a Rectifier

4) Battery: **Figure:9** and **Figure:10** describe the state of the storage system used in the model. The first one shows the percentages of battery bank state of charging on different times of a day. The second one shows the state of charging on monthly basis. Basically it shows the monthly storage capacity of the battery.

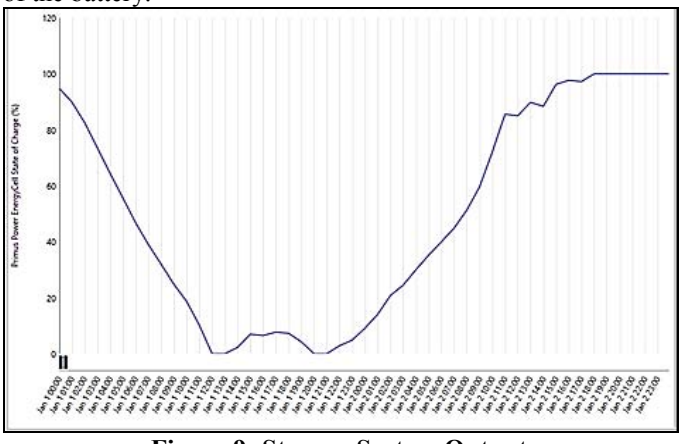

Figure 9: Storage System Output

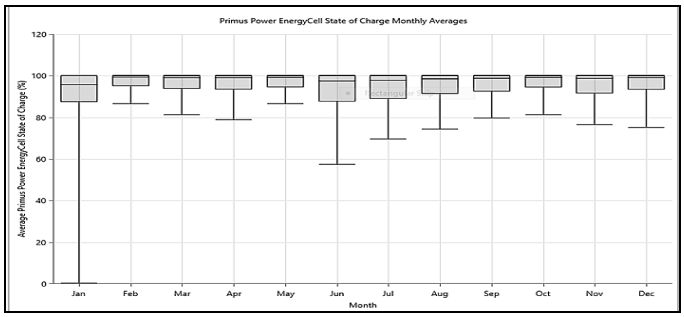

Figure 10: Monthly Storage Capacity of the Battery

V. BACKUP SYSTEM DESIGN

Backup system is provided to assist the central system in case of unforeseen circumstances of low renewable power availability and the period of maintenances. Whereas the source of energy originate from the nature, it could be greatly possible that the weather can vary any time. Therefore, the backup system is considered with diesel generator to meet the load.

A. Model:

This energy model of backup system consist a 25kw generator to meet the 22kw peak load. The load we consider that the community will get 2-fan and 3-light per house. **Figure: 11** shows the energy model of backup system.

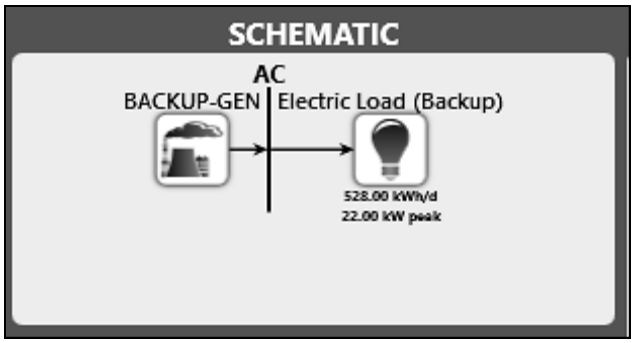

Figure 11: The energy model of backup system.

B. Optimization of Result:

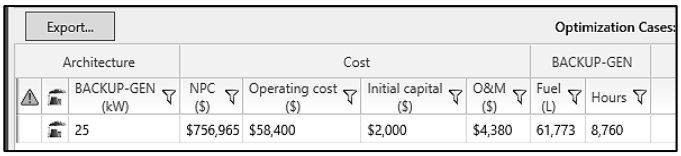

Figure 12: Optimization of Result

The implemented model with proper data shows the optimization analysis of the system. **Figure: 12** shows the optimized output. The results show the equipment sizing, total net present cost (NCP), initial cost, fuel cost, operation and maintenances cost (O&M), total fuel. The system will work only when the central system is not providing enough power

VI. COST ANALYSIS

Cost analysis is a technique used to compare the total cost of a project with its benefits, using monetary unit. This enables the calculation of the net cost or benefit associated with the program. Analysis the cost of the particular project is essential to appraised and compared, as an option for choosing the best approach. A specific approach is followed for the entire cost analysis process that has been done. In this entire analysis process the detail costing information for individual equipment, maintenance and operation cost, and salvage value have been discussed.

A. Initial Cost

The initial cost is divided into three parts such as Electrical Components, Technical Support, and Feasibility study. In electrical components only major electrical parts that has been used in this system is considered. **Figure. 13** shows the value of initial costs.

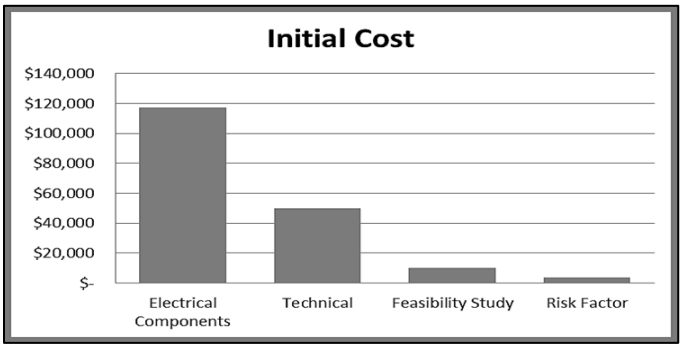

Figure 13: Graphical representation of Initial cost

B. Annual Cost

The fuel cost, operation & maintenance cost and risk value is considered as the annual cost. In O&M cost the general & administration cost, taxes, labor cost, individual equipment maintenance cost are considered**. Figure: 14** shows the detail allocation of annual cost analysis.

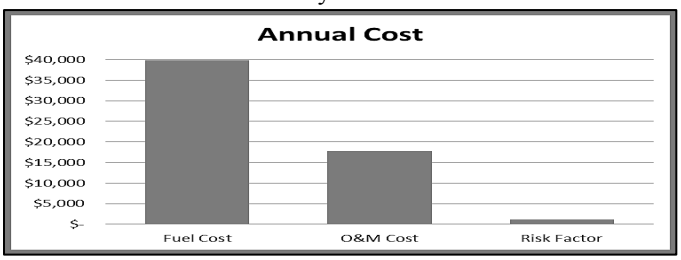

Figure 14: Graphical representation of Annual cost

C. Salvage Value

Salvage cost is actually the estimated cost that an asset will realize upon at the end of its useful life. Salvage value is subtracted from the cost of a fixed asset to determine the amount of the asset cost that will be depreciated. Thus, salvage value is used as a component of the depreciation calculation. Only electrical components salvage cost is taken into account here. The salvage of different components is represented in **Figure: 15.**

Salvage Value		
Electrical Components:		
	Bio-Gas Generator	$ 1,200
	Solar Photovoltaic	$ -
	Inverter	$ 200
	Battery	$ 25
	Diesel Generator	$ 400
		$ 1,825

Figure 15: Salvage Value

D. Total Cost Allocation

With consideration of all the costs like initial cost, annual cost and salvage cost together the total cost allocation is demonstrated in **Figure: 16**.

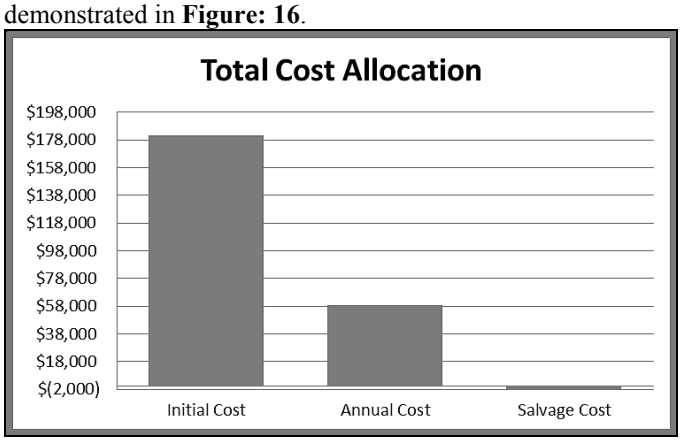

Figure 16: Graphical representation of Total cost allocation

E. Payback Period

Payback period is the time in which the initial cash outflow of invest is expected to be recovered from the cash inflows generated by the investment. Payback period is usually expressed in years. Calculation and graphical representation of payback period has shown in **Figure: 17** and **Figure. 18**.

PAYBACK PERIOD			
Total electricity produce (TEP)		261866kWh	
Cost of Energy (CoE)		$ 0.26	per kwh
Cash Inflow per year (TEP*CoE)		$ 68,085	
Annual Cost for project (Cash Outflow)		$ 58,774	
Estimated Annual Net Cash Inflow:			
(Cash Inflow-Cash Outflow)	$ 9,311		
Initial Cost:			
	$180,906		
PAYBACK PERIOD			
[(Amount to be initially invested)/ (Estimated Annual Net Cash Inflow.)]	19.43	years	

Figure 17: Payback period calculation

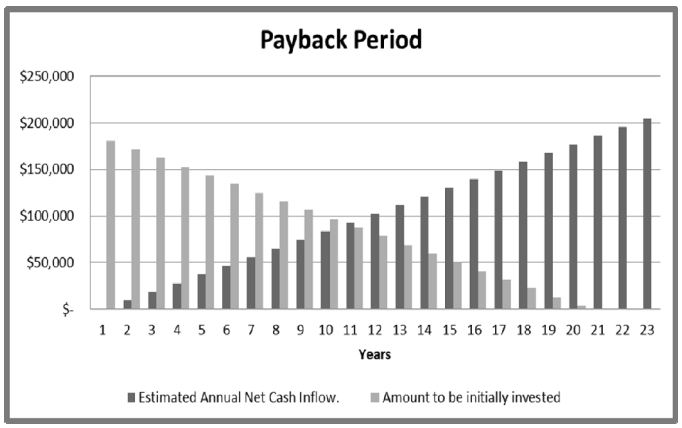

Figure 18: Graphical Representation of Payback period

F. Cost Comparison

The average amount of money spend by the people for electricity is estimated $23688 or BDT 1840761 per year based on the survey. However, the proposed hybrid system will cost them approximately $68,085/year. It is to be noted that the cost of the hybrid system is significantly high than the present cost of electricity. But the hybrid system is expected to be more reliable compare to the existing electricity supply provided by Rural Electrification Board (REB) with very low down time. Moreover, the cost can be reduced by using energy efficient low power appliances.

VII. CONCLUSIONS

Energy solution in Bangladesh is extremely critical and its major power station is run by natural gas and its reservation is now under threat if no new gas mine is identified. The acute electricity crisis along with the conventional fuel crisis is affecting every sector of the country and economy is being crippled. To reduce the dependency on fossil fuels, renewable energy could play vital role in this regard. There are lots of locations and opportunities to establish RES based power plants- which can solve the major electricity problem in Bangladesh. In this paper, through analysis and development the autonomous hybrid renewable energy system power plant can provide a better solution towards developing a sustainable energy solution for rural Bangladesh.

REFERENCES

[1] *ISSN 2278 - 8875 International Journal of Advanced Research in Electrical, Electronics and Instrumentation Engineering ,Vol. 1, Issue 2,* August 2012 , *Economic Feasibility of Hybrid Biomass/PV/Wind System for Remote Villages Using HOMER* , J. K. Maherchandani1, Chitranjan Agarwal2, Mukesh Sahi3 , College of Tech. &Engg., Udaipur1, College of Tech. &Engg., Udaipur 2, Govt. Polytechnic College, Chittorgarh3

[2] *INTERNATIONAL JOURNAL OF RENEWABLE ENERGY RESEARCH* , Md. MeganurRhaman ,*Vol. 3, No. 4, 2013 , Hybrid Renewable Energy System for Sustainable Future of Bangladesh,* Md. MeganurRhama , Department of Electrical and Electronic Engineering, Ahsanullah University of Science and Technology, Tegjaon, Dhaka, Bangladesh.

[3] BANGLADESH POWER DEVELOPMENT BOARD website. [Online]. [Cited: july 6, 2015.]Available:*http://www.bpdb.gov.bd/bpdb/index.php?option=com_content&view=article&id=12&Itemid=126*

[4] International Journal of Precision Engineering and Manufacturing-Green Technology Vol. 2, No. 1, pp. 99-112 JANUARY 2015 / 99

[5] Omar Ellabban, Haitham Abu-Rub, FredeBlaabjerg, *Renewable energy resources: Current status, future prospects and their enabling technology. Renewable and Sustainable Energy Reviews 39, (2014), 748–764, p 749, doi:10.1016/j.rser.2014.07.113.*

An Investigation into the Efficiency of Silicon Carbide Based Power Inverters

A.I. Maswood*, Lazhar Benbrahim**, Pinkymol Harikrishnaraj
Power Electronics Research Laboratory, School of Electrical and Electronic Engineering,
Nanyang Technological University, Singapore, **Qatar University, Qatar
E-mail : eamaswood@ntu.edu.sg

Abstract—In this work, a study of a silicon carbide power modules in power inverter is presented. Voltage/Current/ power and switching energy loss characteristics based on experimental data are detailed. A comparative study of total power losses and efficiency of a silicon carbide based three phase inverter with silicon base is analyzed and studied. The efficiency of the silicon carbide based inverters based on Semi-south manufactured device is found to be about 99%, and is more efficient than known conventional silicon based inverters, especially at high frequency.

***Index Terms*— Efficiency, Silicon Carbide, Power Loss, Inverter.**

I. INTRODUCTION

Si-C (Silicon carbide) based semiconductor devices are currently being researched and developed for use in high-temperature, high-power and high-frequency conditions under which conventional Si-based semiconductors cannot perform adequately [1]. Such features of Si-C material that increase efficiency and make it operate under such extreme conditions are expected to offer significant improvements to systems such as power management, power distribution and on-board motor/actuator drivers due to their superior intrinsic properties in these operating areas. Many such properties and associated results have been reported by Maswood et all [13, 14], and may be re-presented here to convey the idea.

Development results in Si-C development and technological advances have led to a reduction in the relative cost to manufacture Si-C wafers as well as an increase in the yield of dies produced per wafer. The result is a cross over point in the balance of cost versus performance where Silicon gives way to the new material, Si-C, for specific applications that benefit from and require extra performance [2]. As a result of these developments Si-C power devices and modules are becoming popular and readily available commercially, from companies such as Semi-South, Cree, etc. According to the Si-C power devices' manufacturers, there are several perceived advantages with these Si-C-based devices over Si-based devices such as reduced energy losses and high switching frequency, which assist to increase the efficiency and reduce the converter weight and size [3].

In this work, output characteristics and switching energy loss characteristics based on experimental data are established. The losses during conducting state and switching state are calculated, and loss models are developed. The Si-C JFETs (SJEP 120R063) from Semi-South are employed in the inverter, and the Si-C diodes (SDP 30S120) from Semi-South are used as the anti-paralleled diodes for the Si-C JFETs. Then, the efficiencies of the inverter are estimated based on the calculations at different combinations of switching frequencies.

II. SILICON CARBIDE POWER MODULES

A. An assessment of SI-C in inverters

The silicon-carbide (Si-C) inverter modules that can be used in electric and hybrid-electric vehicles can reduce thermal energy losses by about 46% compared with conventional silicon modules currently in use. It is hoped that when employed in electric vehicles these Si-C modules will improve the fuel efficiency by 25 to 40% [4]. Researchers hope to reduce power losses further, and have set a target of cutting losses to 10% of the equivalent Si inverter's losses thus to save energy [5]. Compared to an inverter using Si diodes and IGBT devices, the power loss was claimed to be approximately 70% lower and the volume is approximately 25% of the Si-based design [6].

B. Advantages of SI-C compared to silicon-based devices

Silicon carbide has a higher energy band-gap, critical electric, saturated electron drift velocity and thermal conductivity than silicon material. The wider energy band-gap of Si-C allow it continue to operate up to much higher temperatures. There is evidence that a Si-C JFET can operate through a temperature range of -50 to 400 degrees Centigrade [15]. The Si-C JFET can offer switching frequencies as high as 20MHz.

The ability of Si-C devices to operate with high junction temperature offers the potential to greatly reduce the size and weight of the heat sink, this could also lead to cost savings and smaller space consumption in the electronic circuit. This is particularly important for aerospace applications which are highly sensitive to weight and size requirements. The Si-C devices will be able to operate at a breakdown voltages close to 2500V. The simulation results are suggested that

breakdown voltages of up to 30 times higher can be achieved by some devices [7].

The reduction in switching loss by using Si-C could also enable the converter to operate at higher switching frequency. Hence the size of the output filter and other system costs could be reduced. Si-C devices have lower switching losses than Si devices up to 5 times in the same condition operations.

III. Comparative Study of Total Power Loss of a SI-C JFET with a Silicon IGBT

One of the commercially available Si-C based devices, Si-C JFET (SJEP120R063), from Semi-South, is compared to an IGBT (STGW30NC120HD) which have the same rated current and voltage of 30 A and 1200V respectively [13].

A. Conduction loss

The conductive losses at a number of points (Pcond) were calculated from within the linear region of operation following equation

$$Pcond = V \times I \times T \quad (1)$$

Where V is voltage across device, I is the current through the device and T is duty cycle assumed at 0.5.

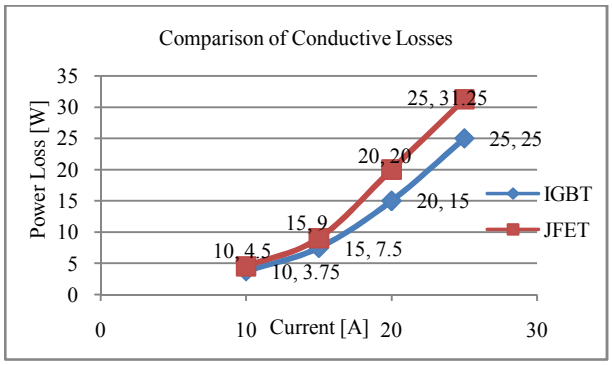

Fig. 1. Comparison of Conductive losses for Si-C JFET and Si IGBT

At higher current ranges from Fig. 1, it can be seen that, the conductive loss of Si-C JFET is higher than that of Si IGBT.

B. Switching loss

The Fig. 2 shows the energy losses during switching with current and gate resistance from 15A to 30A and 10 Ω respectively.

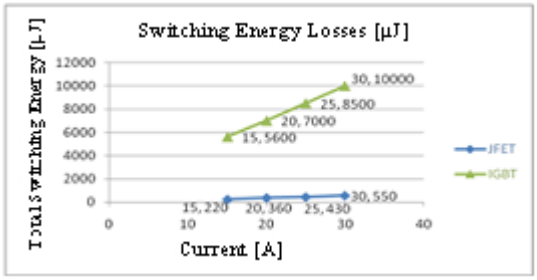

Fig. 2. Comparison of switching losses for Si-C JFET and Si IGBT

It is clear that, the switching energy losses of the Si-C JFET are significantly lower than those of the Si IGBT under the same conditions. It can switch between on-state and off-state with much lower dynamic energy loss per switching cycle. Also at the same allowable switching loss the Si-C JFET could operate at higher frequency.

C. Net energy losses

The total power conductive and switching losses of Si-C JFET and Si IGBT at three different switching frequencies are plotted in Fig. 3 below. It verifies the better performance of Si-C JFET at high switching frequencies. This feature is paramount in the low to mid power level inverter, switching at higher frequencies to shift harmonics to higher orders.

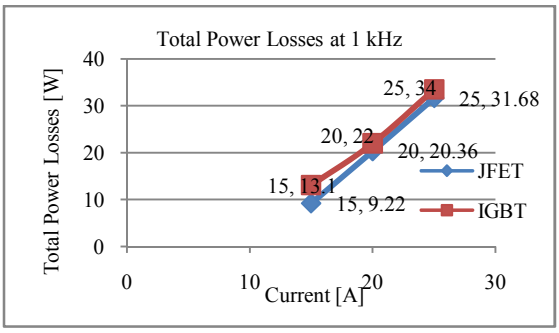

(a) At 1 kHz operating frequency

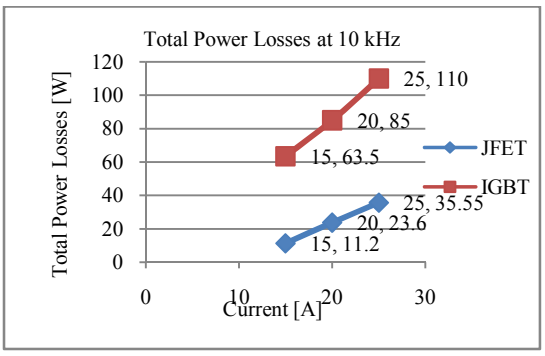

(b) At 10 kHz operating frequency

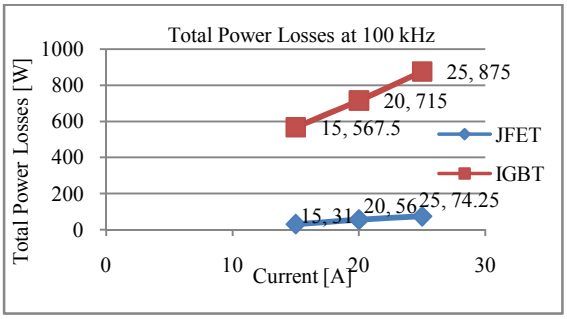

(c) At 100 kHz operating frequency

Fig. 3. Comparison of total losses for Si-C JFET and Si IGBT at three different common inverter frequencies.

IV. Efficiency Comparison of the SPWM Three Phase Inverters Based on SI-C and Silicon Based Devices.

Based on the data sheets of Si-C components (SJEP120R063 JFET and SDP30S120 diode) and Si IGBT module (STGW30NC120HD) the efficiencies of the SPWM three phase inverters are calculated and compared. Here high carrier frequency (20 kHz and 50 kHz) is employed.

The current through switching device in PWM three phase inverters are calculated [8]:

$$I_{G:JFET} = I_{C\_IGBT} = I_0 \times \sqrt{\left(\frac{1}{8}\right) + \frac{m_a \times \cos\varphi}{3\pi}} \cdot \quad (2)$$

Where m_a is PWM modulation index,cosφ is the power factor of load.I_0 is the peak of phase current.

The total losses on switches and reverse diodes in SPWM three phase inverter is:

$$P_{Total\_Loss} = 6 \times \begin{pmatrix} P_{Cond\_Device} + P_{SW\_Device} \\ + P_{Cond\_D} + P_{SW\_D} \end{pmatrix}. \quad (3)$$

Having taken all these losses i.e. switching and conduction loss in diodes and device, the efficiency of SPWM three-phase inverter is calculated by (4).

$$\eta = \frac{P_{out}}{P_{in}} = \frac{P_{out}}{P_{out} + P_{Total\_Loss}} \quad (4)$$

With a m_a= 0.8 and cosφ=0.8, the calculated results at f_c=20 kHz and 50 kHz are shown in Table I. The results from the Table I indicate that, for Si-C based power devices, the inverter efficiencies are always maintained high near 99% for various device currents and power levels.

These prospects are of high importance in inverters used in Fuel cells or PV (Photo-voltaic) applications where due to limited available power, device losses are to be highly minimized

TABLE I: EFFICIENCY COMPARISON OF SI-C BASED INVERTER AND SI BASED INVERTER

Parameters		Total Power Losses [W]		Output Power [kW]	Efficiency [%]	
Operating Current	Inverter	20 kHz	50 kHz		20 kHz	50 kHz
25A	**Si-C JFET**	**44.9**	**95.3**	22.22	**99.50**	**99.28**
	Si-C Diode	**65.2**	**65.2**			
	Si IGBT	811.5	2017.5		95.58	90.45
	Si Diode	214.4	327.9			
20A	**Si-C JFET**	**36.6**	**78**	17.77	**99.55**	**99.32**
	Si-C Diode	**43.9**	**43.9**			
	Si IGBT	666	1656		95.45	90.01
	Si Diode	180.1	293.6			
15A	**Si-C JFET**	**25.9**	**54.8**	13.33	**99.60**	**99.39**
	Si-C Diode	**26.7**	**26.7**			
	Si IGBT	520.5	1294.5		95.25	89.57
	Si Diode	144.2	256.6			

V. Experimental Results and Analysis of Device Characterization of Si-C Junction FET

Si-C JFETs (SJEP 120R063) with Si-C diodes (SDP 20S120) in antiparellel are tested experimentally in this paper. The test method and test results for static and switching states are presented in the following sections.

A. Static test

The Fig. 5 shows the I_D-V_{DS} comparison of experimental data with the manufacturer's data sheet of this device at junction temperature of 125^0C as obtained with the set up of Fig. 4. It consists of a DC voltage source, a variable gating signal, the Si-C JFET itself and a variable load to adjust the current flow.

The key equipments used in the experiment are:

- Circuit breaker: FUJI_SA103A (AC 220V, 35kA)
- Oscilloscope: TEKTROMIX_TDS 7054 (500MHz, 5GS/s)
- DC voltage sources: XANTEX_XKW 300-10 (DC power supply 300V, 10A) Resistors: TERCO_MV 1100 (3.3 kW)
- Variable voltage source: XANTEX_XT (20V-3A and 60V-1A)

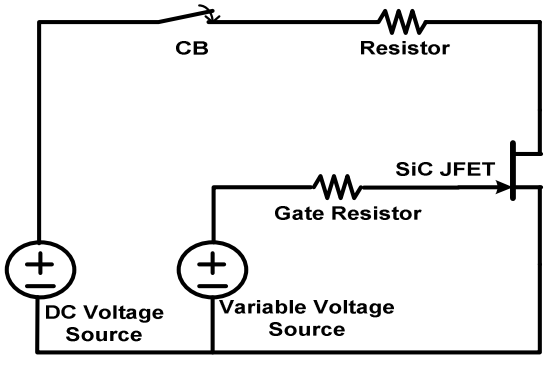

Fig. 4. Circuit topology for testing the Si-C JFET

The gate resistance was selected to be 2.2Ω, 2W. As shown as Fig. 5, when the gate voltage is maintained at 3V and 2.5V the experimental curves closely match the ones extracted from datasheet characteristics. With gate voltages less than 2.5 there is a large mismatch which doesn't create a problem

for low to mid power inverters used in alternative energy, where the typical gate voltage is likely to be much higher.

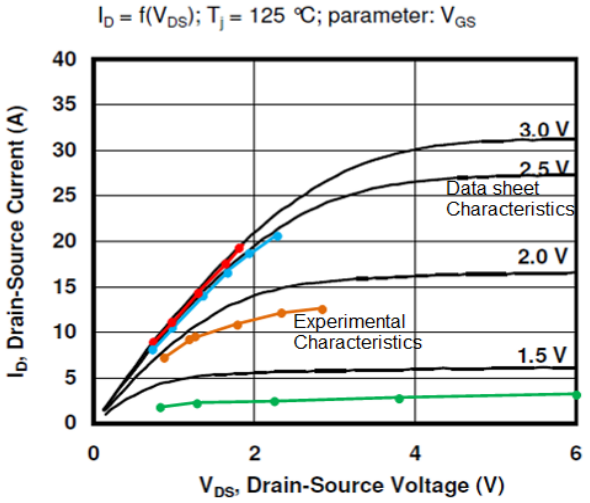

Fig. 5. Comparison of Experimental data with the manufacturer's data sheet at TJ 1250C

B. *Switching test*

The energy loss characteristics are investigated with gate driver SGDR600P1, produced by SemiSouth. The test circuit shown in Fig. 6 is used for switching characteristic test and the ambient temperature was kept constant at 250°C.

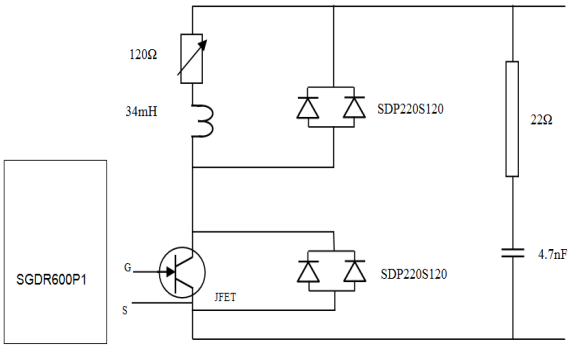

Fig. 6. Test circuit used for the JFET operating with the gate driver

The JFET was tested at voltages up to 300V and currents up to 14A in line with small/mid range inverters. Experimental results for various I_D are calculated and presented in Table II. The magnitude of switching energies was measured by using the area function of the Tektronix TDS 7054 oscilloscope.

TABLE II: SWITCH STATE ENERGY LOSS CHARACTERISTIC

Drain Current [A]	On-Energy Losses [µJ]	Off-Energy Losses [µJ]	Total Energy Losses [µJ]
4	50	30	80
6	52	43	95
8	60	50	110
10	76	74	150
12	90	95	185
14	100	110	210

Fig. 7(a) and (b) expresses switching power loss, the transient drain current and drain-source voltage at switching frequencies of 5 kHz and 20 kHz respectively with a source voltage of 250V. The energy loss is mostly in the distance of the power curve between the two cursors (top of power trace).

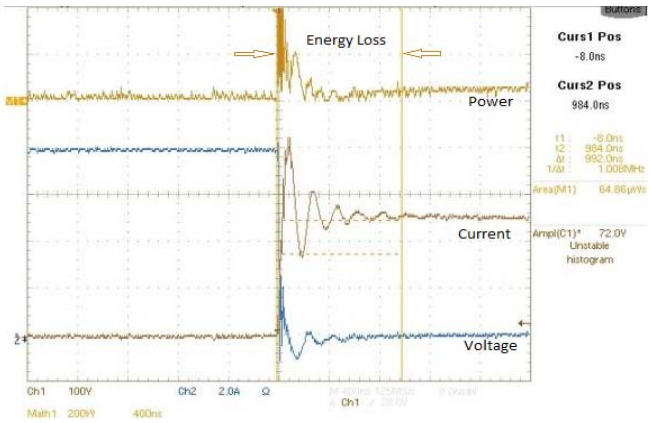

(a) At 5 kHz

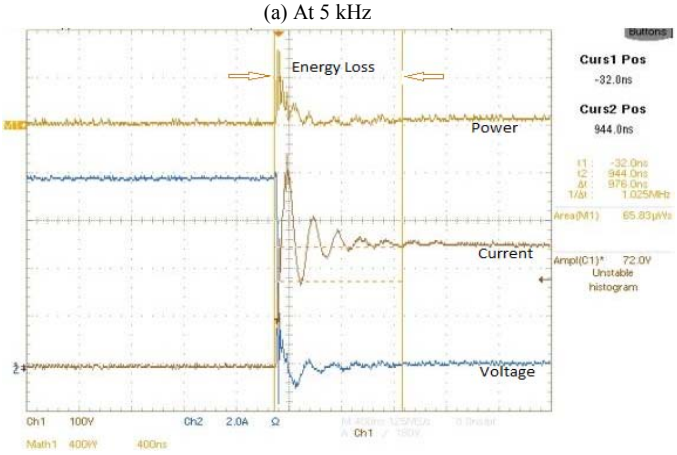

(b) At 20 kHz

Fig. 7. Off State energy losses at 250V, and 8A. (a) At 5 kHz, (b) At 20 kHz switching frequencies.

From Table III, it is possible to see that the switching-energy losses are nearly independent of the operating frequency.

TABLE III: TEST RESULTS FOR SWITCHING LOSSES AT SOURCE VOLTAGE OF 250V AND AT DIFFERENT DRAIN CURRENTS AND FREQUENCIES

Testing Data	On State Energy Losses [µJ]		Off State Energy Losses [µJ]	
Drain Current [A]	5 kHz	20 kHz	5 kHz	20 kHz
2	46.84	45.74	14.48	15.73
4	50.78	48.27	24.74	26.86
6	51.84	50.83	38.85	39.28
8	58.86	58.51	64.86	65.83
10	62.19	61.72	67.33	68.83
12	65.74	63.43	77.47	75.37
14	70.76	68.56	94.76	95.29

With two selected drain voltages (V_{DS}), it is seen that the switching losses of the device do change slightly (approximately less than 5%) when the source voltage increases as shown in Table IV.

TABLE IV: TEST RESULTS FOR THE SWITCHING LOSSES AT 20 kHz AND FOR DIFFERENT V_{DS}

Testing Data	On State Energy Losses [µJ]		Off State Energy Losses [µJ]	
Drain Current [A]	250V	300V	250V	300V
2	45.49	50.83	15.46	17.35
4	49.00	52.61	26.34	26.52
6	50.67	52.87	40.56	43.78
8	59.73	60.45	63.87	61.56
10	62.57	61.79	66.98	69.12
12	63.37	63.66	74.65	74.96
14	65.59	70.63	93.54	94.53

Fig. 8, depicts the on state energy loss characteristics at two selected drain source voltages

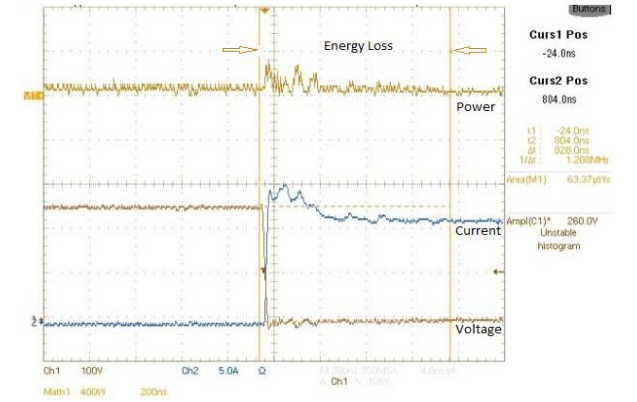

(a) V_{DS}=250V

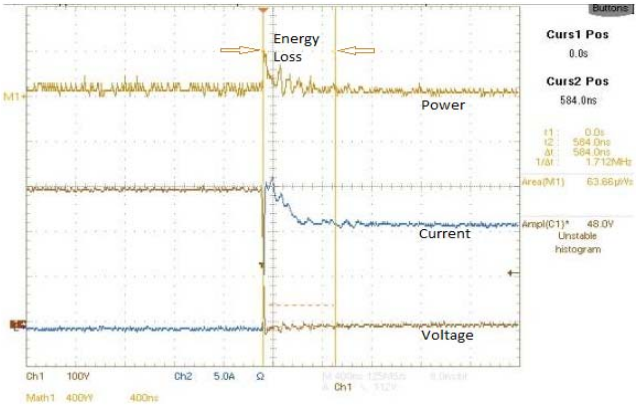

(b) V_{DS}=300V

Fig. 8. On State energy losses at drain current of 12A frequency of 20 kHz and at different voltages :(a) 250V (b) 300V (Details in table IV)

Table V shows the summary of the device switching energy losses at high frequencies, i.e., from 50 kHz to 100 kHz. These results confirm that the switching energy losses are practically independent of the operating frequency. This is a very important fact in high frequency inverters commonly used in fuel cell or PV based rear-ends inverters where energy conservation is paramount.

TABLE V: TEST RESULTS FOR I_D= 6A, V_{DS} =250V AND AT A RANGE OF DIFFERENT FREQUENCIES

Frequency [kHz]	On-Energy Losses [µJ]	Off-Energy Losses [µJ]
50	41.54	40.56
60	39.69	41.37
70	40.92	41.87
80	42.45	41.65
90	41.76	42.34
100	41.41	41.84

Fig. 9 shows the on state and off state loss characteristics at high frequency.

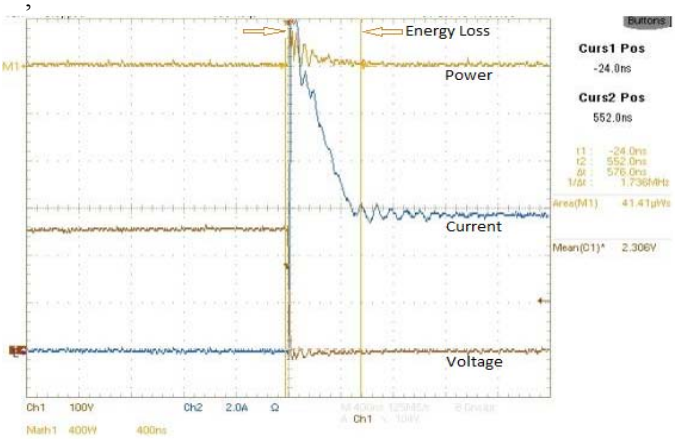

(a) On State

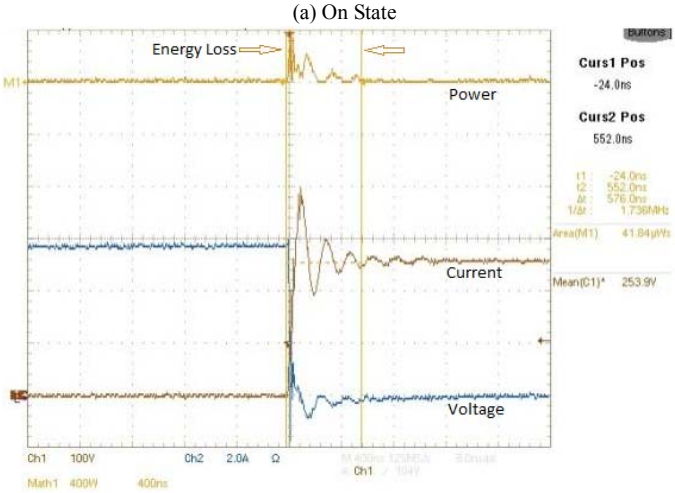

(b) Off State

Fig. 9. Energy loss characteristics at high frequencies (a) On state energy losses (b) Off state energy losses

Due to the maintenance of constant ambient temperature, the junction temperature at 100 kHz is higher than that at 50 kHz in test above. Hence, based on the data in Table V it can be seen that both on-energy loss and off-energy loss at drain current of 6A only increase slightly when the junction temperature changes. Experimental results obtained show that the performance of the Si-C JFET is quite stable having the results tallied with the manufacturer's technical datasheet.

VI. Conclusions

The Si-C JFET especially in the normally-off state is suitable for use in power converter and is reviewed and detailed in this paper. Principal advantages of Si-C power switches like small switching energy loss and high operating junction temperatures over its conventional counterpart, the Si-MOSFET and Si-IGBT are investigated with experimental work. A commercially available Si-C based device, A Si-C JFET from Semi-South is wired for laboratory testing and experimental verification. Thermal as well as electronic properties of Si-C if used as a power device, can lead to inverter devices that can perform excellently at high power levels and high switching frequencies with increased efficiency, reduced inverter weight, size and cost. Having a lower net power loss compared to the Si devices, the efficiency of Si-C inverter is found to be about 99.25%. This is achieved at a high inverter frequency of above 50 kHz.

VII. Acknowledgement

The authors would like to gratefully acknowledge the support of Energy Research Institute @NTU (ERIAN) under their PhD student support program.

VIII. References

[1] H.-R. Chang, R. N. Gupta, C. Winterhalter, and E. Hanna,"Comparison Of 1200v Silicon Carbide Schottky Diodes And Silicon Power Diodes" *Collection of* Technical Papers. 35th Intersociety Energy Conversion Engineering Conference and Exhibit (IECEC) (Cat. No.00CH37022), p 174-9 vol.1, 2000

[2] Maswood, A. I; Yoong, ZK, "Design aspects of a switch-mode transformer under wide input voltage variation", IEEE TRANSACTIONS ON INDUSTRIAL ELECTRONICS Volume: 53 Issue: 3 Pages: 752-758, JUN 2006.

[2] M. Ruff*, et al.*, "SiC Divices: Physics and Numerical Simulation," *IEEE Transactions on Electron Devices,* vol. 41, June 1994.

[3] C.M Johnson, "Comparison of silicon and silicon carbide semiconductors for a 10 kV switching application*", IEEE 35tg Annual Power Electronics Specialists Conference (IEEE Cat. No.04CH37551), p 572-8 Vol.1, 2004*

[4] Ali I. Maswood, "A Switching Loss Study In SPWM IGBT Inverter", *2nd IEEE International Conference On Power and Energy 2008 (PECon 2008), JB, Malayasia 2008* .

[5] Alvin Ong, Joseph Carr, Juan Balda and Alan Mantooth ," A comparison of silicon and silicon carbide MOSFET switching characteristics" , *IEEE Region 5 Technical Conference, TPS, p 273-277, 2007.*

[6] X. Gua, Q Shui, C.W. Myles, M.A. Gundersen, "Comparison of Si, GaAs, Sic and GaN FET-Type Switches for Pulsed Power Applications," *Digest of Technical Papers. PPC-2003. 14th IEEE International Pulsed Power Conference (IEEE Cat. No.03CH37472) 2003.*

[7] A.P. Mihaila , F. Udrea, S.J. Rashid, P. Godignon, J. Millan, " Si-C Junction FETs - A State Of The Art Review", *Semiconductor Conference, 2005. CAS 2005 Proceedings. p 349 - 352*

[8] P. G. Neudeck*, et al.*, "High-Temperature Electronics - A Role for Wide Bandgap Semiconductors?," *Proceedings of the IEEE,* vol. 90, JUNE 2002.

[9] R. Meuret, "The SEFORA project," *presentation to the academic partners,* 2007.

[10] O. Nowak, "Markets for Silicon Carbide Devices," *Wicht Technologie Consulting (WTC), Munich EPE,* 2005.

[11] P. Friedrichs and R. Elpelt, "Layout considerations for improving the on-state performance of vertical SiC switching devices," *PESC, 17-21 June Orlando, Florida, USA 2007.*

[12] A. I Maswood, Pinky Hari, "Efficiency of Silicon Carbide Based Power Inverters Analytical Results", IEEE International Conference on development of Renewable Energy System, Dhaka, Jan 4-6, 2012.

[13] Maswood, A. I.; Al-Ammar, E.; Liu, F. "Average and hysteresis current-controlled three-phase three-level unity power factor rectifier operation and performance". IET POWER ELECTRONICS Volume: 4 Issue: 7 Pages: 752-758 2011

[14] Maswood, A. I; Yusop, AK; Rahman, MA, "A novel suppressed-link rectifier-inverter topology with near unity power factor' IEEE TRANSACTIONS ON POWER ELECTRONICS Volume: 17 Issue: 5 Pages: 692-, SEP 2002.

Biogas Based Chain Business: A Road to Sustainable Rural Development

M. A. Ehsan[1], C. K. Das[2]
Dept. of Electrical and Electronic Engineering
CUET
Chittagong, Bangladesh
[1]amimul66@gmail.com

Mahadi Hasan[3]
Dept. of Biomedical Science
CityU of HK
Hong Kong

Abstract— **Bidirectional business concept where both parties are seller and buyer at the same time is termed as chain business. No one dominates on other in a chain business, so everyone is benefited at the same time. In this paper, a biogas based chain business model is designed for a community of 500 families, where people sell various wastes (organic waste, cow dung and chicken manure) to biogas plant authority, in contrast buy electricity, cooking gas and bio-fertilizer at affordable price. The model is abstracted based on developing countries like Bangladesh and analyzed for rural community, although it is also applicable for developed countries. Proper electrification is still not satisfactory and natural gas for home application facilities are totally absent in rural areas of Bangladesh. Use of chemical fertilizers in agriculture causes serious environmental and health hazards. However, this model eventually ensures financial gain, electrification, biogas for homestead use, agricultural growth, proper waste management and therefore, sustainable development of rural community in the long run as well as economic benefit of the entrepreneurs.**

Keywords—chain business; biogas; rural community; sustainable development.

I. INTRODUCTION

Energy business is escalating with daily expanding energy demand. Energy markets are mostly fossil fuel centered which is the decisive reason of environmental menaces including global warming and other climate changing effects [1-3]. Besides, nuclear power is extensively in practice as well in some developed countries that is enormously risky considering recent events [4]. Even though some business have been grown based on renewable energy sources like solar PV, windmill etc., but most of them are mainly related to equipment manufacturing and supply or installation [5].

Among all renewable sources biogas is not very popular in energy business till now [6]. But biogas has incredible business potential as it yields gas, electricity and fertilizer at the same time [7].

Bangladesh is a country of high energy demand and this demand is vigorously intensifying in recent years [8]. Almost 70% of total populations live in rural areas and more or less all rural areas are still out of proper and reliable electrification [9]. Contrariwise, only 4% of total people have natural gas cooking facility and others burn wood for cooking which consequences alarming devastation of green territory of the country, as a result severe environmental impacts have been seen in recent years [10] and may be one of the major causes of global warming [11-13]. For household lighting, people still depend on kerosene burners. As a result, children of rural areas stay behind in education perspective [14]. Again due to rapidly increasing population, agricultural lands are being altered into living places to facilitate this huge habitat [15]. Furthermore, chemical fertilizers are used to increase agricultural production, which leads to environmental pollution as well as destruction of biodiversity [16]. Then again, backyard farming (cattle and poultry) is very common in rural areas in each family and a constant source of everyday waste. Recently, poultry business gained popularity, which is another huge source of chicken manure. One more common waste source in community areas is daily household organic waste. Normally, these wastes are dumped elsewhere in open and causes severe odor and a variety of pollutions. However these available wastes (main sources of biogas) could be used in biogas plant to produce biogas for cooking in addition to electricity generation. After producing biogas, remnant of waste comes out of the digester in the form of wet slurry which could be turned into high quality bio-fertilizer for agriculture (in both land and fishing) through little processing and conditioning [17, 18].

In this research, a chain business model is designed based on biogas plant for rural areas of Bangladesh and likely countries for 500 houses consisting community and its long term benefits are studied.

The contents of the paper are organized as follows. The chain business concept and its benefits are described in Section II. The proposed chain business model is developed in Section III. Section IV describes the corresponding calculations and results of the proposed model, followed by conclusion in section V.

II. CHAIN BUSINESS CONCEPT AND ITS BENEFITS

The main concept of this chain business is- all people of a certain rural area are interrelated and act as key players. There introduced a business entity who invests in a specific area to set up biogas plants (stated as “plant authority” in Fig. 1).

People sell their domestic organic waste and animal manure to the biogas plant authority. Biogas plant authority produces biogas from that wastes, generates electricity and at the end of the digestion, produces bio-fertilizer, in addition, sells these

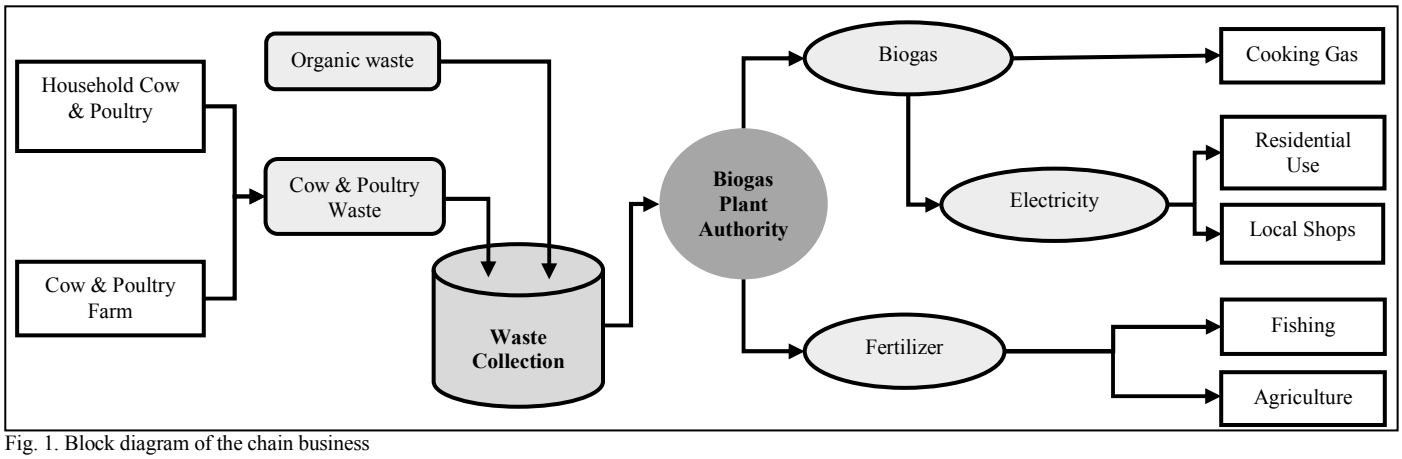

Fig. 1. Block diagram of the chain business

products to the people. There also kept provision for electricity supply to shops and other business individuals of the local market. Henceforth, at the end of the month, people save a reasonable amount of money as they do not need to buy wood and kerosene. Again, production of fishing farm and agricultural field increase with the use of bio-fertilizer and in turn enhances profit.

On the other hand, waste management in rural society becomes eco-friendly which upshots clean and healthy environment. Plant authority has to sell products at minimum price so that poor people can afford. The simplified block diagram of this model is shown in Fig. 1. Every family of rural areas always raises some domestic animals commonly cow and chicken to meet their primary egg, milk and meat demand. Some people have their own small scale poultry or cattle farm when some group of people have cooperative large scale farm through joint venture. Waste management of this vast extent of manure from those large numbers of chicken and cow is a gigantic problem and correspondingly a crucial threat to environment. Another common source of waste is organic waste. Organic waste is yet again two in types – food waste and fresh waste (kitchen wastes, unused vegetable and fruit residues, peelings etc.). Other than household, additional common and immense source of fresh waste is local market where people sell vegetables, fruits etc. and agricultural residues of those. Again, these fresh wastes are sometimes seasonal as in summer and rainy season many indigenous fruits, while in winter various vegetables are available in rural Bangladesh. Hence, enough fresh waste is accessible over the year. The business authority buys all these organic wastes and manure, transports them to their waste storage facility to retain the biogas plants in production. Wastes are kept in different storage depending on waste type and the storage is channeled to digester inlet of each kind.

A portion of produced gas is used for electricity generation by gas generators and remaining is supplied through pipeline as cooking gas.

Another noteworthy benefit of this concept is- it ensures good study environment at houses for children. Cooking with

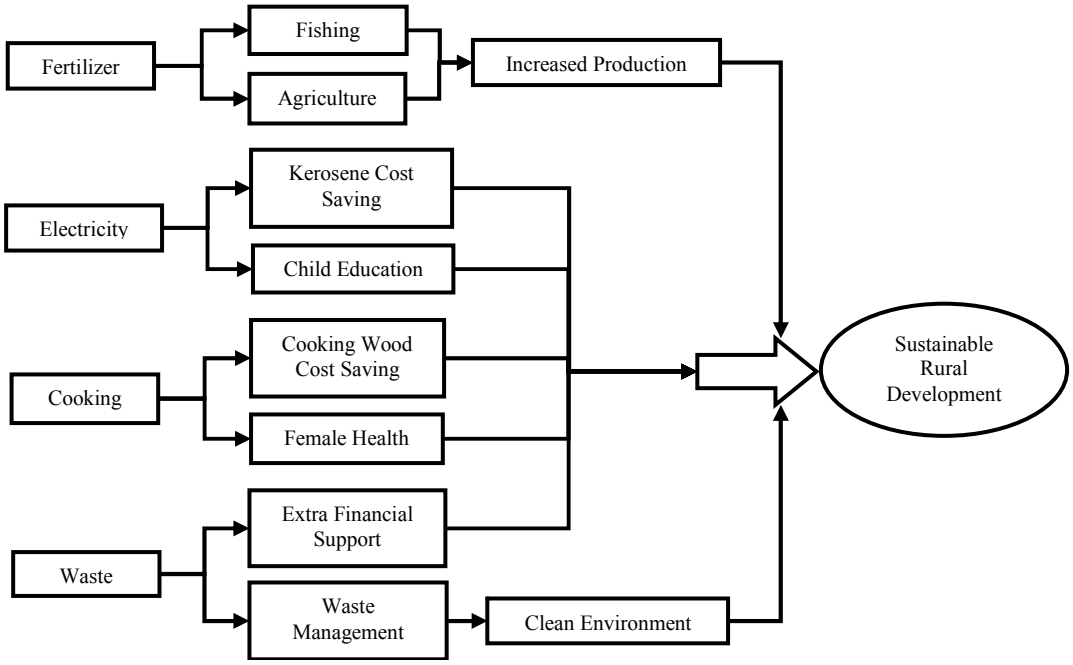

Fig. 2. Benefits of biogas based chain business in rural community

biogas likewise improves women's health and saves time from collecting wood.

All the benefits of this concept are visualized in Fig. 2 for easy understanding at a glance. Proper waste management is possible in this system which results an extra source of income along with clean environment.

Cooking gas facility not only saves wood cost along with other environmental benefits but also ensures healthy cooking environment at kitchen. Electricity provision also saves a good amount of money from lighting which provides sound study environment for children. Use of bio-fertilizer increases both fish and other agricultural production and also saves environment from several pollutions. Finally, these benefits ensure overall developments of rural community in a sustainable manner.

Sustainable cash flow means money flow between plant authority and rural people in terms of their corresponding products from the selling point of view. That signifies money flows in a cyclic manner rather unidirectional. Fig. 3 briefs this cash flow in a cyclic manner. In this system, biogas plant authority buys waste from people which flows a significant amount of money to people's pocket from business entity. On the other hand, from selling the plant products (biogas, electricity and bio-fertilizer) to the people, a reverse flow of money occurs. Thus, both parties are benefited at the same time from this chain business.

III. Chain Business Model Development

The chain business concept is modelled for a typical rural community of Bangladesh and 500 families are taken into account for the study.

Electricity and cooking gas demand of the designed model is estimated based on the standard home of rural community [19]. For standard home, 6 m^3 biogas is necessary per day for both cooking and electricity. 2.5 hour (Hr) cooking with a two-burner stove requires 2 m^3 biogas and 1.4 kWh electricity generation entails 1 m^3 biogas [20]. Electricity demand of a standard home is tabled in Table 1. Hence load curve of the designed model is shown in Fig. 4 and calculated electricity requirement is 1,450 kWh per day on an average, which requires nearby 1,040 m^3 biogas. Total cooking gas demand is 1,032 m^3 including some food shops in local market.

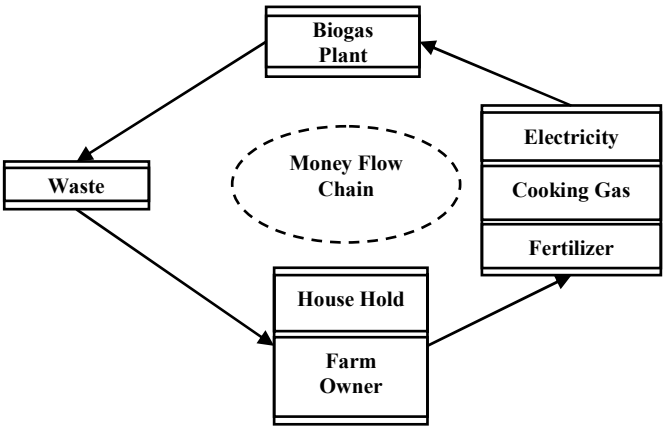

Fig. 3. Sustainable cash flow

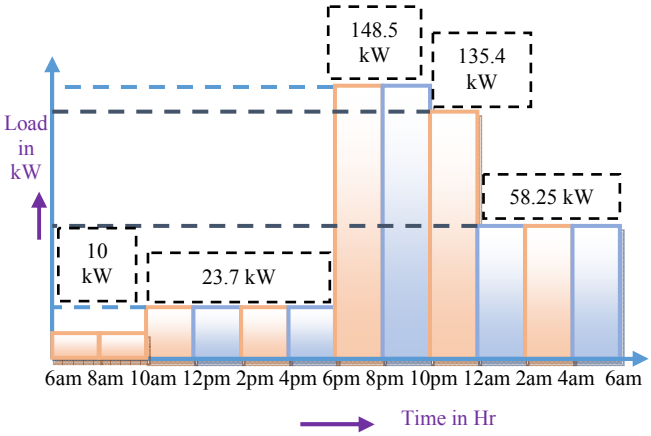

Fig. 4. Load curve of the designed

Electricity price is 5 BDT[1] (≈0.06 USD)[2] per kWh and cooking gas charge is 300 BDT (≈4 USD) per month for each family.

In this design, 3 different biogas plants are proposed for all 3 kinds of wastes.

Total daily waste requirements are 1,200 kg organic waste, 14,500 kg cow dung and 20,250 kg chicken manure.

Plant authority is responsible for collecting waste in daily basis or in a particular interval. Total 485 cows and 40,500 chickens are needed to produce stated amount of waste.

Organic waste is priced 3 BDT/kg (≈0.04 USD) while fresh cow dung and chicken manure are 1 & 2 BDT/kg (≈0.013 & 0.03 USD) respectively. Schematic of a typical biogas plant is presented in Fig. 5 and digester, hydraulic chamber, mixer etc. are designed based on IDCOL standards for this model [20].

Design parameters are shown in Fig. 6 for all three digesters. Digesters are pictured in (a), (b) and (c) part for organic waste, cow and chicken manure respectively. Aimed at reliable system operation, total 6 generators (ratings- 1.2 kW, 5 kW, 10 kW, 20 kW, 40 kW & 76 kW) are incorporated in this model. Generator operations are scheduled based on electricity demand.

Biogas contains H_2S, moisture, vapor etc. which are toxic and corrosive to generator core [21, 22]. So, purifier is obligatory before each generator to lengthen generator lifetime.

TABLE I. Energy Demand of a Standard Home

Load	Rating (Watt)	Number	Total Power (Watt)
Energy Saving Bulb	15	2	30
Energy Saving Bulb	25	2	50
Energy Saving Bulb	12	2	24
Ceiling Fan	75	3	225
Color TV	100	1	100
Refrigerator	150	1	150
Computer	80~90	1	90
		Total	669

1. BDT stands for "Bangladeshi Taka", which is the currency of Bangladesh
2. 1 BDT = 0.013 USD (where USD abbreviates "US Dollar")

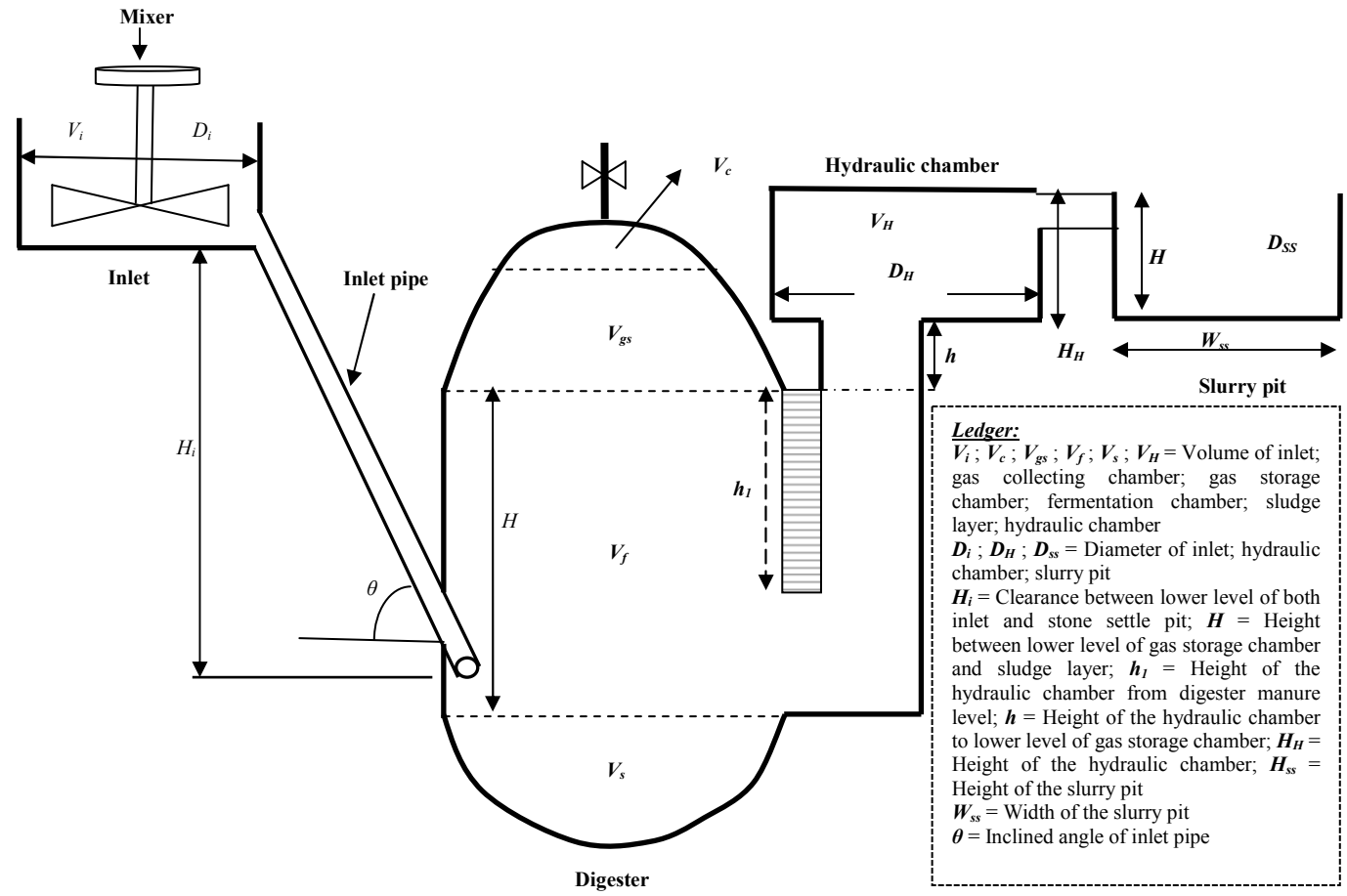

Fig. 5. Schematic diagram of biogas plant

IV. Calculation and Result

Lifetime of the designed model is considered 20 years. Total installation cost of the whole model is analyzed to 1.95 crore BDT (≈0.253 million USD) including plant construction cost (digester, inlet and hydraulic chamber), pipeline and purifier cost, electricity generation, transmission and protection cost.

Repairing and overhauling costs of generators are calculated to 52 lac BDT (≈0.67 million USD). Overhauling cost includes both top and major overhauling costs. Top overhauling is 15% of generator cost and it is required after 10,000 hours of operation. After further 10,000 hours of operation major overhauling has to be done which is 50% of generator cost [23].

Waste price for the designed model for 20 years of operation is about 43 crore BDT (≈5.6 million USD) which in turn brings about financial gain of the people of this area.

Raw slurry output from the digester is semi-liquid in type and can be used directly as fish food and after some processing as land fertilizer. Total 262,500 ton slurry output is analyzed for 20 years and processing cost is 26 crore BDT (≈3.37 million USD).

To operate the plant effectively some personnel are mandatory in permanent basis and time to time temporary labors

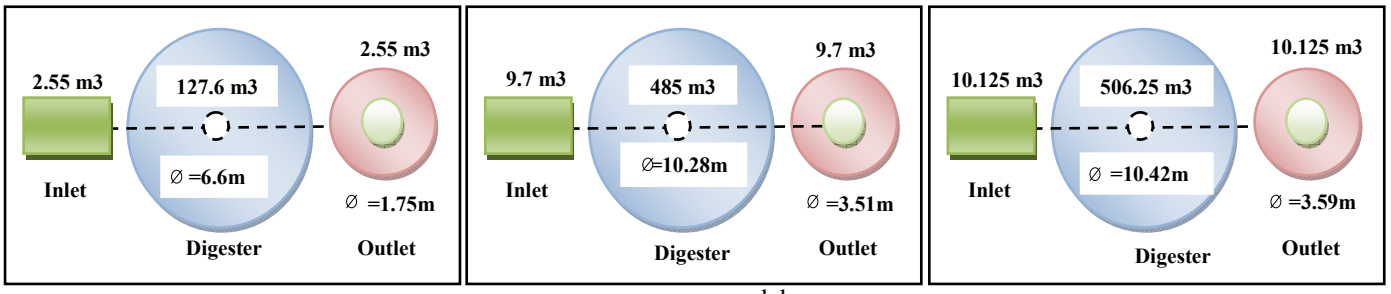

(a) (b) (c)

Fig. 6. Digester design for (a) Organic Waste; (b) 485 Cows; (c) 40,500 Chickens

labors are too requisite. Total waging cost for plant operation and maintenance is calculated 134,000 BDT (≈1750 USD) per month and so 3.2 crore BDT (≈0.415 million USD) for 20 years.

Thus total plant cost for estimated lifetime is about 75 crore BDT (≈9.73 million USD).

Main income of plant authority comes from electric bill, cooking gas charge and fertilizer selling.

Total electric bill in 20 years is about 6 crore BDT (≈0.778 million USD) including service charge. Similarly, cooking gas bill is calculated as 3.72 crore BDT (≈0.48 million USD). Outcome from fertilizer selling is quite large and calculated to 110 crore BDT (≈14.3 million USD) considering 3 & 5 BDT/kg (≈0.04 & 0.06 USD) for fresh slurry and bio-fertilizer respectively.

Hence, net income of the plant authority in this model is 120 crore BDT (≈15.56 million USD).

Income of each individual other than plant investors only from waste selling are as follows-

Household individuals = 10,000 BDT (≈130 USD) per annum

Small scale poultry farm = 60,000 BDT/month (≈780 USD)

Large scale poultry farm = 300,000 BDT/month (≈3900 USD)

Small scale cow farm = 9,000 BDT/month (≈117 USD)

Large scale cow farm = 90,000 BDT/month (≈1170 USD)

Food hotel = 1,800 BDT/month (≈24 USD)

Local market = 9,000 BDT/month (≈17 USD)

Survey in rural Chittagong (Unosottur Para, Raozan), shows that, for a typical family cooking wood cost is 800-1,000 BDT/month (≈10~13 USD) and kerosene cost per month is 400-600 BDT (≈5~8 USD). Therefore, every family saves an amount of 1,200-1,600 BDT (≈15~21 USD) per month only from cooking and lighting sectors.

V. Conclusion

In this designed business model, both people and business authority (entrepreneurs) are dependent on each other and hence benefited mutually. This model not only exonerates a way to develop rural life style but also economic and environmental benefits as well. Further detailed analysis and simulation modelling of this chain business concept could be done in future for comprehensive validation of the proposed concept at the field level.

References

[1] N. Abas, A. Kalair, and N. Khan, “Review of fossil fuels and future energy technologies”, Futures, vol. 69, pp. 31-49, May 2015.

[2] A. Schmidt, B. E. Law, C. Hanson, and O. Klemm “Distinct global patterns of strong positive and negative shifts of seasons over the last 6 decades” Atmospheric and Climate Sciences, vol. 2 (1), pp. 76 -88, Jan. 2012.

[3] A. Oberheitmann, “Some remarks on the individual contribution to climate change” American Journal of Climate Change, vol. 2 (3), pp. 198-202, Sep., 2013.

[4] (2015) IEEE Spectrum page. [Online]. Available: http://spectrum.ieee.org/static/fukushima-and-the-future-of-nuclear-power

[5] A. Aslani, and A. Mohaghar, “Business structure in renewable energy industry: Key areas”, Renewable and Sustainable Energy Reviews, vol. 27, pp. 569-575, Nov. 2013.

[6] M. Richter, "Utilities’ business models for renewable energy: A review", Renewable and Sustainable Energy Reviews, vol. 16 (5), pp. 2483-2493, Jun. 2012.

[7] S. A. Gebrezgabher, M. P. M. Meuwissen, B. A. M. Prins, and A. G. J. M. O. Lansink, "Economic analysis of anaerobic digestion—A case of green power biogas plant in the Netherlands", NJAS - Wageningen Journal of Life Sciences, vol. 57 (2), pp. 109-115, Jun. 2010.

[8] (2015) Bangladesh Power Development Board website. [Online]. Available: http://www.bpdb.gov.bd/bpdb/index.php?option=com_content&view=article&id=12&Itemid=126

[9] (2015) World Bank Indicators: Country Chapter- Bangladesh page. [Online]. Available: http://data.worldbank.org/country/bangladesh

[10] L. Gomes, “Natural gas in Pakistan and Bangladesh - Current issues and trends”, Univ. of Oxford, The Oxford Institute for Energy Studies, 2013.

[11] H. Herich, M. F. D. Gianini, C. Piot, G. Močnik, J. L. Jaffrezo, J. L. Besombes, A. S. H. Prévôt, and C. Hueglin, "Overview of the impact of wood burning emissions on carbonaceous aerosols and PM in large parts of the Alpine region", Atmospheric Environment, vol. 89, pp. 64-75, Jun. 2014.

[12] O. Favez, H. Cachier, J. Sciare, R. S. Estève, and L. Martinon, "Evidence for a significant contribution of wood burning aerosols to PM2.5 during the winter season in Paris, France", Atmospheric Environment, vol. 43 (22-23), pp. 3640-3644, Jul. 2009.

[13] W. Maenhaut, R. Vermeylenb, M. Claeysb, J. Vercauterenc, C. Matheeussenc, and E. Roekensc, "Assessment of the contribution from wood burning to the PM10 aerosol in Flanders, Belgium", Science of The Total Environment, vol. 437, pp. 226-236, Oct. 2012.

[14] J. Aguirre, “Impact of rural electrification on education: A case study from Peru”, Universidad del Pacífico, Peru, 2014.

[15] K. Makitaa,E.M. Fèvreb, C. Waiswac, M.D.C. Bronsvoortd, M.C. Eislera, and S.C. Welburna, "Population-dynamics focussed rapid rural mapping and characterisation of the peri-urban interface of Kampala, Uganda", Land Use Policy, vol. 27 (3), pp. 888-897, Jul. 2010.

[16] A.K. Dahiya, and P. Vasudevan, "Biogas plant slurry as an alternative to chemical fertilizers", Biomass, vol. 9 (1), pp. 67-74, 1986.

[17] T. Bond, and M. R. Templeton, "History and future of domestic biogas plants in the developing world", Energy for Sustainable Development, vol. 15 (4), pp. 347-354, Dec. 2011.

[18] S. Savci, “Investigation of effect of chemical fertilizers on environment”, in proc. APCBEE Procedia ICESD’12, 2012, vol. 1, p. 287-292.

[19] C. K. Das and M. J. Alam, “An innovative Energy Neutral Home system for rural areas of Bangladesh”, in proc. IEEE ICECE’12, 2012, p. 888-891.

[20] IDCOL Biogas Plant Construction Manual, Infracture Development Company Limited, 2007.

[21] S. M. Zicari, "Removal of hydrogen sulfide from biogas using cow-manure compost", M. Sc. thesis, Cornell University, New York, USA, Jan. 2003.

[22] (2015) Biogas process for sustainable development page. [Online]. Available: http://www.fao.org/docrep/T0541E/T0541E0b.htm

[23] Rahman Renewable Energy Co. Ltd, Local Office of IDCOL (Infrastructure Development Company Limited), Gajipur, Bangladesh, 2015.

Assessing a rural electrification program in Malaysia: system performance analysis on 11 solar PV-diesel hybrid systems

Abdul Muhaimin Mahmud[1], Richard E. Blanchard[2]
Centre for Renewable Energy Technology System
School of Electronic, Electrical & System Engineering
Loughborough University
United Kingdom
[1]A.M.Mahmud@lboro.ac.uk, [2]R.E.Blanchard@lboro.ac.uk

Abstract— **In 2006, there was a significant numbers of schools in rural Sabah in Malaysia that had no access to 24-hours electricity. Extension of grid electricity networks becomes uneconomical because of the geographical conditions of these areas and the low electrical energy density demand of the population. Malaysia's rural development policies, therefore, emphasizes on the need to improve the learning and living condition at the rural schools. The abundant solar energy resource in the region is used for providing alternative power supply for these schools. 160 schools in rural Sabah were installed with solar photovoltaic (PV)-diesel hybrid systems. Even though the systems have been in operation for some years, knowledge informing the systems performance is difficult to find. Thus, understanding the system operation is a highly valuable experience and lessons can be learned for implementation of the rural electrification program (REP). This paper describes the finding from a field study at 11 solar PV-diesel hybrid systems. It highlighted some parameters that define the reliability of a solar PV system. The solar PV systems installed at schools in rural Sabah were found to be reliable. They reduced dependency on the diesel fuel consumption and fully utilized clean energy from the sun. It is essential to have reliable solar PV system that can provide sufficient energy for the load demand.**

Keywords—Solar PV, rural electrification program (REP), system performance, reliability

I. INTRODUCTION

Rural electrification is the process, plans, programs or initiatives by government, private sectors, institution or organization that bring electricity to the rural and remote areas where 24-hour electricity connection does not exist. People and communities can develop towards modern civilization if electricity is made available because it can benefit their lifestyle by improving the level of health, education, economy and technology [1]. Renewable energy technology system is recognized as the alternative technology to grid electricity network and solar photovoltaic (PV) system is a popular option [2].

Malaysia, in recent years has achieved 96.86% of 24 hours electricity access. The electricity access coverage in Peninsular Malaysia is the highest at 99.72% as compared to Sarawak (88.01%) and Sabah (92.94%). The geographical conditions and the low electricity energy density demand, of the remaining none electrified areas, has made extension of grid electricity networks uneconomical and in some areas impossible.

The Malaysian government shows high commitment in extending modernization to rural areas. However planning, initiatives and strategies in REP for community need longer time for its complexity to be implemented. Barriers like geographical isolation, inadequate community and social integration risk the implementation of any REP [3]. The aspiration to reduce the gap in education excellence between urban and rural areas lead to the initiative of 160 school solar PV-diesel hybrid systems being implemented in rural Sabah. 78 systems were installed and in operation during 2009, with the remaining coming online in the time period 2010-2014.

The system comprises of solar PV modules as the primary energy generator, battery as the energy storage, diesel generator to support the system and inverter that convert DC and AC voltage in both direction. 78 systems use charge controller and bidirectional inverter. The other systems use two types of inverter systems, grid inverter and bidirectional inverter. The systems were installed with standard capacity depending on the school load demand (10 kWp, 15 kWp, 20 kWp, 30 kWp, 40 kWp, 45 kWp, 50 kWp, 55 kWp and 60 kWp).

A study to determine the success of the solar home system in Bangladesh was conducted by [4] which used quantitative and qualitative survey methods. For long term performance of solar PV system, [5] observed the load consumption, energy productivity, diesel usage and energy generation strategies. Evaluation of solar home systems was conducted by [2] to confirm the specification of the installation. It is envisaged that the installation will be analyzed after the systems are in

operation for several years. The information is valuable for knowledge and learning purposes and provides understanding on the systems operation. Thus, this paper (1) describes system performance indices as tools in determining the reliability of the solar PV systems and (2) evaluate 11 solar PV systems using the system performance indices.

II. METHODOLOGY

A. Scope of Study

11 schools were selected and characterized into several categories which are system capacity, geographical condition and year of operation to ensure the population is defined in several homogeneous subgroups [6]. The locations are shown in Fig. 1.

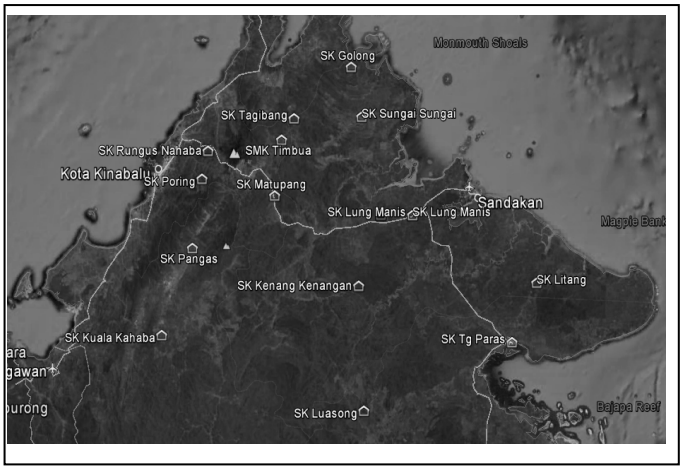

Fig. 1. Location of the 11 systems.

A field study was conducted from August 2014 to September 2014. The detail of the solar PV-diesel hybrid capacity of each school is shown in Table 1 below and Fig. 3 shows the installed system. The system operation was measured and recorded using a Sunny Webbox data logger. Sunny Sensor Box is used to record meteorological data as reference parameters. The data was recorded every 15 minutes for parameters including the meteorology data; DC and AC voltage and current at the solar PV array, inverter and battery system; operation of diesel generator; and schools load consumption to examine the system's energy balance and performance indices.

B. System Performance Indices

System performance indicators are identified and the reference values are defined from standard, specification and literatures and describes below.

a) *Charge factor* [5], [8]-[10]
- An overcharge capacity of the previous discharge output receives by battery.
- **Reference value:** 1.1 – 1.4. It is essential to have lower charge factor due to energy losses during the charge-discharge process

b) *PV generator capacity (Ca)* [8], [11]
- Ratio of energy produced by PV divided by energy consumed by load in a period of time.
- **Reference value:** 1.0 – 1.2.

c) *Accumulator capacity (Cs)* [8]
- Ratio of maximum energy available from the battery divided by energy consumed by load in a period of time with respect to actual battery energy efficiency.
- **Reference value:** $3 \leq C_S \leq 5$ (for rural electrification)

d) Solar PV fraction
- Fraction of energy produced by solar PV as compared to the total energy generation from all sources. The ratio of solar PV and diesel generator is expected to be 9:1 as specified from the design.
- **Reference value:** > 90%

e) *Balance of system (BOS) efficiency* [12]
- Overall efficiency of the other components of the system.
- **Reference value**: No specific value but the higher the efficiency indicates lower losses within the system components (excluding the PV panel).

III. RESULT AND ANALYSIS

A. Energy Resources

The irradiation level at each school is higher than the region average [13] (Fig. 2) except at SK Poring due to its location at highland (836 m) and the area is always surrounded with cloud especially in the afternoon.

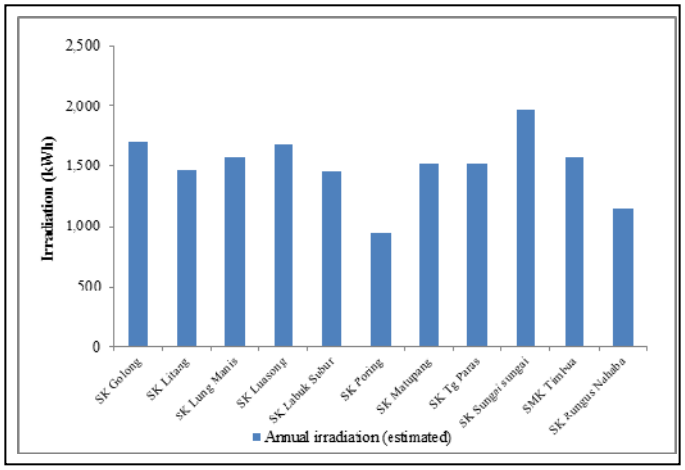

Fig. 2. Annual irradiation recorded at 11 schools.

A. System performance analysis

The recorded data obtained from 11 systems were analysed. In general, the system operation was recorded for one to two years for each system. Data losses were found to have occurred during some periods of time for some systems. Table 2 describes the performance values of the systems.

TABLE I. LIST OF THE 11 SCHOOLS AND THE SOLAR PV-DIESEL HYBRID SYSTEMS CAPACITY. (SK MEANS PRIMARY SCHOOL AND SMK MEANS SECONDARY SCHOOL)

School name	District	Geographical (*elevation from sea level)	Year operation	Capacity			
				Solar PV (kWp)	Grid Inverter / Bidirectional inverter (kW)	Battery (Ah)	Genset (kVA)
SK LUASONG	TAWAU	LAND (62 m)	2011	30	32 / 20	4500	24
SK LABUK SUBUR	SANDAKAN	LAND (4 m)	2011	20	20 /15	3000	13
SK LITANG	KINABATANGAN	LAND (13 m)	2011	20	20 /15	3000	13
SK GOLONG	BELURAN	LAND (11 m)	2011	30	32 / 20	4500	24
SK LUNG MANIS	SANDAKAN	LAND (51 m)	2011	40	44 / 30	6000	30
SK MATUPANG	RANAU	LAND (216 m)	2011	40	44 / 30	6000	27
SK PORING	TUARAN	LAND (836 m)	2009	15	13.7 / 10	1500	12
SK TANJUNG PARAS	LAHAD DATU	ISLAND (10 m)	2011	30	32 / 20	4500	24
SMK TIMBUA	RANAU	LAND (38 m)	2011	60	64 / 45	9000	33
SK SUNGAI SUNGAI	BELURAN	LAND (17 m)	2014	60	60 / 45	9000	30
SK RUNGUS NAHABA	RANAU	LAND (614 m)	2011	20	20 /15	3000	13

Fig. 3. (left) Solar PV structure and power house at SK Labuk Subur, (centre) solar PV panels at SK Sungai sungai, (right) system power house for batteries, inverters, diesel generator and other accessories at SK Lung Manis.

TABLE II. SYSTEM PERFORMANCE OF 11 SOLAR PV SYSTEMS

Parameters	Unit	Mean	SD
BOS efficiency	%	95.79	1.89
PV fraction	%	90.99	9.29
Charge factor		1.34	0.08
PV generator capacity		1.13	0.09
Accumulator capacity		3.13	0.57

[a]*SD = standard deviation*

The BOS efficiency for all systems were more than 90% with average at 95.79% (SD = 1.89). The systems were installed to high quality and complied with standards and specifications [14].

Overall, 328 MWh of electricity energy were generated by the solar PV panels to meet the load demand and to charge the batteries. In contrast, 25.5 MWh was produced by diesel generators which contributed 7.22% of the total energy produced by the systems. Three systems (SK Golong, SK Litang and SK Poring) did not meet the reference value of 90% solar PV fraction. The load ratio for SK Golong and SK Litang was almost 100% as describes in Fig. 4 and battery problem at SK Poring are the reasons for higher usage of diesel generator. The lowest diesel generator usage was observed at SK Labuk Subur with 181 hours of running hours recorded. Teachers and staff live off site at a nearby village is the reason for low load at 22.69 kWh/day. The other two systems with the same capacity have a load double that of SK Labuk Subur. The charge factor was a mean 1.34 and SD 0.08. The highest charge factor was found at SK Poring (1.58).

Standalone PV system requires high reliability and can be determined by the capacity of the PV and the batteries with the amount of load consumed in a period of time (daily, monthly or annually) [8]. The PV generator capacity is found at 1.13 (SD=0.09) and the accumulator capacity at 3.13 (SD=0.57). The solar PV systems generate sufficient electrical power that meet the demand by the load and the batteries. Furthermore, the batteries contain adequate capacities which compensate the period of low or zero energy production from the solar PV, as well as supporting the diesel generator operation.

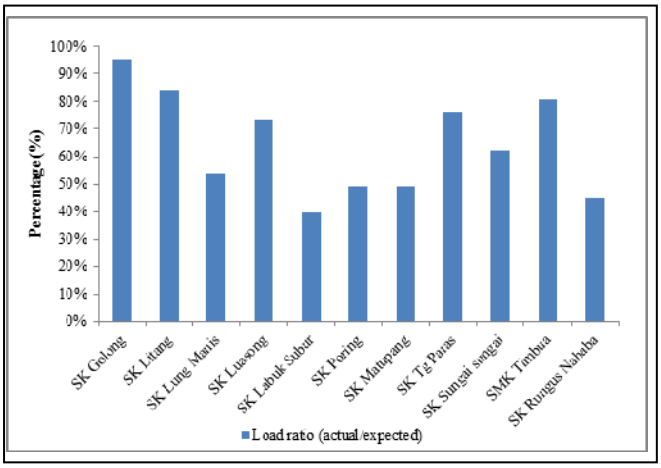

Fig. 4. The ratio of the actual load and the expected load.

Fig. 5 below describes the energy generation from solar PV and diesel generator at SK Poring in January 2011. The diesel generator was in operation every weekday of the month – the same situation was observed in other months. The actual load was recorded at 14.12 kWh/day, which is half the expected value at 28.8 kWh/day. The battery SOC level dropped to just 20%. This happened after midnight, which initiated the diesel generator for the charging process (Fig. 6). The battery voltage was at low voltage level (1.8 V_{dc} per cell) even though the SOC level was more than 50%. The batteries were unable to produce sufficient energy as its actual capacity was lower than the nominal value. Hence, this condition reduces the reliability of the solar PV system.

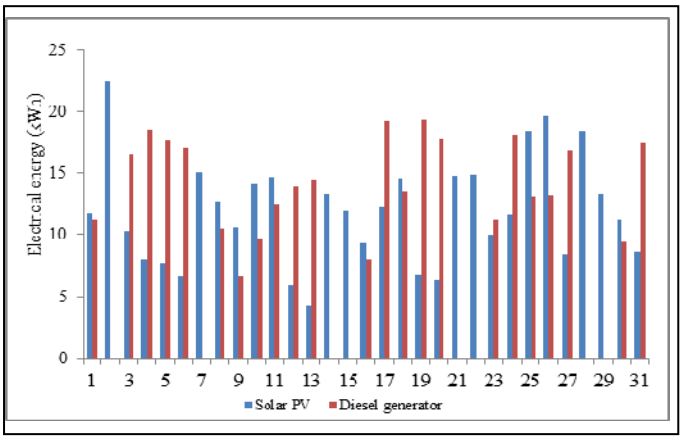

Fig. 5. Energy generation from solar PV and diesel generator for January 2011 at SK Poring.

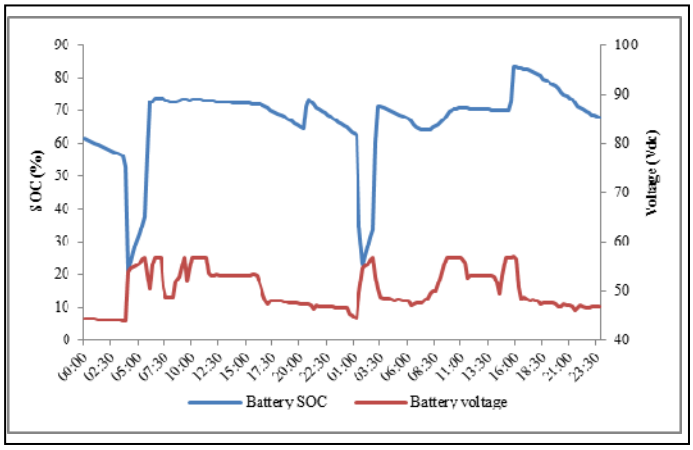

Fig. 6. Battery state of charge (SOC) and voltage on 17-18/1/2011 at SK Poring.

IV. CONCLUSION

This paper gives an understanding of off-grid solar PV system operation. The fact that information on field performance data is not easily found in literatures makes findings from this paper valuable.

This paper reports on the work to evaluate the performance of 11 solar PV systems which have been installed at schools in rural Sabah. Methods in evaluating the system performance indices that determine the reliability of the system have been presented. 10 systems were found to be highly reliable and give sufficient power for the schools load demand. Though the system at SK Poring could meet the load demand, the issues in higher consumption of the diesel generator is highlighted. In this case the problem was found to have occurred because the battery system did not have sufficient capacity.

The information from this paper is to be used in constructing guidelines for evaluating solar PV system performance. In the future, several milestones are to be achieved such as defining the effectiveness of the REP in transforming the education excellence in rural areas and developing a REP model that is high in sustainable value.

ACKNOWLEDGMENT

The authors would like to thank officers at Electrical Engineering Branch, Public Works Department of Malaysia, for their assistances and supports during the field study. Abdul Muhaimin Mahmud wishes to thank the Public Service Department of Malaysia for sponsoring the study.

REFERENCES

[1] F. S. Javadi, B. Rismanchi, M. Sarraf, O. Afshar, R. Saidur, H. W. Ping, and N. a. Rahim, "Global policy of rural electrification," Renew. Sustain. Energy Rev., vol. 19, pp. 402–416, Mar. 2013.

[2] S. A. Chowdhury, M. Mourshed, S. M. R. Kabir, M. Islam, T. Morshed, M. R. Khan, and M. N. Patwary, "Technical appraisal of solar home

systems in Bangladesh: A field investigation," Renew. Energy, vol. 36, no. 2, pp. 772–778, Feb. 2011.

[3] J. Hazelton, A. Bruce, and I. MacGill, "A review of the potential benefits and risks of photovoltaic hybrid mini-grid systems," Renew. Energy, Dec. 2013.

[4] T. Urmee and D. Harries, "Determinants of the success and sustainability of Bangladesh's SHS program," Renew. Energy, vol. 36, no. 11, pp. 2822–2830, Nov. 2011.

[5] P. Díaz, R. Peña, J. Muñoz, C. A. Arias, and D. Sandoval, "Field analysis of solar PV-based collective systems for rural electrification," Energy, vol. 36, no. 5, pp. 2509–2516, May 2011.

[6] M. K. . Trochim, Research Methods Knowledge Base. Statistic's Solution Consulting. [Online]. Available: http://socialresearchmethods.net.

[7] SMA Solar Technology AG, SunnyBoy 3000TL/3600TL/4000TL/500TL with reactive power control. SMA Solar Technology AG, Niestetal, Germany.

[8] A. Luque and S. Hegedus, A handbook of photovoltaic science and engineering. Chichester:Wiley, 2003.

[9] R.-S. Liu, L. Zhang, X. Sun, H. Liu, and J. Zhang, Electrochemical Technologies for Energy Storage and Conversion. Weinham, Germany: Wiley-VCH Verlag & Co. KGaA, 2012.

[10] B. Espinar and M. Didier, "The role of energy storage for mini-grid stabilization : IEA PVPS Task 11 Report," France, 2011.

[11] T. Khatib, A. Mohamed, K. Sopian, and M. Mahmoud, "Optimal sizing of building integrated hybrid PV/diesel generator system for zero load rejection for Malaysia," Energy Build., vol. 43, no. 12, pp. 3430–3435, Dec. 2011.

[12] British Standards Institution, Photovoltaic system performance monitoring — Guidelines for measurement , data exchange and analysis. 1998.

[13] S. Shaari, A. M. Omar, A. H. Haris, R. Abdul Rahman, and S. I. Sulaiman, Solar Photovoltaic Power : Irradiation data for Malaysia. Ministry of Energy, Green Technology & Water, Malaysia / Malaysia Building Intergrated Photovoltaic Project, 2010.

[14] A. M. Mahmud, R. Blanchard, and R. Gottschalg, "Impact Study on Rural Electrification Program Using Solar PV-Diesel Hybrid System for Rural Schools in Sabah, Malaysia," 4th Symposium small PV-application - Rural electrification and commercial use, 2015, p. 145.

RET SCREEN Based Feasibility Study on the Prospect of Wind Power Generation along the Coastal Region of Chittagong, Bangladesh.

Sadreza Mohammad Nizam Uddin[1] , Md. Bodrudduza[2] , B.K.M. Mizanur Rahman[3], M. Fayyaz Khan[4]

Department of EEE United International University, Dhaka, Bangladesh

E-mail: nir23zher@gmail.com

***Abstract*— In this paper, a study has been made on the cost and performance analysis of wind power plant in the coastal region of Chittagong of Bangladesh using RET Screen software. Till to date, no reliable data on wind power is available on Bangladesh. Very recently, some organizations named BPDB, Bangladesh Metrological Department and CWET of India have taken up projects to study wind potential along the costal belt of Bangladesh. Among them BPDB has taken up several programs named WERM, SWERA and WRAP in the country [1]. As reliable data of wind is not available, proper design on wind power plant is not feasible. As a result, harnessing energy from wind remains a remote possibility. The power development board, Bangladesh (BPDB) installed 50 numbers of turbines in the costal belt of Kutubdia in the year March 2008 [2]. Unfortunately vary little amount of energy could be extracted so far and most of pillars and turbines are rushed and has become inoperative. The main reason for such set back is due to lack of proper feasibility study and reliable data on wind. Taking all those points in serious consideration, author in this paper have tried to collect a reliable data on wind along the costal belt of Chittagong and based on this data, possible power generation from wind is analysed through RET Screen. With this user friendly software, optimum number of units together with cost of energy (COE).**

***Keywords*— RE, Wind Turbine, RET Screen, BPDB, GHG, COE.**

I. INTRODUCTION

Bangladesh is situated between 20°34' and 26°38' N latitudes and 88°01' and 92°41' E longitudes with about 150 million people living on 144,000 sq km area [3]. Mainly we are depending on our fossil fuel to met up our energy demand. Our energy demand is mainly met from natural gas (61.76%), Furnace Oil(21.28%), Diesel(7.89%), Coal(2.31%) and Hydro(2.13%) according to the higher percentage of use [4]. Demand of these fossil fuels is increasing day by day with the increase in energy demand. If this situation is continuing, there will be no fuel for our future generation. On the other hand, Green House Gases (GHG) gases are also emitted when we burn the fossil fuels which are harmful for our environment. To overcome this situation, we have to turn on to Renewable Energy (RE). There are many forms of Renewable Energy like Solar, Wind, Geo-thermal, Tidal, Hydro etc. Among those Solar is a good source of energy but it takes huge land space. As a result our harvesting land will reduce rapidly to met our demand. On the other hand we have to setup many batteries to store energy which is also harmful for our environment. Considering all the facts, the prospect of wind energy as an alternative source of Renewable Energy in Bangladesh needs to be examined because the oil and gas reserve of the country is very small. In this paper, an attempt has also been made to investigate the application of wind energy for generation of electricity in coastal region of Bangladesh. In this regard, primarily we have chosen wind speed data of Chittagong for investigation. To complete analysis we have used RETScreen software. Using this software, we have analysed Energy Model, Cost Analysis, Emission Analysis and Financial Analysis. In this paper we take all the price of component considering current market as much as possible.

II. WIND POWER SYSTEM

There are four main parts of a wind turbine: the base, tower, nacelle and blades that shown in figure 1. The blades capture the wind's energy, spinning a generator in the nacelle. The tower contains the electrical conduits, supports the nacelle and provides access to the nacelle for maintenance. The base made of concrete and steel, supports the whole structure [5]. We have chosen a Turbine from 'PowerWind' Manufacturer Company. The model number of this Turbine is 'PowerWind 500' and attached with SCADA system. Nacelle and Blade both are made of glass fibre reinforced plastic. Its electrical and mechanical specifications are shown in table 1 [6].

TABLE 1: SPECIFICATION OF WINDPOWER 500 TURBINE:

Rated Power Output	500 kw
Grid connection	50 Hz / 690 V
Power Factor	0.9 Ind. to 0.9 Cap.
Generator	Asynchronous, air-cooled
Rotor Swept Area	2463 m^3
Rotor Speed	6-249 rpm

Gear ratio	1:54.2
Nominal rotation	1,350 rpm

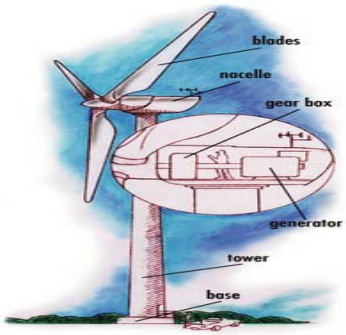

Figure-1

III. WIND DATA OBSERVATION

We have observed the average velocity of six coastal regions in Bangladesh that is collected from a journal [7]. Among those, the avarage data of Potenga is good for wind power. All the data is calculated at 50 m height. We know that the velocity of wind is varied with the height and it depends upon the roughness of the terrain. It is calculated by the following power law expression and calculated data shown in table 2.

$$\frac{v_z}{v_{Ref}} = \left(\frac{h}{h_{Ref}}\right)^{\alpha}$$

Where, v_z and v_{Ref} are the average velocity at h and h_{Ref} meter height. Here α is the roughness parameter and it is varies from 0.1~0.4 depending on the weather of the terrain [8]. We have assumed the roughness parameter 0.4 to calculate velocity at 50m height.

TABLE 2: WIND VELOCITY DATA OF THREE DISTRICTS IN m/s [7]:

Location → Month ↓	Chittagong	Cox's Bazar	Khepupara	Kutubdia	Sondip	Potenga
Jan	5.25	5.42	6.06	2.55	3.35	8.97
Feb	4.15	5.53	6.33	2.63	4.34	9.15
Mar	7.14	6.52	6.97	3.35	4.62	10.63
Apr	7.95	8.05	10.23	3.90	6.97	11.43
May	7.95	5.53	8.41	4.00	3.52	12.22
Jun	9.94	5.97	6.80	5.27	5.53	12.54
Jul	10.23	5.53	5.97	5.21	4.89	13.27
Aug	9.85	5.70	5.70	4.53	3.90	12.32
Sep	6.70	4.62	5.15	3.04	3.35	10.79
Oct	4.07	4.70	5.34	2.09	2.35	10.00
Nov	4.89	3.71	4.26	1.72	2.45	9.68
Dec	3.17	4.70	3.71	1.86	2.45	8.53
Mean	6.71	5.50	6.12	3.35	3.98	10.79

IV. PERFORMANCE AND COST ANALYSIS USING RETSCREEN

The RETscreen International Wind Energy Project Model can be used world-wide to easily evaluate the energy production, life-cycle costs and greenhouse gas emissions reduction for central-grid, isolated-grid and off-grid wind energy projects, ranging in size from large scale multi-tribune wind farms to small scale single-tribune wind systems. In this paper we analyze the feasibility of a central–grid wind energy project. We analyzed our project at Potenga in Chittagong district. The climate data of Chittagong district is shown in table 3.

TABLE 3: DETAILS ABOUT THE LOCATION :

	Unit	Climate data location	Project location
Latitude	°N	22.3	22.3
Longitude	°E	91.8	91.8
Elevation	m	13	13
Heating design temperature	°C	16.5	
Cooling design temperature	°C	29.9	
Earth temperature amplitude	°C	9.0	

V. ENERGY MODEL

In a wind turbine velocity of wind is converted into electric energy. According to the calculation of Wind Velocity, the annual average wind velocity of Potenga is 10.79 ms^{-1}. We can calculate the Energy by using below equations –

Power, $P = \frac{1}{2} \rho A V^3 C_p$

And, Energy = Power × Time

Therefore, $Energy = \frac{1}{2} \rho A V^3 C_p \times Time$

Where, ρ is the density of air that creates pressure on the blade of the turbine. A is the swift area of the turbine blade, V is the velocity of the wind and C_p is a Betz constant that refers

efficiency of a wind turbine. A German Physicist Albart Betz find out that no wind turbine can convert more than 59.3% of the kinetic energy of the wind into mechanical energy turning a rotor [9]. Considering 40 turbines having 0.5 MW power of each, the total power become –

Power = Number of Turbines × Turbine Capacity
= 40 × 0.5
= 20 MW

Now,

Energy per Year = 20 × 24 × 365
= 175,200 MWh

Considering all the parameters, we have calculated total electricity exported to grid in MWh using RETscreen software which is shown in following table.

TABLE 4: PER MONTH ELECTRICITY EXPORT TO GRID:

Month	Wind speed m/s	Electricity exported to grid MWh
January	9.0	7,537
February	9.2	6,885
March	10.6	8,593
April	11.4	8,685
May	12.2	9,267
June	12.5	9,056
July	13.3	9,591
August	12.3	9,291
September	10.8	8,325
October	10.0	8,150
November	9.7	7,755
December	8.5	7,136
Annual	**10.8**	**100,271**

According to the calculation of RETscreen software, electricity exported to grid 100,271 MWh per year. Thus the power efficiency C_p of the Turbine is 57.23%.

VI. COST ANALYSIS

The cost for a utility scale wind turbine range from about $1.3 million to $2.2 million per MW of nameplate capacity installed [10]. We have considered the price of each half MW turbine $ 0.80 million or BDT 64 million. The different types of cost are shown in table 5.

Table 5: INSTALATION COST OF COMPONENT FOR WIND TURBINE:

Name of Cost Types	Amount (BDT)
Wind Turbine Cost	1,280,000,000
Feasibility Study	1,398,675
Development	2,331,126
Engineering	1,864,901
Balance of System & Miscellaneous	76,651,943
Total	1,438,594,143

For maintenance of the plant, different types of employees are required. Some cost has to be earmarked for this. Also Bangladesh is stormy country, every year two or more medium or heavy storm hit on the coastal region. So we have to be prepared to repair the wind turbine after storm. The salaries of the employers are fixed according to the pay commission scale 2015 [11]. Total annual cost required for manpower and spares is shown in the table 6.

Table 6: ANNUAL COST DETAIL:

Post	Qunt.	Salary/Month(BDT)	Salary/yr (BDT)
Plant Manager	1	80,000	96,0000
A. Plant Manager	1	60,000	72,0000
Engineer (Mechanical)	10	30,000	36,00000
Engineer (Electrical)	10	30,000	36,00000
Technician	10	15,000	18,00000
Store Manager	1	17,000	2,04000
Cleaner	5	9,000	54,0000
Parts in Reserve (Approximately)	NA	NA	10,000,000
Total Annual Cost			2,14,24000

The per unit cost of the wind power

As a developing country, the cost of wind power per unit of energy is a vital issue. We can calculate the price of per unit wind power by using the following formula [12].

$$\text{Cost per unit} = \frac{\text{Turbine \& other fixed cost} + (\text{Annual recent cost} \times \text{life time})}{365 \times 24 \times \text{life time} \times P_m(U_m)}$$

Where, $P_m(U_m)$ is the value of power at mean velocity. The project's life time is considered to be 15 years. Hence,

$$\text{Cost per unit} = \frac{1,438,594,143 + (21,424,000 \times 15)}{365 \times 24 \times 15 \times 310(KW)}$$

If we calculate it then the cost will be BDT 43.21 per unit.

VII. EMISSION ANALYSIS

In this step we only consider the emission reduction of GHG gases compare to the Natural gas. A **greenhouse gases** (sometimes abbreviated **GHG**) is a gas in an atmosphere that absorbs and emits radiation within the thermal infrared range. This process is the fundamental cause of the greenhouse effect [13]. The major greenhouse gases in the Earth's atmosphere are water vapour, carbon dioxide, methane, nitrous oxide, and ozone. Greenhouse gases mainly affect the temperature of the Earth. Without them, Earth's surface temperature would average about 33 °C colder, which is about 59 °F below the present average of 14 °C (57 °F) [14][15][16]. As we know that Natural gas is mostly used fuel to generate electricity therefore we consider it for base case system analysis. After comparing both Natural gas and Wind, we get that the emission of Natural gas is 65,866.3 Tons of CO_2 per year and the proposed case emits 7,904 Tons of CO_2 per year. Finally GHG emission reduction is 57,962.4 Tons of CO_2

per year. Thus we see that it is not harmful for our environment.

VIII. FINANCIAL ANALYSIS

This is most important part to set up a project. Without Financial analysis we can't verify whether a system is viable or not. In this paper we have analyzed the worksheet contains in five sections: Financial parameters, Annual income, Project costs and savings/income summary, Financial viability, yearly cash flow and Cumulative cash flow graph.

In financial parameter section we consider some terms and factors that are shown in table 7.

TABLE 7: FINANCIAL ANALYSIS PARAMETERS:

Financial parameters		
General		
Fuel cost escalation rate	%	8.0%
Inflation rate	%	6.1%
Discount rate	%	12.0%
Project life	yr	15
Finance		
Incentives and grants	BDT	
Debt ratio	%	100.0%
Debt	BDT	1,438,594,143
Equity	BDT	0
Debt interest rate	%	16.00%
Debt term	yr	8
Debt payments	BDT/yr	331,199,272

According to the table 7, we see that we continue this project for 15 years and we borrow full amount from any national or international Bank where interest rate is 16 percent. We will pay to the bank BDT 331,199,272 per year and will continue for 8 years.

Annual income for the plant is shown in Table 8 to calculate annual savings.

TABLE 8: ANNUAL INCOME:

Annual income		
Electricity export income		
Electricity exported to grid	MWh	100,271
Electricity export rate	BDT/MWh	43,206.02
Electricity export income	BDT	4,332,304,561
Electricity export escalation rate	%	5.0%

We see that we will export 100,271MWh electricity every year at BDT 43206.02 per MWh. We will earn about BDT 43.32 billion per year at BDT 43.21 per unit.

Summary of total cost and income is shown in table 9.

TABLE 9: COST AND SEVINGS OR INCOME SUMMARY:

Project costs and savings/income summary			
Initial costs			
Feasibility study	0.1%	BDT	1,398,675
Development	0.2%	BDT	2,331,126
Engineering	0.1%	BDT	1,864,901
Power system	89.0%	BDT	1,280,000,000
Balance of system & misc.	10.6%	BDT	152,999,441
Total initial costs	**100.0%**	**BDT**	**1,438,594,143**
Annual costs and debt payments			
O&M		BDT	21,424,000
Fuel cost - proposed case		BDT	0
Debt payments - 8 yrs		BDT	331,199,272
Total annual costs		**BDT**	**352,623,272**
Periodic costs (credits)			
Annual savings and income			
Fuel cost - base case		BDT	0
Electricity export income		BDT	4,332,304,561
Total annual savings and income		**BDT**	**4,332,304,561**

Now we see the yearly cash flow data in table 10. To calculate data we ignore income tax which is normally waived by the government.

Table 10: TOTAL CASH FLOW DATA:

Yearly cash flows			
Year	Pre-tax	After-tax	Cumulative
#	BDT	BDT	BDT
0	0	0	0
1	4,194,987,510	4,194,987,510	4,194,987,510
2	4,421,044,513	4,421,044,513	8,616,032,023
3	4,658,388,948	4,658,388,948	13,274,420,971
4	4,907,584,245	4,907,584,245	18,182,005,217
5	5,169,221,948	5,169,221,948	23,351,227,165
6	5,443,923,116	5,443,923,116	28,795,150,280
7	5,732,339,796	5,732,339,796	34,527,490,076
8	6,035,156,571	6,035,156,571	40,562,646,648
9	6,684,291,450	6,684,291,450	47,246,938,098
10	7,018,100,486	7,018,100,486	54,265,038,583
11	7,368,575,195	7,368,575,195	61,633,613,778
12	7,736,547,347	7,736,547,347	69,370,161,125
13	8,122,890,208	8,122,890,208	77,493,051,334
14	8,528,520,609	8,528,520,609	86,021,571,943
15	8,954,401,118	8,954,401,118	94,975,973,061

According to this data we see that after starting generation we will earn money and at 15th year the cumulative amount will be about BDT 949.54 billion. It's corresponding graph also shown in figure 3.

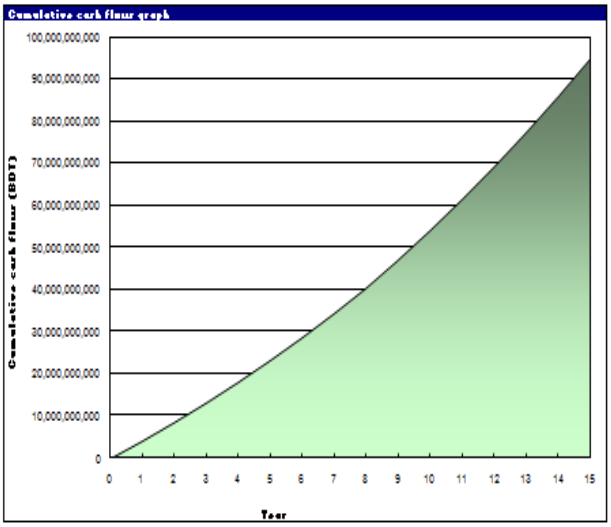

Figure 3

We have to pay total amount of money to the bank in 8 years is,

$$= 331,199,272 \times 8$$

$$= 2,649,594,176$$

Our total income of one year is BDT 4,194,987,510 which is greater than the bank payment.
Now,

Breakeven point

= Revenues - Total Expenses

= Revenues - (Total bank payment + Annual cost)

= 4,194,987,510 - (2,649,594,176 + 21,424,000)

= 1,523,969,334

According to the breakeven point calculation, we can make profit from the commissioning year [17]. So we can say that the system is feasible because of reaching breakeven point within a short time.

IX. CONCLUSION

Although the investment cost for installation of a wind turbine system is quite high, but still it may be a good option for thriving business activities on it. To make the analysis more feasible, we use here RETScreen software. One of the primary benefits of using this software is that it facilitates the project evaluation process for decision makers. The *GHG Analysis* worksheet, with its emission related input items (e.g. fuel mix) and its calculated emission factor output items (e.g. GHG emission factor) allows the decision-maker to consider various emission parameters with relative ease. However, the user should be aware that, this ease of use may give a project developer a too opstimistic and simplified view of what is required in setting a baseline for a proposed project. As such, it is suggested that the user take a conservative approach in calculating the base line emission factor for the project, particularly at the pre-feasibility analysis stage. In order to determine the net benefits of obtaining carbon finance for the project, the user can evaluate the project using two methods, once including the value of the carbon credits and the associated transaction costs and secondly without it, and then make a comparative result out. So the government should come forward with soft term loans to install wind power plant. For coastal areas installation of power plant could be a good decision. Major advantage of wind power that it take low place for setup and also give 24 hours electricity depending on wind without back up.

REFERENCES

[1] http://www.google.com.bd/url?sa=t&rct=j&q=&esrc=s&source=web&cd=1&cad=rja&uact=8&sqi=2&ved=0CCAQFjAA&url=http%3A%2F%2Fwww.buet.ac.bd%2Ficece%2Fpub2004%2FP118.pdf&ei=HExkVdD2B9OPuASJ6oHYCw&usg=AFQjCNH5Wq-1BIsk3hAxB0Kagj9F1GSJKQ&bvm=bv.93990622,d.c2E

[2] http://forum.daffodilvarsity.edu.bd/index.php?topic=26196.0

[3] http://www.academia.edu/2094424/Green_Energy_Financing_in_Bangladesh

[4] http://www.bpdb.gov.bd/bpdb/index.php?option=com_content&view=article&id=5&Itemid=6

[5] http://www.ecw.org/windpower/web/cat2a.html

[6] http://www.powerwind.co.in/pdf/PI_PW500_DataSheet_en.pdf

[7] http://www.buet.ac.bd/icece/pub2004/P048.pdf

[8] http://es.ucsc.edu/~jnoble/wind/extrap/

[9] http://www.raeng.org.uk/publications/other/23-wind-turbine

[10] http://www.windustry.org/how_much_do_wind_turbines_cost

[11] http://boxnews24.com/new-pay-scale-bangladesh-2015-2016-gov-non-gog-teacher/

[12] http://www.wind-power-program.com/turbine_economics

[13] "IPCC AR4 SYR Appendix Glossary" (PDF). Retrieved 14 December 2008.

[14] Karl TR, Trenberth KE (2003). "Modern global climate change". Science **302** (5651): 1719–23. Bibcode:2003Sci...302.1719K. doi:10.1126/science.1090228. PMID 14657489.

[15] Le Treut H., Somerville R., Cubasch U., Ding Y., Mauritzen C., Mokssit A., Peterson T. and Prather M. (2007). Historical overview of climate change science. In: Climate change 2007: The physical science basis. Contribution of Working Group I to the Fourth Assessment Report of the Intergovernmental Panel on Climate Change (Solomon S., Qin D., Manning M., Chen Z., Marquis M., Averyt K. B., Tignor M. and Miller H. L., editors) (PDF). Cambridge University Press. Retrieved 14 December 2008.

[16] "NASA Science Mission Directorate article on the water cycle". Nasascience.nasa.gov. Retrieved 2010-10-16

[17] http://www.accountingcoach.com/break-even point/explanation/2

100% Electrification and Renewable based Ethiopian Power Sector Development Strategies

Md. Alam Hossain Mondal[#], Elizabeth Bryan, Claudia Ringler, Mark Rosegrant

Environment and Production Technology Division (EPTD), International Food Policy Research Institute (IFPRI)
2033 K Street, NW Washington DC, USA
[#]a.mondal@cgiar.org

***Abstract*— This study presents an assessment of future electricity supply strategies for Ethiopia. This study also examines opportunities to diversify the energy supply-mix in ways that meet the country's goals of sustainable energy system development and improved energy security, using the MARKAL energy system model. National policies, such as universal electrification, zero carbon emissions and export options are integrated in this modeling work to find the least-cost mix of technologies to meet the country's rising demand for energy given rapid socio-economic development. The model allocates renewable energy technologies (RETs) for electricity production, as their potential is relatively high in Ethiopia. Hydro, Solar PV and wind contribute significantly to improve energy security. The total system cost with RETs is not significantly higher than the base case to meet the policy targets. Alternative policy options show higher investment costs in the near term but have long-term benefits in terms of sustainable energy system development and access to modern sources of energy for all.**

***Keywords*— energy policy, renewable energy, MARKAL model, power sector, Ethiopia**

I. INTRODUCTION

The main barriers to widespread electricity access in Ethiopia are financing, planning, governance and institutional capacity [1]. The Government of Ethiopia has a plan to achieve universal electrification, clean energy generation from renewable energy resources and electricity exports to neighboring countries [2], [3]. To analyze the techno-economic feasibility of diversification of the energy supply-mix over the long term, optimization energy models can provide valuable insights for energy policy design and investment. Energy policy and investment decisions consider all expected energy supply and demand side options that are consistent with national development goals. Long-term comprehensive energy system planning is required to improve access to modern sources of energy, increase energy security and mitigate greenhouse gas (GHG) emissions. Energy planning based on comprehensive modeling tools enables policy-makers to anticipate and respond to the rapid changes that are occurring and to take advantage of new innovations. This type of investigation in Ethiopia is currently lacking.

In this study, the MARKAL (MARKet ALlocation) energy system model was developed to find the least-cost solution for alternative technology selections for next 30 years (2015-2045) in the Ethiopian power sector. The design of this model allows for a wide range of hypothetical assessments to be carried out, such as different sets of strategy, energy or technology availability or climate constraints [4].

Based on Ethiopia's Growth and Transformation Plan (GTP), the green economy strategy, the sustainable energy for all (SE4All) plan, and strategies of the Ethiopia Electric Power Corporation (EEPCo) for further development of the power sector [3], [5]–[7], the following policy scenarios were developed in MARKAL:

i) Reference scenario: This scenario assumes a continuation of current energy and economic dynamics without imposing any policy constraints and serves as the reference scenario.

ii) Targeted electrification (electrification) scenario: This policy scenario is based on government's Growth and Transformation Plan to provide electricity access to all household by 2030.

iii) Renewable energy development (renewable) scenario: This policy scenario assumes that the government targets to produce 100% of the country's electricity from renewable energy resources by 2025.

iv) Electricity export (export) scenario: This alternative policy scenario assesses the impact of exporting electricity to neighboring countries. Based on the Ethiopian electricity development plan, this scenario considers an upper bound of electricity export to be 20% of national total demand from 2020 onwards to determine the impacts on power sector development.

v) Renewable, electrification and export (combined) scenario: This scenario assumes that the specific policy interventions are carried out to ensure that the following targets are met: 100% renewable energy-based electricity by 2025, electricity exports are permitted up to a maximum limit of 20% of national demand beyond 2020, and 100% electrification by 2030.

II. MARKAL MODEL

MARKAL (MARKet ALocation) is an energy system planning optimization tool. The model was developed in 1974 by a consortium of members of the International Energy Agency. The Brookhaven National Laboratory, New York, USA, and the Kernforschungsanlage Juelich, Juelich, Germany, were the hosts of the program. MARKAL is an extensive model used for longer term analyses and can be used for cities, provinces, countries or regions. About 250 institutes across 70 countries have adopted this model [8]. Based on user specified technological and energy availability limitations, MARKAL classifies technological allocation to

meet the specified energy demand of an energy system. It determines the optimal energy supply mix and finds the least-cost solution based on the techno-economic parameters of the selected technologies [9]. To meet this objective, the model calculates a partial equilibrium of the supplied reference energy system (RES) [10], [11].

MARKAL is a demand-driven, linear programming model. The schematic structure of the MARKAL model for Ethiopia is given in Fig. 1. Energy demand is driven by the provided conversion technologies including existing and forthcoming and the supplied energy resources factors that to be exploited. The model determines the amount of energy required to meet projected demand and the associated investment needs. It also determines the capacity for technology integration by year, the level of utilization of selected technologies and environmental effects. The environment is an important restriction for any energy conversion process and this issue is considered in this modeling approach.

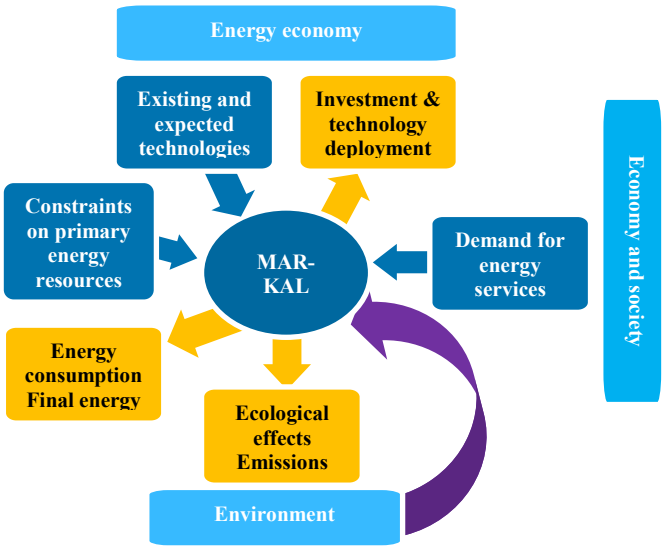

Fig. 1: Schematic structure of MARKAL model [4], [12]

III. Ethiopia-MARKAL Framework Development

The development of the reference energy system (RES) is the key contribution of this study. The developed RES for Ethiopia can be used for any energy planning analysis with minor updates to the database. The MARKAL model mainly consists of a large set of energy technologies, linked together by energy flows that jointly form the RES, which is why RES is called the backbone of MARKAL for any specific energy system [10]. This reference system is able to allocate primary energy resources based on technologies selected by capacity and year, considering technologies performance to meet the year-wise specific energy demand.

Electricity demand for each sector is projected (2012-2030) using the Long-range Alternative Planning system (LEAP) model [13]. In the LEAP model, an energy intensity method was applied to project Ethiopian energy demand. The annual average growth rate of electricity demand estimated by LEAP is applied to estimate electricity demand for 2035, 2040 and 2045 in the MARKAL model. Electricity demand is projected to increase from 6690 GWh in 2015 to about 80160 GWh in 2045 in the reference scenario and to about 119680 GWh in the targeted electrification scenario.

Energy price, primary energy resource availability and their boundary limits are supplied in the model based on a synthesis of previous studies. All costs in this study are presented in US Dollars (1 USD = 20.80 Ethiopian Birr in 2015). Characteristics of all conversion technologies need to be supplied to design the reference energy system. These technologies convert energy from primary resources to electricity to meet the specified electricity demand. A fairly representative set of conversion technologies is developed for the Ethiopian power sector, which includes a total of 11 different conversion technology types: pulverized coal, oil-based steam turbine (ST) and simple cycle, gas ST and combined cycle (CC), large hydro, small-medium hydro, solar photovoltaics (PV), concentrated solar power (CSP), wind, and geothermal.

Transmission and distribution (T&D) losses was amounted to 23% in 2012 and are expected to decrease to 14% by 2045 [3][14]. For each of the technology types, values are given for efficiency, capital cost, operation and maintenance (O&M) costs, NO_2 and SO_2 emissions per unit of energy production, introduction year and residual capacity. Based on the Ethiopian Research Group report [15] and the Eastern Nile Power Trade Program (ENPTP) study report [16], transmission and distribution (T&D) costs are also incorporated in the model. Only centralized-grid electricity has been considered in the Ethiopia-MARKAL model as the main aim is to cover all power plants to feed to the national grid. End use demand technologies have been merged into their respective sector-wise electricity demand that refers to the gross demand of each sector.

IV. Optimization Results

Ethiopian power generation capacity is expected to grow from 3,190 MW in 2015 to 24,890 MW in 2045 to meet the electricity demand which amounts to an average growth rate of about 7% per year in the reference scenario (Table 1). The structure of generation technologies also changes significantly with the introduction of natural gas-, coal- and solar PV-based technologies. CSP is not selected by the model until the end of the analysis period. Moreover, oil-based and geothermal plants do not get additional capacity for investment. Large hydro capacity is projected to increase from the current capacity of 1,660 MW to 6,160 MW in 2045, an average growth rate of 4.5% per year. The model shows an opportunity to introduce solar PV and wind power plants due to their learning cost effects on investment over the long term. In the reference scenario, the contribution of renewable energy technologies decreases from 94% in 2015 to 85% in 2045.

Electricity production grows from 10,590 GWh in 2015 to 94,090 GWh in 2045 in the reference scenario. The share of renewable electricity decreases from about 99% in 2015 to 93% in 2045. Electricity production from large hydropower rises from 6,270 GWh in 2015 to 44,670 GWh in 2045, which amounts to 47.5% of total electricity production in 2045. The MARKAL model suggests that the country import 1,200 GJ of

fuel oil in 2015 for electricity production. Fossil fuel energy consumption increases dramatically from 1,200 GJ in 2015 to 57,270 GJ in 2045.

TABLE I
TECHNOLOGY CAPACITY DEVELOPMENT, ELECTRICITY PRODUCTION AND FOSSIL FUEL DEMAND IN THE REFERENCE SCENARIO

	Base scenario (no policy)		
	2015	2030	2045
Technology capacity (MW)			
Coal-fired plant	-	20	20
Fuel oil based steam turbine	30	30	-
Diesel oil-based simple cycle	160	160	160
Natural gas based combined cycle	-	1180	3610
Large hydro (over 100 MW)	1660	2109	6160
Small hydro (1-100 MW)	180	180	180
Geothermal	10	10	10
Solar PV	-	150	7510
Wind	1150	2480	7240
Total (GW)	3190	6400	24890
Electricity production (GWh)			
Coal-fired based plant	-	130	130
Oil-based plants	122	-	-
Natural gas combined cycle	-	5000	6690
Large hydro (over 100 MW)	6270	16280	44670
Small-medium hydro (1-100 MW)	1260	940	840
Geothermal	50	50	50
Solar PV	-	460	23530
Wind	2890	6220	18170
Total (TWh)	10590	29080	94090
Fuel (fossil) requirement (TJ)			
Mined coal	-	1200	1200
Imported oil	1200	-	-
Mined natural gas	-	41900	56070
Total	1200	43100	57270

Figure 2 shows the least-cost selection of capacity levels for all considered alternative policy scenarios. Model results show that electricity production is still dominated by the large hydropower plants in in all scenarios. Large hydropower capacity decreases significantly in the renewable and export scenarios where wind and solar PV contribute to electricity generation. Due to of the large increase in solar PV and wind power generation capacity, the total capacity for the combined scenario is bit higher (due to limited production from these technologies) than the electrification scenario, although the total demand is the same. Maximum generation capacity is required by 2045 in the combined scenario is 32,400 MW to meet the specific 100% electricity demand as well as to meet 100% renewable-based production.

The model findings reveal that between 2015 and 2045 cumulative CO_2 emissions from the total energy system are about 80.4 million tons (mt) in the reference scenario. Emissions reach 0.93 mt in 2015 and are expected to increase to 3.2 mt in 2045, about 3.5 times more emissions than in the base year due to a greater number of fossil fuel-based power plants in the system. CO_2 emissions are expected to decrease by 96% and 94% in the renewable and combined scenarios, respectively, compared to the reference scenario.

The model estimated the total system cost to be about 21.66 billion USD (discounted total during 2015-2045) in the reference scenario. The total system cost increased by about 22% and 25% in the targeted electrification and combined scenario, respectively, compared to the reference scenario. The system cost is enlarged slightly by about 5% in the renewable scenario compared to the reference scenario. Interestingly, the export scenario shows a decrease of about 3% in the total system cost compared to the reference scenario, which suggests that greater exports would provide substantial savings over the long term. The yearly investment cost in the export scenario (except 2025) is also low compared to the other scenarios.

V. CONCLUSIONS

Several policy conclusions can be drawn based on the results in this study. Choosing technologies based on their capacity and primary energy sources enables the Ethiopian power sector to meet their projected electricity demand, achieve electricity access for all, export electricity, and promote sustainable energy development through the utilization of renewable energy resources.

The current supply of energy resources would need to diversify from hydropower to a mix of hydro, solar, and wind. Solar PV has significant potential to supply Ethiopian power due to its learning cost effects. The model result shows alternative technologies that are highlighted in generation planning by the Ethiopian Electric Power Corporation are feasible for investment. The estimated total discounted system costs for the alternative policy scenarios are not much higher than the reference scenario. Furthermore, the electricity export scenario shows a decrease in total system cost from the export of electricity. Although, the initial investment cost in the early period (2020-2030) is higher than in the reference scenario, investment costs in the renewable energy development scenarios (renewable and combined) decline over the longer term.

The model results show that higher investment cost in the near future will be paid back over the long term for these alternative policy scenarios. Achieving these objectives requires a strong long-term vision and robust policy support.

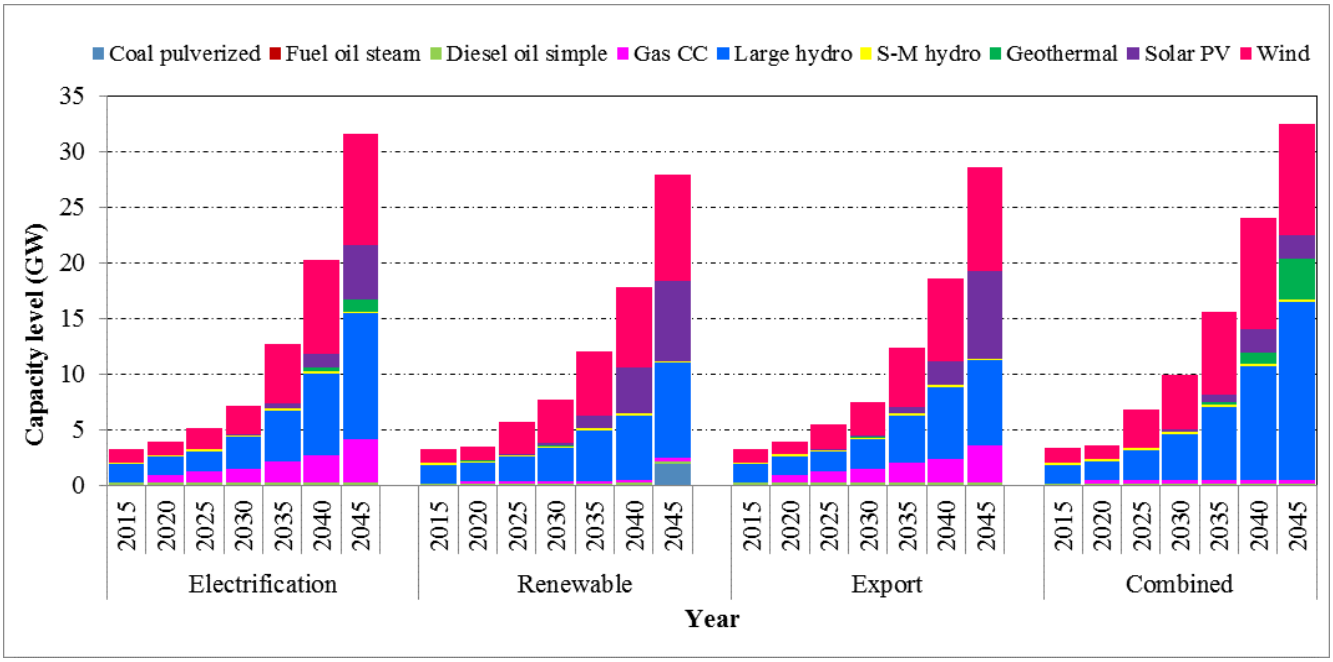

Fig. 2: Technology capacity selection in alternative policy scenarios

An energy strategy focusing on renewable energies can well be more water-intensive than a strategy that relies on fossil fuels. As a result, it is important to assess the implications for water resources of the various energy development strategies as well as the implications of changing water availabilities, in response to growing demand and climate change, on Ethiopia's energy development strategies. As water is also essential for food production, interactions with food security strategies are also important. The International Food Policy Research Institute is assessing these water-energy-food nexus challenges in Ethiopia and the Eastern Nile Basin under a new, German Government supported project titled "The water-energy-food nexus: global, basin and local case studies of resource use efficiency under growing natural resource scarcity".

REFERENCES

[1] M. Bazilian, P. Nussbaumer, H. H. Rogner, A. Brew-Hammond, V. Foster, S. Pachauri, E. Williams, M. Howells, P. Niyongabo, L. Musaba, B. ó Gallachóir, M. Radka, and D. M. Kammen, "Energy access scenarios to 2030 for the power sector in sub-Saharan Africa," *Utilities Policy*, vol. 20. pp. 1–16, 2012.

[2] MoFED, "Growth and Transformation Plan (GTP) 2010/11-2014/15, Ministry of Finance and Economic Development (MoFED)," 2010.

[3] EEPC, "Ethiopian Electric Power: Power Sector Development Powering Africa 2014, Presented by Ethiopian Electric Power Corporation (EEPC)," 2014.

[4] M. A. H. Mondal, S. Kennedy, and T. Mezher, "Long-term optimization of United Arab Emirates energy future: Policy implications," *Appl. Energy*, vol. 114, pp. 466–474, 2014.

[5] MoFED, "Growth and Transformation Plan: Annual Progress Report for F.Y. 2012/13, Ministry of Finance and Economic Development (MoFED)," 2014.

[6] FDRE, "Ethiopia's Climate-Resilient Green Economy: Green economy strategy, Federal Democratic Republic of Ethiopia (FDRE)," 2011.

[7] MoWIE, "Updated Rapid Assessment and Gap Analysis on Sustainable Energy for All (SE4All): The UN Secretary General Initiative, Ministry of Water, Irrigation and Energy (MoWIE)," 2013.

[8] D. Connolly, H. Lund, B. V. Mathiesen, and M. Leahy, "A review of computer tools for analysing the integration of renewable energy into various energy systems," *Applied Energy*, vol. 87. pp. 1059–1082, 2010.

[9] R. Weijermars, P. Taylor, O. Bahn, S. R. Das, and Y. M. Wei, "Review of models and actors in energy mix optimization - can leader visions and decisions align with optimum model strategies for our future energy systems?," *Energy Strateg. Rev.*, vol. 1, pp. 5–18, 2012.

[10] M. A. H. Mondal, *Implications of renewable energy technologies in the Bangladesh power sector: long-term planning strategies. Ecology and Development Series No. 74*. 2010.

[11] J. Mathur, N. K. Bansal, and H. J. Wagner, "Investigation of greenhouse gas reduction potential and change in technological selection in Indian power sector," *Energy Policy*, vol. 31, no. 12, pp. 1235–1244, 2003.

[12] C. Changhong, W. Bingyan, F. Qingyan, C. Green, and D. G. Streets, "Reductions in emissions of local air pollutants and co-benefits of Chinese energy policy: A Shanghai case study," *Energy Policy*, vol. 34, pp. 754–762, 2006.

[13] C. G. Heaps, "Long-range Energy Alternatives Planning (LEAP) system, Stockholm Environment Institute. Somerville, MA, USA." 2012.

[14] MoWE, "Scaling - Up Renewable Energy Program Ethiopia Investment Plan (Draft Final); Ministry of Water and Energy (MoWE), Ethiopia," 2012.

[15] ERG, "Solar energy vision for Ethiopia: Opportunities for creating a photovoltaic industry in Ethiopia, Ethio Resource Group (ERG), Ethiopia," 2012.

[16] ENPT, "Eastern Nile Power Trade (ENPT) Project: Power Studies; Nile Basin Initiative, Eastern Nile Subsidiary Action Program Eastern Nile Technical Regional Office," 2009.

P-Spice Based Study of Environmental Effect on the Performance of the Solar PV Module

Avijit Saha[#1], Naznin Nahar Nipu[#2], Md. Fayyaz khan[#3]

[#]*Dept. of Electrical and Electronic Engineering, United International University*
Dhaka, Bangladesh

[#1]avijitsaha720@gmail.com

***Abstract*—Normally, I-V characteristic of a solar PV under STC is a standard curve plotted through a sun simulator. However, in real life situation, the performance of the module is often affected by different environmental parameters that are not taken into account while plotting the curve. The open circuit voltage and short circuit current are directly dependent on irradiance and temperature. Due to dust accumulation, the overall temperature of a solar cell increases when compared under standard operating conditions. Again, due to partial shading, the temperature of the shaded cells increases thereby reducing the output of the shaded cells. This paper focuses on the environmental effects on the performance of a solar PV module through simulation by P-Spice based on experimental data. Through P-Spice simulation, it has been found that the overall output of the solar PV decreases substantially with the generation of hot spots due to accumulation of dust and partial shading of the solar panels.**

***Keywords*— STC; I-V Characteristic; P-Spice; Hot Spot, Sun Simulator etc.**

I. INTRODUCTION

Photovoltaic system is one of the most promising renewable energy sources in the world. It is the most sustainable solution for the upcoming energy crisis. Photovoltaic (PV) industry is experiencing rapid growth due to improved technology, declining cost and government subsidies [1]. Also, standardized interconnection to the electric utility grid and public enthusiasm for an environmentally benign energy source also plays a vital role in the expansion of solar PV [2].

The optimum solution for power output from a solar PV can be achieved by the installation of a PV system properly which is free from shading and other negative environmental conditions. The output of PV is rated by manufacturers under Standard Test Conditions (STC), temperature = 25ºC; solar irradiance= 1000 W/m^2, and solar spectrum as filtered by passing the atmosphere of air mass 1.5. These conditions are easily recreated in a factory through sun simulator but the situation is different for outdoor environments.

With the increasing use of solar PV, it is vital to know what effect active meteorological parameters such as light intensity, dust, temperature; shading etc. has on its efficiency. This paper investigates the effect of these parameters on the performance of solar PV. The main purpose of this study is to find out the impact of dust and partial shading on the performance of a solar PV module.

II. PREVIOUS STUDY ON IMPACT OF DUST AND PARTIAL SHADING ON SOLAR PV

Light intensity is one of the factors that changes all solar cell parameters, including the short-circuit current, the open-circuit voltage, the fill factor, the efficiency and the impact of series and shunt resistances. At low light levels, the effect of the shunt resistance becomes increasingly important. Consequently, under cloudy conditions, a solar cell with a high shunt resistance retains a greater fraction of its original power than a solar cell with a low shunt resistance.

Solar cells are sensitive to temperature. Increase in temperature reduces the band gap of a semiconductor, thereby affecting most of the semiconductor material parameters. In a solar cell, the most affected parameter by an increase in temperature is the open-circuit voltage (Voc). As the temperature increases, the open-circuit voltage decreases, thereby decreasing the fill factor and finally decreasing the efficiency of a solar cell [3, 4].

The PV modules are generally placed on the rooftop of a house. Therefore, shadows were observed on the modules created by the nearer buildings and trees. Thus, the concept of partial shading on PV system arises. The impact of partial shading on PV system performance has been studied at great length in the past [5, 6, 7]. Past experiences assume that the decrease in power production is proportional to the shaded area and reduction in solar irradiance, thus highlighting the necessity to consider the effect of shading on the performance of the solar PV, introducing the concept of shading. Partial shading of a solar photovoltaic module is one of the main causes of overheating of shaded cells and reduced energy output of the module. When a module is partially shaded, the shaded cells produce less photon current. Therefore, all the cells in a series array are forced to carry the same current. The shaded cells may get reverse biased, acting as loads, draining power from fully unshaded cells. If the system is not appropriately protected, hot-spot problem can arise and in several cases, the system can be irreversibly damaged.

Dust is the lesser acknowledged factor that significantly influences the performance of the PV installations. The accumulation of dust particles on a PV module is found to exponentially reduce the available area for transmission of incident photons [8]. A major problem facing by scientists is sand accumulation and numerous researches proved that, more than 50% of solar module performance reduction was caused by unclean panels within a period of one month [9], [10]. It is a well-established fact that PV output power is affected by

ambient temperature. The cleaner and cooler the PV is, higher is the power generated with enhanced efficiency [11].In the new trend of integrated PV arrays, it is difficult to avoid the impacts on PV module. This makes the study of environmental effects on the performance of the solar PV module a key issue. With a physical Solar PV module, it is difficult to study the environmental impacts considering all the environmental factors. A P-Spice model of a PV module consisting of 24 cells has been developed to carry out this study. The model is used to study the effect on PV due to variation in irradiation, change in temperature, shading, dust etc.

III. ANALYTICAL MODEL OF A PRACTICAL SOLAR CELL

An ideal solar cell can be modelled as a current generator in parallel with a photodiode.This simple model is then generalized to take into account series and shunt resistive losses and recombination losses. Temperature effects are then introduced and the effects of space radiation are also studied. A behavioral model is introduced which allows the solar cell simulation for arbitrary time profiles of irradiance and temperature.

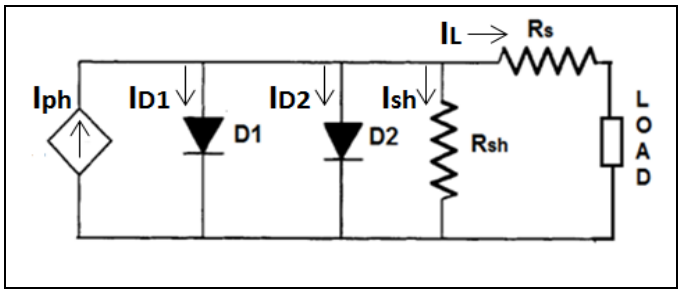

Fig. 1. Analytical Model of a Practical Solar Cell

Here,
I_{ph}= Photo current, D1=Photodiode, D2=Recombination diode, Rs=Series resistance, Rsh=Shunt resistance.

To find out the parameters of a practical solar cell, some common terms used are [12]:

J_{sc}= Short circuit current density at STC = 0.031 A/cm^2,
J_o= Saturation current density = 10^{-11}A/cm^2,
J_{02}= Recombination current density = 10^{-9} A/cm^2,
A = Area of the solar cell, G = Irradiance in W/m^2,
C_{Isc}= Temp. Co-efficient of short circuit current= 6.4×10^{-6},
T = Operating temperature, V_T= Thermal voltage=25 mV,
E_g = Band gap energy = 1.17 ev,
Rs=10^{-4} Ω, Rsh=10^5 Ω

Here,

Load Current, $I_L = I_{ph} - I_{D1} - I_{D2} - I_{sh}$ (1)

Photocurrent, $I_{ph} = \frac{J_{sc}AG}{1000} + AC_{Isc}(T-25)$ (2)

Current through photodiode, $I_{D1} = AJ_0(e^{\frac{V_L - I_L R_s}{nV_T}} - 1)$ (3)

Current through recombination diode, $I_{D2} = AJ_{02}(e^{\frac{V_L - I_L R_s}{nV_T}} - 1)$ (4)

Current through shunt resistance, $Ish = \frac{V_L - I_L R_s}{R_{sh}}$ (5)

Open circuit voltage, $V_{oc} = V_T \ln(1 + \frac{J_{sc}}{J_o})$ (6)

In this paper, to study the environmental effect on solar PV module, we have chosen a poly crystalline silicon PV module (Model: SLP2.5-04H) marketed by Solarland Bangladesh with following specifications:

Total no. of cells=24, Cell Area= 7.5 cm^2
Voc=7.0 V, Isc=0.46A
Vm=5.7 V, Im=0.43 A, Pm=2.5 W

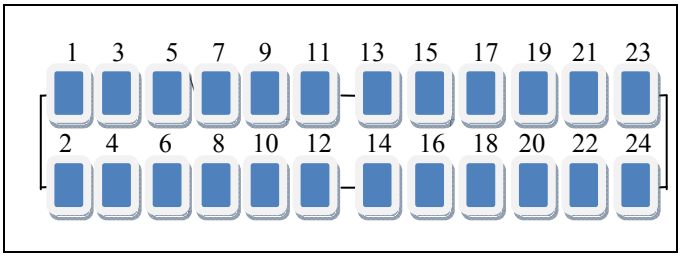

Fig. 2. Schematic of Solar PV Module Chosen for Study

From Figure 2, we can see that odd numbered cells are connected in series. Again, even numbered cells are connected in series. These two strings are connected in parallel which means an odd numbered cell is connected in parallel with its subsequent even numbered cell.

Taking the required parameters into consideration, we have designed a P-Spice model to simulate the performance of the above mentioned solar PV module. Throughout the paper, the term panel or module will refer to this panel. The P-Spice model gives the following I-V characteristics curve of the module:

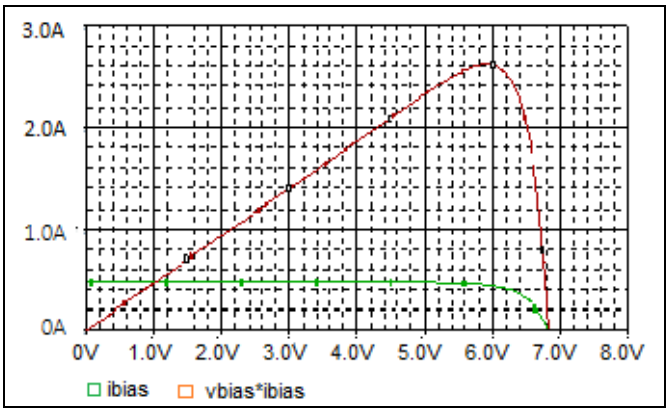

Fig. 3. I-V Characteristics of a Solar PV Module under STC

Here,
Voc=6.85 V, Isc=465 mA
Vm=6 V, Im=435 mA
Pm=2.6 W

From Figure 3, we can see that the simulated value is slightly different from the given specifications of the panel. This can happen due to various technical reasons including the value of short circuit and recombination current density, series and shunt resistance etc. But this slight deviation is quite acceptable.

IV. PERFORMANCE OF SOLAR PV MODULE DUE TO DUST ACCUMULATION

To realize the impact of dust on the performance of a solar PV module, we kept two identical solar PV modules at the rooftop. One of the panels was regularly cleaned, whereas the other was left uncleaned to accumulate dust. After a week, when dust accumulated uniformly over the panel, temperature of both the clean and dusty panels was recorded together with solar irradiance.

Ambient temperature= 35.5 ºC
Irradiance=900 W/m^2

TABLE I. CELL TEMPERATURE (ºC) OF CLEAN PANEL

Cell no.	Temperature	Cell no.	Temperature	Cell no.	Temperature
1	40.1	9	36.7	17	37.4
2	41.2	10	34.5	18	36.4
3	38.5	11	34.8	19	40.4
4	42.2	12	33.9	20	36.0
5	44.4	13	36.4	21	39.9
6	40.0	14	35.8	22	39.7
7	39.4	15	41.1	23	38.1
8	38.7	16	42.3	24	40.5

TABLE II. CELL TEMPERATURE (° C) OF DUSTY PANEL

Cell no.	Temperature	Cell no.	Temperature	Cell no.	Temperature
1	42.7	9	37.2	17	39.7
2	43.0	10	36.7	18	39.6
3	39.4	11	36.2	19	42.5
4	43.5	12	35.4	20	39.0
5	46.3	13	38.3	21	41.6
6	41.6	14	37.5	22	42.9
7	40.0	15	43.1	23	38.7
8	39.4	16	44.6	24	42.6

Then we plotted the I-V characteristics curve of the PV module using P-Spice for the recorded set of data.

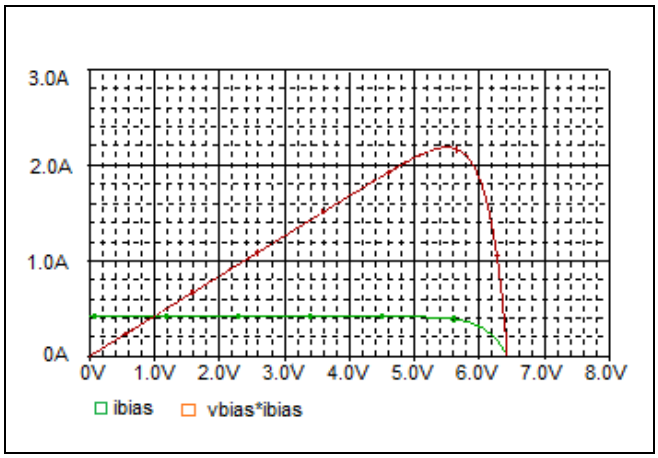

Fig. 4. I-V Characteristics of a Clean PV Module

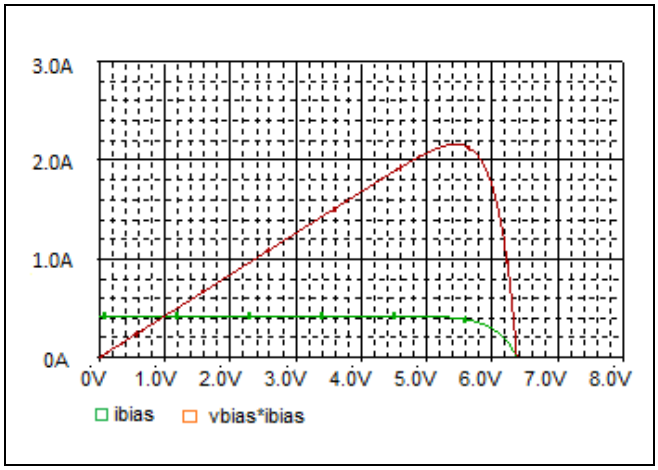

Fig. 5. I-V Characteristics of a Dusty PV Module

TABLE III. SPECIFICATIONS OF CLEAN AND DUSTY PANEL

Parameter	Clean Panel	Dusty Panel
Avg. Cell Temperature(° c)	38.68	40.69
Voc (V)	6.42	6.37
Isc (mA)	420	420
Vm (V)	5.5	5.4
Im (mA)	397	394
Pm (W)	2.18	2.13

From Table III, we can see that due to dust accumulation, the overall cell temperature of the dusty panel has increased. An increase in temperature has little effect on short circuit current. So the current is almost the same for both clean and dusty panel. But increase in temperature results in decrease of open circuit voltage. Therefore, Voc of clean panel is higher than that of dusty panel. As a result, the maximum power generated by the dusty panel reduces by 2.3 % compared to that of the clean panel.

V. PERFORMANCE OF A PARTIALLY SHADED SOLAR PV MODULE

To understand the impact of partial shading, we have partially shaded a panel with tree leaves. Cell no. 6, 8, 9, 10, 11, 12, 16, 17, 18, 19 and 20 has been partially shaded. Then we measured the irradiance, and the temperature of both the unshaded and partially shaded panels.

Ambient temperature=30.9º c
Irradiance=900 W/m^2

TABLE IV. CELL TEMPERATURE (° C) OF AN UNSHADED PANEL

Cell no.	Temperature	Cell no.	Temperature	Cell no.	Temperature
1	30.5	9	31.3	17	29.7
2	31.6	10	31.7	18	31.6
3	32.7	11	32.2	19	33.5
4	30.5	12	33.7	20	32.4
5	29.6	13	31.3	21	32.4
6	31.7	14	32.5	22	32.5
7	31.9	15	32.1	23	32.3
8	34.4	16	30.6	24	27.6

TABLE V. CELL TEMPERATURE (° C) OF A PARTIALLY SHADED PANEL

Cell no.	Temperature	Cell no.	Temperature	Cell no.	Temperature
1	31.7	**9**	**36.6**	**17**	**42.9**
2	30.5	**10**	**40.7**	**18**	**41.4**
3	32.9	**11**	**35.2**	**19**	**40.8**
4	32.1	**12**	**39.9**	**20**	**35.3**
5	30.6	13	32.5	21	32.4
6	**38.7**	14	31.3	22	32.9
7	33.9	15	30.1	23	32.7
8	**36.4**	16	33.6	24	28.6

TABLE VI. CELL IRRADIANCE (W/M^2) OF A PARTIALLY SHADED PANEL

Cell no.	Irradiance	Cell no.	Irradiance	Cell no.	Irradiance
1	900	**9**	**888**	**17**	**60**
2	900	**10**	**492**	**18**	**210**
3	900	**11**	**888**	**19**	**420**
4	900	**12**	**552**	**20**	**840**
5	900	13	900	21	900
6	**150**	14	900	22	900
7	900	15	900	23	900
8	**540**	16	900	24	900

From Table V and VI, we can see that the temperature of the partially shaded cells is higher than other unshaded cells of the same panel. Also the irradiance is less. Considering these facts, we have defined the parameters of the behavioural model of the PV module and plotted the I-V characteristics using developed P-Spice model.

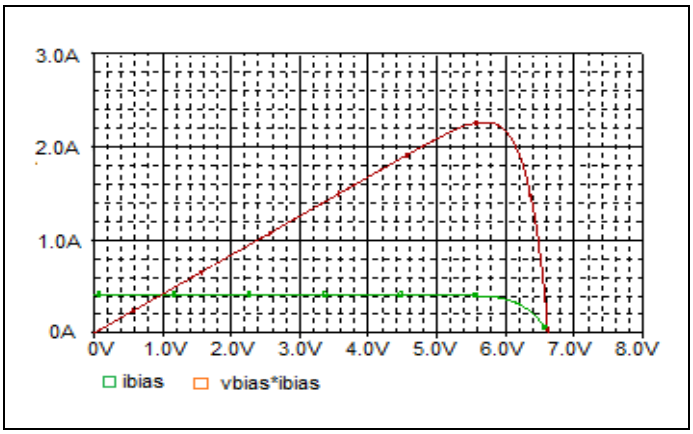

Fig. 6. I-V Characteristics of an Unshaded Solar PV Module

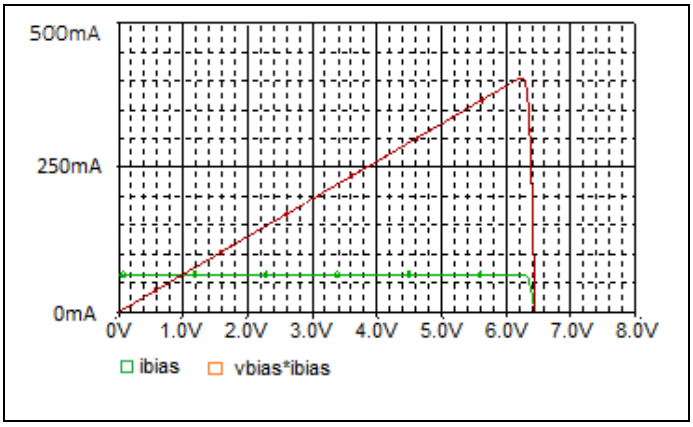

Fig. 7. I-V Characteristics of a Partially Shaded Solar PV Module with No Bypass Diode

Then we considered the impact of bypass diode under partial shading conditions. This section will reveal that position of by-pass diode is important as far as the performance of the cell is concerned. Here, cell no. 6, 8, 9, 10 and 11 are partially shaded. Again cell no. 17, 18, 19 and 20 are partially shaded. So, we have considered two bypass diodes across cell no. 1 & 11 and 13 & 23. Similarly we have considered 4 bypass diodes across cell no. 1 & 5, 7 & 11, 13 & 17 and 19 & 23.

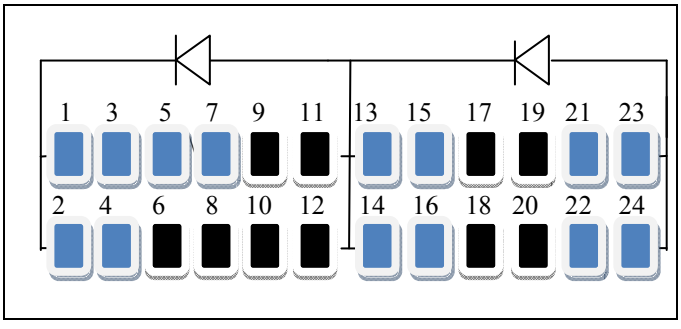

Fig. 8. Schematic of Solar PV with Two Bypass Diodes

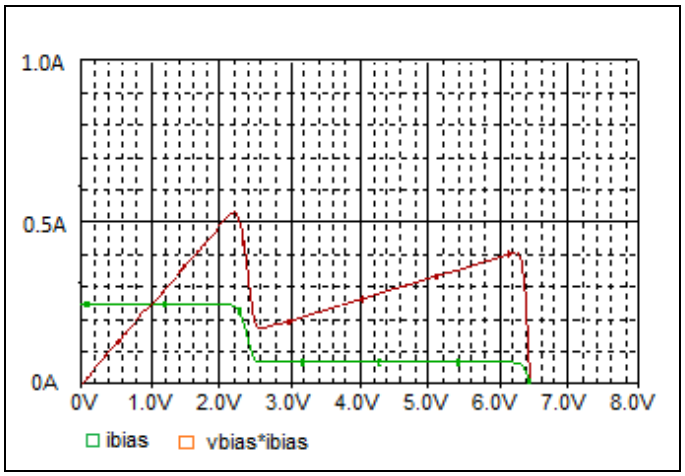

Fig. 9. I-V Characteristics of a Partially Shaded Solar PV Module with Two Bypass Diodes

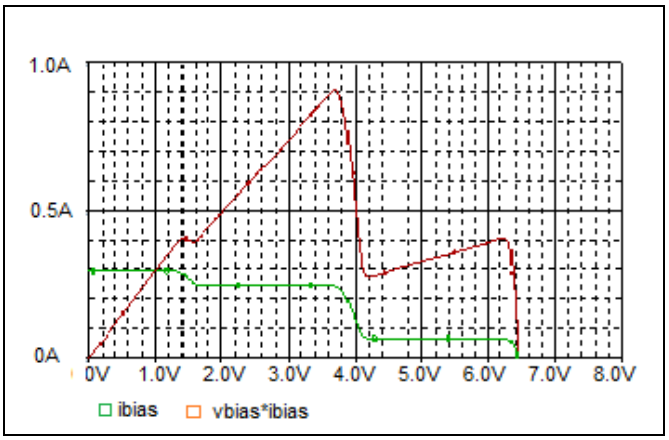

Fig. 10. I-V Characteristics of a Partially Shaded Solar PV Module with Four Bypass Diodes

TABLE VII. SIMULATION RESULTS OF UNSHADED AND PARTIALLY SHADED PANELS

Parameter	Unshaded	Partially Shaded (No Bypass)	Partially Shaded (Two Bypass)	Partially Shaded (Four Bypass)
Voc (V)	6.62	6.44	6.44	6.44
Isc (mA)	419	66	245	295
Vm (V)	5.72	6.24	2.20	3.70
Im (mA)	396	65	241	244
Pm (W)	2.26	0.41	0.53	0.90

From Table VII, we can see that generation of hotspots due to partial shading of some of the cells leads to an increased cell temperature and thereby reducing Voc. But, this impact on Voc is not that significant as Voc changes very little with increase in temperature. But the impact on Isc is very significant. The panel with no bypass diode supplies very small current compared to that of unshaded panel. This happens due to partial shading of some of the cells as they get less exposure to sunlight which results in less current generation by those cells. For series connected cells, with no bypass diode, the delivered current is equal to the minimum current generated by the cell that is heavily shaded. Therefore, the maximum power generated by a partially shaded panel with no bypass diode is the lowest.

To understand the impact of hotspot on a partially shaded panel with bypass diode, we have simulated the I-V characteristics of the solar PV module considering two and four bypass diodes. From Table VI, we can realize that as the number of bypass diode increases, the current generation by the panel increases. Also, the overall power supplied by the panel gradually increases.

VI. CONCLUSION

This paper focuses on the impact of different environmental factors that directly or indirectly decreases the output power of a module. We have discussed the I-V curves of a solar panel under different conditions and highlighted the basic factors that are responsible for the reduction in output power. The overall analysis was illustrated by experimental data which we have collected under different environmental conditions. The partial shading and dust increase the temperature of the affected cells, decreases the irradiance thus reducing the output power. The photovoltaic systems which have small modules are less affected by dust, temperature or shading than that of the systems with larger modules. In the study, it was also shown that the relative differences of PV module performance parameters between the cases where the modules were dusty and shaded and the cases where they are cleaned and unshaded under the same environmental condition are generally very high. Therefore, the efficiency can be improved by proper periodic maintenance of the PV modules. Voc, Isc, Vmax, Imax and Pmax are the most affected parameters due to dust and shading which has been found through simulation and experimental data. The paper will be of great use to the PV system designers in minimizing the environmental impacts on the PV modules.

REFERENCES

[1] International Energy Agency, “Cost and Performance trends in grid-connected PV systems and case studies”, *Technical Report EA PVPS T2-06*, Dec, 2007.

[2] International Energy Agency, “Trends in photovoltaic applications” - survey report of selected by countries between 1992 and 2005, Technical Report IEA PVPS T1-15, 2006.

[3] Masaki Shima, Masao Isomura, Ken-ichiro Wakisaka, Kenji Murata, and Makoto Tanaka, "The influence of operation temperature on the output properties of amorphous silicon-related solar cells", Solar Energy Materials & Solar Cells, Vol. 85, 2005, pp. 167–175.

[4] Shingo Nagae, Masanori Toda, Takashi Minemoto, Hideyuki Takakura, and Yoshihiro Hamakawa. “Evaluation of the impact of solar spectrum and temperature variations on output power of silicon-based photovoltaic modules", Solar Energy Materials & Solar Cells, Vol. 90, 2006, pp. 3568–3575.

[5] H. Rauschenbach, ”Electrical output of shadowed solar arrays”, IEEE Transactions on Electron Devices, vol. 18, no. 8, pp. 483–490, 1971.

[6] A. Kovach and J. Schmid, “Determination of energy output losses due to shading of building-integrated photovoltaic arrays using a ray-tracing technique”, Solar Energy, vol. 57, no. 2, pp. 117–124, Aug. 1996. IEEE Photovoltaic Specialists Conference, 1990, pp. 1005–1010.

[7] N. van der Borg and M. Jansen, “Energy loss due to shading in a bipv application”, 3rd World Conference on, in Photovoltaic Energy Conversion, 2003. vol. 3, 2003, pp. 2220–2222.

[8] Neil S. Beattie, Robert S. Moir, Charlslee Chacko, Giorgio Buffoni, Simon H. Roberts, Nicola M. Pearsalla. “Understanding the effects of sand and dust accumulation on photovoltaic modules”, Renewable Energy, Vol. 48, 2012, pp. 448-452.

[9] B.marian, J.adelstein, and others "Performance parameters for grid connected PV system. IEEE. Photovoltaic's specialist conference – Florida, January 3-5 (2005).

[10] J. Bishop, “Computer simulation of the effect of electrical mismatches in photovoltaic cell interconnection circuits”, Solar cells, vol. 25, pp. 73–89, 1988.

[11] A. Abete, E. Barbisio, F. Cane, and P. Demartini, “Analysis of photovoltaic modules with protection diodes in presence of mismatching,” 21st IEEE Photovoltaic Specialists Conference, 1990, pp. 1005–1010.

[12] L.D. Partain, “Solar Cells and their applications”, Wiley *1995* page 16.

A study on Data Accuracy by Comparing Between the Weibull and Rayleigh Distribution Function to Forecast the Wind Energy Potential for Several Locations of Bangladesh

Syed Enam Reza, Pallabi Zaman
Division of P & D, Bangladesh
Power Development Board (BPDB)
Dhaka, Bangladesh
Email: rsyedenam@yahoo.com
pallabi65_program@ymail.com

[2]Arif Ahammad, Ifrat Zaman (Ifty)
[2]Dept. of EEE, IBAIS University
Dhaka, Bangladesh
Email:arif08eee@gmail.com
Email: ifrat.zaman@gmail.com

Md. Faysal Nayan
Department of EEE, Ahsanullah
University of Science & Technology,
Dhaka, Bangladesh
Email: faysal.nayan@gmail.com

***Abstract*— This paper focuses the behaviour of wind speed pattern in some selected locations of Bangladesh in order to forecast the wind energy potential of Bangladesh. In our study, the wind speed data for Cox's Bazar, Kuakata, Swandip, Hatiya and Sydpur between 2004 and 2007 have collected from several organizations i.e. Bangladesh Meteorological Department (BMD), Local Government Engineering Development (LGED) and Infrastructure Development Company Ltd (IDCOL) and processed on daily, monthly and hourly basis. The data have been examined by Weibull distribution function using Weibull Graphical method in order to find the shape parameter (k) and scale parameter (c) and thus compared between the Weibull and Rayleigh distribution functions to deduce the wind availability of the selected locations. Moreover, statistically Correlation Coefficient (R_2), Root Mean Square Error (RMSE), and Coefficient of Efficiency (COE) methods have also employed based on the data in order to evaluate the performance of the Weibull probability density function.**

Keywords*— *Weibull distribution function, Rayleigh distribution function, Weibull Shape Parameter, Wind Pattern forecasting, Model Performance Parameters.

I. INTRODUCTION

Wind energy is an alternative clean source of energy which can replace the finite source of fossil fuels to meet the increasing energy demand throughout the world. Utilization of wind energy is very imperative for the future development of power sector of Bangladesh [1]. As other neighbouring countries are showing solid economic growth, Bangladesh, despite having abundant resources is lagging behind due to the power crisis [2]. To mitigate energy crisis; relying solely on the fossil fuels would not be a cost-effective proposition, so it needs to explore renewable resources like wind, solar etc. [3]. Wind power technology in Bangladesh has been growing significantly in the last few years because it has moderate wind speed during the summer and winter seasons i.e. for the six months period of the year starting from March to the August [4]. Till July 2015, the wind energy comprises of only 2 MW of out of 405 MW total renewable production [5]. Already the Bangladesh Government has announced a renewable energy policy which emphasizes to increase its share in renewable power generation from 5% in 2015 to 10% by 2020 [6]. With a view to achieve this target government has undertaken a project called Sustainable and Renewable Energy Development Authority (SREDA) which is on its voyage to install more wind power plants with the aid of Bangladesh Power Development Board (BPDB). Wind power is a very unpredictable source of energy, so the modeling of wind speed variation of a particular location is essential requirement in the estimation of wind energy potential for a typical site [7].

In this study, Weibull distribution function has been compared with the Rayleigh distribution in order to predict the accuracy of the collected data for errorless prediction of wind availability of the mentioned locations. The amount of error between the two models has also been calculated for the given locations. The mean speed data has also been verified by employing other statistical methods like Correlation Coefficient (R^2), Root Mean Square Error (RMSE) and Coefficient of Efficiency (COE) as well. The value of Weibull shape factor (k) and Weibull scale factor (c) have been calculated by using Weibull Graph Paper method which is described in [10, 11 and 12].

II. LITURATURE REVIEW

Several studies have performed so far addressing the feasibility study of wind energy along with the analysis of investment, operation and maintenance cost [8] but now it is high time to explore and point out the most suitable sites for wind energy generation which leads us the requirement of statistical analysis based on different models i.e. Weibull Distribution, Maximum Likelihood Estimation (MLE), Method of Moments (MOM), Density Power Method (DPM) etc. Few studies shows the wind speed frequency analysis using the Weibull Distribution Method where they used the Graphical Method i.e. Weibull Paper Method [10, 11 and 12] to find Weibull parameters. In addition to this, they [10, 12] have compared the accuracy of the site by finding the Scale

parameter (c) and Shape parameter (k) using Energy Pattern Factor Method, Weibull Paper Method and Standard Deviation Method. Most of the analyses were done based on the coastal areas of Bangladesh for having higher wind speed than the other parts of the country. In this study, Weibull and Rayleigh distribution functions have been compared to predict the wind pattern for the mentioned locations.

III. Wind Speed Modelling

Usually wind speed constantly varies, so it is necessary to know exactly how often and how strongly wind blows to be able to predict a wind turbines production. Normally, wind speed is measured and recorded in every 10 minutes and the data can be sorted into wind speed classes of 1 m/s each. It is necessary to have only a few key parameters that can explain the behavior of a wide range of wind speed data. The simplest and most practical method for this is to use a distribution function [10] because it describes the energy contained in the wind at a certain site. K is the Weibull parameter and it specifies the shape of a Weibull distribution which takes on a value of between 1.0 and 3.0. A small value for k signifies very variable winds, while constant wind is characterized by a larger k [13]. Turbine manufacturers randomly chose the value of shape parameter, k=2 for turbines to be installed at any given site as a standard specification. Comparing the Weibull parameter with Rayleigh function gives a clear view for wind speed forecasting because at k=2, Weibull distribution gives the Rayleigh distribution [14].

IV. Calculation Methodology

Weibull function is the most reliable method for wind analysis to describe the wind speed frequency curve. In statistical modeling of wind speed variation, it has been widely applied by many researchers. The Weibull distribution $f_W(v)$ equation can be expressed as [9, 10, 11 and 12]:

$$f_W(v) = \left(\frac{k}{c}\right)\left(\frac{v}{c}\right)^{K-1} \exp\left(-\left(\frac{v}{c}\right)^{k}\right) \quad (1)$$

Where, v is the wind speed (m/s), K is the Weibull Shape parameter (dimensionless) a measure for the characteristics wind speed of the distribution and C is the Weibull Scale Parameter (m/s).

The Rayleigh $f_R(v)$ distribution is a special case of the Weibull distribution in which the shape parameter k is assumed to be equal to 2. From Equation (1) the probability density functions of the Rayleigh distribution given by:

$$f_R(v) = \frac{2v}{c^2} e^{-\left(\frac{v}{c}\right)^2} \quad (2)$$

Where, v is the wind speed (m/s) and C is the Weibull Scale Parameter (m/s). The curves for the Rayleigh function have been obtained from the Equation (2).

The prediction accuracy of the model in the estimation of the wind speeds with respect to the actual values was evaluated based on the Correlation Coefficient (R^2), Root Mean Square Error (RMSE) and Coefficient of Efficiency (COE). These parameters were calculated based on the following equations [15, 16]:

$$R^2 = \frac{\sum_{i=1}^{N}(y_i - z)^2 - \sum_{i=1}^{N}(x_i - z)^2}{\sum_{i=1}^{N}(y_i - z)^2} \quad (3)$$

$$RMSE = \left[\frac{1}{N}\sum_{i=1}^{N}(y_i - x_i)^2\right]^{\frac{1}{2}} \quad (4)$$

$$COE = \frac{\sum_{i=1}^{N}(y_i - x_i)^2}{\sum_{i=1}^{N}(y_i - z)^2} \quad (5)$$

Where, y_i is the i^{th} actual data, x_i is the i^{th} predicted data with the Weibull distribution, z is the mean of actual data, N is the number of observations.

V. Results & Discussion

This study compares between Weibull function and the Rayleigh Function in order to find the data accuracy and to predict the wind pattern of the given locations. The comparison between Weibull density function and Rayleigh density function; for Cox's Bazar, Hatiya, Kuakata, Swandip and Sydpur from the years 2004 to 2007 (March-August) has been made below using the Equations (1) and (2).

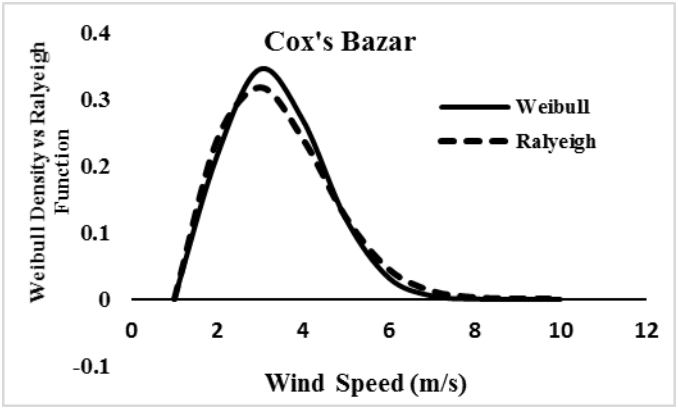

Fig. 1 Weibull Density Function Vs Rayleigh Function Curve for Cox's Bazar

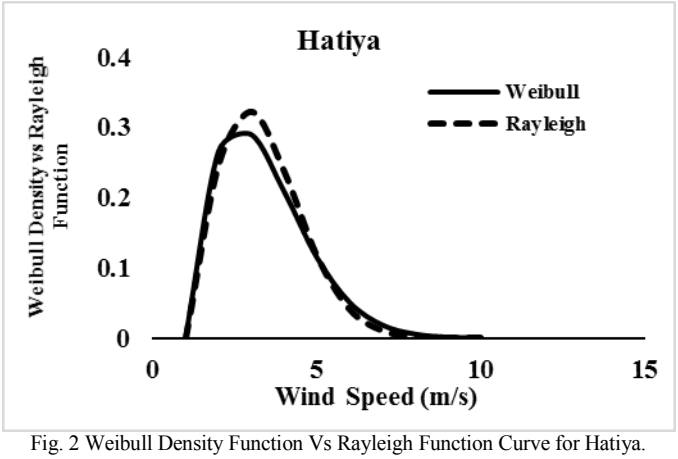

Fig. 2 Weibull Density Function Vs Rayleigh Function Curve for Hatiya.

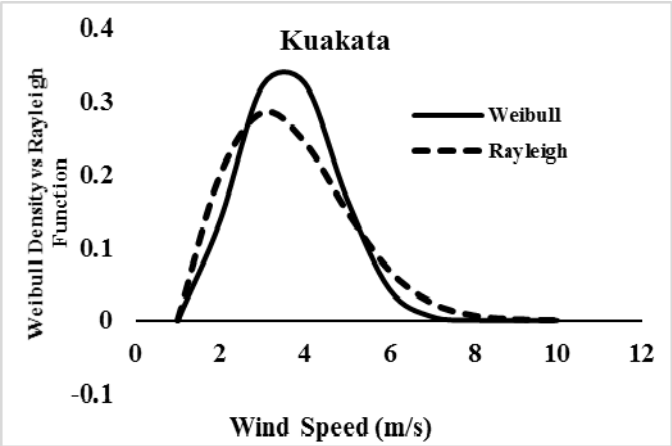

Fig. 3 Weibull Density Function Vs Rayleigh Function Curve for Kuakata

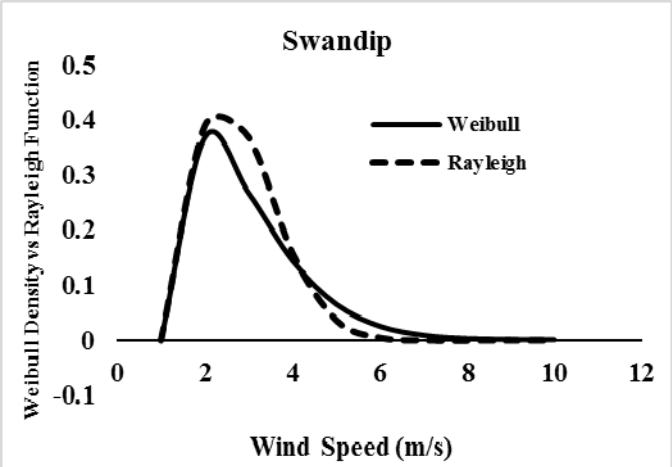

Fig. 4 Weibull Density Function Vs Rayleigh Function Curve for Swandip

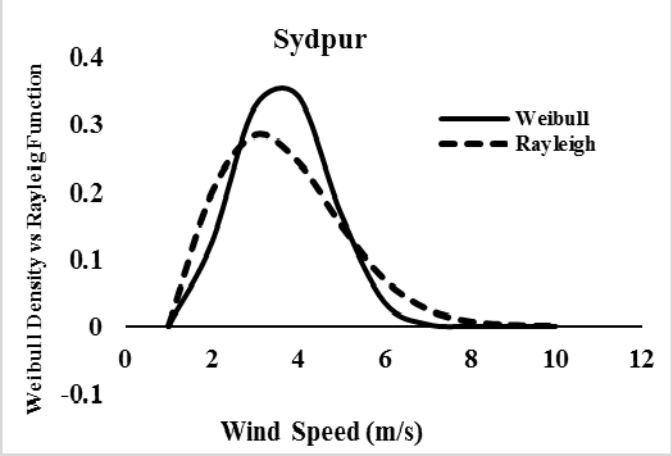

Fig. 5 Weibull Density Function Vs Rayleigh Function Curve for Sydpur

From Fig. 1 to Fig. 5, it is observed that Weibull Distribution Function for Cox's Bazar, Swandip & Hatiya closely fits with the Rayleigh Distribution Function where the ones of Kuakata and Sydpur show slight variation. In order to find the accuracy of the data the percentage of error calculation has been performed to find out the gross deviation of Weibull analysis from the ideal one i.e. Rayleigh Distribution Function. The time frame for this analysis was chosen from the month March to the August.

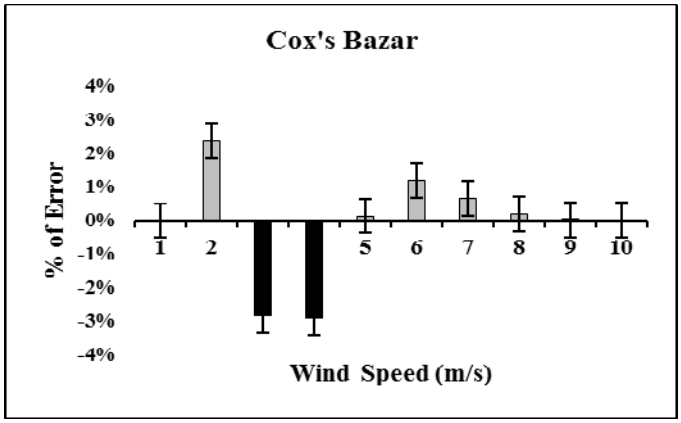

Fig. 6 The % of Error at each wind speed between the calculated Weibull and Ideal Rayleigh Function at Cox's Bazar from March to August

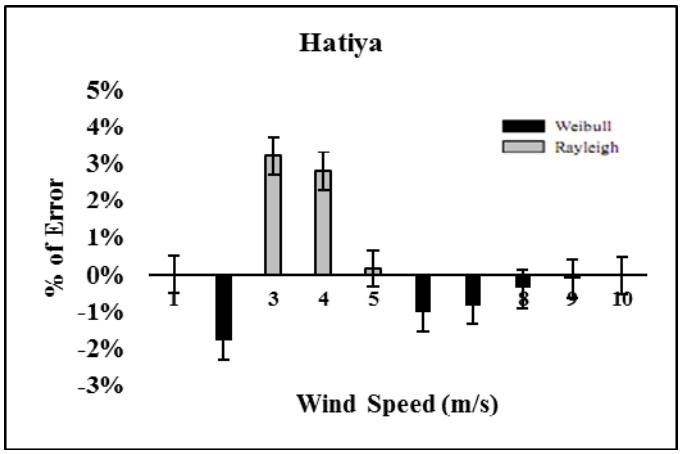

Fig. 7 The % of Error at each wind speed between the calculated Weibull and Ideal Rayleigh Function at Hatiya from March to August

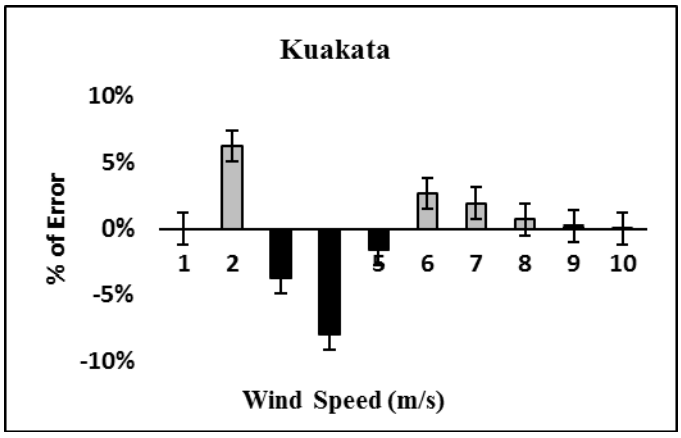

Fig. 8 The % of Error at each wind speed between the calculated Weibull and Ideal Rayleigh Function at Kuakata from March to August

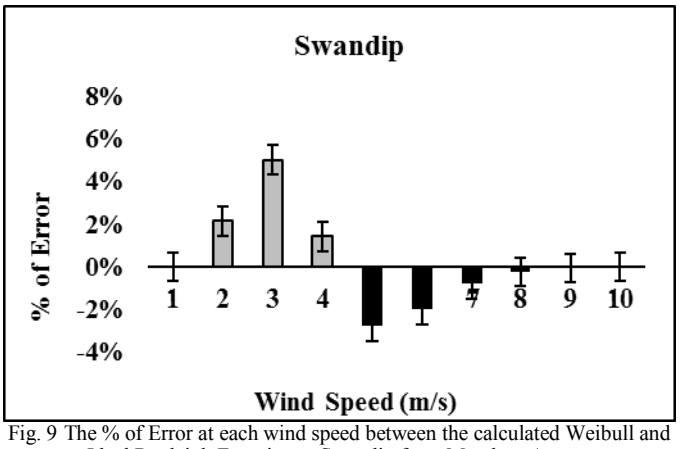

Fig. 9 The % of Error at each wind speed between the calculated Weibull and Ideal Rayleigh Function at Swandip from March to August

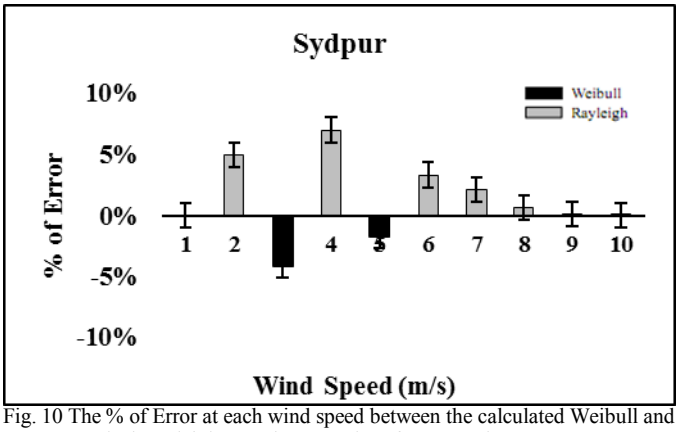

Fig. 10 The % of Error at each wind speed between the calculated Weibull and Ideal Rayleigh Function at Sydpur from March to August

The Fig. 6 to Fig. 10 shows the % of error between the Rayleigh Distribution Function (Ideal) and the Weibull Distribution Function at each wind speed. It is found that Cox's Bazar, Hatiya and Swandip show a minimal difference of around ±3% whereas other two stations differ slightly more than ±3% from the Ideal Rayleigh Distribution Function.

The Table I shows the average Weibull and the performance parameters from March to August between 2004 and 2007. The Weibull distribution parameters (k and c) from the years of 2004 to 2007 (March to August) have calculated using the Weibull Paper Method applying the process used in [10, 11 and 12]. The model prediction performance parameters (R^2, RMSE and COE) were calculated based on Equations (3), (4) and (5) respectively.

TABLE I. WEIBULL SCALE PARAMETER C, SHAPE PARAMETER, K AND MODEL PERFORMANCE PARAMETERS IN ALL SELECTED SITES FROM 2004 TO 2007 FOR MARCH TO AUGUST

Locations	Weibull Parameters		Model Performance Parameters		
	K	C (m/s)	R^2	RMSE	COE
Cox's Bazar	1.75	2.93	0.1258	0.0872	0.0227
Hatiya	1.33	2.82	0.0685	0.0302	0.0019
Sydpur	2.17	2.62	0.0014	0.0620	0.0084
Kuakata	1.27	3.07	0.0215	0.0596	0.0097
Swandip	2.22	2.25	0.0887	0.0319	0.0017

It is seen that the scale parameter (c) varies between 2.25 and 3.07 (m/s) while the shape parameter (K) ranges from 1.27 to 2.17. The most important parameter is the shape parameter (k) as Cox's Bazar, Swandip and Sydpur have the suitable values ranging around k=2 which approximates the Rayleigh function. The predicted model performance parameters (R^2, RMSE and COE) for the all locations during the whole period range from 0.0014 to 0.1258, 0.0302 to 0.0872, and 0.0017 to 0.0227 respectively which is acceptable in terms of accessing the performance of the Weibull Method.

Table II below shows the mean wind speed and standard deviations for the months from March to August for five selected locations. It is seen that Hatiya and Swandip has the lowest standard deviation with 0.036 and 0.033 respectively which is significant, but Swandip has the lowest mean wind speed (2 m/s) among all the stations. Meanwhile, both Kuakata and Cox's Bazar have the highest wind speeds but the standard deviations of those locations (0.26 and 0.27 respectively) are bit high compared to the previous two stations. So it can be concluded that Kuakata has lower standard deviation at higher mean speed (3.32 m/s).

TABLE II:
YEARLY MEAN ACTUAL WIND SPEED AND STANDARD DEVIATIONS IN 5 SELECTED SITES FROM 2004 TO 2007 BETWEEN MARCH AND AUGUST

Locations	Parameters	March	April	May	June	July	August	Whole Period
Cox's Bazar	Vm	3.2409	3.3695	3.1638	3.1252	2.9065	3.4210	3.2045
	δ	0.3023	0.3362	0.2637	0.2444	0.1351	0.3619	0.2739
Hatiya	Vm	2.2120	2.7779	2.7651	2.6107	2.6750	2.5850	2.6043
	δ	0.1472	0.1213	0.1148	0.0377	0.0698	0.0248	0.0369
Sydpur	Vm	3.0480	2.5078	2.3792	2.2763	2.3278	2.3664	2.4843
	δ	0.3461	0.0760	0.0251	0.0263	0.0006	0.0186	0.0731
Kuakata	Vm	2.6493	3.7168	3.1252	3.4981	3.3438	3.6139	3.3245
	δ	0.0551	0.4467	0.1827	0.3374	0.2602	0.3952	0.2612
Swandip	Vm	1.5819	1.6590	2.1349	2.2378	1.9805	2.0063	2.00
	δ	0.2142	0.1756	0.0692	0.1207	0.0067	0.0049	0.0336

VI. Conclusion

The percentage of error between the Weibull & Rayleigh Distribution Function is minimal which satisfactory and this indicates that the data we studied to deduce the Weibull parameters (k & c) was reliable to predict the wind energy prospect of the given locations. It was found that the Weibull distribution for Cox's Bazar, Swandip & Hatiya closely matches the Rayleigh distribution which indicates calculation accuracy for the mentioned time period. The value of Weibull shape parameter (k) remains between 1.27 and 2.17, which also closely follows the Raleigh function (k=2).

It is also observed that the shape parameter (k) of Cox's Bazar (1.75), Swandip (2.22) and Sydpur (2.17) is around the value of 2.0; which is significant because more the value of k approaches to 2.0 the more constantly the wind flows. In terms of standard deviation Hatiya has the lowest (0.033 m/s) among all but it has the lowest wind speed (2.0 m/s). However, Kuakata and Cox's Bazar both have the higher standard deviations (0.26 and 0.27 m/s) but their mean wind speed is far higher (3.32 and 3.20 m/s) than that of Hatiya.

The predicted model performance parameters (R^2 = 0.0014 to 0.1258, RMSE = 0.0302 to 0.0872 and COE = 0.0017 to 0.0227) show slight variation among them and was within the tolerable limit. So considering the overall analyses it can be concluded that, Kuakata, Cox's Bazar and Hatiya can be declared as the most potential windy sites among the all 5 locations.

One of the challenging features of this study is the data collected by the Bangladesh Meteorological Department (BMD) was recorded from 20m above the ground. The Bangladesh Power Development Board (BPDB) is planning to generate a mass scale of power from wind energy and to do so it has already taken steps to install the wind marks at several locations of the country to collect the wind data at higher levels from the ground. The tendering process of this wind mask installation project has already been initiated by the Division of Planning & Design (P & D) of Bangladesh Power Development Board (BPDB).

The future scope of this study could be to apply Least Square Method (LSM) instead of Graphical Model (Weibull Paper Method); as we have applied Graphical Model in this study; to determine the Weibull Distribution Function. In addition to this, the Parameters k and c obtained by using Weibull Distribution Method can also be compared against same the parameters found by employing Energy Pattern Factor Method and Standard Deviation Method for further verification.

Acknowledgment

The authors gratefully acknowledge the support from Division of Planning & Design (P&D) of Bangladesh Power Development Board (BPDB). The assistance from Bangladesh Meteorological Department (BMD) is also gratefully acknowledged for providing some of the wind speed data of several locations.

References

[1] A. Islam, M. S. Islam, M. Zakirul, "Monthly and seasonal assessment of wind energy potential in coastal area of Bangladesh", IEEE Conference on the Developments in Renewable Energy Technology (ICDRET), Dhaka, DOI: 10.1109/ICDRET.2014.6861733, pp.1-6, 29-31 May 2014.

[2] Y. Arafat, S. Chowdhury, "Prospect of Renewable Energy in Bangladesh: A Comprehensive Study of Future Scopes", IEEE Conference on Computer Modelling and Simulation (UKSim), Cambridge, DOI:10.1109/UKSim.2013.82, pp.559 - 562, April 2013.

[3] Md. N. H. Khan, A.M. Rahman, "An extensive overview of present situation of renewable energy practices in Bangladesh, Building renewable electricity supply in Bangladesh", IEEE Conference on the Developments in Renewable Energy Technology (ICDRET), Dhaka, DOI: 10.1109/ICDRET.2014.6861702, pp.1-6, 29-31 May 2014.

[4] S. Mahmud and J. Noviedo, "The need of wind energy in Bangladesh," IEEE Conference ICIEV, Dhaka, Bangladesh, DOI: 10.1109/ICIEV.2013.6572640, pp.1-6, 17-18 May 2013.

[5] Available at: http://sreda.gov.bd/

[6] Available at: http://sreda.gov.bd/index.php/about-sreda

[7] B.G. Kumaraswamy, B. K. Keshavan, Y. T. Ravikiran, "Analysis of seasonal wind speed and wind power density distribution in Aimangala wind form at Chitradurga Karnataka using two parameter weibull distribution function" IEEE Power and Energy Society General Meeting, CA, USA, DOI: 10.1109/PES.2011.6039587, pp. 1 - 4, 24-29 July 2011.

[8] P. Mazumder and V. D. Gupta, "Prospects of wind energy in Chittagong," ICIEV, Dhaka, Bangladesh, DOI:10.1109/ICIEV.2012.6317507, pp.753-758, 18-19 May 2012.

[9] A. Islam, M. S. Islam, M. M. Hasan, A. H. Khan, "Analysis of Wind Characteristics and Wind Energy Potential in Coastal Area of Bangladesh: Case Study-Cox's Bazar", ELEKTRIKA-UTM Journal, Malaysia, vol. 15(2), pp. 1-10, 2013.

[10] M. M. Alam and A. K. Azad, "Analysis of Weibull Parameters for the Three Most Prospective Wind Sites of Bangladesh", Proceedings of the International Conference on Mechanical Engineering, (ICME2009), Dhaka, Bangladesh, 26- 28 December 2009.

[11] A. N. M. M. I. Mukut, M. Q. Islam and M. M. Alam, "Analysis of Wind Characteristics in Coastal Areas of Bangladesh", Transaction Journal of Mechanical Engineering at the Institution of Engineers, Bangladesh, vol. ME39(1), June 2008.

[12] A. K. Azad and Manabendra Saha, "Weibull's Analysis of Wind Power Potential at Coastal Sites in Kuakata, Bangladesh", International Journal of Energy Machinery, Vol. 4, No. 1, pp. 36–45, 2011.

[13] Available at: http://www.wind-data.ch/tools/weibull.php?lng=en

[14] Available at: http://www.wind-power-program.com/wind_statistics.htm

[15] A. N. M. M. I. Mukut, M. Q. Islam and M. M. Alam, "Estimation of Wind Energy Potential in Coastal Areas of Bangladesh by Using Weibull Distribution", 4th BSME-ASME International Conference on Thermal Engineering, Dhaka, Bangladesh, 27-29 December, 2008.

[16] D.A. Fadare, "A Statistical Analysis of Wind Energy Potential in Ibadan, Nigeria, Based on Weibull Distribution Function", The Pacific Journal of Science and Technology (PJST), Vol. 9. No. 1., May-June 2008 (Spring).

Developing an Open Access Monitoring Device for Off-Grid Renewables

Richard Blanchard[#1], Matt Little[*2]

[#]*CREST, Loughborough University, United Kingdom*

[1]r.e.blanchard@lboro.ac.uk

[*]*Renewable Energy Innovation, Nottingham, United Kingdom*

[2]matt@re-innovation.co.uk

***Abstract*— Electricity access is a key driver for developing a modern society. The use of locally generated renewable energy can overcome limitations of expensive grid infrastructure. However, there are still barriers to access particularly for the rural poor in the global south. When individuals or communities invest in electricity provision it is important to know how well the system is performing. Commercial monitoring systems have been developed for large scale renewable energy systems. The cost of these can outweigh the cost of a small decentralised renewable energy system. This paper describes the development of a low cost data logger that is going to be used to monitor the system performance of small photovoltaic nano-grids in Kenya and Bangladesh. The device performs within the expected range for the current, voltage, temperature and irradiance sensors. Data from the data logger device is sent via GPRS to a website where it can be accessed as real time graphical displays and data files.**

***Keywords*— Remote monitoring, photovoltaics, nano-grid, GPRS, current, load, Bangladesh, Kenya**

I. INTRODUCTION

Access to modern energy services limits people's ability to reach their potential. Around 1.3 billion people do not have access to electricity and 2.9 billion make use of traditional heating and cooking fuels [1]. These people are largely living in what can be described as rural locations. Electrification programmes have been developed in a number of countries to bring power to the people. However, even with ambitious schemes such as the Ravi Ghandi Rural Electrification Programme in India, people, especially the rural poor, are still going to be 'under the cable': that is unable to afford to connect to the grid. It is expected that by 2035 the number of people without access to electricity will not decline owing to population growth.

There are alternatives to grid extension which include solar home systems (SHS) and micro-grids. SHS typically consist of a photovoltaic (PV) module, battery, lamps and a socket for powering a small device such as a mobile phone. SHS deployment has been successful in Bangladesh with funding supported through Grameen Shakti. However, SHS are limited in what they can do as they can only support low electrical loads. However, developing micro-grids is another option. Micro-grids are independent distributed generation networks that can be stand-alone or grid-tied. Their capacity can range from a few kilowatts to megawatts as there is no absolute definition. At the smaller end of the scale the term nano-grids can be applied for the 1-4kW range. Nano-grids are proposed to support the space between SHS and micro-grids for small rural communities. The idea behind solar nano-grids (SONG) is not only to provide basic lighting and power for small electrical devices, but also to support some form of economic activity to help develop the community where such a SONG is installed. For example, this could be through milling grain, improving irrigation water pumping, egg incubators, refrigeration or hair clippers.

A key feature of the nano-grid is that it will supply DC current. The principal reason for this was to keep costs down by avoiding the need for a DC-AC inverter. Furthermore, losses associated with DC-AC conversion will be reduced.

In 2013 funding from UK Department for International Development and the Engineering Physical Sciences Research Council was approved to develop SONG[1] systems in Kenya and Bangladesh.

As part of the research two communities were identified in Kenya and two in Bangladesh. These have been widely consulted on their individual and community energy needs and SONG systems have been designed to meet these.

However, as SONG is a new concept and it is important to learn how the systems perform against system models. Furthermore, these locations in Kenya and Bangladesh are remotely located making regular physical monitoring of the SONG systems difficult. Therefore, it was decided to employ remote monitoring technology to ascertain the efficacy of the SONG.

Remote monitoring is not new even in renewable energy technologies such as wind farms or commercial anaerobic digesters where SCADA systems are used. But, these are often expensive costing £10,000s. This would not be applicable for SONG. Experience in developing remote access photovoltaic systems [2-5] and monitoring or rural biogas systems [6-7] led

[1] The SONG partnership is led by Loughborough University UK, with United International University and Grameen Shakti Bangladesh, Intersave Kenya and the University of Oxford UK.

to the concept of developing a low cost device to monitor the SONG systems.

The aim of this paper is to report on the development of an open access monitoring device for off-grid renewable energy systems. The objectives were to scope the system requirements, design and build the monitoring device as well as test the device prior to deployment in Kenya and Bangladesh. Costs, conclusions and future work are reported.

II. METHODOLOGY

The methodology is divided into three sections; system requirements, design and build, and testing.

A. System requirements

The development of the SONG remote monitoring device needed a requirements capture exercise to identify the whole and sub-systems that would be required. The first stage was to consider what was wanted from the device. The key features were to:

- Measure the electricity being produced from the photovoltaic modules
- Measure the irradiance
- Measure the battery state of charge
- Measure user loads
- Measure temperature of the modules and battery
- Have energy autonomy
- Store data
- Send data from the SONG system to an online website and database
- Report problems to the operator

The original specifications were based on a 3kWp DC solar nano-grid supplied by project partner UIU, Bangladesh. The key components were:

- PV 3kWp
- Battery 36kWh
- Optimiser 3kW (input 48V DC, Output 220V DC
- Controller 3kW PWM charging, DR connection GSM connectivity for remote monitoring and controlling, Data logging
- Pre-paid DC energy meter: code programmable up to 500W

B. Design and build

Having established the requirements and system conditions the unit specifications and sensors were identified as shown in Tables 1 and 2

TABLE 1 UNIT SPECIFICATIONS

Parameter	Value
Input supply voltage	6-60V DC
Input current	500mA
Internal battery	2200mAh 3.7V LiPo
Internal power supply	5V nominal 6V max
ADC range	15 bits
ADC sensitivity	0.1mV
Data sample rate	10Hz

TABLE 2 SENSORS

Parameter	Value
Temp. Range	-10^{o}C to 100^{o}C
Temp. accuracy	+/- 1^{o}C
Current sensor range	0-50A DC
Current sensor accuracy	2.5mA
Voltage sensor (low) range	0-60V DC
Voltage sensor (high) range	20-300V DC
SD card size	Up to 32GB

The device is based upon an open source microcontroller Linkit ONE Internet of Things base unit [8] This contains the SD card, GPRS module and GPS module. In addition, WiFi and Bluetooth can be used although they were not implemented for this project. The Linkit One device is connected to a bespoke PCB which contains 3 x analogue to digital converters, ADS1115 [9], the input power supply and the PV input voltage regulator.

Any standard sized SIM card can be used with the adjacent SD card capable of storing up to 32GB. The battery, a LiPo 3.7V 2200mAh for back up, can run the device if input power is lost. The GPS sensor checks the location of the unit every 2 hours. If the unit location has differed by a distance of more than 50m then a text message is sent to SMS phone numbers of the operator.

1) Sensors

Six current sensors were included with the device; these are based upon the ACS758 Allegro Hall effect current sensor [10]. The 50A uni-directional version has been used, namely ACS758-X050U. This was supplied with a regulated 5V supply voltage. The output is 0.6V + 60mV/A.

The voltage sensors measure two voltage ranges; low 0-60V DC and high 0-300V DC. Two different sensors are used for these ranges. For the low voltage sensor, the unit specifications must be able to measure the DC voltage level up to 60V DC for the 48V battery bank. A potential divider is used which is calculated to give the correct conversion range. A 5.1V zener diode protects against potential over voltage.

To measure up to 60V DC, keeping within the 3.3V maximum input and using a 10k resistor as Ra, the potential divider will be comprised of Ra = 10k and Rb > 110k (where Vout = Vmax x (Ra/(Ra+Rb)). Hence 3.3 = 60 x (10/(10+110)). To allow for any higher voltages some headroom can be given. An Rb = 160k could give a voltage range up to 80V. The potential divider of 200k and 10k with 0.1% accuracy resisters are used for this function.

For measuring higher voltages up to 300V DC is more challenging. Indeed, it can be dangerous and damage equipment. An isolation amplifier is used to provide up to 1000V isolation between the 300V signal and the ADC. This is performed using an ACPL-C870 [11-12]. A potential divider of 200k and 1k was used to give the input signal.

2) Temperature sensors

A thermistor is used as part of the potential divider circuit with an accurate and stable reference voltage with low cost and good accuracy. A 10k thermistor is used to record the temperature. The thermistor is characterised as half of a potential divider, with a 10k precision resistor and a precision voltage regulator to supply the potential divider. The thermistor output needs to have the correct interpolation applied so that the temperature reading is accurate. Importantly, the thermistor needs to be thermally bonded to the unit under test.

3) Power supply

The device is powered by a 2200mAh 3.7V LiPo battery. The charge is kept through a DC-DC converter power supply from the battery connection or via a solar PV backup. The DC-DC converter changes the input voltage of 6-60V DC down to the 5V used by the data logger. The solar PV backup uses a small PV module (1.5Wp) to top up the device battery.

4) Data monitoring

Data is monitored via a web interface. This uses a bespoke version of ThingSpeak [13]. A specific data logger channel to present the outputs as graphs and record the data was set-up[14].

5) Software and hardware License

The work is released under a Creative Commons By-Attribution Share-Alike 4.0 (CC BY-SA 4.0) license [15]. Fig. 1 shows the schematic of the device and Fig 2 the completed prototype.

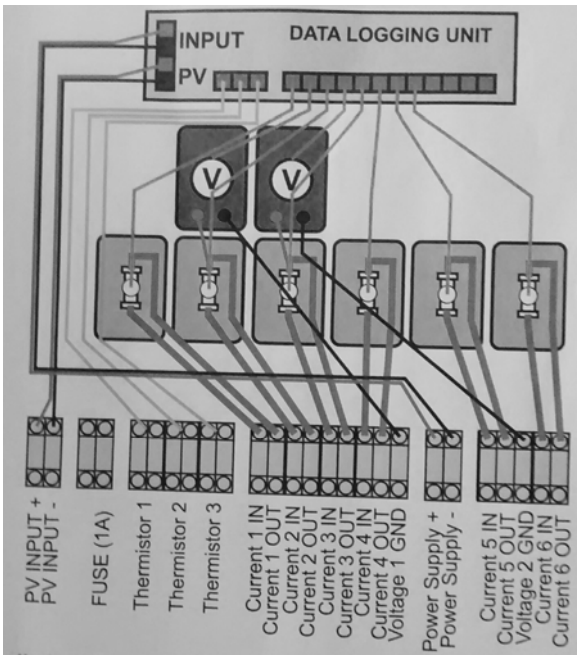

Fig. 1 Remote monitoring device wiring schematic

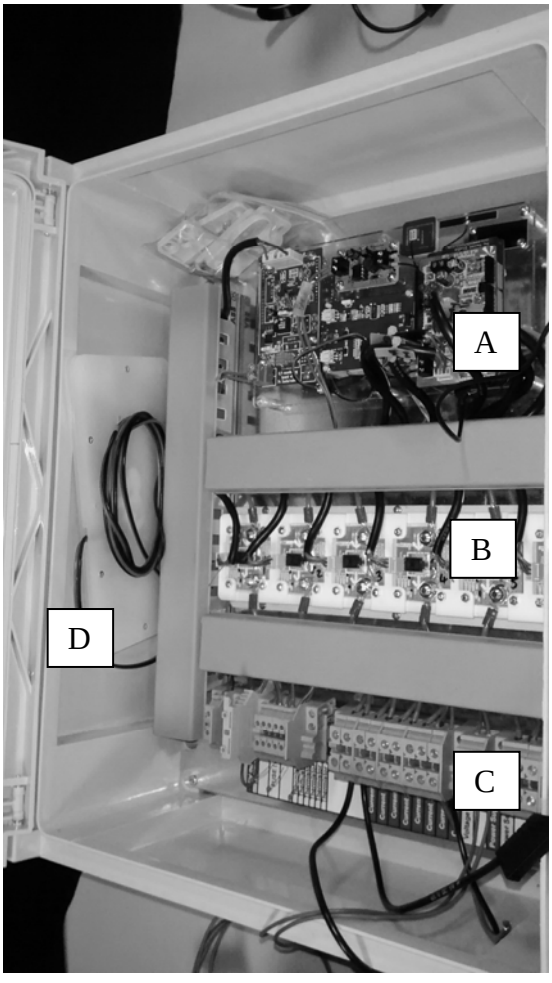

Fig.2 The prototype device. A=Data logger unit, B=Current sensors, C=Cable connectors, D=Packed back up 1.5Wp PV module

6) Embedded Software

The embedded software has been written in C programming language. It is designed for upload to the LinkIt ONE unit via the Arduino IDE. An overview flow diagram is shown in Fig. 3 that indicates the steps in the data acquisition process for different sub-systems.

Users are able to configure the monitoring device by a simple text configuration file which is described here. This can be edited and copied to the data logger SD card which sets the instructions by which the Linkit ONE operates. The data logger application has several configurable options. The details of those options and how the configuration file was written is described here. The configuration file is a small file on the root of the SD card.

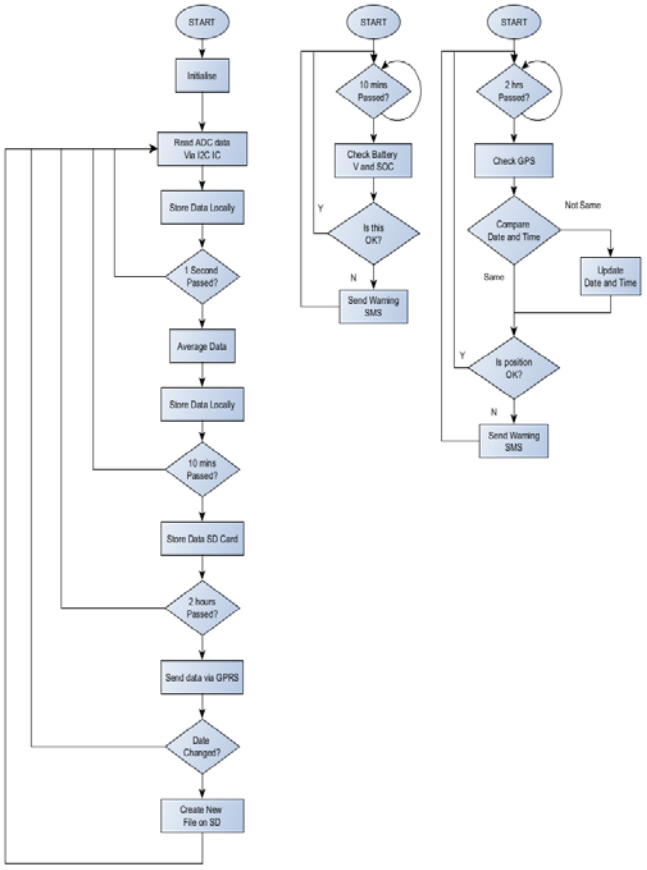

Fig. 3 Software overview flow diagram

a) Filename & Location

The configuration file **MUST** be stored on the root of the SD card under the name "Datalogger.settings.conf".

b) File Structure

The configuration file has one setting per line.

Each line has a setting name, an equals sign, and a setting value, e.g.:

THINGSPEAK_URL=agile-headland-8076.herokuapp.com

Setting names are all uppercase. Words in the name are separated with underscores.

Setting values are either strings or numbers. All numbers are read as signed integers.

Spaces on either side of the equals sign are ignored. For example:

THINGSPEAK_URL=agile-headland-8076.herokuapp.com

and

THINGSPEAK_URL = agile-headland-8076.herokuapp.com

will be treated identically.

c) Comments

Lines starting with a # are treated as comments. The entirety of the line will be ignored.

Comments at the end of a line are not supported. e.g.:

GPRS_APN=giffgaff.com # Some comment here

is **NOT** valid and would result in the comment becoming part of the GPRS_APN setting.

d) GPRS Settings

There are three settings for GPRS connections shown in Table 3:

TABLE 3 GPRS SETTINGS

Setting Name	Notes
GPRS_APN	The APN of the data provider
GPRS_USERNAME	The username for the data provider.
GPRS_PASSWORD	The password (sometimes not required).

These settings are readily available online for various data providers.

e) Data Storage Services

The datalogger can upload data to remote online data storage services. Due to differences in how each service works, the settings for one service may differ from another. Currently the only supported service is Thingspeak, see table 4. Other services may be added in the future.

TABLE 4 CONFIG FILE UPLOAD SETTING

Setting Name	Notes
THINGSPEAK_URL	The URL of the thingspeak service
THINGSPEAK_API_KEY	The write API KEY for the thingspeak channel.

f) Telephone Numbers

The datalogger can send text messages to inform users of its status. There are two sets of telephone numbers, see Table 5. General numbers are for basic status information. Maintenance numbers are for "alarm" type messages such as low battery warning. Up to four numbers may be specified for each set. Messages will be sent to all numbers in the set.

TABLE 5 CONFIG FILE PHONE NUMBERS

Setting Name	Notes
GENERAL_PHONE_NUMBER_1 GENERAL_PHONE_NUMBER_2 GENERAL_PHONE_NUMBER_3 GENERAL_PHONE_NUMBER_4	Up to 4 general numbers.
MAINTENANCE_PHONE_NUMBER_1 MAINTENANCE_PHONE_NUMBER_2 MAINTENANCE_PHONE_NUMBER_3 MAINTENANCE_PHONE_NUMBER_4	Up to 4 maintenance numbers.

Exact phone number format will depend on country of use. Known formats:

g) Upload Settings

Raw data is read 5 times per second. This data is averaged, stored in RAM and uploaded. Available configuration settings are:

For example, settings of

UPLOAD_AVERAGING_INTERVAL_SECS = 30
DATA_UPLOAD_INTERVAL_SECS = 180

would result in a single average of 150 readings being taken and stored in RAM every 30 seconds. These readings would be uploaded every 180 seconds. This means that 6 averages would be uploaded every 180 seconds.

h) Local Storage Settings

Raw data is read 5 times per second.

This data is averaged, stored in RAM and stored to SD card. Available configuration settings are:
For example, settings of:

STORAGE_AVERAGING_INTERVAL_SECS = 5
DATA_STORAGE_INTERVAL_SECS = 60

would result in a single average of 25 readings being taken and stored in RAM every 5 seconds. These readings would be stored to SD card every 60 seconds. This means that 12 averages would be stored every 60 seconds.

Note: data storage and data upload are **entirely independent functions**. They both use the same raw data, but the uploading and storage are not dependent on each other to function.

i) Battery Level Warning

The battery level is checked every hour unless this is overridden in settings. If the battery level is equal to or less than the level set, the maintenance phones numbers are sent a warning message, see Table 6.

TABLE 6 CONFIG FILE BATTERY WARNING

Setting Name	Notes
BATTERY_WARN_INTERVAL_MINUTES	Number of minutes between checking the battery (defaults to 60)
BATTERY_WARN_LEVEL	Battery warning level in percent (not including % sign). e.g to warn at 80% or below use BATTERY_WARN_LEVEL = 80

C. Testing

In order to ascertain whether the device had been correctly constructed and the sensors were working within their design parameters the machine was tested using a Fluke voltage and

current generator. Sensors performed within expected tolerances.

D. Economics

The idea behind developing this data logger was to provide a tool to enable the performance of small scale renewable energy systems to be monitored. Data enables operators to check on whether the system is performing within expected parameters and also to indicate whether maintenance is needed.

The data logging device has been developed from scratch. A budget of approximately £6,000 was allocated to building five of the devices. The learning meant that approximately £3,000 was spent developing the first prototype. Subsequently an additional five data loggers were developed for the remaining £3,000 budget. Clearly there is a learning curve from the initial £3,000 per unit cost for the first prototype to £600 per unit for the subsequent five devices. In the SONG project, a budget of £10,000 was assigned to each nano-grid that is being developed. Thus the cost of the data loggers being deployed is only 6% of the total SONG installation budget. Further iterations should in theory be cheaper.

An interesting advantage for future developments is the data logger, communications and power management sub-systems can be attached to any sensors to transmit data to the operator website.

III. Conclusions

The development of low cost monitoring devices for remote renewable energy applications will help in the understanding of the performance of systems and how end-users make use of the energy available. The aim of the project, to develop such a remote monitoring device has been successfully achieved and has been described in this paper. The system requirements were developed into the design and subsequent construction of the data logger, communications, sensors and power subsystems. In addition, data can be sent to a website where it can be accessed and operators can be contacted by SMS text should problems arise with the SONG or the monitoring device. This has been rigorously tested prior to deployment.

Interestingly, the data logger, communications platform and power sub-systems have the real potential to be used in monitoring other energy or environmental parameters where sensors are available as the sensor specific code can be rewritten for bespoke applications. Furthermore, the data gained from the available irradiance can also help validate published irradiation databases.

Following the installation of the first two devices in Kenya the next stage of the project will be to deploy two devices in Bangladesh. Future publications will report on the operation of the nano-grids.

IV. Acknowledgment

This work is part funded by UK Engineering and Physical Research Council Projects EP/J000361/1 and EP/L002612/1.

V. References

[1] International Energy Agency. World Energy Outlook 2014. IEA Paris.

[2] Williams, S. R., Blanchard, R. E., Mohammed, A., Bliss, M., Pancholi, R., & Clowes, M. (2013). The development of a remote laboratory for distance learning at Loughborough University. In *Can we do it? Yes we can! Recognising, promoting and developing flexible learning in HE* (pp. 1). University of Westminster, Marylebone Campus, London

[3] Blanchard, R. E., Williams, S. R., Bliss, M., Clowes, M., Mohammed, A., & Pancholi, R. (2014). Educating the World: A Remote Experiment in Photovoltaics. In *1st International Conference on Non-Conventional Energy* (pp. 1-5). JIS College of Engineering, Kalyani, India.

[4] Williams, S. R., Blanchard, R. E., Mohammed, A., Bliss, M., Pancholi, R., & Clowes, M. (2014). The Development of a remote laboratory for distance learning at Loughborough University. In *HEA Annual Conference 2014* (pp. 1). Aston, UK.

[5] Blanchard, R. E., Williams, S. R., Bliss, M., Clowes, M., Mohammed, A., & Pancholi, R. (2014). The Development of a Photovoltaic Remotely Operated Laboratory Experiment: A Contribution to Meeting the Challenge of the Renewable Energy Skills Shortage. In *World Renewable Energy Congress XIII* (pp. 1-7). University of Kingston, London.

[6] Radu, T., Blanchard, R. E., Wheatley, A., Yadav, D., Bora, D., Purkayastha, R., Ghatak M, Barbora L, Mahanta P, Collins F, and Diamond, D. (2014). Providing energy for rural Indian communities. Anaerobic digestion at Loughborough University. In *UK AD & Biogas 2014* (pp. 1). Birmingham.

[7] Blanchard, R.E., Radu, T., Collins, F., Diamond, D. & Wheatley, A.D. (2015). Real-time autonomous remote biogas monitoring. Bioenergy: an engine for economic growth in the global South workshop. Wellcome Trust, London 28/01/2015.

[8] www.seeedsstudio.com/wiki/Linkit_ONE Accessed 15/9/15

[9] www.ti.com/lit/ds/symlink/ads1115.pdf Accessed 15/9/15

[10] www.allegromicro.com/~/media/files/datasheets/ACS758-datasheet.ashx Accessed 15/9/15

[11] www.avagotech.com/docs/AV02-3563EN Accessed 15/9/15

[12] www.re-innovation.co.uk/web12/index.php/en/information/electronics-information/244-voltage-measurement Accessed 15/9/15

[13] http://thingspeak.com Accessed 15/9/15

[14] http://agile-headland-8076.herokuapp.com/channels/7 Accessed 22/9/15

[15] http://creativecommons.org/licenses/by-sa/4.0/ Accessed 15/9/15

Computational and Experimental Study of an Ultra-Low Head turbine

Pradeep Parajuli*[1], Pratik Koirala[1], Nischal Pokharel[1],
Dr. Hari Prasad Neopane[1], Sailesh Chitrakar[1]
[1]Department of Mechanical Engineering
Kathmandu University, Dhulikhel, Kavre, Nepal
*E-mail: pra_deep_ppt@yahoo.com

Dr. Ing.– Ramesh Kumar Maskey[2]
[2]Department of Civil and Geomatics Engineering
Kathmandu University, Dhulikhel, Kavre, Nepal
E-mail: rmaskey@ku.edu.np

***Abstract*— As the threat of limited energy has reached its peak, a system that utilizes majority of the unutilized sites to extract energy is demanded. The project work, presented here, aims to propose an efficient system to exploit the low head sites, test and verify the technical feasibility and economical affordability of thus proposed system. The research was carried out to develop ultra-low head turbines that exploits the sites with lower head and lower discharge using only limited hydraulic and mechanical components satisfying the economic viability [1]. Three models were prepared and one was successfully tested to verify the operating principle called "Static Pressure Difference principle". Focusing on blade profile, mesh generation CFX package was used to analyze the fluid flow through turbine hub and blade. This approach was carried out on three different turbine models with straight, twisted and curved blade profiles and results were used for efficiency evaluation of each turbines. The simulation result showed curved profile to be best efficient profile than other two with 87.03 % efficiency and well distinguished pressure and suction side within a blade. The produced power was 3 W at rotational speed 12 rpm anticlockwise with torque of 2.45 N-m at the flow rate of 6 l/s.**

The computational analysis was ensued by scaled model testing in a small irrigation canal with a channel system. The testing showed curved blade turbine model's efficiency of 64.36 % with output power of 2 W at rotational speed of 15 rpm anticlockwise with torque of 1.28 N-m at the flow rate of 6.4 l/s. The head difference was maintained at 5 cm for both type of analysis.

Keywords*— *Computational Fluid Dynamics (CFD); Froude number; Static Pressure Difference and Ultra-Low Head turbine

I. INTRODUCTION

The literature research, in the areas of the hydropower sector, signifies that the installation of the project is dependent of the head and the discharge of the site. Usually high head refers to Pelton turbine installation: moderate head and moderate discharge for Francis turbine: low head and high discharge for Propeller and Kaplan turbine [2]. Concern, now, is shifted on the utilization of unutilized sites i.e. low head and low discharge on which this project was focused. A new technology of Ultra-Low Head turbine (ULH), which can be installed even in irrigation canal, waste water treatment plant and other small man made canals, was employed that works in the principle of static pressure difference unlike conventional turbine [1]. Studying about the blade profile optimization of ULH turbine is still an immature field as very little research–research performed by James A. Senior (till 2008) – has been performed regarding it. This project, thus, was focused on the use of commercial software for simulation part to optimize the blade profile.

II. OVERVIEW OF ULTRA-LOW HEAD TURBINE

A. Structure of Ultra-low head turbine

ULH turbine is a low head to energy convertor, which is devoid of large number of hydraulic and mechanical components, with structure similar to traditional waterwheels: breast-shot type [3]. The turbine consists of central hub–a cylinder that blocks the upstream water– and blades–a surface that allows the passage of water through its own rotation– mounted radially on the hub surface. The blades are attached at an inclined angle to the axis, preferably 20^0, in order to maintain the depth of downstream water level [1]. Side walls, mounting for bearings, may be present in some as an essential component to prevent the leakage from the side of the hub [1].

B. Static pressure difference principle

The ULH turbine is fitted to a channel system and as the water flows in the channel and strikes the turbine: the continual rotational motion of the turbine occurs that allows the energy conversion in the system. As the water flows from upstream to the downstream, flow area decreases, due to blockage by hub, and downstream velocity increases as per the continuity equation. This dissimilar depths of water results in hydraulic pressure difference on either side of the wheel, as a result, forces

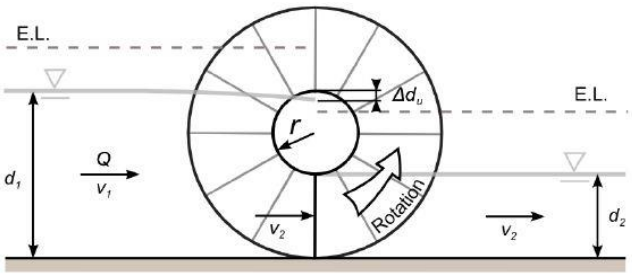

Fig. II.1 Static pressure difference in Ultra-low head turbine [1]

are generated once the flow passes beneath the hub. This force is counteracted by the reaction force, once the flow is accelerated as it undergoes nozzle effect beneath the hub. These two forces simply act on the model as shown in the Fig. II.1 to illustrate operating principle namely "Static Pressure Difference principle" [1].

III. Computational Study And Results

Computational fluid dynamics (CFD) refers to the branch of fluid dynamics that simulates the real flows by the numerical simulation of the governing equations– Navier Stokes equation [4]. This technique deduce the complex governing equations into a system of simpler algebraic equations easier to solve. A CFD process includes three steps: pre-processing–specify boundary conditions, solver–define convergence criteria and post processing–analyze results.

A. Design of different models

Three models each with eight blades were designed namely straight, twisted and curved blade profile over which CFD analysis is performed. The former two are the existing design whereas the latter one was selected as it resembles the blade configuration of cross flow turbine and creates enough pressure difference generating the lift inducing streamline flow too.

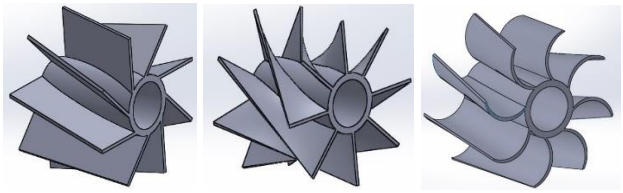

Fig. III.1 Design of straight, twisted and curved turbine respectively

B. Domain creation and meshing

Two fluid domains were created in SolidWorks: stationary domain– one over which fluid flows– and rotating domain– one over which the turbine model rotates.

These domains were imported in ANSYS CFX and then discretized to generate smaller units by hex dominant meshing with free face mesh type set to "All Quadrilaterals" to produce uniform meshing. Similar domain creation and meshing process were used for all aforementioned three turbine models.

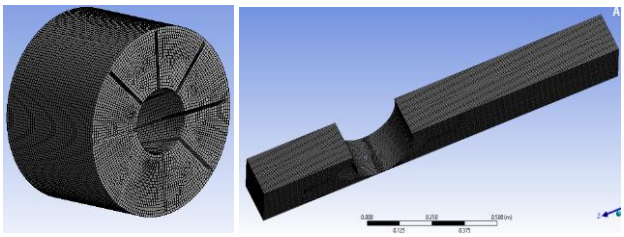

Fig. III.2 Meshing of rotating and stationary domain respectively

C. Boundary conditions and convergence criteria

The inlet boundary condition for stationary domain was specified with bulk mass flow rate of 6 kg per sec and outlet condition was characterized for static pressure of 1 atm. As the multiple domain was used: water and air, fluid values of water= 1 and air at 25ºC= 0 was set at inlet of stationary domain and vice versa at opening of rotating domain. The domain motion for rotating domain was changed to rotating type with angular velocity 12 rpm in anticlockwise direction. The water flow being considered as incompressible, the turbulence model k-Epsilon had been used for validation process.

The maximum iteration was set to 300 with RMS residual type and residual target of 1.E-4.

D. Simulation result

The flow distribution along the flow path from inlet to outlet along pressure variation and velocity distribution, at the different sections of the domain, are interpreted in this section. Also, torque acting on each blades for each turbine was evaluated to calculate the total power output for efficiency calculation. Viewing the flow pattern, pressure variation in pressure and suction side and comparing the efficiency calculated in each model, a turbine with suitable blade profile was chosen.

1) Streamline flow and velocity distribution

Flow pattern was viewed to minimize splash (volumetric) loss and to check turbulence–hindrance for larger power output– of the output flow.

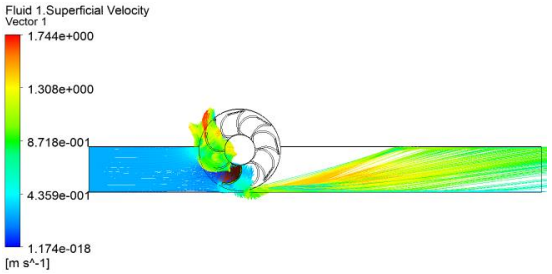

Fig. III.3 Flow visualization in curved blade profile

It is observed from Fig. III.3 that velocity of water when it just stroke the turbine, 0.44 m/s is increased to 1.74 m/s when it just leaved the turbine: the decrease in flow area as per continuity equation.

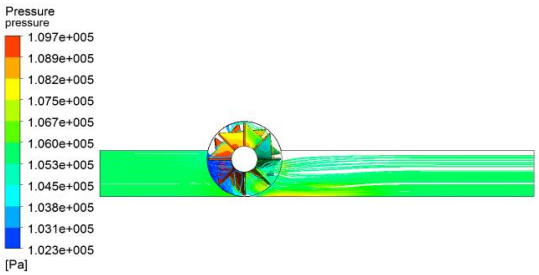

Fig. III.4 Use of cover to decrease splash loss

Further, water splash was observed just above the rotating domain that accounts for volumetric loss– a factor that decreases efficiency. Also, larger volumetric loss was observed in twisted profile due to oppositely twisted blade on two ends due to which streamline tends to rotate the model in clockwise direction at far end. This loss could be minimized by the use of cover in the rotating domain as below.

2) Pressure variation

Simulation showed that the pressure was largest for the blade profile facing the upstream flow. The reason for larger pressure is low velocity at upstream and the dominancy of static force.

This pressure variation was observed clearly in the curved profile.

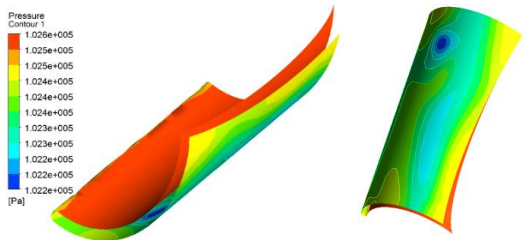

Fig. III.5 Pressure and suction side in curved blade profile

3) Torque comparison and efficiency calculation

For each of the turbine model, resultant torque is the summation of torque produced by each blades mounted on the hub and hub itself taken in the direction along the axis of rotation. From this, power output and efficiency was calculated. The result obtained showed: the curved profiled turbine with efficiency 87.03% as the best one in comparison with straight blade and twisted. The efficiency of straight blade turbine and twisted blade turbine were 61.78% and 36.87% respectively. The torque and power output variation for input power of 3.53 W (head difference 5 cm and discharge 6 l/s) among straight, twisted and curved blade profile are given below.

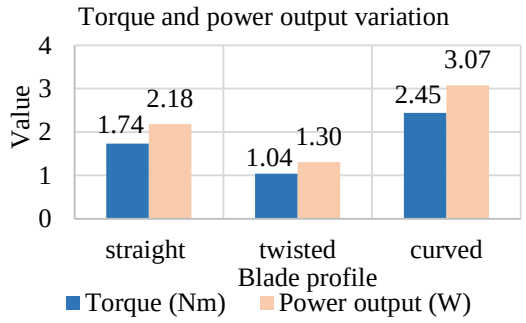

Fig. III.6 Torque and power output in each of three different turbines

4) Conclusion drawn

The result matches the theoretical concept of impacts of free jets on different profiled blades as the curved profile blade is best one due to presence of high pressure side to impinge the flow and low pressure side to increase velocity of water. The straight profile is less efficient because it has no high pressure and low pressure side. Also, the variation, if occurs is quite less nearly equal to about 100 Pa as compared to 300 Pa that occurs in curved blade profile. The twisted profile blade is least efficient amongst three because of varying high pressure side and low pressure side along the same face of the blade profile. Viewing the pressure contour and torque obtained from the simulation process, curved blade profile was selected as best blade profile for the ULH turbine.

5) Optimization of curved profile

Simulation was carried out by varying the blade number and its angle along the hub axis. The former simulation showed, with the increase in blade number, upstream flow acted on two or more blades at same time, thereby, creating insignificant high and low pressure side and disturbing the flow pattern. The latter one was carried to calculate best blade inclination.

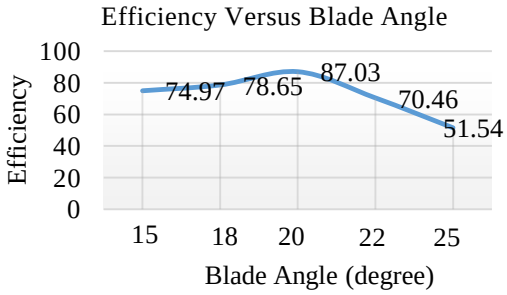

Fig. III.7 Efficiency Vs Blade Angle graph

It is observed that the turbine is best efficient for blade angle range of 18^0 to 22^0 being maximum at 20^0. Lesser the blade angle below 20^0, depth of downstream flow cannot be maintained up-to blade hub low level on regular basis, hence desirable head isn't achieved. Greater the blade angle above 20^0, condition of turbulence may occur.

IV. Experimental Testing And Results

A scaled down model following geometric, kinetic and dynamic similarity is prepared in the workshop and testing procedure is facilitated by the preparation of setup canal for testing in reduced discharge. The model has a width of 15 cm and outside diameter of 30 cm, and hub diameter blade chord length of 10 cm each.

A. Model and set preparation

The computational analysis was ensued by experimental study to validate the results obtained. The turbine model was prepared by cutting poly vinyl pipe to desired shapes of hub and blade with shaft attached to it. Then, canal set up was built using wooden planks with hinges provided at inlet and outlet to form door like structure which accounts to overcome the varying discharge. A small pulley was attached to shaft as shown in Fig. IV.2 in order to measure the stopping load- a load that ceases the motion of rotating turbine.


Fig. IV.1 Model for testing

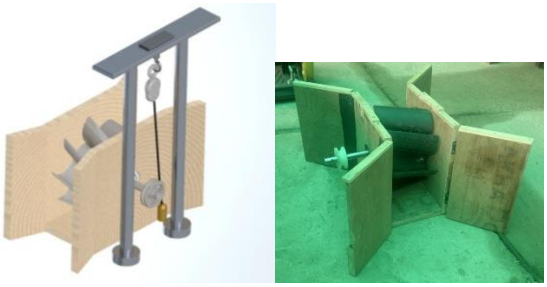
Fig.IV.2 Design and fabrication of complete test setup respectively

B. Model testing and result.

The turbine model was tested in an irrigation canal on the way to "*Khopasi*" and parameters like velocity of flow, head difference, canal dimension, stopping load etc. were measured.

Floatation method was used to measure the flowing velocity and discharge obtained was 6.38 l/s. The rotational speed obtained was 15 rpm anticlockwise for head difference of 5 cm.

Fig. IV.3 Testing site (left) and torque measurement, head difference (right)

"Prony Brake"–a means that uses weight and counterweight mass scale and a frictional belt to apply the stopping load– was used to calculate the output power by multiplying the stopping torque by angular velocity [1].

$$P_{out} = \left(m_{weight} - m_{counterweight} \right) * g * r * 2\pi * f \quad (1)$$

Stopping load of m_{weight}= 2 kg ceased the rotating motion of the turbine for which spring balance reading obtained was $m_{counterweight}$= 0.91 kg. As a result, efficiency of 64.36 % was obtained with power output of 2.02 W.

C. Model scaling

Scaling down of a prototype reduces the time consumption and eases the computational processing. It is difficult to simulate under the actual condition in CFD. Various experimental tests can be conducted on the scale down model and similitude concept can be used to relate with the large prototype. For the flow that occurs through open channels and where gravitational force is most significant Froude number governs the dynamic similarity [5]. From the equivalence of Froude number

$$\frac{V_m}{\sqrt{gL_m}} = \frac{V_p}{\sqrt{gL_p}} \quad (2)$$

Table IV.1 Full scale estimation

S. N	Head difference m	Hub diameter, m	Flow rate, m^3/s	Power output kW
1.	0.05	0.1	0.00638	2.02*E-03
2.	0.25	0.5	0.356	0.56
3.	0.5	1	2.01	6.375
4.	0.75	1.5	5.49	25.89
5.	1	2	11.42	72.12

The table shows that mechanical power output of 6.37 W is obtained under the head difference of 0.5 m and discharge around 2 m^3/s which is easily available in irrigation canal.

D. Results comparison

Computational study showed curved blade model to be best efficient one with 87.03 % efficiency. The testing result showed the acceptance of curved model with efficiency percentage of 64.36 % as leakage losses account for 8 – 10% of efficiency value, although it has a negligible effect once rotor speeds reach peak power and above [6]. This efficiency of 64.36 % is viewed as satisfactory one as most of the ULH turbine (esp. straight and twisted one) installed in sparse parts of the world have the efficiency equivalent to this. Further, the deviation from computational analysis might be due to flow acceleration, increase in revolution (15 rpm in testing while 12 rpm in simulation) and turbulence. Though there may exists certain errors, these errors could be minimized in prototype building and testing and larger amount of power output is expected as indicated by the model scaling table.

V. Conclusion

Theory and practical analysis suggests that ULH is driven directly by the pressure difference between two dissimilar depths of water on either side of the installation. CFD analysis in three different profile of the blades showed that curved blade profile is best suitable in the case of ULH turbine among straight, twisted and the curved profile. The best angle between hub and the blades was found to be 20 degree. The experimental testing was acceptable to the results obtained from the computational study. The reasonable deviation in efficiency was mainly due to leakage losses and increase in revolution. Model test showed that the efficiency of the machine was 64.36 % and the output power generated was 2 W. The scaling of the model data suggests that power output of 6 kW can be generated for hub diameter of 1 m which is quite a large amount in itself.

Acknowledgment

We are very much thankful to Turbine Testing Laboratory and Department of Mechanical Engineering of Kathmandu University for providing us this opportunity to carry out this research. We would also like to acknowledge the whole staffs of Technical Training Centre for facilitating out in experimental setup preparation.

References

[1] Senior, J., Wiemann, P., & Muller, G. "The rotary hydraulic pressure machine for very low head hydropower sites", University of Southampton, U.K.

[2] Harvey, A, & Brown, A (1992). Micro-Hydro Design Manual.Stockholm: ITDG Publishing

[3] Müller, G. & Kauppert, K. (2004), "Performance Characteristics of water wheels", Journal of Hydraulic Research, 42, 451 -460.

[4] Sayma, A. (2009), "Computational Fluid Dynamics".Abdulnser sayma & Venus Publishing Aps.

[5] Kumar, Dr. D.S. (2012),"Fluid Mechanics and fluid power engineering".S.K. Kataria & Sons.

[6] Linton, N. P. (2013), "Field trisls and development of a hydrostatic pressure machine", University of Southampton, Page 126

Performance Comparison of Mirror Reflected Solar Panel with Tracking and Cooling

Sheikh Md. Shahin Alam[1], Dr. A.N.M. Mizanur Rahman[*2]

[1]*UG Student,* [2]*Professor*

Department of Mechanical Engineering

Khulna University of Engineering & Technology, Khulna-9203, Bangladesh

[1]sasumon52@gmail.com; [2]drmizan84@gmail.com

Abstract: **Dwindling nature of fossil fuels led many countries to search for new and alternative sources of energy. Solar energy is a clean, eco-friendly and abundantly available energy source. The useful forms of solar energy are either heat or electricity. The electricity demand is increasing every day. The conversion of solar energy to electricity through PV module is becoming popular but overprice of cells and lower efficiency hinder its use in developing countries. To reduce high cost per unit electricity, one way is to improve the performance of PV systems. New cost effective mirror reflecting linear focusing solar concentrator may be a good solution. As mirror boosted radiation intensity over the panel is more, the consequence is increased temperature of the panel. But panel temperature above 25°C reduces the open circuit voltage and decrease efficiency. Thus, proper cooling is needed to improve the panel performance. This paper presents the comparison of performance of a mirror reflected solar panel (MRSP) with automatic cooling and tracking. As the mirrors are fixed to the panel the incident radiation will be obstructed by the booster. Thus, a tracking mechanism is developed to focus the sun light approximately in perpendicular direction. The MRSP with automatic tracking and cooling was designed and constructed from locally available materials. The values of current and voltage were measured under different conditions of tracking. The output power was calculated and the values were compared for various combinations. From the results it could be depicted that tracking with only reflection and only cooling give higher power than tracking without reflection or cooling; but while tracking with reflection plus cooling the power increase is much more than any other combination. The average increment of power by using tracking with reflection plus cooling is about 59.71%.**

***Keywords*— Mirror reflected solar panel; Panel cooling; Panel tracking, Panel performance.**

I. INTRODUCTION

Solar energy is a clean, environment-friendly and abundant resource available everywhere almost all the year. Indeed, in just one hour, the solar energy intercepted by the earth exceeds the world's energy consumption for the entire year [1]. The potential of solar energy to mitigate climate change is equally impressive. Except for the modest amount of CO_2 emissions generated during the manufacture of energy conversion devices, the direct use of solar energy produces a very little greenhouse gases and it has the potential to displace large quantities of non-renewable fuels. Solar energy conversion is manifested in a family of technologies having a broad range of energy applications viz., lighting, comfort heating, water heating, distillation and production of fuels like hydrogen or synthesis gas.

Extracting useable electricity from the sun was made possible by the discovery of photoelectric mechanism and subsequent development of solar cells. Solar panels are being used widely especially popular in remote areas where establishment of electricity distribution lines is not economically feasible. This alternative power source is continuously achieving greater popularity. Extraction of energy from sun is being heavily researched and solar electricity costs have now reached within a few cents per kWh. It becomes comparable to other forms of electricity generation and will drop in future with the adoption of new technologies such as titanium oxide cells with a peak laboratory efficiency of 32% and average efficiency of 15-20% [2]. To make this source competitive, it is necessary to recover energy as much as possible from a solar power system. The solar energy is still more expensive than the classical fossil burned electricity [3].

The distribution of solar energy over an area is not linear with time rather it varies from morning to evening with a peak at noon. Also, if the panel is fixed to receive maximum radiation in the noon, the morning and afternoon radiation will again be reduced because of its incidence angle. For this reason it is desired that the solar panels should be mounted in such a way that it faces the sun most of the time or there should be a tracking system for the panel. Sun-tracking systems are designed in a way to track the sun on a single axis (based on azimuth angle) or on two axes (based on azimuth and altitude angles). As the amount of electricity obtained from PV systems is directly proportional to the radiation intensity, so a concentration system may be a good solution to increase the efficiency. This would significantly reduce the cost of electricity generation by photovoltaic panels [4]. Sungur C. [5] investigated multi-axes sun-tracking system and found that 42.6% more energy is available compared to fixed panel system.

To improve the performance of PV system a new cost effective mirror reflecting linear focus type solar energy concentrating system has been developed. Due to simplified assembly of concentrating mirrors, the standard technologies

facilitate low-cost manufacturing. As the mirror boosted radiation intensity over the PV panel is more than its normal value the temperature of the panel will increase. Temperature above 25^{o}C reduces the band gap of a semiconductor material, thereby affecting the properties of most semiconductor materials, ultimately reduce the open circuit voltage and thereby decrease the efficiency. Temperature increase of 1°C of the PV cells decreases 0.4 to 0.5% efficiency for crystalline silicon based cells [6, 7] and 0.25% for amorphous silicon cells [8]. Thus, an effective cooling system may be a good solution for increasing efficiency of a photovoltaic system. Concentrators, trackers and cooling system offer opportunities to increase output power in a cost-effective manner. Today the theoretical efficiency of a solar PV cell is said to be around 25% to 30% and a practical efficiency around 17% [8]. Xiao Tang et al. [9] experimentally investigated the effect of cooling using both air-cooling and water-cooling of solar panel and found maximum temperature reduction of 4.7^{o}C and 8^{o}C respectively.

II. Design of MRSP with Tracking and Cooling System

Keeping the objectives in mind the MRSP was designed in a cost effective manner considering some factors like minimum dimensions so that it would be easily portable, easy setting of the reflectors, fast cooling mechanism, selection of best cooling side, locally available materials and the design of the circuit for automatic adjustment.

A. Design Consideration

The design of MRSP involved mechanical and electrical parameters and they were addressed in a cost effective manner. The important parameter that led to fix some other parameters was the available solar panel size. The work was conducted at Mechanical Engineering Department of KUET and the solar panel was taken from the lab. However, some other points were given emphasis and these were: total weight of the system for easy portability, facing the panel towards the sun, utilizing an effective and replaceable cooling system, minimizing the torque on motor for small power input and using reduction gear for smooth rotation.

B. Design of Minimum length of reflector

As the weight of whole system ultimately dictates the load on tracking motor, while designing the reflector two things were considered: the weight of the reflector and to evenly distribute the reflected rays over the panel to avoid uneven voltage generation. To make it light weight it was important to minimize its size by calculating the minimum inclined length of the booster mirror. From the laws of reflection of light, the geometry of light rays with booster mirror (BE) and PV panel (BC), it was observed that if the mirror is fixed at an angle of 120° with the panel then it will cover the whole panel surface in AB side. The sides AB and CD are similar in dimension so the mirror size was same for that two sides. The height of the mirror was calculated as 29 cm. The same analogy was applied for side AD. This is demonstrated in Fig. 1.

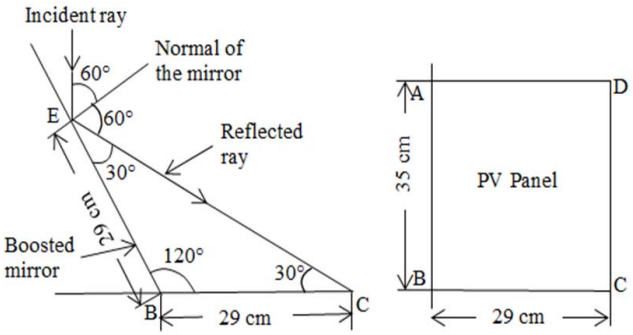

Fig.1. Geometry of light ray with boosted mirror and PV panel

C. Selection of Cooling Site

As the panel surface gets heated, it needs fast cooling for better performance. Cooling of the panel could be performed either from underside or from topside. There are different types of PV modules among them glass to tedler and glass to glass module are available in Bangladesh. So, it is important to estimate which side would be more effective for cooling. The schematic arrangement of PV cell construction is shown in Fig. 2.

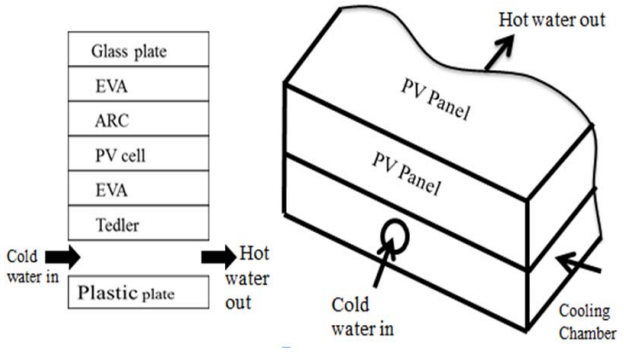

Fig. 2 Schematic arrangement of cooling unit

For the glass to tedler module the equivalent thermal resistance from tedler to PV cell (bottom-side) is 2.4537×10^{-3} K/w and the glass plate to PV cell (top-side) is 6.2931×10^{-3} K/w. As the equivalent thermal resistance of bottom-side of the panel is less than that of the top-side, therefore cooling from bottom-side of the panel was chosen for better cooling. In practice, a cavity was formed with the help of a plastic sheet from the bottom-side of the panel. Cold water was passed through cavity from the lower end to the upper end with the help of potential energy of water in the storage tank.

D. Design of Control System

To control the whole system smoothly a proper control system was designed. The schematic arrangement of the circuit diagram of the control system is shown in Fig. 3 with the help of a block diagram. The microcontroller controls the solenoid valve through relay operation with the help of a LM35 sensor. It also controls the stepper motor through motor controller with the help of defined programme to complete 15° rotation of the PV module every hour.

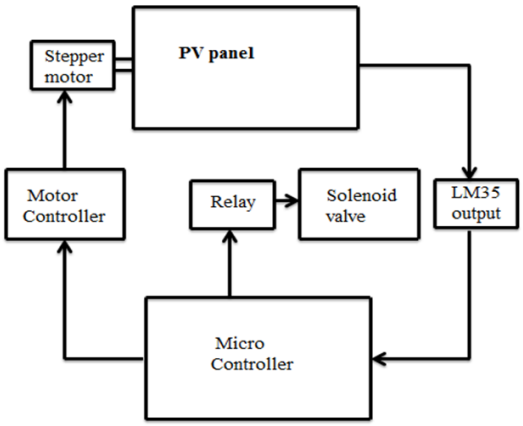

Fig. 3 Schematic arrangement of control unit

E. Design of the Mirror Reflected Solar Panel System

Tracking of panel was accomplished by using six stepper motor. An Arduino UNO microcontroller and a motor controller driver were used to control the stepper motor. A reduction gear was used to minimize the torque. An azimuthal tracking system was used to truck the panel from 9 am to 5 pm. To rotate the whole system every15° per hour from East to West the stepper motor needed 525 steps. Program was made to one step in 55 second. The cooling system added to the bottom side of the PV panel maintained the PV panel temperature within 25°C. The LM35 temperature sensor was placed at the outlet of the cooling system to monitor the outlet temperature. As the outlet temperature in the cooling system exceeds 26°C, the microcontroller would open the solenoid valve and if the temperature is less than 25°C, it would close the solenoid valve through relay operation. The whole system was mounted over a structure with ball bearing arrangement so that it could maintain 15° angle with horizontal and truck the sun as needed.

III. Construction And Working Procedure

A. Construction of Proposed Module

The Mirror reflected solar panel with automatic tracking and cooling system was constructed using locally available raw materials to make it cost effective. At first the cooling system was made attached to the solar panel. A frame was constructed to support the reflectors made to the sizes as mentioned earlier. The reflectors, panel with cooling system were mounted on the frame that can rotate in a horizontal as well as in a vertical axis. Fig. 4 shows the photographic view of the MRSP with automatic tracking and cooling system.

B. Working Procedure

The stepper motor with controller and solenoid valve were connected with power supply unit through relay. The inlet pipe was connected through the solenoid valve and the outlet pipe was connected to the cooling unit in lower portion of PV panel. Cold water was preserved in a reservoir tank at a height of 1.5 m to facilitate water to flow through the annular space by gravity. To run the experiment the whole system was put under sunlight. At first, the open circuit voltage and short circuit current were measured as a data of tracking with reflection system. After that the mirror was closed by a cover of opaque material and data was taken as only tracking system. Switching on the power supply, the solenoid valve would open and water was circulated through the cooling unit unless the outlet temperature of water drops down to 25°C. When the outlet temperature came down to 25°C microcontroller shut down the solenoid valve and data were taken as tracking with cooling system. Finally, the mirror cover was again removed and data were taken as tracking with reflection plus cooling.

Fig. 4 Constructed mirror reflected solar panel

C. Working Procedure

The stepper motor with controller and solenoid valve were connected with power supply unit through relay. The inlet pipe was connected through the solenoid valve and the outlet pipe was connected to the cooling unit in lower portion of PV panel. Cold water was preserved in reservoir tank at a height of 1.5 m to facilitate water to flow through the annular space below the panel by gravity. To run the experiment the whole system was put on under sunlight. At first the open circuit voltage and short circuit current from PV panel was measured as a data of tracking with reflection system. After that the mirror was closed by a cover of opaque material and data was taken as only tracking system. Switching on the power supply, the solenoid valve would open and water was circulated through the cooling unit unless the outlet temperature of water drops down to 25°C. When the outlet temperature came down to 25°C microcontroller shut down the solenoid valve and data were taken as tracking with cooling system. Finally, the mirror cover was again open and data were taken as tracking with reflection plus cooling system.

IV. Experimental Result

A. Data Collection

The experiments were conducted for a total of 10 days from 27-04-2015 to 07-05-2015 and the data was collected as described in section III. Among them data taken on 30-04-2015 is presented in Table I as representative. The table shows open circuit (OC) voltage and close circuit (CC) current for

various mode as: tracking only; tracking and reflection; tracking and cooling; tracking, reflection plus cooling system.

TABLE I

Time in hour	Tracking only		Tracking and reflection		Tracking and cooling		Tracking, reflection plus cooling	
	OC V	CC A	OC V	CC A	OC V	CC A	OC V	CC A
9	18.4	0.70	18.8	0.90	21.4	0.68	21.7	0.90
10	19.0	0.72	19.0	0.91	21.4	0.72	21.8	0.93
11	18.5	0.77	19.0	0.95	21.4	0.75	22.0	1.02
12	18.8	0.77	18.3	0.94	21.4	0.75	22.0	1.03
13	18.9	0.79	17.2	0.86	21.8	0.77	22.0	1.06
14	18.2	0.74	17.8	0.87	21.3	0.73	22.0	0.98
15	17.54	0.65	18.2	0.89	20.6	0.64	21.21	0.97
16	16.2	0.53	17.1	0.71	16.3	0.57	19.6	0.86
17	13.8	0.37	15.6	0.56	13.6	0.37	16.1	0.70

B. Calculated Values from Data

The data obtained from the experiments [11] on each day were calculated for various parameters like power from tracking system (P_{TS}), power from tracking with reflection system (P_{TRS}), power from tracking and cooling system (P_{TCS}), power from tracking, reflection plus cooling system (P_{TRCS}). Then a comparison was made between P_{TS} and P_{TRS}, P_{TS} and P_{TCS}, P_{TS} and P_{TRCS} for the values obtained from data on various dates.

C. Graphical Representation of Data

The power calculated for various days from the data collected on experimental days for various modes as mentioned earlier are plotted as power versus time of the day. Among them the graphs for 29-04-2015 is presented in Fig 5.

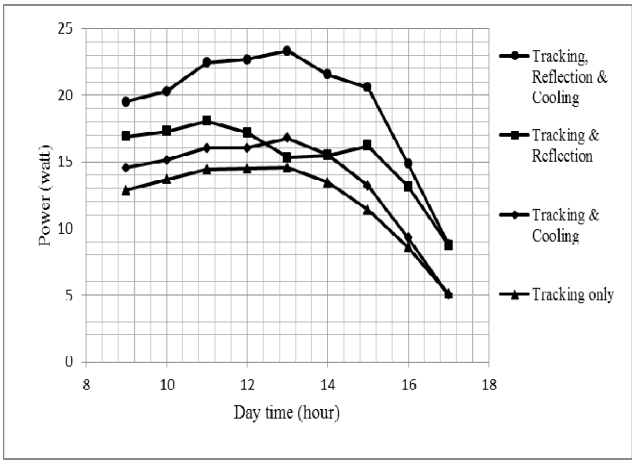

Fig. 5 Distribution of power along the day on 29-04-2015

V. DISCUSSION

In Fig. 5 it is apparent that the power varies with time of the day. It shows a maximum during the noon time which is obvious because the radiation is the maximum. The powers obtained for only tracking system, tracking with cooling system are changing linearly. The nature of the curve is almost similar. Normally on a clear sunny day the radiation intensity as well as power is maximum at noon. Before noon, power gradually increases and in the afternoon it decreases as well. But with increasing solar intensity through mirror reflection the panel temperature increases. Thus, open circuit voltage decreases and finally output power decreases. So, power curve with tracking and reflection system becomes downwards at noon time. As the temperature decreases during afternoon the power curve with tracking and reflection system becomes upward. Maintaining lower temperature by means of cooling system with tracking plus reflection system the output power was more than other process and power curve became linearly upward during morning to noon and linearly downward during noon to afternoon. From the figure it is evident that cooling system was not effective between 4 pm to 5 pm. All the figures are not identically same because of the variation of intensity from day to day. Sometimes because of cloudy sky the radiation decreases which causes a decrement of power.

VI. CONCLUSIONS

From the experimental result it could be concluded as:

- Power increases for tracking with reflection system lowest 1.34% to highest 93.07% and average 30.89%.
- Power increases for tracking with cooling system lowest 0% to highest 80.79% and average 11.36%.
- Power increases for tracking with reflection plus cooling system lowest 8.27% to highest 123.33% and average 59.71%.

REFERENCES

[1] A special report on direct solar energy. Available Web-link: http://srren.ipccwg3.de/report/IPCC_SRREN_Ch03.

[2] Mitchell K, Rizk J, Nagrial M, Development of planning procedures with embedded solar systems, Australian Journal of Electrical & Electronics Engineering, vol 3, no.1, pp 57-64, 2006.

[3] Jiménez V. 2004 [online]. World Sales of Solar Cells Jump 32 Percent. Earth Policy Institute. Retrieved: August 7, 2000.

[4] Özge Demir Başak, Bekir Sami Sazak, Effect of components on a solar panel system Efficiency, Volume: 03, Special Issue: 17, page: 8,| IACEIT-2014 | Dec-2014, Available @ http://www.ijret.org.

[5] Sungur, C., Multi-axes Sun-tracking System with PLC Control for Photovoltaic Panels in Turkey, Journal on Renewable Energy, vol. 34, pp. 1119-1125, 2009, Published by Elsevier Publications.

[6] Brinkworth et al. Thermal regulation of photovoltaic cladding. Solar Energy 1997; 61:16978.

[7] Kranter et al. Combined photovoltaic and solar thermal systems for façade integration and building insulation. Solar Energy 1999; 67:239–248.

[8] Kalogirou SA, Tripanagnostopoulos Y. Hybrid PV/T solar systems for domestic hot water and electricity production. Energy Convers Manage 2006; 47:3368–82.

[9] Tang, X., Zhenhua. Q., Zhao, Y., Experimental Investigation of Solar Panel Cooling by a Novel Micro Heat Pipe Array, Journal of Energy and Power Engineering, vol. 2, pp. 171-174, 2010.

[10] K. Mitchell; M. Nagrial and J. Rizk – 'Simulation and Optimization of Renewable Energy Systems' International Journal of Power & Energy Systems, Vol 27, pp 177-188, 2005.

[11] Sheikh Md. Shahin Alam, Design and Construction of Cooling System for Mirror Reflected Solar Panel, Undergraduate Research Report, Department of Mechanical Engineering, KUET, 2015.

Study of Traditional and Z-source Converter under Variable Fuel-Flow-Rate of PEMFC

[1]Muhammad M. Roomi, *Student Member, IEEE,* Ali I. Maswood, *Senior Member, IEEE* and Md Shafquat Ullah Khan, *Student Member, IEEE*, Mohd Tariq, *Student Member, IEEE*
School of Electrical and Electronic Engineering, Nanyang Technological University, Singapore
Email: [1]muhammad137@e.ntu.edu.sg

***Abstract*— Renewable energy sources integrated with power electronic converters plays an important role in satisfying the energy demands in variable applications. Fuel cell being a promising technology to use as a source of electricity, the mathematical modeling of the fuel cell is studied and testing of power electronic converters are carried out in this paper. Matlab/Simulink models of the fuel cell integrated with the converters are developed. Results show the changes in the fuel utilization, stack consumption and efficiency of a 65kW fuel cell integrated with the traditional and Z-source converters. Key output waveforms of the fuel cell, dc link voltage, three phase output voltages and currents of the inverter are also presented.**

Keywords*— boost converter, dc link voltage, proton exchange membrane fuel cell stack, regulator, Z-source inverter.

I. INTRODUCTION

In past few decades the worldwide energy demand has grown leaps and bounds causing more strains on the availability and sustainability of the naturally found energy sources. Current consumption rates of energy from non-renewable makes it doubtful to sustain beyond this century [1]. Also the main drawback with the conventional way of energy production is the carbon-di-oxide emissions. The global carbon-di-oxide emissions have been drastically increasing which can be seen from Figure 1 [2]. So as an alternative to enhance the energy production, distributed energy resources (DER) are introduced. Distributed energy resources are small, modular, energy generation and storage technologies that provide energy capacity when needed [3]. DER systems may be connected to either to the local electric power grid or can be used in stand-alone applications by isolating it from the grid. This technology includes wind turbines, photovoltaics, fuel cell, micro-turbines, cogeneration and energy storage systems. These can be used to delay, reduce or even eliminate the need to obtain additional power generation by conventional ways if needed. The DER system can provide power conditioning and also enhance reliability. But care should be taken to regulate the power flow as it consumes real and reactive power which may cause network instability. In [4], a power flow control for a single DER system was proposed. A typical structure of a grid integrated to various distributed energy resources system is shown in Fig. 2.

Among the DERs, natural-gas-fed fuel cell which generates electrical energy directly through chemical reactions assures a promising technology. Fuel cells can be classified into many types based on the type of fuel used, electrodes and also the

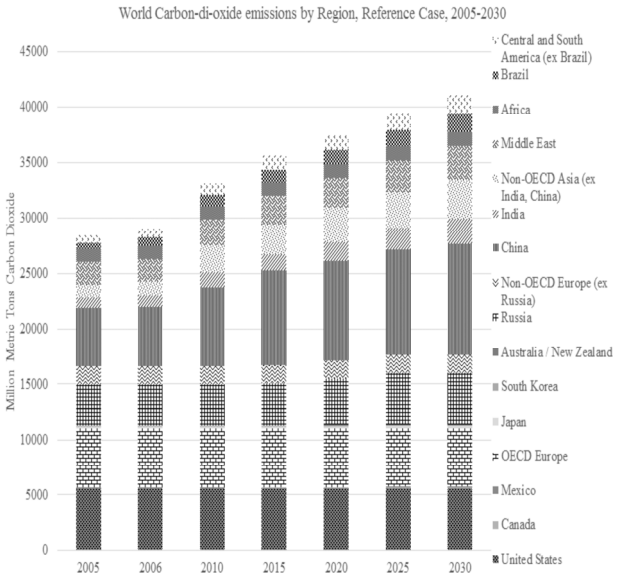

Figure 1. World CO_2 emissions by countries 2005-2030

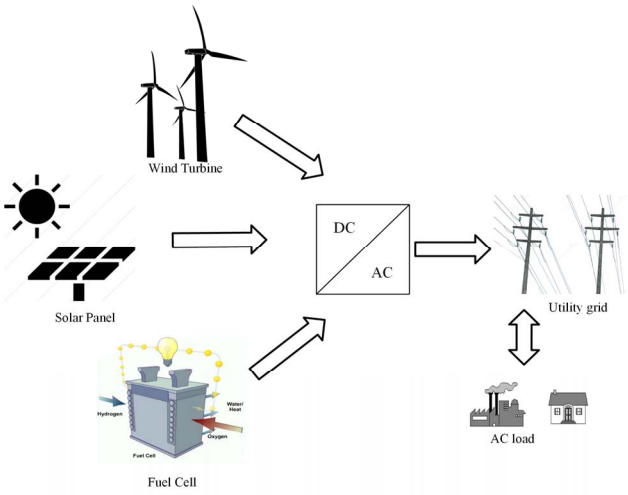

Figure 2. DER Electricity Paradigm

construction. In recent years, fuel cells finds its way to a lot of applications including stationary power sources, portable power sources, micro power sources and electric vehicles [5]. Also, one of the main quality of the fuel cell is that it doesn't have geographic limitations when compared to other DER

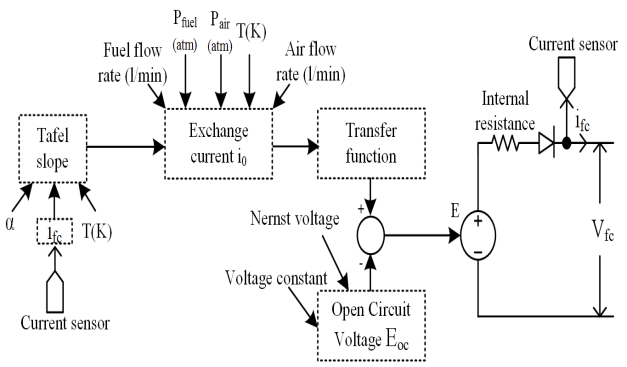

Figure 3. Fuel cell stack schematic representation

sources like solar and wind. But one of main drawback associated with fuel cells are that it's not effective in responding to load transients as fast as required because of its slow internal process. So to make the fuel cell work efficiently, researches have been made on the steady state and dynamic modelling of the fuel cell [6-9].

Even though fuel cell has advantages over the conventional means of power generation, the output voltage of a fuel cell stack is considerably low. So in order to meet the required grid or load voltage, a transformer or a power electronic converter must be connected as a medium between the fuel cell and the grid. When compared to transformers, characteristics like light weight, compactness and cost makes the power electronic converters to be more preferred for energy conversion. Therefore, in this paper two different power electronic converters, traditional boost converter and Z-inverter are connected to the fuel cell and the changes in the fuel cell characteristics, dc link voltage and the three phase ac-output voltage and current are studied for variable fuel flow rate condition.

II. Fuel Cell Modeling

Fuel cell being the topic of the study and comparing the different types of fuel cell, proton exchange membrane fuel cell (PEMFC) delivers high power density and also possess advantages like low weight and volume. Adding to the above mentioned advantages, PEMFC also shows great operating capability at low temperatures, which makes it easy to start and hence resulting in better durability. Also, PEM fuel cell uses hydrogen as a fuel which is processed at anode to general the electrical output for the system. As the byproduct obtained from the reaction is only water, this is found to be environment-friendly.

The fuel cell model used in this study is based on the generic fuel cell model developed in [10]. The detailed model of the fuel cell is considered so that the pressures, temperature, compositions and fuel flow rates can be varied. These variations affects the exchange current and the open circuit voltage of the fuel cell. Considering all these variations, in this simulation study the converters are designed to meet the load demands irrespective of the change in the fuel. A schematic representation of the model been used is shown in Fig.3.

Generally controlled fuel cell voltage is given by the equation [11]

$$E = E_{OC} - NA.\ln\left(\frac{i}{i_0}\right) \quad (1)$$

With the changes in pressure and flow rates, E_{OC}, i_0, A will be modified as:

$$E_{OC} = x.V_N \quad (2)$$

$$i_0 = \frac{zFk(P_{fuel} + P_{air})}{R.h}.\exp\left(\frac{-\Delta G}{RT}\right) \quad (3)$$

$$A = \frac{RT}{z\alpha F} \quad (4)$$

where,
E_{oc} – Open circuit voltage
N – Number of cells
A – Tafel slope (V)
i – Fuel cell current (A)
i_0 – Exchange current (A)
x – Voltage constant at nominal operating condition
V_N – Nernst voltage (V)
z – Number of moving electrons (=2)
F – 96485 A s/mol
k – Boltzmann's constant ($1.38*10^{-23}$ J/K)
P_{fuel} – Partial pressure of fuel (hydrogen) (atm)
P_{air} – Partial pressure of air (oxygen) (atm)
R – 8.3145 J/(mol K)
h – Planck's constant ($6.626*10^{-34}$ Js)
ΔG – Activation energy barrier (J)
T – Temperature (K)
α – charge transfer coefficient

III. Modulation Technique of Converters

This paper analyses the operation of traditional dc-dc boost converter and Z-source inverter. As lot of researches has been done on boost converter and its topologies, this section presents only the Z-source inverter topology and modulation technique that has been implemented for Z-source inverter. Z-source inverter [13] consists of an impedance network as shown in Fig. 4 with two inductors and capacitors connected in X-shape whose source can be either dc voltage or dc current. This inverter has multiple advantages over the traditional VSI and CSI. One such is its ability to operate both as buck and boost whenever needed. Also, Z-source can be used for all sorts of energy conversion.

Unlike VSI, Z-source has nine switching states (six active states when dc source is connected to the load, two zero states when load is shorted by the upper or lower switches in any one phase and an additional state when either two phases or all phases are shorted). This additional state which is also known as shoot-through state provides the buck-boost feature to the Z-source inverter. Also, the main advantage of this inverter is this inverter doesn't need any dead time protection i.e., turning any switch can be turned on irrespective of other turned on switches without damaging the circuit. But the challenge lies in inserting the shoot-through states to the inverter switches at

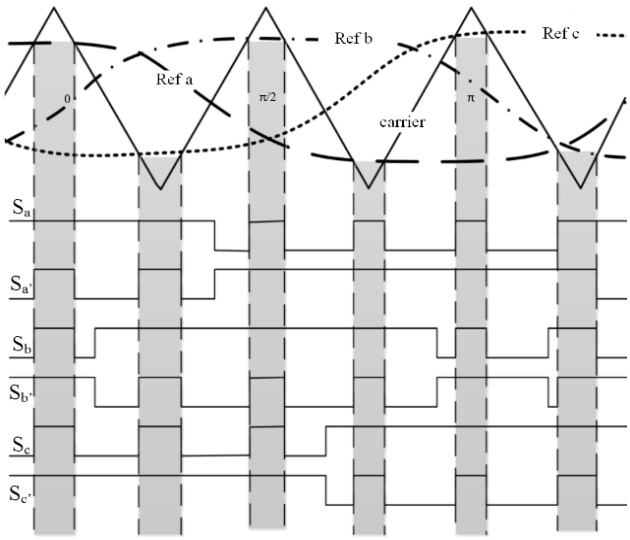

Figure 4. Maximum boost control switching

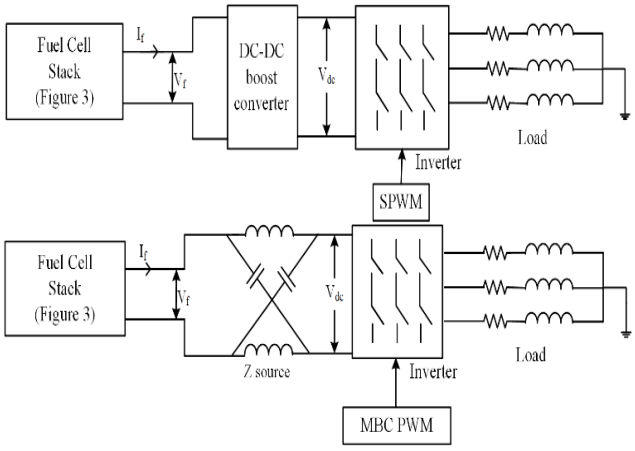

Figure 5. System under study (fuel cell stack represented in Fig.3)
Upper: Boost converter with traditional SPWM
Lower: Z-source inverter with MBC PWM

regular intervals. To insert the shoot-through, various modulation techniques like simple boost, maximum boost, maximum constant boost and modified space vector modulation technique has been proposed [13-16].

Among the modulation techniques, maximum boost control [16] provides maximum operating range for the converter. Hence this paper uses maximum boost control modulation scheme, in which the shoot-through states are inserted just by comparing the triangular wave with the reference waves. The six active states and two zero states operate in the same switching pattern as that of the traditional inverter. In addition whenever the triangular waves are greater or lesser than the positive or negative peak of the three phase reference waves, the circuit enters into shoot-through mode. A simplified diagram of the insertion of shoot-through and the activation of switches for maximum boost control method is shown in Fig. 4.

When choosing a particular modulation technique, parameters like shoot-through duty ratio, modulation index, boost factor, voltage gain and voltage stress has to be taken into account. For MBC, these parameters are designed based on [12], [13] and [16]. In order to obtain the voltage gain, the shoot-through duty ratio average value is calculated as it varies for each cycle. From Fig. 4 it can be seen that the shoot-through duty repeats every π/3. So the shoot-through duty ratio (T_0/T) for an interval (π/6, π/2) is given by,

$$\frac{T_0(\theta)}{T} = \frac{2 - (M\,sin\theta - M\sin\left(\theta - \frac{2\pi}{3}\right))}{2} \tag{5}$$

Integrating (5) within (π/6, π/2) to obtain average value,

$$\frac{\overline{T_0}}{T} = \frac{2\pi - 3\sqrt{3}M}{2\pi} \tag{6}$$

From (6), boost factor B can be calculated as mentioned in [12],

$$B = \frac{1}{1 - 2\frac{\overline{T_0}}{T}} = \frac{\pi}{3\sqrt{3}M - \pi} \tag{7}$$

The voltage gain is obtained by multiplying modulation index M with the boost factor B.

$$G = MB = \frac{\widetilde{v_{ac}}}{V_0/_2} = \frac{\pi M}{3\sqrt{3}M - \pi} \tag{8}$$

From boost factor, voltage stress V_s across the inverter switches can also be calculated by using,

$$V_s = \frac{\widetilde{v_{ac}}}{V_0/_2} \tag{9}$$

where,
$\widetilde{v_{ac}}$ – output ac peak phase voltage
V_0 – fuel cell output voltage

The modulation index and the boost factor determines the boosting level of the dc link voltage. For higher voltage levels, the shoot-through duty ratio has to be adjusted. However, the shoot-through duty ratio doesn't affect the normal operation of the inverter.

IV. Simulation Results

The schematic diagram of the system is shown in Fig. 5. The system comprises of fuel cell stack with the fuel flow regulator, boost converter or Z-source inverter implementing maximum boost and load. PEMFC being used for this study has a nominal operating power of 6kW. The stack is operated with at two fuel rates, 5lpm and 10lpm, which is regulated by the fuel flow regulator. Thereby, the hydrogen flow rate to the fuel cell stack is not maintained constant and is varied after a particular instant of time. With the different flow rate, the performance of the fuel cell stack with both the boost converter and the Z-source are investigated and the changes in the output of the fuel cell and DC link voltage are studied. The corresponding waveforms are presented in this section.

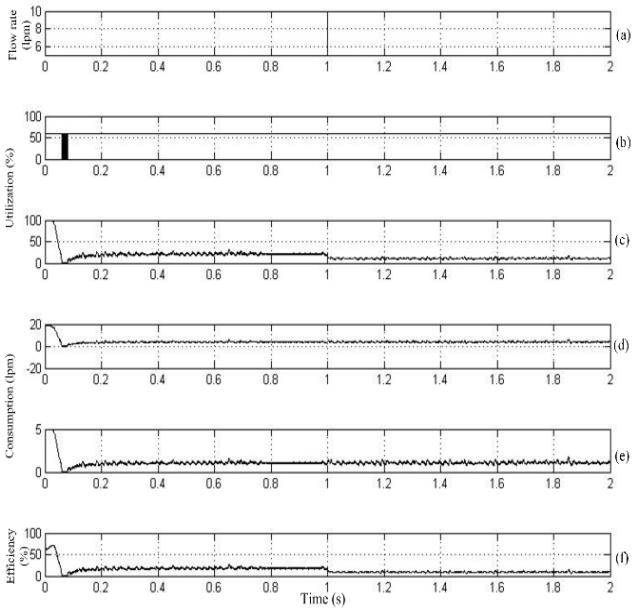

Figure 6. Fuel Cell Characteristics
(a) Fuel flow rate (lpm)
(b) Oxygen Utilization (%)
(c) Hydrogen Utilization (%)
(d) Stack Consumption [Air] (lpm)
(e) Stack Consumption [Fuel] (lpm)
(f) Stack Efficiency (%)

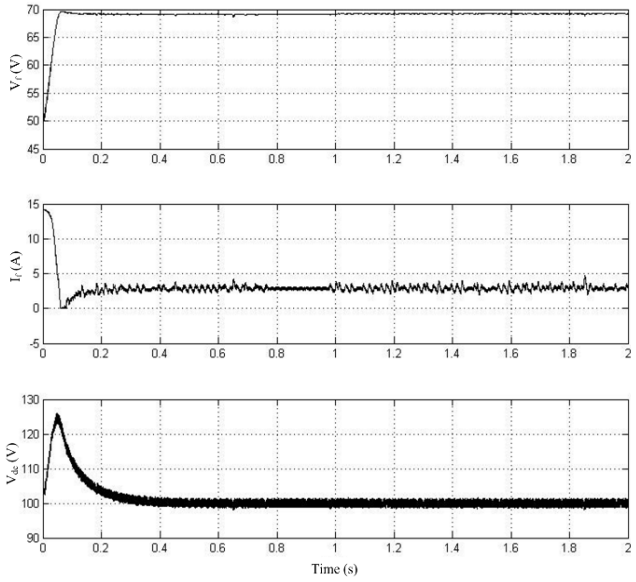

Figure 7. Output waveforms of fuel cell and dc-link
Top: Fuel cell output voltage
Middle: Fuel cell output current
Bottom: DC link voltage

A. Operation of fuel cell with boost converter

The fuel flow rate is initially maintained at 5lpm and changed to 10lpm after an instant of time. During the first 1 sec, the utilization of the hydrogen is maintained constant to a nominal value of 99.56% by a fuel flow rate regulator. After 1 sec, the fuel flow rate regulator is bypassed and the rate of the fuel utilization is varied which is shown in Fig. 6(a). Now the fuel flow rate is increased to 10lpm. Now the variation in the

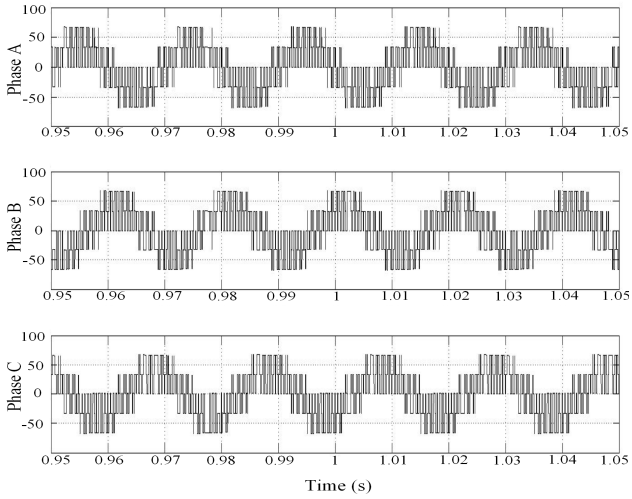

Figure 8. Three phase ac output voltages

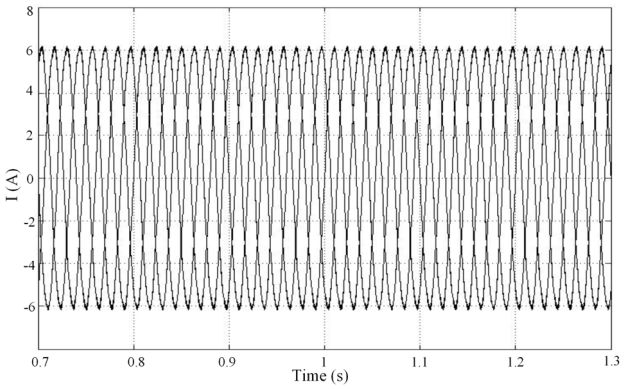

Figure 9. Three phase output currents

stack voltage is observed. The changes in the fuel utilization will definitely affect the stack efficiency, fuel consumption and the air consumption. With the increase in the fuel flow rate, the hydrogen utilization is also reduced. This causes an increase in the Nernst voltage thereby resulting in the decrease of the fuel cell current. Therefore the stack consumption and the efficiency of the fuel cell stack also decreases. The changes in utilization, consumption and efficiency of the fuel cell stack for different flow rates are shown in Fig. 6(b)&(c), (d)&(e) and (f) respectively. The change in the fuel flow rate has its impact only the fuel cell stack output. From Fig. 6(b), it can be observed that the utilization of the air goes to zero for some instant of time, which is reflected in the output current of the fuel cell. The output voltage, output current of the fuel cell and the dc-link voltage are shown in Fig. 7. Also, it can be observed that the dc-link voltage is maintained at 100V by the boost converter; thereby delivering the required power to meet the demand. The peak of 125V at the beginning of the dc-link voltage is mainly due to the transient effect of the regulator. The corresponding three phase inverter output voltages and current are shown in Figs. 8 and 9 respectively. The inverter outputs are uninterrupted even when there is a change in the fuel.

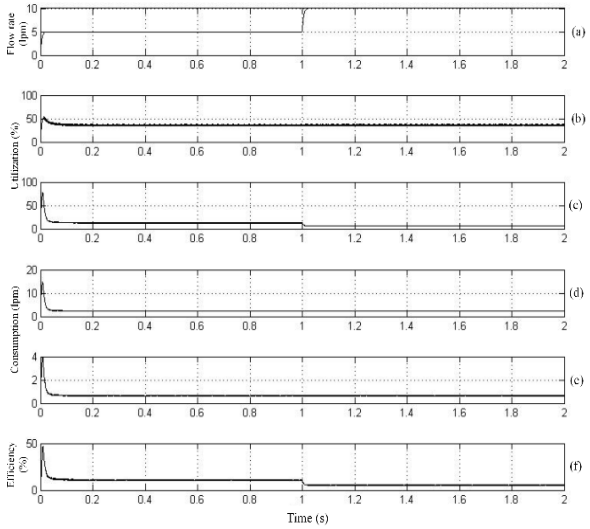

Figure 10. Fuel Cell Characteristics
(a) Fuel flow rate (lpm)
(b) Oxygen Utilization (%)
(c) Hydrogen Utilization (%)
(d) Stack Consumption [Air] (lpm)
(e) Stack Consumption [Fuel] (lpm)
(f) Stack Efficiency (%)

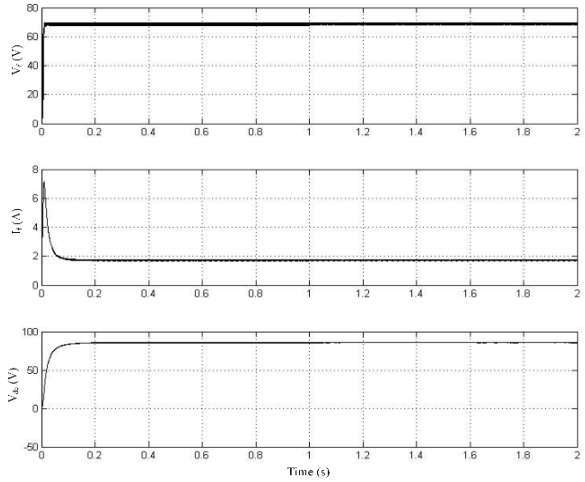

Figure 11. Output Waveforms of fuel cell and dc-link
Top: Fuel cell output voltage
Middle: Fuel cell output current
Bottom: DC link voltage

B. *Operation of fuel cell with Z-source converter*

In this section, the performance of the fuel cell stack and Z-source inverter with variable fuel flow rate is analyzed. As observed from Fig. 10, the change in fuel rate from 5lpm to 10lpm at 1 second of the simulation results changes the stack efficiency and % fuel utilization of H2 decreases as the load demand is not changed, and the fuel consumption does not get affected as the load demand is not changed. This illustrates that the fuel flow rate has to be controlled optimally for a given load demand to utilize the fuel cell efficiently. The changes in utilization, consumption and efficiency of the fuel cell stack for different flow rates are shown in Fig. 10(b)&(c), (d)&(e) and (f) respectively. The change in the fuel flow rate has its impact only the fuel cell stack output. Unlike boost converter, the utilization of the air doesn't goes to zero at any point of time, hence maintaining a steady fuel cell output current. The output voltage, output current of the fuel cell and the DC link voltage are shown in Fig. 11. The dc-link voltage doesn't have any peak at the beginning, proving that transient effect of the regulator is completely eliminated with Z-source converter. Also from Figure 11, the dc-link voltage is boosted to around100V by the Z-source converter; thereby delivering the required power to meet the demand. Z-source achieves the boosted voltage by utilizing less fuel to deliver the same output as that of the boost converter. The corresponding three phase inverter output voltages and current are shown in Figs. 12 and 13 respectively. From Fig. 12 and 13, with the amplitude and magnitude respectively remaining the same, it can be understood that Z-source inverter can maintain the output voltage and current irrespective of the change in the fuel rate.

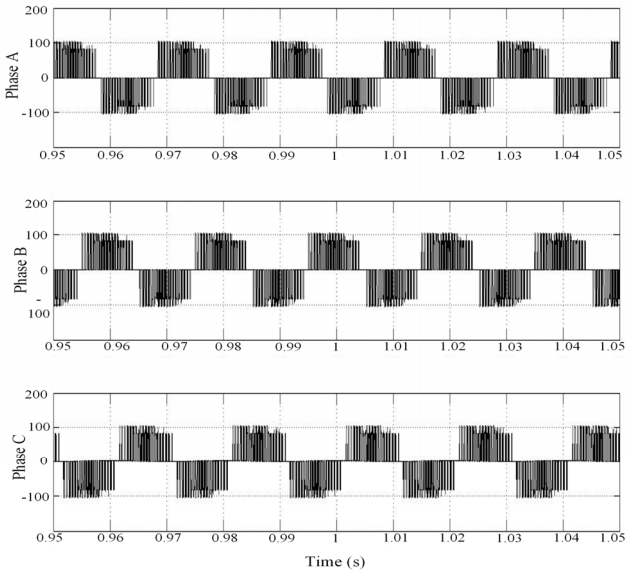

Figure 12. Three phase ac output voltages

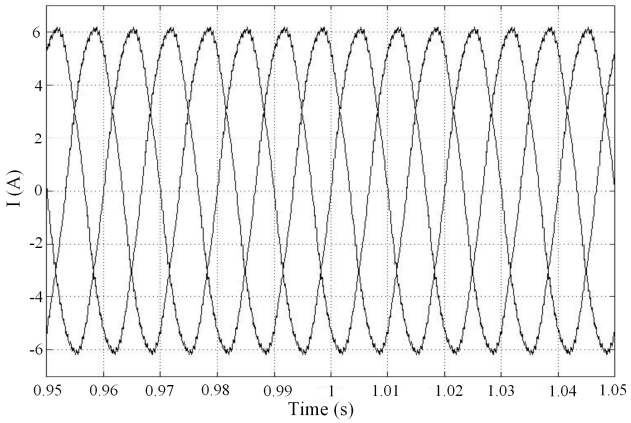

Figure 13. Three phase output currents

The performance results of the PEMFC stack with both the boost converter and also the Z-source converter under variable fuel flow condition is investigated and results are shown in Figs. 6, 7, 10 and 11. The fuel flow rate is increased from 5lpm

to 10lpm as seen from Fig. 6(a). The percentage of oxygen utilized in this report is maintained constant and only the utilization of the hydrogen is varied. The utilization of hydrogen in Figs. 6(c) and 10(c) decreases when the fuel flow rate is increased. This affects the efficiency in both of the fuel cell stack in both the cases as the efficiency is calculated based on the utilization of the fuels. From Figs. 7 and 11, it can be seen that the output voltage of the fuel cell and the dc link voltage remains unaffected.

V. CONCLUSION

This paper presents the performance evaluation of traditional boost converter and the Z-source inverter for variable fuel flow rate. From the results obtained, it is evident that the boost converter and the Z-source converter deliver the same voltage irrespective of the change in the fuel flow rate. But from the results, it can be seen that the peak voltage of $125V_{dc}$ is noticed at the beginning of the simulation in boost converter which is due to the transient effect of the voltage regulator. But Z-source converter because of the capacitor networks eliminates the peak and provides smooth transition. Z-source network provides same voltage boost as that of the boost converter by utilizing less fuel. Also, with the advantage of Z-source converter like the voltage level can be increased to any higher level by adjusting the shoot-through duty ratio, which is restricted in boost converter, makes it a promising choice for distributed generation system.

ACKNOWLEDGMENT

The authors gratefully acknowledge the support provided by Energy Research Institute at NTU (ERI@N) for this work.

REFERENCES

[1] R. Anderson. [Online]. Available: http://www.resilience.org
[2] Energy Information Administration. [Online]. Available: http://rainforests.mongabay.com/09-carbon_emissions.htm
[3] (2014) N.R. Friedman. [Online]. Available: http://www.nrel.gov
[4] M. Dai, M. N. Marwali, J. W. Jung and A. Keyhani, "Power flow control of a single distributed generation unit" *IEEE Trans. Power Electronics*, vol.23, no.1, pp.343-352, Jan. 2008.
[5] K.Y. Lee, "The effect of DG using fuel cell under deregulated electricity energy markets," *IEEE Power Engineering Society General Meeting, 2006.*
[6] C. E. Chamberlin, "Modeling of proton exchange membrane fuel cell performance with an empirical equation," *J. Electrochem. Soc.,* vol. 142, no. 8, pp. 2670–2674, Aug. 1995.
[7] R. Cownden, M. Nahon, and M. A. Rosen, "Modeling and analysis of a solid polymer fuel cell system for transportation applications," *Int. J. Hydrogen Energy*, vol. 26, no. 6, pp. 615–623, Jun. 2001.
[8] J. C. Amphlett, R. F. Mann, B. A. Peppley, P. R. Roberge, and A. Rodrigues, "A model predicting transient responses of proton exchange membrane fuel cells," *J. Power Sources*, vol. 61, no. 1–2, pp. 183–188, Jul./Aug. 1996.
[9] J. Hamelin, K. Agbossou, A. Laperrière, F. Laurencelle, and T. K. Bose, "Dynamic behavior of a PEM fuel cell stack for stationary applications," *Int. J. Hydrogen Energy*, vol. 26, no. 6, pp. 625–629, Jun. 2001.
[10] S. M. Njoya, O. Tremblay and L. -A. Dessaint, "A generic fuel cell model for the simulation of fuel cell vehicles", *Proc. VPPC*, Sept. 7–10, 2009, pp. 1722–29.
[11] J. Larminie and A. Dicks, *Fuel Cell Systems Explained*, 2nd ed. John Wiley and Sons Ltd.
[12] M. M. Roomi and A. I. Maswood, "Investigation of Z-source inverter for fuel cell system in a zero energy building," in *Proc. ICDRET,* 2014.
[13] F. Z. Peng, "Z-source inverter", *IEEE Trans. Industry Applications,* vol. 39, no.2, pp. 504-510, March/April 2003.
[14] S. Miaosen, W. Jin, A. Joseph, F. Z. Peng, L. M.Tolbert, D. J. Adams, "Constant boost control of the Z-source inverter to minimize current ripple and voltage stress" *IEEE Trans. Industry Applications*, vol.40, pp. 770-778, 2006.
[15] K. Yu, F. L. Luo, M. Zhu, "Space vector pulse-width modulation based maximum boost control of Z-source inverters," *IEEE ISIE*, pp.521,526, 28-31 May 2012.
[16] F.Z.Peng, S. Miaosen, Q. Zhaoming, "Maximum boost control of the Z-source inverter", *IEEE Trans. Power Electronics*, vol. 20, pp. 833-838, 2005.

Incorporating the Institutions' Perspective into a Proposed Model for Assessing Success of Solar Home System Implementations

Hans Holtorf, Tania Urmee, Martina Calais, Trevor Pryor
School of Engineering and Information Technology
Murdoch University
Murdoch, WA, 6150 Australia
h.holtorf@murdoch.edu.au *(corresponding author)*

***Abstract*—Solar Home Systems can supply basic electricity services in Sunbelt countries. About 20 % of the world's population lack of access to these services. A preliminary model to evaluate the success of a SHS implementation has been proposed previously. The views of a range of institutional stakeholders related to SHS were explored by problem centered interviews and by participatory observation. An improved model of success is developed which is capable of providing a quantitative measure of success for SHS implementations. Five groups of key stakeholders have been determined. The most important self-set goals for the institutional stakeholders are profit, quality and social benefit. The most important success factors that encourage the achievement of self-set goals were retrieved and are discussed. Measuring the level of achievement of the defined self-set goals is the largest challenge in this process. The refined model of success demonstrates the complexity of measuring the success of Solar Home System implementations. The next phase of the research is to survey the Users' views on the SHS's success.**

Keywords—Success; Solar Home System (SHS); SHS key-stakeholder.

I. INTRODUCTION

Electricity services contribute to the reduction of poverty and to human development. Of the approximately 7 billion inhabitants of the world, 20 % do not have access to electricity [1] and for many of these, electrification by grid extension is very costly. Wiedemann gives figures in the range of USD 1,200 for an urban grid connection and USD 2,000 for a rural grid connection in developing countries [2]. In terms of required rural electricity services Adkins et. al. list illumination, telecommunication (mobile phone operation) and information (radio & TV) as the key demands, none of which require large amounts of electricity [3]. The costs of grid connection for many of these potential electricity Users, combined with their low electricity consumption, make this approach a cost-ineffective option [4].

To meet the low electricity demand of remote households in developing countries, the Solar Home System (SHS) has been proven to be a cost effective solution for such dispersed potential Users and is being widely used for off grid electrification [5]. Solar Home Systems (SHSs) have been implemented since the 1980s [6, 7] and have also proven themselves to be a reliable solution [8]. Additionally, the success and failure of SHS projects has been investigated, e.g. by Urmee [9]. Asif and others report that Bangladesh's SHS regime is the most successful at present [10]. It seems that there is a lack of tools available to measure the overall success of a SHS implementation. The measurement of implementation success would provide a feedback loop to improve future activities in this area. The importance of such a tool is justified by the desire of project implementers and donors to improve their performance. For example, the Paris Declaration on Aid Effectiveness includes a desire to see improvement in the delivery of such aid projects [11].

This research addresses the question of how to measure the success of a SHS implementation. To date, isolated indicators such as the number of SHSs installed, the SHSs in operation as compared to the total number of SHSs installed, or the Users' satisfaction have been applied to measure the success of SHS implementations [12]. In an earlier phase of this research, a model of success was developed based on literature review and personal experience [13].

This model of success addresses the success of key-players involved in the implementation of SHSs. Thereby success is defined as the achievement of self-set goals. It is assumed that players engaging in SHS have different self-set goals (SSG). These SSG have different importance and they have different levels of achievement (LoA). To grade the success of a SHS implementation the weighed arithmetic mean of the importance of SSGs (I_{SSG}) and the LoAs determine the overall success ($Success_{impl.}$):

$$Success_{impl.} = \frac{\sum_{i=1}^{o} I_{SSG_i} \cdot LoA_{SSG_i}}{\sum_{i=1}^{o} I_{SSG_i}} \qquad (1)$$

Various players are involved in the SHS environment. They can be grouped into institutional players and into Users of SHSs. Institutional players deal with SHSs on different levels and for multiple reasons, e.g. technology optimization or economic feasibility. By contrast Users of SHSs invest in these systems for private purposes.

This paper explores the institutions involved in SHSs and presents their views relating to the success of SHS implementations. In this research the concept of Freeman on stakeholders is applied for the classification of the respective players [14]. The results of this exploration of institutional stakeholders are then incorporated into the existing model of success to generate an improved model.

After setting the scene for this work in this section, the paper proceeds to discuss the methodology (Section II). The *RESULTS AND DISCUSSION* section discusses the responses of the questioned participants on each section of the model of success (SSG, I_{SSG}, success factors and LoA), with conclusions being drawn that can be taken forward to the development of an improved model (Section III). Thereafter an improved model of success is presented and discussed (Section IV), and finally conclusions are drawn and the necessary next steps for this research are outlined (Section V).

II. METHODOLOGY

After the development of the abstract model of success it was necessary to determine the real world elements within the sections of the model of success. The research being in the stage of development of a model (a model is the representation of objects and processes [15]) therefore applies qualitative methods [16]. The paper's focus is on institutions dealing with SHSs. Problem centered interviews (PCI) [17, 18] and participatory observation (PO) [19] were applied to best adapt to the participant's capability of communicating meaningful content [20, 21]. The research directs the attention towards a broad exploration on elements necessary for the modelling of success rather than on the statistical coverage of known elements. Therefore 12 respondents were selected covering a wide range of institutional experience on SHSs. TABLE I gives an overview of the target respondents. They were grouped into three categories based on the nature of their involvement in the implementation of SHSs.

PCIs were conducted with most of the participants. A guiding diagram based on the model of success was presented to the interviewees with the following guiding questions:

- Who are the key-stakeholders in the SHS environment?
- What are SHS related self-set goals of the interviewee's institution?
- How important are these goals (please rank from 1 to 5)?
- What are the success factors (SF) to achieve the self-set goals and what are their weights?
- How do you measure the level of achievement of the self-set goals?
- What are further challenges related to success of SHSs?

The interviewees were requested to narrate on the items shown on the model diagram (the key-stakeholders, self-set goals of their institutions, their importance and so on). Key-words and key-sentences were noted on this diagram by the interviewer while he confined himself to focus on the key questions of the interview and to clarify uncertainties within the narration. In parallel the interview was audio recorded.

TABLE I. RESEARCHED RESPONDENTS

Group	Notes	Range of Operation
International Supply Chain	2 manufacturers (PCI)[c] 2 system integrators[a] (PCI)[c]	International
National Supply Chain	2 system implementers[b] (PCI)[c] 2 local entrepreneurs (PO)[c]	National
Donors and Consultants	2 donors (PCI)[c] 2 consultants (PCI)[c]	International

a. System integrators design systems from components on the intl. market and disseminate them on the intl. market.

b. System implementers design systems from components on the natl. and intl. market and implement those systems on the national market.

c. PCI = Problem Centered Interview, PO = Participatory Observation

The PO approach was applied to the local entrepreneurs since they had difficulties in reading, writing, and dealing with modern technology and abstract graphs. The researcher accompanied an installation team during the realization of an entire SHS installation project. A local dealer, who supplied automotive spare parts, electrical appliances for households, and components for SHSs as well as complete Solar Home Systems, was observed for an entire day in his shop while he was dealing with his customers. The observations from the PO activities were documented in a notebook in order to reduce the biasness due to behavior modification triggered by modern observation technologies.

III. RESULTS AND DISCUSSION

The following sections present the results from the first five key questions outlined above in section *METHODOLOGY*. Each sub-section focusses on a key question and provides the results of the research with the respondents (PCI and PO), a discussion of these results, and some summarizing conclusions derived from this discussion.

A. Key-Stakeholders

The first information sought from the respondents was on the key-stakeholders in the SHS environment. Fig. 1 shows the result. The respondents identified 16 different stakeholders in the SHS environment. The most important stakeholder is the *local entrepreneur* followed by the *national system implementers*, the *users*, the *intl. donors* and so on.

Fig. 1 also shows stakeholders which were mentioned by multiple respondents and stakeholders which were mentioned only by a minority of respondents. It was decided that stakeholders mentioned by at least 25% of the participants to be key-stakeholders. However, due to the discussion below some single nominations were included to the final list of key-stakeholders in TABLE II.

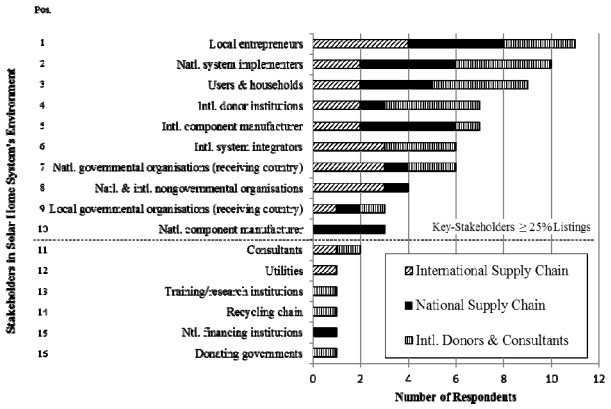

Fig. 1. Key-stakeholders in SHS environment listed by institutions.

At least one member in each of the 3 responding groups listed in TABLE I agreed that positions 1-5, 7 & 9 in Fig. 1 are stakeholders related to SHSs. It was noticed that *international system integrators* (pos. 6), *national and international nongovernmental organizations* (pos. 8), and *national component manufacturers* (pos. 10) were not recognized by all groups as stakeholders. This indicates that these potential stakeholders are of minor importance to those particular interviewed groups. Only 75% of the respondents mentioned *users* as a stakeholder. However, in most of the literature users are referred to as an important, if not the major stakeholder [12, 22]. All respondents from the *national supply chain* mentioned the *international manufacturers* as key-stakeholders indicating that SHSs often cannot be implemented without international products. *Training/research institutions* and *national financing institutions* were listed by a minority of respondents. However, literature mentions lack of these items as barriers to successful SHS implementation [23]. The *recycling chain* for lead acid batteries was a major issue in the past [24] but it was mentioned by only 1 respondent.

TABLE II. FIVE GROUPS OF KEY-STAKEHOLDERS

Group	Stakeholders
International Supply Chain	Intl. component manufactures[a] Intl. system integrators[a]
National Supply Chain	Local entreprepreneurs[a] Natl. system implementers[a] Natl. component manufacturers[a]
Donors	Intl. donor institutionsa
Other Institutions	Natl. governmental organizations[a; c] Natl. & intl. nongovernmental institutions[a] Local governmental organisations[a] Training/research institutions[b] Recycling chain[b] Natl. financing institutions[b]
Users	Users and households[a]

a. Included as no. of nominations > 25%

b. Included because of the importance highlighted in the discussion

c. Natl. governmental organizations refer to organizations in receiving countries.

B. *Self-Set Goals and Importance of Self-Set Goals*

Next the respondents were queried about the SSG and the I_{SSG} of their particular institution. Twenty different SSGs were identified and their importance was attributed by the respondents on a scale of 1 to 5. The totals for all the groups were also summed and the results of this section are depicted in Fig. 2.

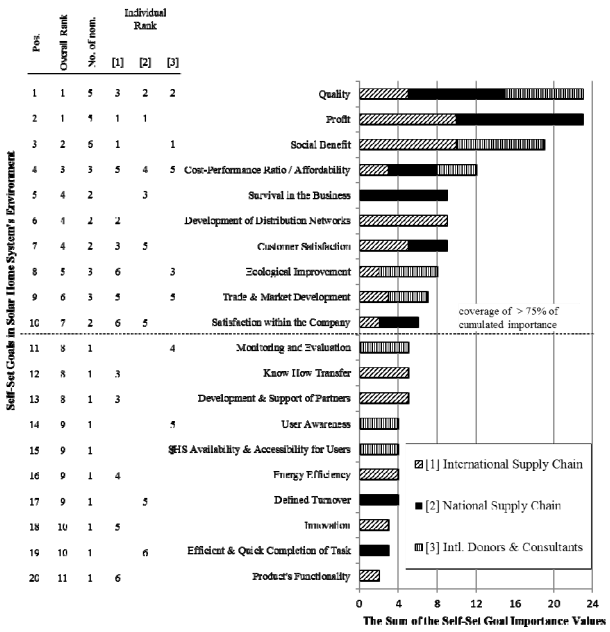

Fig. 2. Group's self-set goals ranked by the sum of the self-set goal importance values.

As shown in Fig. 2 *profit* and *quality* were ranked as the most important SSG and *product's functionality* was ranked as the least important SSG. *Quality* was explained as the capability to serve for a long period without fault, while *functionality* was understood as a SHS having many features. *Social benefit* (less indoor pollution, brighter light, improved communication and leisure by cell phone, radio and TV) was ranked as the most important SSG by the *international donors and consultants*. *Social benefit* was also given high priority by the *international supply chain*.

Some SSGs are quantifiable and their LoA is measurable in numbers whereas others are qualitative (not distinguished in Fig. 2). An example are *profit* and *customer satisfaction* respectively. According to Schmalen et. al. both types of self-set goals and their measurement are important for success analysis [25].

SSGs exist which are listed exclusively by a single group of respondents. *Survival in the business* was exclusively listed by the members of the *national supply chain*; while the *international supply chain* group members exclusively listed the *development of distribution networks* (both rank 4 in Fig. 2). This behavior correlates to the explanations on success stating that views on success are specific to the position of the enterprise in the market [26].

The distinction between a self-set goal and a success factor (SF) is difficult and under specific circumstances impossible.

In the discussion of the model of success some respondents would categorize certain items as self-set goals while the same items were rated as SFs by other respondents. Quality is an example of an item that was considered both as SSG and SF. The top ranking of quality as a SSG reflects the respondents' awareness of this issue. Quality was listed as a very important SF for enterprises [27]. Literature on SHSs confirms the correlation of quality and success [8, 28, 29].

The international donor institutions and consultants are in a different position than the natl. and intl. supply chain. Donor institutions pointed out that they play the role of executing implementers on behalf of commissioning organizations, e.g. a donating government. The goals of international donor organizations would therefore be highly influenced by the commissioning organizations. In the interviews, no SSGs were listed by the international consultants; they mainly focused on SFs of SHSs.

It was concluded that the most important SSGs in the SHS environment are those within the top 75% of the overall cumulative importance values (see Fig. 2). This limit excludes individual nominations or multiple nominations given, but with low values for the importance of the nominations. Next, the summed importance of SSGs for each group of key-stakeholders (TABLE I) is used for the selection of the most important SSGs for that group. The groups' goals are ranked by the total of the group's importance values and the ranks 1 and 2 are then selected as the most important SSGs. The procedure recognizes the absolute importance of SSGs given by multiple stakeholders or a very high importance given by individual stakeholders and it considers the views of the stakeholder groups on their SSGs with highest importance.

TABLE III. MOST IMPORTANT SELF-SET GOALS FOR THE INSTITUTIONAL KEY-STAKEHOLDER GROUPS

Group	Ranked Self-Set Goals
International Supply Chain	1. Profit; social benefit and its facets 2. Development of distribution network
National Supply Chain	1. Profit 2. Quality
Intl. Donors	1. Social benefit and its facts 2. Quality

C. Success Factors

In the next step of the query, the participants were requested to list the SFs related to their SSGs and to weigh these according to their importance. In the model of success, SFs have a significant impact on the LoA

of SSGs. Many articles have discussed the idea of SFs on general success, e.g. [25, 26, 30] and on SHS success [10, 31]. A number of conclusions can be drawn from the interaction with the respondents on success factors.

Success factors can be categorized in a number of ways, for example by:

- their sphere of impact (which stakeholders are affected?),
- their controllability (are SFs endogenous or exogenous),
- their impact nature (do the SFs impact on one or on several goals, are they general SFs?)
- their interconnectedness (does a variation of one SF impact on another SF?)
- their compensability (how far can an unmet SF be compensated for by other factors?) and
- their dependency on specific situations (are the SFs generally valid or do they only hold in a specific situation?).

According to the results of the survey and the literature review, some key general SFs for Solar Home Systems were determined:

- quality of systems and services;
- balancing of the costs and the quality of systems and services in order to ensure affordability and long term operation;
- communication across all stakeholder groups and on all levels;
- education and training on all levels;
- solving the existent causality dilemmas in the SHS environment;
- the uniqueness of stakeholders;
- contextualization on multiple levels.

In summary, numerous SFs are critical to the process of assessing the success of SHS implementations. The above mentioned SFs will be added in the final model of success.

D. Measurement of the Level of Achievement

The last part of the survey focused on the measurement of the LoA of SSGs. For the respondents this proved to be the most difficult element of the presented model.

The determination of the LoA often depends on a quantitative measurement (e.g. 1000 SHSs installed in one month). The measurement scale for such a LoA can be time and situation dependent. SSGs are prone to change for multiple reasons which impacts on the measurement of the LoA. For example, one interviewee reported on the development of a new market (storage equipment for grid connected PV systems) which had reduced the importance of the initial SHS market for his company. As a consequence of such influences, the focus of a company may change. The initial SSG is modified, the measurement scale for excellent is revised, and, in the instance mentioned above, reduced. An opposite effect can also be observed.

SSGs may have quantitative or qualitative properties. Quantitative SSGs may be evaluated linearly, exponentially/logarithmically or by threshold. A quantitative, SSG linked to a threshold of a local installer was to finalize an installation, including travelling efforts, within one day. If achieved, this would render the grading *excellent*. Not finalizing the task within one day would be graded *failure*.

The achievement of a certain turnover of systems or components is another version of a quantitative SSG. However, the manner in which this is measured in terms of LoA can vary. Consider a situation where the SSG is to install 1000 SHSs in a month, and assume that, in practice, 900 systems were installed in a particular month. One respondent used a simple linear approach in assessing this and gave a LoA of 90%. In an exponential approach the LoA would render 63%, in a logarithmic approach the LoA would be 98%. The calculation process for assessing the LoA of such quantitative goals needs to allow for such different approaches.

Qualitative SSGs are either measured indirectly by a derived variable or merely by subjective judgement. Two interviewees listed the qualitative SSG *satisfaction in the company* which can be measured indirectly by the time employees stay in a company before they seek to apply for other employment. The problem in the case of gauging the LoA of a purely qualitative SSG is the reduced comparability to other stakeholders or projects, because of the subjective nature of the assessment.

A respondent pointed out that the LoA can only be given with very coarse resolution. The use of such a coarse scale may assist in ensuring some uniformity in comparing different projects or implementations, because results could be more amenable to being judged in a similar manner. It may provide a useful way to quantify the LoA of quantitative and qualitative SSGs. The approach provided by this respondent was incorporated into the model. In order to be consistent with the maximum grading of "five", which is used for the weight of the success factors and the importance of SSGs, and in order to reflect failure by a "zero", we propose: 5=excellent / fully achieved, 4=good, 3=satisfactory, 2=poor, 1=very poor and 0=failure. Thereby we accept the inconsistency of having a six tier system as compared to the five tier system for the grading of the success factors and SSGs, in order to allow the value of 0 for failure.

This section has indicated the different approaches that participants can take in assessing the achievement of goals. Irrespective of different individual metrics used, stakeholders need to apply the six tier scale as above for their levels of achievement in order to apply a common scale across all LoA values and to make the model of success work.

The conclusions from this part of the participant's interrogation are:

- the measurement scale for the LoA is time and situation dependent;
- quantitative and qualitative measurement indicators exist;
- stakeholders can apply different measurement scales for both quantitative and qualitative indicators;
- the measurement resolution, in terms of LoA, needs to be rather coarse because of the difficulty in providing "exact" measurements of many of these levels of achievement;
- the evaluation of the achievement of SSGs depends on the type of SSG (quantitative versus qualitative) and on the specific stakeholder;
- in order to apply the model of success, stakeholders need to provide a numerical grading of the LoA;
- we propose a six tier numbering system with 5=excellent and 0=failure.

However, some flexibility in gauging the SSGs and/or the LoA of these goals throughout the course of a project must be built into the model due to the volatility of SSGs over time.

IV. The Improved Model of Success

Based on the results of the research described in this paper, the original model of success described in [13] has been improved. Key-stakeholders have been determined, specific SFs have been detected, and general key features of SFs have been explained. In addition, the challenges of measuring the LoA have been highlighted. Fig. 3 depicts the improved model of success. The modifications compared to the initial model of success are highlighted and described below.

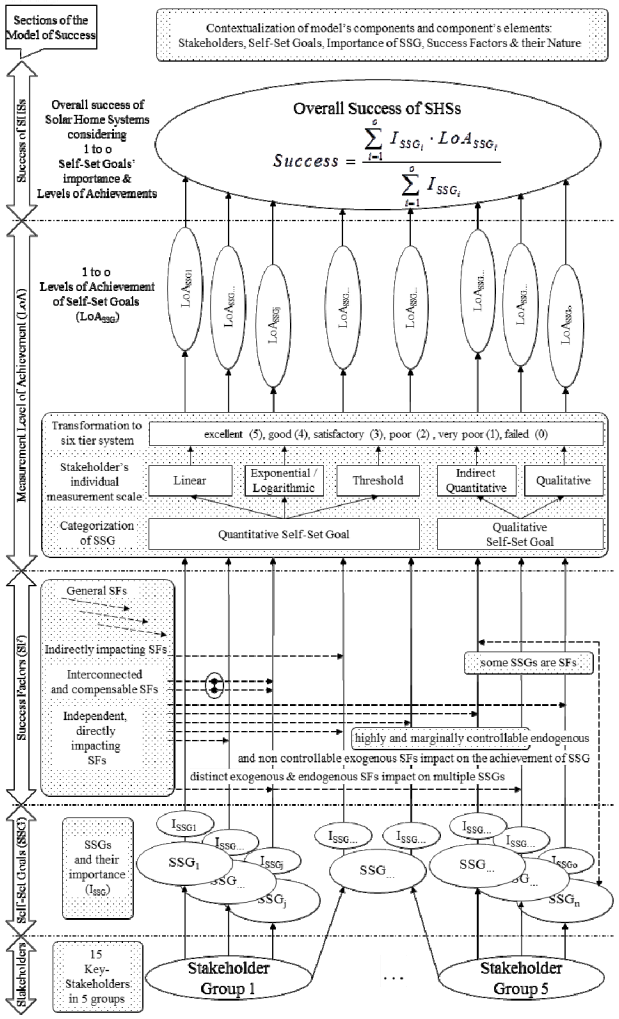

Fig. 3. Improved model of success.

Five stakeholder groups and their members, as stated in TABLE II, are incorporated in the improved model of success.

Manifold self-set goals were listed by respondents. From this the most important SSGs were derived (TABLE III).

Success factors have been sorted into general, indirectly impacting, and independent, directly impacting SFs. They may be of endogenous (highly or marginally able to be influenced by stakeholders) or of exogenous nature (not influenceable). Some SFs impact on the achievement of distinct, others on multiple SSGs. In addition, the SFs may be interconnected. To a certain extent the stakeholder may be able to compensate for an interconnected SF by focusing on the other SFs that are linked to it.

Some SSGs can be SFs – for example quality.

The measurement of the level of achievement remains a major challenge: for one, stakeholders' SSGs may change over time. Then, self-set goals need to be sorted into quantitative and qualitative SSGs. Next, stakeholders internally decide on the evaluation scale (linear, exponential/logarithmic, and threshold) for the quantitative SSGs, and on indirect quantitative indicators for the qualitative SSGs. Finally, stakeholders are required to transform their grading into the six tier system of the model of success with an excellent LoA equaling a grading of 5, a failure equaling a grading of 0 and the four levels in between respectively.

A formula is used in Fig. 3 to calculate a final quantitative value for the success of a SHS implementation which represents the weighted arithmetic mean of the importance of the self-set goal's I_{SSG} values, with the weighting provided by the level of achievement of these goals LoA_{SSG}.

A superordinate level is the contextualization. The note on contextualization in Fig. 2 reminds the model's user that all of the elements within the model's components are situation, location and time dependent. Therefore, the components need to be carefully defined for each SHS implementation considered, although it would be expected that some of the components would be common to many SHS implementations.

V. Conclusion and Outlook

Measuring the success of Solar Home System implementation is very complex. A multidimensional construct is necessary for the appraisal of success. This study has resulted in a methodology to evaluate the success of Solar Home System implementation by proposing a model of success. The research addresses the components of this model and their linkages. The considerations necessary when examining the model's components have been described.

This explorative research gives a starting point for the application of the model of success when investigating the success of institutions involved in the dissemination of SHSs. For the application of the model quantitative methods will be applied to determine success of SHS implementation.

This model of success can be applied to different SHS dissemination approaches to allow comparison of the successfulness of these different implementations. Likewise it can be used to observe the development of success in a particular SHS implementation by applying it at different points in time in the project cycle. Last but not least, the model includes the individual stakeholders' level of success, and so can be applied to each stakeholder individually.

This model of success will need continuous adaptation as SHSs and their appliances undergo further development. Some elements of the model of success may vanish while new elements may appear.

Human Research Ethics

This research was approved by the Human Research Ethics Committee of Murdoch University. The approval was granted under the Project Number 2012/076, Project Title: "Success factors of rural electrification through Solar Home Systems in developing countries using African case studies".

Acknowledgment

This research is financially supported by the School of Engineering and Information Technology at Murdoch University, Western Australia, and the International Relations Office at University of Oldenburg, Germany, through scholarships. It has also been supported by a Fellowship for Tania Urmee at the Hanse-Wissenschaftskolleg in Delmenhorst, Germany.

References

[1] IEA. (2012, 16.06.2012). The electricity access database. Available: http://www.iea.org/weo/electricity.asp

[2] K. Wiedemann. (2012, 24.01.2015). Electrification Challenges in Rural Areas. Available: https://energypedia.info/wiki/Electrification_Challenge_in_Rural_Areas

[3] E. Adkins, K. Oppelstrup, and V. Modi, "Rural household energy consumption in the millennium villages in Sub-Saharan Africa," Energy for Sustainable Development, vol. 16, pp. 249-259, 9// 2012.

[4] W. Fulkerson, M. D. Levine, J. E. Sinton, and A. Gadgil, "Sustainable, efficient electricity service for one billion people[1]," Energy for Sustainable Development, vol. 9, pp. 26-34, 6// 2005.

[5] S. Bhattacharyya, Rural Electrification Through Decentralised Off-grid Systems in Developing Countries: Springer, 2013.

[6] K. Pertz, Nutzung erneuerbarer Energiequellen in Entwicklungsländern vol. 89. Bonn: Bundesministerium für wirtschaftliche Zusammenarbeit, 1988.

[7] R. Acker and D. Kammen, "The quiet (energy) revolution. Analyzing the dissemination of photovoltaic power systems in Kenya," Energy Policy, vol. 24, p. 31, 1996.

[8] F. D. J. c. a. Nieuwenhout, v. A. Dijk, P. E. Lasschuit, v. Roekel, G, v. V. A. P. Dijk, D. Hirsch, et al., "Experience with Solar Home Systems in Developing Countries: A Review," Progress in Photovoltaics: Research and Applications, vol. 9, 2001, p. 20, 2001c.

[9] T. Urmee, "Solar PV electrification programs in developing countries : towards an holistic approach," PhD, Faculty of Minerals and Energy, Murdoch University, Perth, 2009a.

[10] M. Asif and D. Barua, "Salient features of the Grameen Shakti renewable energy program," Renewable and Sustainable Energy Reviews, vol. 15, pp. 5063-5067, 12// 2011.

[11] OECD, "The Paris Declaration on Aid Effectiveness and the Accra Agenda for Action," OECD2009.

[12] S. Komatsu, S. Kaneko, P. P. Ghosh, and A. Morinaga, "Determinants of user satisfaction with solar home systems in rural Bangladesh," Energy, vol. 61, pp. 52-58, 17.05.2013 2013.

[13] H. Holtorf, T. Urmee, M. Calais, and T. Pryor, "A model to evaluate the success of Solar Home Systems," Renewable and Sustainable Energy Reviews, vol. 50, pp. 245-255, 10// 2015 a.
[14] R. E. Freeman and J. McVea, Strategic Management: A Stakeholder Approach. Boston: Pitman, 1984.
[15] P. Atteslander, "Operationalisierungsvorgang," in Methoden der empirischen Sozialforschung, ed Berlin, Germany: Schmidt Verlag, 2008, pp. 33-36.
[16] S. Lamnek, Qualitative Sozialforschung. Weinheim, 2006.
[17] L. Van Audenhove, "Expert interviews and interview techniques for policy analysis," I. a. T. SMIT Studies on Media and I. I. I. o. B. Technology, Eds., ed. Brussel: Vrije Universiteit Brussel, 2007.
[18] H. A. Mieg and B. Brunner, "Experteninterviews," ed. Zuerich, Switzerland: ETH Zuerich,, 2001, p. 33.
[19] N. Mack, C. Woodsong, K. MacQueen, G. Guest, and E. Namey, "Module 2 Participant Observation," Family Health International (FHI)2005.
[20] P. Mayring. (2002, 10.03.2014). Einführung in die qualitative Sozialforschung. Eine Anleitung zu qualitativem Denken (Oelkers, Jürgen; Hurrelmann, Klaus ed.).
[21] M. Sewell. (2014, 25.08.2014). The Use of Qualitative Interviews in Evaluation. Available: http://ag.arizona.edu/sfcs/cyfernet/cyfar/Intervu5.htm
[22] C. Hellpap, "Kernherausforderungen beim Aufbau ländlicher Verbreitungssysteme für Pico PV Systeme," presented at the Im Abseits der Netze, Bonn, 2011.
[23] C. A. Friebe, P. v. Flotow, and F. A. Täube, "Exploring the link between products and services in low-income markets—Evidence from solar home systems," Energy Policy, vol. 52, pp. 760-769, 05.11.2012 2013.
[24] H.-G. Bloos and K. Haars, "Umweltbilanz von Photovoltaischen Familiensystemen," presented at the 10. Symposium Photovoltaische Solarenergie, Bad Staffelstein, Germany, 1995.
[25] H. Weindlmaier, C. Schmalen, and M. Kunert, "Erfolgsfaktorenforschung: Theoretische Grundlagen, methodische Vorgehensweise und Anwendungserfahrungen in Projekten für die Ernährungsindustrie," presented at the Tagung der Gesellschaft für Wirtschafts- und Sozialwissenschaften des Landbaues e.V. 2006, Gießen, 2006.
[26] C. V. Bullen and J. F. Rockart, "A primer on critical success factors," ed, 1981, p. 75.
[27] R. D. Buzzell and B. T. Gale, Das PIMS-Program - Strategien und Unternehmenserfolg. Wiesbaden, Germany: Gabler, 1989.
[28] T. Urmee and D. Harries, "Determinants of the success and sustainability of Bangladesh's SHS program," Renewable Energy, p. 9, 2011.
[29] M. Bazilian, P. Nussbaumer, A. Cabraal, R. Centurelli, R. Detchon, D. Gielen, et al., "Measuring energy access: Supporting a global target," The Earth Institute Columbia University2010.
[30] W. H. Hoffmann and R. Schlosser, "Success Factors of Strategic Alliances in Small and Medium-sized Enterprises—An Empirical Survey," Long Range Planning, vol. 34, pp. 357-381, 2001.
[31] D. C. Barua, "Strategy for promotions and development of renewable technologies in Bangladesh: experience from Grameen Shakti," Renewable Energy, vol. 22, pp. 205-210, 1// 2001.

.

Analysis of Air Foils and Design of Blades for a Low-Speed 250W Horizontal Axis Wind Turbine Suitable for Coastal Areas of Bangladesh

Mahtab Murshed[1], Md. Yeasin Arafat[2], M. Abdur Razzak[3]
Department of Electrical and Electronic Engineering
Independent University, Bangladesh
Plot-16, Block-B, Bashundhara, Dhaka-1229, Bangladesh

E-mail: [1]Mahtab_murshed@hotmail.com, [2]nealmagik@gmail.com, [3]razzak@iub.edu.bd

***Abstract*—Implementation of wind turbines has been expanded fundamentally on account of its accessibility and simple and easy generation techniques all around the globe. In the interim in Bangladesh wind energy conversion techniques are exceptionally late idea contrasted with other renewable energy conversion techniques but then in numerous spots research are going on to study and investigate the wind speed. Bangladesh has reasonably wind energy potential. In the present study, wind attributes and wind energy capability in the coastal regions including Chittagong, Cox's Bazar, Hatiya, Teknaf, Kutubdia, Mongla and Patenga are been investigated. The main focus of this research is to study the wind prospects of coastal regions in Bangladesh by building up a measurable examination of wind speed and available power calculation at diverse seaside areas at 15m height, analyzation of air foils and design of turbine's blades for a 250W low-speed horizontal axis wind turbine (HAWT).**

Keywords—Wind Turbine; Bangladesh; Coastal areas; Blade design; Wind power

I. INTRODUCTION

The best possible use of energy demonstrates the best possible social advancement alongside the nation's financial development. As indicated by the world energy reports, the significant amount of the world's energy necessity has been supplied by renewable energy sources. The customary non-renewable energy sources and transformation methods are bringing about genuine negative effects on our surroundings, for example, an unnatural weather change, acid rain, ozone layer exhaustion and so on. Keeping in mind the end goal to build up a clean energy source there is no substitute of renewable energy on the grounds that renewable energy sources are clean, environment friendly and free of cost. In Bangladesh fundamentally we are relying upon fossil fuel to take care of our energy demand. Our energy interest is basically met from natural gas (62.76%), furnace oil (20.45%), diesel (8.29%), coal(2.17%) and hydro (1.99%) as indicated by the higher rate of utilization [1]. Interests of these fossil fuels are expanding day by day with the increment of energy demand. On the off chance that this circumstance is proceeding, there will be no fuel for our future era. Then again, green house gases (GHG) are likewise transmitted when we blaze the fossil energizes which are destructive for our surroundings. To beat this circumstance, we need to swing on to renewable energy. There are numerous types of renewable energies like wind, solar, geo-thermal, tidal, hydro etc. Wind energy plays one of the key roles among the renewable energy sources. It has been utilized earlier for a long time to move boats, pump water, watering systems, windmills and so on. Keeping in mind the end goal to produce power from the kinetic energy of wind, obliges a base normal wind velocity of 6 m/s. In Bangladesh the average annual wind speed is too low (under 2.5m/s) to develop vast scale wind turbines. Generation of power utilizing the wind turbines is a more current innovation in the nation contrasted with other use of the energy because of the low-speed wind turbine holds less possibility for commercial usage. However, different researches have been performed and a significant number of them are presently under process to analyze the wind attributes of the seaside territories in Bangladesh [2-4]. The greater part of them finished up by concluding that Bangladesh has reasonably wind energy potential at coastal areas and some hilly areas located in Chittagong [2].

A small, low-speed and off-grid wind turbine can be a great energy solution for the citizens of remote waterfront ranges in Bangladesh focusing on wind turbines driven pumps for drinking water and watering systems, businesses along the narrows of Bengal coastline like ice making, shrimp/fish cultivating, fish preparing and salt creation commercial ventures, incubation centers and so forth. Numerous commercial enterprises in those regions are off-grid, as of now utilizing diesel generators. However, the advancement of little off-grid wind turbine at those areas is very low because of a few confinements, such as, absence of adequate and solid information about wind velocity, lack of interest by the government and non-government organization because of the lower proficiency as a result of low wind speed [2, 3].

In view of those, the primary goal of this research work is set to focus on the wind prospects of coastal region in Bangladesh by building up a measurable examination of wind speed at that locale at distinctive statures over the ground, hypothetical investigation of wind force accessibility, and lastly, the analysis of foils and design of blades for a 250W low-speed horizontal axis wind turbine (HAWT) by utilizing Qblade software, an open source foil analysis and blade designing software by Hermann Föttinger Institute of TU Berlin. The outline methodology includes analyzing airfoils,

designing and developing of poles and blades for a low-speed wind turbine, which is suitable for seaside regions of Bangladesh including Chittagong, Cox's Bazar, Teknaf, Hatiya, Patenga, Kutubdia and Mongla.

II. Wind Prospects in Coastal Areas of Bangladesh

The geographical area of Bangladesh is in the scope between 20°34'- 26°38'N and the longitude between 88°01-92°4E. Fig. 1 shows the coastal regions Bangladesh. There are numerous hilly and coastal regions of Bangladesh which have possibilities for small scale wind turbines as per previous research works [2, 3]. The southern part of the nation has a 724 km long, angular coastline alongside more than 200 km long hilly coastline territories and more than 50 islands situated in the Bay of Bengal, where strong wind flows with a tremendous amount of energy [4]. In the coastal regions of Bangladesh, the annual average wind velocity at 25-30m height has been recorded more than 5 m/s, which holds a great prospect for small off-grid wind turbines, as research shows that for the low-speed wind turbines the minimum average wind velocity is 3.5m/s [4-6]. The velocity of wind gets enhanced when it enters the beach front line of the southern part of the nation. As per research pursued by some non-government organizations, local government engineering department (LGED) and Bangladesh University of Engineering and Technology (BUET) indicates the wind speed for power generation in Bangladesh is marginally available from the late March till the beginning of October where the maximum wind speed has been recorded during June-July. Many waterfront areas of the nation such as Chittagong, Cox's Bazar, Teknaf, Hatiya, Patenga, Kutubdia and Mongla have immense potential to produce electricity from the wind energy [7]. The geographical loacation of Chittagong is (22°22′N 91°48′E), Cox's Bazar (21°35′0″N 92°01′0″E), Teknaf (20°52′N 92°18′E), Hatiya (22°22′N 91°7.5′E), Patenga (22° 15'N 91° 47'E), Kutubdia (21°49′N 91°51.5′E) and Mongla (22°29′20″N 89°35′43″E) as shown in Fig.1 where the average wind speed recorded as 3.5m/s [2, 4, 8].

III. Wind Velocity Analysis for Coastal Areas of Bangladesh

A. Wind Data

In order to study the wind prospect and available energy it is necessary to analyze the wind data especially the wind velocity (maximum, minimum and the average) available at the coastal regions in Bangladesh. Wind data (monthly) measured at a height of 20m at different coastal areas listed in Table I [8] have been considered for this research work. From Table I it is onserved that the maximum wind velocity has been recorded at Patenga (9.20m/s) in July and the minimum velocity at Mongla (1.01m/s) in December at a height of 20m above the ground. With further analysis the yearly average maximum and minimum have been measured as 5.51m/s and 2.43m/s. respectively. Finally, the yearly average of those areas has been recorded as 3.86m/s, which holds a near good wind prospect in that region.

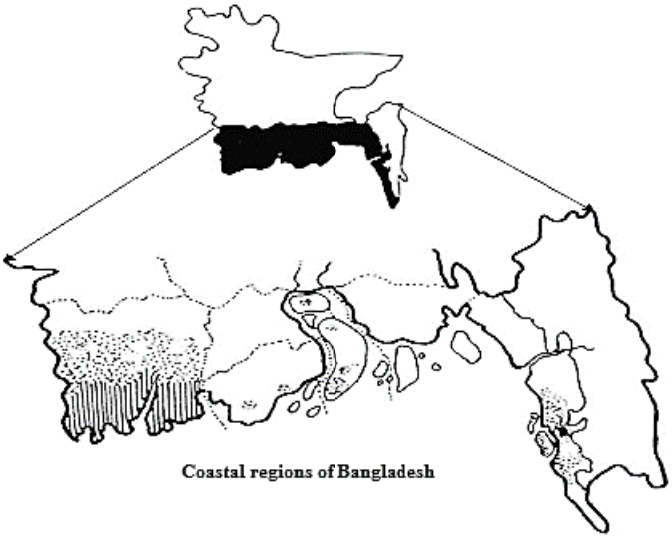

Fig. 1. Coastal regions having wind energy prospect in Bangladesh

B. Wind Shear Exponent Calculation

By determining the wind speed, v at reference point, h_{ref} the wind velocity at desired height, h can be calculated by using wind shear exponent [8, 11-13] as

$$\mathrm{v} = v_0 \left(\frac{h}{h_{ref}}\right)^{\alpha} \quad (1)$$

where v_0= average wind speed, h = desired height and h_{ref}= reference height and α = coefficient, which changes along with the stability of the atmosphere. $\alpha = 0.143$ when the atmosphere is relatively stable like coastal areas. A theoretical wind speed calculated at different height using the wind shear exponent shown in eq. (1) has been listed in Table II. For the reference height of 20m with an average wind speed of 3.86m/s, the wind velocity for the wind turbine at the proposed height of 15m is found to be

$$\mathrm{v} = v_0 \left(\frac{h}{h_{ref}}\right)^{\alpha} = 3.2375 \left(\frac{15}{20}\right)^{0.143} = 3.7 ms^{-1}.$$

Table II. Height vs. wind velocity (reference height 20m)

Height from ground (m)	Wind velocity (ms^{-1})
5	3.17
10	3.50
15	3.70
20	3.86
25	3.99
30	4.10
35	4.20

C. Air Density

Power extraction from a wind turbine depends on some air factors like moisture, air density and air regulation. For this research air density has been considered since the air density impact is the most during power extraction. Air densities at different temperature for a stable atmospheric pressure are listed in Table III [14]. The average temperature (℃) of coastal areas in Bangladesh is around 30℃ at which the average air density is found to be 1.16 kg/m^3.

Table I. Wind Velocity (m/s) at 7 Different Coastal Locations of Bangladesh (Reference Height 20m)

Locations	Monthly wind velocity (m/s)												Yearly Maximum	Yearly Minimum	Yearly Average
	Jan	Feb	Mar	Apr	May	Jun	Jul	Aug	Sep	Oct	Nov	Dec			
Chittagong	3.64	2.88	4.95	5.01	5.51	6.89	7.09	6.83	4.64	2.82	3.39	2.2	7.09	2.20	4.65
Cox's Bazar	3.76	3.86	4.51	5.58	3.83	4.14	3.83	3.95	3.2	3.26	2.57	3.26	5.60	2.57	3.81
Teknaf	3.7	4.01	4.39	4.01	3.32	3.89	3.83	2.7	2.44	2.2	1.57	1.76	4.39	1.57	3.15
Hatiya	3.04	2.64	4.16	3.97	4.82	6.47	5.75	2.64	2.96	2.77	3.06	2.57	5.75	2.57	3.74
Patenga	6.22	6.34	7.37	7.92	8.47	8.69	9.2	8.54	7.48	6.93	6.71	5.91	9.2	5.91	7.48
Kutubdia	1.77	1.82	2.32	2.7	2.77	3.65	3.61	3.14	2.11	1.45	1.19	1.29	3.65	1.19	2.32
Mongla	1.07	1.25	1.72	2.51	2.92	2.63	2.48	2.35	1.83	1.27	1.02	1.01	2.92	1.01	1.84

Table III. Temperature vs air density

Temperature(℃)	Air Density (Kg/m^3)
35	1.14
30	1.16
25	1.18
20	1.21
15	1.23
10	1.25
5	1.27
0	1.29

D. MaximumAvailable Power Calculation

According to Betz Law theoretically no wind turbine can extract more than 59% of the available kinetic energy of wind into mechanical energy, in practice the power extraction often measured less than 40% [8]. Te maximum output power availability is given by

$$P_{available\ (max)} = \frac{1}{2}\rho A v^3 C_P \qquad (2)$$

where $A(=\pi r^2)$ is the swept area by the HAWT rotor blade and C_p(=0.59) is the Betz limit (theoretical), ρ is the air density and v is the air velocity.

Considering the wind speed, v= 3.70 ms^{-1} (calculated in section III.B), pole height= 15m, blade's radius, r = 3m each, $\pi = 3.1416$, and swept area, $A = \pi r^2 = 12.6\text{m}^2$, air density, ρ = 1.16 kg/m^3 (found from Table III), theoretical Betz coefficient, C_p = 0.59 and practical Betz coefficient, C_p = 0.30, the maximum available output power for the proposed horizontal axis wind turbine (HAWT) can be calculated using eq. (2) as

$$P_{available\ (max)} = \frac{1}{2}\rho A v^3 C_P$$

$$= \frac{1}{2} \times 1.16 \times 28.27 \times 3.70^3 \times 0.59 \approx 490W \text{ (theoretical)}$$

$$P_{available\ (Max)} = \frac{1}{2}\rho A v^3 C_P$$

$$= \frac{1}{2} \times 1.16 \times 28.27 \times 3.70^3 \times 0.30 \approx 250W\ (practical)$$

IV. Design of Blades for a 400W Wind Turbine

A. Calculation of Blade Radius

Considering the wind speed, v = 3.70 ms^{-1} (calculated in section III.B), pole height = 15m, maximum available output power, $P_{available\ (Max)}$= 250W (calculated in section III.D), air density, ρ = 1.16 kg/m^3 (found from Table III), and the practical Betz coefficient, C_p ≈0.30, the blade radius, r can be determined using eq.(1) as

$$r = \sqrt{\frac{2P_{available\ (max)}}{\rho v^3 C_P \pi}} = \sqrt{\frac{2\times250}{1.16\times(3.70)^3\times0.30\times3.1416}} \approx 3.0\text{m}$$

B. Foil Selection

Study indicates that NACA 63215 is the most durable and shapeable air foil for low-speed horizontal axis wind turbine (HAWT). Shape is the primary reason to consider this airfoil as the tip foil for the research, meanwhile NACA 0021 air foil is one of the most efficient NACA foils in terms of its commercial availability, which has been considered as the root foil for the research. These two NACA airfoils perform one of the maximum turbine efficiencies with wide operating range [14, 15]. The air foil selection in Qblade simulation software with the measurements is shown in Fig. 2. The core analysis (operational view point) of root foil NACA 0021, tip foil NACA 63215 is shown in Figs. 3 and 4, respectively, where α = incidence angle, D = drag, L = lift, C_m = pitching moment coefficient, C_l = lift coefficient and C_d = drag coefficient.

For this study, the airfoil simulation for the blade analysis using Qblade software has been limited to a small inflow angles (taken as -20° to +20°), although the practical blades of HAWT operate in higher inflow angles. In order to converge in practice and produce a near accurate analysis it is necessary to extrapolate the airfoil execution 360° polar for the wind flow. The polar extrapolation for tip foil NACA 63215 and root foil NACA 0021 is shown in Fig. 9, where α = incidence angle, D = drag, L = lift, C_m = pitching moment coefficient, C_l = lift coefficient and C_d = drag coefficient.

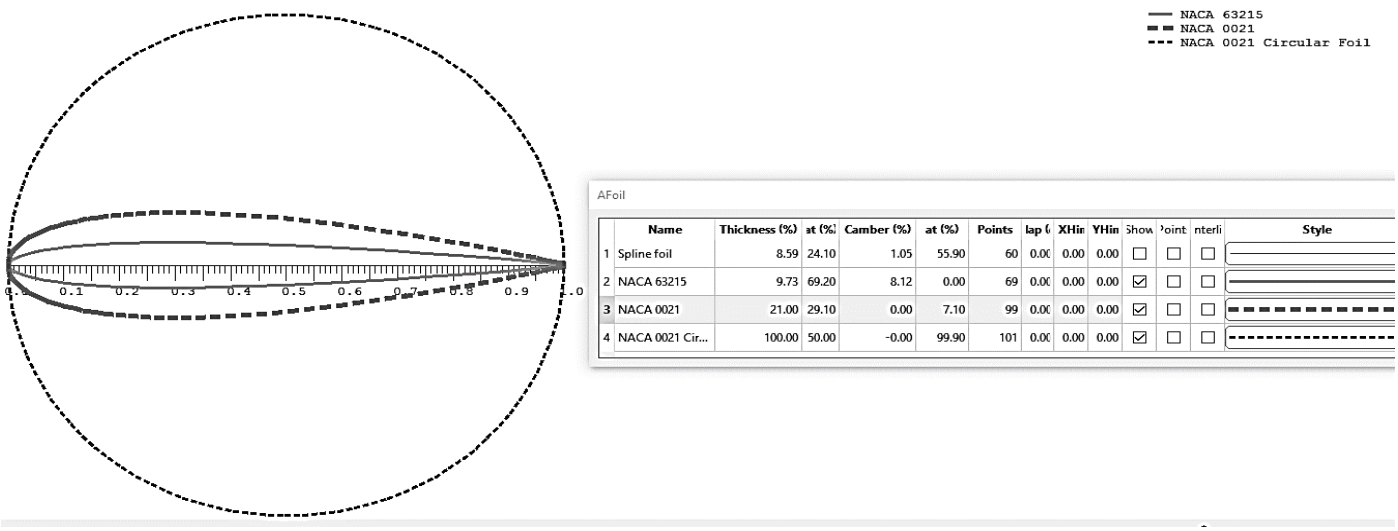

Fig. 2. Foil Selection root Foil (Circular) NACA 0021, root Foil NACA 0021, tip Foil NACA 63215

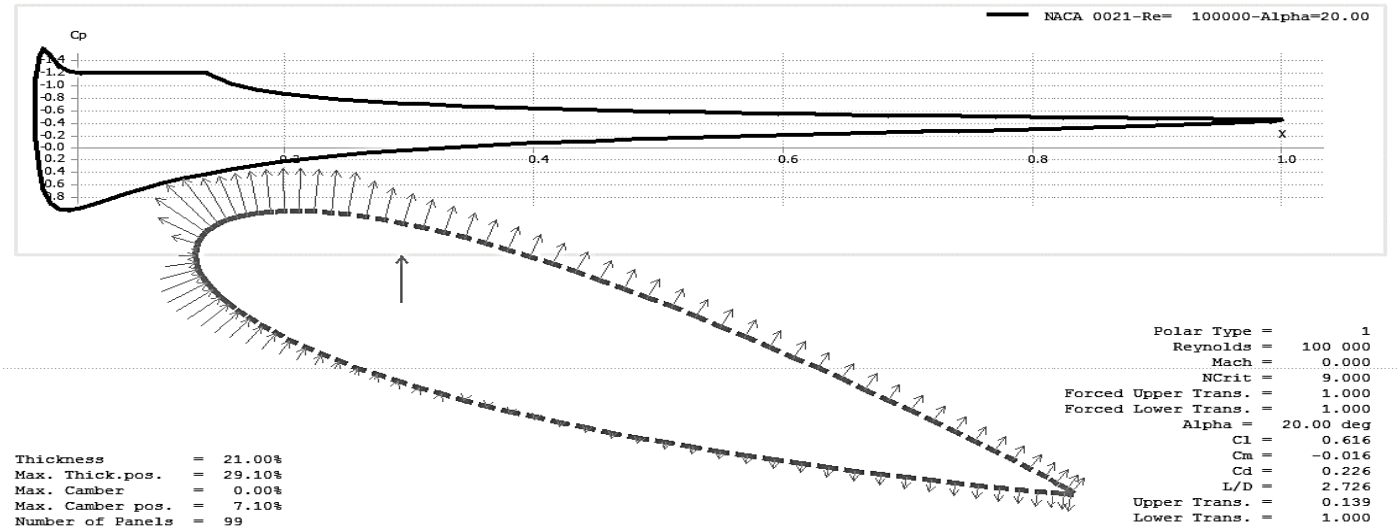

Fig. 3. NACA 0021 core analysis (Root foil operational point view)

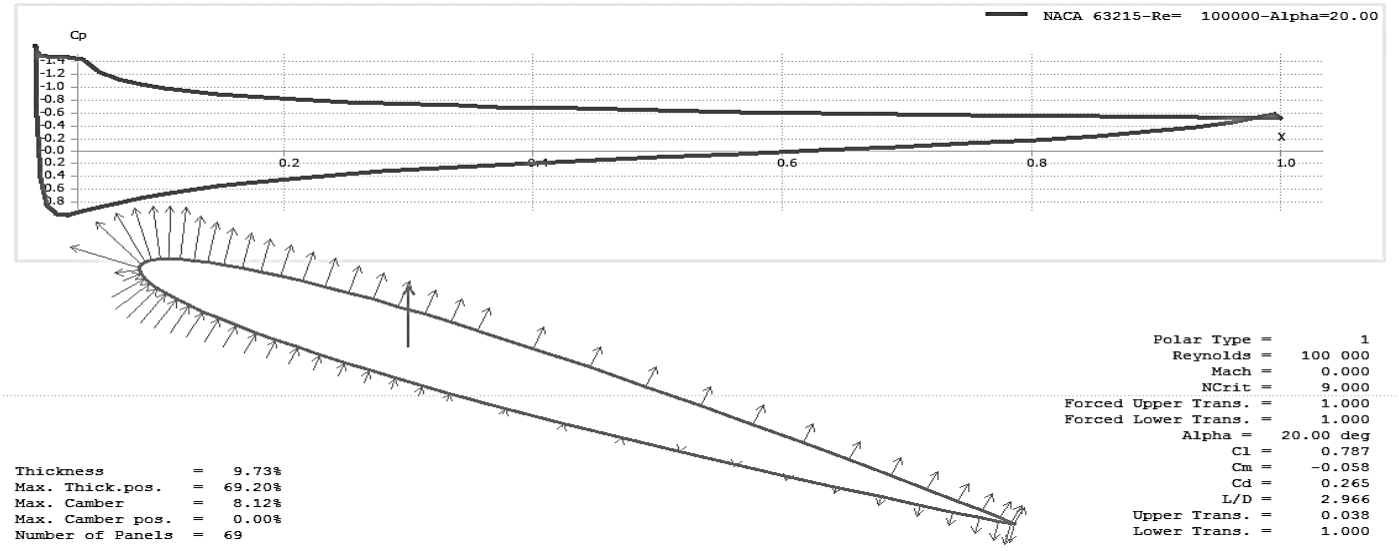

Fig. 4. NACA 63215 core analysis (Tip foil operational point view)

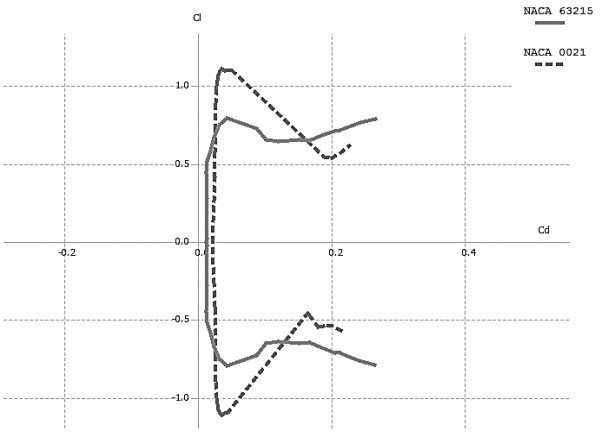

Fig 5. Tip foilNACA 0021 and root foil NACA 63215 analysis (inflow angle -20° to +20°) (Lift coefficient, C_l vs. drag coefficient, C_d)

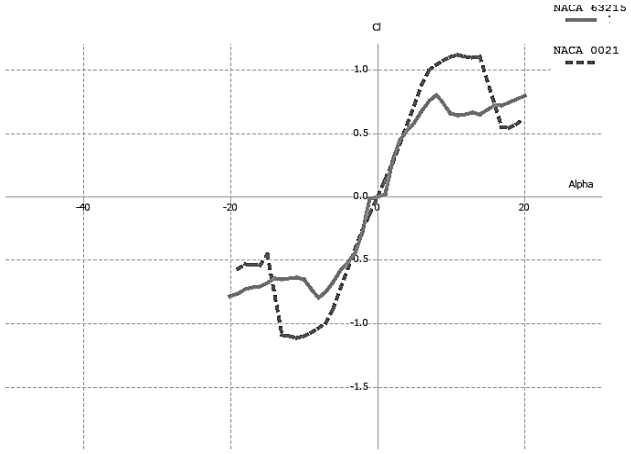

Fig. 6. Tip foilNACA 0021 and root foil NACA 63215 analysis (inflow angle -20° to +20°) (Lift coefficient,C_l vs. Pitching moment coefficient, α)

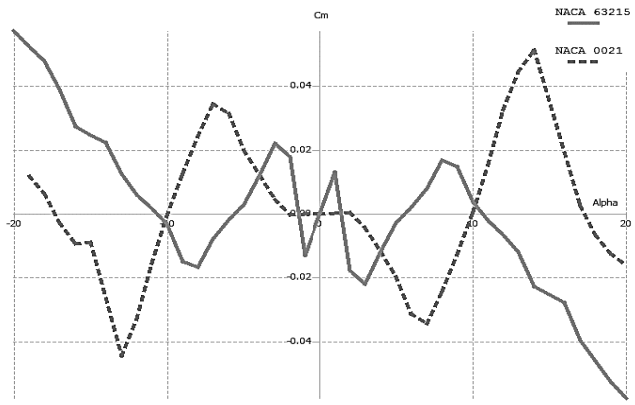

Fig. 7. Tip foilNACA 0021 and root foil NACA 63215 analysis (inflow angle -20° to +20°) (Incidence angle, α ; vs.Pitching moment coefficient, C_m)

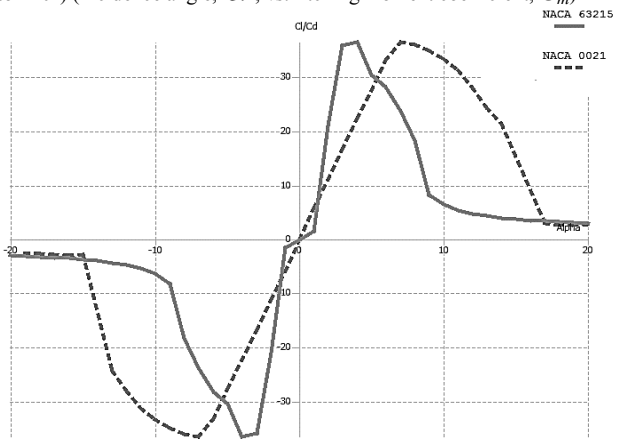

Fig. 8. Tip foilNACA 0021 and root foil NACA 63215 analysis (inflow angle -20° to +20°) (Glide ratio C_l/C_d vs. Incidence angle, Alpha)

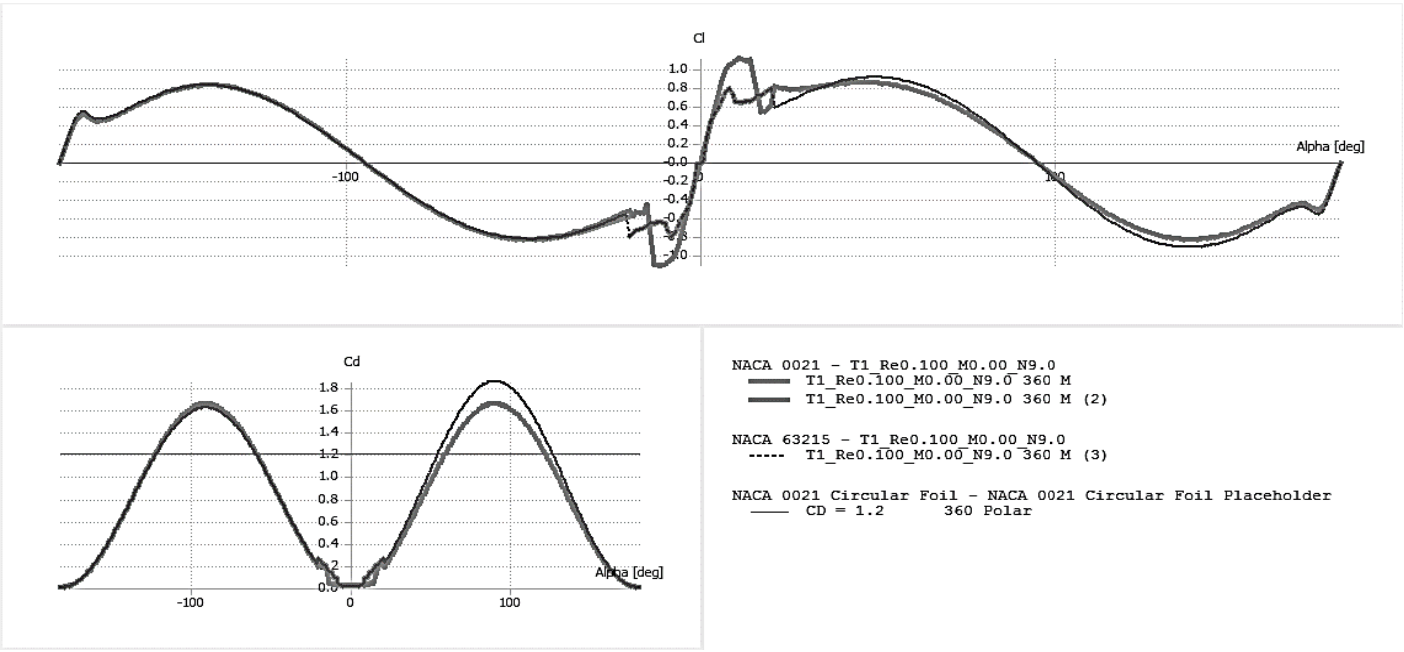

Fig. 9. Tip foilNACA 0021 and root foil NACA 63215 analysisresult polar extrapolation

In the simulation, the blade foils (NACA 63215 and NACA 0021) and the foil responses (such as lifts, drags, angles of incidence, different coefficients) have been analyzed in order to compare with blade element momentum theory. Various blade properties for root foil NACA 0021 and tip foil NACA 63215 are shown in Figs. 5-8, where α = incidence angle, D = drag, L = lift, C_m = pitching moment coefficient, C_l = lift coefficient and C_d = drag coefficient. The designed blade for single view and rotor view with placement of foils at different section of blades are shown in Figs. 11 and 12, respectively, which can be considered for the proposed low-speed 250W wind turbine.

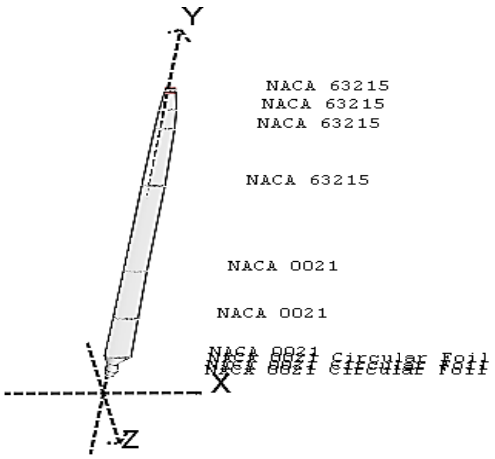

Fig. 10. Blade design (single blade view)

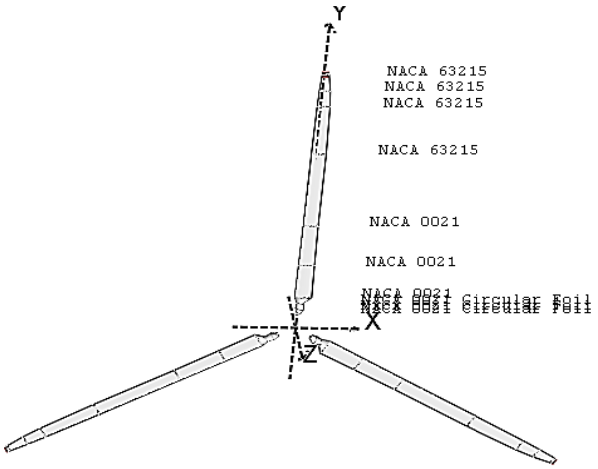

Fig. 11. Blade design (rotor view)

V. CONLUSION

In this paper, a statistical analysis of wind speed at different height above the ground at coastal areas of Bangladesh, the power availability based on average wind speed of 3.86m/s over the region, the analyses of NACA 63215 and NACA 0021 airfoils and the design of blades for a 250W low-speed off-grid horizontal axis wind turbine have been studied. The wind velocity data over the coastal areas (Chittagong, Cox's Bazar, Teknaf, Hatiya, Patenga, Kutubdia, Mongla) shows a near good prospect for wind power generation in the region throughout the year. Considering the fact that with a decent amount of kinetic energy available for low wind velocity over the region, the blades of 3m radius for a low-speed 250W wind turbine have been simulated using Qblade software after analyzing the air foils of NACA 63215 and NACA 0021. This research can be useful for developing a small scale low-speed horizontal axis wind turbine in the coastal areas of Bangladesh.

References

[1] "Installed capacity report- BPDB", Bangladesh power development board, Available at: http://www.bpdb.gov.bd/bpdb/index.php?option=com_content&view=article&id=5&Itemid=6 [May 21, 2015]

[2] A.N. M. Mominul Islam Mukut, Md. Quamrul Islam, Muhammad Mahbubul Alam "Analysis of Wind Characteristics in Coastal Areas of Bangladesh" Journal of Mechanical Engineering, The Institution of Engineers, Bangladesh, Vol. ME39, No. 1, June 2008.

[3] Dr. Anwar Hossain, "Wind Energy in Bangladesh", Sustainable Development Networking Programme. Available at: http://www.sdnbd.org/wind.htm [June 19, 2015]

[4] M.J. Khan, M.T. Iqbal, S. Mahboob, "A wind map of Bangladesh", Renewable Energy (2004),Volume: 29, Issue: 5, Publisher: Elsevier, Pages:643-660.

[5] T.V. Ramachandra, B.V. Shruti, "Wind energy potential mappings in Karnataka, India, using GIS", Energy Conversion and Management 46 (2005) pp. 1561-1578.

[6] "Record Year for Wind Energy: Global Wind Power Market increased by 43% in 2005", Global Wind Energy Council Press Release, Brussels, 17th February, 2006.

[7] "Final Report of Solar and Wind Energy Resource Assessment (SWERA)- Bangladesh", Renewable Energy Research Centre (RERC), university of Dhaka, Bangladesh, Available at: http://xa.yimg.com/kq/groups/14503985/2014718169/name/SWERA_Bangladesh_FullReport.pdf[July 18, 2015]

[8] Sultan Ahmmed and Quamrul islam "Wind power for rural areas of Bangladesh", 3rd international conference on Electrical and Computer Engineering ICECE, 2004, 28-30 December 2004

[9] Md. Habib Ullah, Tamzi dul Hoque, Md Mus addaqul Hasib "Current Status of Renewable Energy Sector in Bangladesh and a Proposed Grid Connected Hybrid Renewable Energy System" International Journal of Advanced Renewable Energy Research, Vol.1, Issue.11, pp. 618-627, 2012.

[10] Ajinkya Padate, "Tidal and wind energy and wind energy conversion duo". International Journal of Renewable and Sustainable Energy 2013; 2(4): 163-166.

[11] M. L. Kubik, P. J. Coker, C. Hunt, "Using meteorological wind data to estimate turbine generation output: a sensitivity analysis" World Renewable energy congress 2011, 8-13 May 2011, Linkoping, - Sweden.

[12] H. Panofsky and J. Dutton, "Atmospheric Turbulence: models and methods for engineering applications", Pennsylvania State University: John Wiley and Sons, 1984.

[13] Wikipedia web-based encyclopedia project supported by the Wikimedia Foundation "Density of air" Available at: http://en.wikipedia.org/wiki/Density_of_air [June 11, 2015]

[14] John McCosker "Design and Optimization of a Small Wind Turbine" An Engineering Project Submitted to the Graduate Faculty of Rensselaer Polytechnic InstituteAvailable at: http://www.ewp.rpi.edu/hartford/ ~ernesto/SPR/McCosker-FinalReport.pdf [June 23, 2015]

[15] M.H. Mohamed, A.M. Ali, A.A. Hafiz, "CFD analysis for H-rotor Darrieus turbine as a low-speed wind energy converter", International Journal of Engineering Science and Technology, 18 (2015) 1-13.

Design and Analysis of an In-Runner Permanent Magnet Alternator for Low-Speed Wind Turbine

Md. Yeasin Arafat[1], Mahtab Murshed[2], M. Abdur Razzak[3]
Department of Electrical and Electronic Engineering
Independent University, Bangladesh
Plot-16, Block-B, Aftabuddin Road, Bashundhara R/A, Dhaka-1229, Bangladesh

E-mails: nealmagik@gmail.com[1], mahtab_murshed@hotmail.com[2], razzak@iub.edu.bd[3]

***Abstract*—The in-runner permanent magnet alternator (PMA) is adequately utilized as a part of wind power generation system specially for its robust and conventional structural configuration. In this research, the execution investigation of an in-runner outspread flux PMA intended for direct driven, extremely low-speed and small capacity wind power system has been examined with numerous modificationshave taken into account e.g. changing some mechanical parameters such asuse of effective and robust material, fractional slotting per pole, improving the slot fill factor and mounting of the magnets for reduction of cogging torque. The proposed configuration has been analyzed by finite element analysis (FEA) technique keeping in mind the end goal to observe the real time performance with several loss counting and cogging torque calculation.A good slot fill factor improves the thermal condition in the slot of the stator by reducing the copper losses. Considering all the point, an in-runner radial flux permanent magnet alternator (RFPMA) has been achieved with minimum losses and higher efficiency.**

Keywords—in-runner PMA; low-speed wind turbine system; finite elements analysis (FEA); cogging torque

I. INTRODUCTION

The power prerequisites of the world including Bangladesh are expanding at alarming rate and the demand of power has been running in front of supply. It is also now generally perceived that the fossil powers (i.e., coal, petroleum and common gas) and other traditional resources, presently eye being utilized for generation of electrical energy, may not be either adequate or suitable to keep pace with perpetually expanding interest of the electrical energy of the world. Additionally, generation of electrical power by using cold based steam force plant or atomic force plants causes contamination, which is prone to be more intense in future because of extensive producing limit on one side and more prominent familiarity with the general population in this appreciation.

Small size wind power framework turns out to be more well-known than greater one because of less ecological unsettling influence, small in size and perfect for low wind speed territory. For small size power unit, the mechanical construction should be simple, cost effective and maintenance-free. Also direct driven system reduces thegear up drive components offering the opportunity to cutprices and increases the system efficiency and reliability [1]. Multi-pole configured direct driven in-runner permanent magnet alternator ismaintenance-free and used in severalweather conditions. Since external excitation is not needed in PMA which reduces conductor losses by external excitation and increases the efficiency and reliability of the alternator [2, 3].

In recent time, high-speed permanent magnet machine such as 2000-1500 rpm is used for hybrid electric vehicle (HEV) [4, 5]. On the other hand, low-speed PMA such as 200-1500 rpm rated speed alternator is the first choice for power generation like direct driven wind power or low-speed hydro power generation [6-8].Out-runner PMA is more attractive for wind power generation system for its higher effective output power cross sectional area but the main drawback is higher cogging torque generation due to greater interaction between stator slots and rotor poles [8]. So for robust design, an in-runner PMA is becoming more popularin wind power generation system due to its low cogging torque.

In low wind speed condition, the cogging torque expanded significantly because of higher cooperation or line up between permanent magnet and the stator slot. This torque creates huge amount of noise and vibration while the machine is running. Recent researches shows that several factors like arrangement of the magnetic field, number of slots per pole per phase, slot opening and filling factor, pole pitch and distribution of magnetic flux density are some of the main factors affecting the cogging torque [9].

In this research, adirect driven, small capacity, extremely low-speed, multi pole, in-runner radial flux permanent magnet alternator (PMA) has been studied and its performance like material consumption, improvement of efficiency and minimization of cogging torque has been examined. Finite Element Analysis (FEA) method is adopted to design this alternator for better accuracy which is simulated by ANSOFT Maxwell software. In design issue, reduction of cogging torque was one of the main field of improvement of this alternator. Mainly fractional slot number per pole per phase and mounting type of the magnets in the rotor surface were applied to reduce this cogging torque to reach the maximum efficiency at extreme low-speed. For accurate and better analysis several losses such as frictional loss, eddy current loss, core loss, copper loss werealso taken into account, and some mechanical parameters such asuse of effective and robust material, fractional slotting per pole, slot fill factor etc. are modified.

II. COGGING TORQUE REDUCTION

Cogging effect is an effect arises in permanent magnet alternator which creates an exceptional periodic oscillated torque due to interaction between magnetic poles in the rotor and stator slots. In permanent magnet alternator unbalanced torque pulsation results extra noise and vibration during alternator operation happened only for this effect [10]. Also the torque magnitude is inversely proportional to the rotational speed of the rotor. So in a low-speed wind power system the repulsive cogging torque generated in permanent magnet alternator is much higher than a high-speed alternator.

The magnetic field energy or total co-energy W_C of an PMA is given by [10],

$$W_c = \frac{1}{2} \times L \times i^2 + \frac{1}{2} \times (\Re + \Re_m) \times \phi_m^2 + N \times i \times \phi_m \quad (1)$$

where L = length of stator, i = exciting current, $\Re$ and $\Re_m$ are the reluctances seen by the magneto motive force and the magnetic field respectively; N = rated speed, and ϕ_m= magnetic flux of the magnet linking the exciting coil. The electromagnetic torque T can be determine by differentiating the total co-energy, W_c with respect to rotor angular displacement θ as [10],

$$T = \frac{\partial W_c}{\partial \theta} \quad (2)$$

where exciting current is constant.

By substituting (1) into (2), the torque can then be calculated as

$$T = \frac{1}{2} \times i^2 \times \frac{dL}{d\theta} - \frac{1}{2} \times \phi_m^2 \times \frac{d\Re}{d\theta} + N \times i \times \frac{d\phi_m}{d\theta} \quad (3)$$

Thecoil inductance of second term in equation (3) is fixed, and independent of the rotor angular displacementθ. Therefore, simply the second term will be present in (3) and cogging torque can be calculating by targeting on the magnetic interaction as well as the reluctance variation between the exciting coil and magnet, which yields,

$$T_{cogg} = -\frac{1}{2} \times \phi_g^2 \times \frac{d\Re}{d\theta} \quad (4)$$

where ϕ_g = magnetic flux = ϕ_m. From (4) it shows that, cogging torque appears when the magnetic flux travels through a changeable.

In this research, minimization of cogging torque in a low-speed permanent magnet alternator suitable for small size wind power system has been studied. The most widely and effectively used cogging torque minimization technique is fractional slot per pole per phase which is significantly reduces the magnitude of cogging torque and minimizesthe unwanted noise and vibration in the alternator. Besides the technique of fractional slot mounting of the magnet is also applied in this proposed design to minimize the cogging torque.

Two different approaches are used for cogging torque calculation: the analytical and numerical ones. Due to oversimplification, higher inaccuracy occurred in analytical method. On the other hand, two-dimensional (2D) and three-dimensional (3D) FEA modeling of the alternator are used to measure the cogging torque in numerical method which offers more accurate calculations for complex geometry. Here RMXPRT and MAXWELL 2D is used for numerical analysis.

III. THE FEATURES OF THE MACHINE

In this research work, two main materials which is used such as magnetic poles and steel sheets for rotor and stator are studied and observed their performance to find the efficient and cost effective material. Also to achieve higher efficiency and lower cogging torque several modifications have been done. In the following subsections, the mostly used materials, machine geometry and its modifications are discussed.

A. PMA's Permanent Magnet Materials

The magnetic material should have higher magnetic coercive force, maximum energy product which can give greater energy density, sufficient residual magnetism density and well stability such as magnetic stability, thermal stability, chemical stability and time stability with better economy [11]. The cost of ceramic magnet is lowest but the maximum energy density is low as usual. On the other hand, the rare earth magnet samarium cobalt alloys have better energy density but much expensive. Alnico is preferred for extreme location like coastal area but they are simply demagnetized compared to ceramic magnets due to their lower values of coercive force [12]. To get higher energy density and residual flux density the use of NdFeB type rare earth magnets are increased [13, 14], which are considered for the proposed design. The main parameters of NdFeB are listed in Table I [11].

TABLE I. MAIN PARAMETERS OF NdFeB

Property	**Value**
Residual flux density	1.15 T
Coercive force	915 kA/m
Maximum energy density	263.1 kJ/m3
Relative recoil permeability	1.03

TABLE II. DATA TABLE FOR M19_26G SILICON STEEL SHEET

Property		**Value**
Material Grade		M19_26G or M350-50A
Thickness		0.50 mm
Minimum Magnetic Induction at 1 T, 50 Hz		1.45 W/kg
Minimum Magnetic Induction at 1.5 T, 50 Hz		3.33 W/kg
Minimum Lamination Factor		97%
Core loss at 1.0 T, 50 Hz		1.33 W/kg
Core loss at 1.5 T, 50 Hz		2.94 W/kg
Minimum Magnetic Induction at	H=2500 A/m	1.59 T
	H= 5000A/m	1.69 T
	H= 10000A/m	1.79 T

B. Rotor and Stator Materials

Currently any kind of designing issues for electrical machines specially in alternator design, silicon based electrical steel sheet is widely used due to its low volume and cost. In this designing procedure M19_26G or M350-50A silicon based electrical steel sheet is used. The magnetic properties of M19_26G are provided in Table II [15].

C. In-Runner Radial Flux PMA

There are several types of permanent magnet alternator configurationsavailable.However,an in-runner radial flux PMA has more robust mechanical arrangement due to interior rotor positioned inside the stator than out-runner radial flux PMA. Also higher output power and low cogging torque can be achieved from an in-runner PMA than an out-runner one. In this research work, an in-runner RFPMA is considered to design for the direct driven low-speed small size wind power system, 3D view of which is shown in Fig.1. The design (electrical and dimensional) parameters of the PMA are listed in Table III.

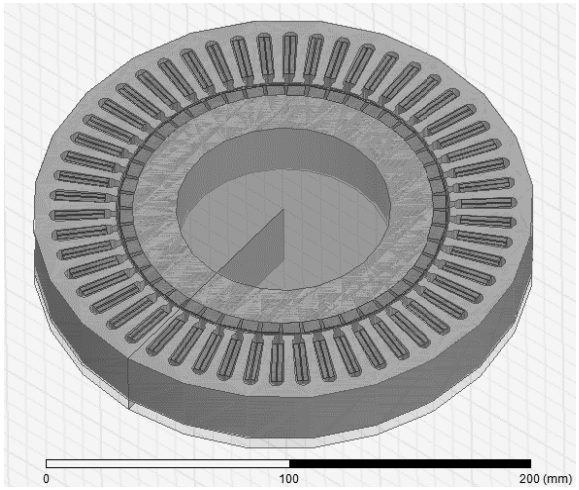

Fig. 1. 3D graphical view of an in-runner permanent magnet alternator

TABLE III. ELECTRICAL AND DIMENTINAL PARAMETERS OF THE MACHINE

Property	Value
Rated power (Pout)	250 W
Reference speed (N)	100 rpm
Frequency (f)	40 Hz
Rated phase voltage (Va)	24 V
Thickness of PM (LPM)	6.0 mm
Number of stator slots (Q)	54
Number of poles (P)	48
Length of the air-gap (g)	1.0 mm
External diameter of the stator (Sout)	210 mm
Internal diameter of the stator (Sin)	140 mm
Length of the stator (L)	50 mm
External diameter of the rotor (Rout)	138 mm
Internal diameter of the stator (Rin)	90 mm

D. Fractional Slot

In conventional machine design, the number of slots per pole per phase must be integer. But in permanent magnet alternator where magnetic pole is involved, integer number of slots can cause higher cogging torque production. That's why in permanent magnet alternator, fractional slots per pole per phase is more suitable. The number of slots per pole per phase cannot be too large due to reduction of the capacity of suppressing the higher harmonic. Similarly, fractional slot winding can significantly decreases the harmonic content to improve the electromotive force (EMF) waveform [16]. Therefore, in this research work, the number of slots per pole per phase is chosen assmall and fractional.

E. Mounting of the Magnet

The impact of mounting of the magnets is significant in permanent magnet alternator with low rotational speed. Several techniques are available for mounting the magnets in the rotor as a pole but surface mounting and surface embedded are the most commonly used due to simple and robust design of the rotor. For high power density, surface mounted radial magnetic poles are commonly used. On the other hand, surface embedded technique is used for high-speed application and has higher torque ripple due to more interaction between stator slots and magnetic poles.

In the present research, surface mounted magnet design is adopted as shown in Fig. 2. The thickness of the magnetic pole is considered as 6 mm and the pole embrace value is taken as 0.8 which is practically easy to build and perfect to get higher efficiency.

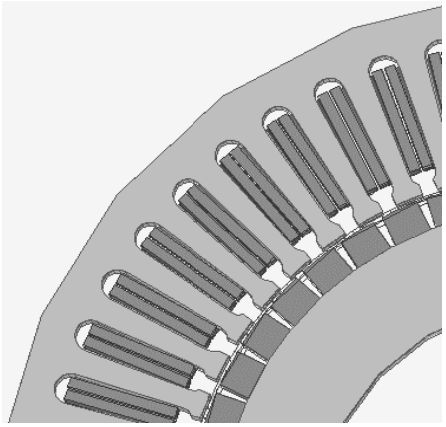

Fig. 2. Surface mounting permanent magnet pole design

IV. RESULTS AND ANALYSIS

Using ANSOFT MAXWELL RMXPRT and MAXWELL 2D software, the proposedPMA was examined where the transient interval is considered as 0.1 second. The alternator wasevaluated at each 0.0005 second. Theresults are discussed in the following paragraphs.

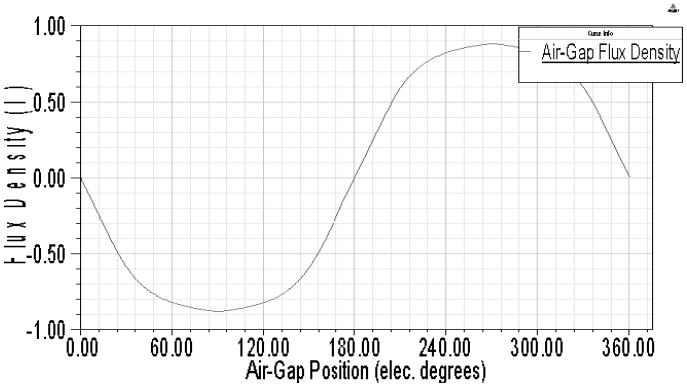

Fig. 3. Air gap flux density of outer rotor PMA (No load condition)

Maximum air gap flux density of this in-runner rotor machine is found around 0.86T where the length of air gap in between stator and rotoris limited as 1 mm as shown in Fig. 3.For 1 mm air gap the amount flux density generation is sufficient.

Fig. 4. Output power vs. torque angle

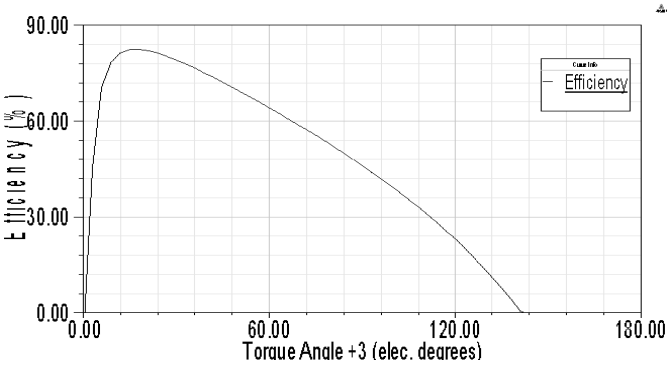

Fig. 5. Efficiency vs. torque angle

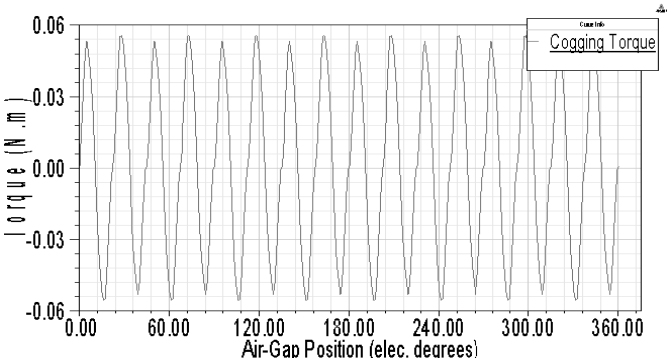

Fig. 6. Cogging torque in two teeth vs. air gap position

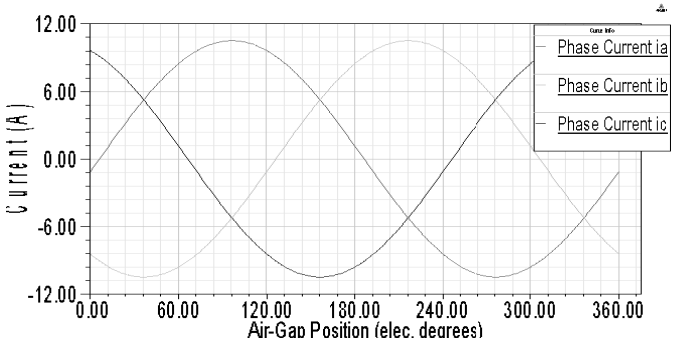

Fig. 7. Winding current vs. air gap position under load

The output power versus torque angle plot is shown in Fig.4 and the maximum output power is found to be approximately 466.4W. Maximum output power can be achieved when the torque angle is 78 degrees and the efficiency is 56%. Generally, conventional low-speed alternator has around 55%-65% efficiency. In this proposed design, higher efficiency of around 80.7% has been achieved,as shown in Fig. 5, by using fractional slot number per pole, modified slot type and good slot fill factor.

In the proposed design, the cogging torque is found to be around 0.051 N-m which can be almost negligible compared conventional low-speed PMA. The cogging torque versus air-gap position plot is shown in Fig. 6.

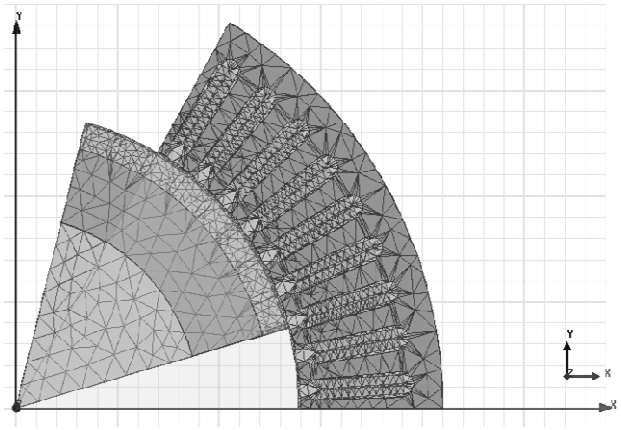

Fig. 8. Mesh detail with air gap region

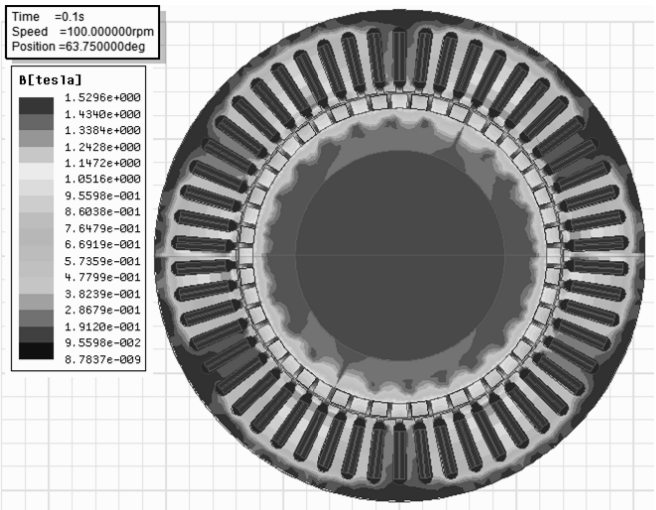

Fig. 9. Magnetic flux density analysis

The three phase RMS current of this proposed PMA is found to be around 7.39 A as shown in Fig. 7. Two layers finite element meshing was applied instead of one-layer meshing to increase the precision of the cogging torque computation as shown in Fig.8.The chart and graphical presentation of the magnetic flux density in the computation domain is shown in Fig. 9. Table IV illustrates the material consumption of the machine. For compact configuration the designed PMA has lower copper weight and armature core steel weight.

Table V shows simulation result of full load operation of the designed PMA. Due to good fill factor which is around 71.3%, the armature copper loss has been reduced. So the overall efficiency and temperature stability of the stator has been improved due to minimization of losses.

TABLE IV. MATERIAL CONSUMPTION DATA

Material consumption	Value
Armature wire density	8900 kg/m3
Permanent magnet density	7550 kg/m3
Armature core steel density	7650 kg/m3
Rotor core steel density	7650 kg/m3
Armature copper weight	2.19645 kg
Permanent magnet weight	0.781091 kg
Armature core steel weight	3.93921 kg
Rotor core steel weight	2.1083 kg
Total net weight	9.02505 kg
Armature core steel consumption	11.1046 kg
Rotor core steel consumption	4.51372 kg

TABLE V. FULL LOAD OPERATION RESULT

Parameter	Value
Peak line induced voltage	30.2052 V
RMS line current	7.39281 A
RMS phase current	7.39281 A
Armature thermal load	71.5114 A^2/mm^3
Specific electric load	25414.6 A/m
Armature current density	2.81379 A/mm^2
Frictional and winding loss	12 W
Iron – core loss	5.41557 W
Armature copper loss	42.4008 W
Total loss	59.8164 W
Output power	250.17 W
Input power	309.987 W
Efficiency	80.7 %
Synchronous speed	100 rpm
Rated torque	23.8895 N-m
Torque angle	22.3709 deg
Maximum output power	466.454 W

V. CONCLUSION

The analysis of an in-runner radial flux permanent magnet alternator (PMA) with multi-pole and fractional slot number has been designed and analyzed for an exceptionally low-speed (100 rpm) direct driven 250W wind power system suitable for low wind speed region. The proposed PMA has higher efficiency and minimum cogging torque compared to similar type of conventional alternator. Also the minimum material consumption provides a compact shape of the alternator. The in-runner type rotor, rare earth type magnetic pole and silicon based electrical steel gives a robust configuration which is perfectly suitable for outdoor type use such as wind power system in coastal areas.

REFERENCES

[1] A. P. Ferreira, A. M. Silva, A. F. Costa, “Prototype of an Axial Flux Permanent Magnet Generator for Wind Energy Systems Applications”, Power Electronics and Applications, 2007 European Conference, pp. 1–9 (2007).

[2] Rizk J., Nagrial M., “Design of permanent-magnet generators for wind turbines”, The Third International Power Electronics and Motion Control Conference Proceedings, IPEMC, Vol. 1, pp. 208–212 (2000).

[3] Chen J. Chemmangot V.N., Longya Xu., “Design and finite element analysis of an outer-rotor permanent magnet generator for directly coupled wind turbines”, IEEE Trans. Magnetics, Vol. 36, No.–5, pp. 3802–3809 (September 2000).

[4] Peter Sergeant, Alex Van den Bossche, “Influence of the amount of permanent magnet material in fractional-slot permanent magnet synchronous machines”, IEEE, pp. 1-11 (2013).

[5] Naghi Rostami, M. Reza Feyzi, Juha Pyrhönen, Asko Parviainen, Vahid Behjat, “Genetic algorithm approach for improved design of a variable speed axial-flux permanent-magnet synchronous generator”, IEEE Trans. Magnetics, Vol. 48, pp. 4860-4865 (2012).

[6] W. Fei, P.C.K. Luk, “A new technique of cogging torque suppression in direct-drive permanent-magnet brushless machines” IEEE Trans. Industry Applications, Vol. 46, No. 4, pp. 1332-1340 (2010).

[7] Tiberiu Tudorache, Leonard Melcescu, Mihail Popescu, “Methods for cogging torque reduction of directly driven PM wind generators”, 12th International Conference on Optimization of Electrical and Electronic Equipment, IEEE, pp. 1161-1166 (2010).

[8] Kyoung-Jin Ko, Seok-Myeong Jang, Ji-Hoon Park, Han-Wook Cho, and Dae-Joon You “Electromagnetic performance analysis of wind power generator with outer permanent magnet rotor based on turbine characteristics variation over nominal wind speed” IEEE Trans Magnetics, Vol. 47, No. 10, pp. 3292-3295 (Ooctober 2011).

[9] Oleg Kudrjavtsev and Aleksander Kilk, “Cogging Torque Reduction Methods”, IEEE, (2014), pp. 251 – 254.

[10] Chun-Yu Hsiao, Sheng-Nian Yeh and Jonq-Chin Hwang, “A novel cogging torque simulation method for permanent-magnet Synchronous machines”, MDPI, pp. 2167 – 2170 (2011).

[11] Ting Liu, Shoudao Huang, Qiul ing Deng, Qingyun Pu, Keyuan Huang, “Effect of the number of slots per pole on performance of permanent magnet generator direct-driven by wind turbine”, College of Electrical and Information Engineering, Hunan University, China.

[12] C. Ocak, D. Uygun, Y. Cetinceviz – E. Demir, Y. Gungor, “Performance aspects and verifications of in-runner and out-runner permanent magnet synchronous generator designs of the same magnet structure for low-speed wind systems”, 11th International Conference On Environment and Electrical Engineering (EEEIC), Venice (2012).

[13] Neumann T.W., Tompkins R.E., “Line start motor designed with NdFeB permanent magnet”, 8th International Workshop on Rare Earth Magnets and their Application, Dayton, Ohio, pp. 77 – 89 (1985).

[14] Ramsden V.S., Nguyen H.T., “Brushless DC motors using neodymium iron boron permanent magnets”, Electrical Energy Conference (1987). Adelaide, pp. 22 – 27 (October 1987).

[15] Typical data for M19_26G Silicon Steel Sheet, http://www.aperam.com/brazil/ing/arquivos/atalogelectricalsteeleng.pdf, [26July 2015]

[16] Dohmeki, H,Shoji Y., “Characteristic comparison of PMSM by slot/pole ratio”, The Eighth International Conference on Electrical Machines and System,. Nanjing, China, pp. 251 – 254 (2005).

Voltage Regulation in Solar-Wind Hybrid Energy System using LTC3784

Tazrin Hassan Rini and M. Abdur Razzak
Department of Electrical and Electronic Engineering
Independent University, Bangladesh
Plot-16, Block-B, Bashundhara, Dhaka-1229, Bangladesh
E-mail: htazrin@yahoo.com

***Abstract*—This paper presents a solar-wind hybrid energy system which consists of a Photovoltaic (PV) array, a wind turbine, a Permanent Magnet Synchronous Machine (PMSM), a three phase diode bridge rectifier, a LTC3784 controller, a grid interface inverter, a LC low-pass filter and a step up transformer. The main objective of the paper is to show that whatever may the input voltage (7V-24V DC) comes from the hybrid system, the controller LTC3784 will always give a constant output voltage of 24V DC which is being inverted at 24V AC using an SPWM-based full-bridge inverter, and stepped up to $312V_{peak}$ ($220V_{RMS}$) using a step-up transformer to feed into the utility grid with a frequency of 50 Hz which is the grid voltage in Bangladesh. The proposed model is mathematically designed and simulated by using PSIM and LTspice software. The simulation results show the effectiveness of the hybrid system.**

Keywords- Solar System, Wind System, LTC3784, Inverter

I. INTRODUCTION

With the world energy demand increasing at an exponential rate, the search for energy sources other than fossil fuels is no longer a luxury. Although the fossil fuels offer a temporary solution to this energy crisis, they cause the emission of carbon dioxide and other greenhouse gases, which are harmful to the environment. Hence scarcity of fossil fuel resources and environmental effects, Bangladesh's energy strategy attempts to raise the reliance on renewable energy resources, primarily in photovoltaic and wind concentrated power [1].

Several configurations of hybrid PV-wind system do exist but these configurations inject high frequency current harmonics (HFCH), so to eliminate HFCH the system needs filtering which makes the system more expensive and bulky. [1-4]. In conventional inverters, transformers are used to match the inverter output voltage with the utility grid voltage [5]. But transformers are heavy weighted and costly equipment.

In this paper, Solar-Wind System is connected together so that if one source is not available, the other one can compensate for it. They can work individually and simultaneously too. Then the output is transferred to the controller LTC3784. The controlled constant voltage is then inverted and the method is described later in detail in this paper. All the parameters of the elements are mathematically derived and the designed values are simulated in PSIM and LTspice software to analyze and verify our proposed model.

II. DESIGN OF SOLAR-WIND HYBRID SYSTEM

A. Solar System

The solar panel used here is Resun Solar Energy's solar panel [6], under Standard Test Condition (STC), with 240W maximum output power. At STC condition of 25º temperatures, and irradiance of 1000 W/m, the panel is simulated to give an output of 24V. The output of the Solar system is shown in Fig.1.

TABLE I. Design parameters of solar system

Parameter	Value
Number of cells	60
Standard Light Intensity, S_0	$1000W/m^2$
Reference Temperature, T_{ref}	25^0C
Series Resistance, R_s	.0155Ω
Shunt Resistance, R_{sh}	1000Ω
Short Circuit Current, I_{sc}	9.09A
Temperature Coefficient, Ct	.005454

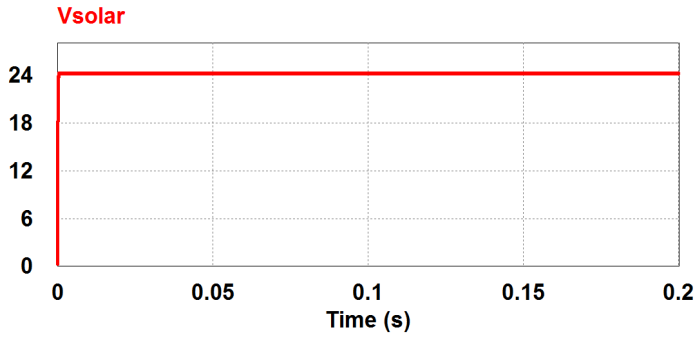

Fig.1. Simulated Output of the Solar System

B. Wind System

In this paper, the system parameters of a 230W Wenzhou SUG New Energy Co., Ltd's SNE-200S [7] wind turbine have been considered for design and simulation. The wind turbine is connected to the gear box and the electrical-mechanical interface and then to permanent magnet synchronous generator to produce an AC output. The system gives 24V output which is shown in Fig.2.

TABLE II. Design parameters of Wind turbine

Parameter	Value
Nominal Output Power	230W
Base Wind Speed	10 m/s
Base Rotational Speed	10m/s
Initial Rotational Speed	0.8
Moment of Inertia	1m kg.m^2
Short Circuit Current, I_{sc}	9.09A
Gear ratio	4.28

Table III. Design parameters of PMSM

Parameter	Value
Stator Resistance, R_s	1mΩ
D-axis inductance	1mH
Q-axis inductance	1mH
V_{pk}/krpm	4000
No. of poles	4
Moment of Inertia	100m kg.m^2

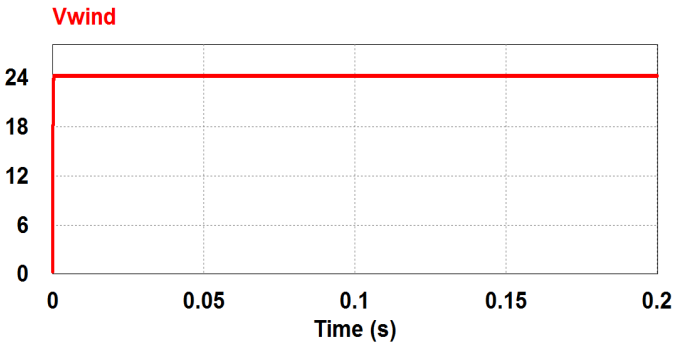

Fig.2. Simulated Output of the Wind System

C. *Combined Solar-Wind System*

Two outputs coming from solar and wind system is added together. The designed model is shown in Fig.3.

III. CONTROLLER LTC3784

The output from both solar and wind system is uncertain. One might give more power and other might give less or both might give same amount of power or one might give full power and other one doesn't give any power. So it becomes essential to control the voltage of this hybrid system. To get a constant voltage from the system, LTC3784 IC has been used in this paper. This IC can take input from 4.5V DC to 60V DC. But to give a fixed output of 24V DC, the input needs to be between 7V DC to 24V DC. It is a product of Linear Technology [8]. The output power of LTC3784 is 240W at 10A. The configuration of LTC3784 is shown below in Fig.4. The simulation has been done with LTspice IV. It is a simulation software of Linear Technology. This IC gives 24V DC output whatever may the input is from 7V to 24V. The outputs from LTC3784 are shown in Fig.5.

IV. PROPOSED GRID TIE INVERTER

To provide power to utility grid there are some requirements [1, 4]. They are:

a) The output voltage should be equal as grid amplitude
b) The phase and frequency of inverter should be same as the utility grid.

In order to simplify the process of synchronization, instead of generating the sine wave from an analog oscillator or from a micro controller and digital-to-analog (DAC), the sine wave for the switching technique is sampled from the power grid using a step-down transformer which steps down the 220V of the grid voltage to 5V. By using a sine wave signal sampled from the grid to generate the SPWM signal, the frequency of the output voltage of the Grid-Tie Inverter (GTI) will have the same frequency as the grid voltage.

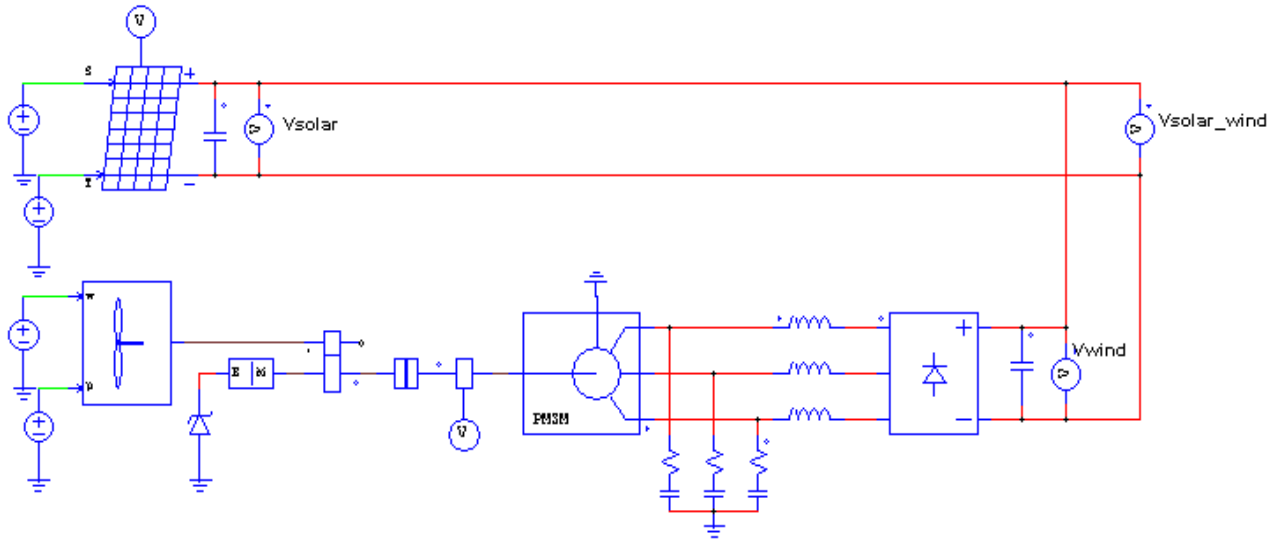

Fig.3.Combined Design of Solar & Wind System

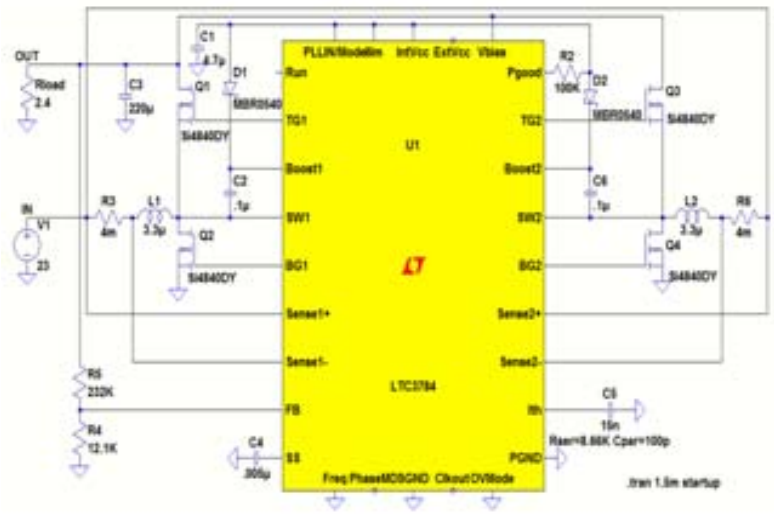

Fig.4. Configuration of LTC3784

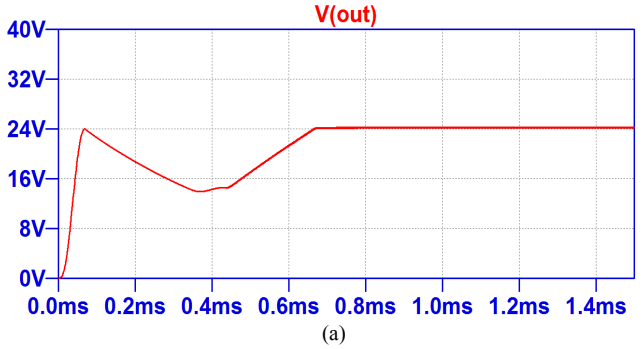

(a)

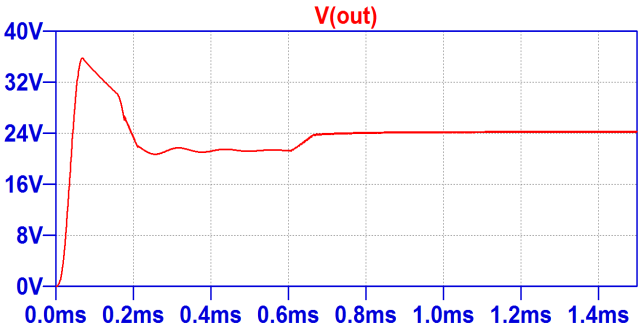

(b)

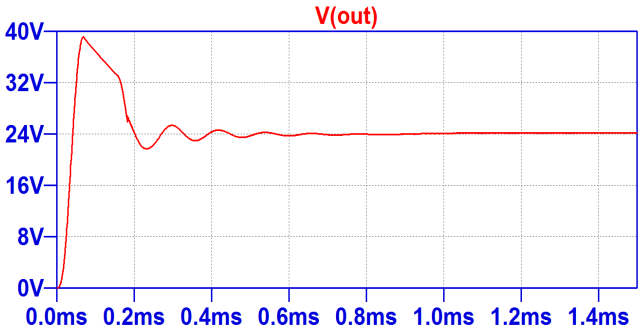

(c)

Fig.5. Simulated Output when input is (a) 10V (b) 20V and (c) 24V

To produce a SPWM signal, a high frequency triangular wave signal is required. In this switching circuit, the high frequency triangular wave is generated using an analog oscillator with a frequency of 10 kHz. Then inverter's phase is synchronized with the grid's phase by employing a 50Hz square-wave pulse taken from the grid and applying AND operation with comparator output which generates four sets of signals [5].

The designed single-phase inverter has four MOSFETs in H-bridge configuration. For M1 & M2 MOSFETs, positive voltage emerges across the load while for M3 and M4 pair, negative voltage emerges across the load [1]. And thus the inverter gives a full square wave output which contains lots of harmonics.

These harmonics are reduced by using LC filter. Here, the cut off frequency, f_c is 50Hz and the characteristic impedance, R is assumed to be 50Ω.So, the values of C and L are calculated using the following equations as C = 63.7μF and L = 0.159 H.

$$f_c = \frac{1}{2\pi\sqrt{LC}} \quad (1)$$

$$R = \sqrt{\frac{L}{C}} \quad (2)$$

A. Inverter with Transformer

The controlled output voltage coming from LTC3784 goes to the inverter. Then it is being inverted using SPWM. And then the output is sent to LC filter to give a harmonic less output and after that it is being stepped up with step up transformer which is shown is Fig.6.

Fig.7 shows the unfiltered voltage from inverter and Fig.8 shows the filtered voltage from inverter. Fig.9 shows the inverter output voltage being stepped up which is 312V (220V RMS).

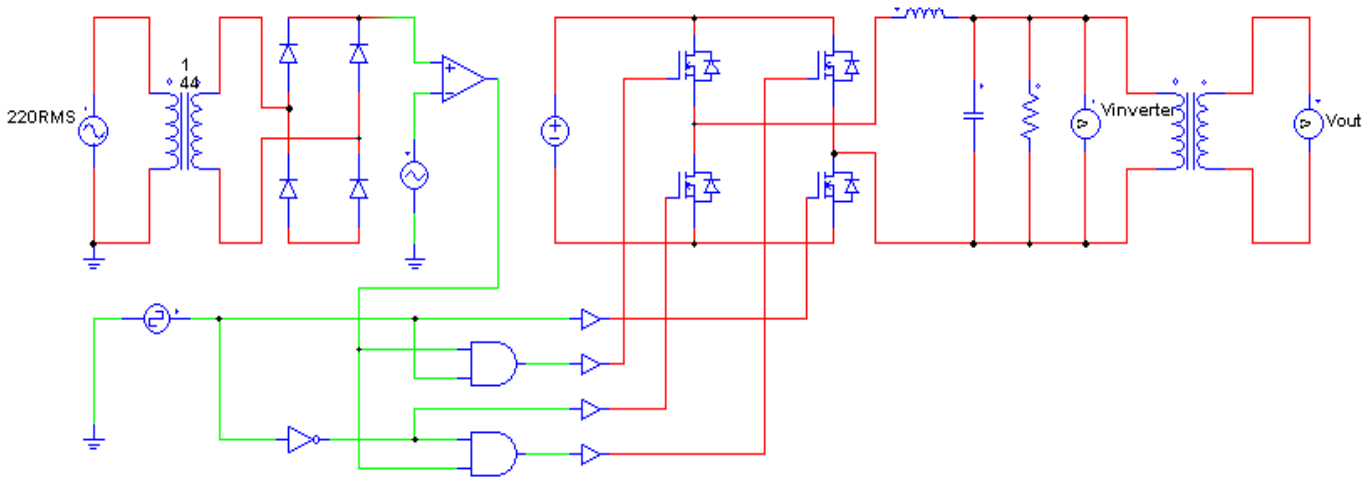

Fig.6.Designed Inverter with Step Up Transformer

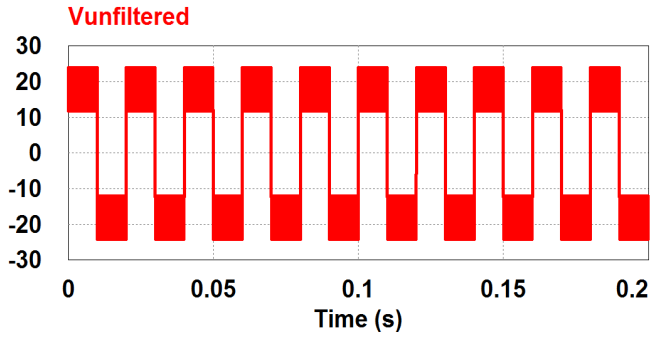

Fig.7. Simulated Output of the Unfiltered Inverter

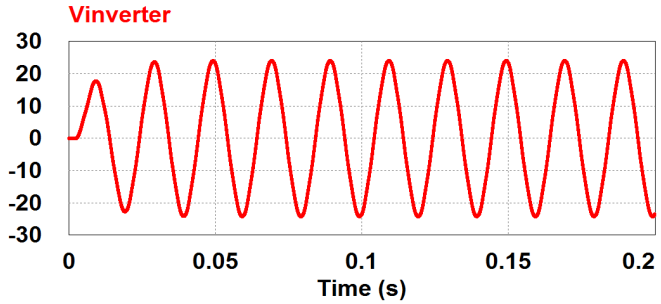

Fig.8. Simulated Output of the Filtered Inverter

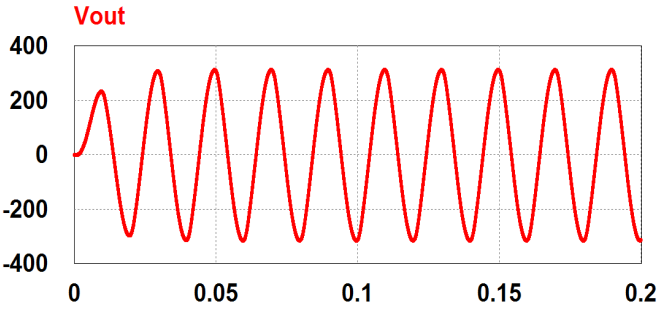

Fig.9. Simulated Output of the Stepped Up

V. CONCLUSION

In this paper a controller for hybrid solar-wind system has been presented. Along with this, grid tie inverter has been discussed and presented with mathematical modeling, analysis and computer simulation. Any voltage coming from solar and wind system can be controlled with LTC3784 and it gives a constant voltage which is being inverted using SPWM to ensure the output voltage has 50Hz frequency with a magnitude of 312V peak (220V RMS) and is in phase with the utility grid voltage. Therefore, it can be said that the simulation results prove that the proposed solar-wind hybrid energy system with controller LTC3784 can be fed to the utility grid with its sinusoidal output voltage.

REFERENCES

[1] S. Chakraborty, M. A. Razzak, "Design of a transformer-less grid-tie inverter using dual-stage buck & boost converters", International Journal Of Renewable Energy Research, Vol.4, No.1, pp. 91-98, March 2014.

[2] Chen et al., "Multi-Input Inverter for Grid-Connected Hybrid PV/Wind Power System", IEEE Transactions on Power Electronics, vol. 22, May 2007.

[3] J. Hui, A. Bakhshai, P. K. Jain, "A Hybrid Wind-Solar Energy System:A New Rectifier Stage Topology"Applied Power Electronics Conference & Exposition (APEC),2010 Twenty-Fifth Annual IEEE.

[4] Abdalrahman, A. Zekry, and A. Alshazly, "Simulation and implementation of grid-connected inverters", International Journal of Computer Applications, vol. 60, no. 4, December 2012.

[5] S. Chakraborty, M. A. Razzak, M. S. U. Chowdhury, S. Dey, "Design of a Transformer-less Grid Connected Hybrid Photovoltaic and Wind Energy System", 9th International Forum on Strategic Technology (IFOST), 21-23 October, 2014.

[6] http://www.alibaba.com/product-detail/240W-24V-Poly-Solar-Panel-with_1176369097.html?spm=a2700.7724857.35.1.owruKK accessed on 21 August, 2015.

[7] http://www.alibaba.com/product-detail/200-watt-wind-turbine_1458919538.html?spm=a2700.7724857.35.1.LoIx91 accessed on 21 August, 2015.

[8] http://www.linear.com/product/LTC3784 accessed on 20 February, 2015.

Socio-economic Impact of a Rural Microgrid

Shailendra Kumar Jha
DoEEE, Kathmandu University
Dhulikhel, Nepal
shailendra@ku.edu.np

Petter Stoa
Sintef Energy Research
Trondheim, Norway

Kjetil Uhlen
Elkraft, NTNU
Trondheim, Norway

***Abstract*—Microgrids are in demonstration phase for rural electrification in Nepal. There are different viable options of forming rural microgrids by the interconnection of distributed energy resources like micro-hydropower plant (MHP), Wind Turbines (WT) and photovoltaic (PV) systems. The rural microgrid under study includes three renewable energy sources MHP, WT and PV system, and battery bank for energy storage. The paper presents the current socio-economic status of rural community fulfilling its electrical need from the rural microgrid. The socio-economic challenges for the sustainability of the rural microgrid are also discussed.**

Keywords- Microgrid; Rural; Socio-economic; Benefits; Nepal

I. INTRODUCTION

Electricity has become the basic need of every society whether urban or rural. The urban communities get their supply from large integrated national grid whereas most of the rural commuinities are out of its reach. Most of the rural communities of Nepal fullfill their electricity need by solar photovoltaic systems or micro-hydropower plants[1,2,3]. In Nepal there are 329849 numbers of solar home systems with total installed capacity of 8.43MWp, 22605 numbers of small solar home systems (>10Wp) with total installed capacity of 113kWp, 2155 numbers of institutional solar PV systems with total installed capacity of 2949.35kWp, and 111 numbers of solar photovoltaic water pumping systems fullfilling the rural electricity demand [1]. 1287 numbers of MHP with installed capacity of 24.606MW, 1634 numbers of pico hydro power plant with installed capacity of 3.703MW, and 24 numbers of small WT with installed capacity of 26.7kW are also deployed for rural electrification in Nepal [1].

There are prospects to interconnect these distributed generators (DG) like MHP, WT or PV systems to supply a larger electrical demand of the rural villages[2,3,4]. The interconnection of two or more distributed energy resources like MHP, WT or PV systems to fullfill the electrical demand of a rural community can be called a rural microgrid[2-7]. The DGs located nearby can be interconnected to supply a larger rural area and provide a relaible supply to the community[2-7]. Interconnection of renewable sources improves the people's living condition and diversify and increase the revenue sources [2,8]. Microgrids offer smaller initial cost, higher efficiency, environmental advantages and less operating cost [2,9,10,11]. Renewable energy microgrid reduces the GHG emissions and improves the environment [10,11,12]. Rural microgrid improves local income generating activities, communication services, education services and agricultural production [13].

There are several possibilities of forming a rural microgrid in Nepal. Some of the interconnection possibilities are as depicted in Fig.1, Fig.2, Fig.3 and Fig.4 [2]. Two MHPs with hydro turbine (HT) and induction generators (IG) or Synchronous generator (SG) can be connected to form a microgrid as shown in Fig.1. A rural microgrid in Nepal can

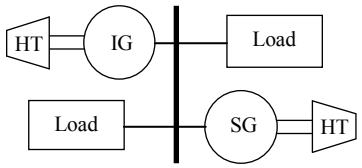

Fig. 1 A microgrid with two MHPs and loads[2]

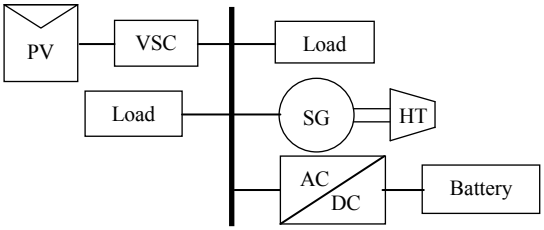

Fig. 2 A hybrid microgrid with PV, MHP, battery bank and loads[2]

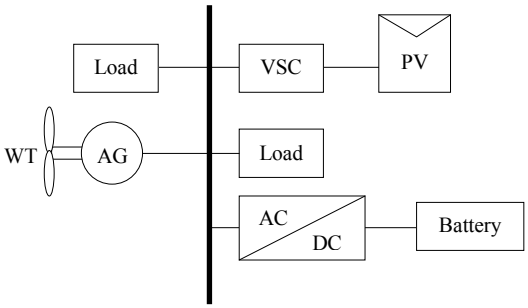

Fig. 3 A hybrid microgrid with PV, WT, battery bank and loads[2]

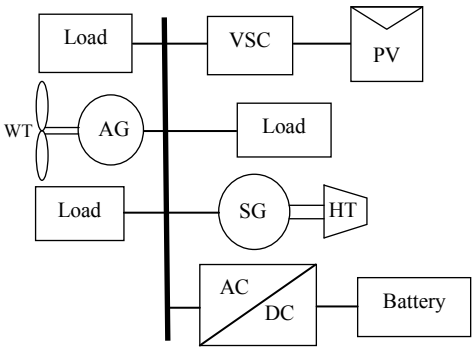

Fig. 4 A hybrid microgrid with PV , WT, MHP, battery bank and loads[2]

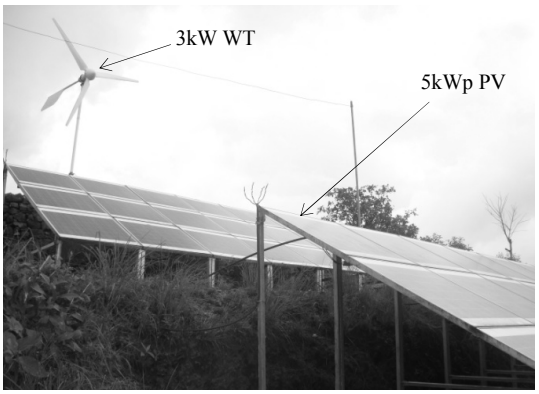

Fig. 5 Installation site of PV and WT at Thingan village

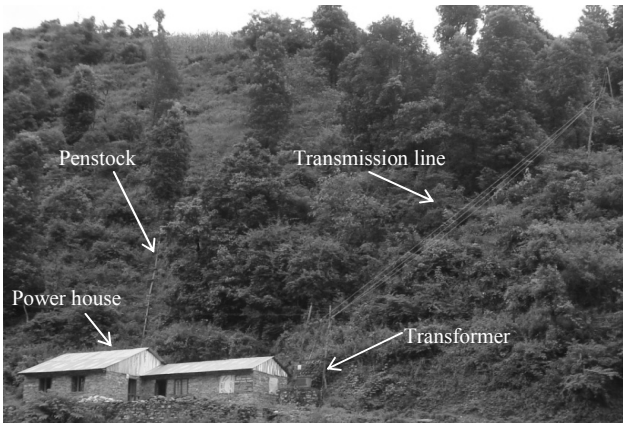

Fig. 6 Installation site of MHP at Kolkhop village

be formed by interconnection of a PV system with a voltage source converter (VSC), a battery bank with DC to AC converter and a MHP as in Fig.2. Also as peresented in Fig.3 PV with VSC, a battery bank with DC to AC converter and a WT can be interconnected to form a microgrid to supply the village load. A MHP, a PV system, a battery bank , WT and local loads would all be connected to form a microgrid as depicted in Fig.4 .

II. System Description

The Thingan-Miteri rural microgrid was installed in 2012 in Makawanpur district of Nepal. It consists of three DGs a 20kW MHP, a 5kWp PV systems, a 3kW WT and a battery bank for storage. The PV systems, WT and battery bank are installed at Thingan village, and the MHP is installed at Kolkhop village 7km away from the PV-WT installation site. Fig.5 shows the installation site of PV and WT, and Fig.6 depicts the installed MHP system. The interconnection of the three DGs to form a microgrid and supply a larger rural load is as depicted in Fig.7. The rural microgrid supplies power to 170 houses, two poultry farm and a grinding mill of the village. Each house has been provided three LED lamps of 8W each. The tariff to be paid by each house is Nepalese rupees 150 (USD 1.47) per month for energy comsumption upto 5kWh. The energy consumed above that is to be paid with a tariff of Nepalese rupees 10 (USD 0.10) per kWh. For

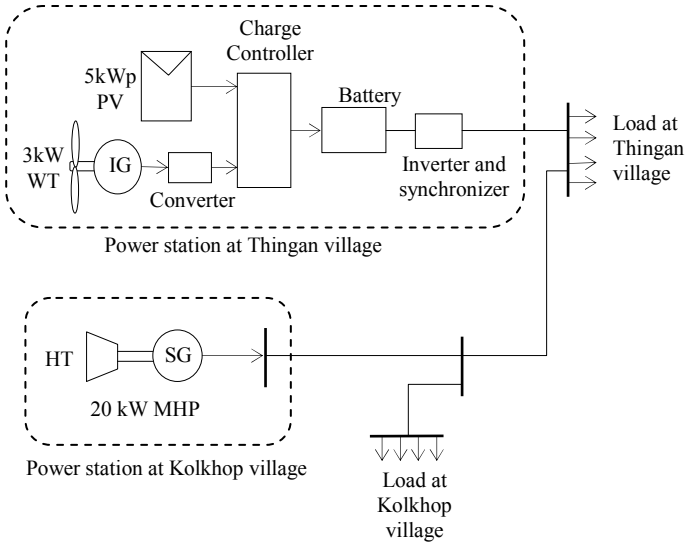

Fig. 7 Thingan-Miteri Rural Hybrid microgrid

industrial comsumers during the day time the tariff is Nepalese rupees 10 (USD 0.10) per kWh.

III. Socio-economic Benefits

As per the survey conducted in the rural villages where the microgrid has been installed, the following socio-economic benefits were observed:

A. Increase of standard of living

Due to surplus power during the day time the use of latest technologies for entertainment, information, communication and household works have increased. The villagers were found using devices like TV, radio, VCR/DVD, laptops, mobile phones, pressing iron, chargable torch lights, refrigerators, sound systems etc. This has increased the living standard of the rural community.

B. Education

Due to the availability of smoke less lights students can do their homework during night time and can study for longer period. This has increased the percentage score of students in exams at school. Computer education has also been introduced at school of the village. Adult education during night time has been made possible due to electricity. Training to villagers about baisic electricity concepts and information on the use of different components of the microgrid has been possible.

C. Improved information access

The use of mobile phones, televisons and radios has increased the information access of the villagers. Previoulsy informations were transferred manually, but now after the microgrid installation villagers convey their messages easily through mobile phones and get national and international informations through radios and televisions sets being used.

D. Women empowerment

Due to electricity, women can work during nigh time and can manage their time for participation in social gathering and adult education. Women do not have to spend a lot of time in bringing water from the river for their daily needs. They utilize this time in working in their gardens to grow flowers and vegetables. Their participation in decision making for children health and education, and household savings is increased.

E. Drinking Water

The availability of surplus electricity has helped people staying on the hills to pump water from the river at the downstreams and store for drinking and household purposes. Also they can use water for vegetation around there houses on the hill.

F. Health

Replacement of kerosene by electricity for lighting, has decreased the inhalation of smoke during work or study. This has decreased respiratory diseases in the community. Childrens are protected from burns while lighting the lamps and poisoning from ingestion of kerosene. Use of sufficient light for study and work was also reduced the eye problems in the villages. Availability of sufficient water has helped villagers to clean their house, clothes and toilets regulary and has reduced sanitation problems.

G. Environmental Impact

The use of clean and renewable sources like solar energy, wind energy and water energy to generate electricity reduces the CO_2 emission by the community. As per Intergovermental Panel on Climate Change(IPCC) the carbon dioxide (CO_2) emission factor by diesel oil based electricity is 0.26676kgCO_2/kWh [14]. The 5kWp PV with average 5 peak sun per day will reduce the CO_2 emission by 2.2tCO_2/year, the 20kW MHP will reduce the emission by 42.25tCO_2/year, and the 3 kW wind turbine with an average generation of 1.8W will reduce the CO_2 emission by 3.8tCO_2/year; considering 330 days of operation per year. Thus, the Thingan-Miteri microgrid reduces the carbon emission of the villages by 48.25tCO_2/year.

H. Local employment

The rural microgrid has created jobs for operators at the two sites of microgrid. In total fours persons are employed for the operation and maintenance of the system. A grinding mill has employed two persons, poultry farms have employed four persons. Also some villagers have started chair or basket weaving during night which has created self employment. Women have started tailoring and stitching job during night hours which have helped to increase their family income.

I. Income generation

The villagers have started grinding mill, poultry farms and basket and chair weaving works. These have generated income to the villagers involved. Also as water pumping on the hills from river has been made possible, villagers are growing cash crops and generating income.

J. Savings

Villagers do not have to purchase their own electricity generation sources like small solar photovoltaic systems or emergencyy torch lights, batteries or kerosene lamps. They do not have to spend money on buying kerosene and batteries regulary for lighting.

IV. Socio-economic Challenges

Although the installation of the rural microgrid has brought many benefits to the villages, some challenges also need to be faced by the community for the proper operation and sustainability of the microgrid. As per the site survey, and discussions with the villagers and operators the followings major challenges were presumed:

A. Tariff collection and updates

The collection of tariff is poor. The villagers do not pay the tariff on time and as the operators are of the same community they cannot force the villagers for the timely payment. This creates problems for providing monthly salary to operators and saving money for regular operation and maintenance works. Also the regular update of tariff is not being possible, which is required in the long run of the microgrid.

B. Insufficient end use during day time

The electricity generated is used mostly for lighting or other purposes during evening 3-4 hours and during morning 3-4 hours. During day time the power consumption is low and during night the power consumption becomes very low. All the power produced by the MHP is fed to the dumped heating load. Thus the plant factor of the system is too low and should be improved for the generating income for maintenance of the microgrid. Also villagers are to be trained and motivated for increasing the end use and creating self employment. End uses like saw mill, furniture shop, electrical and electronic devices repair shops, etc are to be promoted.

C. Limitation of electricity supply during evening hours

The microgrid is designed for lighting of 250 house hold for the evening and morning hours and for other end use during day time. Many of consumers connect fans, TV, radio, mobile phones, laptops during evening hours, and the system becomes overloaded and results in over-current tripping of the system. The consumers have a limited access to electricity during the evening hours to fulfill their need and thus are less satisfied by the system and are less willing to pay the tariff.

D. Service territories

The system is planned to supply power to 250 households of the Thingan and Kolkhop villages. At present only 170 houses have been electrified in the villages and there is surplus power to fulfill the lighting need of the adjoining villages or communities. The cost of extension has been a major challenge, although sufficient power available.

E. Major repair

The rural microgrid has been installed by foreign donation and contribution of the local user community. The regular tariff collected is just for the operators' salary and minor operation and maintenance to be performed periodically. If a major repair is required in the system the village community would be forced to stay in dark until they get some financial support from any donor agencies. Thus a proper step is to be taken prior to the occurrence of such critical event.

F. Microgrid operation after National grid extension

Some of the adjoining villages have electricity from the integrated national grid. After some years, there are possibilities of having national grid supply in the villages where the microgrid is installed. The users getting limited supply and paying high tariff than the national grid will be forced to prefer the national grid supply, and thus the microgrid operation could come to cease. The community should to plan for interconnecting their isolated microgrid to the national grid in future.

G. Regulatory Policies

Proper regulatory policies are to be made for the increase of end use application during the day time. Policies for regular updates of tariff are to be formulated. Plans and actions are to be undertaken for the major repair situations and system expansion. Proper plan and policies are to be formulated for interconnection of the Thingan-Miteri rural microgrid to national grid in future.

V. CONCLUSIONS

The Thingan-Miteri rural microgrid has helped to increase the standard of living of the rural community. The environment, health and education situation of the community has improved. Information access and entertainment has been an added benefit over lighting. Women empowerment and self employment has made the villages a better place to live. Despites of these benefits the community will have to face some socio-economic challenges for the sustainability of the system. The community has to make proper policies for repair and maintenance, extension, up-gradation and if required integration to the national grid in future. With proper future guidelines rural microgrid will be sustainable and would help to improve the livelihood of the rural villages in Nepal.

REFERENCES

[1] AEPC/NRREP(2013), NRREP Baseline Part B: Baseline of Renewable Energy Technology installations in Nepal, Government of Nepal, Ministry of Science, technology and Environment, Alternative Energy promotion Center (AEPC), National Rural Renewable Energy Programme (NRREP), Khumaltar, Lalitpur, Nepal, 2013

[2] Jha, S.K.; Stoa, P.; Uhlen, K., "Microgrid: Prospects and challenges in Nepal," Power and Energy Systems Conference: Towards Sustainable Energy, 2014 , vol., no., pp.1,6, 13-15 March 2014

[3] Maskey, R. K.; Bhandari, V.; Adhikary, B.; Dahal, R.; Shrestha, N., "Prospects for small hydro power plants based mini-grid power systems in Nepal," *Developments in Renewable Energy Technology (ICDRET), 2012 2nd International Conference on the* , vol., no., pp.1,5, 5-7 Jan. 2012

[4] Stoa, P.; Taylor, G.; Chhetri, B.B.; Adhikary, B., "Integrating renewable energy sources in developing countries: A Nepal case study," *Power and Energy Society General Meeting, 2011 IEEE* , vol., no., pp.1,6, 24-29 July 2011

[5] Lasseter, R. H., "MicroGrids," Power Engineering Society Winter Meeting, 2002. IEEE , vol.1, no., pp.305,308 vol.1, 2002

[6] Lasseter, R.H.; Paigi, P., "Microgrid: a conceptual solution," *Power Electronics Specialists Conference, 2004. PESC 04. 2004 IEEE 35th Annual* , vol.6, no., pp.4285,4290 Vol.6, 20-25 June 2004

[7] Litifu, Z.; Estoperez, N.; Al Mamun, M.; Nagasaka, K.; Nemoto, Y.; Ushiyama, I., "Planning of micro-grid power supply based on the weak wind and hydro power generation," Power Engineering Society General Meeting, 2006. IEEE , vol., no., pp.8 pp

[8] Michelon, B.; Nejmi, A.; Dos Ghali, J.; Saidi, A.D.; Bolay, J. -C, "Electrification of isolated areas by interconnecting renewable sources: a sustainable approach," *Clean Electrical Power, 2007. ICCEP '07. International Conference on* , vol., no., pp.33,40, 21-23 May 2007

[9] Solanki, A.; Montoya, L.F.; Fu, Q.; Nasiri, A.; Bhavaraju, V.; Abdallah, T.; Yu, D., "Managing intermittent renewables in a microgrid," *Innovative Smart Grid Technologies (ISGT), 2012 IEEE PES* , vol., no., pp.1,6, 16-20 Jan. 2012

[10] Hatziargyriou, N.D.; Anastasiadis, A.G.; Vasiljevska, J.; Tsikalakis, A.G., "Quantification of economic, environmental and operational benefits of Microgrids," PowerTech, 2009 IEEE Bucharest , vol., no., pp.1,8, June 28 2009-July 2 2009

[11] Anastasiadis, A.G.; Tsikalakis, A.G.; Hatziargyriou, N.D., "Operational and environmental benefits due to significant penetration of Microgrids and topology sensitivity," Power and Energy Society General Meeting, 2010 IEEE , vol., no., pp.1,8, 25-29 July 2010

[12] Mariam, L.; Basu, M.; Conlon, M.F., "Community Microgrid based on micro-wind generation system," Power Engineering Conference (UPEC), 2013 48th International Universities' , vol., no., pp.1,6, 2-5 Sept. 2013

[13] Kirubi, C; Jacobson, A; Kammen, D.M.; Mills, A; "Community-Based Electric Micro-Grids Can Contribute to Rural Development: Evidence from Kenya," World Development, Elsevier Ltd., 2009

[14] http://www.ipcc-nggip.iges.or.jp/public/2006gl/pdf/2_Volume2/V2_1 _ Ch1_Introduction.pdf

Solar Power Controller to Drive Load at Constant Power under Insufficient Solar Radiation

Md. Tanvir Ahammed[#], Md. Rafiqul Islam[*]

Department of Electrical and Electronic Engineering, Khulna University of Engineering & Technology
Khulna-9203, Bangladesh

[#]tanvir.eee10@gmail.com,[*]mri@eee.kuet.ac.bd

***Abstract*—In this paper we have proposed, designed, and practically implemented 125V solar power controller (SPC) capable of driving load at constant power under insufficient solar radiation. The SPC consists of two DC-DC converters along with MPPT controllers and a storage battery. One of the DC-DC converters is connected directly to the solar panel and the other is to the storage battery. To extract the maximum possible electric power from the solar panel MPPT controller is used. The converter steps up unregulated solar panel voltage to a regulated 125V at the load end. The output voltage can be adjusted to any desired level from 20V to 200V DC depending on the application. The proposed controller can provide constant power at 125V and charge the battery when photovoltaic generated power is greater than the load requirements. In contrast, the controller takes additional power from the battery for driving load at constant power with efficiency of about 87% during insufficient solar radiation. The controller can be effectively utilized to drive solar powered loads in real time irrespective of solar radiation.**

***Keywords*— Solar power controller, Insufficient solar radiation, 125V DC-DC converter, Parallel operation, MPPT controller**

I. INTRODUCTION

The demand of electrical energy is increasing tremendously and about 92% of world electrical energy demand is fulfilled by conventional energy resources which utilizes fossil fuels like oil, coal, gas etc. The cost of fossil fuels is increasing day by day as their stocks are limited and they are not available in every part of the world. Continuous use of fossil fuels has severe environmental issues due to global warming [1]. Solar energy, on the other hand, is renewable, environmentally friendly, and unlimited clean source of energy. It is expected that the effective utilization of solar energy can fulfil present and future demand of electric energy.

A photovoltaic (PV) module utilizes intensity of sunlight and converts optical energy into electrical energy. However, the output power of a PV module is not constant, rather, it varies with the variation of intensity of sunlight due to environmental conditions as well as man-made shading [2].

In order to make efficient utilization of solar energy using PV module extensive researches have been carried out. A cost-effective MPPT system is very much promising to harvest maximum electrical energy from solar arrays and reported in [3]. A hybrid system for standalone solar application is presented in [4] which combines wind turbine and PV module. A battery less solar harvesting circuit for low power application was shown in [5]. A directly water pumping system using solar module was reported in [6]. To utilize the PV power completely, it is desirable to use high efficiency power conditioning unit for PV systems [7]. It is well known that the performance of solar powered loads like solar driven water pumps (SDWP), solar powered rice mills (SPRM), solar powered electric vehicles (SPEV), etc. may degrade due to insufficient solar radiation. In previous studies [8-11] driving loads at constant power under insufficient solar radiation were not addressed in details for battery less PV systems. It is therefore very much important to develop solar power controller (SPC) for driving loads efficiently under insufficient solar radiation.

In this paper a power electronics based 125V SPC is proposed, designed, and practically implemented. The performance of the SPC is tested for different solar radiations. The results presented in the present study demonstrate that the proposed SPC is capable of driving loads at constant power with 87% efficiency even under insufficient solar radiation.

II. PROPOSED SOLAR POWER CONTROLLER

Maintaining constant power at the load end for battery less applications, such as, SPEV, SDWP, SPRM, etc. is the main difficulty in PV systems. Here, a SPC is proposed that can provide constant power at the load end even when solar radiation is insufficient.

A. Controller Configuration

The proposed SPC consists of two DC-DC converters (boost converter) along with MPPT controllers and a storage battery. Two DC-DC converters operate parallel and share a load in order to maintain constant power at the load end. The block diagram of the proposed SPC is shown in Fig.1. The arrows, as shown in Fig. 1 indicate the direction of power flow. Converter-1 acts as main source and converter-2 acts as backup source. Converter-1 is connected to the output of an MPPT controller which is connected to a solar panel and converter-2 is connected directly to the terminal of a backup battery. The battery is connected to the solar panel via a MPPT charge controller. The MPPT charge controller protects the backup battery from over-charging and over-discharging. Lead acid battery can be used due to low cost and maintenance. Both of the DC-DC converters are designed for 125V DC applications. A control system is included to adjust the SPC output voltage to any desired value. The main hardware components of the SPC are ferrite core transformer (ETD-39), current mode PWM controller (UC3843), ultrafast-diode (UF-5408), resistors, capacitors etc.

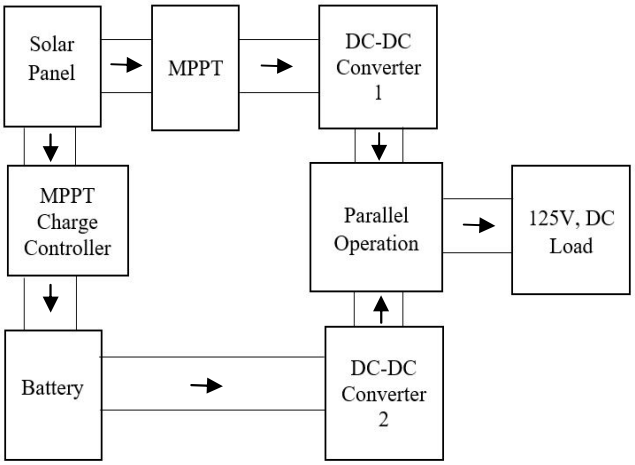

Fig. 1 Block diagram of the proposed SPC.

B. Controller Operation

The controller provides regulated 125V DC terminal voltage at the load end even under insufficient solar radiation. In the proposed SPC, PV module acts as primary source and storage battery is a backup source. The major operation of the proposed SPC are as follows:

- When PV module power generation is higher than load requirements converter-1 remains in operation and drives the load connected to it. Converter-2 remains in idle. The excess PV generated energy is stored in the battery. The charge controller controls charging and discharging operation of the battery.
- When PV module power generation is equal to load requirements converter-1 remains in operation and drives the load connected to it. Converter-2 remains in idle.
- When PV module power generation is lower than the load requirements, converter-1 and converter-2 remain in operation and share the connected load. In this stage the excess energy stored previously in the battery starts discharging.
- When PV module power generation is null, converter-2 remains in operation and drives the connected load. The excess energy previously stored in the battery starts discharging in this stage and converter-1 remains in idle.

The operation schematics of the proposed SPC is listed in Table I.

III. Performance Of The Proposed SPC

The most important part of the proposed solar controller is the DC-DC converters, which steps up the PV module terminal voltage and give regulated 125V DC at the output to drive the load. The voltage stepping up capability and efficiency of the DC-DC converters determines the effectiveness of the proposed SPC. The DC-DC converters are designed using fly-back converter topology, because it requires relatively less components and has better efficiency.

TABLE I
Operational Schematics Of The Proposed SPC.

PV power generation	Battery status
$P_{PV} > P_{Load}$	Battery charging
$P_{PV} < P_{Load}$	Battery discharging
$P_{PV} = P_{Load}$	Battery idle
$P_{PV} =$ Null	Battery discharging

A simplified circuit-diagram of a fly-back DC-DC converter is shown in Fig. 2. The proposed SPC are designed to provide 125V DC at the load end, which reduces transmission loss and enables long distance transmission of power for solar systems.

A. Experimental Results

To determine the performance of the proposed SPC experimentally, a solar panel and a storage battery is used. The solar panel used here has the following parameters: P_{max} = 44W, V_{oc} = 19.2V, I_{sc} = 2.96A, $V_{operating}$ = 16.5V, and $I_{operating}$ = 2.67A for standard operating condition 1000W/m^2 at 25^{0}C. A 12V, 7.5Ah lead acid battery is used as a back-up source. Since the proposed SPC is designed to derive load at constant power under insufficient solar radiation, the effectiveness of the SPC is tested for different solar radiations. In order to vary the incident solar radiation on the panel surface, artificial shading was created by a screen. The solar radiation was varied by changing the shading distance from the solar panel. The dependency of panel terminal voltage, V_{solar}, and current, I_{solar}, as a function of solar radiation measured under different shading conditions is shown in Fig. 3. As seen in Fig. 3 the output characteristics of the panel is highly dependent on the shading conditions i.e. solar radiation. This demonstrates that driving loads at constant power is a vital issue under insufficient solar radiation. Tables II and III show the experimental data obtained from the implemented SPC for 22W DC load. The data are taken in two cases: i) when solar power generation is more than the requirements of the load and ii) when solar power generation is less than the requirements of the load. It is observed from Tables II and III that the solar power generation decreases with decreasing solar radiation. As long as the solar power generation enough to derive the load at rated power, the excess solar energy is used to charge the battery. This is happened when the incident

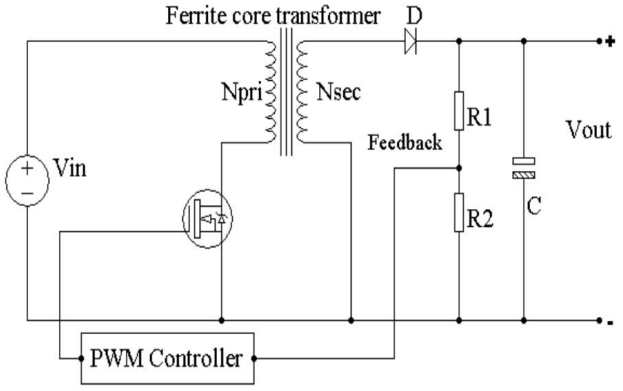

Fig. 2 Fly-back topology for DC-DC converter.

TABLE II
LOAD SHARING CHARACTERISTICS OF SOLAR PANEL AND BATTERY FOR 22W DC LOAD WHEN SOLAR POWER GENERATION IS MORE THAN THE REQUIREMENTS OF THE LOAD

Solar radiation (W/m^2)	Solar			Battery (charging)			Load			Efficiency (%)
	V_{solar} (V)	I_{solar} (A)	P_{solar} (W)	$V_{battery}$ (V)	$I_{battery}$ (A)	$P_{battery}$ (W)	V_{load} (V)	I_{load} (A)	P_{load} (W)	
700.0	13.95	2.20	30.69	13.90	0.61	8.48	125.60	0.17	21.35	86.50
600.0	13.76	1.90	26.14	13.80	0.28	3.86	125.70	0.17	21.37	87.00
580.0	13.46	1.85	24.90	13.80	0.00	0.00	126.00	0.17	21.42	86.00

TABLE III
LOAD SHARING CHARACTERISTICS OF SOLAR PANEL AND BATTERY FOR 22W DC LOAD WHEN SOLAR POWER GENERATION IS LESS THAN THE REQUIREMENTS OF THE LOAD

Solar radiation (W/m^2)	Solar			Battery (discharging)			Load			Efficiency (%)
	V_{solar} (V)	I_{solar} (A)	P_{solar} (W)	$V_{battery}$ (V)	$I_{battery}$ (A)	$P_{battery}$ (W)	V_{load} (V)	I_{load} (A)	P_{load} (W)	
270.0	7.90	1.30	10.27	12.00	1.20	14.40	125.70	0.17	21.37	87.00
200.0	7.90	0.96	7.58	12.00	1.40	16.80	125.60	0.17	21.35	86.50
105.0	7.90	0.50	3.95	12.00	1.73	20.76	125.70	0.17	21.37	87.00
50.0	7.90	0.20	1.58	12.00	1.92	23.04	125.60	0.17	21.35	86.40
30.0	7.90	0.10	0.79	12.00	2.00	24.00	125.60	0.17	21.35	86.40
0.0	0.00	0.00	0.00	12.00	2.05	24.60	125.90	0.17	21.40	86.00

solar radiation more than 580 W/m^2 and clearly observed in Table II. From Table II, it is observed that at 580 W/m^2 solar radiation the whole PV power generated is used to drive the load, for this reason charging current is zero. The situation becomes reverse when solar radiation falls below 500 W/m^2 as seen in Table III. In this situation the SPC takes the remaining amount of power from the storage battery in order to derive the load at rated power. To understand the load sharing characteristics among the solar panel and the battery under different solar radiations Fig. 4 is plotted. It is found in Fig. 4 that the implemented SPC can maintain constant power at the load whatever may be the solar radiation. When solar power is sufficient to derive the load, the battery remains in idle. The battery comes into operation when solar power generation is insufficient to derive the load at rated power. Under no shading condition the maximum solar power generation is 30.69W, so it can easily drive the load without the help of the battery. The turn ON and turn OFF directions of the battery are also shown in Fig. 4. The battery will be in turned ON stage when the amount of solar radiation lies left to point A and it starts discharging for providing surplus of power at the load. The opposite is happened, that is, battery will be turned OFF when the solar radiation is sufficient to drive the load at rated power. Point B in Fig. 4 indicates that solar power generation is null and the load is solely driven by the battery. Between points A and B solar panel and battery derive the load by sharing. Beyond point A, as shown in Fig. 4 the battery remains in charging stage. The power sharing tendency to maintain the constant load power is clearly understood by power curves shown in Fig. 4. The solar radiation dependent SPC efficiency is shown in Fig. 5. From Fig. 5, the overall

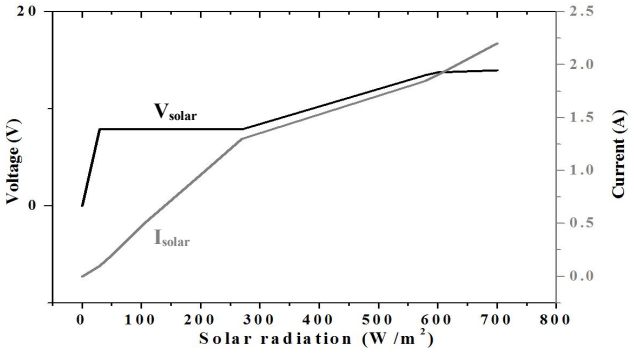

Fig. 3 Dependency of solar panel terminal voltage, and current as a function of solar radiation.

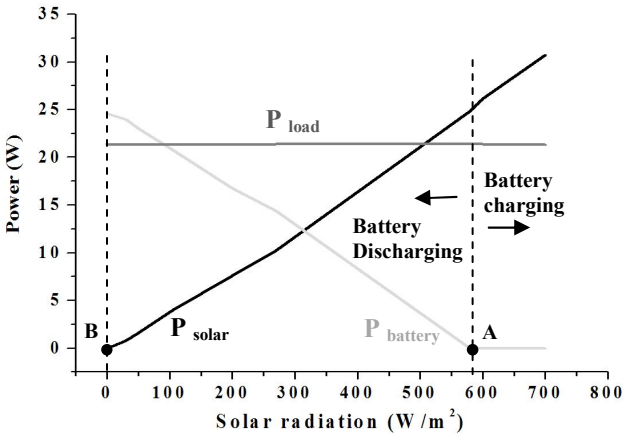

Fig. 4 Solar radiation dependent load sharing status of solar panel and battery along with battery charging and discharging characteristics.

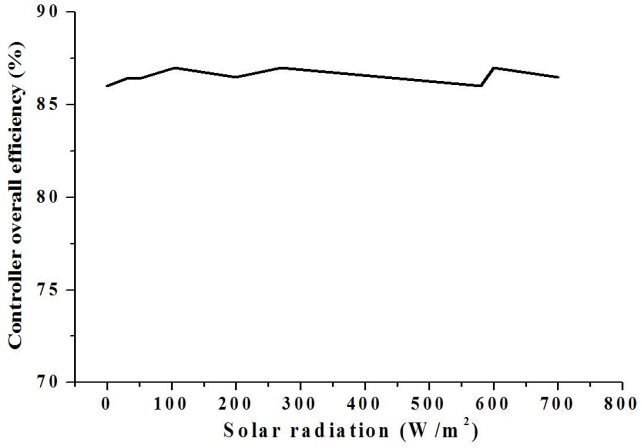

Fig. 5 Solar radiation dependent SPC efficiency.

efficiency of the proposed SPC is found to be about 87% and it is almost constant for the variation of solar radiation from lower to higher value. This demonstrates that the implemented SPC efficiency is independent of solar radiation and it is capable of driving the load at rated power even under insufficient solar radiation.

IV. CONCLUSION

In this work we have proposed, designed and practically implemented a SPC with a view to drive a load at rated power even under insufficient solar radiation. The controller boosts up unregulated solar panel terminal voltage to a regulated 125V at the load side. MPPT controllers are used to obtain maximum available power from the solar panel and to control charging operation of battery. MPPT charge controllers also protects the battery from over charge and over discharge. The controller is capable to switch over the battery from charging to discharging mode depending on the availability of solar radiation. The effectiveness of the controller is tested for 22W load at different solar radiations. It is found that the proposed controller provides constant power at the load side with almost constant efficiency of about 87% and it is independent of solar radiation. It is expected that the implemented SPC can be used to drive solar driven loads in real time at rated power even under insufficient solar radiation.

References

[1] M. Veerachary, "Fourth-order buck converter for maximum power point tracking applications*", IEEE transactions on aerospace and electronic system,* vol. 47, No. 2. pp. 896-911, April 2011.

[2] J. K. H. Hussein, I. Muta, T. Hoshino, and M. Osakada, "Maximum photovoltaic power tracking: An algorithm for rapidly changing atmospheric conditions," in *Proc. Inst. Elect. Eng.—Gen. Tranmiss. Distrib.,* vol. 142, no. 1, pp. 59–64, Jan. 1995.

[3] D. P. Hohm and M. E. Ropp, "Comparative study of maximum power point tracking algorithms using an experimental, programmable, maximum power point tracking test bed," in *Proc. 28th IEEE Photovoltaic Spec. Conf.,* 2000, pp. 1699–1702.

[4] MouS. Tanezaki, T. Matsushima, and S. Muroyama, "Stand-alone hybrid power supply system composed of wind turbines and photovoltaic modules for powering radio relay stations," in *Proc. IEEE INTELEC*, Oct. 2003, pp. 457–462.

[5] Davide Brunelli, Clemens Moser and Lothar Thiele, Member IEEE, "Design of a Solar-Harvesting Circuit for Battery less Embedded Systems". *IEEE Trans. on Circuits and Systems,* vol. 56, 11 Nov. 2009.

[6] H. Dehbonei, S. R. Lee, and H. Nehrir, "Direct energy transfer for high efficiency photovoltaic energy systems. Part I: Concepts and hypothesis,"*IEEE Trans. Aerosp. Electron. Syst*., vol. 45, no. 1, pp. 31–45, Jan. 2009.

[7] T. Esram and P. Chapman, "Comparison of PV array maximum power point tracking techniques," *IEEE Trans. Energy Convers*. vol. 22, no. 2, pp.439-449, June 2007.

[8] S. Zhong Yi He, Hong Chen, "Integrated solar controller for solar powered off-grid lighting system", *Elsevier, Energy Procedia 12*, pp. 570-577, September 2011.

[9] Mo J. Enslin, M. Wolf, "Integrated photo-voltaic maximum power point tracking converter*," IEEE Trans. Ind. Electron. ,* vol. 44, no. 6, pp. 769-773, Dec. 1997.

[10] Rong-Jong Wai, Wen-Hung Wang, "High performance Stand-Alone Photovoltaic Generation System, " *Industrial Electronics, IEEE Trans*. vol. 55, no. 1, pp. 240-250, Jan. 2008.

[11] J Cam Pham, Kerekes, T. Teodorescu, "High efficient bidirectional battery converter for residential PV systems," *Power Electronics for Distributed Generation Systems (PEDG), 2012 3rd IEEE International Symposium on,* vol., no., pp.890-894, 25-28 June 2012.

Electric efficiency of the lighting technology of auto industry: recent development and future prospect

Muhammad Sifatul Alam Chowdhury
Department of Electrical and Electronic Engineering
International Islamic University Chittagong
Chittagong, Bangladesh
m.sifatul.alam@gmail.com

Al Mahmudur Rahman
Institute of Engineering Mechanics
Karlsruhe Institute of Technology
Karlsruhe, Germany
al.rahman@partner.kit.edu

***Abstract*—To meet the increased demand of flexible and technologically advanced lighting system, superior technologies are introduced in the automobile industry. Though initially candle was used for the lighting however lighting technology is now staying at a supreme level of advancement. In 1908 though electric bulb was started to use in the motor vehicle but specifically from 1920 electric bulb were started to use in the passenger car. Technologies like advanced front lighting system or active intelligent lighting system playing the key role to achieve this supreme advancement of automotive lighting technology. Tremendous improvement are achieved both on luminous efficiency and power consumption of the lighting system. Technologies like light emitting diode (LED), Halogen, Xenon made the vehicle lighting system more flexible and secure. Lighting system of vehicle plays the role of lighting, signalling and safety issue. Light emitting diode (LED) and Xenon bulbs are comparatively expensive than halogen bulbs however the efficiency of halogen is comparatively lower than that of LED/Xenon bulbs. To represent the identity of vehicle lighting system play the key role which is directly related to the vehicle safety. That is vehicle lighting system not only used only for illumination but also for vehicle safety. In this paper the technologies used in the vehicle lighting system are deeply reviewed and compared. Besides this comparative discussion of this technologies from economical perspective are done.**

***Keywords*—Automotive lighting system; Lighting electronics; Light emitting diode (LED); Vehicle electrical system; Halogen bulb; Xenon bulb; Efficiency of vehicle lighting system.**

I. INTRODUCTION

Initially illumination was the key concern of the lighting system of motor vehicle however now a days the lighting system of a motor vehicle playing some crucial role including passenger safety and signalling. The rapid growth of the automobile industry also emphasizes on the multipurpose use of vehicle lighting system with minimum energy use. Modern lighting technology of the vehicle using the state of the art technology where the power consumption is minimum. Moreover the astonishing development of electric vehicle made the work much easier.

At the beginning of the auto industry fuel like oil were used for lighting purpose and a vehicle did not maintain a fully electrified system. After the invention of HID headlamps though the massive use of HID seen for headlamp but LED took place of the HID lamp at the first decade of 21st century. Implementation of green technologies in the vehicle reduced the power consumption of the vehicle greatly. Technologies like regenerative braking, fuel cell are performing impressively good to increase the power consumption efficiency of the vehicle [1]. The consumption rate of vehicle is directly related to the emission of vehicle where the key power consuming equipment's of the vehicle is the lighting system of the vehicle. So the more efficient lighting system the more efficient power consumption will happened in the vehicle Lighting system of current vehicles are pretty complex and headlamp of the vehicle plays the key role as it describes the vehicle identity. Now a days safety of the passengers are given the maximum priority while designing an electrical system of the vehicle and the technologies like adaptive front light system made the work more flexible [2]-[3].

II. METHODOLOGY

Due to the supreme advancement in the semiconductor industry more electronics are added in vehicle electrical system. There are fixed regulations about the intensity and types of the light can be used in the different side of the vehicle like front, tail etc. Technological advancement are implemented within this regulation to make the vehicle lighting system more efficient and secure. In this research along with the technological advancement of vehicle lighting system a relation between economical and technical perspective of vehicle lighting system are discussed.
Emphasize are given on the latest advancement of vehicle lighting system, how they implemented in the vehicle, how the use of latest technologies made the vehicle power consumption more efficient. Beside this market statistics and market forecast on the vehicle lighting system are represented so that a detail projection can be gained about the ruling technology of vehicle lighting market. There are a lot of data

about the market research of the lighting system of the vehicle however most authentic and widely accepted data are used in this research.

III. Current Automobile Industry

At present the automobile industry is increasing at an impressive rate. If the focus can be given on the current vehicle production rate than it can be easily sorted out which countries are dominating in this sector [4]. Because the domination not only depends on the large investment but also depends on the technological advancement and the proper implementation of those technologies.

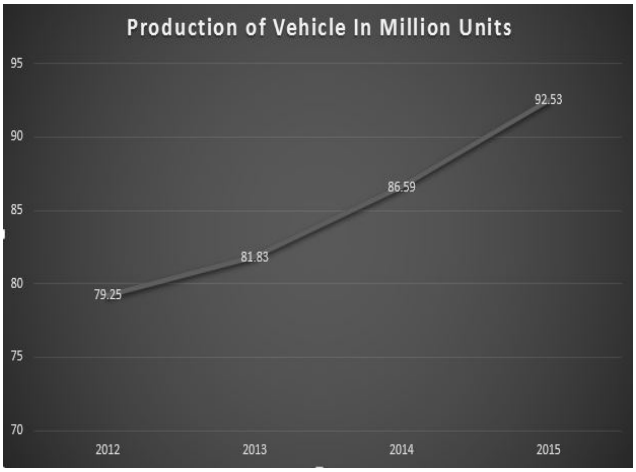

Fig. 1. Worldwide vehicle production forecast

If the focus can be given on the leading automobile giants it can be easily realized that simultaneous research and proper implementation of state of the art technologizes is solely responsible for preserving the leading positions. According to the Fig. 2 a ranking of vehicle manufacturer based on their sales in 2014 it is clear that Toyota is leading the market with securing the 23% of the market share [5]. Continuous research and investment to improve the lighting technologies is one of a key player behind this success of Toyota.

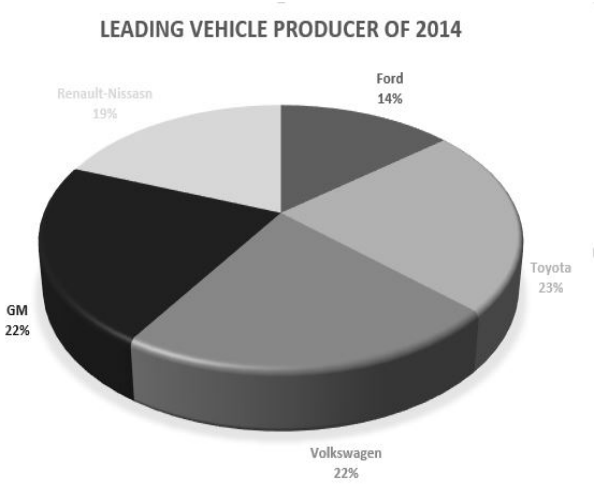

Fig. 2. Worldwide vehicle producers ranking of 2014

IV. Main Electricity Consumers of the Vehicle

There are several parts in the vehicle for consuming the power. A list of major power consuming parts are included below:

TABLE I
Major Electricity Consumer of the Vehicle

Motor
electric fuel-supply pump
Radio
Side-marker lamp
Interior heating fan
Electrical radiator ventilator
Windshield wiper
Stop lamp
Turn signal
Fog lamps
Rear fog lamp
Heated rear window
Indicator lamp
Low beam (dipped beam)
License-plate lamp
tail lamp

This list of consumers can be varied from vehicle to vehicle. If focus can be given on the chart it is easily noticed that lighting system of the vehicle is the major consumer of vehicle power. That is majority of the power of a vehicle is consumed by its lighting system. So the efficiency of vehicle lighting system greatly affect the overall power consumption of the vehicle. The more efficient lighting system the more efficient power consumption

V. Vehicle Standard Light Specification

Standard light specification for car and commercial vehicles are mentioned below:

TABLE II
Vehicle Standard Light Specification [6]

Name	Voltage (V)	Power (W)	Lumen	Category
High beam, low beam	6	45/40	-	R2
	12	45/40	1030/740	
	24	55/40	-	
Fog lamp, high beam, low	6	55	-	H1
	12	55	1550	

beam in 4-headlamps	24	70	1900	
Fog lamp, high beam	6	55	-	H3
	12	55	1450	
	24	70	1750	
High beam, low beam	12	60/55	1450	H4
	24	75/70	1750	
High beam, low beam in 4-headlamp fog lamp	12	55	1500	H7
	24	70	1750	
Fog lamp, static cornering light	12	35	800	H8
High beam	12	65	2100	H9
Fog lamp	12	42	850	H10
Low beam, fog lamp	12	55	1350	H11
	24	70	1600	
Low beam in 4-headlamps	12	55	1100	HB4
High beam in 4-headlamp	12	60	1900	HB3
Stop, turn-signal rear fog, revers lamp	6	-	-	P 21 W
	12	21	460	
	24	21	460	
Stop lamp/ tail lamp	6	21/5	440/35	P 21/5 W
	12	21/5	440/35	
	24	21/5	440/40	
Side-marker lamp, tail lamp	6	5	50	R 5 W
	12		50	
	24		50	
Tail lamp	6	10	125	R 10 W
	12			
	24			
Daytime running light	12	13	250	P 13 W
Stop lamp, turn signal	12	19	350	P 19 W
	12	19	215	PY 19 W
License-plate lamp, tail lamp	6	5	45	C 5 W
	12			
	24			
Reversing lamp	12	21	460	C 21 W
Side-marker lamp	6	4	35	T 4 W
	12			
	24			
Side-marker lamp, license-plate lamp	6	5	50	W 5 W
	12			
	24			
Side-marker lamp, license-plate lamp	6	3	22	W 3 W
	12			
	24			

VI. STATE OF THE ART LIGHTING TECHNOLOGIES

A. Light emitting diode (LED) and OLED

A Light emitting diode is a nothing but a p-n junction. In 1993 for the first time ford installed LED tail lamp. Since then the use of LED in different parts of vehicle are increased at a high rate [7]-[9]. The invention of LED opened a new era to in the field of vehicle headlamp [10]-[11].Though light emitting diodes (LED) leads in the vehicle lighting technology however the invention of organic light emitting diode opened a new era in the field of automotive lighting. Main advantage of OLED is its design option. OLED can be vastly used in the wide space in the vehicle like tail. The thing which attract the users to select a vehicle is the design of that vehicle and light plays an important role to attract the customer. In this sense the use of OLED is a revolutionary addition in the field of automobile. Many companies like Audi, Ford are already started to use OLED in their vehicle.

There are some basic difference between LED and OLED. The main specialty of OLED is its thinness which makes OLED easier to implement in the surface area. But the key difference between the LED and OLED is indicates names that is LED is made up of with inorganic layers whereas OLED is made up of organic layers. Most suitable area for OLED in vehicle is the roof or window. But there are some barriers like price, performance, safety which is still under research. Though the performance of the OLED reached the mark of halogen lamp but the attraction of OLED is not turned yet to the automotive industry.

One of an impressive advantage of OLED is its light weight which enable this to implement in the roll up display. Though organic light emitting diode is an impressive technology in the field of automotive lighting system however the efficiency of OLED is still less than LED considering cost. So it may take time to see mass use OLED in the vehicle.

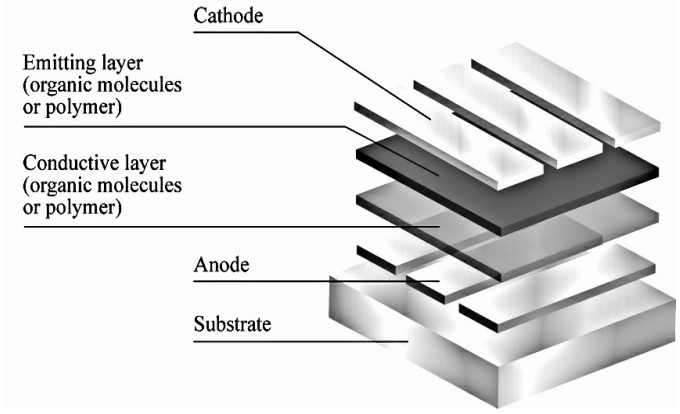

Fig. 3. Basic structure of organic light emitting diode [12]

B. High intensity discharge lamp (HID)

Electric arc is responsible for producing illumination in the high intensity discharge light. High intensity discharge lights are special type of gas discharge light [15]-[16]. Though gas discharge light for the vehicle was introduced in 1990 but high intensity discharge lamp was introduced for the first time in Europe during 1991. It's the widely used lighting technology in the auto industry [17].

There are different types of HID lamp like Xenon short-arc lamp, Sodium vapor lamp etc. however the basic principles behind this almost same. There is an arc tube and the tube is filled with both gas and metal. The gas is responsible for starting the arc and once the arc is started it cause the metal to form plasma which impressively increase the intensity of arc light which is produced by the arc. This will reduce the power consumption.

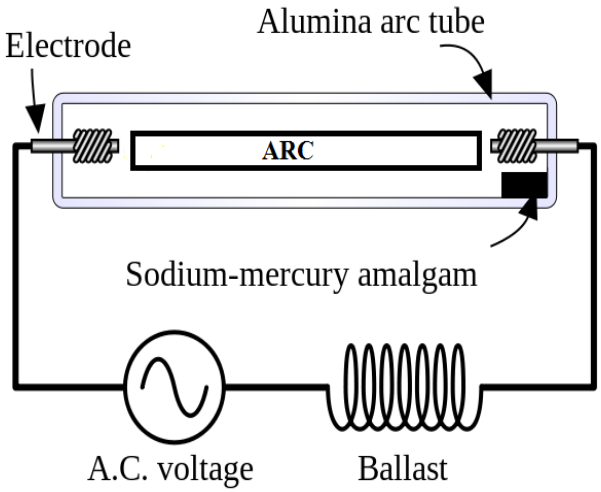

Fig. 4. High pressure sodium lamp [18]

HID lamps can save up to 75% energy if they are replaced with incandescent lamps. The overall efficiency of HID lamp is near 110-120 lumen per watt. However there some losses which are greatly responsible for reduced intensity of HID lamps especially the presence of ballast is the most inefficient part of HID lamps with this the operating temperature which is not perfectly suitable for performance oriented operations.

The major barrier behind the massive use if HID lamps is its efficiency. The efficiency of HID lamps are pretty lower than Light emitting diodes (LED). Various parts of High intensity discharge (HID) lamp are less durable than the parts of LED as LED doesn't contain parts like electrode or filaments. One of a major drawback of HID lamp is its operating temperature which is around -30^0C to 60^0C which pretty tough to maintain simultaneously. Moreover the color quality of the HID lamps are average whereas the color quality of LED is far better than HID lamp. According to the Fig. 5 it is seen that the lumen per watt of HID lamp is 75 and the Lumen per watt of LED is 17.

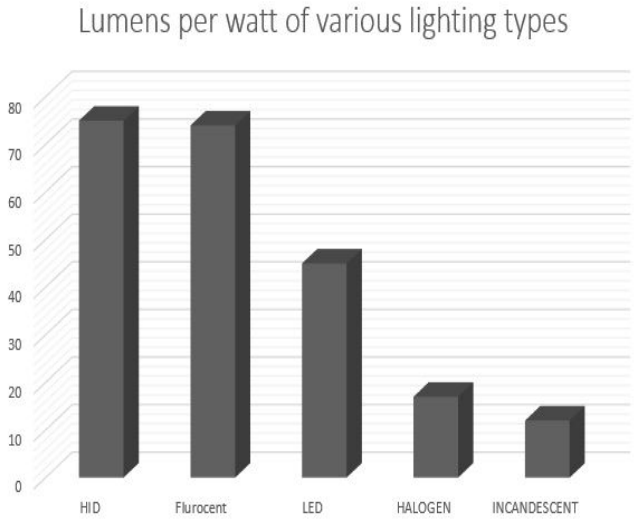

Fig. 5. Lumens per watt of various lighting system

C. Halogen Light

Halogen light mostly known as the tungsten light is the mostly used lighting technology in the automobile industry. It is an incandescent light where a light amount of halogen particle like bromine are mixed. There are no temperature barrier for the halogen lamps and halogen light can be used in the higher temperature. Halogen lamps are mostly used as headlamp of the vehicle. Though halogen lighting system were first introduced in 1960 at Europe however it was introduced at US in 1979.

According to Fig. 6 it is clear that the efficiency of halogen lamp is pretty higher than typical incandescent lamp which is 90 lm/W. The lifetime of the halogen lamp is also higher than incandescent lamp which is approximately 4000 hours. But both the parameter is still lower than that of LED and HID lamp [19].

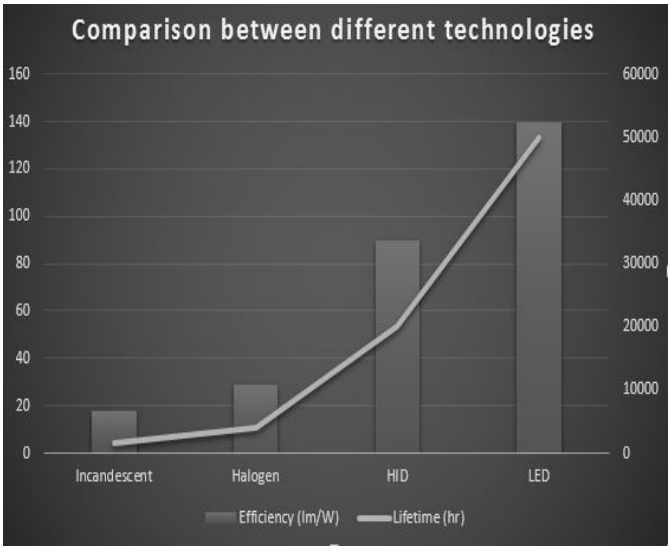

Fig. 6. Comparison between various lighting systems

Halogen lamps are one of the most old and reliable technology in the history of automobile lighting. After implementing polycarbonate to make the exterior casing of the halogen headlamp instead of glass it became stronger and lighter than before which definitely increased the efficiency of the halogen lamps.

According to their life cycle and cost halogen lamp are the most impressive option for automobile manufacturer for vehicle lighting system till now.

CONCLUSION

Light Emitting Diode (LED), High Intensity Discharge (HID) and Halogen lamps are the most common technologies that are enlightens the vehicle lighting system currently. Besides some other technologies like Laser are under research and implemented in a limited way. Lasers are generally used for empowering headlamps [20]. Main advantage of laser is its illumination power which is much more than typical LED or HID lamp and the size and design of Laser headlamp is pretty impressive. However the disadvantage of laser headlamps lies in its advantage because eyes can't tolerate high intensity of light it might be a cause of blindness. So the safety issue of laser headlamp is not fully resolved and till than laser headlamp should not be seen in the vehicle in a massive way.

Except the laser headlamp the other three technologies are currently dominating the automobile lighting market more specifically the halogen lamps are ahead in the domination chart. All the technologies have their own impressive characteristics. At present halogen is the highest revenue earning technology in field of automobile lighting and this will continue till end of this decade. Though technically halogen lamp are leading but when the consideration is given to the lighting of the different side of the vehicle than surely the front lighting will be highest earning side.

In this paper a comprehensive review is done on the automobile lighting system. Detail discussions are done on different technologies used in automobile for lighting purpose. Along with their technical representation their market statistics are also represented to clarify that which lighting technology is currently dominating the current automobile industry. This representations also indicates the future technologies that are awaited to rule the vehicle lighting system.

REFERENCES

[1] Chowdhury, M. S. A., Rahman, A. M., & Samrat, N. H., "A comprehensive study on green technologies used in the vehicle," In Green Energy and Technology (ICGET), 2015 3rd International Conference on (p. 5). IEEE.

[2] Magar, S. G., "Adaptive Front Light Systems of Vehicle for Road Safety," In Computing Communication Control and Automation (ICCUBEA), 2015 International Conference on (pp. 551-554). IEEE.

[3] Wallaschek, J., Boyce, P., & Hoffman, D. D., "Automotive lighting and human vision," (Vol. 178). Berlin (Germany): Springer.

[4] (2015) Global vehicle production forecast is available at : http://www.statista.com/statistics/266813/growth-of-the-global-vehicle-production-since-2009/

[5] (2015) Vehicle producers ranking of 2014 can be available at: http://www.statista.com/statistics/271608/global-vehicle-sales-of-automobile-manufacturers/.

[6] Detail discussion about vehicle standard lighting specification can be found at: http://www.hella.com/hella-za/assets/media_global/HASA_Bulbs_Catalogue_2012_LRes.pdf

[7] Gacio, D., Cardesin, J., Corominas, E. L., Alonso, J. M., Dalla-Costa, M., & Calleja, A. J., "Comparison among power LEDs for automotive lighting applications," In Industry Applications Society Annual Mee ting, 2008. IAS'08. IEEE (pp. 1-5). IEEE.

[8] Young Jr, W. R., & Wilson, W., "Efficient electric vehicle lighting using LEDs," In Southcon/96. Conference Record (pp. 276-280). IEEE.

[9] Zhu, X., Zhu, Q., Wu, H., & Chen, C., "Optical design of LED-based automotive headlamps," Optics & Laser Technology, 45, 262-266.

[10] Bergh, A. A., "Blue laser diode (LD) and light emitting diode (LED) applications," Physica Status Solidi (a), 201(12), 2740-2754.

[11] Kang, B., Yong, B., & Park, K. "Performance evaluations of LED headlamps," International journal of automotive technology, 11(5), 737-742.

[12] (2015) Detail discussion about organic LED can be found at : http://eng.thesaurus.rusnano.com/wiki/article1447

[13] Li, J., Nakagawa, T., MacDonald, J., Zhang, Q., Nomura, H., Miyazaki, H., & Adachi, C., "Highly Efficient Organic Light-Emitting Diode Based on a Hidden Thermally Activated Delayed Fluorescence Channel in a Heptazine Derivative," Advanced Materials, 25(24), 3319-3323.

[14] Koudelka, P., Hanulak, P., Jaros, J., Papes, M., Latal, J., Siska, P., & Vasinek, V.,"Study of LED modulation effect on the photometric quantities and beam homogeneity of automotive lighting," In International Conference on Photonics Solutions 2015 (pp. 96591P-96591P). International Society for Optics and Photonics.

[15] Bergner, A., Groeger, S., Hoebing, T., Ruhrmann, C., Hechtfischer, U., Tochadse, G. & Awakowicz, P., "Investigating the outer-bulb discharge as ignition aid for automotive-HID lamps," Journal of Physics D: Applied Physics, 47(35), 355204.

[16] Volker, S., "Automotive Lighting".

[17] Bullough, J. D., Fu, Z., & Van Derlofske, J., "Discomfort and disability glare from halogen and HID headlamp systems," (No. 2002-01-0010). SAE Technical Paper.

[18] (2015) Detail discussion on high intensity discharge lamp can be found at: https://gearheads.in/showthread.php?5676-All-you-wanted-to-know-about-HID-headlights-(Bi-XENON-H4-H7-etc).

[19] (2015) Comparison between various lighting system can be found at : http://www.eia.gov/todayinenergy/detail.cfm?id=9871

[20] Altingöz, C., "Laser technology in automotive lighting. In SPIE LASE," (pp. 896518-896518). International Society for Optics and Photonics.

Electricity generation form pretreated palm oil mill effluent using *Klebsiella Variicola* as an inoculum in Microbial Fuel Cell.

[1]Md. Amirul Islam, [1]Maksudur Rahman Khan[*], [2]Abu Yousuf
[1]Woon Chee Wai, [1]Chin Kui Cheng
[1]Faculty of Chemical Engineering and Natural Resources
[2]Faculty of Engineering Technology
University Malaysia Pahang
Gambang 26300, Pahang, Malaysia
mrkhancep@yahoo.com

In this study, generation of electricity from pretreated palm oil mill effluent (POME) using *Klebsiella variicola* was investigated. POME wastewater with a COD value 68,360 mg/l was subjected to pretreatment with ultrasonication and used as a substrate. MFCs, enriched with pretreated palm oil mill effluent (POME) were employed to harvest electricity by using inoculation of *K. variicola*, collected from city wastewater. *K. Variicola* was isolated from city wastewater as well as from biofilm of MFC and identified using BIOLOG gene III analysis. The electrochemical activity of *K. variicola* and the performance of the MFC were evaluated by polarization curve measurement. The MFC showed average power density of 1648.70 mW/m^3 and 1280.56 mW/m^3 were obtained from ultrasonication pretrated POME and untreated POME respectively. Apart from electricity production, the COD removal efficiency by *K. variicola* for POME with pretreatment was 74% and that for untreated was 48%. These results showed that the power output and COD removal efficiency can be raised in significant amount using pretreated POME in MFC.

Keywords—component; MFC, K. Variicola, Ultrasonication pretreatment.

I. INTRODUCTION

Microbial fuel cell is promising technology which can be utilize both simple and complex substrates by using fermentative microorganisms. The contemporary world is confronting two major problems i) energy crisis ii) wastewater generation, which can be solved by exploiting MFC technology. Malaysia is the second largest producer of palm oil in the world after Indonesia [1]. Palm oil is one of the main agricultural products of Malaysia and constitutes 49.5% of the total world production [2]. Palm oil mill effluent (POME) is a hazardous liquid waste that comes out extraction of palm oil. It has specific characteristics of high biological oxygen demand (BOD 25 g/L), chemical oxygen demand (COD 53.6 g/L), total suspended solids (SS 19 g/L) and low pH (3.5–4.0) [3]. To reduce pollution with POME, several methods have been investigated such as chemical and physical pretreatment and biological treatment [4].

Application of microbial fuel cells (MFCs) to wastewater treatment for direct recovery of electric energy appears to provide a potentially attractive alternative to traditional treatment processes in an optic of costs reduction, and tapping of sustainable energy sources that characterizes current trends in technology [5]. Energy needs are increasing day by day in contemporary world and in an effort to aid energy availability and also research initiatives are being focused on substitute, renewable and carbon neutral energy sources. Conversion of biological energy to electrical energy using electrochemically active microorganisms through microbial fuel cells (MFCs) is one such environmentally friendly renewable and sustainable technology that is considered to be one of the most effective [5,6] and carbon neutral energy sources [7]. MFCs are fuel cells that are capable of utlizing chemical energy available in organic substrates into electrical energy using bacteria as a biocatalyst to oxidize the bio-degradable substrates. The fact that bacteria capable to oxidized substrates to produce bioelectricity makes MFCs an ideal solution for different types of wastewater treatment and in line with domestic energy production [8].

Biological waste treatment is widely used for energy generation due to low cost of production. Electricity generation from wastewater using MFC is one of the technologies being improved continually to suit the wastewater characteristics which comprise high organic contents. MFC technology utilizes microorganisms present in wastewater to oxidize organic contents through a biochemical process which generates certain amount of electricity. A comprehensive review on the various substrates which have been used and can possibly be used in MFCs had been done by Pant et aJ. [9]. The efficiency and economic viability of converting organic wastes to bioenergy depend on the characteristics and components of the waste material [9]. The chemical composition and the concentrations of the components that can be converted into products or fuels, is of major interest while considering the potential substrates in bioelectrochemical systems [10].

The objective of this research is to study and compare the amount of electricity generated from POME without and with pretreatment using sonication. In this present work, we selected a fermentative facultative anaerobe *K. variicola* collected from city wastewater, as the biocatalyst to construct MFC. Wastewater treatment efficiency of the system in terms of COD removal is also compared between different pretreatment conditions.

II. METHODOLOGY

A. Source of microorganism and sample collection

Palm oil mill effluent (POME) samples were collected from a local palm oil mill factory in Kuantan, Pahang, Malaysia. The sample was collected from final discharge of POME as well as discharge tank. Wastewater was also collected from Kuantan city. All samples were stored in sterilized glass bottle at 4^0 C to minimize the degradation of samples by indigenous microbial activities, thus preserving the quality of the samples.

B. MFC configuration

The air cathode single chamber MFC was built with a cubic plexi glass which has a dimension of 5 cm x 5 cm (Shanghai, Sunny Scientific, China) and a total working volume of 20 mL. Carbon brush was directly used as anode electrode. The membrane electrode assembly (MEA) was placed at the front opening side of the cubic chamber by facing the membrane side to the anode substrate and the PACF side was faced to the air. The whole MFC setup was tighten up with screws. Titanium wire of 5 cm was inserted through the MEA. Electric circuit consisting of resistor was connected from the anode chamber of MFC to the cathode chamber. All experiments were conducted at room temperature. For POME characterization, required amount of sample was withdrawn from anode chamber after two weeks of MFC operation. The COD was determined using digestive solution HR (0 – 1500 mg/L range; Hach, USA) and measured using a COD reactor (ACH DRB 2 00, USA).

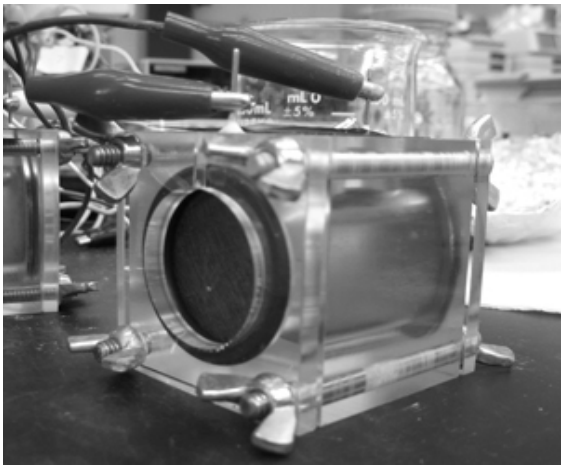

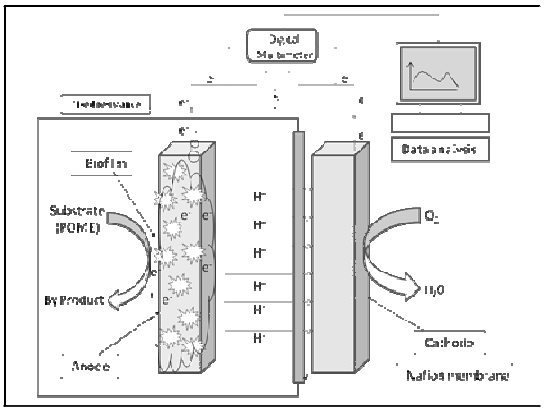

Figure 1. Single chamber air cathode MFC set up and its schematic diagram.

C. Ultrasonic pretreatment of POME

About 20 ml of POME wastewater was poured into an Erlenmeyer flask. The sample was then subjected to ultrasonic bath using a CREST ULTRASONICS (Model 690DAE; 50/60 KHz) for 45 min. This time duration was selected based from a preliminary study which gave the optimum result.

D. Isolation of potential electro-active bacteria from city wastewater

In most MFC research using pure culture bacteria, the bacteria is often isolated from the waste samples containing high population of bacteria. These bacteria are selected based on their ability to grow as biofilm on the anode in the fuel cell environment. For this study, the source of microorganisms was city wastewater. Enrichment of the cultures was carried out by preparing an overnight culture in LB broth (10% v/v) incubated at 370C with shaking at 150 rpm. The overnight culture (10% v/v) was used as inoculum in the anode compartment. After 14 days of MFC batch operation, the anode was taken out and placed in 0.1 M phosphate buffer and shaken vigorously to detach bacteria that grew as biofilm on the anode. The side of the anode was also carefully scraped and resuspended in phosphate buffer. The bacterial suspension was serially diluted and the pure culture bacteria were obtained using the spread plate technique. Biolog gene III was performed to partially identify the isolated bacteria.

E. Biolog gene III analysis

Once the pure cultures from the samples were obtained, BIOLOG GEN III test (Biolog Inc., United States) was done under aerobic conditions to confirm the genus and species of microorganisms by using carbon consumption tests with the isolated microorganisms. Biolog microplate analyzes a microorganism in 94 phenotypic tests: 71 carbon source utilization assays and 23 chemical sensitivity assays. Tetrazolium redox dyes were used to colorimetrically indicate utilization of the carbon sources or resistance to inhibitory chemicals. The isolate was identified by growing on agar medium and then suspended in a special inoculating fluid (IF) at the recommended cell density. Then the cell suspension was inoculated (100 µl per well) into the GEN III microplate, and the microplate was incubated incubated at 33^0 C for 24 h to allow the phenotypic fingerprint to form. Respiration causes

were increase for reduction of the tetrazolium redox dye, forming a purple color. After incubation, the phenotypic fingerprint of purple wells is compared to Biolog's extensive species library and a species level identification of the isolate was made [11].

F. Power measurement and analyses

The voltage (V) and current (I) across an external resistor (1 kΩ) in the MFC circuit was monitored (1 hour intervals) using a digital multimeter with data logger software (Fluke 289 True RMS Multimeter, USA) data was collected from the computer through USB cable adapter. External resistance was varied from 50 to 20,000 X to obtain polarization curve. Current density (I) was noted from I = V/R, and normalized by surface area. Power density normalized by surface area (PA, W m-3) were monitoed and calculated using the following equations

$$P = VI \quad (1)$$

$$P = V^2/AR \quad (2)$$

The COD removal efficiency (mg/l) was calculated as demostrated by Baranitharan et al. [12] and the CE of the complex substrates was calculated following Logan et al. [13].

III. Results and Discussion

A. Identification of predominant microorganisms in the biofilm

The single chambered air cathode MFC was set up to allow natural microorganisms from the city wastewater to grow under facultative anaerobic condition in the anode compartment. After the MFC was operated, the anode was taken out and it was noticed that biofilm was formed on the anodic electrode. Since the isolated bacteria was able to grow and survive in the MFC condition and produced electricity, there is a good possibility that the potential electro active bacteria are able to utilize the rich substrate in POME to generate electricity. Samples of the suspension and the biofilm (scraped from the anode) were taken and bacteria were isolated to obtain pure culture. The identification and characterization was done using Biolog gene III analysis.

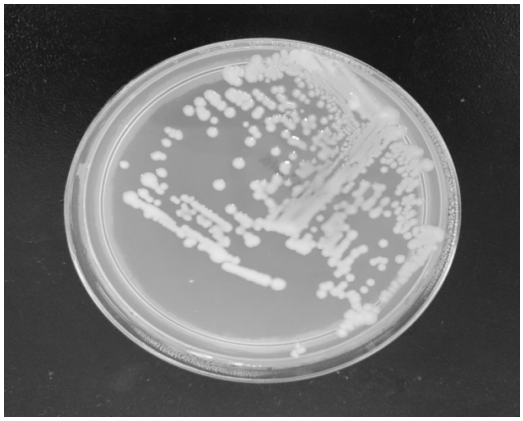

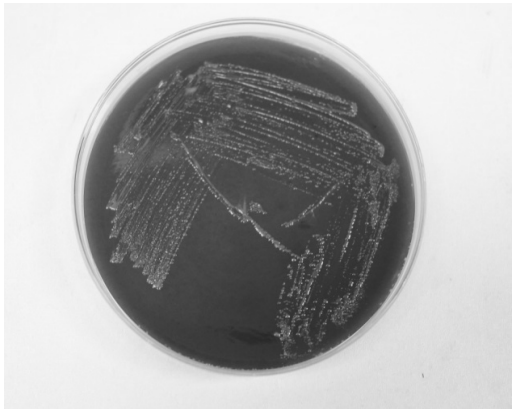

Figure 2. Nutrient agar culture and POME adjustment of *K. variicola*

B. Performance of MFC with pretreated POME

Stable open circuit potential of 550-600 mV was achieved after overnight enrichment. The MFCs were continuously fed with pretreated POME as a substrate. As early as 2 days, the MFCs started to generate electrical current. A maximum closed circuit potential of 753 mV, which is equivalent to a current of 28.39 mA, was recorded after 10 days of enrichment. The MFCs were operated continuously for more than 10 days maximum power density and current density were recorded 1619.86 mW/m3 and 287.53 mA respectively. The anode effluent showed a maximum COD removal efficiency of 74.28%.

C. Performance of MFC with untreated POME

Stable open circuit potential of 450-550 mV was achieved after overnight enrichment. The MFCs were continuously fed with untreated POME as a substrate. As early as 2 days, the MFCs started to generate electrical current. A maximum closed circuit potential of 662 mV, which is equivalent to a current of 23.83 mA, was recorded after 10 days of enrichment. The MFCs were operated continuously for more than 10 days maximum power density and current density were recorded 1236.77 mW/m3 and 216.72 mA respectively. The anode effluent showed a maximum COD removal percentage of 48.37%.

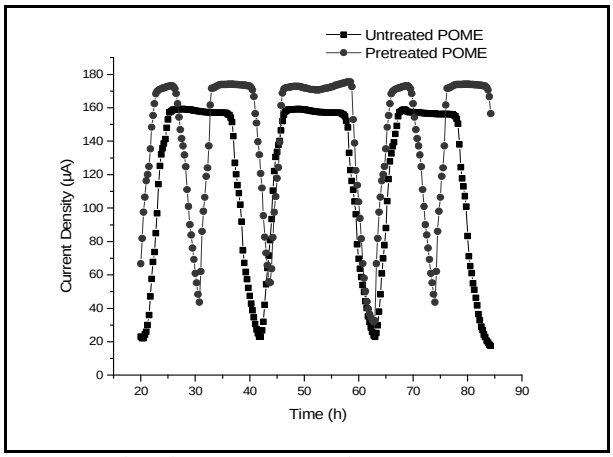

Figure 3. Profile of current densities of MFC using pretreated and untreated POME with time under 1000 Ω resistance.

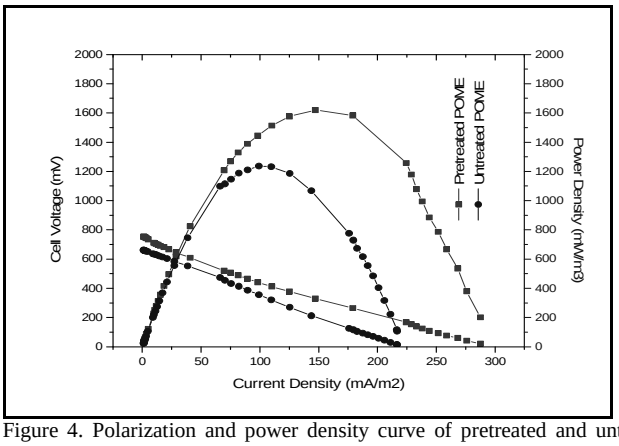

Figure 4. Polarization and power density curve of pretreated and untreated POME.

D. COD removal efficiency

Analysis of the pretreated POME and untreated POME in MFC was evaluated by comparing wastewater parameters. The maximum COD removal efficiency was achieved 74% for pretreated POME as a substrate of MFC. On the other hand, untreated POME was achieved only 48.37% of COD removal efficiency. The COD removal using untreated POME was less than that of pretreated POME. The COD removals of the palm oil mill wastewater in the MFC system over time is shown in Fig. 5. The figure shows that COD removal efficiency sharply increases with the increases of time in first cycle from day 1 to day 5, afterwards day 4 to day 12, COD removal efficiency achieved relatively lower than first cycle.

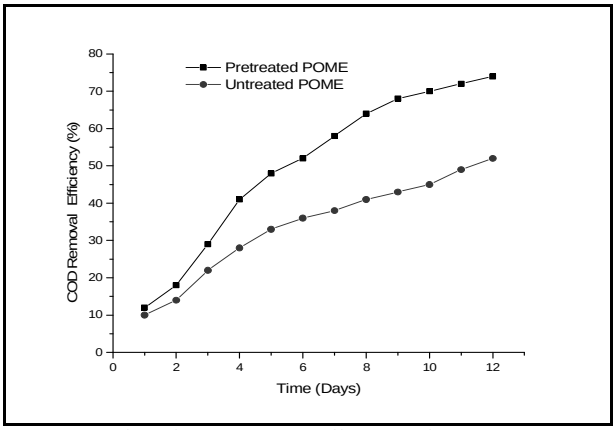

Figure 5. Profile of COD removal efficiency of MFC using pretreated and untreated POME with time.

IV. CONCLUSION

Final discharge POME was successfully utilized to generate electricity in a single chambered MFC without the addition of nutrient. The use of *K. variicola* strain, which was isolated earlier from biofilm on the anode MFC using pretreated POME substrates showed significant electricity generation in MFC compared untreated POME substrate. Although treatment of POME was not efficient at present, efforts to improve the overall performance of the MFC is underway including reactor design, treatment parameters and operational process in order to ensure that MFC would deliver its promise as a potential source of renewable energy and treatment of wastewater.

REFERENCES

[1] M.P.O.B. Malaysian Palm Oil Board. A summary on the performance of the Malysian oil palm industry. http://*econ.mpob.gov.my / economy / Performance 30109.htm* (2008)

[2] Malaysia Palm Oil Board (MPOB), Malaysian Palm Oil Statistics, Economics and Industry Development Division, MPOB, Kuala Lampur, 2004.)

[3] A. Ahmed, S. Ismail and S. Bhatia, "Water recycling from palm oil mill effluent (POME) using membrane technology", Desalination, Vol. 157, pp. 87-95, August 2003.

[4] M. Said, A. Ahmad, A. Wahab, M. Tusirin and S. Abdullah, "Blocking mechanism of PES membrane during ultrafiltration of POME", Industrial engineering chemistry, Vol. 21, pp. 182-188, January 2015.

[5] A. Capodaglio, D. Molognoni, E. Dallago, A. Liberale and R. Cella, "Microbial Fuel Cells for Direct Electrical Energy Recovery from Urban Wastewaters", The Scientific World Journa, pp. 1-8, 2013.

[6] E. Yu, S. Cheng, K. Scott and B. Logan, "Microbial fuel cell performance with non-Pt cathode catalysts", J Power Sources, Vol. 171, pp. 275–281, 2007.

[7] D. Lovley, "Microbial fuel cells: novel microbial physiologies and engineering approaches", Curr Opin Biotechnol, Vol. 17, pp. 327–332, 2006.

[8] A. Salgado, "Microbial fuel cells powered by Geobacter sulfurreducens", Basic Biotechnol, Vol. 5, pp. 96–101, 2009.

[9] D Pant, G. Bogaert G, L. Diels and K. Vanbroekhoven, "A review of the substrates used in microbial fuel cells (MFCs) for sustainable energy production", Bioresource Technology, VOl. 101, pp. 1533-1543, 2010.

[10] L. Angenent and A. Wrenn, "Optimizing mixed-culture bioprocessing to convert wastes into bioenergy", pp. 179-194,2008.

[11] Y. Zuo, D. Xing, J. Regan and B. Logan, "Isolation of the exoelctrogenic bacterium ochrobactum anthropi YZ – 1 by using a U – tube microbial fuel cell", Appl. Environ. Microbiol., Vol. 74, pp. 3130-7, Mar 2008.

[12] B. Logan, B. Hamelers, R. Rozendal, U. Schroder, J. Keller and S. Freguia, "Microbial fuel cells: methodology and technology", Environ Sci Technol, Vol. 40, pp. 5181–5192, 2006.

[13] E. Baranitharan, MR Khan, D. Prasa and J. Salihon, "Bioelectricity generation from palm oil mill effluent in microbial fuel cell using polacrylonitrile carbon felt as electrode" Water Air Soil Pollut Vol. 224, PP. 1–11, 2013.

[14] Andrew, D. E., Lenore, S. C., & Arnold, E. G. (1995). Standard methods for the examination of water and wastewater (19th ed.). Washington, DC: APHA, AWWA.

[15] S. Toshihiroi, N. Chiaki, S. Kohei, S. Toshiya and N. Toshiaki, "Ethanol production from glycerol containing biodiesel waste by *Klebsiella variicola* shows maximum productivity under alkaline conditions", New Biotechnology Vol. 31, pp. 246-253, May 2014.

Bryophyllum Pinnatum Leaf Fueled Cell: An Alternate Way of Supplying Electricity at the Off-grid Areas in Bangladesh

Mehedi Hasan[1], Kamrul Alam[2]

[1] *Department of Electrical and Electronic Engineering*
City University
Dhaka, Bangladesh.
[1]mehedi.physics@gmail.com

[2] *Department of Physics*
Jagannath University
Dhaka, Bangladesh.
[2]kakhan01@yahoo.com

Abstract— **Production of electricity from *Bryophyllum pinnatum* leaf is very cheap and the cells are easy to maintain and operate for any people as this leaf contains some organic acids. The main raw materials to produce electricity in this process are the zinc and copper plates and the juice of *Bryophyllum pinnatum* leaf. This plant can be grown anywhere. As there is plenty of free spaces in off-grid areas, the people can easily get some sort of electricity using this method. In this paper, we provide a comprehensive discussion on the main advancement of Nano-power plant in our off-grid regions using this technique and the estimated the cost to build that electrical source. We also discuss the cost of this kind of renewable power source and how their adaptability can enhancement the progression of new power management solutions, especially for their integration in living environments, making the practical application of such systems economically viable.**

Electricity production technique by using *Bryophillum Pinnatum* Leaf (BPL)

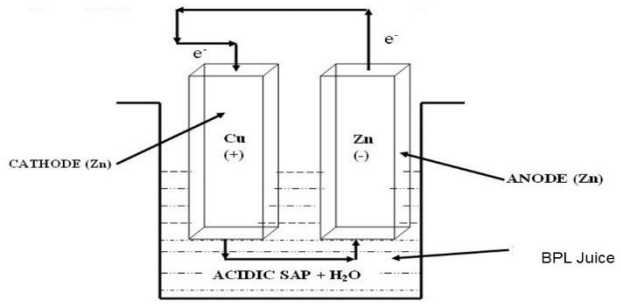

***Keywords*— *BPL cell; PKL cell; Electricity; Bryophyllum pinnatum;* Off-grid; Biomass; Renewable energy.**

I. INTRODUCTION

Bangladesh has 162 million people in a land mass of 147,570 sq. km, already has shown a tremendous growth in recent years [1][2][3]. A flourishing economic growth, rapid urbanization and increased industrialization and development has increased the country's demand for electricity. Statistic says that by 1st July, 2011, almost 111.6 million people lives in rural areas and 39 million in urban areas [4]. Our government is trying to produce electricity at an affordable price. But still now, it is so insufficient to fulfil the total need of electricity for all people. Presently access to electricity has been recorded 62% (including Renewable Energy) and per capita electricity generation recorded which is very low compared to other developing countries [5]. About 3.45 million people have newly been connected and system loss (distribution) is now 12.03%. Uppermost generation so far was 7356 MW recorded on 30/03/2014 and it is snowballing gradually [6]. These information leads us to consider that, still a lot of regions in our country is out of reach of electricity. As a result life is deliberate there. People living with the access of no electricity, are not having a well access of information from mass media. As a result, they are failed to walk with the people who has some access of electricity.

TABLE-1. HOUSEHOLD REPORTING SOURCE OF LIGHT [7].

Locality	Source of Light in percentage				
	Electricity	Solar Energy	Kerosene	Bio Gas	Others
Total	56.60	3.32	39.49	0.13	0.46
Rural	48.48	4.01	46.45	0.15	0.54
Urban	88.70	0.45	10.70	0.04	0.11

(Source: Population Census Sample Survey, 2011, BBS.)

In rural areas, the requirement of electricity is not much, but to operate a small lamp, a radio or to charge a mobile phone. As because they are out of national grid, the BPL electricity can be so cooperative for them in those commitments. No complex requirements are compulsory to produce electricity by themselves. They can grow fuel as a form of *Bryophyllum pinnatum* and can generate electricity at a reasonable price. Moreover, the construction, production, operation and maintenance of *Bryophyllum pinnatum* Leaf Fuelled Cell or BPL cell is very unpretentious as this leaf contains some organic acids which acts like electrolytes [8][9][10]. Anyone can do it, if he or even she is mindful of this method. Although the current ailment and efficiency of BPL electrical energy production is not noteworthy as it cannot produce a lot of electricity at a time with compared to other conventional process for general people, like we, lives in the cities, but for the people to whom the word "Electricity" is just a word of dream and the place where to supply a glance of electricity is still awkward- at least for right now, can get a little amount of electricity, and possibly can get benefited by using the method of BPL electrical energy production.

In our study, we've found that by using the Dynamic-Electrolyte Model, it is promising to have electricity on average 3-4 Watts for more than 6 hours using only 4.5 Litres juice where the percentage of BPL was 50%, i.e. 2.25 Litres, which can be used in the preceding cycles. This statistics leads us to think about the possibility of BPL electricity in off-grid areas.

II. *Bryophyllum pinnatum*: A biomass source for Electricity

Phytochemical analysis of dissimilar fragments of plant citations of *Bryophyllum pinnatum* disclosed the attendance of acids, for instance, mallic acid, amino acid, ascorbic acid, syringic acid, caffeic acid, iso-citric acid etc. [8][9][10] and also some metals like copper, iron etc. [11][12].

At BCSIR (Bangladesh Council for Scientific and Industrial Research), Dhaka, Bangladesh, a quantitative experiments have also been done by Dr. Barun Kanti Saha, Senior Scientific Officer (SSO), Institute of Food Science & Technology (IFST) BCSIR. The Department of Food & Nutrition of BCSIR has tested some specimen *of Bryophyllum pinnatum* leaf and found that the titratable acidity of the *Bryophyllum pinnatum* leaf (BPL) is 0.88% [11][12]. So, if we place a pair of electrode in the solution of *Bryophyllum pinnatum* leaf, we can get electrical energy [09][11].

In our method of constructing BPL cell we use copper and zinc plates as electrodes which are low-priced, comparatively better conductors and available in the local market. Generally when zinc plates come contact with acids, it goes into solution, generating 0.762 V relative to the standard hydrogen electrode; in equilibrium, and when copper comes in contact and goes to the solution it generates -0.345 V [13]. So, the reaction in each electrodes in presence of copper (small amount of copper sulphate used in the juice) in the juice will be-

$$Zn \rightarrow Zn^{2+} + 2\,e^{-}$$
$$Cu^{2+} + 2\,e^{-} \rightarrow Cu$$

And the generating net electromotive force of these reaction in cell or a copper-zinc pair electrodes in an acidic solution is, 0.762V – (-0.345V) = 1.107V, bearing in mind the electrode sides of interface in the electrolyte solution or the juice, where the zinc plates are considered as negative and copper plates are positive electrodes. The flow of electricity depends much on the surface area of the electrodes, solution types, etc. [14].

III. The Model of BPL Nano-Power Plant

A proposed model of BPL Nano-power plant will be based on the Dynamic-Electrolyte Model. In our study, we've found that, 18 Zinc plates and 12 Copper plates can produce 3-5 Watts power, than a combination of more of these plates can produce a remarkable power at a time and for long periods.

In our study, we made the flow of juice using gravitational potential by our hand pulling upward a jar and downward the other. Obviously to make a flow of juice of much greater amount than this we have to introduce an easier way using gravitational potential of juice.

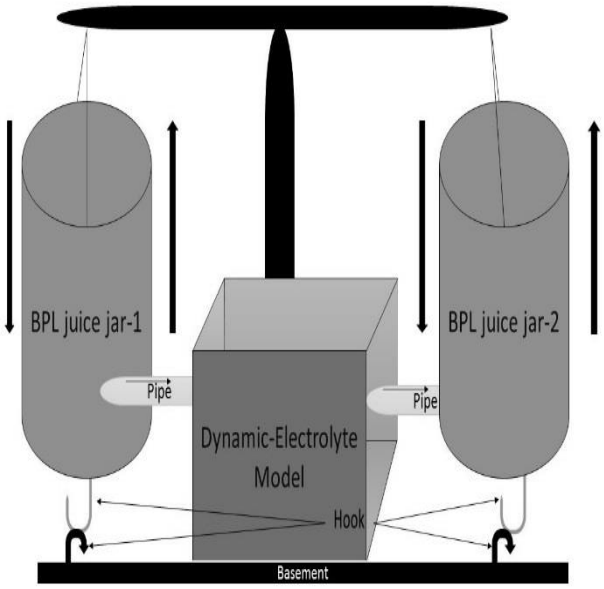

Fig.1. A Dynamic-Electrolyte Model for BPL mini power plant.

For a bigger power source we'll need bigger amount of juice. In that case, two jars of juice will be suspended to the two ends of beam just like a balance. Both jars can go up and down. There will be a hook under each jar. At basement, two hooks

will also be placed. By moving jar-1 and jar-2 up and down we can make flow of juice inside the cell to make the interacting ions (H+, Cu2+) distributed uniformly. There will be holes in zigzag fashions to create a place to flow the through the zinc and copper plates.

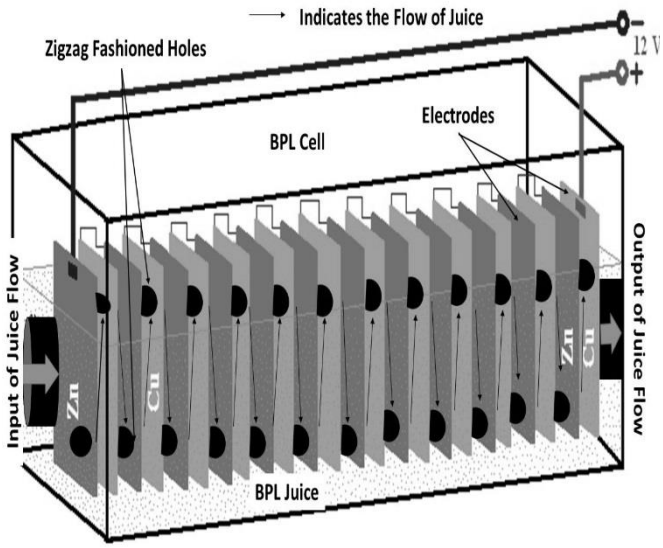

Fig-2. A 12V BPL cell.

When the performances of output power goes down, we need another flow of juice to redistribute reactant ions (H+, Cu2+). For that, the hook of jar-2 will be attached to the hook below that jar in the basement. The juice will start to flow from up to down or jar-1 to jar-2.

We can connect more cell like this in series or parallel combination as BPL module. Then we can connect that module with a charge controller which stores the charge and supplies continuous output.

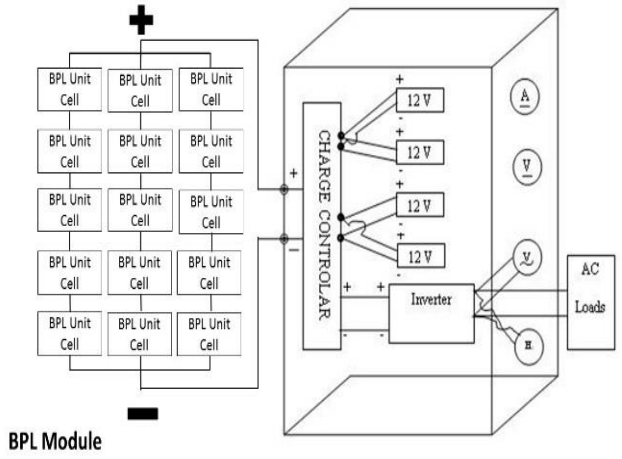

Fig-3. A BPL module.

As BPL can supply electricity 24Hours, we can also store that electrical energy in a rechargeable battery to use other purposes.

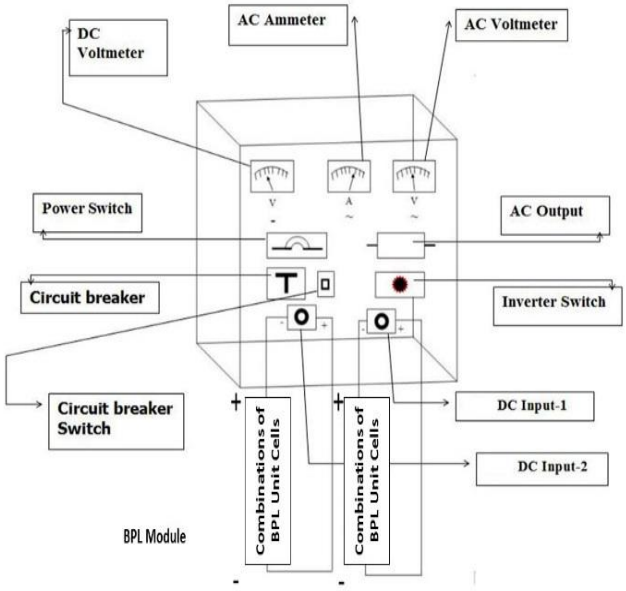

Fig.-4. A schematic diagram of BPL Nano power plant.

BPL cells supply a D.C. current. So, by converting D.C. current to A.C. current, we can increase the output performance or operate A.C. equipment. A voltmeter and an ammeter will be connected to observe the voltage and current of this power plant.

IV. The Cost of Building a BPL Power Source

Right now, we are working to develop cell performance and the longevity of a BPL cell. And we got our answer as Dynamic-Electrolyte Model. We've worked on a 6V cell which gives 3-4 Watts. By the combination of more cell like this, we can multiply the powers on demand.

Generally a 6V cell consists of 12 copper plates and 18 zinc plates. The average area of these electrodes is 1.04cm^2 approximately. So, the total area of zinc and copper plate in a 6V cell is approximately 18.72cm^2 and 12.48cm^2 and the weight of 18 zinc plates is 750gms and for copper is 350gms approximately. This new designed cell also consists of two containers, pipes and wires which are priced negligible and a battery box. The total cost of building a cell like this will be,
Cost of 1Kg Zinc = 250 Taka (In local market)
Cost of 1Kg Copper = 1000 Taka (In local market)

So, the cost of 750gms 18 zinc plates is 187.5 Taka and 350gms or 12 copper plates is 350 Taka.
The price of plastic box is 150 Taka, two jar 10 Taka and the other price, like pipe, gum, wires etc. will be 50 Taka only.

So, total price of a single cell will not be greater than 750 Taka.

10 similar kind of cell will cost not more than 7500 Taka, where the size of the jar will be much bigger than this.

As the fuel or BPL is free of cost, then only less than 9000 Taka will be the cost of a 50W BPL mini power plant. This 50W power source can run 5-10 LED bulbs or other electrical components at a time.

Our study says, a cell like this can work well up to one year. Only by changing zinc plates and washing the copper plates, we can use again these cells.

V. THE COST OF BUILDING A BPL POWER SOURCE

A study says that the total cultivated area of Bangladesh is 13 million hector (ha.). Over 11.5 million hectors are used to grow rice and other crops. Rest of them can be considered as free land.

TABLE-2. LAND PER FAMILY IN AGRICULTURE [15].

Class of family or farmer	**No of owner family (lac)**	**Land size per family**
Marginal	92.43	0.02 to 1.0 ha.
Small farmer	20.92	1.01 to 3.00 ha.
Medium farmer	3.04	10.00 ha.
Large farmer	1.23	10.00 & above

There are a lots of free area in our village. People can cultivate *Bryophyllum pinnatum* and produce electricity by themselves. For that, a little space anywhere around the house are needed.

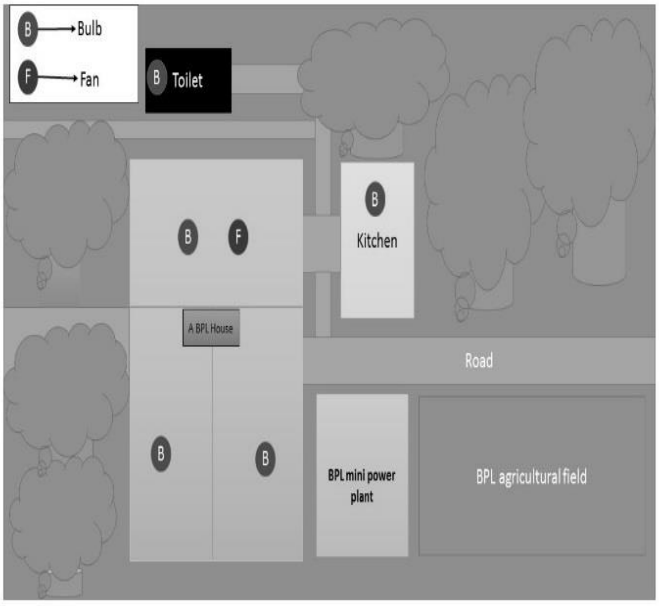

Fig-5. A BPL House.

VI. CONCLUSIONS

BPL cells also produce some bi-products. Generally, there types of bi-products are produced in BPL cells. These are-

1) Methane Gas: It can be used for home system to operate burner in the rural complex areas in Bangladesh. A further study is needed on this.

2) Bio-Fertilizer: Using wastage of the BPL we can get fertilizer which can be used agricultural field. It contains a good portion of zinc, which is a good zinc based fertilizer.

3) Hydrogen Gas: Hydrogen gas is the most valuable gas in world which is possible to generate from this device.

The other benefit of using this technique is that it does not produce CO_2 gas in the environment. Cost is much effective as compared to other renewable technologies. It is also very easy to operate, maintain, no harmful elements produced, environment friendly etc. The other important thing is to produce electricity from BPL cell, we need to grow *Bryophyllum pinnatum*, which is a green plant and produce valuable oxygen.

This study shows an effective way to solve the problem of giving a glance of light in the rural areas in Bangladesh with an affordable price with an easy technique alongside with solar panels. But the maintenance of solar panels are much higher than this kind of cells, which makes an effective and alternate source of electrical energy and may play an important role in socio-economic development. These work will show the guideline of one of the new renewable energy technologies.

ACKNOWLEDGMENT

I would like to express my deepest gratitude to my M.Sc. thesis supervisor Prof. Dr. Md. Kamrul Alam Khan, Department of Physics, Jagannath University, Dhaka, Bangladesh for his valuable suggestion and dedication during this work.

REFERENCES

[1] Geoffrey Hayes, and Gavin Jones, "The Impact of the Demographic Transition on Socioeconomic Development in Bangladesh: Future prospects and Implications for Public Policy", p. 7.

[2] *Statistical Pocket Book of Bangladesh-2013, Bangladesh Bureau of Statistics*, Statistics and Information Division (SID), Ministry of Planning. p. -3.

[3] http://countrymeters.info/en/Bangladesh

[4] *Statistical Pocket Book of Bangladesh-2013, Bangladesh Bureau of Statistics*, Statistics and Information Division (SID), Ministry of Planning. p. 8.

[5] *Statistical Pocket Book of Bangladesh-2013, Bangladesh Bureau of Statistics*, Statistics and Information Division (SID), Ministry of Planning. p. 12.
[6] Bangladesh Power Division.
Available: http://www.powerdivision.gov.bd/site/page/70c0abba-e714-4bd6-b4de-e2c61fb25558 /বদি্যু□-খাতরে-হালনাগাদ
[7] *Statistical Pocket Book of Bangladesh-2013, Bangladesh Bureau of Statistics*, Statistics and Information Division (SID), Ministry of Planning. p. 141.
[8] "*Renewable Energy Policy of Bangladesh*", Power Division, Ministry of Power, Energy and Mineral Resources, Government of the People's Republic of Bangladesh, 6 Nov 2008 (Policy Document).
[9] E.J. Lund and M. Bush, "*Electric correlation potentials in the leaf of Bryophyllum*", Plant Physiology, The American Society of Plant Physiologists, vol. 5, no. 4, p. 491-508. Oct 1930. (article)
[10] Md. Kamrul Alam Khan, "*Studies on electricity generation from stone chips plant (Bryophyllum pinnatum*)", International J. Eng. Tech 5(4); pp. 393-397, Dec 2008
[11] J. Sultana., K.A. Khan., M.U. Ahmed. "*Electricity Generation from Pathor Kuchi Leaf (PKL) (Bryophillum Pinnatum).*" J.Asiat Soc. Bangladesh Sci., 37(4): 167-179, December 2011.
[12] Shuva Paul.,Shdha Chowhury.,Jennifar Akter.,Priyanka Paul.,Nabilah Manzoor. American International University Bangladesh,Dhaka-Bangladesh, "*Performance testing of BKL Electricity Module.*" EIT-2012, IUPUI (Indiana University-Purdue University,Indianapolis),USA.
[13] R. Vasant Kumar and Thapanee Sarakonsri, "*Introduction to Electrochemical Cells*", p. 5.
[14] Muhammad Riazul Hamid, "*Characterization of a Battery cell fueled by Bryophyllum Pinnatum sap*", International Journal of Scientific & Engineering Research, Volume 4, Issue 3, March-2013, ISSN 2229-5518.
[15] Bangladesh Power Division.
Available: http://www.powerdivision.gov.bd/user/brec1/30/1

Internal Quantum Efficiency of Si-Drift Solar Cells with Nonuniformly and Heavily Doped Emitter

Md. Rashedul Huqe and Md. Iqbal Bahar Chowdhury
Department of Electrical and Electronic Engineering
United International University, Dhaka, Bangladesh
Email: rashedul_uiu@yahoo.com, ibchy@eee.uiu.ac.bd

***Abstract*—This work focuses to develop an analytical model of the internal quantum efficiency for a drift-field Si-solar cell with non-uniformly and heavily doped emitter region. The resulting mathematical intractability owing to the consideration of all the non-ideal effects have been resolved by employing an elegant approximation technique. The developed model shows that the drift-field solar cells have significantly higher internal quantum efficiency over the uniformly-doped Si-solar cells, particularly for high energy photons.**

***Index Terms*—Internal quantum efficiency, drift-field solar cells, doping dependency of carrier mobility, non-uniformly doped emitter.**

I. Introduction

In the drift field (DF) solar cells [1] the improvement of current-voltage characteristics can be obtained by appropriate introduction of non-uniform and heavy doping levels in the bulk emitter-base regions to develop an electric field therein in accordance with the built-in field developed in the depletion region. However, heavy and non-uniform doping levels introduce a number of non-ideal effects which include the space dependency of the energy band-gap narrowing and the carrier transport parameters (mobility and lifetime), the electric field dependency of the carrier mobility and the dominance of the Auger recombination mechanisms over the Shockley-Read-Hall recombination mechanism. All these effects degrade the performance parameters of the DF solar cells far from the expectation and hence, need to be analyzed carefully.

However, consideration of all the above-mentioned effects makes the analytical modeling mathematically intractable and the conventional models [2]–[4] found in the literature, therefore, failed to incorporate all these effects. Although Verhoff and Sinke [5] considered almost all these effects in their models, they considered the Auger recombination for the doping levels $\geq 5 \times 10^{18}\ cm^{-3}$ and the SRH recombination for the lower doping levels, they did not consider the field-dependency of the carrier mobility and their model is applicable for the dark saturation current only, not for the internal quantum efficiency. Indeed, mathematical intractability is evolved from the simultaneous consideration of the SRH and the Auger recombination and also, from the consideration of the field-dependency of the carrier mobility. By employing an elegant exponential approximation technique to resolve this mathematical intractability, Rashedul *et al.* [6] developed an analytical model for the dark saturation current in the non-uniformly and heavily doped p-type base region. But this model is not applicable for analyzing the internal quantum efficiency. Recently, M. S. Uddin *et al.* [7] developed an analytical model of the internal quantum efficiency of DF solar cells; but this model is applicable for the base region, not for the emitter region. Therefore, the objective of this work is to develop an analytical model of the internal quantum efficiency of DF solar cells having non-uniformly and heavily doped emitter region by considering all of the above-mentioned non-ideal effects.

II. Analysis

A. Basic Equations and Physical Models

In order to determine the photocurrent generated within the non-uniformly doped emitter region for the development of an analytical model of the internal quantum efficiency of a Si-drift solar cell, the solution of the following equations are necessary.

$$J_p = qp(x)\mu_p(x)E(x) - qD_p(x)\frac{dp(x)}{dx} \quad (1)$$

$$\frac{dJ_p}{dx} = -q(R-G) \quad (2)$$

where $E(x)$ is the electric field that acts on the holes in the emitter region and considering the band-gap narrowing effects can be expressed as [8]

$$\frac{E}{V_T} = -\frac{d}{dx}ln\ N_d(x) + \frac{d}{dx}ln\ n_{ie}^2(x) \quad (3)$$

μ_p and D_p are the hole mobility and the diffusivity and (R-G) is the net recombination rate. Since the emitter region is non-uniformly and heavily doped, the band-gap narrowing effects, the doping dependence of the carrier transport parameters (i.e. the mobility and the lifetime) and the presence of both the Shockley-Read-Hall (SRH) and the Auger recombination mechanisms have to be considered. The physical models

needed to describe these non-ideal effects are as follows:

$$n_{ie}^2(x) = n_{i0}^2 \left[\frac{N_d(x)}{N_{ref}}\right]^{\gamma_2} \quad (4)$$

$$\mu_p = \frac{qD_p(0)}{kT}\left[\frac{N_d(x)}{N_{m,ref}}\right]^{-\gamma_3} \quad (5)$$

$$R_{SRH} = \frac{p}{\tau_{ps}} = \frac{\tau_{p0}}{1+\frac{N_d}{N_{0,ref}}} \quad (6)$$

$$R_{Auger} = \frac{p}{\tau_{pa}} = \frac{1}{C_{An}N_d^2} \quad (7)$$

$$G_p(x) = q\alpha\frac{\lambda I_0}{hc}e^{-\alpha(\lambda)x} = q\alpha G_0 e^{-\alpha(\lambda)x} \quad (8)$$

Eqn. (4) models the effective intrinsic carrier concentration including the band=gap narrowing effects [9], with $n_{i0} = 1.194 \times 10^{10}\ cm^{-3}$, $N_{ref} = 1.3 \times 10^{17}\ cm^{-3}$ and $\gamma_2 = 0.5355$. The doping-dependence of the low-field hole mobility [10] can be described by Eqn. (5), where $D_n(0) = 12.5727\ cm^2\ (V.s)^{-1}$, $N_{m,ref} = 1 \times 10^{17}\ cm^{-3}$, and $\gamma_3 = 0.38$. The doping dependent SRH [11] and Auger recombination rates, under steady-state condition, are given by Eqns. (6) and (7), where τ_{ps}, τ_{pa} are the carrier lifetime for the SRH and the Auger recombination respectively with $N_{0,ref} = 7.1 \times 10^{15}\ cm^{-3}\ sec$, $\tau_{n0} = 3.52 \times 10^{-4}\ sec$ [12] and C_{An} is the Auger coefficient for electrons modeled as [13]

$$C_{An} = 0.67 \times 10^{-31} + 8.16 \times 10^{-34}T - 2.44 \times 10^{-37}T^2$$

Eqn. (8) gives the expression of the steady-state generation rate due to optical illumination, where I_0 is the irradiance at the emitter surface and α is the absorption coefficient of silicon at a given wavelength (λ). Finally, the electron current continuity equation [Eqn. (2)] can be furnished as

$$\frac{dJ_p}{dx} = -\frac{qp}{\tau_{p,eff}} + q\alpha G_0 e^{-\alpha x} \quad (9)$$

where $\tau_{p,eff}$ is the effective electron lifetime given by

$$\frac{1}{\tau_{p,eff}} = \frac{1}{\tau_{p0}} + \frac{N_d}{\tau_{p0}N_{0,ref}} + C_{An}N_d^2 \quad (10)$$

B. Model Derivation

Assuming an normalized hole concentration defined as $p_e = \frac{pN_d}{n_{ie}^2}$ and using Eqn. (3) in Eqn. (1) results in

$$\frac{dp_e}{dx} = -\frac{J_p}{qD_p} \quad (11)$$

Differentiating the above equation w.r.t x results in a second order differential equation (DE) of $p_e(x)$ as

$$\frac{d^2p_e}{dx^2} - \frac{d}{dx}ln\left(\frac{N_d}{qD_pn_{ie}^2}\right)\frac{dp_e}{dx} - \frac{p_e}{D_p\tau_{p,eff}} = -\frac{\alpha G_0 N_d}{D_pN_{ie}^2}e^{-\alpha x} \quad (12)$$

Assuming an exponential doping profile in the emitter region defined as

$$N_d(x) = N_d(0)e^{\frac{-\eta x}{W_e}} = N_d(0)u(x) \quad (13)$$

where 'W_e' is the width of the emitter region, u is a suitable variable and $\eta = log\left[\frac{N_d(0)}{N_d(W_e)}\right]$ is the logarithmic slope of the doping profile, the electric field, the mobility, the effective lifetime and and the DE [Eqn. 12] can be organized as

$$\frac{E_p}{V_T} = \frac{\eta}{W_e}(1-\gamma_2) \quad (14)$$

$$\frac{1}{qD_p} = \frac{1}{qD_p(0)}\left[\frac{N_d(0)}{N_{0ref}}\right]^{\gamma_3}u^{\gamma_3} = F_h u^{\gamma_3} \quad (15)$$

$$\frac{1}{\tau_{p,eff}} = \frac{1}{\tau_{p0}} + \left[\frac{N_d(0)}{\tau_{p0}N_{0ref}}\right]u + C_{An}[N_d(0)u]^2 \quad (16)$$

and

$$\frac{d^2p_e}{dx^2} + G_1\frac{dP_e}{dx} - \frac{P_e}{L_{p,eff}^2} = -\alpha G_0\frac{N_d}{D_pN_{ie}^2}e^{-\alpha x} \quad (17)$$

where $G_1 = -\frac{\eta}{W_e}(1-\gamma_2+\gamma_3)$ and $L_{p,eff} = \sqrt{D_p\tau_{p,eff}}$ is the effective diffusion length. It is evident from the Eqn. (17) that the DE is analytical intractable due to the presence of $\tau_{p,eff}$ and $L_{p,eff}$. Therefore, using the exponential approximation technique [6], the terms ($\tau_{p,eff}$ and $D_p\tau_{p,eff}$ can be approximated as a simple exponential given by

$$\frac{1}{\tau_{p,eff}} \equiv R_0 u^{k_p} \quad (18)$$

$$\frac{1}{L_{p,eff}^2} \equiv \frac{1}{L_{p0}^2}u^{\gamma_3+k_p} \quad (19)$$

The solution of the DE [Eqn. 17] gives the minority hole carrier density $p_e(x)$ as a linear combination of modified Bessel functions of the first kind I_β and of the second kind K_β of order β [Appendix A] as

$$p_e(x) = w(x)\left[(C_1^{'} + v_1^{'})I_\beta(X) + (C_2^{'} + v_2^{'})K_\beta(X)\right] \quad (20)$$

where all the variables and the constants are presented in the Appendix A. The total photocurrent density at a given wavelength can be obtained as [14]

$$J_{ph}(\lambda) = J_{pe}(\lambda) + J_G(\lambda) + J_{nb}(0)(\lambda) \quad (21)$$

where J_{nb} and J_G are the photocurrent generated at the depletion edge of the uniformly doped base region and within the depletion region respectively [14] and J_{pe} is the photo-generated current density obtained from the hole current equation given by (1) at the depletion edge i.e. $x = W_e$. Finally, the wavelength dependent internal quantum efficiency can be obtained as

$$\eta_i(\lambda) = \frac{J_{ph}(\lambda)}{qG_0(\lambda)} \times 100\% \quad (22)$$

III. Results and Discussion

In this section, the simulation results based on the proposed analytical model are presented. The simulations are carried out for a Si-drift solar cells with non-uniformly doped emitter and uniformly doped base. For convenience, the model developed in this work is termed as the 'present model', whereas, the term 'previous model' refers to the model with uniformly-doped Si solar cell [14].

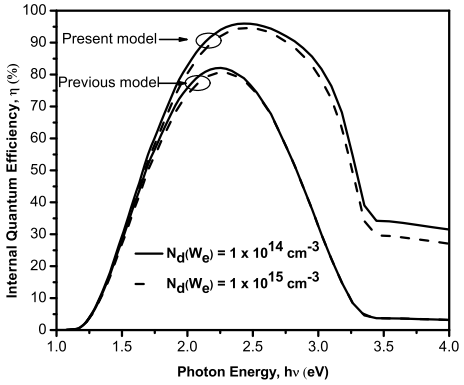

Fig. 1. Internal quantum efficiency vs. photon energy for the present model and the previous model. Here, two base doping densities at $x = W_e$ of $5 \times 10^{14}\ cm^{-3}$ and $1 \times 10^{15}\ cm^{-3}$ are considered, $S_p = 1 \times 10^6\ cm/sec$, $W_e = 0.5\ \mu m$ and $N_d(0) = 1 \times 10^{20}\ cm^{-3}$.

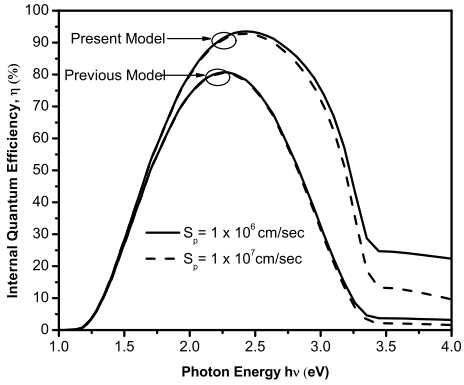

Fig. 2. Internal quantum efficiency vs. photon energy for the present model and the previous model. Here, two surface recombination velocities of $S_p = 1 \times 10^6\ cm/sec$ and $S_p = 1 \times 10^7\ cm/sec$ are considered, $W_e = 0.5\ \mu m$, $N_d(0) = 1 \times 10^{20}\ cm^{-3}$, $N_d(W_e) = 1 \times 10^{15}\ cm^{-3}$.

Two common observations can be made from Figs. (1) to (3). First-the internal quantum efficiency for the present model is higher than the previous model especially for the mid to high energy photons and second- the effect of surface recombination is reduced with the increase of the electric field. The non-uniformity of the emitter doping profile is such that it creates an electric field in the neutral emitter region in the same direction as the field in the depletion region. This field causes photo-generated carriers for mid to high-energy photons in the emitter region to pass with an increased velocity and hence, increases the photo-current. On the other hand, the roughness of the surfaces is represented by the surface recombination velocity. The worse is the roughness of the surface, the higher is the carrier loss at the surface (the higher is the recombination occurred) and hence, the lower is the internal quantum efficiency. However, introduction or increase in the electric field in the quasi-neutral emitter region causes holes to drive away at a faster rate from the surface and lessens the probability of surface recombination resulting in the improvement in η_i.

Electric field introduced in the emitter region with the help of the non-uniform doping profile is directly related with the logarithmic gradient of the doping profile. Increase in the doping level at the junction (at $x = W_e$) i.e $N_d(W_e)$ causes this gradient and hence, the electric field to decrease. Therefore, with the increase in $N_d(W_e)$ while maintaining peak doping level at the surface ($x = 0$) results in lowering of the photocurrent and causes η_i to decrease. This fact is evident from Fig. (1).

Fig. (2) shows that the internal quantum efficiency decreases with the increase of the surface recombination velocity at the emitter surface. Since surface recombination velocity causes carrier loss at the emitter surface, the more the surface recombination, the less will be the photocurrent generated in the emitter region and hence, the internal quantum efficiency.

Fig. (3) shows that increase in the emitter width decreases

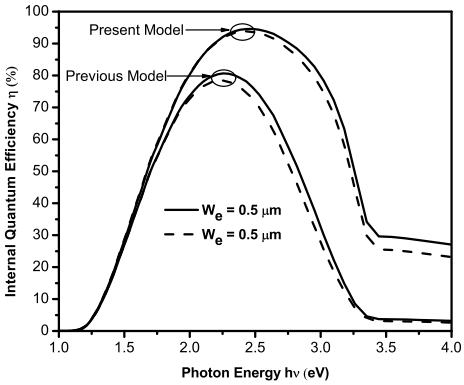

Fig. 3. Internal quantum efficiency vs. photon energy for the present model and the previous model. Here, two emitter widths of $0.5\ \mu m$ and $0.6\ \mu m$ are considered, $S_p = 1 \times 10^6\ cm/sec$ and $N_d(0) = 1 \times 10^{20}\ cm^{-3}$, $N_d(W_e) = 1 \times 10^{15}\ cm^{-3}$.

the internal quantum efficiency. This is due to the fact that increase in the emitter width increases the probability of volume recombination (SRH and Auger) in the emitter region. Moreover, increase in W_e decreases the logarithmic gradient of the doping profile therbey causing the electric field in the emitter region to decrease.

IV. Conclusion

In this work the effects of the non-uniform emitter doping profile on the internal quantum efficiency of a drift-field solar cell have been investigated. In doing so, an analytical model has been developed that includes all the non-ideal effects mentioned in the literature by the judicious application of the exponential approximation technique to resolve the evolving intractability of the governing differential equation. The simulation results obtained from the developed analytical model shows that the non-uniformity of the emitter doping

profile not only increases the internal quantum efficiency for the mid to high energy photons, but also decreases the effect of surface recombination velocity. Therefore, this work will be useful in designing high efficiency solar cells by providing better physical insight.

APPENDIX A
SOLUTION OF THE DE

Letting $p_e(x) = v(x)w(x)$ converts the the second order differential equation (17) to

$$\begin{aligned} \frac{d^2v}{dx^2} &+ \left[\frac{2}{w}\frac{dw}{dx} + G_1\right]\frac{dv}{dx} + \frac{1}{w}\left[\frac{d^2w}{dx^2} + G_1\frac{dw}{dx} + \frac{w}{L_{p,eff}^2}\right]v \\ &= -\alpha G_0 \frac{N_d}{wn_{ie}^2 D_p} e^{-\alpha x} \end{aligned} \quad (23)$$

Letting $\frac{2}{w}\frac{dw}{dx} + G_1 = 0$ and $\frac{2W_e}{\eta(\gamma_3+k_p)}\frac{1}{L_{p0}^2}u^{\frac{\gamma_3+k_p}{2}} = Z$ gives w(x) and v(x) respectively as

$$w(x) = u^{\frac{(1-\gamma_2+\gamma_3)}{2}} \quad (24)$$

$$\begin{aligned} \frac{d^2v}{dZ^2} &+ \frac{1}{Z}\frac{dv}{dZ} - \frac{1}{Z^2}\left[Z^2+\beta^2\right]v \\ &= -\frac{\alpha G_0}{(b_0 Z)^2}\frac{N_d}{wn_{ie}^2 D_p}e^{-\alpha x} \end{aligned} \quad (25)$$

where Eqn. (25) represents a non-homogeneous modified Bessel equation of order β, $b_0 = \frac{\eta(\gamma_3+k_p)}{2W_e}$, $\beta = \frac{1-\gamma_2+\gamma_3}{\gamma_3+k_p}$. Finally, the solutions $p_e(x)$ and $J_p(x)$ cab be obtained as

$$p_e(x) = w\left(C_1^{'} + v_1^{'}\right)I_\beta(Z) + \left(C_2^{'} + v_2^{'}\right)K_\beta(Z) \quad (26)$$

$$\begin{aligned} J_p(x) &= \frac{qD_p n_{ie}^2}{N_d} \times \frac{\eta}{W_E} \times w \\ &\times \left[\left(C_1^{'} + v_1^{'}(x)\right)A_x + \left(C_2^{'} + v_2^{'}(x)\right)B_x\right] \end{aligned} \quad (27)$$

where

$$\begin{aligned} A_x &= \left[(1-\gamma_2-\gamma_3)I_\beta + (\gamma_3+k_p)Z\frac{dI_\beta}{dZ}\right] \\ B_x &= \left[(1-\gamma_2+\gamma_3)k_\beta + (\gamma_3+k_p)Z\frac{dk_\beta}{dZ}\right] \\ v_1^{'} &= -\alpha G_0 V_1,\ v_2^{'} = \alpha G_0 V_2 \\ V_1(x) &= \int K_\beta(Z)e^{-\alpha x}\left[\frac{2W_E}{\eta(\gamma_3+k_p)}\right]dx \\ V_2(x) &= \int I_\beta(Z)e^{-\alpha x}\left[\frac{2W_E}{\eta(\gamma_3+k_p)}\right]dx \end{aligned}$$

Using the boundary conditions at $x = 0$ and $x = W_E$ given by $p(0) = -\frac{J_p(0)}{qS_p}$ and $p(W_e) = 0$ [5], where S_p is the surface recombination velocity at the emitter surface, one obtains $C_2^{'} = -\beta_s C_1^{'}$, where

$$\begin{aligned} C_1^{'} &= \alpha G_0 \times \frac{V_{1W}I_{\beta W} - V_{1W}K_{\beta W}}{I_{\beta W} - \beta K_{\beta W}} = \alpha G_0 C_1 \\ \beta_s &= \frac{\frac{S_p}{D_p(0)}I_{\beta 0} + \frac{\eta}{2W_E}A_{x0}}{\frac{S_p}{D_p(0)}k_{\beta 0} + \frac{\eta}{2W_E}b_{x0}} \end{aligned}$$

Finally, the photo-generation current in the non-uniformly doped emitter can be calculated as the hole current generated at $x = W_E$ as

$$J_{pe} = \frac{\eta\alpha G_0}{2W_E w} \times \left[(A_x - \beta_s B_x)C_1 - A_x V_1 + B_x V_2\right] \quad (28)$$

REFERENCES

[1] M. Wolf, "Drift fields in photovoltaic solar energy converter cells", *Proc. of the IEEE*, vol. 51, no. 5, pp. 674-693, May 1963.

[2] R. V. Overstraeten and W. Nuyts, "Theoretical investigation of the efficiency of drift-field solar cells", *IEEE Trans. Electron Devices*, vol. 16, no. 7, pp. 632-641, Jul 1969.

[3] F. A. Lindholm and Y. H. Chen, "Current-voltage characteristic for bipolar p-n junction devices with drift fields, including correlation between carrier lifetimes and shallow-impurity concentration", *J. Appl. Phys.*, vol. 53, no. 12, pp. 8863-8866, Dec. 1982.

[4] J. A. Del Alemo and R. M. Swanson, "The Physics and Modeling of Heavily Doped Emitters", *IEEE Trans. Electron Devices*, vol. 31, no. 12, pp. 1878-1888, Dec. 1984.

[5] L. A. Verhoef and W. C. Sinke, "Minority-carrier transport in nonuniformly doped silicon-an analytical approach", *IEEE Trans. Electron Devices*, vol. 37, no. 1, pp. 210-221, Jan. 1990.

[6] M. R. Huqe, S. I. Reba, M. S. Uddin and M. I. B. Chowdhury, "Analytical Modeling of the Base Dark Saturation Current of Drift-Field Solar Cells Considering Auger Recombination", *Int. J. of Renew. Energy Res.*, vol. 3, no. 2, pp. 420-426, 2013.

[7] Md. Shihab Uddin, Md. Rashedul Huqe and Md. Iqbal Bahar Chowdhury, "Analytical Model of the Internal Quantum Efficiency of Non-uniformly and Heavily Doped Silicon Solar Cells Including Non-ideal Effects", *International Conference on Materials, Electronics and Information Engineering (ICMEIE 2015)*, University of Rajshahi, Rajshahi, Bangladesh, June 5-6, 2015.

[8] R. J. van Overstraeten, H. J. Deman and R. P. Mertens, "Transport equations in heavy doped silicon", *IEEE Trans. Electron Devices*, vol. ED-20, no. 3, pp. 290-298, Mar. 1973.

[9] D. B. M. Klaassen, J. W. Slotboom and H. C. de Graaff, "Unified apparent bandgap narrowing in n- and p-type Silicon", *Solid-State Electron.*, vol. 35, no. 2, pp. 125-129, 1992.

[10] M. M. Shahidul Hassan, Orchi Hassan and Md. Iqbal Bahar Chowdhury, Effect of Majority Carrier Current on the Base Transit Time of a BJT, *Journal of Electron Devices*, vol. 10, pp. 511- 514, 2011.

[11] J. G. Fossum and D. S. Lee, "A physical model for the dependence of carrier lifetime on doping density in nondegenrate silicon", *Solid-State Electron.*, vol. 25, no. 8, pp. 741-747, 1982.

[12] J. G. Fossum, "Computer-aided numerical analysis of silicon solar cells", *Solid-State Electron.*, vol. 19, pp. 269-277, 1976.

[13] J. Dziewior and W. Schmid, "Auger coefficient for highly doped and highly excited silicon", *Appl. Phys. Lett.*, vol. 31, no. 5, pp. 346-348, May 1977.

[14] S. M. Sze, *Physics of Semiconductor Devices*, John Wiley & Sons. Inc., New York, 2nd Edition, ch. 14, pp. 800-805, 1981.

Ramp Rate Analysis of Roof-top PV on Distribution Grids for Large Cities in Australia

Md Rabiul Islam

Postgraduate Program Renewable Energy, University of Oldenburg
Oldenburg, Germany

mrabiul_eee_eng@hotmail.com

Hans-Peter (Igor) Waldl

Overspeed GmbH & Co. KG
Oldenburg, Germany

***Abstract*—Aggregation of PV power plants can mitigate electricity demand as well as reduce consumption of fossil fuels. Due to high penetration of roof-top PV power into the Australian electricity market, utility planners and grid operators have to deal with short time variability of output power which can be a potential limiting factor in deploying PV systems. In this Paper, PV variability between different large cities will be analysed due to large there size and various climatic zones within Australia. In order to examine the smoothing effect of geographically distributed roof-top plants, output electricity data of five (05) minutes resolution for 200 sites are analysed. A significant smoothing effect are observed compare to a single site but it depends on the number of aggregated roof-top PV plants and relative correlation between them. Overall PV variability and the amount of smoothing are not the same in all cities within Australia.**

Keywords— Distributed generation, PV variability, Ramp Rate, Smoothing, Australia

I. INTRODUCTION

The sun is an enormous energy source. Conversion of a small fraction of this solar radiation can mitigate much of the world's energy demand. Solar photovoltaic modules are the medium to convert photon energy to electricity. For the last five years, PV module prices have been reducing rapidly which reflects increasing PV energy into the Australian electricity market [1] [2]. The growth in solar PV system has come from the roof-top sector [3]. But rapidly increasing PV roof-top plants are also a concern of utility providers due to PV variability and its uncertainties. PV variability is mainly caused due to the movement of the sun which can be precisely predicted from solar geometry. Another reason for variability is movement of clouds which cannot always be predicted. Within a short time scale (from seconds to minutes) PV's output variability on the Grid causes local voltage flickering issues. For longer time scale (minutes to hours) less PV power output into the Grid requires a balancing reserve to meet the demand. In other words, uncertainty of PV power due to cloud movement's into the Grid should be predicted in order to maintain power quality and continuous electricity supply [4][5]. To deal challenges into the Grid, the Australian Energy Market Operator (AEMO) operates the National Electricity Market (NEM) through a gross pool Market system where electricity is traded 24 hours a day, 7 days a week. Dispatch bids occur every five minutes to maintain power quality issue, and spot bids occur every thirty (30) minutes by averaging six dispatch bids [6] [7]. In other words, uncertainties of PV power production due to cloud movement the Grid should be predictable in order to maintain power quality and a continuous supply of electricity. For this reason, PV variability is a considerable topic for research as well as power system planners and market operators. Several studies(Wiemken et al. (2001), Kawasaki et al. (2006), Murata et al. (2009), Mills and Wiser (2010), Hoff and Perez (2010), Golnas and Voss (2010), Golnas et al. (2011), Golnas and Bryan (2011)) have been completed by considering varying PV scenarios within Germany, Japan and USA [4, 5, 8-14]**.** So far in Australia only a few studies have been done to characterize PV variability and geographic smoothing and this is what encourages me to study PV roof-top plants output variability from different regions in Australia.

II. OBJECTIVES

The objective of this research work is to analyse roof-top PV electricity output in order to characterize PV variability through variability metric (Ramp Rates), level of probability (P95, Fraction of % Installed Capacity) on distribution Grid of large cities in Australia for developing effective measures to manage variability in different levels of penetration for system planners (Generation-Load prediction), operators and the Energy Market. This study also focuses on smoothing benefits after the aggregation of PV roof-top plants. The aim of this study can be described as –

- Analysis of variability metric Ramp Rate (RRs) within same geographical locations. And between different geographical locations in Australia.
- Analysis of smoothing benefits after the aggregation of PV roof-top plants.

III. METHODOLOGY

To quantify solar variability, Ramp Rate (RR) is one of the most important metrics. Ramp Rate is an important metric for Grid operators and energy market planners because a large change in power output introduces instability on the Grid. The Ramp Rate of a PV plant is defined as the ratio of power changes in PV power output time series and time interval. It can be expressed mathematically –

$$\text{Ramp Rates (RRs)} = (P(t+\Delta t) - P(t)) / \Delta t \qquad (1)$$

$$\text{Ramp Rates (RRs) (\% of Installed capacity / Time Scale)} = 1/\Delta t * (P(t+\Delta t) - P(t)) / (\text{Installed Capacity}) \qquad (2)$$

Δt = Time Interval (5 minutes)

PV roof-top output electricity data of 5 minutes resolution is considered from October, 2013 to September, 2014. A time scale of 5 minutes resolution is used.Statistical analysis addressing probability distribution of ramps with respect to fraction of installed capacity per time scale resolution is considered. From the probability distribution graph, a certain threshold (P95) can be analyzed. In this study, P95 probability threshold is considered for analysis. http://pvoutput.org is used here as a source of PV roof-top output electricity data. Data is processed and analyzed with the help of R-studio software (Version 0.98.1056).

IV. ANALYSIS OF RAMP RATES (RRS)

A. *Ramp Rates within Same Geographical Location*

1) *Data:* To analyze variations in PV roof-top power plant's output (Ramp Rates) within the same geographical areas, two PV roof-top Plants (VIC_SITE_V1 and VIC_SITE_V1N) of Melbourne, Australia is considered. They are 400 m far from each other. Both sites are equal installed capacity (5000 Wp) and orientation (North).Output electricity data in five (05) minutes interval (Data recording Time interval which is defined as Timescale in this paper) of 24 hours from October, 2013 to September, 2014 considered for analysis.

2) Results and Discussion: To understand PV variability within the same geographical location (Melbourne, Australia), power output of VIC_SITE_V1 and VIC_SITE_V1N are shown in Fig-1. Fig-1 shows a histogram representation (The number of ramps VS power step changes in watt). VIC_SITE_V1 and its neighbor site VIC_SITE_V1N shows most of the fluctuations in between 0 to ±500 watt with nearly the same number of ramps. Both sites are showing a nearly equal occurrence of fluctuations. It is also noticeable that most of the fluctuations occur within 10% of the installed capacity.

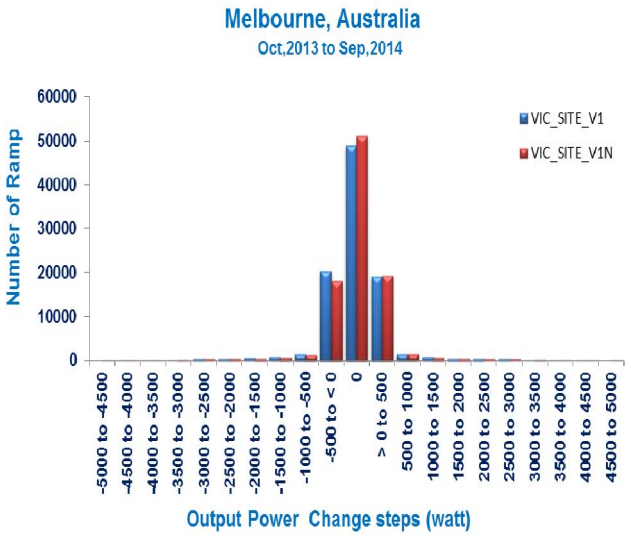

Fig. 1 Number of Ramps VS Power step change (watt) of two sites in Melbourne

B. *Ramp Rates between different cities in Australia*

1) Data: To analyze PV roof-top plant's output (Ramp Rates) between different regions in Australia. NSW_SITE_ N (Sydney), ACT_SITE_ A (Canberra), VIC_SITE _V (Melbourne), QLD_SITE _Q (Brisbane), SA_SITE_ S (Adelaide) are considered with the same duration (October, 2013 to September, 2014, most fluctuating period - 10 Hour to 15 Hour of each day). All of these sites are equal installed capacity (5000 Wp) and orientation (North). The Cumulative Probability Distribution analysis of Ramp Rates (% of installed capacity) is analyzed to describe PV variability to understand regional diversity.

2) *Results and Discussion:* Fig-2 shows Cumulative Probability Distribution of Ramps with respect to ramp rate (%) of installed capacity for different cities in Australia. From Fig-2, it can be observed that NSW_SITE_N is located in Sydney and has a probability of 11.12% to exceed 10% of installed capacity, whereas only 2.66% probability to exceed 30% of installed capacity. An analysis of P95 means 95% probability of variation smaller than 20% of installed capacity. ACT_SITE_A is located in Canberra, Australian Capital Territory shows a 15.23% probability to exceed 10% installed capacity of the plant and 8.16% probability to exceed 20% installed capacity of the plant. It also shows 95% variability smaller than 28.96% installed capacity of the plant. VIC_SITE_V is located in Melbourne, Victoria shows 15.27% probability to exceed 10% installed capacity of the plant and only 2.75% probability to exceed 30% installed plant capacity. 95% variability is smaller than 5.8% installed plant capacity. SA_SITE_S shows 17.52% probability to exceed 10% installed capacity of the plant and 10.82% probability to exceed 20% installed capacity of the plant. They have 5% probability to exceed 40% installed capacity of the plant. QLD_SITE_Q shows 22.55% probability to exceed 10% installed plant capacity and

11.62% probability to exceed 30% of installed capacity. They have only 5%

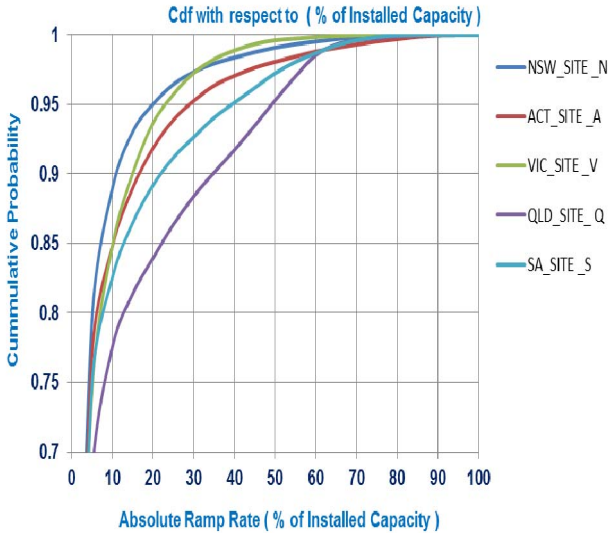

Fig. 2 Cumulative probability distribution of different cities with respect to absolute ramp rate (% of installed capacity)

Probability to exceed 50% installed plant capacity. Table- I give a summary of observations from Figure-2. After individual observation of different city's PV variability, Brisbane is belonging to subtropical climatic zone which has higher fluctuation comparatively other cities of Australia. Melbourne, Sydney and Canberra are belonging to temperate climatic zone which shows nearly the same PV output power variability but Adelaide shows higher fluctuation. After individual observations of different city's PV variability, Brisbane is belonging to subtropical climatic zone which has higher fluctuation comparatively other cities of Australia.

TABLE I
SUMMARY OF RAMP RATE BETWEEN DIFFERENT CITIES IN AUSTRALIA

Site Name of different City in Australia	**Probability to exceed of 10 % installed Plant Capacity (%)**	**Probability to exceed of 20 % installed Plant Capacity (%)**	**Probability to exceed of 30 % installed Plant Capacity (%)**
NSW_SITE _N	11.12	5.00	2.66
ACT_SITE _A	15.23	8.16	4.74
VIC_SITE _V	15.27	6.36	2.75
SA_SITE _S	17.52	10.82	7.36
QLD_SITE_ Q	22.55	16.06	11.62

From Figure-2, it is observed that the maximum variability within 30% installed capacity of the plant whereas Brisbane shows 50% installed plant capacity. Individual PV roof-top plant of one location shows higher fluctuation due to clouds movement.

V. SMOOTHING EFFECT AFTER AGGREGATION OF PV ROOF-TOP PLANTS

Australia as a country shows diverse geographical characteristics due to its size and demand of electricity is also increasing. To meet increasing demand, penetration of PV power into Australian Energy Market as a promising source of green energy but hindering due to its variability of nature. To predict short term (less than 10 minute) fluctuation on the Grid in order to maintain power quality (frequency fluctuation) is also required. Aggregation of PV roof-top plants can mitigate fluctuations. Benefits of aggregation may vary geographically due to diverse characteristics of clouds. In this study, PV roof-top plant's data from different cities will be analyzed and will discuss amount of smoothing after aggregation compared to single site.

1) Data: In this chapter, smoothing effects after aggregation of PV roof-top plants from different regions are analyzed. Twenty (20) PV roof-top plants within 150 km of Victoria, thirty five (35) PV roof- top plants within 110 km of Queensland, twenty (20) PV roof-top plants within 60 km in South Australia, thirty five (35) PV roof-top plants within 40 km are analyzed to understand smoothing after aggregation of PV roof-top plants. All of the roof-top plants are equal in size (5000 Watt) and north oriented. PV electricity output data of 5 minutes resolution is considered from October, 2013 to September, 2014 by considering the highest fluctuating period (10 Hour to 15 Hour) of the day.

2) Results and Discussion: Figure-3 shows the probability to exceed 10% installed capacity for different regions in Australia. In Victoria, after aggregation of 20 sites there are also reducing probabilities of Ramp Rates from 15.27% to 1.46% to exceed 10% of installed capacity. Queensland has comparatively larger PV variability than Victoria. After aggregation of 35 sites in Queensland are reducing probabilities from 22.55% to 1.87% to exceed 10% of installed plant capacity. In South Australia, Single site shows 17.52% probability to exceed 10% installed capacity whereas aggregation of 20 sites show only 3.94% probability to exceed 10% installed capacity. In South Australia, single site shows 17.52% probability to exceed 10% installed capacity whereas aggregation of 20 sites show only 3.94% probability to exceed 10% installed capacity.

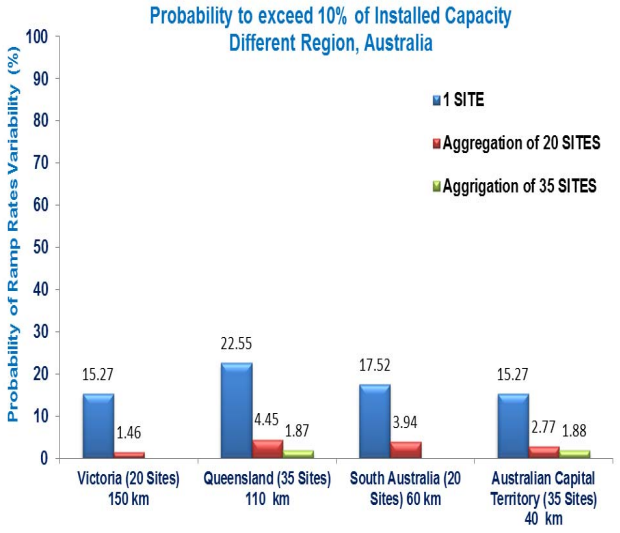

Fig. 3 Probability of Ramp Rates between different regions in Australia

A shorter distance of 40 km is considered for Australian Capital Territory and it is observed that an aggregation of 35 sites show only 1.88% probability to exceed ramp rates of 10% total plant capacity whereas single site shows 15.27% probability.

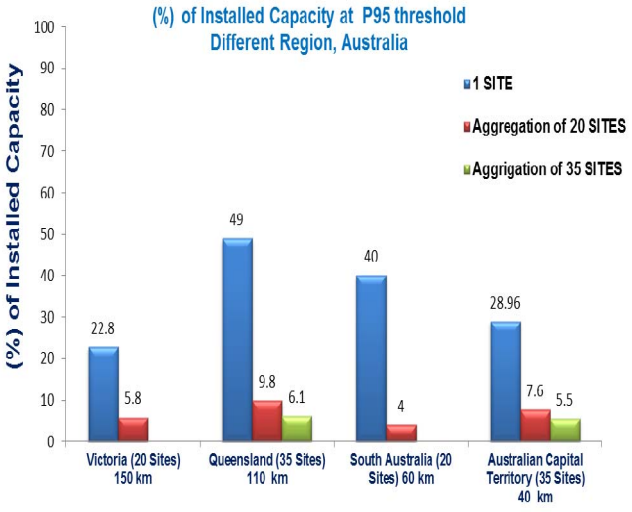

Fig. 4 (%) of Installed Capacity at P95 threshold of different regions in Australia

From Figure-4, it is observed that 95% probability (P95 threshold) of fluctuation smaller than 290 Watt (5.8% of installed capacity) after aggregation of 20 sites whereas single site in Victoria show 1140 watt (22.8% of installed capacity). In Queensland, aggregation of 35 sites show 95% probability of ramp rate smaller than 305 watt (6.1% of installed plant capacity) whereas single site shows 2450 watt (49% of installed plant capacity). In spite of fluctuation in all year, South Australia shows significant results after aggregation of 20 sites which show only 5 % probability to exceed 200 watt (4% of installed capacity) whereas single site has 10 times the Ramp (40 % of installed capacity). In Australian Capital Territory, there is a chance of 5% to exceed Ramps of 275 watt (5.5 % of installed capacity) after aggregation of 35 sites whereas 1448 watt (28.96% of installed capacity) of a single site. Though smoothing depends on a number of aggregated roof-top plants, co-located plants shows lower smoothing than uncorrelated sites.

VI. Conclusions

An analysis of PV output variability in Australia is presented. Several regions are (Victoria, Queensland, South Australia, and Australian Capital Territory) having a majority number of the PV roof-top plants are analyzed during this period. PV variability metric Ramp Rates (RRs) from October, 2013 to September, 2014 are considered for this analysis period.

The key findings are associated with the objectives of this study are as follows –

- Co-located PV roof-top plants show similar PV variability.
- Temperate climatic regions (Victoria, Australian Capital Territory and New South Wales) show less PV variability than subtropical region (Queensland) of Australia.
- A significant smoothing effect was observed during the analysis. In this study, it is observed that there is 95% variability smaller than 10% installed capacity in different regions of Australia :
- Amount of PV variability reduction depends on aggregated number of sites and Aggregation of geographically distributed plants which shows significant PV variability reduction than aggregation of co-located plants.

Overall Aggregation of geographically distributed PV roof-top Plants provide natural mitigation of PV output variability and site pair correlation which is a function of distance and time interval. Analyze results are consistent with previous studies regarding PV variability. As PV penetration is increasing into electricity Grids, statistical approach of Cumulative distribution portfolio (Cdf) of PV variability from different regions are efficient for the electricity market operators in order to set operating thresholds, estimation of operating reserves and peak saving potential of PV.

Acknowledgment

Special thanks to Overspeed GmbH & Co. KG, Oldenburg, Germany for making data available to this study and for their Master thesis program. My sincere gratitude is dedicated to my supervisor Dr. Hans-Peter (Igor) Waldl for his critical and generous suggestions have given for my work. This is worth mentioning that his conceptual ideas and guidance at every stage in my work have shaped my work to a perceptible direction.

REFERENCES

[1] HTTP://WWW.SOLARCHOICE.NET.AU/BLOG/RESIDENTIAL-SOLAR-SYSTEM-PRICES-APRIL-2015 INTERNET ACCESS DATE: 29TH MAY, 2015.

[2] http://www.pv-magazine.com/news/details/beitrag/solar-energy-prices-to-drop-by-up-to-12-in-2014_100016875/ Internet Access Date: 29th May, 2015.

[3] *ROOFTOP PV FORECASTING, ANDREW REDDAWAY*, August 2012, Australian Energy Market Operator (AEMO).

[4] Book – *Renewable Energy Sources and Climate Change Mitigation*, First Published 2012, ISBN- 978-1-107-60710-1.

[5] Jan Kleissl, Book – *Solar Energy Forecasting and Resource Assessment*, First Edition 2013, ISBN: 978-0-12-397177-7.

[6] Australian Energy Market Operator (AEMO), http://www.aemo.com.au/ , Internet Access Date: 29th May, 2015.

[7] Australian Energy Market Commission (AEMC), http://www.aemc.gov.au , Internet Access Date: 29th May, 2015.

[8] "An evaluation method of the fluctuation characteristics of photovoltaic systems by using frequency analysis", Kawasaki, N., T. Oozeki, K. Otani, and K. Kurokawa (2006) , Solar Energy Materials and Solar Cells, Volume 90, Issues 18-19, pp. 3356-3363 .

[9] "A Method of Estimating the Output Fluctuation of Many Photovoltaic Power Generation Systems Dispersed in a Wide Area", Murata, A., H. Yamaguchi, and K. Otani (2009) , Electrical Engineering in Japan, Volume 166, No. 4, pp. 9-19.

[10] Understanding Variability and Uncertainty of Photovoltaics for Integration with the Electric Power System, Andrew Mills, Mark Ahlstrom, Michael Brower, Abraham Ellis, Ray George, Tom Hoff, Benjamin Kroposki, Carl Lenox, Nicholas Miller, Joshua Stein, Yih-huei Wan, Environmental Energy Technologies Division, December 2009.

[11] "Quantifying PV Power Output Variability", Hoff, T. and R. Perez, (2010, conditionally accepted for publication in Solar Energy (1/2010).

[12] "Short-term Irradiance Variability: Station Pair Correlation as a Function of Distance", Perez R., S. Kivalov, J. Schlemmer, K. Hemker, Jr. and T. E. Hoff, (2011) , Proc. ASES National Conference, Raleigh, NC.

[13] "POWER OUTPUT VARIABILITY OF PV SYSTEM FLEETS IN THREE UTILITY SERVICE TERRITORIES IN NEW JERSEY AND CALIFORNIA", A. Golnas, S. Voss, SunEdison, Beltsville, MD, USA.

[14] A report on "Implications of Wide-Area Geographic Diversity for Short-Term Variability of Solar Power", Andrew Mills and Ryan Wiser, Ernest Orlando Lawrence Berkeley National Laboratory, September 2010, LBNL - 3884E.

[15] Australian Government and info services, http://www.australia.gov.au/about-australia/our-country , Internet Access Date: 29th May, 2015.

[16] Australian Government and info services, http://www.australia.gov.au/about-australia/australian-story/austn-weather-and-the-seasons , Internet Access Date: 29th May, 2015.

[17] *Bureau of Meteorology, Australia.* http://www.bom.gov.au/ , Internet Access Date: 29th May, 2015.

[18] "THE AUSTRALIAN NATIONAL ELECTRICITY MARKET: CHOOSING A NEW FUTURE", Mr John Pierce, World Energy Forum 13-16 May 2012 (Conference), Quebec City, Canada.

A Snapshot of Energy Efficient Off Grid Appliance Market in Bangladesh

Hasna J. Khan[1], Asma J. Huque, Mohammad S. Hoque
Kaysar Ahmed, Rafiur Rahman, Tanvir Ahmed, and Rashedul Alam

[1]*Prokaushali Sangsad Limited (PSL), Dhaka, Bangladesh*

[1] hasnajkhan@gmail.com

***Abstract*— The study focuses on off-grid appliance market in Bangladesh, which is expected to grow at a rapid pace in the upcoming years. Survey of upstream and downstream sales agents along with the off-grid appliance consumers have revealed many barriers for energy efficient appliances in the nascent market, including a gap in information and awareness on energy efficient products with a need for enabling environment for market development. Under the circumstances price of the appliance is the leading decision criterion for the rural consumers, which is followed by other features including warranty, longevity, and performance.**

Keywords— Bangladesh; solar; energy efficient appliance; off-grid appliance; market survey

I. INTRODUCTION

The vast majority of 25 million rural households in Bangladesh are not connected to the national grid electrification services. Since grid service has not reached many locations, Small Power Producers (SPP) using diesel gensets with micro-grid service fill up a significant part of this gap on an adhoc basis. Whereas diesel micro grids are widespread in serving the rural markets for more than two decades, most recent advancement in solar mini grids has created a new opportunity for clean energy solutions for the commercial markets in particular [1] [2]. While such off-grid services meet the need of the rural commercial markets, there appears to be a strong demand for off-grid household electrification service, which is mostly met with alternatives like Solar Home System (SHS) [3]. Since early 2000 Bangladesh has made remarkable achievement as one of the largest off-grid service users for rural electrification, where over 4 million SHS are in use. Alongside the national SHS program implementation by IDCOL, there exists a growing market for retail sales of SHS. Together, the service users of these alternatives constitute the current off-grid appliance market in Bangladesh. This market will experience significant growth in the coming years with the rising trend in off-grid electrification. Hence timing is optimum for introducing high quality and super efficient appliances into the market through Clean Energy Ministerial's Global Lighting and Energy Access Partnership (Global LEAP) [4] [5].

The demand for off-grid electrification is evidenced through the rising sale of appliances in Bangladesh. Dhaka being the capital city, it has major commerce for off-grid appliances that include wholesale importers, and retailers. With the onset of broader access to electricity, the overall market for off-grid appliances has grown at a rapid pace within the recent years. This paper elaborates on the main features of the off-grid appliance market that will lead to a market growth in the upcoming years where energy efficiency has received noticeable recognition among the users in the context of energy and cost savings.

II. METHODOLOGY

In order to identify the nature of the off-grid appliance market, information was collected from individuals at (a) upstream, (b) midstream and (c) the user level. Such appliances include LED light, mobile charger, fan, television, and refrigerator, having the highest likely demand in the off-grid areas. Within the upstream level are manufacturers, importers and other suppliers who procure appliances in bulk quantity and forward them to the retailers. The wholesale importers face import related regulations imposed on items; hence their views reflect the policy trends. The retailers are widespread nationwide serving the central markets to the rural shops. The survey received responses from whole sellers and importers of appliances that have potential use in the rural off-grid electrification market. Since the retailers interface the consumers directly, their interviews and opinion provide a deeper understanding of the market scenario from the consumers' choice and preference perspective.

III. RESULTS

A. Survey of Whole Sale Market:

The survey provides a list based on priority of market demand and supply volume, along with consumer's selection criteria. The market price of energy efficient (EE) appliances is different from other traditional appliances, since it is based on the product's efficiency and consumer's knowledge base about the merits of EE. Some of the manufacturers are assembling their products locally and selling them in the retail market through agents or SHS companies. Whereas the appliances used in IDCOL's SHS are pre-approved on the basis of performance, the commercial market is oblivious to the performance and service life. The survey finds that except for refrigerator, the market price of most appliances has a decreasing trend, which also relates to the import duty structure. Table-1 shows, the present market prices of EE appliances in $/Watt.

There is growing market for appliances in Bangladesh. All over the country many manufacturers, importers and suppliers are offering new energy efficient appliances suitable within grid and off grid area. The survey finds that the upstream level samplers are offering their energy efficient appliances by many

TABLE-1: THE MARKET PRICE OF SAMPLED PRODUCTS (PRICE PER WATT) IN LAST THREE YEARS

Appliance	2015		2014		2013	
	Max.	Min.	Max.	Min.	Max.	Min.
LED Light	$2.17	$0.50	$1.37	$0.67	$1.50	$0.57
Fan	$1.65	$1.20	$1.72	$1.40		
TV	$13.75	$10.10				
Refrigerator	$15.60		$9.80		$9.80	
Mobile Charger	$0.45					

TABLE-2: THE SELECTION CRITERIA FOR PURCHASING ENERGY EFFICIENT APPLIANCES FROM THE MARKET (1 HIGHEST)

Light	Fan	TV	Refrigerator
1. Lower Price 2. Performance 3. After Sales Service	1. Performance 2. Longevity 3. After sales service	1. Performance 2. Longevity 3. Brand Value 4. Attractive outlook	1. Performance 2. Longevity 3. Environment friendly

features. Table-2 shows the preference of people while making a selection of the appliances. Performance of the appliance is a very important criterion which reflects the value of their investment.

Most upstream level sellers are offering incentive to the customers to increase their sales and profit with better efficiency appliances. The type of incentive being offered is different and depends on the business pattern. The survey finds that in most cases the incentives include (a) Cash discount, (b) Gift with purchase, (c) After sales service, or (d) Sales commission to the sales representative. The sellers of off-grid appliances at the upstream level mentioned major barriers faced in the business of manufacturing, importing for supplying EE appliances, which include:

- Lack of legal and regulatory step for removing lowest technologies from the market and promoting energy-efficient technologies by the authority.
- High VAT & Tax on import items
- Huge shipment charge and duration
- CNF clearance harassment
- Lack of awareness raising for the organization who implement projects
- Lower quality products in local market
- Piracy/sticker business

Other barriers include:

- Lack of Institutional and individual capacity to promote EE products.
- Lack of knowledge within policy makers, customs, NBR and financial institutions.

Considering the upstream level sellers play an important role in spreading out the off grid appliance to the retailers in the country, the survey team wanted their opinion on addressing those barriers and improving the sales of EE appliances. The survey collected some recommendation from the whole sellers, which include:

- Strengthening of Policy Context for EE
- Provide training and develop practice to select EE products by the importers
- Tax benefit for EE products, provide training to related customs, NBR
- Provide training and aware IDCOL and others to select efficient products.
- Have continuous monitoring and random testing in BUET, BSTI, other government institutions
- Penalty should be implemented for stickered and lower quality products
- Campaign on EE products and how to save money by using EE products
- Swift CNF and Port clearance

B. Survey of Retail Market:

Although off-grid appliance market in Bangladesh is broadly distributed from central Dhaka to the rural areas, the retail market for energy efficient appliances is more localized within retailers in the capital city and the POs of IDCOL. Interviews with the retailers indicate that their consumers are willing to switch toward energy efficient appliances irrespective of the prices after they have been explained about their performance life and potential economic benefit. In the view of retail sellers of the appliances, the impact of increased availability of energy efficient appliances is to reduce sales of less efficient products.

High price was identified as the greatest challenge faced by the retailers in selling EE products. Among others, it is noted that product warranty cannot be maintained since manufacturers often leave the market after few months posing a problem for product replacement. In certain cases, products are immediately copied and reproduced in local shops bringing product price, as well as quality, down significantly. Therefore, same products can be found at a lower price, even in the rural areas. It has been suggested that providing door to door delivery of product and/or information may assist in accelerating dissemination of energy efficient off-grid appliances to the customers residing in rural areas. In response

TABLE-3 RATE THE CUSTOMERS' PREFERENCE OF CRITERION FOR PURCHASE (1 HIGHEST)

	Light	Fan	TV	Mobile charger	Fridge
Necessity	1	1	1	1	2
Price	2	2	2	4	1
Energy Efficiency	7	7	Does not care	Does not care	4
Warranty	3	3	3	2	3
Attractive outlook	6	6	Does not care	Does not care	Does not care
Brand value	5	4	Does not care	Does not care	5
Others (specify)	4 - Performance	5 - Performance	4 - Performance	3 – Dual functionality (Mobile + Portable lamp charging)	

to recommendations for removing barriers for improving sales of energy efficient appliances, it has been proposed that the manufacturers should be legally bound to be in the market for at least one year and there should be incentives to manufacturers for reducing product cost giving discounts to the consumer.

C. Survey of End-user consumers

The demand for appliances in the off grid areas depend on the geographic region and socio-economic status of the population. Residents of an off-grid area named Nalitabari, Sherpur were interviewed where most households have solar home system (SHS's) ranging from 40Wp to 85Wp. The very basic electrical appliances used are 3 Watt LED light, 5 Watt CFL light, 18 Watt TV, 3 Watt mobile charger & 12-8 Watt DC stand fan. As shown in Table 4, according to these respondents, light, fan, mobile phone charger, TV and fridge appear to have the highest demand, in order. Within a broader appliance survey, response from Africa [5] showed similar demand but in a different order, where light, phone charger, TV, radio, refrigeration was followed by fan and solar water pump.

TABLE-4: THE DEMAND FOR APPLIANCES IN THE MARKET (1 HIGHEST)

Item	Light	Fan	TV	Mobile charger	Fridge
Rating	1	2	4	3	5

Within each category of appliance, the consumers have selection criteria a basis for willingness to pay. Table 3 shows the order of selection for each appliance. Necessity followed by price and warranty appear to be the highest ranking, whereas branding and energy efficiency have no significant impact on the choices. The latter may be attributed to the lack of knowledge and information on the benefits of high quality energy efficient products. This reveals the need for awareness building on merits of EE among the rural consumers.

Some ideas regarding energy efficient product, incentives etc. were shared with them, and the survey found some common outcomes, including:

- At the time of purchasing any new product, majority households consider the price issue as a first criterion. Brand, product quality and then warranty coverage are other issues that they consider.
- Most of the households' use the energy efficient product like LED light at the time of replacement of the old CFL light. They are not interested to change all existing appliances with the new energy efficient product though the product is incentivized.
- Availability of information on new efficient technology and product is the key market challenge and lack of awareness and insufficient marketing of new product are the barriers for buying energy efficient appliances.

Most of the people prefer to receive the incentive on direct product price. Some of them are interested to receive it as extended product warranty.

IV. CONCLUSION

The off-grid appliance market in Bangladesh is expected to grow at a rapid pace in the upcoming years. Survey of upstream and downstream sales agents along with the off-grid appliance consumers have revealed the many barriers existing in introduction of energy efficient appliances in the nascent market. In general price of the appliance is the leading decision criteria for the rural consumers, which is followed by warranty, brand name, and performance. There is a large knowledge gap in information and awareness on energy efficient products. Many of existing barriers can be overcome by creating an enabling environment in which existing and new off-grid energy appliance manufacturers and retailer would find it easier to serve the market. Lack of institutional and individual capacity to promote EE products by policy makers and financial institutions also need to be addressed. The underlying lack of knowledge of energy efficiency should be removed for accelerating penetration of energy efficient appliances in the rural areas of Bangladesh.

REFERENCES

[1] Hasna J. Khan, Asma J. Huque, Kaysar Ahmed Sagor, Tanvir Ahmed, Rashedul Alam, M. Riazul Hamid, "Experience from First Solar Mini Grid Service in Bangladesh," in *Decentralized Solution for Developing Economies Springer Proceedings in Energy*, pp 43-52, March 2015

[2] Khan, H.J.; Huque, A.J., "Reliable power supply with solar mini grid in Sandwip Island of Bangladesh," in *Developments in Renewable Energy Technology (ICDRET), 2012 2nd International Conference on the* , vol., no., pp.1-4, 5-7 Jan. 2012

[3] Expanding Energy Access Beyond the grid, Sierra Club, 2014 http://action.sierraclub.org/site/DocServer/Final_Beyond_the_Grid_report__web_.pdf?docID=16729.

[4] http://www.cleanenergyministerial.org/

[5] Globar Leap Off-grid Appliance Market Survey, April 2015, Clean Energy Ministeria

Prototype Design and Overview of a Low Price Microbial Fuel Cell

Uddin Sheikh Shehab, Abu Hena MD Shatil
Electrical and Electronic Engineering Department
American International University Bangladesh
Dhaka 1213, Bangladesh
usshehab@gmail.com, abu.shatil@aiub.edu

Roni Kazi Shoffiuddin, Walid Abdullah Bin
Electrical and Electronic Engineering Department
American International University Bangladesh
Dhaka 1213, Bangladesh
xeonr@ymail.com, pb.walid@gmail.com

***Abstract*—Non conventional sources of energy are one of the society's greatest demands. On the other hand almost 2 billion people in this earth shortage of enough sanitation and economic means to yield it. Waste water treatment energy costs are also a pivotal issue. Microbial fuel cell represents a new method of renewable energy recovery. It's like a bio reactors that converts the chemical energy into electricity by using bacteria. However expensive and toxic materials needed to run the electrons from the bacteria to the electrode. Because of high initial cost and low output, government and private companies are not investing money in this sector. In this paper we are working to minimize the cost by using different types of chemical elements with a brief overview of microbial mechanism. We have also implemented a practical model and discussed about the actual data we found from the prototype.**

Keywords— Microbial fuel cell, Nafion, Membrane, Salt bridge, Agar, Sodium chloride

I. INTRODUCTION

Alternative sources of energy are in high demand because developed as well as developing countries are facing serious energy crisis [18, 19]. In Bangladesh 62.11% (7280 MW) [installed capacity-11683MW] of the electricity comes from the gas [22]. The country's gas reserves stand at 14.16 trillion cubic feet (tcf) as of June 2015 the parliament was told yesterday. If the current rate of extraction remains unchanged the reserve would last until 2031, Nasrul Hamid, state minister for power, energy and mineral resources, said in reply to lawmaker's queries [Source: The Daily Star 29 june,2015]. So the conventional power plant which are run by gas would be shut down and the economic growth of Bangladesh would be collapsed after 2031 as electricity is the driving force of our promising economy. So we have to concentrate on renewable energy sources to ensure our energy security as well as to accelerate economic growth. In recent years, fuel cells have emerged as a renewable energy sources. Among different kinds of fuel cells, microbial fuel cells (MFCs) defined as devices which directly converts microbial metabolism into electricity have attracted researcher's attention [17]. In an MFC, bacteria are separated from a terminal electron acceptor at the cathode so that the only means for respiration is to transfer electrons to the anode. An MFC is thus a bio electrochemical system that derives electricity by mimicking bacterial interactions in nature. Microorganisms 'catabolise compounds such as glucose [1], acetate or wastewater [2]. Microbial fuel cells use biocatalysts for the conversion of chemical energy to electrical energy ([4], [6] and [5]). We can produce Hydrogen from MFC. The most effective hydrogen production is observed upon fermentation of glucose in the presence of Clostridium butyricum [7].

$$C_{12}H_{22}O_{11} + 13H_2O \text{ ---> } 12CO_2 + 48H^+ + 48e^-$$

II. WORKING MECHANISM OF MFC

Microbial fuel cells (MFCs) are devices that use bacteria as the catalysts to oxidize organic and inorganic matter and generate current[20].Electrons produced by the bacteria from these substrates are transferred to the anode (negative terminal) and flow to the cathode (positive terminal) linked by a conductive material containing a resistor or operated under a load. Electrons can be transferred to the anode by electron mediators or shuttles by direct membrane associated electron transfer or by so-called nanowires produced by the bacteria or perhaps by other as yet undiscovered means. Chemical mediators such as neutral red or anthraquinone-2, 6-disulfonate (AQDS) can be added to the system to allow electricity production by bacteria unable to otherwise use the electrode.

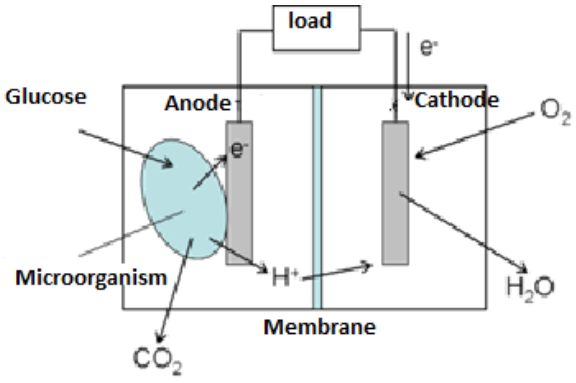

Fig. 1. MFC mechanism

Figure1 shows that bacteria in the anode compartment transfers electrons obtained from an electron donor (glucose) to the anode electrode. This occurs either through direct contact, nanowires or mobile electron shuttles. During electron production protons are also produced in excess. These protons migrate through the cation exchange membrane (CEM) into the cathode chamber. The electrons flow from the anode through an external resistance (or load) to the cathode where they react with the final electron acceptor (oxygen) and protons [21].

III. Materials and Construction

A. Anode

First anodic materials must be conductive, bio compatible and chemically stable in the reactor solution. Metal anodes consisting of noncorrosive stainless steel mesh can be used but copper is not useful due to the toxicity of even trace copper ions to bacteria. The most versatile electrode material is carbon, available as a compact graphite plates, rods, granules. The simplest materials for anode electrode is graphite plates and rods as they are relatively inexpensive, easy to handle and have a defined surface area.

B. Cathode

Due to its good performance, ferricyanide ($K_3[Fe(CN)_6]$) is very popular as an experimental electron acceptor in microbial fuel cells. The greatest advantage of ferricyanide is the low over potential using a plain carbon cathode, resulting in a cathode working potential close to its open circuit potential. The greatest disadvantage, however, is the insufficient reoxidation by oxygen, which requires the catholyte to be regularly replaced. In addition, the long term performance of the system can be affected by diffusion of ferricyanide across the CEM and into the anode chamber. Oxygen is the most suitable electron acceptor for an MFC due to its high oxidation potential, availability, low cost (it is free), sustainability, and the lack of a chemical waste product (water is formed as the only end product). The choice of the cathode material greatly affects performance, and is varied based on application. For sediment fuel cells, plain graphite disk electrodes immersed in the seawater above the sediment have been used [3].

C. Membrane

The majority of MFC designs require the separation of the anode and the cathode compartments by a CEM. Exceptions are naturally separated systems such as sediment MFCs or specially designed single-compartment MFCs. The most commonly used CEM is Nafion (Dupont Co., USA), which is available from numerous suppliers (e.g., Aldrich and Ion Power, Inc.). Alternatives to Nafion, such as Ultrex CMI-7000 (Membranes International Incorp., Glen Rock, and NJ) also are well suited for MFC applications [3]. In comparison with Nafion, Ultrex with great mechanical stability and more affordability is a common alternative for CEMs [8, 9]. As a further instance, Ultrex CMI 7000 is another commonly utilized CEM [10, 11, 9] are considerably more cost-effective than Nafion. Zirfon[12] and Hyflon (Solvay-Solexis, Italy)[13] are another alternative cut-rate CEMs. In comparison with Nafion, Zirfon is of higher oxygen permeability (penetrability) which is detrimental to anodic reactions, but its specific resistance is much lower[12].In addition to Zirfon, Arico et al. reported that in conductivity and chemical stability, Hyflon is better than Nafion[16]. When a CEM is used in an MFC, it is important to recognize that it may be permeable to chemicals such as oxygen, ferricyanide, other ions, or organic matter used as the substrate [3].

D. Mediator

If oxygen is present, it will collect all the electrons as it has a greater electronegativity than the mediator. A number of mediators have been suggested for use in microbial fuel cells. These include natural red, methylene blue, thionine or resorfuinetc. [15]. Thionine has been used extensively as a mediator of electron transport from Escherichia coli ([14], [15]). If no exogenous mediators are added to the system, the MFC is classified as a "mediator-less" MFC even though the mechanism of electron transfer may not be known [3].

IV. Fundamentals of Voltage Generation

Electricity is generated in an MFC only if the overall reaction is thermodynamically favourable. The reaction can be evaluated in terms of Gibbs free energy expressed in units of Joules (J), which is a measure of the maximal work that can be derived from the reaction calculated as

$$\Delta G_r = \Delta G^o_r + RT\ln(\Pi) \quad (1)$$

where ΔG_r (J) is the Gibbs free energy for the specific conditions, ΔG^o_r (J) is the Gibbs free energy under standard conditions usually defined as 298.15 K, 1 bar pressure and 1 M concentration for all species, R (8.31447 J mol-1 K-1) is the universal gas constant, T (K) is the absolute temperature and Π (dimensionless) is the reaction quotient calculated as the activities of the products divided by those of the reactants. The standard reaction Gibbs free energy is calculated from tabulated energies of formation for organic compounds in water available from many sources. For MFC calculations, it is more convenient to evaluate the reaction in terms of the overall cell electromotive force (emf), E_{emf} (V), defined as the potential difference between the cathode and anode. This is related to the work W (J), produced by the cell or

$$W = E_{emf} Q = -\Delta G_r \quad (2)$$

where Q = nF is the charge transferred in the reaction, expressed in Coulomb , which is determined by the number of electrons exchanged in the reaction, n is the number of electrons per reaction mol and F is Faraday's constant (9.64853×10^4 C/mol). Combining these two equations, we have

$$E_{emf} = -\Delta G_r / nF \quad (3)$$

If all reactions are evaluated at standard conditions, $\Pi = 1$, then

$$E^{o}_{emf} = -\Delta G^{o}_{r}/nF \quad (4)$$

Where E^{o}_{emf} (V) is the standard cell electromotive force. We can therefore use the above equations to express the overall reaction in terms of the potentials as

$$E_{emf} = E^{o}_{emf} - (RT/nF) \ln (\Pi) \quad (5)$$

The advantage of equation (5) is that it is positive for a favourable reaction, and directly produces a value of the emf for the reaction. This calculated emf provides an upper limit for the cell voltage; the actual potential derived from the MFC will be lower due to various potential losses like (i) Ohmic losses, (ii) Activation losses, (iii) Bacterial Metabolic losses and (iv) Concentration losses [3].

V. Standard Electrode Potentials

The reactions occurring in the MFC can be analyzed in terms of half-cell reactions, or the separate reactions occurring at the anode and the cathode.

$$2CH_3COO^- = CH_3CH_3 + CO_2 + 2e^- \quad (6)$$

For sucrose oxidation, we therefore have,

$$E_{AN} = E^{0}_{AN} - (RT/2F) \ln [(CH_3COO^-)^2 / (CH_3CH_3)] \quad (7)$$

For the cathode potential E_{cat} if we consider the case where ferricyanide is used as the electron acceptor for the reaction, we can write

$$Fe(CN)_6^{3-} + e^- = Fe(CN)_6^{4-} \quad (8)$$

$$E_{cat} = E^{0}_{cat} - (RT/2F) \ln [(Fe(CN)_6^{4-})^2 / Fe(CN)_6^{3-}] \quad (9)$$

The Cell EMF is calculated as,

$$E_{emf} = E_{cat} - E_{An} \quad (10) [3]$$

VI. Average Chemical Components use for Cell Design With Pricing

The model shown in figure 1 is the ideal configuration to construct a Microbial Fuel Cell (MFC).It is efficient than any other models of MFC as of now. But the unavailability as well as the price of the elements discourages to construct such model. It also increases the payback duration of project which is the vital obstacle to make it popular as a new source of renewable energy. Table 1shows the price of the elements which are so much costly.

TABLE I. Price of Elements [24]

Elements	Price
Nafion 117 (10cm ×10cm)	$33.00
NADH (1 gm)	BDT. 5000
Potassium Ferricyanide(250 gm)	BDT. 1500

As the construction cost is high enough so we need to concentrate on finding new model of MFC.

VII. Proposed Model With New Chemical Component

The model shown in figure 2 may be a replacement of ideal expensive model of MFC. In this model we are not using any coenzyme such as NADH (Sodium Salt) in anode. The function of coenzyme is to make reaction fast. But in MFC the performance of coenzyme is not convincing. So we try to

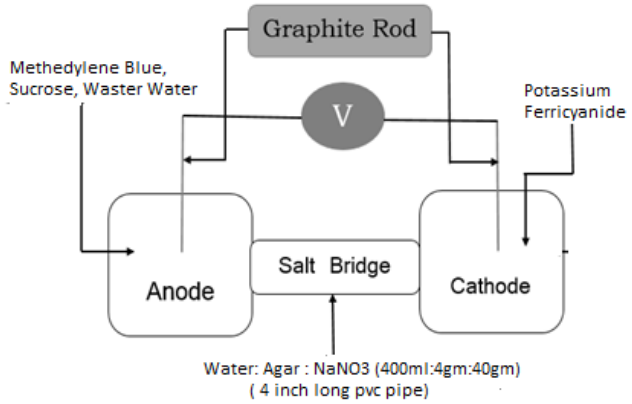

Fig. 2. An alternative model of MFC

eliminate this element to reduce the cost. Then we replace the Proton Exchange Membrane (PEM) with a salt bridge. The high cost of Nafion and unavailability of other PEM elements such as Ultrex CMI-7000, zirfon, Hyflon forces us to make this replacement. The salt bridge is made of a composition of water, agar (bacteriological-$C_{14}H_{24}O_9$) and sodium nitrate ($NaNO_3$).This salt bridge is permeable to chemicals such as oxygen, ferricyanide, other ions, or organic matter used as the substrate like glucose or sucrose. Table 2 represents the price of the alternative elements. We can also replace potassium ferricyanide ($K_3[Fe(CN)_6]$) with salt water (H_2O+NaCl) as it has the required properties to be used in cathode

TABLE II. Proposed Chemical Price from Hatkhola Bazar

Elements	Price
Agar(500 gm)	BDT.3500
Sodium nitrate(500 gm)	BDT.650
Sodium chloride(500 gm)	BDT.14

VIII. Practical Setup & Data Analysis

We set up a prototype design in our lab with all the arrangement possibly we could manage. We had used two bottles of different diameter and length as anode and cathode chamber. The bottle having the larger length and diameter than the other one was used as anode chamber. The mixture of drain water and cow dung is treated as waste water. At first we mixed 1 litre of drain water with 0.5 litre of liquid. We used 10 mL of methylene blue as mediator and 25gm of sucrose as organic material. Our salt bridge was 6.5 inch long and 0.5 inch thick. We took 6.5 gm agar, 32.5gm sodium nitrate and 325mL of water for constructing the salt bridge. At first we took all the components in a pot then mixed the materials during the heating process. We heated the mixture until it become adhesive. Then we put the mixture inside a pipe of 6.5 inch long and 0.5 inch diameter at the time of cooling. 250 mL potassium ferricyanide is used at cathode chamber. Both of the electrodes are graphite rods. All the components are pretty much available in our local market like Hatkhola Bazar, old Dhaka.

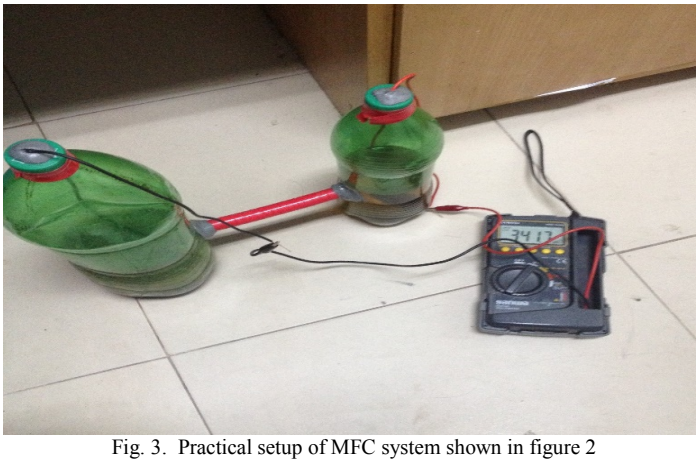

Fig. 3. Practical setup of MFC system shown in figure 2

TABLE III. VOLTAGE (MILI VOLT) OBTAINED FROM MODEL

Day	Voltage output from Waste (Cow dung + Drain water) 0.5 litre
01	87.8
02	114.5
03	341.1
04	234.4
05	190.1
06	178.8
07	145.7

IX. COMPARISON WITH AN IDEAL CASE

At department of aerospace and mechanical engineering in University of southern California, a practical model was implemented by using Nafion 117 as a membrane. Test data's and graph are given below. [23]

Chambers:	Anode and cathode
Length	3.3 cm = 33 mm
Diameter	3.9 cm = 39 mm
Projected surface area	11.94 cm^2
Membrane:	**Nafion 117**
Thickness	177.8 um = 0.1778 mm
Projected surface area	11.94 cm^2
Electrodes:	**Anode and cathode**
Thickness	0.6 cm = 6 mm
Projected surface area (large)	11.94 cm^2
Surface/ Volume ratio	10 666*

Fig. 4. Specific data for MFC experiments at University of Southern California [23]

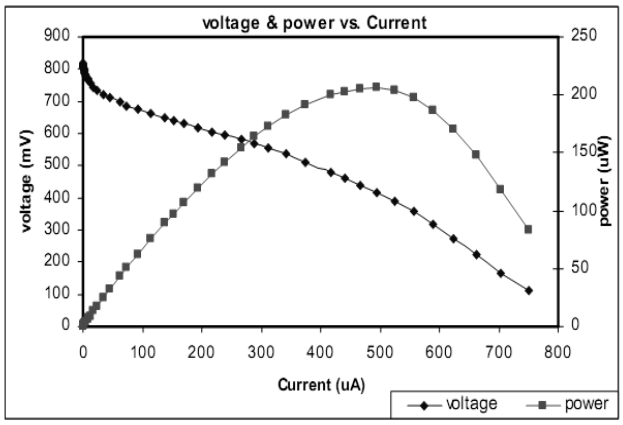

Fig. 5. Graphical presentation for voltage and power vs current for an MFC [23]

With a projected electrode surface area of 11.94 cm^2 the max Power attained was approximately 206.4 microwatts [23]. For prototype set up in our lab, the values are given below.

TABLE IV. OUR LAB EXPERIMENTAL DATA FOR MFC CELL

Chambers	Anode	Cathode
Length	35.5 cm	30.5 cm
Diameter	10.16 cm	7.6 cm
Surface Area	1133.11 cm^2	728.22 cm^2
Salt bridge Length	16.5 cm	
Salt bridge Diameter	1.3 cm	
Electrode Length	14 cm	
Electrode diameter	1.3 cm	
Electrode Surface Area	57.2 cm^2	

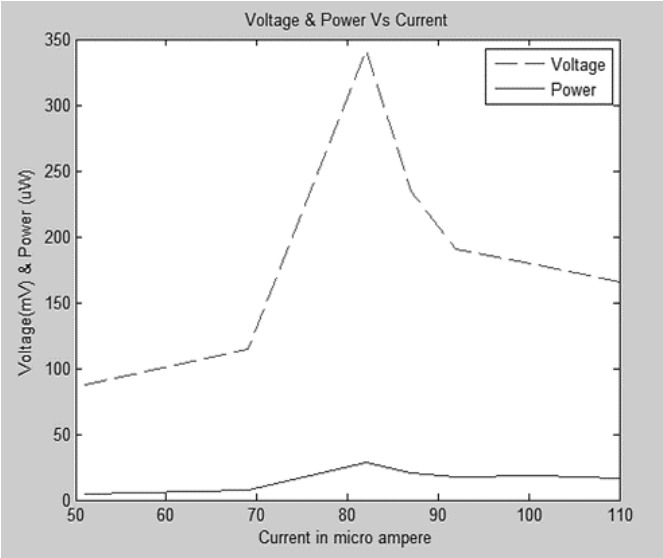

Fig. 6. Voltage and Power Vs Current for proposed model

Figure 6 shows that we had achieved highest 28.02 micro watts amount of power

X. Conclusion

Microbial fuel cell is showing us the future energy system. It could be used in biomass based energy harvesting technique. But still we need to achieve many things to make it feasible and practical. The most prompt demand for an MFC-based idea is a scalable or standard technology that can provide, in a cost-effective manner, the large surface areas needed for the anodes and cathodes. We must address these materials issues related to MFC development, and we must also advance our understanding of the biological basis for the process. In the future, MFCs will have to contend with more on grid renewable-energy technologies, such as wind and solar power. The operating costs needed for electricity production with MFCs will probably be too great if the substrate for the MFC is grown as a crop in a manner similar to that for ethanol production from corn.

Acknowledgment

We would like to express our deepest gratitude towards our teacher and mentor Mr A S M Anwar Hasan, Assistant Professor, Dept. of Chemistry, Adamjee Cantonment College for share his outstanding idea about our research.

References

[1] Chen, T., S.C. Barton, G. Binyamin, Z Gao, Y. Zhang, H.-H. Kim & A. Heller, A Miniature Biofuel Cell, *J. Am. Chem. Soc*. Vol.123,No.35,2001,8630-8631.

[2] Habermann, W. & E. H. Pommer, "Biological Fuel Cells with Sulphide Storage Capacity,"*Appl. Microbiol. Biotechnol.*, Vol.35,pp.128-133,1991.

[3] B.E. Logan, B. Hamelers, R. Rozendal, U. Schro ¨ der, J. Keller,S. Freguia, P. Aelterman, W.Verstraete, K. Rabaey,"Microbial fuel cells: methodology and technology,"*Environ. Sci. Technol.*, Vol. 40,pp. 5181–5192,2006.

[4] Sisler F. D., Biochemical Fuel Cells, in Progress in Industrial Microbiology, D. J. D. Hockenhull (Ed), J. &A.Churchill, London, Vol. 9, pp.1–11,1971.

[5] Palmore G. T. R. and G. M. Whitesides, Microbial and Enzymatic Biofuel Cells in Enzymatic Conversion of Biomass for Fuels Production, M. E. Himmel, J. O. Baker and R. P. Overend (Eds), ACS Symposium Series No.566, American Chemical Society, Washington, DC, 1994, 271–290.

[6] Turner A. P. F., W. J. Aston, I. J. Higgins, G. Davis and H. A. O. Hill, Applied Aspects of Bioelectrochemistry: Fuel Cells, Sensors, and Bioorganic Synthesis, in Fourth Symposium on Biotechnology in Energy Production and Conservation, C. D. Scott (Ed), Interscience, New York, 401, 1982.

[7] Suzuki S. and I. Karube, Energy Production With Immobilized. Cells, *Appl. Biochem. Bioeng*., Vol. 4,pp. 281 – 310,1983.

[8] R. Rozendal, T. Sleutels, H. Hamelers, C. Buisman, Effect of the type of ion exchange membrane on performance, ion transport, and pH in biocatalyzed electrolysis of wastewater,Water Sci. Technol. 57 (2008) 1757–1762.A. Karnik, "Performance of TCP congestion control with rate feedback:TCP/ABR and rate adaptive TCP/IP," M. Eng. thesis, Indian Institute ofScience, Bangalore, India, Jan. 1999.

[9] F. Harnisch, U. Schro ¨ der, F. Scholz,"The suitability of monopolar and bipolar ion exchange membranes as separators for biological fuel cells,"*Environ. Sci. Technol.*,Vol.42,pp.1740–1746, 2008.

[10] J.R. Kim, S. Cheng, S.E. Oh, B.E. Logan,"Power generation using different cation, anion, and ultrafiltration membranes in microbial fuel cells, "*Environ. Sci. Technol.*, Vol.41 ,pp.1004–1009,2007.

[11] K. Rabaey, P. Clauwaert, P. Aelterman, W. Verstraete,"Tubular microbial fuel cells for efficient electricity generation,"*Environ. Sci. Technol.* ,Vol.39,pp.8077–8082,2005.

[12] D. Pant, G. Van Bogaert, M. De Smet, L. Diels, K. Vanbroekhoven, Use of novel permeable membrane and air cathodes in acetate microbial fuel cells, Electrochim. Acta 55 (2010) 7710–7716.

[13] I. Ieropoulos, J. Greenman, C. Melhuish, Improved energy output levels from small-scale Microbial Fuel Cells, Bioelectrochemistry 78 (2009) 44–50.

[14] Roller S. D., H. P. Bennetto, G. M. Delaney, J. R. Mason, S. L. Stirling and C. F.Thurston,"Electron Transfer Coupling in Microbial Fuel Cells : 1. Comparison of Redox Mediator Reduction Rates and Respiratory Rates of Bacteria,"*J. Chem. Technol. Biotechnol.*, Vol. 34, Issue 1, pp.3-12,1984.

[15] Bennetto, H. P., Stirling, J. L., Tanaka, K. and Vega C. A., Anodic Reaction in Microbial Fuel Cells, *Biotechnology and Bioengineering*, Vol. 25, pp.559-568,1983.

[16] A. Arico, V. Baglio, A. Di Blasi, V. Antonucci, L. Cirillo, A. Ghielmi, V. Arcella, Proton exchange membranes based on theshort-side-chain perfluorinatedionomer for high temperature direct methanol fuel cells, Desalination 199 (2006) 271–273.

[17] Daniel, D.K., B. Das Mankidy, K. Ambarish and R. Manogari, 2009. Construction and operation of a microbial fuel cell for electricity generation from wastewater. *International Journal of Hydrogen Energy*, 34(17): 7555-7560.

[18] D.R. Bond and D.R. Lovley, *Appl. Environmental Microbiology*, 2003, 69, pp. 1548–1555.

[19] T. Catal, K. Li, H. Bermek and H. Liu, *Journal of Power Sources*, Vol.175, pp.196-200,2008.

[20] B. E. Logan, *Microbial fuel cell*, John Wiley & Sons, 2008.

[21] K. Rabaey, W. Ossieur, M. Verhaege and W. Verstraete, Wat., *Sci. Tech*.,Vol.52, pp. 59-66, 2005.

[22] (2015)Bangladesh Power Development Board Website, [Online] Available At:http://www.bpdb.gov.bd/bpdb/index.php?option=com_content&view=article&id=150&Itemid=16.

[23] Michael Alexander Calder, "Modelling of a Microbial Fuel Cell," M. Eng. thesis, Norwegian University of Science & Technology, Trondheim, Norway, August. 2007.

[24] (2015) Fuel cell store website, [online], Available at : http://fuelcellstore.com/fuel-cell-components/membranes/nafion-117

Prospect of Karanja (Pongamia pinnata) Biodiesel as an Alternative Energy Source in Bangladesh

Rumana Subnom[1], Md. Zihadul Alam[*2], Jannatul Fardous Mugdho[3]

[1,2,3]*Department of Mechanical engineering*

Rajshahi University of Engineering & Technology

Rajshahi 6204, Bangladesh

[*2]xihadratul@gmail.com

***Abstract*—Bangladesh is an agriculture based country, where any edible and non-edible seeds can be grown. As a result biodiesel can be an effective solution to the increasing price and shortage of petroleum fuels. Every year Bangladesh imports about 5.5 million tons of different types of oil. Due to which Bangladesh has to pay a huge currency every year. Karanja, a sustainable source of biodiesel, can be cultivated for the socio-economic developments of the country. Karanja petrodiesel up to 20% blend with diesel fuel does not require any engine modification and sometimes even gives better performance than pure diesel fuel. It is found that, with the utilization of unused lands about 0.52 million tons of biodiesel can be produced annually. Moreover, the use of biodiesel can reduce CO_2, CO, HC, NO_x and SO_x emissions compared to pure diesel.**

***Keywords*— Biodiesel; Petroleum fuel; Karanja; sustainable source; Bangladesh**

I. INTRODUCTION

Emissions due to fossil fuel ignition leads to different destructive effects including sea level rise, climate change, loss of biodiversity, receding of glaciers, greenhouse gas (GHG) emissions etc. The energy crisis due to increasing urbanization and motorization leads to price hike in petroleum based fuels and consequently it is affecting the global economy. So an alternative, sustainable, renewable, cost-effective and less emission producing source of energy is desirable. Among all other energy sources biodiesel is found as the most environment friendly for their excellent combustion properties [1].

Biodiesel is mono-alkyl esters extracted from vegetable oils or animal fats which is produced by transesterification method. Using this method high viscosity and low volatility of vegetable oils are removed. Nowadays, developed countries all over the world are being interested in biodiesel utilization. In Malaysia, palm is being considered as the raw material for biodiesel production. Following a report of 2007, European countries are consuming 350 million gallons and USA is consuming 50 million gallons biodiesel annually. France is using 50% of bio-diesel mixing with diesel fuel. In Zimbabwe, Jatropha is being cultivated for biodiesel production. In Nicaragua, 1000 ha land has been used to plant one million *Jatropha curcas*. In Nepal, 40,000 *Jatropha curcas* has been planted in 22.5 ha area. In Bangladesh, biodiesel can be easily produced as the sources of vegetable oil such as Soyabean, Neem, Coconut, Sunflower, Mustard, Jatropha, Cotton seed etc. can be easily grown. By using these oils for the production of biodiesel, the shortage of conventional fuels can be reduced considerably [2].

Among the sources of vegetable oils (both edible and non-edible) Jatropha, Karanja and Putranjiva have found as the most economical for their little domestic practices. Karanja oil is obtained from seeds of *Pongamia pinnata* which belongs to the family Leguminaceae or papilionaceae. Karanja biodiesel reduces the emissions of carbon monoxide (CO), hydrocarbons (HC), sulphur dioxide (SO_2) and NO_x after combustion. B20 (blend of 20% Karanja biodiesel and 80% diesel) have shown maximum efficiency at all compression ratios and properties are almost same as diesel fuel [3]. In this paper, the prospect of Karanja biodiesel as an alternative fuel in Bangladesh has been discussed. At present, some initial projects on biodiesel production are going on but commercial production should be started as early as possible to meet the energy scarcity and economic development.

II. KARANJA: AS AN ALTERNATIVE FUEL

A. *Alternative Fuel for Kerosene*

In 2014, Bangladesh has imported about 5.5 million tons of different petroleum products. Among them, about 1.3 million tons were crude oil, 2.9 million tons were diesel, 0.33 million tons were jet fuel and 0.9 million tons were petrol and octane. Moreover, the total consumption of kerosene was 290 million liters as shown in figure 1 [4]. In Bangladesh, only 49% of the total population can access to electricity and few has services of LPG gas for domestic works.

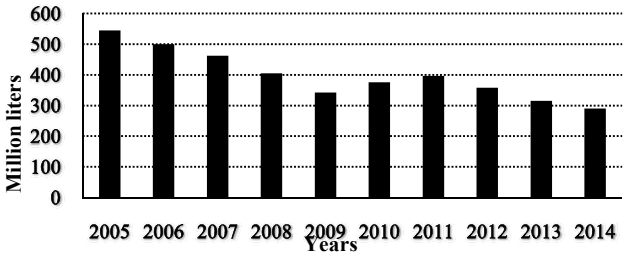

Fig. 1 Kerosene consumption pattern in Bangladesh [4].

Therefore, huge population of rural areas use kerosene lamp and hurricane for cooking and lighting purposes. As the reserve in the country is very limited, huge amount of liquid fuel is imported every year. Bangladesh Petroleum Corporation (BPC) pays about USD 134.53 per barrel for importing kerosene and jet fuel. The crude Karanja oil shows promising effect in the traditional cooking stoves although the method is not commercially well known. Therefore, Karanja oil can be an suitable alternative for kerosene [5].

B. As Alternative Fuel for Diesel Engine

The seeds of Karanja contains approximately 30-40% oil which can be easily converted to biodiesel or fatty acid methyl esters (FAME) by transesterification process with methanol in the presence of KOH. The important properties of FAME for Karanja are: flash point (135 to 150°C), cloud point (8.3°C), pour point (2.1°C), saponification number (196.7), iodine value (80.9), cetane number (55.84), viscosity (3.8 to 4.8 mm^2/s at 40°C), which indicates that it can be used in diesel engine up to 20% blend without considerable engine modification [6]. This source of diesel is getting more attention as a renewable, eco-friendly, biodegradable and non-toxic fuel. Moreover, biodiesel can be an alternative for reducing the greenhouse gas (GHG) emissions and shows no sulfur emission. It was reported that, at full load condition 80% CO emission was decreased by using pure Karanja oil in diesel engine at the place of diesel fuel [7].

III. Numerous Applications of Karanja

Almost all the parts of *Pongamia pinnata* such as leaf, root, flower, seed, and other parts have been utilized as a source of traditional medicines, animal fodder, fish poison, timber and bio-fuel etc.

A. Medicinal Values of Karanja

Almost all parts of Karanja are used as medicine traditionally. Juice of Karanja root mixed with lime water and coconut oil is very effectual for gonorrhea treatment. It is also good in various skin diseases and for cleaning gums, ulcers, and teeth. Its leaves play a powerful role for the treatment of diarrhea, gonorrhea, dyspepsia, leprosy, flatulence, cold, cough etc. Stem bark shows antipyretic and CNS sedative actions. Fruits are effective for leprosy, tract, piles, tumors, ulcers and abdominal decease etc. Flowers are useful to reduce dipsia in diabetes. Seeds are helpful for the treatment of keloid tumors, chronic fevers, anemia, hypertension, hemorrhoid, pectoral diseases, inflammations, whooping cough etc. [8].

B. *Uses of Karanja Plant*

Karanja tree can be used as animal fodder, fish poison, timber, green manure and fuel [8]. Moreover, soils fertility can be increased by addition of Karanja leaves and the seed cake. *Pongamia* species work as atmospheric nitrogen fixer. For the widespread set-up of lateral roots of Karanja, it works to control erosion of soil. For windbreak of tea plantation *Pongamia pinnata* is also grown in Sri Lanka. [9]. It is also planted as a shade or ornamental tree for avenue plantings along roadsides and canal banks [8].

C. Uses of Karanja Oil

Karanja oil is an enormous source of biodiesel. It can be used as cooking fuel and for lightening lamps. It can also be used as pesticides, lubricant, water paint binder and in tanning and soap making industries [9]. Karanja Oil is also useful in liver pain, piles, chronic fever, leprosy, ulcers and so on [8].

D. Uses of By-products

The de oiled cake consists of furan derivatives, flavonoids and uranoflavonoids and is used in skin diseases. The cake can also be used as bio pesticide, fertilizer, and for organic farming. Seed shells are considered as combustibles. Additionally, the de oiled cake has pesticidal value, particularly against nematodes [10].

IV. Requirement of Alternative Fuel

Kerosene and diesel has huge applications for domestic purposes and automobile vehicles. Karanja oil, an alternative source of conventional fuels, can be consumed for low cost of production and nonfood use.

A. High Depletion Rate of Principal Resources

Coal, crude oil, petroleum and natural gas all are fossil fuels and none of them are renewable. Their depletion rates have been analyzed and result showed that by the year 2042, coal will be the only remaining fossil fuel [11]. Several other studies also predicted that the reserves of crude oil will come to an end between 2050 and 2075 which does match with the recent statistical review of world energy of BP [12, 13]. In south Asia, 90 percent of the total energy demand is fulfilled by fossil fuel and about one-third of it is petroleum [14]. According to the World Bank in 2011, the consumption rate of fossil fuel was about 71.53 percent of the total energy in Bangladesh [15]. To meet the consumption rate, the south Asian countries import more than 70 percent of the demanded oil which is estimated to be doubled by 2020 [14]. The Financial Express recently revealed with the information that Bangladesh is to import 1.3 million tones crude petroleum oil from Saudi Arabia and UAE in this year and it would cost approximately 1.129 million USD [16].

B. Emission Problems

In several researches, it has been found that Karanja biodiesel blend with diesel fuel can reduce exhaust gas emission compared to diesel fuel considering different conditions. Among all other emissions NO_x, CO and smoke emissions for pure diesel fuel and Karanja biodiesel have been discussed.

TABLE I. COMPARISON BETWEEN EMISSION CHRACTERISTICS OF DIESEL FUEL AND KARANJA BIODIESEL

Engine category	Testing condition	Fuels used	NO_x emissions	HC emissions	Smoke emissions	References
Kirloskar single cylinder, 4-stroke (Model-DAF 8)	80% load	Diesel	About 1550 ppm	-	4% opacity	[17]
		B20KOME (Karanja Oil Methyl Ester)	About 990 ppm	-	About 1.5% opacity	
Kirloskar single cylinder, 4-stroke (Model-AV1)	80% load	D100	972 ppm	42.3 ppm	55 HSU of opacity	[18]
		KB50 (Karanja Biodiesel)	952 ppm	54 ppm	71 HSU of opacity	
Kirloskar single cylinder, 4-stroke (Model-TV1)	Full load	Diesel	About 240 ppm	About 38 ppm	About 32% HSU of opacity	[19]
		KME (Karanja Methyl Ester)	About 150 ppm	About 22 ppm	About 19% HSU of opacity	
Kirloskar single cylinder, four stroke diesel engine (model-ALV)	100% load and 200 bar of injection pressure	Diesel	About 1350 ppm	About 70 ppm	-	[20]
		B20	About 850 ppm	About 62 ppm	-	
Single cylinder, 4-stroke, water-cooled & compression ratio 17.5:1 diesel engine	Constant speed of 1500 rpm & at different load conditions	Diesel	48% lower compared to diesel fuel emission	50% lower compared to diesel fuel emission	20% lower compared to diesel fuel emission	[21]
		Karanja biodiesel				
Single cylinder, water-cooled & compression ratio 17.5 diesel engine	1500 rpm of engine speed and about 4.8 kg load	Diesel	About 1010 ppm	About 60 ppm	-	[22]
		B20	About 1100 ppm	About 48 ppm	-	
Kirloskar single cylinder, 4-stroke, water cooled diesel engine (model-AVL)	At 2.5 kW of brake power	Diesel	About 125 ppm	About 235 ppm	About 250 Hu	[23]
		100% Karanja biodiesel	About 77 ppm	About 170 ppm	About 180 Hu	

V. PRESENT AND FUTURE CONDITION OF BIODIESEL PRODUCTION IN BANGLADESH

The reserve of non-renewable fossil fuels will deplete in next 150 years according to present consumption rate. However, 95% of this demand can be fulfilled by biodiesel. Being a densely populated country Bangladesh cannot consume edible oil seeds for biodiesel production. At this condition, biodiesel obtained from non-edible seeds is the only reliable field [24]. Although the future is promising, biodiesel and bioethanol production are still in their initial stage in Bangladesh [25].

During 2009, a project had been run by plant Biotechnology Division under Bangladesh Atomic Energy Commission for cultivating Jatropha and cassava but due to the lack of policy and insufficient fund it did not progress [25]. Due to the scarcity of cultivable lands, Bangladesh can use about 47750 km rail and road side areas for the cultivation of non-edible seeds. The possible places for non-edible seeds plantation in Bangladesh are shown in table II. The country can save about $6 billion per year by reducing dependency on importing crude oil. From an estimation, it is found that about 2387,500 ton non-edible seeds can be produced each year which can supply 1322,235 ton oil leading to 1001,881 ton biodiesel. It was also found that including cultivation, the cost of biodiesel will not exceed 120tk/liter [24].

At present for the production of biodiesel there is no project running in Bangladesh. But in near future biofuel is going to be a prominent sector. As stated by Energy-Bangla, Japanese company Honda Denki Co. Ltd has shown interest for investing up to 1 billion USD in Bangladesh for biofuel, green power and sugar sector.

TABLE II. POSSIBLE PLACES FOR NON-EDIBLE OIL SEEDS CULTIVATION IN BANGLADESH [24].

Total road line	= 21040 Km
Total rail line	= 2835 Km
Total amount of road side	= 42080000 m
Total amount of rail line side	= 5670000 m
Distance between two trees	= 2 m
Types of seeds	= 10
Total number of each kind of seeds planted both sides of road and rail line	= 2387,500

In the vulnerability list of global climate change, Bangladesh has placed 1st for meeting the huge demands of

energy using conventional fuel which indicates we should step towards eco-friendly biodiesel. Moreover, Biofuel has the ability to decrease the greenhouse compared to petroleum alternatives [26]. With the cooperation of scientific researchers, institutes, advanced technologies, enterprises and improvement of relevant laws and regulations it would be possible to produce biodiesel in near future. For the social and economic developments and to meet the energy scarcity Bangladesh should set up small and medium sized biofuel industry. Major obstacles such as low oil yield non-edible plant, lack of biofuel production policy, enzymatic and chemical breakdown are needed to overcome. Both government and non-government organizations should also collect huge fund for researching on renewable energy from international bodies [25].

VI. Concluding Remarks from the Overview

Bangladesh is a developing country with increasing population. The main problems of the country are power crisis and high cost of fossil fuels which are rapidly increasing. Moreover, Bangladesh is fully depended on petroleum fuels which will deplete in a few decades. To meet the huge gap between demand and insufficient supply, the government of Bangladesh imports about 916,000 tons of diesel and furnace oil every year [24]. Among all other oil bearing seeds Bangladesh should start producing Karanja as it can be easily grown in any type of soil and climate. Besides the cultivation of Karanja does not require additional lands and reduces the emissions of harmful gases. Proper investments for biodiesel industries and plantation of Karanja in the available wastelands are desired. Although further investigations are imperative for the availability of biodiesel at low cost. So it can be concluded that for safe, renewable and environment friendly source of energy Karanja biodiesel can be a viable alternative fuel for diesel engine. To reduce the environmental degradation and huge dependence on petroleum fuels Bangladesh should start cultivating Karanja and other non-edible oil plants commercially.

References

[1] Poonam Singh Nigam, A.S., *Production of liquid biofuels from renewable resources.* Progress in Energy and Combustion Science, 2011. **37**: p. 52-68.

[2] Md. Abdul Wakil, Z.U.A., Md. Hasibur Rahman, Md. Arifuzzaman, *STUDY ON FUEL PROPERTIES OF VARIOUS VEGETABLE OIL AVAILABLE IN BANGLADESH AND BIODIESEL PRODUCTION.* International Journal of Mechanical Engineering, 2012. **2**(5): p. 10-17.

[3] Raghavendra Prasada S.A, K.V.S., *Pongamia Pinnata (karanja) Biodiesel as an Alternative fuel for Diesel Engine: A Review.* Advanced Engineering and Applied Sciences: An International Journal, 2014. **4**(4): p. 52-61.

[4] *Bangladesh Petroleum Corporation (BPC)*. 2015; Available from: http://www.bpc.gov.bd/contactus.php?id=46.

[5] P. K. Halder, N.P., and M. R. A. Beg, *Prospect of Pongamia pinnata (Karanja) in Bangladesh: A Sustainable Source of Liquid Fuel.* Journal of Renewable Energy, Hindawi Publishing Corporation, 2014: p. 1-12.

[6] Paul T. Scott, L.P., Ning Chen, Johanna S. Hadler, Michael A. Djordjevic, Peter M. Gresshoff, *Pongamia pinnata: An Untapped Resource for the Biofuels Industry of the Future.* Bioenerg. Res., 2008. **1**: p. 2-11.

[7] Baste S.V., B.A.V.a.C.S.B., *Emission Characteristics of Pongamia Pinnata (Karanja) Biodiesel and Its Blending up to 100% in a C.I. Engine.* Research Journal of Agriculture and Forestry Sciences, 2013. **1**(7): p. 1-5.

[8] Savita Sangwan, D.V.R.a.R.A.S., *A Review on Pongamia Pinnata (L.) Pierre: A Great Versatile Leguminous Plant.* Nature and Science, 2010. **8**(11): p. 130-139.

[9] Gaurav Dwivedi, S.J., Mahendra Pal Sharma *Pongamia as a Source of Biodiesel in India.* Smart Grid and Renewable Energy, 2011. **2**: p. 184-189.

[10] Bobade S.N. , K.V.B., *Detail study on the Properties of Pongamia Pinnata (Karanja) for the Production of Biofuel.* Research Journal of Chemical Sciences, 2012. **2**(7): p. 16-20.

[11] Shahriar Shafiee, E.T., *When will fossil fuel reserves be diminished?* Energy Policy, 2009. **37**(1): p. 181-189.

[12] *World Fossil Fuel Reserves and Projected Depletion*. 2002: The Colorado River Commission of Nevada: p.1-3. Available from: http://crc.nv.gov/docs/world%20fossil%20reserves.pdf

[13] *BP: World Reserves of Fossil Fuels*. 2015; Available from: http://knoema.com/smsfgud/bp-world-reserves-of-fossil-fuels.

[14] K.V.Raju, *Biofuels in South Asia: An Overview.* Asian Biotechnology and Development Review, 2006. **8**(2): p. 1-9.

[15] *Fossil fuel energy consumption (% of total) in Bangladesh*. Available from: http://www.tradingeconomics.com/bangladesh/fossil-fuel-energy-consumption-percent-of-total-wb-data.html.

[16] *BD to import 1.3m tonnes of crude oil from Saudi, UAE*. 2015; Available from: http://www.thefinancialexpress-bd.com/2015/02/12/80799.

[17] B. Baiju, M.K.N., L.M. Das, *A comparative evaluation of compression ignition engine characteristics using methyl and ethyl esters of Karanja oil.* Renewable Energy, 2009. **34**: p. 1616-1621.

[18] Singh, Y., Singla, A., *Comparative analysis of jatropha and karanja-based biodiesel properties, performance and exhaust emission characteristics in an unmodified diesel engine.* Pollution, 2015. **1**(1): p. 23-30.

[19] S. Jindal, B.P.N., Narendra S. Rathore, *Comparative Evaluation of Combustion, Performance, and Emissions of Jatropha Methyl Ester and Karanj Methyl Ester in a Direct Injection Diesel Engine.* Energy Fuels, 2010. **24**: p. 1565–1572.

[20] Nagarhalli M. V., N.V.M., Mohite K.C., *EMISSION AND PERFORMANCE CHARACTERISTICS OF KARANJA BIODIESEL AND ITS BLENDS IN A C.I. ENGINE AND IT'S ECONOMICS.* ARPN Journal of Engineering and Applied Sciences, 2010. **5**(2): p. 52-56.

[21] A.M. Ashraful, H.H.M., M.A. Kalam, I.M. Rizwanul Fattah, S. Imtenan, S.A. Shahir, H.M. Mobarak, *Production and comparison of fuel properties, engine performance, and emission characteristics of biodiesel from various non-edible vegetable oils: A review.* Energy Conversion and Management, 2014. **80**: p. 202-228.

[22] P. L. Naik, D.C.K., *Performance Analysis of CI Engine using Pongamia Pinnata (Karanja) Biodiesel as an Alternative Fuel.* International Journal of Science and Research, 2013. **2**(8): p. 445-450.

[23] Yashvir Singh, A.S., Nitin Lohani, *Production Of Biodiesel From Oils Of Jatropha, Karanja And Performance Analysis On CI Engine.* INTERNATIONAL JOURNAL OF INNOVATIVE RESEARCH & DEVELOPMENT, 2013. **2**(3): p. 286-294.

[24] Kaniz Ferdous, M.R.U., Rehnuma Islam, Maksudur R. Khan, M. A. Islam, *Potentiality of Biodiesel Production From Non-Edible Oil: Bangladesh Perspective.* Journal of Chemical Engineering, IEB, 2012. **27**(2): p. 1-5.

[25] Alam, M.A., *Alternative Energy Source. Exploring environment friendly biofuel option.*http://archive.thedailystar.net/newDesign/news-details.php?nid=268377; 2013.

[26] I. B. Muhit, D. Baidya, Nurangir Nahid, Prospect of Algal Biodiesel Production in Bangladesh: Overview from Developed Countries. *IOSR Journal of Mechanical and Civil Engineering (IOSR-JMCE),* 2014. 11(1): p. 49-54.

Comparative Analysis of Carrier Schemes for PWM in Multilevel PUC Inverter for PV Applications

Mohd Tariq[1], Mohammad Tauquir Iqbal[2], Atif Iqbal[3],
Mohammad Meraj[4], Muhammad M. Roomi[5], Md Shafquat Ullah Khan[6]
[1, 5, 6] School of Electrical and Electronic Engineering, Nanyang Technological University, Singapore, 639798
[2]Damodar Valley Corporation, Kolkata, India, 700052
[3, 4,] Department of Electrical Engineering, Qatar University, Doha, Qatar, 2713
[1, 2] Formerly at, Department of Electrical Engineering, Indian Institute of Technology, Kharagpur, India, 721302
mohd0017@e.ntu.edu.sg,tauquir.iqbal@gmail.com, atif.iqbal@qu.edu.qa,

***Abstract*— This paper presents an evaluation of two modulation methods for the seven-level packed U cell (PUC) inverter for photovoltaic applications. The PUC is a multilevel inverter which has less number of switching devices than the conventional multilevel inverters. The PUC inverter is in modular configuration consisting of one U-cell and four additional power switches, one dc link and an auxiliary capacitor. A U cell is called an arrangement of two power switches and one flying or clamping capacitor. In this paper, the level-shifted (LS-PWM) and phase-shifted PWM (PS-PWM) for triangular carrier are presented and compared. Harmonic analysis for both the cases has been performed and phase–shifted triangular carrier has been found to have the minimum harmonics. The difference in harmonics of the two modulation methods for the triangular carrier is confirmed by the theoretical approach and verified by simulation in MATLAB® Simulink environment, and simulation results are presented and discussed in the paper.**

Keywords*— *Packed U cell (PUC), Photo Voltaic, Level Sifted, Phase Shifted, Triangular.

I. INTRODUCTION

Recently, renewable sources of energy such as solar, geothermal and wind have gained popularity due to increase in pollution level and depletion of conventional energy sources like coal etc. [1]. To meet the environmental challenges and depletion of fossil fuels, Photovoltaic (PV) presents a highly attractive energy source during the last two decades. The widespread use of single-phase grid-connected photovoltaic (PV) systems for low power level, installed near customers can be noticed in many countries [2]. Present research is focused mainly in the three areas: 1) decreasing the installation cost (by increasing production and installations); 2) increasing the system efficiency (by reducing THD and voltage ripple of the capacitors); 3) increasing the reliability.

The investigated topology in this paper is able to meet the above requirements of increasing the system efficiency and reliability. With respect to power quality, a sinusoidal current as the output of the grid-connected PV system is required. Unfortunately, harmonics are present in the output current because of the use of power semiconductor devices and the variable power flow of the PV panels [3-6]. The IEEE standard 519-1992 "Recommended Practices and Requirements for Harmonic Control in Electrical Power Systems" sets limits of harmonic voltage and current at the point of common coupling (PCC). This standard establishes limits equal to 5% for the current and voltage THD factors, that the producer should deliver to the customer [7]. Multilevel inverters (MLI) have many advantages with respect to the traditional two-level configuration such as low switching loss, low THDs, is fault tolerant, and overall better power quality [8]. But main disadvantages of MLI are increased components count thus increasing the cost and decreasing the reliability, beside requirement of more number of DC sources. Packed U Cell (PUC) multilevel inverter topology is introduced in [9] working with only one DC source and having high power quality using a small number of passive and active components. Other needed DC sources are supplied by capacitors that acts as auxiliary DC source. PUC inverter is suggested for PV application in [10] as it offers high efficiency.

There are two modulation methods in the multicarrier PWM schemes; level shifted PWM (LS-PWM) [11] and phase shifted PWM (PS-PWM) [12]. Combination of the level-shifted PWM (LS-PWM) and the phase-shifted PWM (PS-PWM) is reported in [13]. It is called "level- and phase-shifted PWM (LPS-PWM)." The LPS-PWM realizes low voltage ripple on the capacitors. In this paper a comparison between level shifted and phase shifted PWM methods for triangular carrier is done using MATLAB® Simulink environment. In previous research, the PUC invention [9], novel control technique[14-17] and analysis [9],[17] are presented. Evaluation of Level- and Phase-Shifted PWM for Multilevel PUC Inverter is not reported in the

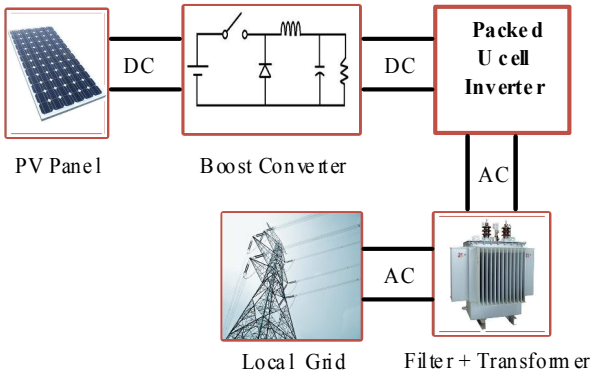

Figure 1 Block diagram of the single-phase grid-connected PV systems.

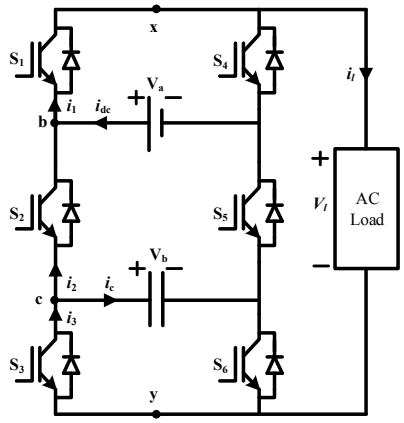

Figure 2. Packed U-cell topology.

literature and hence presented in this paper. The comparative evaluation of level and phase shift based PWM carrier generation will help in better understanding of the subject eventually helping its implementation in the real world. The block diagram of the single-phase grid-connected photovoltaic (PV) systems is shown in figure 1, which consists of: 1) a boost converter stage to perform maximum power point tracking (MPPT) [18]; 2) single phase multilevel packed U cell inverter; 3) an inductive filter and a step-up transformer for interfacing with the local grid..

The paper is organized as follows: operation of the PUC inverter is explained in section 2. Theoretical analysis of triangular carrier based PWM is presented in sections 3. Simulation results are presented and discussed in section 4 and the conclusions in section 5.

II. OPERATION OF PUC INVERTER

A seven level single-phase voltage source inverter with packed U-cell topology is shown in figure 2. This is called Packed U-cell because each unit of the inverter is of U shape. Depending upon the number of capacitors in the investigated topology different level of voltages can be achieved. In the investigated topology two capacitors have been used to obtain seven levels (V_{dc}, $2V_{dc}/3$, $V_{dc}/3$, 0, $-V_{dc}/3$, $-2V_{dc}/3$, $-V_{dc}$). The Voltage across second capacitor (C_2) i.e. V_b must be maintained at one-third of the voltage of the first capacitor (C_1) i.e. V_a. The relation between number of voltages level achieved and number of capacitors used can be represented by equation (1).

$$N_v = 2^{Nc+2} - 1 \tag{1}$$

Where: N_v is number of voltage levels and N_c is number of capacitors used.

In the investigated topology, the number of power switching devices and the number of capacitor/neutral voltage clamping devices are reduced when compared with the existing Neutral Point Clamped (NPC), Flying capacitor (FLC) and Cascaded H-bridge (CHB) multilevel inverter solutions. The numbers of devices for different types of inverters are shown in Table 1. Six

$$N_p = 2^{Ns} \tag{2}$$

Table 1: 7 – Level single phase inverter

Components	NPC	FLC	CHB	PUC
Power Switches (IGBTs)	12	12	12	6
Capacitors	6	21	3	2
Clamping Diodes	12	0	0	0

IGBTs have been used in the investigated topology for achieving 7 levels. These 6 IGBTs are subdivided into two legs, hence only three switches form one leg. Number of possible states can be given by equation (2). N_p is number of possible states and N_s is number of switches in one leg in equation 2.

In the investigated topology 8 states are possible in which two states are redundant when all the switches are ON or OFF. The redundant states represent Zero voltage. Table 2 shows switching combination for one leg for the investigated topology. The switches in other leg are complimentary.

The switching function of the PUC inverter can be defined by equation (3) and the inverter output voltage can be defined by equation (4). The points x, b, c and y are shown in figure 2.

$$S_j = \begin{cases} 0 & \text{if } S_j \text{ is Off} \\ 1 & \text{if } S_j \text{ is On} \end{cases} \qquad j = 1, 2, 3 \tag{3}$$

$$V_{xy} = V_{xb} + V_{bc} + V_{cy} \tag{4}$$

Based on the switching function shown in table 2, each voltage can be represented as given in equation (5) to equation (8).

$$V_{xb} = V_1 (S_1 - 1) \tag{5}$$

$$V_{bc} = (V_1 - V_2)(1 - S_2) \tag{6}$$

$$V_{cy} = V_2 (1 - S_3) \tag{7}$$

$$V_{xy} = V_1 (S_1 - S_2) + V_2 (S_2 - S_3) \tag{8}$$

III. TRIANGULAR CARRIER LEVEL SHIFTED AND PHASE SHIFTED PWM ANALYSIS

The phase voltage of a two level inverter with natural sampled PWM and triangular carrier can be described by

Table 2 Switching Combination for one leg

State	Voltage	S_1	S_2	S_3
0	Va	1	0	0
1	Va- Vb	1	0	1
2	Vb	1	1	0
3	0	1	1	1
3’	0	0	0	0
4	-Va	0	1	1
5	Vb - Va	0	1	0
6	-Vb	0	0	1

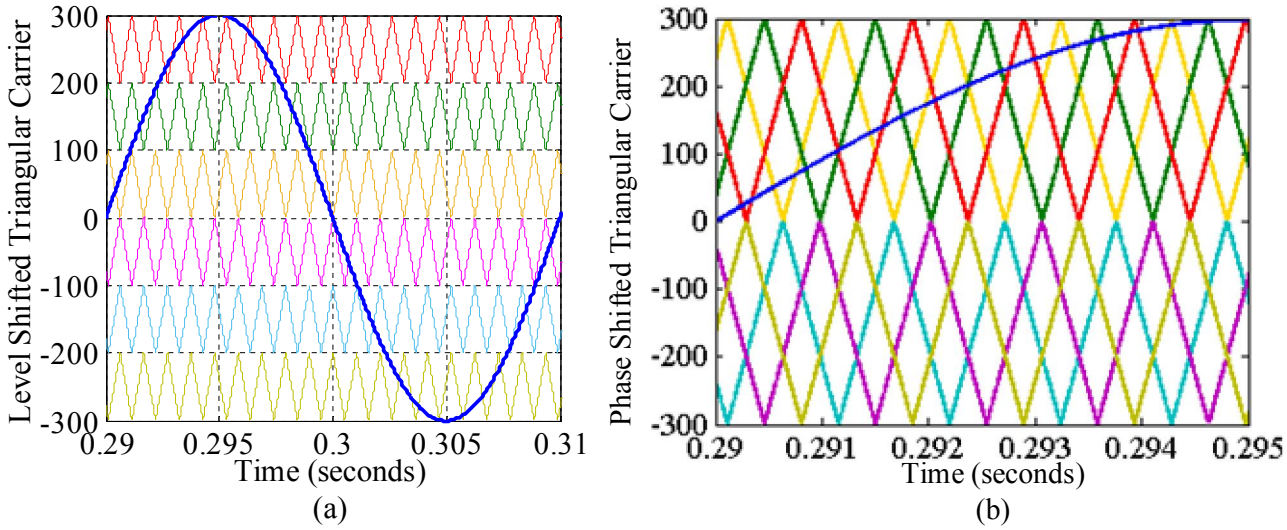

Figure 3. (a) Level Shifted Triangular Carrier. (b) Phase Shifted Triangular Carrier.

equation (9). Equation (9) is derived in [19] using the expression given in the works of Black in [20].

In [19], explanation of three terms in equation (9) has been explained as: a) Term 1 gives the amplitude of the fundamental and it is directly proportional to the modulation index; b) Term 2 gives the amplitudes of the harmonics at the carrier frequency and multiples of the carrier frequency and it is due to the presence of the sin [mt/2]; c) Term 3 gives the amplitudes of the harmonics in the sidebands around each multiple of the carrier frequency. Figure 3 (a) and figure 3 (b) shows level shifted and phase shifted triangular carrier and sinusoidal reference signal for generation of PWM signals for IGBT switches of inverter.

$$F(t)=\frac{MV}{2}\cos(\omega_F t)+\frac{2V}{\pi}\sum_{m=1}^{\infty}J_o\left(mM\frac{\pi}{2}\right)\sin\left(m\frac{\pi}{2}\right)$$
$$.\cos(m\omega_c t)+\frac{2V}{\pi}\sum_{m=1}^{\infty}\sum_{n=\pm1}^{\pm\infty}\frac{J_n\left(mM\frac{\pi}{2}\right)}{m} \quad (9)$$
$$.\sin\left((m+n)\frac{\pi}{2}\right)\cos(m\omega_c+n\omega_F t)$$

modulation index. Whereas the second and third term shows that all harmonics of the carrier frequency is existing in the phase voltage. In equation (9);

ω_F = frequency of the fundamental (reference)

ω_c, = frequency of the carrier signal (rad/s),

M = modulation index, V= value of the dc supply voltage,

J_o, J_n, = Bessel functions of the first kind.

IV. Simulation Results and Discussion

The PUC inverter model is built using MATLAB® Simulink simulation software package to verify the performance of different PWM modulation schemes. PUC inverter connected to PV module is discussed in [10]. In [10], PV supplies the PUC inverter with 48 V and 3.4 A at maximum power point. A DC/DC boost converter is used to extract the PV maximum power and step up its voltage to 150 V. In line to the above, single DC source is selected of 150 V. The second capacitor has the voltage rating of 1/3rd of the DC source. Figure 4 details the control structure for generation of switching signals. One third of the voltage across capacitor 1(dc link capacitor) was compared with the voltage across capacitor 2 (auxiliary capacitor) to generate the error. The generated error was passed through a PI controller to generate reference current. The reference current was again compared with the actual current to generate the reference sinusoidal signal. The generated reference sinusoidal signal was then compared with a triangular carrier signal divided into six zones comprising three positive and three negative zones as shown in figure 3 (a) and 3 (b). The generated reference signal, is compared with different modulation schemes as detailed in figure 3. The Fourier analysis has been done to obtain the total harmonic distortion (THD) of voltage and current for all the cases. The THD for voltage and current has been calculated based on equations (10) and (11) respectively.

Figure 5 (c) shows the capacitor voltages. Seven level output voltage {shown in figure 5 (a)} is obtained using table 2 switching combination. Table 3 outlines the simulation parameter for operating condition of PUC inverter. The value of inductor and resistance at the load is 12mH and 40 ohm respectively. At 0.3 seconds the load was reduced to half and

Table 3. The operating conditions for simulation

Simulation Set up Parameters	Rating
Capacitors	4700 µ F
Load Resistance	40 Ω
Load Inductance	12 mH
Modulating Frequency	1 kHz
Load Change (at time)	0.3 seconds

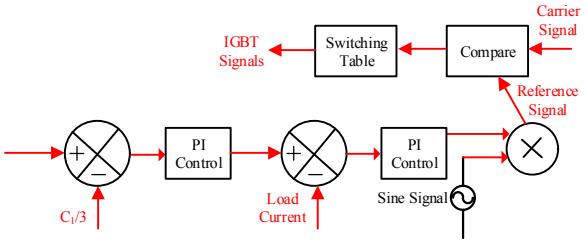

Figure 4 Control structure for generation of switching signals

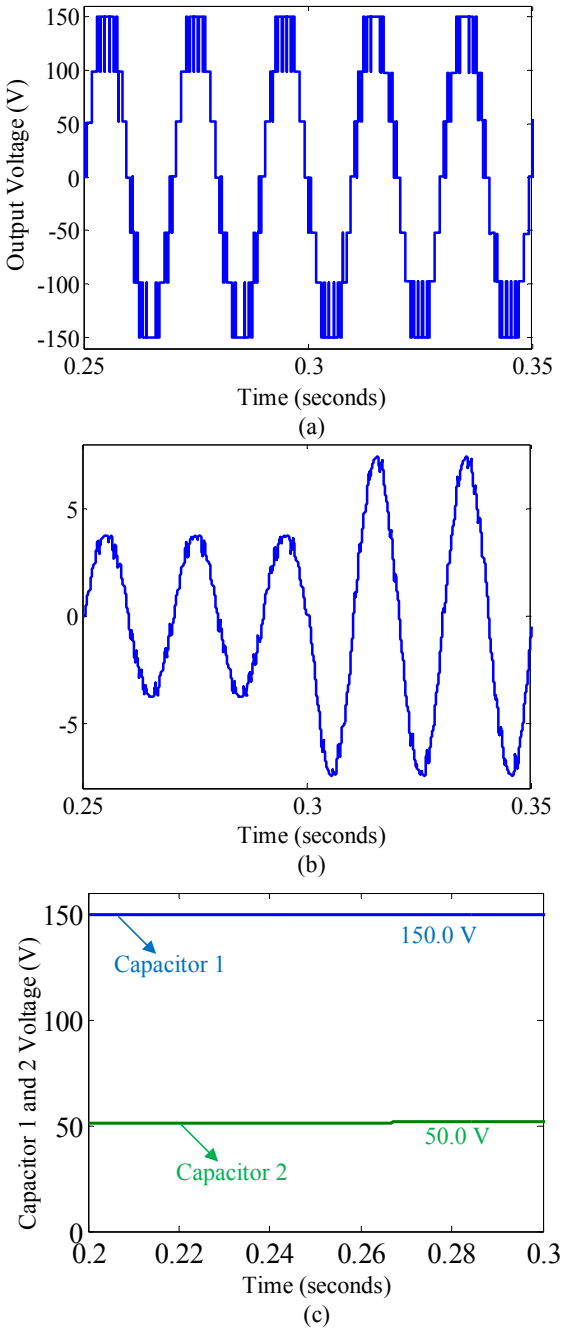

Figure 5. (a) Output Voltage (b) Output Current (c) Capacitor Voltage.

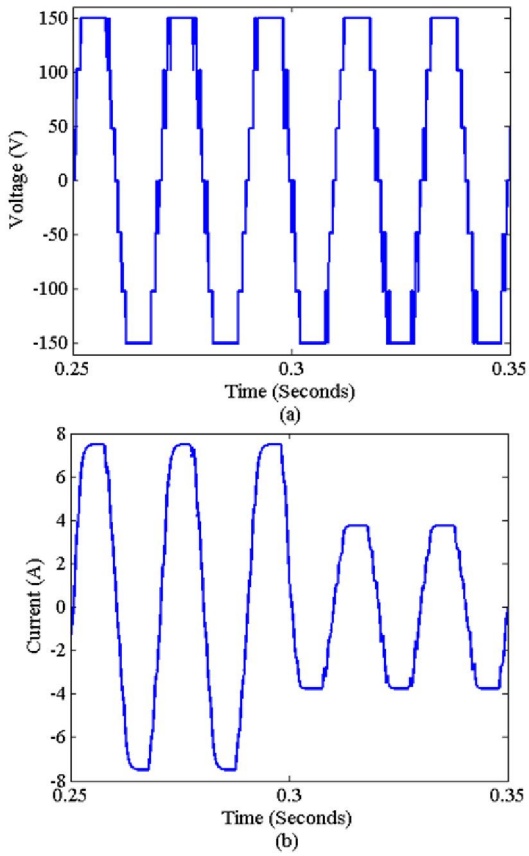

Figure 6. Output (a) Voltage (b) Current, when Load is increased

increased to double in figure 5 (b) and figure 6 (b) respectively, hence the current doubles at 0.3 seconds {as shown in figure 5 (b)} and decreases to half at 0.3 seconds {as shown in figure 6 (b)}. At 0.3 seconds, two 40 ohm resistors were connected in parallel to make 20 ohm effective resistance for decrease in load

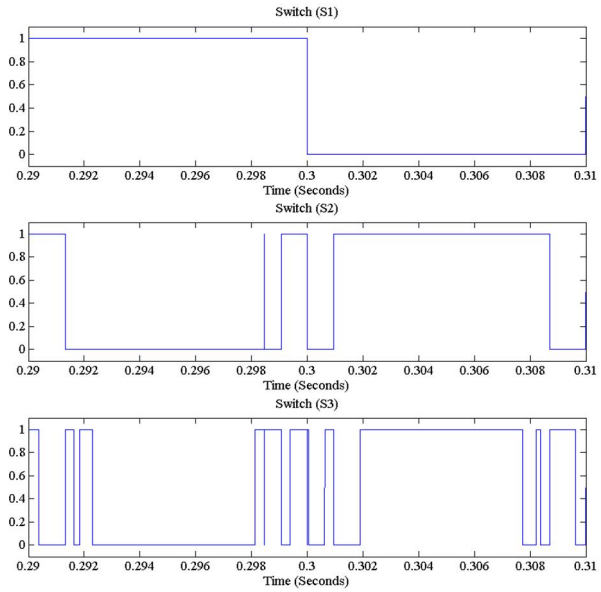

Figure 7 PWM Signal for the three switches of the PUC inverter

and for increase in load two 40 ohm resistors were disconnected from parallel to make 20 ohm effective resistance into 40 ohm resistance. The switching signals generated using control structure shown in figure 4, are shown in figure 7. When triangular level shifted carrier PWM is applied the THD in output voltage is 18.01% The THD in output current {shown in figure 8 (b)} for same PWM scheme is 7.78%. The THD in output voltage {shown in figure 8 (c)} when triangular phase shifted carrier PWM is applied is 17.96%. The THD in output current for same PWM scheme shown in figure 8 (d) is 2.79 %.

$$THD_V = \frac{\sqrt{V_2^2 + V_3^2 + V_4^2 + ...}}{V_1} \quad (10)$$

$$THD_I = \frac{\sqrt{I_2^2 + I_3^2 + I_4^2 + ...}}{I_1} \quad (11)$$

It is observed from figure 8, summarized in table 4 that the THD for phase shift carrier is less in comparison to level shift carrier. Whereas overall, the least THD in current is also observed with triangular phase shifted carrier PWM.

Table 4. FFT results for different modulation schemes

Particulars		THD (in %)
Triangular Carrier		
Level-Shifted	Voltage	18.01
	Current	7.78
Phase-Shifted	Voltage	17.96
	Current	2.79

V. CONCLUSIONS

The paper has presented the comparison of different PWM schemes which can be applied to the PUC inverter. Investigating the suitable modulation schemes is very essential with respect to grid integration, as the power quality is directly dependent on THD. Triangular phase shifted carrier PWM scheme can be applied for integrating the PUC inverter with PV and grid systems. Triangular phase shifted carrier PWM scheme for PUC inverter has been suggested based on observing the THD in current which is just 2.79 %. The THD of voltage in both the cases are almost similar and are 17.96 % and 18. 01 %, with triangular phase shifted carrier PWM showing the minimum value. The whole system i.e. solar panel, boost converter with PUC inverter will be very cost effective, besides having good

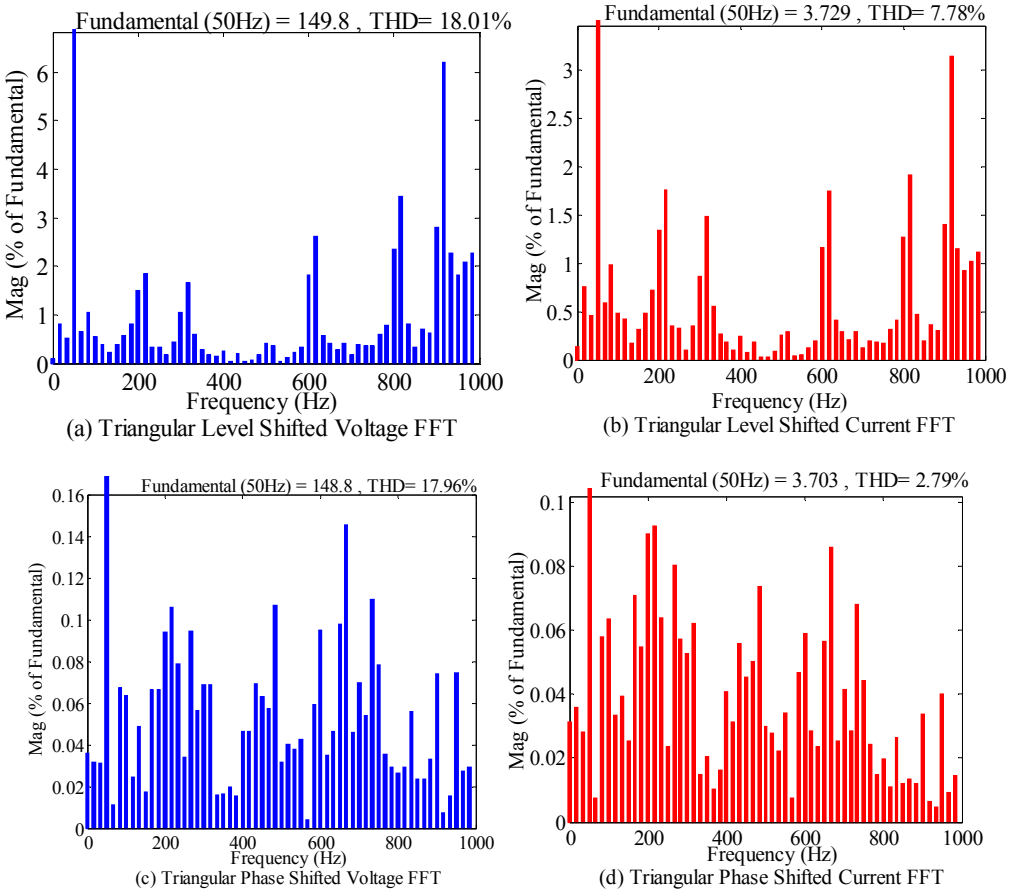

(a) Triangular Level Shifted Voltage FFT
(b) Triangular Level Shifted Current FFT
(c) Triangular Phase Shifted Voltage FFT
(d) Triangular Phase Shifted Current FFT

Figure 8. FFT of Voltage and Current for different PWM schemes. (a) – (d) description given below each figures.

reliability and power quality as it has the minimum number of power electronics devices compared to previously introduced multilevel inverter topologies. With reduced no. of capacitors and power switches seven levels of voltages have been achieved for PUC inverter. The control of PUC inverter was also successfully implemented and shown for load change at 0.3 seconds in figures. The concept was verified by MATLAB® Simulink simulation and results are presented and discussed in the paper.

ACKNOWLEDGEMENTS

This publication was made possible by NPRP-EP grant # X-033-2-007 from the Qatar National Research Fund (a member of Qatar Foundation). The statements made herein are solely the responsibility of the authors.

REFERENCES

[1] M. Tariq, S. Bhardwaj and M. Rashid, "Effective battery charging system by solar energy using C programming and microcontroller", American Journal of Electrical Power and Energy Systems, 2(2), 41-43. 2013.

[2] M. Tariq and K. Shamsi. "Application of RET to Develop educational infrastructure in Uttar Pradesh." International Journal of Recent Trend In engineering, ACEEE (USA) Vol. (4), pp 187-190, 2010.

[3] A. I. Maswood, A. K. Yusop, M. A. Rahman, "A novel suppressed-link rectifier-inverter topology with near unity power factor," IEEE Trans. Power Electronics, vol.17, no.5, pp.692-700, Sep 2002.

[4] M. Aiello, A.Cataliotti, S. Favuzza and G. Graditi, "Theoretical and experimental comparison of total harmonic distortion factors for the evaluation of harmonic and interharmonic pollution of grid-connected photovoltaic systems," in *Power Delivery, IEEE Transactions on* , vol.21, no.3, pp.1390-1397, July 2006.

[5] A. I. Maswood, S. Wei, M. A. Rahman, "A flexible way to generate PWM-SHE switching patterns using genetic algorithm," IEEE Applied Power Electronics Conf., vol.2, pp.1130-1134, 2001.

[6] A.I. Maswood, E. Al-Ammar, F. Liu, "Average and hysteresis current-controlled three-phase three-level unity power factor rectifier operation and performance," IET Power Electronics, vol.4, no.7, pp.752-758, Aug. 2011.

[7] IEEE Recommended Practices and Requirements for Harmonic Control in Electrical Power Systems, IEEE Standard 519-1992, 1992.

[8] A. Tariq, M. A. Husain, M. Ahmad and M. Tariq, ""Simulation and study of a grid connected multilevel converter (MLC) with varying DC input," *Environment and Electrical Engineering (EEEIC), 2011 10th International Conference on* , pp.1-4, 8-11 May 2011.

[9] Y. Ounejjar, K. Al-Haddad and L. A Gregoire., "Packed U Cells Multilevel Converter Topology: Theoretical Study and Experimental Validation," *in Industrial Electronics, IEEE Transactions on* , vol.58, no.4, pp.1294-1306, April 2011.

[10] A. Sheir, M. Orabi, M. E. Ahmed, A. Iqbal, and M. Youssef, "A high efficiency single-phase multilevel packed U cell inverter for photovoltaic applications," *in Telecommunications Energy Conference (INTELEC), 2014 IEEE 36th International* , pp.1-6, Sept. 28 -Oct. 2 2014.

[11] B. P. McGrath, D. G. Holmes, "Multicarrier PWM strategies for multilevel inverters," *in Industrial Electronics, IEEE Transactions on*., vol. 49, no. 4, pp.858-867, Aug. 2002.

[12] Y. Hinago and H. Koizumi, "A modulation method for capacitor voltage ripple reduction of the switched-capacitor inverter using series/ parallel conversion," *in Proc. IEEE Int. Conf. Ind. Technol*., pp. 105–109, Mar. 2011.

[13] A. Tsunoda, Y. Hinago and H. Koizumi, "Level- and Phase-Shifted PWM for Seven-Level Switched-Capacitor Inverter Using Series/Parallel Conversion," *in Industrial Electronics, IEEE Transactions on* , vol.61, no.8, pp.4011-4021, Aug. 2014.

[14] Y. Ounejjar, K. Al-Haddad and L. A. Dessaint, "A Novel Six-Band Hysteresis Control for the Packed U Cells Seven-Level Converter: Experimental Validation," *in Industrial Electronics, IEEE Transactions on* , vol.59, no.10, pp.3808-3816, Oct. 2012L

[15] A. Iqbal, M. Tariq, K. Rahman, and A. Al-qahtani. "Control Of Packed U-cell Multilevel Five-phase Voltage Source Inverter." *In Qatar Foundation Annual Research Conference*,. ITPP0493. 2014

[16] H. Vahedi, K. Al-Haddad and H. Y. Kanaan, "A new voltage balancing controller applied on 7-level PUC inverter," *in Industrial Electronics Society, IECON 2014 - 40th Annual Conference of the IEEE* , pp.5082-5087, Oct. 29 2014-Nov. 1 2014.

[17] Y. Ounejjar, K. Al-Haddad, A. I. Alolah, "Averaged model of the 31-level packed U cells converter," *in Industrial Electronics (ISIE), 2011 IEEE International Symposium on* , pp.1831-1836, 27-30 June 2011

[18] A. Tariq, M. Asim, and M. Tariq. "Simulink based modeling, simulation and Performance Evaluation of an MPPT for maximum power generation on resistive load." *2nd International Conference on Environmental Science and Technology IPCBEE*, Singapore, vol.6, Feb. 2011

[19] J. Hamman, F. S. Van Der Merwe, "Voltage harmonics generated by voltage-fed inverters using PWM natural sampling," *in Power Electronics, IEEE Transactions on* , vol.3, no.3, pp.297-302, July 1988.

[20] H. S. Black, Modularion Theor?;. Princetown, NJ: Van Nostrand & Co., 1953.

Prospect of Solar PV based Power Generation in the Marshy Lands of Bangladesh: An Analysis Through RETScreen Software

Kashfia Naz Nikita[1], Sk Nazmul Islam[2], Md. Sarafat Islam[3], Mithun Saha[4] and Md. Fayyaz khan[5]

Dept. of EEE, United International University, Dhaka, Bangladesh

[1]kashfia.nikki@gmail.com

[2]skshohel1991@gmail.com

[3]sabuj.ahmed499@gmail.com

[4]mithun.saha0@gmail.com

[5]fyk@eee.uiu.ac.bd

***Abstract*– Bangladesh receives an average daily solar energy of 4-6.5 kWh/m^2/day [1] which is highly suitable for generation of electricity through solar PV. As Bangladesh is one of the highly densely populated countries in the world [2], so, it is difficult to get empty space for generation of solar PV based power. Population growth is quite high, approximately 1.6% per year [3] and the available space is shrinking at a very fast rate. Also, as the livelihood of around 70% [4] of the population depends on agriculture, so arable lands cannot be used for solar PV based generation. However, there are some marshy lands in Bangladesh whose soil structure is mainly sandy in nature and such soil is not suitable for harvesting crops or vegetation [5]. The main aim of this paper is to focus on such lands of Bangladesh which are suitable for PV based generation. In this context, the authors have surveyed some areas in the north western zone of Bangladesh to study the possibility of solar PV based power generation. A suitable marshy land was found in the district of Sirajganj. The approximate area of the proposed land is around 44 acres where around 13MW of solar PV based power can be generated. The most advantageous part of the location of the land is that a 230kV grid line is situated together with a North West Power Generation Co., Ltd (NWPGCL) sub- station within 1km from the northern edge of the proposed area. The generated power can be directly hooked up with the 230kV grid line. Hence significant amount of energy can be extracted from Solar PV power plant to feed the national grid. The Renewable Energy Policy of the Power Ministry, Government of Bangladesh (GOB) has fixed the target to produce 5% of the total power generation by 2015 and 10% by 2020 from renewable energy sources. This means that at least 800MW power has to be generated from renewable sources by 2015 and 2000MW by 2020, taking into consideration of the predictive load growth for the coming years [6]. Relevant financial data found through RETScreen software shows that such project is quite feasible and the cost of energy stands at Tk 7.70/kWh.**

***Keywords*—COE, Equity, GHG, IRR, MEMPR, NWPGCL, RETScreen**

I. INTRODUCTION

Bangladesh is located in Southern Asia with the geographical coordinates 24^{0}N, 90^{0}E having total area of 143,998 sq km. The population of Bangladesh till the year 2014 data is 159,077,513 [7]. According to Bangladesh Power Development Board (BPDB), the power demand for this huge population in Fiscal Year (FY) 2015 is around 10,283MW and it will rise up to 17,304MW by FY2020 [8]. Presently there is a shortfall of power to the tune of 1000MW in the peak summer seasons. To meet up this gap between generation and demand, Bangladesh has already started to import electricity from neighbouring India and wants to import further 500MW from India within 2018 [9]. Under the existing generation scenario of Bangladesh, generation from renewable sources is only a small fraction of the total power generation. Presently, the share of renewable energy is slightly more than 1% of total generation [10]. Already, year 2015 is at the fag end and much more to be done to increase the generation from the renewable sources to meet the target set by the government. As solar PV is an effective source for renewable energy based power generation in Bangladesh, extensive study has to be made in this sector. TABLE I shows the total percentage of generated power by different fossil fuels separately and also the de-rated power output of the plants under present conditions [11].

TABLE I: TOTAL PERCENTAGE OF INSTALLED CAPACITY OF FUEL BASED POWER PLANTS

Installed Capacity of BPDB Power Plants as on October 2015			
Fuel Type	**Capacity (Unit)**		**Total (%)**
Coal	250.00	MW	2.14 %
Gas	7280.00	MW	62.31 %
HFO	2507.00	MW	21.46 %
HSD	916.00	MW	7.84 %
Hydro	230.00	MW	1.97 %
Imported	500.00	MW	4.28 %
Total	11683.00	MW	100 %

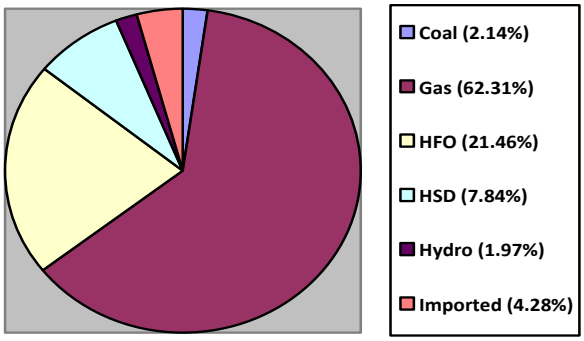

Fig. 1: Pie chart of the generated power by different fossil fuels

TABLE II: AMOUNT OF POWER GENERATION FROM DIFFERENT FUELS

De-rated Capacity of BPDB Power Plants as on October 2015			
Fuel Type	**Capacity (Unit)**		**Total (%)**
Coal	200.00	MW	1.8 %
Gas	6811.00	MW	61.43 %
HFO	2450.00	MW	22.1 %
HSD	897.00	MW	8.09 %
Hydro	230.00	MW	2.07 %
Imported	500.00	MW	4.51 %
Total	11088.00	MW	100 %

From TABLE II, it is seen that major power generation is from natural gas which is depleting at a very fast rate. For other hydro carbon sources, the cost of energy becomes appreciably high. In some cases, cost of energy (COE) becomes cheaper for solar PV when compared to fossil fuel sources like HFO, HSD, Diesel, etc due to continuous fall in the price of solar PV. In this paper, a feasibility study has been made to generate power from solar PV for a large area. The area chosen for such generation is a sandy land near Banga Bandhu bridge, Sirajganj district of Bangladesh. A 230 kV line runs very near to the proposed area (less than 1km). There is also NWPGCL (North West Power Generation Company Ltd.) 230 kV substation near to the proposed land. The longitude and latitude of the land are 24.8^0N & 89.4^0E respectively.

Fig.2: Proposed Land

Fig. 3: NWPGCL 230kV substation near the proposed land

As the land is predominantly made up of sandy soil, so, there is absolutely no chance for crop cultivation. Also during monsoon season, the land is inundated by water to a height of 3~4 feet. A complete analysis has been made by RETScreen software to determine the total investment cost, internal rate of return (IRR), COE, etc together with the amount of power that can be generated from PV panels installed on the land for an approximate area of 44 acres.

I. ANALYSIS THROUGH RETSCREEN

To evaluate the amount of energy production, life-cycle costs and greenhouse gas emissions reduction, the RETScreen International Photovoltaic Project Model can be used efficiently. This evaluation can be done for three basic PV applications: on-grid; off-grid; and water pumping systems. For on-grid applications, the model can be used to evaluate both central-grid and isolated-grid PV systems. In this paper, the feasibility of a central-grid connected solar PV project has been analysed for the proposed land at Sirajganj. The NASA climate data of Bogra (nearest district of Sirajganj) is shown in TABLE III.

TABLE III: GEOGRAPHICAL SPECIFICATION & CLIMATE DATA OF THE PROPOSED LAND

	Unit	Climate data location	Project location
Latitude	°N	24.8	24.8
Longitude	°E	89.4	89.4
Elevation	m	17	17
Heating design temperature	°C	14.0	
Cooling design temperature	°C	31.7	
Earth temperature amplitude	°C	15.0	

Bogra is the nearest area from the proposed location and thus the above table shows the latitude and longitude of the prospective location which are 24.8°N and 89.4°E respectively. Heating design temperature represents the minimum temperature that has been measured for a frequency level of at least 1% over the year for a specific area, cooling design temperature represents the maximum temperature that has been measured for a frequency level of at least 1% over the year for a specific area and Earth temperature amplitude represents half the difference between the maximum and minimum of the earth temperature (i.e. skin temperature) at the depth of measurement.

II. ENERGY MODEL

In solar PV, solar radiation is converted into electrical energy. In this analysis, the annual average solar radiation is 1.88 MWh/m². The corresponding electricity exported to grid is shown in TABLE IV.

TABLE IV: MONTHWISE AVERAGE ELECTRICITY EXPORTED TO GRID FROM THE PROPOSED PV PLANT

Month	Daily solar radiation - horizontal kWh/m²/d	Daily solar radiation - tilted kWh/m²/d	Electricity export rate $/MWh	Electricity exported to grid MWh
January	4.34	5.69	170.0	1,759
February	5.07	6.09	170.0	1,672
March	5.87	6.38	170.0	1,903
April	6.05	5.98	170.0	1,731
May	5.51	5.13	170.0	1,552
June	4.74	4.34	170.0	1,281
July	4.26	3.96	170.0	1,212
August	4.30	4.14	170.0	1,263
September	3.91	3.99	170.0	1,179
October	4.36	4.93	170.0	1,498
November	4.39	5.59	170.0	1,653
December	4.17	5.63	170.0	1,737
Annual	**4.74**	**5.15**	**170.00**	**18,440**

The table shows that the annual electricity exported to grid is 18,440 MWh. The global formula to estimate the electricity generated from a photovoltaic system is:

$$E = A * r * H * PR$$

E = Energy (kWh)
A = Total solar panel Area (m²)
r = solar panel yield (%)
H = Annual average solar radiation on tilted panels (shadings not included)
PR = Performance ratio, coefficient for losses (range between 0.5 and 0.9, default value = 0.75)

Here total 44,175 solar panels of 290Wp are used with total 12.81 MW power capacity and inverters of total 15 MW power capacity are used to convert the dc output power of the panels into ac and feed the power to the national grid. The specifications of solar panel and inverter are shown in TABLE V.

TABLE V: SPECIFICATIONS OF PHOTOVOLTAIC & INVERTER

Photovoltaic			
Type		poly-Si	
Power capacity	kW	12,810.75	
Manufacturer		Yingli Solar	
Model		poly-Si - YGE - YL290P-35b	44175 unit(s)
Efficiency	%	14.9%	
Nominal operating cell temperature	°C	45	
Temperature coefficient	% / °C	0.40%	
Solar collector area	m²	86,152	
Miscellaneous losses	%	15.0%	
Inverter			
Efficiency	%	98.0%	
Capacity	kW	15000.0	
Miscellaneous losses	%	0.0%	

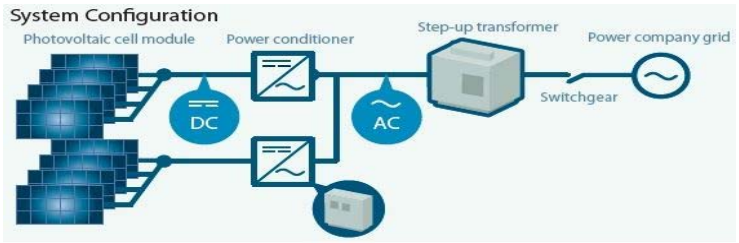

Fig. 4: Single line diagram of the system

III. COST ANALYSIS

Estimation of initial cost is very essential for a feasible project plan. In this paper, five types of costs have been considered as initial cost which is given in TABLE V.

TABLE VI: INSTALLATION COST OF SOLAR PV POWER PLANT

Name of Cost Types	Amount (USD)	Amount (BDT)
Feasibility Study	$36,650	28,31,579/=
Development	$144,000	1,11,25,440/=
Engineering	$79,000	61,03,540/=
Power System	$10,868,885	83,97,30,055/=
Balance of System & Miscellaneous	$11,877,351	91,76,44,138/=
Total	$23,005,886	177,74,34,752/=

Feasibility studies typically include site investigation, resource assessment, environmental assessment, preliminary project design, detailed cost estimate, greenhouse gases (GHG) baseline study and monitoring plan (MP) and final report. Project development activities typically include cost for such items as contract negotiations, permits & approvals, site survey & land rights, GHG validation & registration, project financing, legal & accounting, project development management and travel costs. The engineering phase includes costs for the proposed case project site & building design, mechanical design, electrical design, civil design, tenders & contracting, and construction supervision. The power system includes the associated road construction, photovoltaic, transmission line, substation and power-related energy efficiency measures costs. The balance of system & miscellaneous includes inverter, collector support structure, installation, building & yard construction, spare parts, transportation, training & commissioning, contingencies and interest during construction.

Operation & maintenance cost of the plant and some other specific costs can be enlisted in annual cost such as land lease & resource rental, property taxes, insurance premium, parts & labor, GHG monitoring & verification, community benefits, general & administrative expenses and contingencies. Taking all these costs in consideration, the annual cost for the plant becomes **$377,513** or **BDT 2,91,66,654**.

A periodic cost should be considered as recurrent cost that must be incurred at regular intervals to maintain the project in working condition. As the replacement of the inverters are required once over the life cycle, a periodic cost of **$1,500,000** or **BDT 11,58,90,000** has been considered in this project after first 10 years.

IV. FINANCIAL ANALYSIS

The financial analysis is the most essential part for developing any project. It ensures whether the project will be profitable or not. It contains six sections: Financial parameters, Annual income, Project costs and savings/income summary, financial viability, Yearly cash flows and Cumulative cash flows graph. TABLE VII shows the financial parameters which have been considered in this project.

TABLE VII: FINANCIAL PARAMETERS

Financial parameters		
General		
Fuel cost escalation rate	%	3.0%
Inflation rate	%	5.0%
Discount rate	%	0.0%
Project life	yr	20
Finance		
Incentives and grants	$	0
Debt ratio	%	40.0%
Debt	$	9,202,354
Equity	$	13,803,532
Debt interest rate	%	13.00%
Debt term	yr	15
Debt payments	$/yr	1,423,989

From TABLE VII it is seen that the project life is of 20 years where no grants has been considered. The debt ratio is considered 60:40 which means equity will be 60% and debt will be 40% of the total initial cost. The debt will be paid back within 15 years with 13% interest.

According to all the parameters that have been considered, the annual income is shown in TABLE VIII.

TABLE VIII: ANNUAL INCOME

Annual income		
Electricity export income		
Electricity exported to grid	MWh	18,440
Electricity export rate	$/MWh	170.00
Electricity export income	$	3,134,757
Electricity export escalation rate	%	3.0%

TABLE VIII shows that the annual income for exporting electricity to the grid is $3,134,757 based on total annual energy exported to grid is 18,440 MWh. The projected annual average rate of increase in electricity export rate over the life of the project is considered 3%.

Summary of total project cost & annual savings/income is given in TABLE IX.

TABLE IX: PROJECT COSTS & ANNUAL SAVINGS/INCOME

Project costs and savings/income summary			
Initial costs			
Feasibility study	0.2%	$	36,650
Development	0.6%	$	144,000
Engineering	0.3%	$	79,000
Power system	47.2%	$	10,868,885
Balance of system & misc.	51.6%	$	11,877,351
Total initial costs	**100.0%**	**$**	**23,005,886**
Annual costs and debt payments			
O&M		$	377,513
Fuel cost - proposed case		$	0
Debt payments - 15 yrs		$	1,423,989
Total annual costs		**$**	**1,801,501**
Periodic costs (credits)			
User-defined - 11 yrs		$	1,500,000
Annual savings and income			
Fuel cost - base case		$	0
Electricity export income		$	3,134,757
Total annual savings and income		**$**	**3,134,757**

From TABLE IX, it is seen that the total annual savings and income will be **$3,134,757** or **BDT 24,21,91,326**. As the electricity will be directly exported to the national grid, no fuel cost has been considered.

TABLE X: FINANCIAL VIABILITY

Financial viability		
Pre-tax IRR - equity	%	12.7%
Pre-tax IRR - assets	%	6.8%
After-tax IRR - equity	%	12.7%
After-tax IRR - assets	%	6.8%
Simple payback	yr	8.3
Equity payback	yr	8.1
Net Present Value (NPV)	$	35,923,240
Annual life cycle savings	$/yr	1,796,162
Benefit-Cost (B-C) ratio		3.60
Debt service coverage		1.99
Energy production cost	$/MWh	99.61
GHG reduction cost	$/tCO2	No reduction

TABLE X shows the financial viability of the project where COE is **$99.61/MWh** or **$0.099/kWh** which is **BDT 7.70/kWh**. The benefit-cost ratio is 3.60. Therefore, the project is profitable as ratio greater than 1 is indicative of profitable projects. IRR means Internal Rate of Return and the break-even point of equity payback is 8.1 years. No carbon emission has been considered in this project.

The yearly cash flow and the cumulative cash flow graphs are given in TABLE XI & figure 5 respectively.

TABLE XI: YEARLY CASH FLOWS

Yearly cash flows			
Year	Pre-tax	After-tax	Cumulative
#	$	$	$
0	-13,803,532	-13,803,532	-13,803,532
1	1,408,423	1,408,423	-12,395,108
2	1,485,468	1,485,468	-10,909,641
3	1,564,427	1,564,427	-9,345,214
4	1,645,339	1,645,339	-7,699,874
5	1,728,242	1,728,242	-5,971,632
6	1,813,172	1,813,172	-4,158,460
7	1,900,169	1,900,169	-2,258,291
8	1,989,270	1,989,270	-269,021
9	2,080,513	2,080,513	1,811,492
10	2,173,935	2,173,935	3,985,427
11	-295,935	-295,935	3,689,491
12	2,367,467	2,367,467	6,056,959
13	2,467,652	2,467,652	8,524,610
14	2,570,164	2,570,164	11,094,774
15	2,675,039	2,675,039	13,769,814
16	4,206,303	4,206,303	17,976,116
17	4,316,010	4,316,010	22,292,127
18	4,428,185	4,428,185	26,720,312
19	4,542,860	4,542,860	31,263,173
20	4,660,067	4,660,067	35,923,240

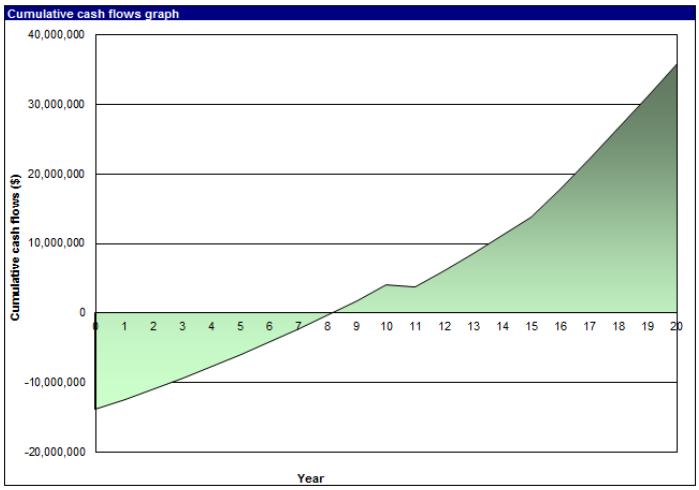

Fig. 5.Cumulative Cash flow

From the graph of figure 5, it is clearly seen that the break-even point is at 8.1th year and after that the flow of profit increases. But after 10 years the cash flow decreases at a small rate till year 11 due to the periodic cost and then it again increases at a fast rate through the rest of the project life.

VI. CONCLUSION

Bangladesh is a densely populated riverine country where most of the people earn their livelihood through agriculture. With the increase of population, the arable land is decreasing at a fast rate. At the same time, demand for power is increasing exponentially with fast depletion of natural gas reserve. Alternative energy sources will have to be found out to meet the energy challenges for years to come. Solar based PV power generation is a lucrative option and with gradual decay of solar PV price, power generation from this source has become attractive and competitive when diesel is considered as the fuel for power generation. Bangladesh government has set a target of meeting 5% of the total generation to be met from R/E sources by 2015 and 10% by 2020. Only few months left for the year 2015; roughly 1% of government's target has been fulfilled till to-date. Due to fair amount of sunshine received in Bangladesh throughout the year, solar PV based generation has to be seriously considered. Only problem with the solar PV is the requirement of large chunk of land for generation in terms of mega watt. In this paper, a detailed study has been made through RETScreen software to generate 13MW of power in the marshy land of Sirajganj district; that can be directly hooked with a 230KV line running nearly 1km from the proposed site. As the proposed area is a marshy land; so the land cannot be used for agricultural harvest and is highly suitable for installation of solar PV. A series of calculations have been made through RET Screen to calculate major parameters like COE, IRR, equity, payback period etc. With the debt equity ratio of 40:60 and annual interest rate of 13%, the cost of energy stands at Tk.7.70 with the benefit-cost ratio of 3.60. The cost benefit ratio shows that the project will be highly feasible. Calculations have been made based on the prevailing land

price for the area. As the proposed land is owned by the government; the COE will further be reduced if the land price is considered at the government rate. Also, carbon trading for the project will bring down the COE further.

REFERENCES

[1] Vision of Solar Power Development through Asia Solar Energy Initiative (ASEI), Renewable-Energy, Power Division, Ministry of Power, Energy and Mineral Resources, Government of Bangladesh. Available: http://www.pd.gov.bd/user/brec/50/91

[2] The World Bank database. Available: http://www.worldbank.org/en/country/bangladesh/overview

[3] The World Fact Book - Central Intelligence Agency. Available: https://www.cia.gov/library/publications/the-world-factbook/fields/2002.html

[4] Agriculture Sector Development Strategy: "Background Paper for Preparation of 7th Five Year Plan"- (17-02-2015), Planning Commission, Ministry of Planning, Bangladesh.

[5] A.B.M.S Islam & M.S.Hussain, "Mineralogical Characterization of Clay fraction of Chalan Beel soils of Bangladesh," Journal of Bangladesh Agriculture University 6(2), 253-260, 2008

[6] Appointment of consultant for feasibility study on 60 MW Solar Park at Rangunia, Chittagong. Power Cell, Power Division, Ministry of Power, Energy and Mineral Resources, Government Of Bangladesh.

[7] The World Bank population database. Available: http://data.worldbank.org/indicator/SP.POP.TOTL

[8] Power System Master Plan. Bangladesh Power Development Board (BPDB). Available: http://www.bpdb.gov.bd/bpdb/index.php?option=com_content&view=article&id=12&Itemid=126

[9] Power Grid Company of Bangladesh Ltd (PGCB). Available: http://www.pgcb.org.bd/PGCB/?a=user/ongoing_project_details.php&id=58

[10] Development of Renewable Energy by BPDB, Bangladesh Power Development Board (BPDB). Available: http://www.bpdb.gov.bd/bpdb/index.php?option=com_content&view=article&id=26&Itemid=24

[11] Power Generation Units (fuel type wise), October 2015, Bangladesh Power Development Board (BPDB). Available: http://www.bpdb.gov.bd/bpdb/index.php?option=com_content&view=article&id=150&Itemid=16

Simulink Based Performance Analysis of Lead Acid Batteries with the Variation of Load Current and Temperature.

Md. Abdul Gaffar[#1], Md. Enamul Huq Sabuj[#2], Fatima Mostafa[#3] , Tanvir Istiaque[#4] and Md. Fayyaz Khan[#5]

Department of Electrical and Electronics Engineering
United International University, Dhaka
Bangladesh.

[1]m.a.gaffar012@gmail.com
[2]enamulsabuj@gmail.com
[3]fatimamostofa@rocketmail.com
[4]tanvir_istiaque@yahoo.com
[5]fyk@eee.uiu.ac.bd

***Abstract*— Storage device in renewable energy applications plays an important role for efficient operation. For solar PV applications, storage device is an integral part during post sun shine hours to supply power to the load. For Solar Home System (SHS), approximately 60% of the total cost is due to storage battery and the battery needs replacement in every five years or so. If the performance of the battery can be enhanced, not only the cost of energy will come down appreciably but the reliability of the system will improve. Battery is needed in PV system to store the excess energy from the sun and release the power to the system again when it is needed. In other words, to enhance a system performance we have to increase the battery performance. In this paper, the parameters which play important role for optimum performance has been studied. The major two parameters that affect the battery performance are load current and temperature. It has been found that, when the discharge current is high, battery capacity reduces and the vice-versa. Again in case of temperature, when temperature increases more than the rated standard value of 25˚C, capacity increases but the life time of the battery decreases. On the other hand, when the ambient temperature goes down, capacity of battery decreases but lifetime of the battery is increased. To analyse the effect of temperature and load current on battery performance, the standard equivalent circuit of battery is considered first and then the equivalent circuit is simulated using Simulink under MATLAB environment.**

***Keywords*— SOC, DOC, DOD, SHS, Simulink, PV, Simscape.**

I. INTRODUCTION

It is commonly thought that renewable energy will play an important role for future power generation. But the question is why we consider it as a future power generation source together with conventional energy sources. The energy demand is increasing with the growth of population. We believe that this spectacular growth of energy can't be met with traditional energy system alone without strongly increasing pressure on renewable energy. Now if we want to completely depend on renewable energy then we must need to consider an energy storing device to store this energy for times when the sun is not shining or the wind is not blowing. So, in this situation, battery is considered as prominent storage device. Again with regard to reliability and cost of standalone or grid connected PV (photovoltaic) power systems, storage battery represents main, important and costliest component. So battery is a pivotal component in respect of overall PV system performance and economic analysis for the system.

II. BATTERY

There are different types of rechargeable battery which can be used as storage device of standalone solar PV systems like Lead acid, Li-ion, Ni-Cd, Ni-Mh battery etc [1] . Among them Lead acid battery is the technology of choice for most of the PV systems. Although there are performance limitations which results in excessive replacement costs, work-place occupational health and safety issues and operational maintenance issues. As lead acid batteries are widely used in different countries including Bangladesh, so in this paper performance of battery under different load conditions and variable temperature has been studied for lead acid batteries.

III. PARAMETERS AFFECTING PERFORMANCE OF BATTERY

As battery is a very important component, we should know about its efficiency and the parameters which are responsible for degrading the performance of this storage device. The degradation of battery capacity mostly depends on areas under charging/discharging phases, DOD (Depth of Discharge) of the battery, exposure to the prolonged periods of low discharge and average temperature of the battery over its lifetime. Among these, two important parameters namely charging current & load current and temperature are discussed here.

A. Effects of charging current &Load current:

The charging or discharging currents affect the battery capacity. If the discharge current is high then the amount of energy that can be extracted is reduced and the battery capacity is low. This occurs as the necessary components

required for the reaction to occur do not have enough time to attain their status for chemical reactions. Again if discharge current is low, more energy can be extracted from the battery and the battery capacity is higher [2]. So depth of discharge and rated battery capacity is strongly affected by the charging and load current rate.

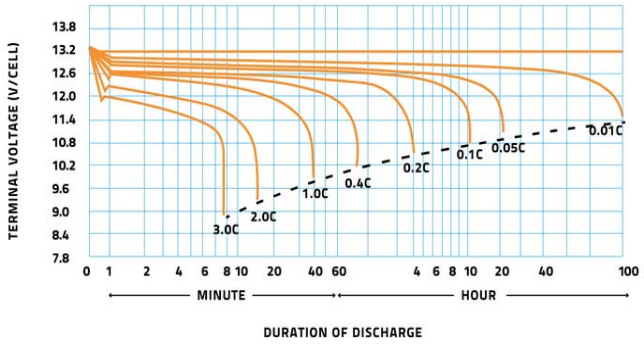

Figure 1: Terminal voltage Vs duration of discharge curve.

If we concentrate in figure-1[3], we can see that if discharge rate is high, duration of discharge of battery is low and vice versa. Again it is also true in the perspective of terminal voltage, at high discharge rate, terminal voltage reduces quickly.

B. Effects of Temperature:

The standard rating for battery is considered at room temperature of 25˚C. The battery temperature should be corrected by applying a temperature compensation coefficient if operating temperature is other than 25˚C [4].

TABLE I
TEMPERATURE COMPENSATION COEFFICIENTS

Temperature	-20⁰C	-10⁰C	0⁰C	10⁰C	20⁰C	25⁰C	30⁰C	40⁰C
Compensation coefficient for a 120-hr discharge	0.58	0.72	0.83	0.91	0.98	1.00	1.02	1.05

Temperature and battery capacity maintain an inverse relationship. When temperature goes down capacity of the battery decreased. And the capacity increases with increase in temperature. The below graph represent how the lead acid battery capacity vary over years with operating temperature. Here we can see, at running temperature of 35 ˚C the battery will deliver more than its rated capacity but their life is relatively short. Where at 15 ˚C, lifetime increases with condensation in capacity.

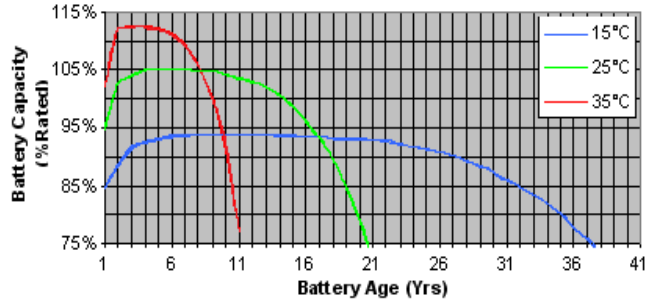

Figure 2 [5]: Capacity Vs. Battery Age curve with temperature variation.

So, high temperature will increase capacity, shorten life, increase internal discharge rate with the increase of charging current. On the other hand, by lowering temperature, capacity will decrease but life of the battery will increase. Capacity at lower temperature reduces the available battery capacity by 0.5% per F [6].

IV. BATTERY EQUIVALENT MODEL

As we already mentioned, battery is the key component for renewable energy systems. And there are different parameters which deteriorate battery capacity and its lifetime. Now to perceive this parameter well, we have to test the battery. But testing a battery takes several hours and good number of testing components like suitable battery charger, stopwatch, voltmeter, ammeter etc [7]. To reduce this long testing time and amount of physical testing components, electrical battery equivalent circuit model is necessary and battery performance can be simulated through simulation software. So for the purpose of capacity determination and optimum component selection, modelling and simulations of battery system are developed to predict the battery performance. There are number of battery equivalent mathematical models available for simulation purposes like thevenin battery model, coppetti model, third order model, fourth order model etc described in ref [8], [9].

In this study, we used a model which described in ref [10], which is constructed using the Sims cape example library Lead AcidBattery_lib. This example shows how to model a lead acid battery cell using the Sims cape language to implement the non-linear equations of the equivalent circuit. In this model, proposed equation contains several parameters that have to be identified. This identification can be simplified by considering some of the parameters as constants. In Ref [11] this parameters and equations are defined. It has been proved that this model was capable of providing accurate simulation results at a very fast simulation speed.

A. Battery Model Structure:

The battery model was designed to accept inputs as current and ambient temperature respectively. And the output is voltage, SOC and electrolyte temperature.

Figure 3: Battery model.

A diagram of overall battery model is shown below-

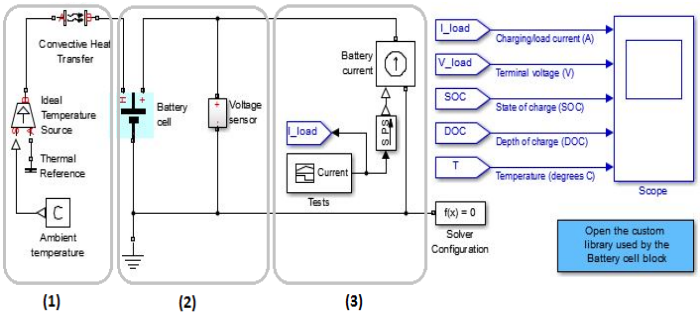

Figure 4: Overall lead acid battery model.

It contains three major blocks which is shown in figure 4.

1) Thermal model:

Thermal model block represents ambient and battery electrolyte temperature. This simple thermal model is used to model battery temperature. It is assumed that cooling is primarily via natural convection and the heating is primarily formed around the battery due to charging and discharging phases of the battery.

2) An equivalent circuit model:

This structure consisted of two main parts: a main branch which approximated the battery dynamics under most condition and a parasitic branch which accounted for the battery behaviour at the end of the charge.

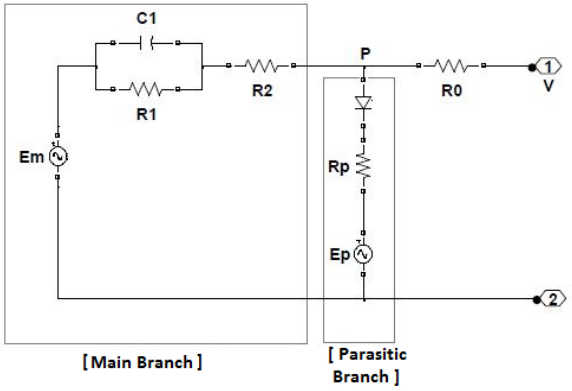

Figure 5 [11]: Battery Equivalent Circuit.

This battery equivalent circuit represent one cell of the battery. The output voltage is multiplied by six, the number of series cells, to model a 12 volt battery. Each equivalent circuit was based on nonlinear equations as found in ref [11]. Different parameters and states are included in these non-linear equations and the parameters depend on empirically determined constants.

3) Block model for simulation of Charge and capacity of battery:

This block tracks the battery's capacity, state of charge (SOC), depth of charge (DOC) etc.

The battery is simulated to see the effect of acid battery by varying current and temperature using this battery model.

V. BATTERY SIMULATION

To estimate battery capacity is a challenge because of variable parameters of battery. To ensure whether a battery is fully charged or fully discharged is difficult to assess. So these difficulties should be taken into consideration during the lab testing process. The model as discussed in the previous section represents the model of a cell of a battery. So if we want to simulate a 12V battery, we will have to connect 6 pieces of 2V battery cell blocks in series. The initial value of SOC and DOC are taken as 20% and the final value is considered as 80% to simplify the battery modelling in charging and discharging states. As we already mentioned, to observe the effect of charging/load current and temperature variation we used MATLAB Simscape example [12].

A. Variation of charging and discharging current:

In this study, we simulate a lead acid battery specified as nominal voltage of 12V, nominal capacity of 20Ah, and charging and discharging rate C/10. So our charging and discharging current is 2A.

Here, battery was first discharged under 2A constant load and then charged under 2A constant current to bring the battery to the initial state of charge. This is shown figure 6.

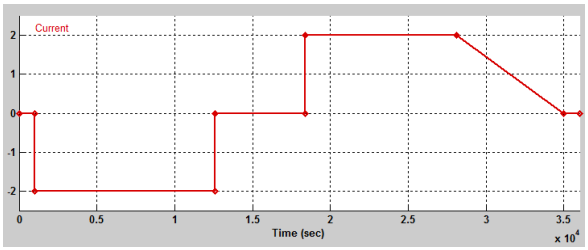

Figure 6: Charging cycle.

Corresponding to the charge cycle, the terminal voltage, SOC, DOC and Temperature are shown in figure-7

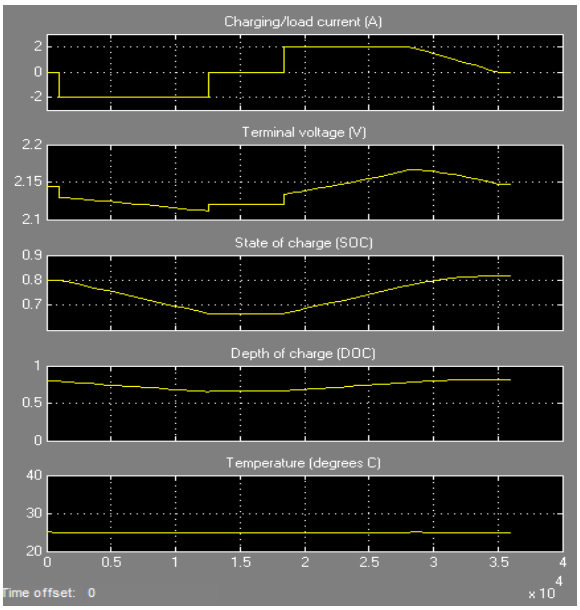

Figure 7: simulation Results of lead acid battery 20AH battery.

These figures reveal that the cell terminal voltage at the first phase of discharge process is equal to 2.15V (so, for a 12V battery, terminal voltage will be 12.9V). SOC and DOC both are equal to 80%. When we place a load, SOC and DOC start to decrease until the cell voltage is 2.11V thus reducing the terminal voltage of the battery to 12.66V and the values of SOC and DOC came down to 67% and 65% respectively. Then the battery is charged again until the cell voltage is equal

to 2.18V (For a 12V battery, it is 13.1V) and both SOC and DOC were 80%, a slight increase in the values of SOC and DOC.

In the case of electrolyte temperature, we considered the room temperature of 25˚C as shown in figure 7.

B. Variation of Temperature:

At first we increase the ambient temperature 25˚C to 40˚C.

Figure 8: Input for change of temperature from 25˚C to 40˚C.

For this temperature range, following changes occurred in SOC and DOC.

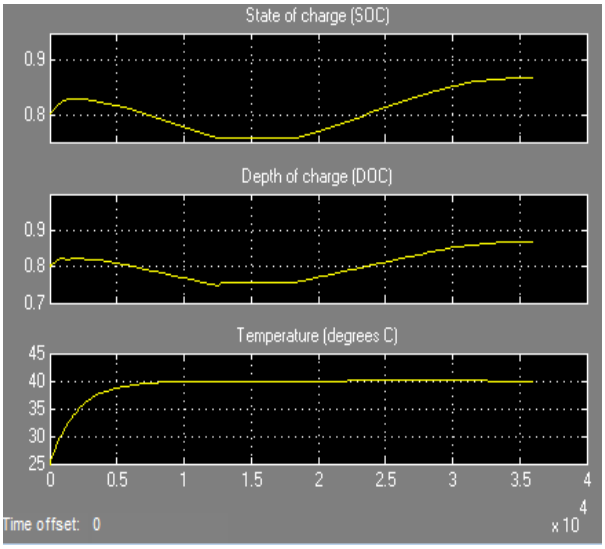

Figure 9: Simulation results for variation of temperature from 25˚C to 40˚C.

In this case also, initial value of Terminal voltage, SOC and DOC remained same. When we placed a load, SOC and DOC started to decrease but this time the value of SOC and DOC is 76% and 75% respectively whereas at 25˚C it was 67% and 65% respectively. So increase in temperature increases the capacity. Again the value of SOC and DOC is also increased after recharging the battery. Whereas at 25˚C, the value of SOC and DOC were 82%, here the value increased to about 86%.

Now if we decrease the temperature from 25˚C to 0˚C, in this case when we placed a load the value of SOC and DOC is decreased, with respect to temperature at 40˚C. For this condition, the value of SOC was 46% and the value of DOC is only 43%. So we can see that this value is much lower than the initial values of SOC and DOC at 25˚C. So decrease in temperature decreases the capacity which can be observed through figure 9.

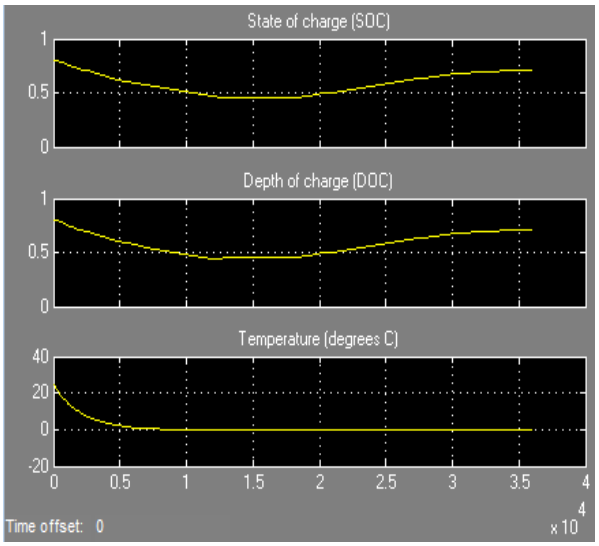

Figure 10: Simulation results for decreasing temperature from 25˚C to 0˚C.

VI. Conclusions

Lead acid battery is being used worldwide in standalone or nano/mini grid solar PV systems. Whatever the PV system is small or large, battery is one of the key factors to realize an efficient system. So the parameters which affect the battery performance have been studied in this paper. To know about this parameter well various model of battery equivalent circuit also has been studied. Two important parameters load current and temperature has got huge impacts on the performance of lead acid battery. So the battery performance was critically studied with the variation of ambient temperature and load current. During discharge cycle of the battery, terminal voltage, SOC, DOC parameters reduce substantially. Also variation of temperature above and below 25^0C has been studied through the simulation software. Increase of temperature above 25^0C shows increment for both SOC & DOC while the terminal voltage of the battery almost remained the same. Lowering temperature below 25^0C, both SOC and DOC decreased with no appreciable change in terminal voltage. So we introduced the Simscape examples of lead acid battery and used this example to simulate the lead acid battery in perspective of load current and temperature. And the simulation with this battery model is absolutely real time simulation. So with this simulation technique, one can predict major variation in the parameters of a battery without under going into time consuming battery tests.

Acknowledgment

We would like to express our sincere gratitude to Math Works family for keeping the SIMSCAPE example of lead acid battery in MATLAB 2014a and Mr. Jackey, R for his research on battery electric equivalent model. Without this model we won't be able to write this paper.

REFERENCES

[1] Wikipedia- the free encyclopaedia, (2015). [online] Available: https://en.wikipedia.org/wiki/List_of_battery_types.

[2] Depth of discharge and battery capacity. [Online]. Available: http://pvcdrom.pveducation.org/BATTERY/charlead.htm

[3] Lead crystal batteries. [Online]. Available: https://www.gliderpilotshop.com/lead_crystal.

[4] Mr. Shah Md. Sazzad Hossain, (2015) "Energy storage- Battery", Rahimafrooz batteries limited, Dhaka.

[5] Battery and energy technologies-(2005) Battery life and (death). [Online]. Available: http://www.mpoweruk.com/life.htm.

[6] John Kim, Enersys (2013). [Online]. Available: https://ewh.ieee.org/r3/nashville/events/2013/Lead%20Acid%20Battery%20Training%20by%20EnerSys%20at%20IEEE%2002-21-13.pdf

[7] Battery basics- (2009). [Online]. Available: http://www.gearseds.com/files/determining_battery_capacity3.pdf

[8] Quree Bajracharya- "Dynamic modelling, monitoring and control of energy storage system", Karlstad University-2013.

[9] Wenxin Peng, "Accurate circuit model for predicting the performance of lead acid AGM batteries" University of Nevada, Las Vegas, August 2011.

[10] Ola Subhi Waheed Al-Quasem. "Modeling and simulation of lead acid storage batteries within Photovoltaic power system" An-Najah National University, Nablus, Palestine, 2012.

[11] Jackey, R. "A Simple, Effective Lead-Acid Battery Modeling Process for Electrical System Component Selection", SAE World Congress & Exhibition, April 2007, ref. 2007-01-0778.

[12] Mathworks (r2014a) –MATLAB and SIMULINK/SIMSCAPE example library LeadAcidBattery_lib.

A Study on Anaerobic Co digestion of Municipal solid waste and tannery solid waste

Md. Abdul Mazed
Sr. Project Officer (Engineer),WASH Department
ACF
Cox's bazar, Bangladesh
mazed.sust@gmail.com

Shilpy Rani Basak
Assistant Professor, Department of Civil and Environmental Engineering, SUST.
Sylhet, Bangladesh
shilpy_basak@yahoo.com

Abstract
Covering an area of 25ha. Hazaribagh in the area of Dhaka city is the center of the entire leather industry of Bangladesh. During the peak period (3 to 4 months) based on Eid-ul Ajha industries emitted effluent of 21600 m3, and solid wastes about 170 ton/day discharging to the municipal drain, that being released into the Buriganga River, Causing irreparable damage to the Environment. Fleshing, this is a major portion of the tannery solid wastes discharging into the drain and creates clogs. Finally it is discharged into the Buriganga River and rising BOD value in water. It is also causes surface and ground water pollution [1]. Municipal solid waste management is also a major problem in our country. That is also responsible for so many environmental pollution. Biogas generation is one of the most promising renewable energy sources in Bangladesh. On the other hand anaerobic digestion is one of the effective ways of generating Biogas. This study shows that fleshing contain significant quantity of volatile solids amenable for biodegradation [5]. Different Properties of waste fleshing were subjected to anaerobic digestion. The studies were carried out in a laboratory scale reactor. Water displacement method was followed to measure the amount of gas. Municipal solid waste was mixed with tannery solid waste based on C/N ratio. All the parameters were checked properly to satisfy anaerobic co-digestion method. The temperature was controlled inside the reactor within 32±2ºc. The range of P^H was observed 6.4 to 8.22. The value of COD reduced to 38%, so it is a green signal to reduce the bad impact on environment. The maximum volume reduction was 53% and reduction of volatile solid (VS) was up to 40% which ensure a stable degradation of the substrates. Total amount of gas was found 143.6cm3/kg. This value is an indication of renewable energy source.

I. Introduction

There are at present 214 Tanneries in Bangladesh, 200 of them in the city of Dhaka and 14 others scattered all over the country. Covering an area of 25 ha. Hazaribagh is the Centre of the entire leather industry of Bangladesh. Nearly 149 tanneries of the 200 produces of leather and leather products are located in the Hazaribagh area [3].

Solid wastes generated at various unit operations of the tanning process considerably vary in quantity and composition. Fleshing is a type of animal tissue waste generated during the preparatory leather processing stage in relatively larger quantities that mainly contains fat and protein [2]. All the solid wastes including toxic water eventually make its way into the Buriganga River, which is considered to be Dhaka's lifeline. Thousands of people depend on the river daily for their daily need. The river has suffered extreme biodiversity loss and has now turned black [6]. The pollutants have eaten up all oxygen in the Buriganga and we call it biologically dead.

Municipal solid waste management is also a tough job in Bangladesh as its producing huge amount every day. To manage it as useful way study included municipal solid waste with tannery solid waste in production of renewable energy.

II. METHODOLOGY

A. Study area:

The study area is Hazaribagh Tannery Estate in Dhaka. The area is of 3.58 sq km and Buriganga River is situated on the west. The town has a population of 55338; density per sq km is 35247. It has about 300 tannery industry.

B. Collection of Sample and Data:

The study has been included visit to observe present management condition of Hazaribagh area for proper selection of sampling stations. Sample was collected from a prominent tannery industry named "Lien Enterprise" with the help of professional worker from their definite discharge point. The sample of municipal solid wastes (MDW) were collected from two residential building and dried at the roof.

C. Method of analysis TSW and MSW

All parameters are as measured using methods described in "Standard methods for the examination of water and wastewater", published jointly by APHA, AWWA, and WEF. In the term of determining BOD_5 and COD the recent fresh sample were collected for exact result.

The sludge was dried at 34^0C for about 64 hours to find actual moisture content. The samples OF TSW were collected with the help of professional worker of the tannery from their definite discharge point. Municipal Wastes were collected from two residential building to use as substrate in digestion reactor. Municipal Solid wastes contains two types of component degradable (organic) and non-degradable (inorganic) wastes. Only degradable (organic) portion excluding plastic. Rubber, glass and leather were separated from municipal solid wastes. Wastes were shredded to ensure efficient function of mixing and digestion process [4].

D. **Experimental Setup of Biogas Unit**

Digestion Reactor-1

A reactor of volume 510 in3 was implemented in laboratory. The reactor was ensured anaerobic condition and surrounded by 2 inch layer of husk (paddy). An effluent pipe was fixed in the lower portion. It was used as leached outlet. A gas reading meter was fixed at the top. All the parameter like temperature, P^H, COD, VS and volume reduction etc. were checked and measured during the active period of reactor. All parameters were worked with satisfaction but the amount of gas yield comparatively bellows the lower limit of meter reading. It was impossible to get reading from this reactor.

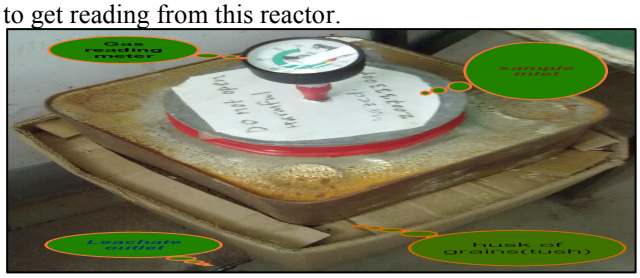

Figure 2.1: Digestion Plant

Digestion Reactor-2

Second digestion reactor was implemented based on water displacement method instead of meter reading. Two units were connected by 8.6 mm dia pipe. First unit is of 317 in3 volume that used as main plant and second unit as connected to contain displaced water. Units were ensured air tied condition. A measuring scale was connected with pipe to take water displacement reading from the scale. Water was placed in equal condition in the beginning. Water started to displace with time when gas yielding started that measured with the help of measuring scale shown in figure 2.2.

Water Displacement Measurement

Water displacement indicates yielding of gas. The displacement reading was taken every days using meter scale that adjusted with experimental unit. Gas production rate has been calculated based on the water displacement reading.

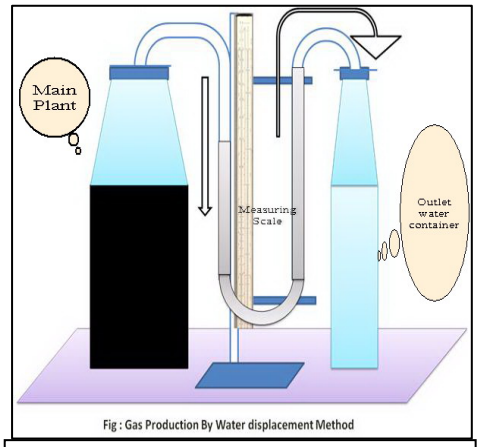

Figure 2.2: Digestion Plant 2

III. RESULT AND DISCUSSION

Two types of digestion plant were setup in the laboratory. It was not possible to collect the rate of generation of gas from first plant. The data has been analyzed here based on second digestion plant.

Characterization of Tannery Solid Waste:

Parameter	Tannery solid Waste
Moisture Content	85.26
P^H	7.38
BOD	417 mg/l
COD	1465 mg/l
TS (%)	18.62

E. **Daily Gas generation**

The production of Biogas during anaerobic digestion process is presented in figure 4.1. The biogas production increases from 1.94 to 4.17cm3/kg. Gas yielding started 12 day later from initial time. Gas yielding was stopped at 53th day of digestion process. Minimum yielding rate is 1.94 Cm^3/day at the end .The maximum gas yielding rate is 4.17cm^3/day.

Organic matter + H_2O + nutrients ⟶ new cell + resistant organic matter + CO_2+ CH_4 +NH_4 + H_2S + Heat

The typical reaction that takes place in hydrolysis process is:

$C_6H_{10}O_5 + 2H_2O \longrightarrow C_6H_{12}O_6$

$C_6H_{12}O_6 + 2H_2O \longrightarrow 2CH_3COOH$ (acetate) + $2CO_2 + 4H_2$

CH_3COOH (acetate) ⟶ $CH_4 + CO_2$

Daily gas generation are shown in figure 3.1

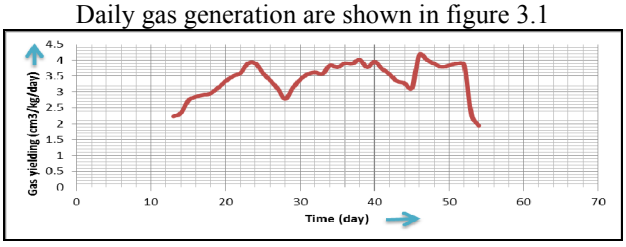

Figure-3.1: Gas Yielding rate with time

The parameter which is important in evaluating the microbial environment is the P^H of the Slurry. The P^H was varied with time during the digestion process and this parameter was the good indicator to evaluate the extent of decomposition. The optimum P^H range for most bacteria is between 6.0 and 7.5 and P^H should not rise above 8.5 [13]. It was seen that the values were in the favorable range. The standard limit of P^H is 6-9 and recorded limit is from 6.9 to 8.22.

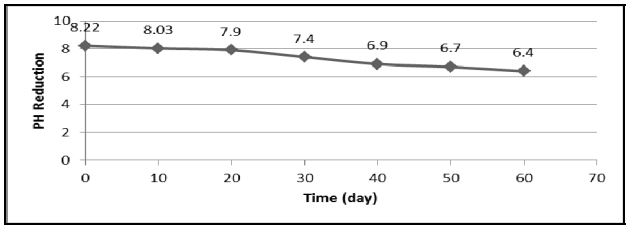

Figure 3.2: Reduction of PH with time

F. Effect of Temperature

Anaerobic breakdown of waste occurs at temperature lying between 0^oc and 69^oc, but the action of the digestion bacteria will decrease sharply below 16 ^{o}c . Production of gas is most rapid between 29 ^{o}c and 41 ^{o}c. The temperature was maintained between 32 ^{o}c ±2 ^{o}c. So the temperature was favorable for the digestion process.

G. Volatile Solid Degradation

The figure 3.3 shows time versus VS relationship. VS are an important parameter for measuring biodegradation, which directly indicate the metabolic status of some of the most delicate microbial groups in the anaerobic system. In term of VS determination the sample were taken every 10 days interval from digester and kept in oven for 24 hour at 110^oc. After 24 hour the sample were kept at 550 ^{o}c for two hour. Each time weight was measured and from weight difference VS was determined. The initial value of VS was 72% and finally reduced to 32% with time. Total VS reduction was 40%. The activities of microorganism increases with the increase of temperature, reflecting stable degradation of the substrate. The reduction of VS denotes the process of stabilization.

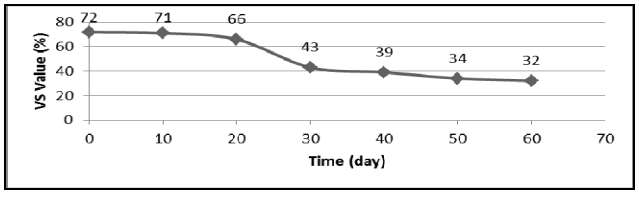

Figure-3.3: Time versus VS relationship

H. Chemical Oxygen Demand (COD) degradation

The figure 3.4 represents the COD reduction in percentage versus time relation graph. The reduction of COD started from 1.05% and finally maximum COD removed up to 37.263%. As the relation coefficient is near to 1 (positive) reduction of COD is directly related with time. The value of COD reduction is increases with time.

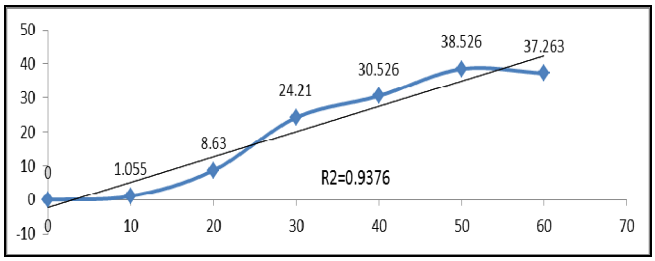

Figure -3.4Time versus reduction of COD (%) relationship

IV. CONCLUSION AND RECOMMENDATIONS

Conclusions

Tannery solid waste and municipal solid wastes have a bad impact on water body and surrounding environment. Municipal solid wastes that are thoroughly discharges from kitchen, industry etc. to the environment and polluting the environment. The study was conducted to search a proper management option for the reduction of that impact by removing their existence in environment also using them in a useful way. From this point of view my main objective of this thesis work was to recover energy from these wastes by a suitable energy recovery method. The favorable environment created by the addition of MSW and domestic sewage can explain this enhancement. The addition of domestic sewage to MSW has an inhibitory effect on Methane gas production from the mixed anaerobic cultures in slurry form in the reactor. While MSW is increases the microorganism's population, domestic sewage addition increases the concentration of available soluble substrate required by the microorganisms.

The temperature was in favorable condition that was about 32^oc±2^oc. Total VS value reduction was 40%. Volume of sludge was reduced to 53%. The maximum amount of methane production is 143.41cm3/kg. The effluent contains high nutrient content i.e. N, P, K, and sludge, respectively. These nutrients can be used as natural fertilizers in the agriculture. Successful implementation of anaerobic digestion method of waste treatment leads to the regional utilization of renewable energy resources with site-specific application depending upon local resources, energy requirements and costs. The disposal problem of MSW and domestic sewage can also be solved substantially.

A. Major findings of this study

- Tannery industry of Bangladesh producing huge amount of solid waste in which Flesh is about 50 to 60%.
- At normal temperature of 30± 2^0C; gives a good yielding rate of gas. It is ensure that at controlled supply of temperature it will give better yielding rate.

- Maximum reduction of VS up to 88% which ensure a stable degradation of the substrate in anaerobic digestion method.
- It is observed that COD value is reduced to 38% so it is a green signal not to be a bad impact on environment.
- The maximum volume reduction is of 53%. This may be due to the stable degradation of the substrate, as well as the addition of domestic sewage to stabilize the anaerobic degradation.
- Cumulative gas yielding of anaerobic co-digestion method is of 143.6cm3/Kg.
- Based on the experimental result it can be concluded that fleshing and municipal waste is potential enough for gas generation by anaerobic digestion method and it can be a good option for waste management.

B. **Limitations**

- Sample has been collected from only one tannery unit.
- Only two anaerobic digestion plants has been established where first plant did not give reading due to improper configuration of the unit.
- Tannery sample have been dried in the sun instead of oven dry to determine dry weight.
- Domestic wastes has been collected only from two domestic building

C. Recommendations

- Finally it can be said that tannery wastes can be used as a raw material to produce bio-gas through anaerobic co-digestion method with MSW.

D. Recommendation for future study

- A digestion plant can be set up changing the percentage of raw materials.
- Other raw materials can be added into the digestion plant.
- A study can be run on residual of co-digestion plant to use as compost in agricultural field.

ACKNOWLEDGMENT

First of all the author wishes to express his great thanks to almighty Allah. Then the author wishes to express his heartiest respect to his supervisor Shilpy Rani Basak, Department of Civil and Environmental Engineering Shahjalal University of Science and Technology, Sylhet for her continual supervision, precious suggestions and requisite recommendations at every stage of this study.
Author is also great full to his thesis examiner Dr. Mushtaq Ahmed, Professor and Dr. Md. Tauhidur Rahman, Associate Profesor, Department of Civil and Environmental Engineering for their invaluable guidance and sympathetic advice throughout the thesis work.

Assistance provided by Md. Nazrul Islam, Assistant instrument Engineer and A.H.M Humayun Kabir, Assistant Technical Officer throughout the thesis work is duly acknowledged.

Author is deeply indebted to his family, friends, and younger brothers for their cordial help to complete this research.

REFERENCES

1. M.Z. Hossain, S.M. Shahnewaz, “A study on existing Management of Tannery Solid Waste”, BSc thesis, Department of Civil and Environmental Engineering, Shahjalal University of Science and Technology, Sylhet, Bangladesh, 2011.
2. S. Booth, A.J. Long and V.L. Laddy, “Converting tannery waste to Energy”, BLC Leather technology Centre, UK,1995.
3. E.A.K. Hague, I.M. Faisal and A. Bayes, “Human Health and Human Welfare Costs of Environmental pollution from the tannery Industry in Dhaka”- an EIA study, Report presented at the midterm review workshop ill Yogyakarta, Indonesia, Sept1977.3-8.
4. CADDET, “Food waste disposal using anaerobic digestion”, Technical brochure No.66, Centre for the Analysis and Dissemination of demonstrated Energy Technologies (CADDET), Oxford shire, UK1998.
5. I, Raihan and S.A., Bhuya, (2006), A Study on treatment of tannery waste water, BSc thesis, Department of Civil and Environmental Engineering, Shahjalal university of Scinence and Technology, Sylhet, Bangladesh.
6. M.R.,Islam, A.S. Akmal, and S.M. Shafiq, (2006), Renewable energy resources and technologies practices in Bangladesh, Renewable and Sustainable Energy, Reviews, doi:10, 1016/j. rser.2006.07.003

Economic and Environmental Assessments of Solar Home Systems in Bangladesh

Md. Mustafizur Rahman[#1], Sayedus Salehin[#2], A.K.M. Sadrul Islam[#3]

[#] *Department of Mechanical and Chemical Engineering, Islamic University of Technology, Board Bazar, Gazipur-1704, Dhaka Bangladesh*

[1] rahman23@iut-dhaka.edu

[2] sayedus@iut-dhaka.edu

[3] sadrul@iut-dhaka.edu

Abstract— **Only about 55% of the population have access to grid electricity in Bangladesh. Diesel generator is the main source of energy supply in the off-grid regions. Use of diesel leads to increased greenhouse gas (GHG) emissions which is a big environmental concern all over the world. Solar Home Systems (SHSs) offer promising solution to the off-grid locations in the developing countries like Bangladesh. More than 3 million Solar Home Systems are installed in rural areas across the country. Most SHSs in Bangladesh use small tube lights as the lighting source. However, the recent SHSs make use of LED bulbs instead of the tube lights in order to decrease the PV panel size which would lower the initial capital cost and annualized cost. In this study, two different Solar Home Systems were analysed having tube lights and LED bulbs as the lighting source, respectively. Each of the SHSs consists of 6 lights (Tube light/LED bulb) and 2 fans with operating hours of 4 daily. The analysis shows that the SHS with tube lights requires initial capital cost of $432, which is 48% higher than the system having LED bulbs as the lighting source. As the SHSs do not use any fossil fuel, there is no operational GHG emission. However, a large amount of energy is used to manufacture PV panels, which needs to be quantified to understand the environmental impact. Energy consumption to manufacture the solar panels of Solar Home System with LED bulbs is 1.44 MWh_t which is 25% lower than the SHS with tube lights.**

Keywords— **Solar Home System (SHS); greenhouse gas (GHG); LED bulb; emission factor; solar energy**

Nomenclature

LED- Light-emitting diodes
CFL- Compact fluorescent
SHS- Solar Home System
LCA- Life cycle assessment
PV- Photovoltaics
GHG- Greenhouse gas
MWh_t- Mega-watt hour thermal energy
CO_2eq- Carbon-di-oxide equivalents

I. INTRODUCTION

Bangladesh is a small country with a huge population of 154.7 million (2013 data) [1]. Due to increasing population, economic and industrial growth, and aspiration for better living standards, the demand for energy is increasing day by day. Natural gas and coal are the main sources of primary energy supply. In Bangladesh, electricity is mainly produced from natural gas, which is accounted for 61.26% of the total installed electricity production (9821 MW), followed by furnace oil (20.87%) and diesel (8.40%) [2]. The unsatisfied demand for electricity is increasing alarmingly which causes load shedding. Only 55.2% of the population has access to grid electricity [3]. Areas that are not connected to the national grid, mainly use stand-alone diesel generators for electrification purpose. Combustion of fossil fuel releases greenhouse gases (GHGs) into the atmosphere which is a big environmental concern worldwide. In Bangladesh, power sector is responsible for producing 40% of the total CO_2 emissions [4, 5]. The country already started to face problems due to global warming. To save the environment and supply electricity to the mass people who do not have access to grid electricity, it is very important to think about the alternative renewable energy sources. Bangladesh government has a plan to generate 10% of the total electricity from renewable resources (e.g. solar, wind, biomass, hydro, etc.) by 2020 [6]. There is a huge potential of solar energy in Bangladesh with a daily solar insolation of 4.67 kWh/m^2 [7]. In different places around the country people have started to extract energy from the sun to generate electricity using photovoltaic cells. Solar Home System program has been started to ensure the access of clean electricity to the rural people. About 9% of the total population are getting electricity from 3 million SHSs that have already been installed in different areas of Bangladesh. Every month about 65,000 SHSs are now being installed [8]. Electricity generation using PV panels are free from GHG emissions. However, materials used to manufacture the components of SHSs consume energy and produce GHGs.

Many studies have been carried out that conducted the techno-economic assessment of renewable energy systems. Zubair et al. [9] designed a wind-PV-diesel hybrid energy system for a coastal area of Bangladesh. The authors found production of electricity from renewable resources is not feasible but a wind-PV-diesel hybrid energy system is financially viable. Islam et al. [10] performed a techno-economic assessment of hybrid renewable energy systems for Saint Martin's Island, Bangladesh. Using a PV-wind-diesel generator system, electricity can be produced for the location at the cost of $0.345/kWh. The hybrid system can reduce CO_2 emissions by about 14 tons/year. Different combinations of

hybrid energy systems were considered by various studies [11-14] to find the cost effective system to produce electricity from the renewable resources around the globe. There are few studies that conducted techno-economic analysis of solar photovoltaic plants. A viability study of a grid connected solar PV system in Bangladesh was carried out by Mondal and Islam [15]. Several different economic and financial indicators (e.g. internal rate of return, net present value, benefit-cost ratio, etc.) were calculated in the study. Chandel et al. [16] did an assessment of solar power plant in India and found the levelized cost of electricity and discounted payback period of $0.24/kWh and 15.53 years, respectively. Dale [17] performed a life cycle assessment of energy cost of three technologies - solar photovoltaic, concentrating solar power and wind, and found wind energy has the lowest energy cost. Mondal and Islam [18] conducted a feasibility study of a grid connected PV system of 500 kW and found the unit cost $0.2. A study by Abdulkarim [19] performed a techno-economic analysis of solar energy for electric power generation in Nigeria. There are few studies that perform environmental impact assessment of solar photovoltaic systems.

Solar Home Systems of capacity 10-130 watt are most common in Bangladesh. SHS consists of 2-7 bulbs, 1 or 2 D.C. fans, and sometimes a 15" LED television. There have been few studies that conduct techno-economic assessments of SHSs. Chaurey et al. [20] found PV micro grid financially more feasible than Solar Home System for 500 densely located households using 3–4 low power appliances (e.g. 9 W CFLs) for an average of 4 h daily. Gustavsson [21] and Mondal [22] conducted feasibility studies of SHSs in Lundazi, Zambia, and Bangladesh, respectively. The author [22] found that the SHS is financially attractive and sustainable for small rural businesses and household lighting.

Life cycle assessment (LCA) is an important tool to quantify GHG emissions of a product from cradle-to-grave. Utilization of fossil fuel releases GHGs which is responsible for ozone layer depletion. Solar Home Systems are free from fossil fuel use and GHG emissions. Production of materials used in SHSs consumes energy which ultimately results in GHG emissions. There are few studies that perform LCA of PV systems of different capacities. According to a study by Peng et al. [23], GHG emission rate of thin film PV systems are within the range of 10.5–50 g-CO_2eq/kWh. Kannan et al. conducted an LCA of a 2.7 kWp distributed solar PV system in Singapore and found 217 g-CO_2/kWh GHG emissions from electricity generation from the solar PV system. 9.4 to 104 g-CO_2/kWh life cycle GHG emissions are reported by different studies [24-28] for poly-crystalline solar PV system. Ahiduzzaman et al. [29] conducted GHG emissions assessments of different renewable energy systems (solar, wind, biomass, hydro, etc.) in Bangladesh. The authors concluded that renewable energy is the key solution for mitigation of GHG emissions as well as sustainable development.

There is a scarcity of assessment of Solar Home Systems with different lighting sources (e.g. tube lights and LED bulbs) in Bangladesh. The recent SHSs make use of LED bulbs instead of the tube lights (CFL) in order to decrease the PV panel size which will ultimately affect the initial capital cost and GHG emissions. There is very limited study on techno-economic and life cycle assessments of SHSs in Bangladesh. The purpose of this study is to find the cost parameters and GHG emissions for a typical Solar Home System in Bangladesh. Techno-economic assessment and emissions assessment for a SHS consisting 6 lights (tube lights/LED bulbs) and 2 fans with daily operating hours of 4 were carried out. Techno-economic assessment was conducted using HOMER (Hybrid Optimization Model for Electric Renewables) developed by NREL (National Renewable Energy Laboratory) of the U.S. It is expected that the SHSs with LED bulbs provide an environmentally friendly and cost-effective solution for the electricity supply for off-grid communities in Bangladesh.

II. Modelling Solar Home Systems with Different Lighting Sources

In order to obtain techno-economic comparison between Solar Home Systems consisting different lighting sources, HOMER (Hybrid Optimization Model for Electric Renewables) software developed by NREL has been utilized. HOMER is an optimization software and can be used for stand-alone and grid-connected renewable energy systems. During the optimization, the tool simulates several system configurations to match the electricity supply with the load demand input within the given set of constraints. It discards the system configurations that do not adequately supply the load demand and presents the suitable configurations categorically based on the total net present cost.

The modelling of the Solar Home Systems require input data for solar radiation, solar PV sizes and costing, battery size and costing and other appropriate input values. In this study, a typical village- Char King, Hatiya (22°22' N, 91°7' E) in Bangladesh has been considered. The monthly solar irradiation data for this location has been obtained from National Aeronautics and Space Administration (NASA). Fig. 1 shows the average monthly solar radiation profile, generated from HOMER, with a scaled annual average radiation of 4.34 kWh/m^2/day and an average clearness index of 0.468.

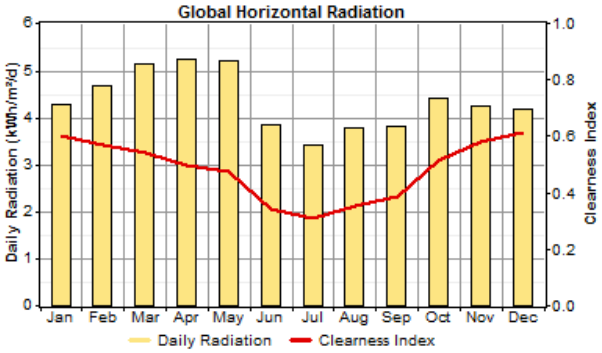

Fig. 1. Average monthly solar radiation profile for the study area

In this study, using different lighting sources (tube light and LED bulb) in Solar Home Systems were assessed. Two different SHSs for a single family home have been analysed having tube light and LED bulb as lighting sources, respectively. Fig 2 shows the energy models for SHS1 and SHS2, respectively. Each of the SHSs consists of 6 lights (Tube light/LED bulb) and 2 fans with operating hours of 4 daily. The ratings of the electrical devices are: tube light (7 watt), LED bulb (3 watt) and fan (12 watt). The operating hours for lights and fans are 1900-2300 daily. The estimated daily working hours for the fans and lights are divided into two seasons (Season 1: October – February) (season 2: March – September). In season 1, the fans are non-operational due to comparatively cool weather. Figs. 3 and 4 show the seasonal load profile for two Solar Home Systems having different lighting sources. Table I shows the load comparison between the Solar Home Systems.

TABLE I.
LOAD COMPARISON BETWEEN SOLAR HOME SYSTEMS

Lighting Source in SHS	Average Load (Wh/d)	Peak Load (W)
Tube Light	223	116
LED Bulb	128	74

Solar Home System 1 (SHS1) and Solar Home System 2 (SHS2) have been modelled in HOMER to supply the peak load demand of 116 W and 74 W, respectively. In this study, 10 W_p PV panels have been considered with a capital cost of $25 and replacement cost of $25. Vision 6FM55D battery (capital cost of $33) with nominal voltage of 12V and nominal capacity of 55 Ah has been considered for electricity storage.

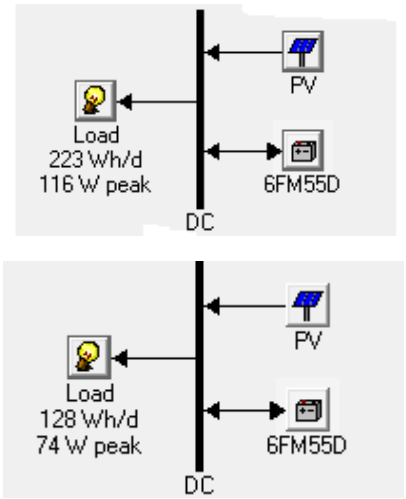

Fig. 2. Energy system models for SHS1 and SHS2, respectively

The simulations reveal the optimized system configuration for SHS1 and SHS2 and the values are presented in Table II. In SHS1 (with tube light), PV panels having 120 W_p rated capacity are required to supply the load demand whereas SHS2 (with LED bulb), 90 W_p PV panels are required. The optimized result shows that SHS2 (with LED bulbs) requires initial capital cost of $291, which is 48% lower than the system having tube lights as the lighting source. Also SHS2 has a total net present cost of $313 as compared to $475 for SHS1.

TABLE II.
SYSTEM CONFIGURATIONS FOR SHS1 AND SHS2

Lighting Source in SHS	PV (W_p)	Battery (Ah)	Initial Capital ($)	Operating Cost ($/yr)	Total Net Present Cost ($)
Tube Light	120	220	432	6	475
LED Bulb	90	110	291	3	313

III. LIFE CYCLE ASSESSMENT

Life cycle assessment (LCA) is an extremely useful tool to evaluate environmental impacts of a product through its entire life, well-to-wheel. ISO 14040 [30] and ISO 14044 [31] talk about principles and framework, and requirements and guidelines of LCA, respectively. According to ISO 14040 [30] and ISO 14044 [31], there are four phases of life cycle assessment which are shown in Fig. 5.

For an LCA, the first step is to clearly articulate the goal and scope followed by inventory analysis and environmental impact assessment. The goal and scope definition includes identifying the purpose of the LCA study and defining the system boundary and functional unit (i.e., kg-CO_2eq). The inventory analysis involves the quantification of inputs (i.e., energy use) and outputs (i.e., emissions) of each stage inside the system boundary. The interpretation phase of the LCA conveys the results that are in consistent with the defined goal and scope of the study.

A. Goal and Scope

The purpose of the study is to quantify energy consumption and GHG emission reduction if tube lights are replaced by LED bulbs in the Solar Home Systems. Solar PV is the most energy intensive component of the solar home system. In this study energy consumption and resulting GHG emissions were quantified to manufacture solar PV used in Solar Home Systems (e.g. with tube lights and with LED bulbs). Energy consumption to manufacture charge regulator, batteries are out of the scope of this research.

B. Method

Solar home system consists of 6 lights (tube lights/LED bulbs) and 2 fans with daily operating hours of 4. Tube lights are 7 watt each, LED bulbs are 3 watt each, and fans are of 12 watts D.C. Daily loads were given as input to HOMER software. Homer performs the simulation and found the sizing of PV for the both solar home systems. SHS1 with tube light

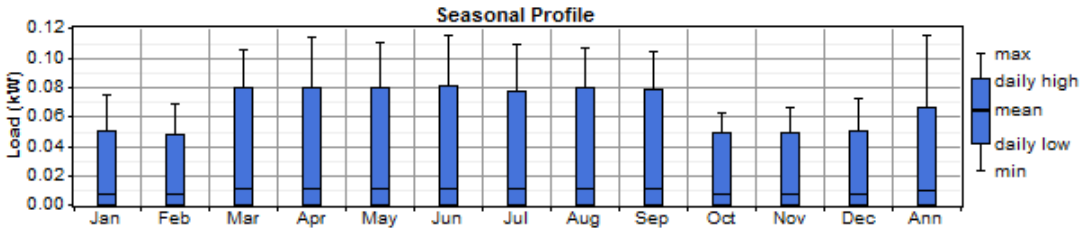

Fig. 3. Seasonal load profile for Solar Home System 1 (tube light as lighting source)

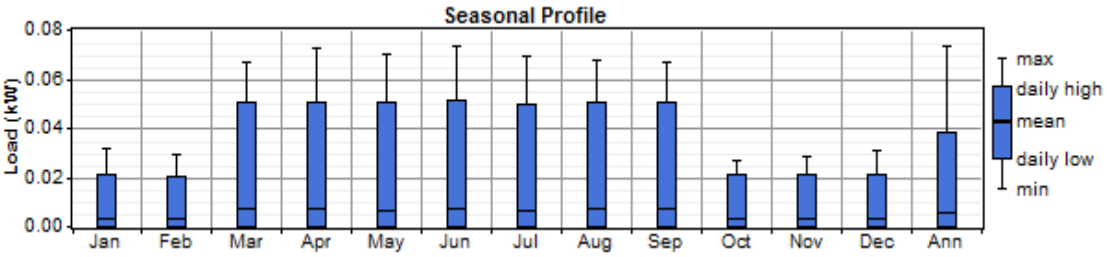

Fig. 4. Seasonal load profile for Solar Home System 2 (LED bulb as lighting source)

(CFL) need 0.12 kW_p PV panel and SHS2 with LED bulbs need a PV panel of 0.09 kW_p.

Numerous studies [32-35] have been carried out to quantify the energy consumption in manufacturing of mono-crystalline solar PV modules. The energy consumption to manufacture PV modules varies from 11-45 kWh_t/kW_p. Karl et al. [35] quantified energy consumption to manufacture the solar PV module used in the solar PV system and its specific energy consumption is 16 MWh_t/kW_p. This value is used in this research. Thermal energy was converted to electrical energy with an assumed thermoelectric conversion efficiency of 35% [36]. To get the total GHG emissions, the energy consumption was multiplied by the grid emission factor of the country where the PV panels are manufactured.

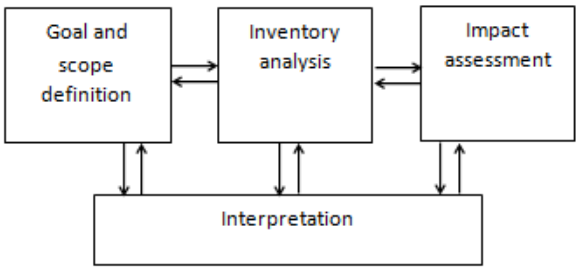

Fig. 5. LCA framework. Adapted from ISO 14040 [30]

C. Results and Discussion

The energy consumption to manufacture the PV panels used in SHS1 (with tube lights) is 1.92 MWh_t. Use of LED bulbs instead of tube lights (CFL) lowers the sizing of PV panels by 25% which is a big advantage from environmental point of view. The energy consumption is reduced by 25% when LED bulbs are used. Solar PV panels are imported to Bangladesh mainly from Germany, France, China, and Japan. In this study these countries were considered. Grid emission factors were taken from ref. [37] for the countries considered. Table III represents the energy consumption and resulting GHG emissions from solar PV manufactured in Germany.

TABLE III.
THE ENERGY CONSUMPTION AND GHG EMISSIONS FROM MANUFACTURING OF PV PANELS (GERMANY) USED IN SHS1 AND SHS2

Parameters	SHS1	SHS2
Energy Consumption (MWh_t)	1.92	1.44
Grid Emission Factor (kg-CO_2eq/kWh_t)	0.675	0.675
GHG Emissions (kg-CO_2eq)	453.68	340.26

Table IV represents the energy consumption and resulting GHG emissions from solar PV manufactured in France.

TABLE IV.
THE ENERGY CONSUMPTION AND GHG EMISSIONS FROM MANUFACTURING OF PV PANELS (FRANCE) USED IN SHS1 AND SHS2

Parameters	SHS1	SHS2
Energy consumption (MWh_t)	1.92	1.44
Grid Emission Factor (kg-CO_2eq/kWh_t)	0.071	0.071
GHG Emissions (kg-CO_2eq)	47.81	35.86

Tables V and VI represent the energy consumption and resulting GHG emissions from solar PV manufactured in China and Japan, respectively.

TABLE V.
THE ENERGY CONSUMPTION AND GHG EMISSIONS FROM MANUFACTURING OF PV PANELS (CHINA) USED IN SHS1 AND SHS2

Parameters	SHS1	SHS2
Energy Consumption (MWh_t)	1.92	1.44
Grid Emission Factor (kg-CO_2eq/kWh_t)	0.973	0.973
GHG Emissions (kg-CO_2eq)	653.59	490.19

TABLE VI.
THE ENERGY CONSUMPTION AND GHG EMISSIONS FROM MANUFACTURING OF PV PANELS (JAPAN) USED IN SHS1 AND SHS2

Parameters	SHS1	SHS2
Energy Consumption (MWh_t)	1.92	1.44
Grid Emission Factor (kg-CO_2eq/kWh_t)	0.443	0.443
GHG Emissions (kg-CO_2eq)	297.90	223.42

Greenhouse gas emissions do not only depend on the energy consumption but also on regional electricity mix. It can be seen that, if the PV modules are manufactured in Germany, GHG emissions are increased by 89% compared to the case of France. Instead of using CFL lights, if LED bulbs are used, GHG emissions can be reduced by 25%.

IV. CONCLUSIONS

This paper estimates the cost of two different Solar Home systems (SHSs) consisting tube lights and LED bulbs, respectively. The analysis shows that the SHS with tube lights requires 48% higher initial cost than the system having LED bulbs as the lighting source. Using LED bulbs as the lighting source in the SHSs is also proved to be environmentally friendly.

REFERENCES

[1] Bangladesh Country Report. 2014 [cited 2015 June 06]; Available from: www.bti-project.org/uploads/tx_itao.../BTI_2014_Bangladesh.pdf.

[2] Annual Report. 2013-2014, Bangladesh Power Development Board. [cited 2015 June 06]; Available from: http://www.bpdb.gov.bd/bpdb/index.php?option=com_content&view=article&id=75&Itemid=81.

[3] The World Bank. [cited 2015 June 29]; Available from: http://data.worldbank.org/indicator/EG.ELC.ACCS.ZS.

[4] ADB. Asia least-cost greenhouse gas abatement strategy (ALGAS) Bangladesh. Asian Development Bank. Manila; 1998.

[5] R.M. Shrestha, G. Anandarajah, and M.H. Liyanage, "Factors affecting CO_2 emission from the power sector of selected countries in Asia and the Pacific," *Energy Policy*, vol. 37(6), pp. 2375-2384, 2009.

[6] M.A.H. Mondal and M. Denich, "Assessment of renewable energy resources potential for electricity generation in Bangladesh," *Renewable and Sustainable Energy Reviews*, vol. 14(8), pp. 2401-2413, 2010.

[7] NASA Surface Meteorology and Solar Energy. [cited 2015 June 29]; Available from: https://eosweb.larc.nasa.gov/sse/.

[8] IDCOL, Solar Home System Program. [cited 2015 June 29]; Available from: http://idcol.org/home/solar.

[9] A. Zubair, A.A. Tanvir, and M.M. Hasan, "Optimal Planning of Standalone Solar-Wind-Diesel Hybrid Energy System for a Coastal Area of Bangladesh," *International Journal of Electrical and Computer Engineering*, vol. 2(6), pp. 731-38, 2012.

[10] A.K.M.S. Islam, M.M. Rahman, M.A.H. Mondal, and F. Alam, "Hybrid energy system for St. Martin Island, Bangladesh: An optimized model," *Procedia Engineering*, vol. 49(0), pp. 179-188, 2012.

[11] C. Li, X. Ge, Y. Zheng, C. Xu, Y. Ren, C. Song, and C. Yan, "Techno-economic feasibility study of autonomous hybrid wind/PV/battery power system for a household in Urumqi, China," *Energy*, vol. 55(0), pp. 263-272, 2013.

[12] G. Rohani and M. Nour, "Techno-economical analysis of stand-alone hybrid renewable power system for Ras Musherib in United Arab Emirates," *Energy*, vol. 64(1), pp. 828-841, 2013.

[13] M.S. Ngan and C.W. Tan, "Assessment of economic viability for PV/wind/diesel hybrid energy system in southern Peninsular Malaysia," *Renewable and Sustainable Energy Reviews*, vol. 16(1), pp. 634-64, 2012.

[14] A. Ghasemi, A. Asrari, M. Zarif, and S. Abdelwahed, "Techno-economic analysis of stand-alone hybrid photovoltaic–diesel–battery systems for rural electrification in eastern part of Iran –A step toward sustainable rural development," *Renewable and Sustainable Energy Reviews*, vol. 28(0), pp. 456-462, 2013.

[15] A.H. Mondal and A.K.M. Sadrul Islam, "Potential and viability of grid-connected solar PV system in Bangladesh," *Renewable Energy*, vol. 36(6): pp. 1869-1874, 2011.

[16] M. Chandel, G.D. Agarwal, S. Mathur, and A. Mathur, "Techno-economic analysis of solar photovoltaic power plant for garment zone of Jaipur city," *Case Studies in Thermal Engineering*, vol. 2(0), pp. 1-7, 2014.

[17] M. Dale, "A Comparative Analysis of Energy Costs of Photovoltaic, Solar Thermal, and Wind Electricity Generation Technologies," *Applied Sciences*, vol. 3(2), pp. 325-37, 2313.

[18] M.A.H. Mondal and A.K.M.S. Islam, "Techno-economic feasibility of grid connected solar PV system in Bangladesh," *1st International Conference on the Developments in Renewable Energy Technology (ICDRET)*.IEEE Xplore, pp. 1-4, 2009.

[19] H.T. Abdulkarim, "Techno-economic analysis of solar energy for electric power generation in Nigeria," http://www.journal.au.edu/au_techno/2005/apr05/vol8no4_abstract09.pdf.

[20] A. Chaurey and T.C. Kandpal, "A techno-economic comparison of rural electrification based on solar home systems and PV microgrids," *Energy Policy*, vol. 38(6), pp. 3118-3129, 2010.

[21] M. Gustavsson, "With time comes increased loads—An analysis of solar home system use in Lundazi, Zambia," *Renewable Energy*, vol. 32(5), pp. 796-813, 2007.

[22] M.A.H. Mondal, "Economic viability of solar home systems: Case study of Bangladesh," *Renewable Energy*, vol. 35(6), pp. 1125-1129, 2010.

[23] J. Peng, L. Lu, and H. Yang, "Review on life cycle assessment of energy payback and greenhouse gas emission of solar photovoltaic systems," *Renewable and Sustainable Energy Reviews*, vol. 19(0), pp. 255-274, 2013.

[24] R. Battisti and A. Corrado, "Evaluation of technical improvements of photovoltaic systems through life cycle assessment methodology," *Energy*, vol. 30(7), pp. 952-967, 2005.

[25] Y. Tripanagnostopoulos, M. Souliotis, R. Battisti, and A. Corrado, "Energy, cost and LCA results of PV and hybrid PV/T solar systems," *Progress in Photovoltaics: Research and Applications*, vol. 13(3), pp. 235-250, 2005.

[26] M. Ito, K. Kato, H. Sugihara, T. Kichimi, J. Song, and K. Kurokawa, "A preliminary study on potential for very large-scale photovoltaic power generation (VLS-PV) system in the Gobi desert from economic and environmental viewpoints," *Solar Energy Materials and Solar Cells*, vol. 75(3–4), pp. 507-517,2003.

[27] H. Hondo, "Life cycle GHG emission analysis of power generation systems: Japanese case," *Energy*, vol. 30(11–12), pp. 2042-2056, 2005.

[28] S. Pacca, D. Sivaraman, and G.A. Keoleian, "Parameters affecting the life cycle performance of PV technologies and systems," *Energy Policy*, vol. 35(6), pp. 3316-3326, 2007.

[29] M. Ahiduzzaman and A.K.M.S Islam, "Greenhouse gas emission and renewable energy sources for sustainable development in

Bangladesh," *Renewable and Sustainable Energy Reviews*, vol. 15(9), pp. 4659-4666, 2011.

[30] ISO 14040: 2006 - Environmental management - Life cycle assessment - Principles and framework. 2006, International Organization for Standardization. Available from: http://www.iso.org/iso/catalogue_detail?csnumber=37456.

[31] ISO 14044: 2006 - Environmental management- Life cycle assessment- Requirements and guidelines. 2006, International Organization for Standardardization. Available from: http://www.iso.org/iso/catalogue_detail?csnumber=38498.

[32] K. Kato, A. Murata, and K. Sakuta, "An evaluation on the life cycle of photovoltaic energy system considering production energy of off-grade silicon," *Solar Energy Materials and Solar Cells,* vol. 47, pp. 95–100, 1997.

[33] G. Hagedorn, "Hidden energy in solar cells and photovoltaic power station," *Proceedings of 9th PV specialist conference*, Germany, pp. 542–546, 1989.

[34] J. Mathur, N.K. Bansal, and H.J. Wagner, "Energy and environmental correlation for renewable energy systems in India," *Energy Sources,* vol. 24, pp. 19–26, 2002.

[35] E.K. Karl and L.J. Theresa, "Initial empirical results for the energy payback time of photovoltaic modules," Siemens Solar Industries, Camarillo, 2002.

[36] R. Garcı´a-Valverde, C. Miguel, R. Martı´nez-Be´jar, and A. Urbina, "Life cycle assessment study of a 4.2kW$_p$ stand-alone photovoltaic system," *Solar Energy,* vol. 83, pp 1434–45, 2009.

[37] Technical Paper, Electricity-specific emission factors for grid electricity. [cited 2015 June 06]; Available from: http://ecometrica.com/assets/Electricity-specific-emission-factors-for-grid-electricity.pdf.

Five Years of Solar Minigrid Service in Sandwip Island of Bangladesh

Hasna J. Khan[1], Asma J. Huque[2]
Kaysar Ahmed[3], Rafiur Rahman[4], Tanvir Ahmed[5], and Rashedul Alam[6]
[1, 2, 3, 4, 5, 6]Prokaushali Sangsad Limited (PSL), Dhaka, Bangladesh
[1]hasnajkhan@gmail.com

***Abstract*— PGEL is the only utility company in the country operating as a solar mini grid service provider for five years. Its pioneering experience has become a learning platform for other private investors, financing and development agencies, in addition to the policy makers. Some of the national clean energy policy decisions for off-grid rural electrification business models are being made using the experience gained from solar mini grid service to Enam Nahar Market. It is observed that the solar PV hybrid is a viable technical option for rural electrification of rural markets; however, a discounted loan term of 15 years minimum is needed to keep such investments attractive and profitable to the private investors.**

Keywords— Bangladesh; Solar mini-grid; Off- grid electrification service; Sandwip island.

I. INTRODUCTION

Distributed power has shown its favored place in Bangladesh in the past decade through the widespread use of Solar Home Systems. Application of SHS, predominantly in the rural areas, has created the industrial base for the components that go along with them. Investors have leaned toward manufacturing various parts of a SHS, while import of solar modules have sky rocketed in the past decade. In a country where solar energy was established as a complementary solution to grid electrification in the early 2000 (REF), national interest has proven it to be the most viable alternative today.

Similar to SHS, solar mini grid is now viewed to have the capability of providing a solution for rural off-grid areas. Although rural markets show the maximum potential for solar mini grid application, clustered households adjacent to the markets are also additional consumers to any service provider. A comprehensive cost benefit analysis of the service delivery model for solar mini grid shows the necessary mix of the customer types. This includes a balance of large consumers with high rate of daily turnover, consumers of medium demand mainly offices and businesses, and small consumers which represent small shops and households. An optimum blend of these categories is desirable for getting maximum socio-economic return on investment.

Most recent advancement in solar mini grids has created a new opportunity for clean energy solutions for the commercial markets in particular [1] [2]. It has also been observed that mini grid electrification can become more cost effective in certain situations as compared to its alternatives [3], [4]. Privately owned utility Purobi Green Energy Limited (PGEL) has provided reliable power supply to the remote Sandwip island community since 2010, receiving technical support from Prokaushali Sangsad Limited (PSL). Reliable electrification from PGEL has resulted in more investment in economic activities and new housing within the electrified area.

TABLE-1: ENERGY CONSUPMTION OF PGEL CONSUMER TYPES

Consumer Type	Total Number	Total kWh
Small and medium enterprise	169	204,512
Institutions	60	165,970
Households	53	31,106
Small Industry	6	7,863

II. RESULTS

Commercial businesses, medical clinics, banks, and others, need reliable electricity to use adequate lights, fans, electrical appliances, and computers. PGEL currently provides solar mini grid service to 288 consumers in Enam Nahar market. Up to August 2015, the plant has generated more than 410 MWh energy with a specific yield of 86.8 kWh/kWp displacing 290 Ton of CO2 since the commissioning month of October 2010. Though the plant is running with full capacity, still several people or organizations or shops are coming to PGEL office to get the connection. Under the circumstances PGEL management has adopted strict measures for demand side management and decided to provide new connections with ensuring specific terms & condtions like; usages of energy efficient appliances (LED light), and running the motor based appliances only at day time. Up to August 2015 the service was being offered to a 288 consumers who had taken connection gradually over five years, as shown in Figure 1 and Figure 2.

Monthly Load pattern: Monthly energy consumption has been shown in Figure 3 up to August 2015. The early growth in energy demand is related to the increase in the consumer base of PGEL (Figure 1). Overall trend in energy consumption has a periodic nature which follows the seasonal demand for energy. During the winter months of November to January there is less

TABLE-2: ENERGY CONSUMPTION OF PGEL CONSUMER CATEGORIES

	Consumer		Energy	
Consumer Class	**Nos.**	**%**	**Total kWh/Mon**	**%**
Large Consumers (>100 kWh)	22	8%	5,038	44%
Medium Consumers (41-100 kWh)	49	17%	3,087	27%
Small Consumers (1-40 kWh)	217	75%	3,255	29%
Total Consumers	288	100%	11,380	100%

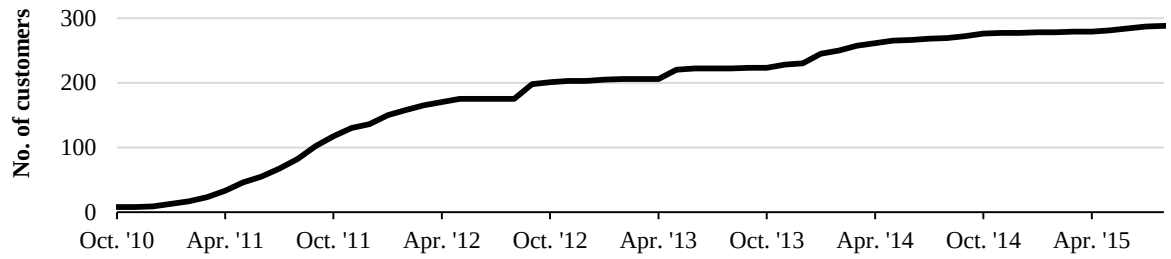

Fig 1: PGEL consumer growth rate (2010-2015)

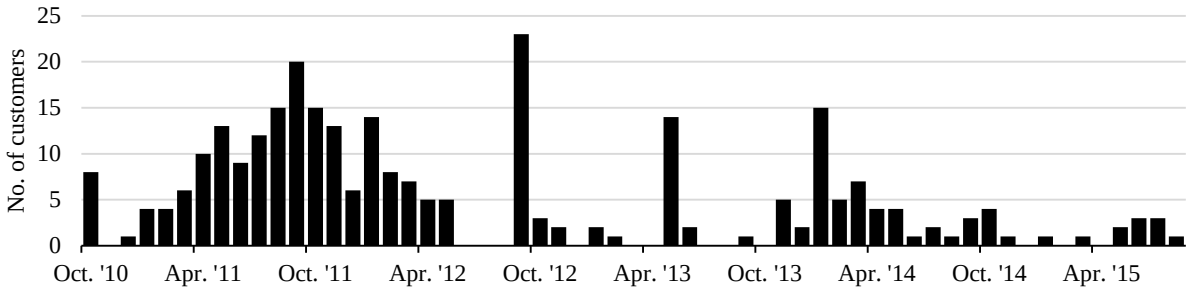

Fig 2: Consumer connection rate for PGEL(2010-2015)

use of fans, hence peak consumption during winter is nearly 20 percent less than peak energy in summer. Unfortunately, this timing coincides with the onset of overcast days from monsoon. An energy service provider like PGEL has to be prepared to meet this increasing demand in June through September in spite of the decreasing generation from solar. In peak energy season April to October, the maximum consumption of energy is more than 13,000 kWh and in winter November to March, it is about 7,500 kWh per month. Diesel backup system is operational during this gap period, which results in higher operating cost for the plant.

Daily Load Pattern: Average daily load pattern of a day in June is shown in Fig 4, showing two identifiable peaks in total energy usage pattern. One peak appears at 12 noon when the offices, health centers and institutions are in full operation, and major fraction of energy is going into fan with other appliances like computers, motorized equipment. Another peak appears between 7 to 8 PM, mainly for evening lighting and other commercial activities of the SMEs in the market. Most energy consumed by the load during the peak daytime is directly supplied by the grid tied inverters. During this period the bi-directional inverters are expected to feed surplus energy to the battery bank. The direct chargers are also designed to feed into the batteries, which are an important resource for evening load. Any shortage of energy from PV or battery will kick-start the generator based on battery management system. Hence, an ideally designed PV hybrid plant should balance the available resources from solar PV, battery bank and generator. Figure 5 demonstrates the revenue earned by PGEL during its five years of operation. The profile is quite identical to the load profile for the period; PGEL has collected approximately USD 3000 per month.

The financing plan of IDCOL has required PGEL to repay its loan within a short time compared to the usual 20 year lifecycle of solar projects. PGEL paid only the interest on its loan during the first 2 years. The capital has to be paid back in the next 8 years, which creates a heavy financial burden for the private investors. In addition to the debt service payments, continuously increasing maintenance cost for the generator and need for creating a fund for replacement of battery and generator, are matters of real concern for the operator. It is therefore recommended that similar initiatives should be designed for a tenor of minimum 15 years at a discounted rate in order to promote interest among the private sector investors engaged in energy services to the remote off-grid locations.

III. Conclusion

Solar electrification service to the remote rural market it Bangladesh is the primary activity of PGEL. It demonstrates technical and business viability for operating solar mini grid in the remote, off grid locations of Bangladesh. PGEL is the only utility company in the country, which is operating as a solar mini grid service provider for over five years, receiving technical support from Prokaushali Sangsad Limited (PSL). Hence, this pioneering experience has become a learning platform for other investors, financing and development agencies, in addition to the policy makers. Some of the national clean energy policy decisions for off-grid rural electrification business models are being made using the experience gained from Enam Nahar Market in Sandwip. However, it is evident that financial viability of the solar PV hybrid mini grid service requires extended loan tenor of at least 15 years to make such services attractive to the private investors.

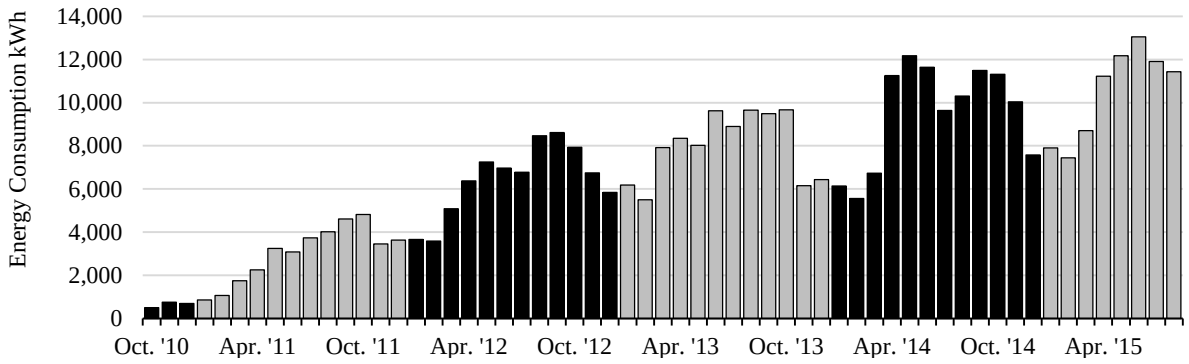

Fig-3: monthly energy consumption (kwh) pattern in sandwip minigrid

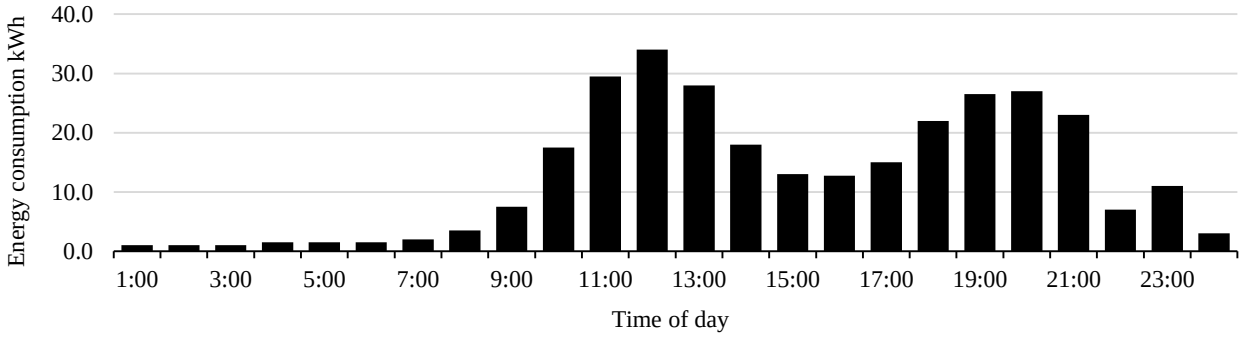

Fig 4 daily energy consumption (kWh) pattern on a summer day in Sandwip mini grid

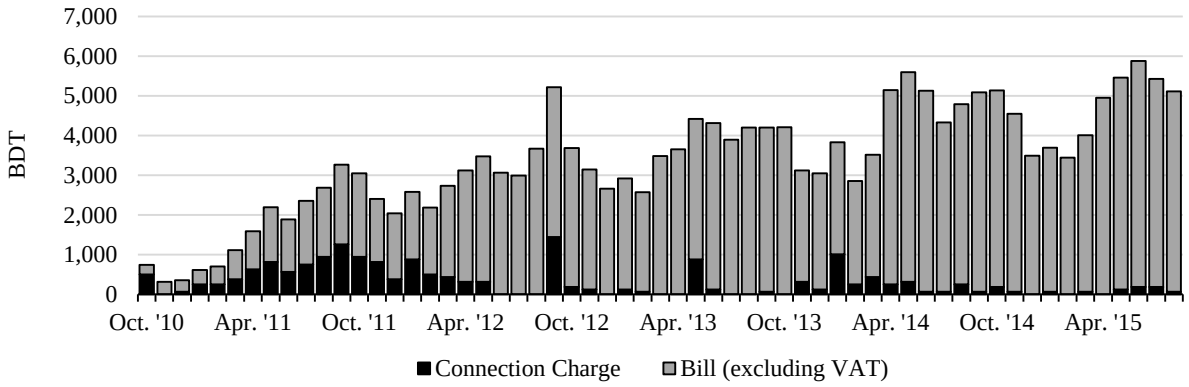

Fig 5 month-wise revenue earned by Sandwip mini grid

REFERENCES

[1] Hasna J. Khan, Asma J. Huque, Kaysar Ahmed Sagor, Tanvir Ahmed, Rashedul Alam, M. Riazul Hamid, "Experience from First Solar Mini Grid Service in Bangladesh," in *Decentralized Solution for Developing Economies Springer Proceedings in Energy*, pp 43-52, March 2015

[2] Khan, H.J.; Huque, A.J., "Reliable power supply with solar mini grid in Sandwip Island of Bangladesh," in *Developments in Renewable Energy Technology (ICDRET), 2012 2nd International Conference on the* , vol., no., pp.1-4, 5-7 Jan. 2012.

[3] Kirubi C,Jacobson A,Kammen D, and A Mills."Community-based electric micro-grids can contribute to rural development: Evidence from Kenya". World Development 37:1208–1221. 2009.

[4] Leena Chandran-Wadia, Shruti Mahajan Deorah, Sameer Nair and Anshuman Lath, "Prospects for Electricity Access in RuralIndia Using Solar Photovoltaic Based Mini-Grid Systems," in Decentralized Solution for Developing Economies Springer Proceedings in Energy, pp 52-64, March 2015.

Performance Study of Lead-Acid Battery in a Solar Car under Different Traffic and Weather Conditions

Abdullah Al Mahmud[1], Imran Bin Jafar[2], Asif Zaman[3], Mosaddequr Rahman[4]

School of Engineering and Computer Science, BRAC University
66 Mohakhali C/A, Dhaka-1212, Bangladesh

[1]mahmud.abdullah@bracu.ac.bd, [2]imranjafar@bracu.ac.bd, [3]asifzaman007@gmail.com, [4]mosaddeq@bracu.ac.bd

Abstract— **In this paper performance of lead-acid battery in a solar car, proposed earlier for Dhaka city dwellers, has been studied under different traffic and weather conditions while the car travels in a long route of Dhaka city. A model of the electric drive system of the proposed car, developed in Matlab Simulink, is used to investigate the battery response. It has been observed that the energy required by the car when it travels 30% of the road at the top speed of 60 km/hour is about 65% of the energy required when it travels 90% of the road at that speed, which further decreases with the increase of number of stoppages. Because of this feature, the proposed solar car appears to be an appropriate means of transport in Dhaka, the city with quotidian traffic congestion. In addition of being emission free, it also ensures less energy consumption during heavy traffic congestion compared to a fuel driven car which burns more fuel and releases more toxic gases under the same road conditions.**

Keywords— **Solar car, SIMULINK, Batteries, Modelling, State of charge.**

I. INTRODUCTION

Fuel driven cars remain one of the major modes of transportation of Dhaka city despite their detrimental effects to environment and public health due to emission of toxic gases. Particularly during rush hours, high traffic congestion brings the cars to standstill position for long period of time, causing them to burn more fuel and emits more gases. To help mitigate this problem, a solar powered lightweight and economically affordable car was proposed in [1] for the Dhaka city dwellers. The car was designed to run mostly on solar power under bright sun of summer and spring, and with a supportive source for charging of the batteries during winter and under cloudy sky.

In a solar car, batteries are critical parts requiring special care to ensure long life and a safe journey. Moreover, batteries cannot be charged quickly, unlike fuel driven cars which can be refueled quickly. It is therefore important to investigate the performance of the battery on the road under different traffic and weather conditions before a real trip is made. This paper targets to investigate the response of lead-acid battery which is widely available and low prices, in the proposed solar car for different road and weather context, when the car travels from home to office on one of the longest routes of Dhaka city measured as 18 km long.

Performance analysis has been carried out by simulating a model of the electric drive system of the car in Simulink, using different specifications parameters collected from a solar car under development in BRAC University workshop [2]. Discharge characteristics of the batteries, i.e., the change in the state of charge (SOC) and the terminal voltage (V_t) during the course of the trip under different traffic and weather conditions have been investigated. Solar panels are not included in the analysis as they do not affect the discharge characteristics of the batteries. Aging effect and loss due to internal discharge of the batteries have also been excluded from the analysis. In the forthcoming sections, section II describes the models used for the battery and the motor power, section III outlines their implementation in Simulink, observation and analyses of the results under changing traffic and weather condition are provided in section IV. Lastly, section V draws the conclusion of the outcomes.

II. MODELING OF SOLAR CAR

Fig. 1 shows the block diagram of the electric drive system of the solar car consisting of solar panels charging the battery through a charge controller. Here the charge controller controls dissipation of energy. However, a controller does not impact discharge characteristics of battery in the operating range, it only works when SOC goes to any of the extreme ends. Detailed of the battery modeling and motor power calculation are discussed in the following subsections.

A. *Modelling of Battery*

The lead-acid battery model used is based on Thévenin battery model [3] as shown in Fig. 2, where R_0 and C_0 are the resistance and capacitance between the electrodes of the battery, R_S is the series resistance, V_{OC} is the open circuit voltage and I_L is the load current. All of the three parameters namely V_{OC}, R_S and V_d in Fig. 2 are functions of SOC and have been evaluated experimentally for our batteries [4].

The load current, I_L for a load which draws out power P can be calculated as [3],

$$I_L = \frac{(V_{OC} - V_d) - \sqrt{(V_{OC} - V_d)^2 - 4R_S P}}{2R_S} \quad (1)$$

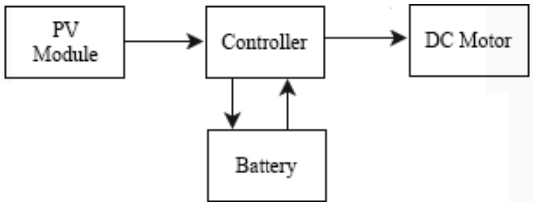

Fig. 1 Block diagram of electric drive system of the solar car

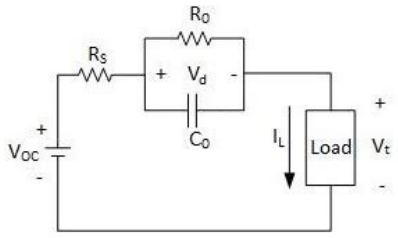

Fig. 2 Thévenin battery model

With I_L known, the terminal voltage V_t and the total charge dissipated from battery Q_{dis} in time t can be calculated as,

$$V_t = V_{OC} - I_L R_S - V_d \tag{2}$$

$$Q_{dis} = I_L t \tag{3}$$

The new SOC of the battery after time t is then given by,

$$SOC(new) = SOC(old) - \frac{Q_{dis}}{C(\theta)} \tag{4}$$

where $C(\theta)$ is the capacity of the battery which also depends on ambient temperature θ. According to [5], a relationship between the battery capacity and the ambient temperature is derived as, using a linear fitting aprroximation,

$$C = C_0(0.0082\theta - 0.77) \tag{5}$$

where C_0 is the discharge capacity at 25 ℃.

With the new SOC as calculated in (4), V_{OC}, R_S and V_d are re-evaluated according to the following relations which were determined experimentally in [4].

$$\left.\begin{aligned} V_{OC} &= 1.4667SOC - 11.0233 \\ V_d &= 0.086SOC - 0.011 \\ R_S &= -0.0531SOC + 0.066 \end{aligned}\right\} \tag{6}$$

Then the algorithm recurs with the calculation of I_L until SOC gets low enough for the process to cease.

B. *Power Calculation of DC Motor*

Power required by the motor to drive the car can be estimated by adding together individual force components that arise from different physical effects. The major three forces are the force of acceleration F_A, aerodynamic drag force F_D, force exerted by the air against the movement of the car, and the frictional force F_R, force required to overcome the frictional resistance between the wheel and the road [7]. Summing up, total driving force, F_T is obtained as,

$$F_T = F_A + F_D + F_R \tag{7}$$

The car will have a force of acceleration only when it is accelerating, otherwise it will be zero when running at a constant velocity. In (9),

$$\left.\begin{aligned} F_A &= ma \\ F_D &= \frac{1}{2} C_D \rho A_{CROSS} v^2 \\ F_R &= \mu_R mg \end{aligned}\right\} \tag{8}$$

In (8), m is the mass, A_{CROSS} is the frontal cross sectional area, v is the velocity and a is the acceleration of the car; ρ is the air mass density, C_D is the coefficient of aerodynamic drag force, g is the gravitational acceleration and μ_R is the coefficient of rolling resistance.

If the car is running at velocity v then the power exerted by the shaft of the motor can be expressed as,

$$P_T = F_T v \tag{9}$$

If the efficiency of the motor is η_m, the power to be supplied by the battery to the motor is given by,

$$P = \frac{P_T}{\eta_m} v \tag{10}$$

III. Implementation in Simulink

The implementation of the aforementioned models of battery, motor power and charge controller are described in the following subsections.

A. *Implementation of Battery Model*

Fig. 3 shows the battery model in Simulink where the required power P and charging current I_{CH} are the inputs to battery. It calculates I_L, V_t and SOC after dissipating power for a certain time and gives out as outputs. As the panels are not included in the analysis and the batteries are assumed to be fully charged at the beginning, I_{CH} remains zero throughout the analysis.

Eq(1), Eq(2) etc. labelled in the diagram refer to the corresponding equation numbers in this paper. The time interval after which the model calculates dissipated charge and records a new SOC can be fixed by the mask parameter dialog box along with the nominal capacity of the battery, initial state of charge, temperature and number of batteries in series.

B. *Implementing Load Block in Simulink*

The Simulink block of load, named 'Load' in Fig. 4, takes inputs of variable velocity on different time frames and some invariants related to the car e.g. its weight, frontal area, etc. If the car moves at velocity v_1 for time t_1, comes to a halt and rests for time t_1^r, and then starts again at v_2 for another time t_2, the input format is $v = [v_1 \quad 0 \quad v_2]$ and $t = [t_1 \quad t_1^r \quad t_2]$.

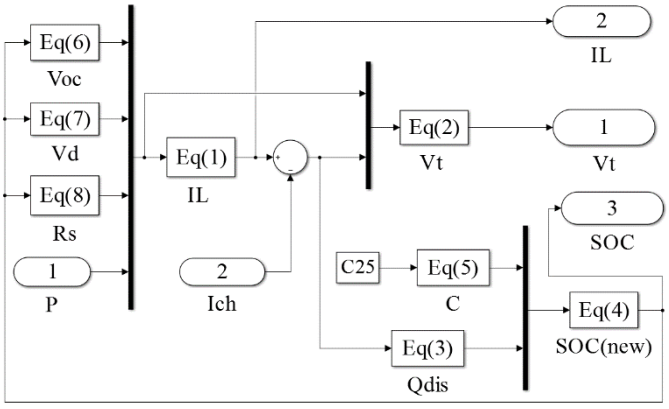

Fig. 3 Implementation of Battery model in SIMULINK

Time t_1 consists of the time at which the car accelerates from static position to reach v_1, the time it runs at constant velocity v_1, and the fall time when the car decelerates to a halt position. The inputs are transferred to a MATLAB program which gives a time-series variable *P* using the equations (7) to (10). The signal building block of load has some presets e.g. Busy road, Highway, Empty road etc. to select easily or the users may produce one according to their concern.

C. *Implementation of Charge Controller*

The charge controller works as conditional switches. In the charge controller block in Fig. 5, there is a switch between output 'P' of the load block and input 'P' of the battery block. A second switch is there in between the current 'I_{CH}' and the input 'I_{CH}' of the battery block of the same figure. When SOC goes down below a certain level, the first switch mentioned is triggered to open to disconnect the load, thereby avoid over-discharging of the batteries. The switch will close again after SOC reaches a certain level. In case of charging, the second switch is closed and is turned open after SOC reaches a high enough value to avoid overcharging.

D. *Combining the Components*

All the components portrayed in earlier sections are packed inside subsystems and combined together to build a complete model of vehicle as in shown Fig. 4. All data found by the simulation are transfered to the MATLAB workspace to plot and analyze the results.

IV. Results and Discussions

An itinerary is assumed for a Dhaka city dweller from his home to office, which is 18 km long. For the sake of convenience, it is assumed that the person leaves his home in the morning with his car fully charged and reaches his office by driving 10% of the distance at 10 kilometre per hour (kph) and rest of the road either at 30 kph or 60 kph depending on the road condition. Simulation is carried out using the parameters values as listed in Table I.

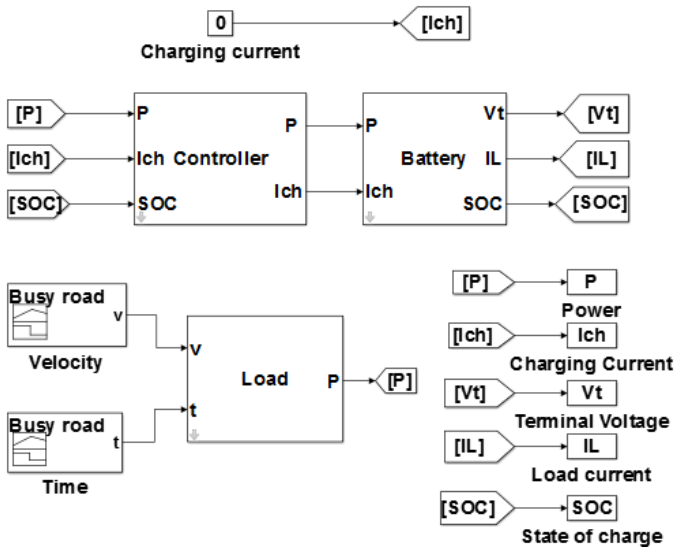

Fig. 4 The Model of the solar car combining all individual components

TABLE I Properties of Solar Car

Components	Parameters	Value
Battery [6]	Capacity of the Battery, *C* (AH)	40
	Number of Batteries in Series	5
Vehicle Platform [1]	Mass of the car, *m* (kg)	500
	Maximum velocity, v_{max} (kph)	60
	Time to get max. velocity, t_{max} (min)	1.5
	Frontal Area, A_{CROSS} (m^2)	1.1
Environment [7]	Coeff. of Rolling Resistance, μ_R	0.01
	Coeff. of Aerodynamic drag force, C_D	0.035
	Air Density, ρ (kg/m^3)	1.2

Fig. 5 shows the plots of (a) car speed, (b) required power by the motor P, (c) battery state of charge SOC and (d) the terminal voltage V_t with respect to time as the car travels at different velocities from its origin to destination. In this plot the car travels 60% of the distance at the top speed of 60 kph, 30% at 30 kph and the rest 10% at 10 kph.

For the sake of simplicity a constant acceleration and deceleration are assumed with which the car reaches the maximum speed from its rest position and comes to a halt from its maximum speed. For higher speed higher acceleration and deceleration are assumed than those at lower speed. The power required increases gradually with car speed and drops abruptly whenever it reaches the target speed, as can be seen from the power plot, plot (b) in Fig. 5. This is because as the car reaches the target speed and starts moving at constant speed, force of acceleration becomes zero requiring less power to drive. SOC plot, plot (c) of Fig. 6, shows gradual decrease in SOC with a faster drop in SOC at higher car speed.

The solid lines in Fig. 6 show how the SOC varies for a 500 kg car when it travels at the top speed of 60 kph for different lengths of the road. It can be observed that SOC drops to 77% when the car runs 90% of the road at the top speed, compared to only 85% when it runs 30% of the road at the top speed, indicating an energy requirement for the latter case which is about 65% of that required when the car travels more distances at higher speed. The requirement of higher energy at higher speed is due to the higher aerodynamic drag force which increases as the square of the velocity according to (8).

Though a car weight of 500kg is assumed initially, it is worth examining how a change in car weight will affect the battery performance, as the actual car weight can vary depending on different factors, such as, weight of passengers and baggages. The dashed line in Fig. 7 shows the variation of SOC for a 800 kg car, travelling 90% of the road at 60 kph. SOC is found to drop to about 70% at the end of the trip. This shows about 30% increase in the energy requirement for about 60% increase in the car weight when the car is running 90% of the road at the peak speed and is well within the battery capacity limit to complete the round trip.

A city like Dhaka where traffic congestion is the norm, it is also important to examin how a heavy traffic congestion would affect the battery performance. During heavy traffic congestion, the car would experience frequent stops. Fig. 7 shows how the SOC varies as the number of stoppages are increased with the car traveling 30% of the road at the top speed for all the cases. It is evident from the plots that energy

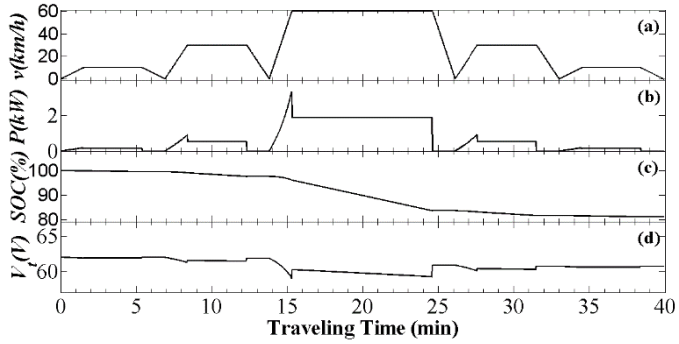

Fig. 5 Plots of (a) car speed, (b) required power, (c) state of charge and (d) terminal voltage with the car moving 30% distance at $30kph$, 60% distance at $60kph$ and 10% at $10kph$.

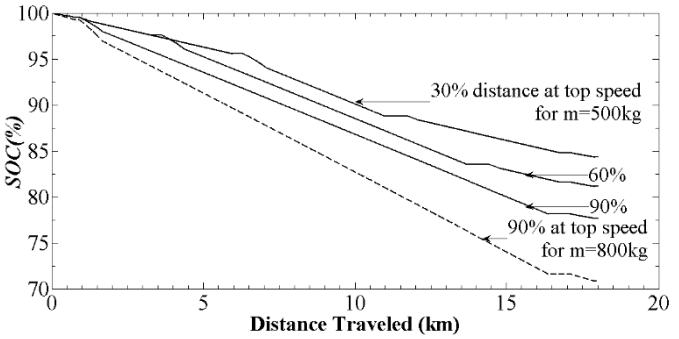

Fig. 6 Solid lines show the variation in SOC during the trip for a 500kg car travelling different lengths (30%, 60% & 90%) of the road at the top speed. Dashed line is that for a 800kg car travelling 90% of the road at the top speed.

requirement of the car will reduce with increased number of stoppages, this is due to the fact that the car covers more distances at lower speed with increased number of stoppages thus requiring less energy to overcome reduced air drag at lower speed.

Consumption of less energy at slower speed will be an added advantage over the fuel driven cars. Furthermore, fuel driven cars will keep burning fuel thus producing more pollution whenever in traffic congestion or waiting at a traffic signal, while the solar car, instead of consuming energy, will harness energy from the sun.

Seasonal temperature variation also affects the battery performance [5] and this is investigated in Fig. 9 which shows the SOC variation for different ambient temperatures, starting from 10℃ , a typical winter temperature, to 40℃ which is the temperature for a hot summer day. With the increase in the ambient temperature, the effective capacity of the battery rises according to (5). Though there is no change in the consumed energy, SOC drops to a maximum of 77% at 10℃ in winter, compared to 83% at 40℃ in summer.

V. Conclusion

Performance of lead-acid battery in a propsed solar car for Dhaka city has been investigated under different road and weather conditions, using a model developed in Simulink. It has been observed that energy requirement decreases significantly when the car runs at a slower speed than that at higher speed, which is attributed to lower air drag force at

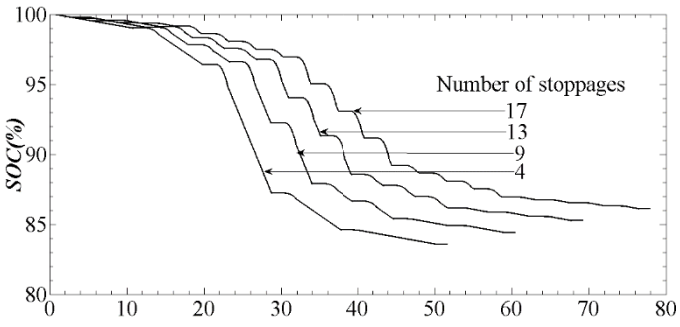

Fig. 7 Variation of SOC during a trip for different number of stoppages with the car travelling 30% of the road distance at the top speed

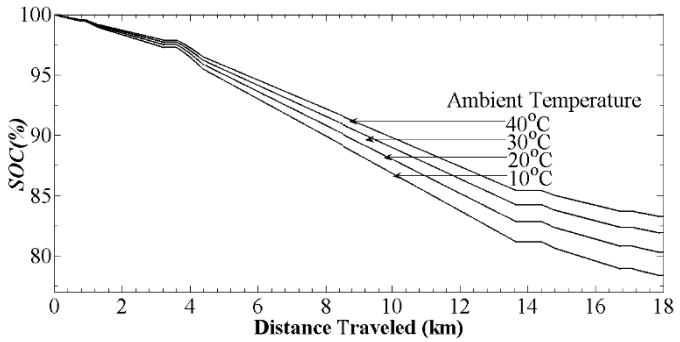

Fig. 8 Variation of SOC during the trip for different ambient temperatures with the car travelling 60% of the road distance at the top speed.

lower velocity. Thus for a city like Dhaka, where traffic congestion is a daily occurrence, solar/electric car will be a perfect mode of transportation as it is not only emission free but also consumes less energy under heavy traffic congestion. The effect of the ambient temperature on SOC elucidates the usability of the car during winter as well as during summer time. A detailed performance study of the proposed solar car under different traffic and weather conditions that also includes the solar panels is currently under way.

References

[1] S. Ahmed, A. H. Zenan and M. M. Rahman, "A two-seater light-weight solar powered clean car: Preliminary design and economic analysis," in *3rd Int. Conf. on the Develop. in Ren. Energy Tech. (ICDRET), 2014*.

[2] T. M. A. Khan, S. Rahman, M. K. Afgani and K. E. Fahim, Solar car, Dhaka: BRAC University, 2014.

[3] R. Carter, A. Cruden, P. J. Hall and A. S. Zaher, "An improved Lead-Acid battery pack model for use in power simulations of electric vehicles,"," *IEEE Trans. Energy Convers.,* vol. 27, no. 1, pp. 21 - 28, Mar. 2012.

[4] R. Tariq, S. Sabbir and S. Afrin, Dynamic electrical model of sealed Lead-Acid battery for EV simulation, Dhaka: BRAC University, 2014.

[5] M. Coleman, C. B. Zhu, C. K. Leel and W. G. Hurleyl, "A combined SOC Estimation Method Under Varied Ambient Temperature for a Lead-Acid Battery," in *Appl. Power Elect. Conf. and Exposition, 2005. APEC 2005. Twentieth Annual IEEE*, 2005.

[6] S. Leitman and B. Brant, Build Your Own Electric Vehicle, Third Edition, McGraw Hill Professional, 2013.

[7] J. P. Dunlop, "Batteries and charge control in stand-alone photovoltaic systems fundamentals and application," Florida Solar Energy Center, Cocoa, 1997.

Differential Evolution Algorithm Based Load Frequency Control in a Two-Area Conventional and Renewable Energy Based Nonlinear Power System

Muhammad Ahsan Zamee[#1], Kazi Khairul Islam[*2], Ashik Ahmed [*3] Kazi Rehnuma Zafreen[#4]

[#]*Department of Electrical and Electronic Engineering, Bangladesh University*
15/1, Iqbal Road, Mohammadpur, Dhaka-1207

[1]zamee.official@gmail.com

[4]rehnumazafreen@gmail.com

[*]*Department of Electrical and Electronic Engineering, Islamic University of Technology*
Board Bazar, Gazipur

[2]kkislam@iut-dhaka.edu

[3]ashikhmd@yahoo.com

***Abstract*— Load Frequency Control (LFC) for any power generating station is a subject of great concern for power system researchers. With the changes of load demand, frequency starts fluctuating which results in deviation in tie line power flow and frequency deviation at consumer end. To overcome this problem, many control techniques have been adopted. In early days fixed value integral/proportional-integral control, Optimal Control, Quantitative feedback theory, pole placement etc. methods were applied. In recent times, neural network, fuzzy logic, genetic algorithm controllers are replacing the conventional techniques. All the control techniques are used to find the optimal values of the PID/PI controller gain parameters (K_p, K_i, K_d) for which system stability is confirmed with minimum of Area Control Error (ACE). Differential Evolution (DE) which is a newer branch of genetic algorithms has been successfully applied in this problem. In this paper DE based PI controller has been implemented for Hydro-Thermal power plants to find out the optimal value of gain parameters for system stability. Nonlinearity has been considered in governor part of the thermal area for practical scenario. 1% step load changes have been applied to both areas simultaneously and individually to confirm its performance. Desired set of controller gain parameters (K_p, K_i) are selected based on eigenvalue and minimum value of Objective Function. All simulations are done in the MATLAB/SIMULINK environment.**

Keywords—***Load Frequency Control, Automatic Generation Control, Eigenvalue, Objective Function, Differential Evolution Algorithm, Proportional-Integral Controller.***

I. INTRODUCTION

Load Frequency Control (LFC) plays a crucial role in power system in maintaining the system frequency and power flow through tie-line at their scheduled values both under normal operating circumstance and under a small step load perturbations. Everywhere throughout the world, a large portion of the power utilities have been operating in interconnected manner because of various practical, technological and ecological considerations. Load Frequency Control is also known as Automatic Generation Control (AGC). The major goal of AGC is to balance the entire system generation against system load losses so that the preferred frequency and power interchange with neighbouring system are maintained. Any variance between generation and demand causes the system frequency to diverge from the nominal value. This high frequency deviation may lead to system breakdown.

Automatic generation control of an interconnected hydrothermal system in continuous and discrete modes considering generation rate constraints has been proposed by Nanda, J *et al* in 1983 [1]. Using the Genetic-Algorithm Based Fuzzy Gain Scheduling of PI Controllers for Load Frequency Control has been discussed by C. S. Chang *et al* in 1998 [2]. Artificial Neural Network technique based three-area power system load-frequency control was developed by Demiroren, A et al [3]. Superconducting magnetic energy storage based Automatic generation control of an interconnected hydrothermal power system was discussed by Rajesh Joseph Abraham *et al* in 2007 [4]. Fuzzy Logic Control Based Steam-Hydraulic Turbines Load Frequency Control has been developed by Ali M. Yousef *et al* [5]. Design of Robust Controller for Load Frequency Control in Deregulated Hydro-Thermal System Using Sliding Mode Controlled Strategies has been proposed by L. Shanmukha Rao *et al* [6]. M. Elsisi *et al* proposed Model Predictive Control of Nonlinear Interconnected Hydro-Thermal System Load Frequency Control Based on Bat Inspired Algorithm [7]. Recently A modified harmony search algorithm for solving load-frequency control of non-linear interconnected hydrothermal power systems is developed by Mojtaba Shivaie *et al* in 2015 [8].

Differential Evolution (DE) is a branch of evolutionary algorithms developed by Rainer Stron and Kenneth Price in 1997 for optimization problems [9]. It is a population based direct search algorithm for global optimization, which is proficient of handling non-differentiable, non-linear and multi-modal objective functions, with a small number of easily chosen control parameters. DE differs from other Evolutionary Algorithms (EA) in the mutation and recombination phases. DE uses weighted differences between solution vectors to alter the population whereas in other stochastic techniques, perturbation occurs in accordance with

an arbitrary amount. DE employs a greedy selection process with inherent elitist features In view of the above, an attempt has been made in this paper for the optimal design of DE based PI controller for LFC in two area interconnected power system considering small step load perturbation occurring in all the areas.

.

II. SYSTEM MODELLING

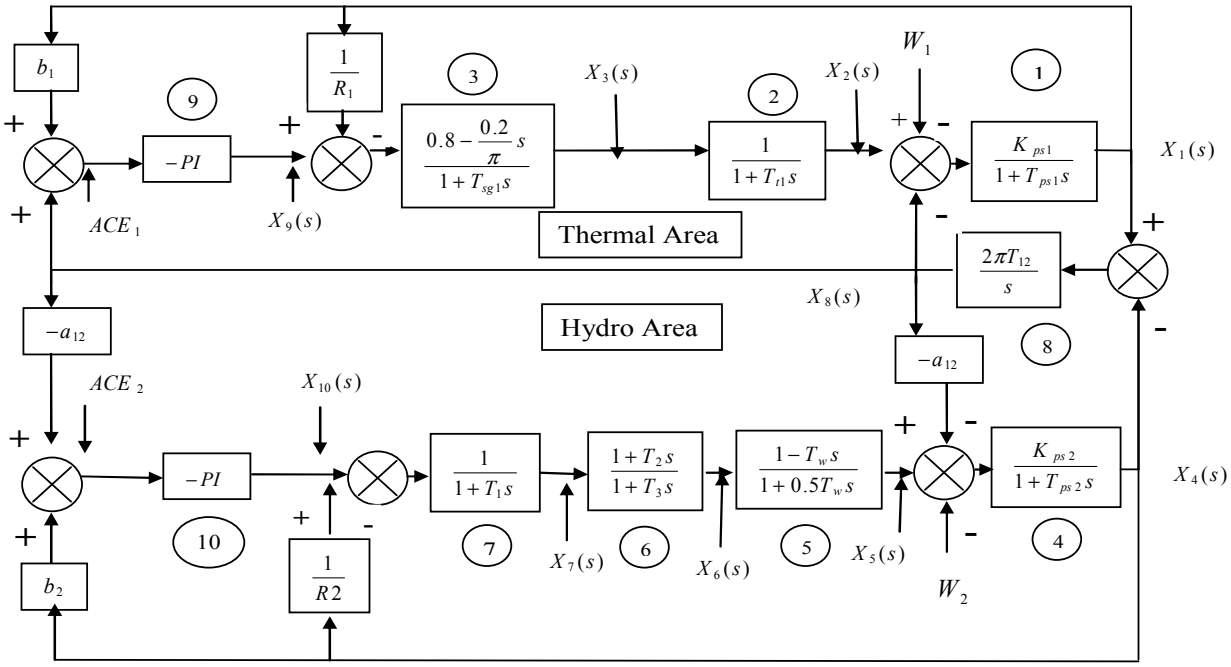

Fig. 1 Transfer function model of two area nonlinear hydro-thermal power system

Fig. 1 represents the transfer function model of an interconnected two area hydro-thermal power system. Governor deadband is considered in thermal area as nonlinearity. The model of thermal and hydro area is adopted from [10] and [4] respectively. In Fig. 1 numbers in the circle represents the block number. Physical significance of each blocks are listed in Table I with respect to the block numbers.

TABLE I

PHYSICAL SIGNIFICANCE OF BLOCKS OF TRANSFER FUNCTION MODEL

Block Number	Physical Significance
1 and 4	Transfer functions of power system and load model
2 and 5	Transfer functions of turbine of thermal and hydro power systems respectively.
3 and 7	Transfers functions of speed governor of thermal and hydro power systems respectively.
6	Transfer function of transient droop compensator of hydro power plant
8	Transfer function for deviation in tie line power flow
9 and 10	Transfer functions of PI controller of thermal and hydro power plant

Now from transfer function block diagram model it is possible to get time domain representation of each block applying the differential equation technique.

$$\dot{x}_1 = -\frac{1}{T_{ps1}}x_1 + \frac{K_{ps1}}{T_{ps1}}\left(x_2 - x_8 - w_1\right) \tag{1}$$

$$\dot{x}_2 = \frac{1}{T_{t1}}\left(-x_2 + x_3\right) \tag{2}$$

$$\dot{x}_3 = \left\{\frac{1}{T_{sg1}}\left(-\frac{0.8}{R_1} - \frac{0.2}{\pi R_1 T_{ps1}} - \frac{0.2K_{p1}b_1}{\pi T_{ps1}} + \frac{0.2K_{p1}2\pi T_{12}}{\pi} + \frac{0.2K_{i1}b_1}{\pi}\right)\right\}x_1$$
$$+\left\{\frac{0.2K_{ps1}}{\pi T_{sg1}T_{ps1}}\left(\frac{1}{R_1} + K_{p1}b_1\right)\right\}x_2 - \frac{1}{T_{sg1}}x_3 \tag{3}$$
$$-\frac{0.2K_{p1}2\pi T_{12}}{T_{sg1}}x_4 + \left\{\frac{0.2}{\pi T_{sg1}}\left(-\frac{K_{ps1}}{R_1T_{ps1}} - \frac{K_{p1}b_1K_{ps1}}{T_{ps1}} + K_{i1}\right)\right\}.$$
$$\frac{0.8}{T_{sg1}}x_8 + \left\{\frac{0.2K_{ps1}}{\pi T_{sg1}T_{ps1}}\left(-K_{p1}b_1 - \frac{1}{R_1}\right)\right\}W_1$$

$$\dot{x}_4 = \frac{1}{T_{ps2}}\left(-x_4 + K_{ps2}x_5 + a_{12}K_{ps2}x_8 - K_{ps2}W_2\right) \tag{4}$$

$$\dot{x}_5 = \frac{2T_2}{T_1T_3R_2}x_4 - \frac{2}{T_w}x_5 + 2\left(\frac{1}{T_w} + \frac{1}{T_3}\right)x_6 + \frac{2}{T_3}\left(\frac{T_2}{T_1} - 1\right)x_7 - \frac{2T_2}{T_1T_3}x_{10} \tag{5}$$

$$\dot{x}_6 = -\frac{T_2}{T_1 T_3 R_2} x_4 - \frac{1}{T_3} x_6 + \frac{1}{T_3}\left(1 - \frac{T_2}{T_1}\right) x_7 + \frac{T_2}{T_1 T_3} x_{10} \quad (6)$$

$$\dot{x}_7 = -\frac{1}{R_2 T_1} x_4 - \frac{1}{T_1} x_7 + \frac{1}{T_1} x_{10} \quad (7)$$

$$\dot{x}_7 = 2\pi T_{12}\left(x_1 - x_4\right) \quad (8)$$

$$\dot{x}_9 = \left(\frac{K_{p1} b_1}{T_{ps1}} - K_{p1} 2\pi T_{12} - K_{i1} b_1\right) x_1 - \frac{K_{p1} b_1 K_{ps1}}{T_{ps1}} x_2 + K_{p1} 2\pi T_{12} x_4 + \left(\frac{K_{p1} b_1 K_{ps1}}{T_{ps1}} - K_{i1}\right) x_8 + \frac{K_{p1} b_1 K_{ps1}}{T_{ps1}} W_1 \quad (9)$$

$$\dot{x}_{10} = K_{p2} a_{12} 2\pi T_{12} x_1 + \begin{pmatrix} \frac{K_{p2} b_2}{T_{ps2}} - K_{p2} a_{12} 2\pi T_{12} x_4 \\ - K_{12} b_2 \end{pmatrix} x_4 - \frac{K_{p2} b_{12} K_{ps2}}{T_{ps2}} x_5 + \left(K_{12} a_{12} - \frac{a_{12} K_{ps2} K_{p2} b_2}{T_{ps2}}\right) x_8 + \frac{K_{p2} b_2 K_{ps2}}{T_{ps2}} w_2 \quad (10)$$

The state variables (x_1-x_{10}) and inputs (W_1-W_2) of the system are listed in Table II.

TABLE II

STATE VARIABLES AND THEIR DESCRIPTION

State Variables	Description
$x_1 = \Delta f_1$	frequency Deviation of area 1
$x_2 = \Delta P_{t1}$	Change in turbine power output of area 1
$x_3 = \Delta Y_{E1}$	Steam valve displacement of area 1
$x_4 = \Delta f_2$	frequency deviation of area 2
$x_5 = \Delta P_{t2}$	Change in turbine power output of area 2
x_6	Transient droop compensator
$x_7 = \Delta Y_{E2}$	Steam valve displacement of area 2
$x_8 = \Delta P_{tie}$	Tie line power deviation
$x_9 = \Delta P_{c1}$	Control signal ouput of area 1
$x_{10} = \Delta P_{c2}$	Control signal output of area 2
$w_1 = \Delta P_{D1}$	Load Disturbance of Area 1
$w_2 = \Delta P_{D2}$	Load Disturbance of area 2

All together (1)-(10) can be represented as

$$\dot{x} = Ax + Bu$$

This is known as the generalized state space equation.
The controller equation used here is:

$$\Delta P_c = -\left(K_P + \frac{K_i}{s}\right) ACE \quad (11)$$

The signal ΔP_c generated by proportional-integral action must be of opposite sign to Δf.

III. DIFFERENTIAL EVOLUTION ALGORITHM

Differential Evolution Algorithm is consists of four basic strategies. They are described below

III.1 Initialization

Initial values of parameters vectors are created using the (12)

$$x_0 = x_{\min} + rand(Pop\_Size, D) \times \left(x_{\max} - x_{\min}\right) \quad (12)$$

Where, x_{max} and x_{min} is the upper and lower bound of the search space respectively. Each parameter vector contains the equal number of data as the number of population. The Number of population (NP) does not change amid the minimization process. After the initialization the DE will iterate for maximum number of generations to obtain the best result. Each population of each generation will run through the process of Mutation, Crossover and Selection sequentially.

III.2 Mutation

New parameter vectors are created by adding the weighted difference between two population vectors to a third vector. This operation is called mutation. For each target vector $x_{i,G}, i = 1,2,.....NP$, Where NP=Number of population. Equation for mutation is written below

$$v_{i,G+1} = x_G^{best} + F\left(x_{r_2,G} - x_{r_3,G}\right) \quad (13)$$

Where, $r_2, r_3 \in \{1,2,.....NP\}$, are integers and mutually different. The randomly chosen integers r_2 and r_3 are also chosen to be different from the running index i. F is a real and constant factor $\in [0,2]$ which controls the amplification of the differential variation $\left(x_{r_2,G} - x_{r_3,G}\right)$ also known as step size.

x_G^{best} = Value of target vector of previous generation for which minimum value of objective function occur. [9]

III.3. Crossover

So as to expand the diversity of the perturbed parameter vectors, crossover is introduced. To this end, the trial vector:

$$u_{i,G+1} = \left(u_{1i,G+1}, u_{2i,G+1}, ...u_{Di,G+1}\right)$$

is formed, where

$$u_{ji,G+1} = \begin{cases} u_{ji,G+1} & if\ (randb(j) \le CR)\ or\ j = rnbr(i) \\ x_{ji,G} & if\ (randb(j) > CR)\ and\ j \ne rnbr(i) \end{cases} \quad (14)$$

$j = 1,2,....., D.$

Where, $randb(j)$) is the j[th] evaluation of a uniform random number generator with outcome $\in [0,1]$ .CR is the crossover constant $\in [0,1]$ which has to be determined by the user. $rnbr\ (i)$) is a randomly chosen index $\in 1,2,.....D$ which ensures that $u_{i,G+1}$ gets at least one parameter from $v_{i,G+1}$. [9]

III.4. Selection

To choose whether or not it ought to become a member of generation G+1, the trial vector; $u_{i,G+1}$ is contrasted to the target vector $x_{i,G}$ using the greedy criterion. If vector $u_{i,G+1}$ yields a smaller cost function than $x_{i,G}$ then $x_{i,G+1}$ is set to $u_{i,G+1}$ otherwise, the old value $x_{i,G}$ is retained. [9]

IV. Steps of System Analysis

Steps of investigation utilizing Differential evolution are depicted in the Fig. 2. For evaluation process 1% step load changes are applied in both areas simultaneously. The selection operation requires objective function to compare present set of data with previous set of data. The objective function used in this work is:

$$J = IAE = \int_0^{T_{sim}} |e(t)| dt \tag{15}$$

Where, $e = \Delta f_1 + \Delta f_2 + \Delta P$

and T_{sim}=simulation time

The values of Δf_1, Δf_2 and ΔP is found using state space equations. To evaluate these parameters using state space equation in time domain Euler's method is used. That is

$$x_i(t+1) = \frac{dx_i}{dt} \times T_s + x_i(t) \tag{16}$$

Where, $x_i = i^{th}$ state variable and $T_s =$ Step size of simulation.

After the completion of a DE cycle, there are numerous solutions for which minimum value of the objective function has occurred, as DE inherits the best results from its previous generations. But not all of them are the satisfying set of data. The values of PI controller gain parameters are found using eigenvalue and minimum value of objective function.

Eigenvalue calculation of system matrix (A) of state space equations defines the stability of the system. Eigenvalues of A matrix represents the poles of the system. A matrix is found from using (1)-(10). Eigenvalue of A matrix with all negative real parts provides stable system. Minimum value of objective function confirms the minimum amount of error in the system response.

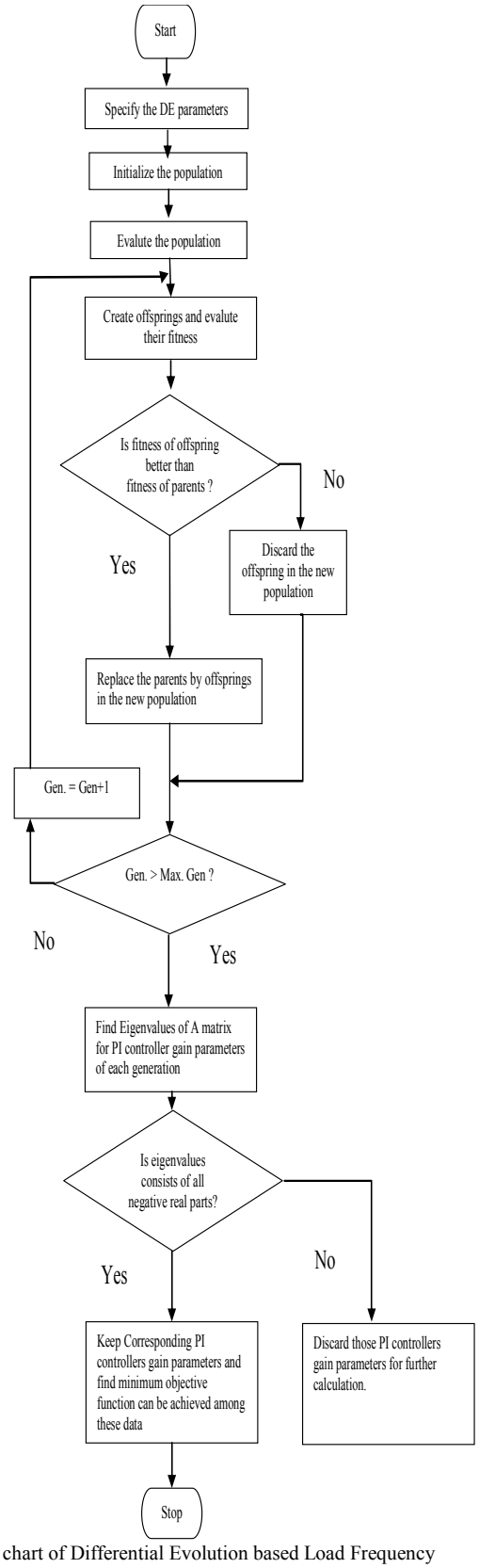

Fig. 2 Flow chart of Differential Evolution based Load Frequency Controller

After getting the optimized sets of PI controller gain parameters (K_p and K_i), the proposed controller is tested for different types of load disturbances to examine its robustness over various loading conditions.

The developed system is simulated using MATLAB. Results are published in terms of system matrix eigenvalue, objective function, transient responses (Settling time, percentage overshoot) and Area control error.

V. SIMULATION RESULTS AND ANALYSIS

The parameters for DE are initialized as follows:
Number of generation: 50, Number of Population: 50,
Initial range of search space: -1~2
Crossover rate: 0.8, Step size: 0.8.
The optimal set of PI controller gain parameters are given in the Table III.

TABLE III

OPTIMIZED VALUE OF GAIN PARAMETERS OF PI CONTROLLER USING DE

PI CONTROLLER			
THERMAL AREA		HYDRO AREA	
K_P	K_I	K_P	K_I
-0.23295	0.191703	-0.1027	1.059465

Corresponding set of eigenvalues are listed in Table IV.

TABLE IV

CORRESPONDING EIGENVALUE SET FOR OPTIMIZED PI CONTROLLER

EIGENVALUE OF SYSTEM MATRIX (A)
-13.4630
-5.9039
-0.2424 + 2.8333i
-0.2424 - 2.8333i
-0.2554 + 0.8536i
-0.2554 - 0.8536i
-1.0696 + 0.1274i
-1.0696 - 0.1274i
-0.2333 + 0.1092i
-0.2333 - 0.1092i

1% step load disturbance has been applied in the system to check the performance of the controller for small perturbation of load.

The transient responses for Fig. 3-5 are listed and showed numerically in Table V. The acceptable limits are taken as ±0.005 Hz and ±0.0005 P.U. deviations for frequency and tie line power flow deviations respectively. In general case settling time is defined as the time required for the response curve to reach and stay within a range of 5% or 2% of the final value. But in this case it is considered as 0.01% for frequency deviation and hence confirms robustness of the controller. The system is found to be stable faster for 1% step load change.

The transient responses for the above set of data are represented from Fig. 3-5.

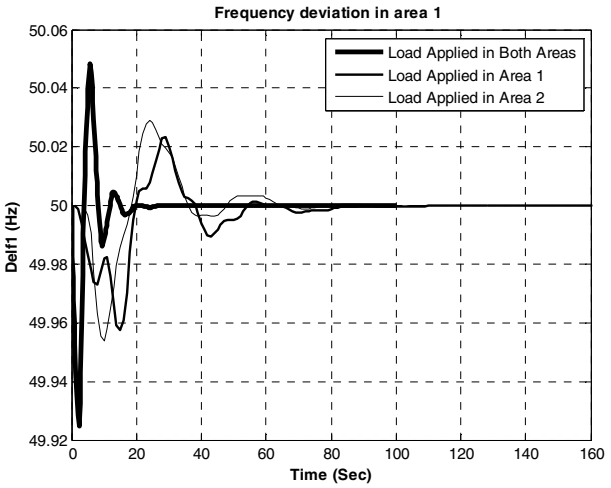

Fig. 3 Frequency Deviation in area 1 due to 1% step load change

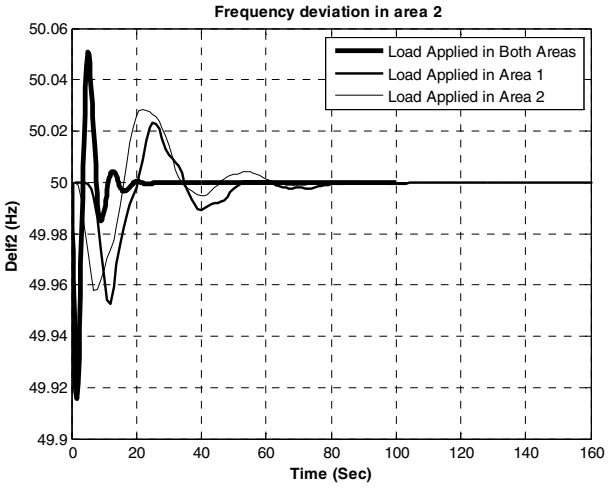

Fig. 4 Frequency Deviation in area 2 due to 1% step load change

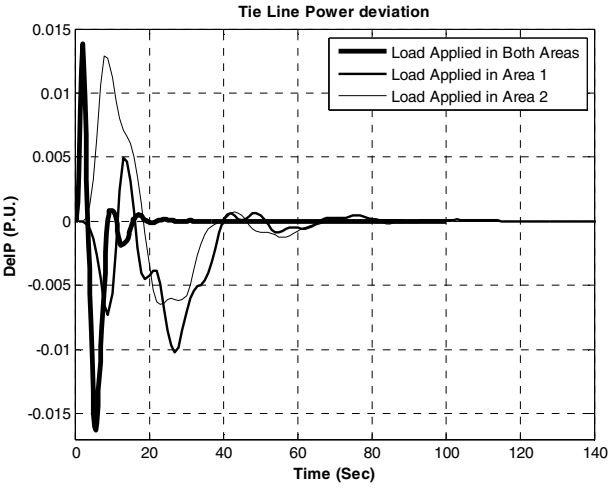

Fig. 5 Tie line power flow deviation due to 1% step load change

TABLE V
TRANSIENT RESPONSES FOR 1% STEP LOAD CHANGES

%Step load changes		1% in Both areas	1% in Thermal area	1% in Hydro area
Settling Time (Sec)	ΔF_1	11.2996	10.8066	7.9843
	ΔF_2	11.0156	11.0756	9.7271
	ΔP	17.6564	14.7726	14.8681
Peak overshoot ~ Peak Undershoot	ΔF_1(Hz)	50.0483~ 49.9248	50.0235~ 49.9574	50.0291~ 49.9536
	ΔF_2(Hz)	50.0510~ 49.9159	50.0233~ 49.9527	50.0283~ 49.9576
	ΔP(PU)	0.0138~-0.0163	0.0049~-0.0102	0.0129~-0.0065
Objective Function		0.6152	0.3161	0.3194

1% step load change is applied on the system considering three different cases. In first case step load change is applied on both the areas. In second and third case only either of the areas is applied with load change. The maximum settling time required for 1% step load changes is found 11.2996 seconds and 17.6564 seconds for frequency and tie line power flow deviation respectively.

The maximum peak overshoot and peak undershoot applying 1% step is found 50.0510 Hz and 49.9159 Hz. using DE based PI controller. As in this research positive load changes are applied, so the first and maximum peak has occurred at negative side. DE based PI controller provides peak over and undershoot within the acceptable limits (49.5~50.5 Hz).

The objective function used in this problem is Integral of Absolute Error (IAE). The values of objective function imply the condition of the system using the proposed controller. The objective of the proposed controller is to minimize the error of the system. The maximum value of objective function found using the proposed controller is 0.6152 for 1% step load change. Thus maximum values are attained when loads are applied in the both areas simultaneously.

So from the Table V it can be said that, the proposed controller can be effectively used for small (1%) load changes in both or either of the areas.

VI. CONCLUSION

In this paper design and simulated execution of DE based PI controller is examined. The proposed controller is applied on a combined conventional (thermal) and renewable energy (hydro) based power system. The execution of the proposed controller has been assessed taking into account the settling time, peak over/undershoots and minimum values of objective function. The stability of the proposed controller is additionally measured utilizing eigenvalue calculation, which implies the robustness of the controller mathematically. The DE based PI controller is found satisfactory over various loading conditions.

APPENDIX

The case study parameters are defined below:
Thermal Area:
Time Constant of Speed Governor, T_{sg1}=0.08 Sec;
Time constant of turbine, T_{t1}= 0.3 Sec;
Time constant of power system, T_{ps1}= 20 Sec
Gain constant of Power system, K_{ps1}= 120 (p.u. MW/Hz)
Frequency bias setting, b_1=0.425 (p.u. MW/ Hz)
Speed regulation, R_1=2.4 (Hz/ p.u. MW)

Hydro Area:
Time Constant of Speed Governor, T_1=0.2 Sec;
Resetting time, T_2=5 Sec;
Transient droop time constant, T_3= 28.75 Sec;
Water Starting Time, T_w=1 Sec;
Time constant of power system, T_{ps2}=20 Sec;
Gain constant of Power system, K_{ps2}=120 (p.u. MW/Hz)
Frequency bias setting, b_2=0.425 (p.u. MW/ Hz)
Speed regulation, R_2=2.4 (Hz/ p.u. MW)
Synchronization coefficient, T_{12}=0.0867
Ratio of power capacity between two areas, a_{12}=1

References

[1] Nanda, J. ; Kothari, M.L. and Satsang, P.S. "Automatic generation control of an interconnected hydrothermal system in continuous and discrete modes considering generation rate constraints", In IEE Proceedings D Control Theory and Applications, Volume:130 , Issue: 1 , January , 1983

[2] C. S. Chang, Weihul Fu and Fushuan Wen, "Load Frequency Control Using Genetic-Algorithm Based Fuzzy Gain Scheduling of PI Controllers", Electric Machines & Power Systems, Volume 26, Issue 1, 1998

[3] Demiroren, A., Zeynelgil, H.L. and Sengor, N.S., "The application of ANN technique to load-frequency control for three-area power system", IEEE Porto Power Tech Proceedings, 2001 (Volume:2)

[4] Rajesh Joseph Abraham, D. Das, and Amit Patra, "Automatic generation control of an interconnected hydrothermal power system considering superconducting magnetic energy storage", International Journal of Electrical Power & Energy Systems Volume 29, Issue 8, October 2007, Pages 571–579

[5] Ali M. Yousef, Jabril A. Khamaj and Ahmad Said Oshaba, "Steam-Hydraulic Turbines Load Frequency Controller Based on Fuzzy Logic Control", Research Journal of Applied Sciences, Engineering and Technology, Volume 4, Issue 15: 2375-2381, 2012

[6] L. Shanmukha Rao and N. Venkata Ramana, "Design of Robust Controller for Load Frequency Control in Deregulated Hydro-Thermal System Using Sliding Mode Controlled Strategies", International Review on Modelling and Simulations, Vol 6, Issue 3, 2013

[7] M. Elsisi , M. Soliman , M. A. S. Aboelela and W. Mansour, "Model Predictive Control of Nonlinear Interconnected Hydro-Thermal System Load Frequency Control Based on Bat Inspired Algorithm", International Electrical Engineering Journal (IEEJ) Vol. 6 (2015) No.7, pp. 1953-1961

[8] Mojtaba Shivaie, Mohammad G. Kazemi and Mohammad T. Ameli, "A modified harmony search algorithm for solving load-frequency control of non-linear interconnected hydrothermal power systems", Sustainable Energy Technologies and Assessments, Volume 10, June 2015, Pages 53–62

[9] Rainer Storn and Kenneth Price, "Differential Evolution – A Simple and Efficient Heuristic for Global Optimization over Continuous Spaces", Journal of Global Optimization, 1997, Vol. 11, No. 4, pp. 341–359.

[10] Gozde, H, Taplamacioglu, M.C. and Kocaarslan, I., "A Swarm Optimization Based Load Frequency Control Application in a Two Area Thermal Power System", International conference on Electrical and Electronics Engineering, 2009, Bursa, Turkey, pp: 124-128.

Fuzzy Logic Control of Buck Converter for Photo Voltaic Emulator

Mohammad Tauquir Iqbal*^, Mohd Tariq[+]^, Md Shafquat Ullah Khan[+]
* Damodar Valley Corporation, Kolkata, India, 700052
[+]School of Electrical and Electronic Engineering, Nanyang Technological University, Singapore, 639798
^ Formerly at, Department of Electrical Engineering, Indian Institute of Technology, Kharagpur, India, 721302
tauquir.iqbal@gmail.com, tariq.iitkgp@gmail.com

***Abstract*— This paper analyses the digital simulation of a buck converter to emulate the photovoltaic (PV) system with focus on fuzzy logic control of buck converter. A PV emulator is a DC-DC converter (buck converter in the present case) having same electrical characteristics as that of a PV panel. The emulator helps in the real analysis of PV system in an environment where using actual PV systems can produce inconsistent results due to variation in weather conditions. The paper describes the application of fuzzy algorithms to the control of dynamic processes. The complete system is modelled in MATLAB® Simulink SimPowerSystem software package. The results obtained from the simulation studies are presented and the steady state and dynamic stability of the PV emulator system is discussed.**

***Keywords*— Fuzzy Control, Buck Converter, DC-DC Converter, Photo Voltaic Emulator, Simulink.**

I. INTRODUCTION

Electricity has become one of the basic needs of life. Electricity is being produced from non-renewable source of energy like fossil fuels, coal etc. As power demand is rising day by day and we cannot depend solely on non-renewable energy sources because it is depleting day by day, we must look for alternative sources of energy. Therefore, extensive research is going for renewable source of energy [1]. Renewable Energy is defined as the energy obtained from naturally repetitive and persistent flows of energy occurring in the local environment. Solar energy is an example of renewable energy as it persists and repeats day after day [2]. Solar energy is being seen as one of the best renewable source of energy especially in disconnected/isolated/remote areas [3]. Power obtained from solar array depends upon solar insolation, climate etc. [4].

The development of the PV emulator was initiated for the testing of PV applications such as inverters or MPPT charge controllers as shown in figure 1. These tests were initially conducted on physical PV arrays. However, there were issues associated with these types of tests [5]. Firstly, outputs from an actual PV array are dependent on environmental conditions. Shadings, temperature differences, and different irradiance levels affect the performance of the cell. Therefore, consistent repeated readings cannot be measured. In addition, as inverters were improving rapidly in terms of their efficiency, more precise MPPT measurements were needed. Hundreds of solar panels are available for purchase. Therefore, a large number of different solar panel is needed to check MPPT algorithm and solar inverters. It is not economical to test on each individual solar panel [6, 7]. It is not economical to buy every types of solar panel and test them. A PV emulator should give I-V characteristics of different kinds of solar panel at different temperature and climate. By simply changing the PV panel type within the emulator, a new solar panel can be simulated without the hassle of purchasing a new PV panel and connecting the panel to the PV hardware to be tested. The mathematical model approach allows for the simulation of a solar panel under various irradiances and temperatures [8, 9].

A solar Photo voltaic emulator should be well designed so that it has the following features: 1) It should predict nearly same static I-V characteristics of real solar arrays and panel under various weather condition and load conditions. 2) It should be able to give satisfactory result under partial shading condition with more than one peak and step [10]. PV emulator is required to study new PV inverters and MPPT tracking algorithm in the laboratory to improve their performance [11]. Control algorithm has been implemented on field programmable gate array (FPGA) for grid connected full-bridge single phase inverter [6]. In Photovoltaic systems, switched power DC-DC converters are widely used to transform power between one voltages to other and also mainly used in maximum power point tracker (MPPT) [12]. DC-DC converter has property of variable resistance which plays an important role to emulate solar I-V characteristics and its respective P-V curves of PV array. The DC/DC converter

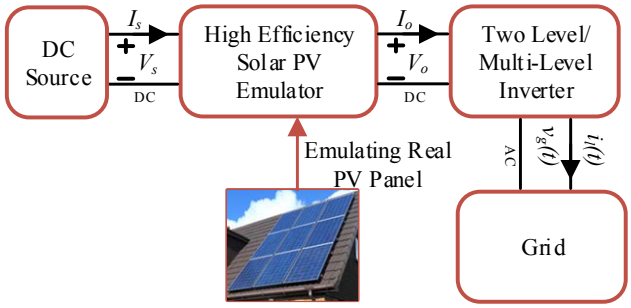

Figure 1. PV emulator connection to a grid connected inverter.

when designed properly can precisely describe the voltage-current and voltage-power characteristics of PV cell/array [13].

Nowadays, many practical industrial applications have been obtained from Fuzzy control [14-15]. From various applications, we have seen that fuzzy control has many advantages: 1) Multi-objective control can be realized. 2) Expert control can be realized. 3) Robust control can be realized [16]. Fuzzy logic control (FLC) has inherited adaptive characteristics. It can be used to a system where we need robust response having uncertainty, variation in parameter and disturbance in load. Fuzzy logic control gives a very good response to those systems which are ill defined, highly non-linear or imprecise. FLC has been already used to regulate DC-DC converters, DC-AC inverters and also in MPPT algorithm and gives very good steady state and dynamic response [14-15]. The dc–dc converter application is different from motor drives application in the sense that in dc-dc converter an electrical quantity (converter output voltage) is controlled whereas in motor, variations in input supply and load transients are controlled. In dc-dc converter, time constant is smaller (orders of magnitude) than for motor drives. Thus, the selection of sampling frequency is of greater concern [17].

The paper is organized as follows: different control schemes for buck converter based PV emulator is explained in section 2. Control strategy of the simulator and fuzzy logic control of buck converter are presented in sections 3 and 4 respectively. Simulation results are presented and discussed in section 5 and the conclusions and future work are presented in section 6.

II. Different Control Schemes for Buck Converter Based PV Emulator

Different control algorithms are used for buck converters like hysteresis control, voltage mode control, current mode control, fuzzy logic control etc. Current mode control (CMC) and voltage mode control (VMC) are very simple and are very old technique. Fuzzy logic control (FLC) is an approach to computing based on how much true is something i.e. between “0 to 1” rather than the usual "true or false" (1 or 0) on which the today’s computer is designed. Fuzzy logic changed true or false to partially true, partially false, values in between 0 to 1 rather than 0 or 1. Now true value can have any value between completely true (1) and completely false (0).As shown in fig.2, Fuzzy logic control have an input stage, intermediate stage and output stage. The input stage sense the output voltage and in the intermediate stage all the fuzzy logic operation takes place like generating membership function and truth values. The intermediate stage, invokes every appropriate rule and generates an outcome for every input, then combines the solution of the rules. Finally, output stage transform the whole result back in to respective control output value. Three types of control namely voltage mode control, current mode control and fuzzy logic control are given in next section. For photo voltaic emulator, a controller is required in order to get full I-V characteristics accurately i.e. having very less percentage of deviation from its actual characteristics.

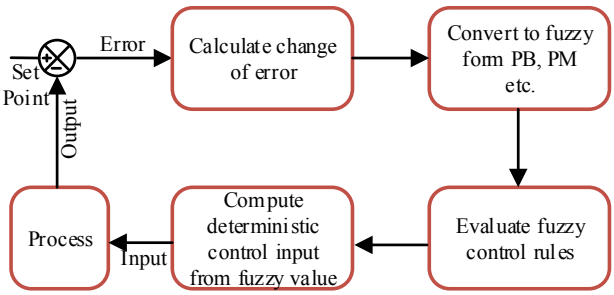

Figure 2. Control System using Fuzzy rules.

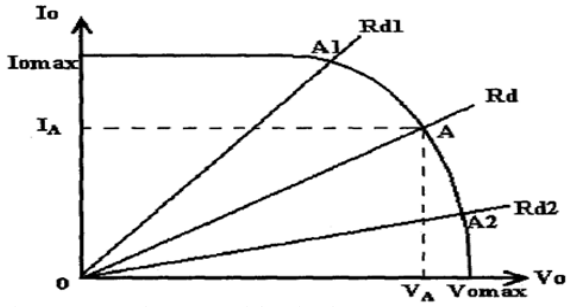

Figure 3. Control Strategy of the Simulator

The advantages which the fuzzy logic control technique offers include the following, 1) Mimics human control logic 2) Uses imprecise language 3) Inherently robust 4) Fails safely 5) Modified and tweaked easily. There are also some limitation of fuzzy based control. 1) Operator's experience required 2) System complexity. 3) To properly develop a fuzzy system, many data and expertise are required 4) Generalizable results are unavailable, has to be programmed for individual application.

III. Control Strategy of the Simulator.

For a Solar panel module, there are infinite number of operating points depending upon the output voltage and output current. Operating point at x axis (Output current = 0) is called open circuit while operating point at y axis is known as short circuit condition. (Output voltage = 0). A PV emulator therefore must meet both the specification of real load characteristics and I-V curve of different photo voltaic modules. As shown in figure 3, under different operating points, the intersection point of the inverse of slope of the load(static resistance) “1/Rd” and actual I-V characteristics of the solar panel will give the very operating point at which emulator is expected to operate.

For every I-V curve which the emulator is supposed to simulate, the actual I-V curve is converted in to look up table and stored in the memory of the memory of the FPGA. The data in the look up table can be discrete values or numerical value depending upon the control scheme used for PV emulator when the current changes from min (0) to Short Circuit current (I_{SC}). In the practical operation, we sense both output voltage and current then calculate load resistance using ohm’s Law. The point of intersection of slope of inverse of load resistance and real I-V curve gives operating point as shown in figure 3. Here the control system ensures that the

performance of the DC-DC Converter is adequate so that the real output voltage can match the reference one under any load conditions. Suppose load resistance is R_d, then after sensing its both output voltage and current, we will ensure load resistance equal to R_A by using ohm's law. R_A=Vo/Io. Then slope of 1/RA will intersect the I-V curve on point A which will produce reference voltage for the controller. As load resistance will change, different reference voltage will be produced. For load resistance (R_d=0), output voltage will be zero, while for load resistance to be infinite, reference value of output voltage will be V_{OC}. In this fashion, whole I-V characteristics can be easily obtained.

IV. Fuzzy Logic Control of Buck Converter

In fig.4 a general structure of fuzzy based control is shown. It has mainly four principal constituents: 1) A fuzzification world, which transfroms data taken from input to respective suitable semantic values. 2) A knowledge base which composed of a data base with the necessary semantic meaning and make proper control rule set. 3) A decision making logic, which emulates a human decision process, it deduce the control action of fuzzy from the understanding of the semnatic variable definitions and control rules. 4) A defuzzification world, which produce a no control fuzzy action from deduced action of fuzzy control.

Fuzzy logic or rule based non-linear controller can be designed easily since its control function is explanied by utilizing fuzzy sets and "if-then" predefined rules rather than convoluted mathematical equation or big look-up table. It will subtantially diminish the cost of development and time and needs little storage for data in the membership fuction and its rules. It has inherited adaptive characteristics which means it is more reliable and more robust when there is change in internal circuit parameter, external disturbance, etc.

Design of Fuzzy Controller for DC-DC Converters:-

The inputs of the fuzzy controller are the error e(k) and the change of the error $\Delta e(k)$ which are given in equation (1).

$$e(k) = v_{ref} - v_o(k) \quad (1)$$

and $\Delta e(k) = e(k) - e(k-1)$

The output of the fuzzy controller is the change of the reference signal $\Delta(k)$. The reference signal is determined by equation (2). Where $(k-1)$ is the previous reference signal.

$$e(k) = (k-1) + \Delta(k)\ ; \quad (2)$$

(k) is sent to the PWM generator. PWM generator generates the necessary switching signal for the gate of the MOSFET in the converter.

Simulink block diagram of FLC of buck converter is shown in fig.5. Change in load is achieved by switching on the timer connected to the corresponding resistance as shown in fig.5. Output voltage and current is sensed and then load resistance is calculated. The slope of inverse of resistance is drawn and it intersects with the operating point of the I-V characteristics as

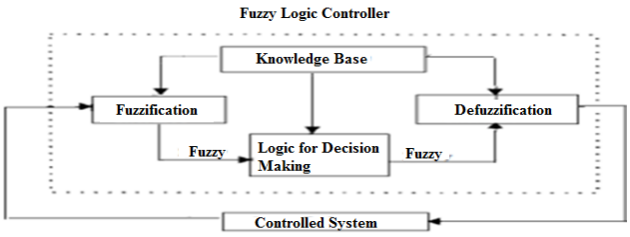

Figure 4. Basic Configuration of FLC.

shown in fig.3, which generates reference voltage as shown in Fig.5. There are many types of fuzzy based controller like fuzzy PI, hybrid PI which is mixture of conventional and fuzzy logic etc. Fuzzy based PID control is used for this application. Block diagram of fuzzy logic based PID control is shown in Fig.6.

Fuzzy rules and its respective 3D visuals are shown in fig. 6 and 7. When the error and change in error is positive large (PB), it means that output is far from its reference voltage; therefore, output also needs to be positive large (PB) to reach its reference quickly. Same will happen when the error and change in error is negative large (NB). When error or change in error is very less or zero then output value is very close to its reference value and output control signal will be small or zero as shown in rules (Table.1).

Table 1. Rules for fuzzy

Error/ Δ Error	NB	NM	NS	Z	PS	PM	PB
NB	NB	NB	NB	NB	NB	NB	NB
NM	NB	NB	NM	NM	NB	NB	NB
NS	NB	NB	NM	NS	Z	PS	PM
Z	NB	NB	NS	Z	PS	PM	PB
PS	NB	NS	Z	PS	PM	PB	PB
PM	NS	Z	PS	PM	PB	PB	PB
PB	Z	PB	PB	PB	PB	PB	PB

Table 2. The operating conditions for simulation

Simulation Set up Parameters	**Rating**
Input voltage	30 Volts
Output voltage	0-21 volts
Switching frequency	10 kHz
Output current	0 -4 Amp
Percentage ripple in current	less than 1%
Percentage ripple in voltage	less than 1%
Inductance of the converter (L)	12 mH
Capacitance of the converter (C)	2.2mf

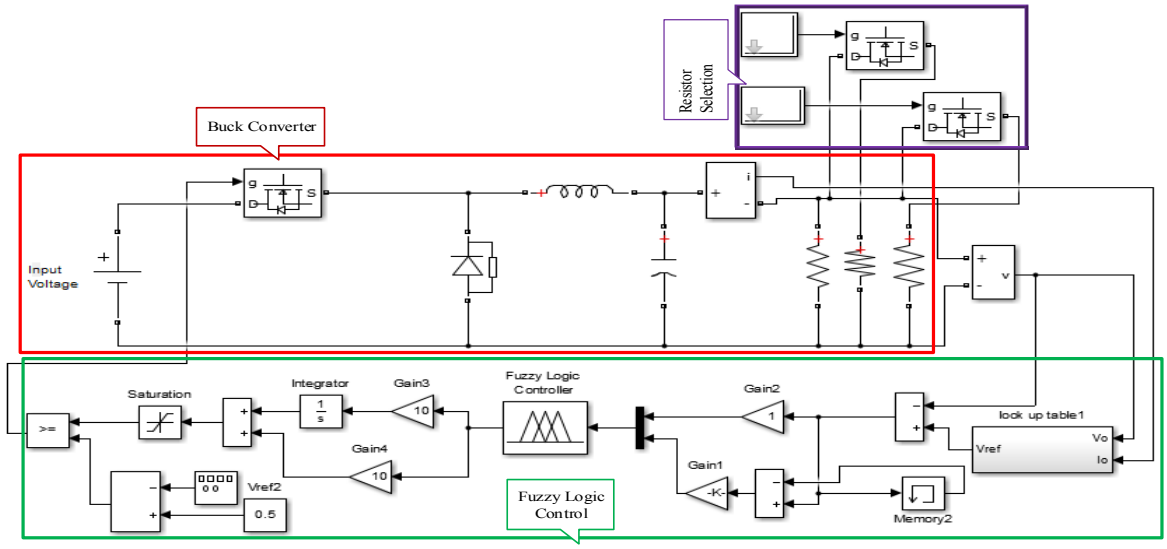

Figure 5. Simulink block diagram of Fuzzy logic control of buck converter

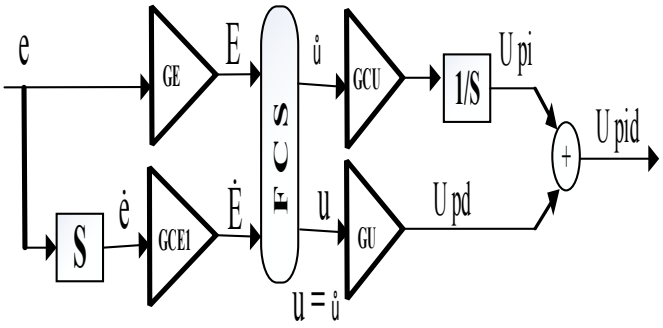

Figure 6. Block diagram of Fuzzy logic based PID control

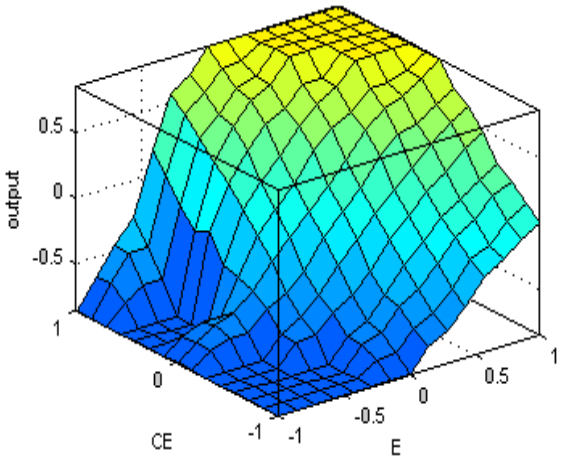

Figure 7. 3D visuals for rules

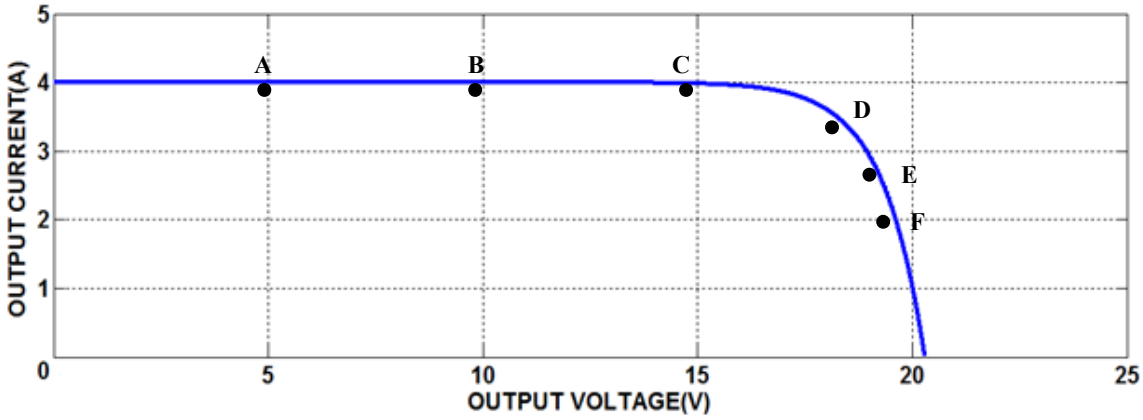

Figure 8. Operating point at different value of load resistance.

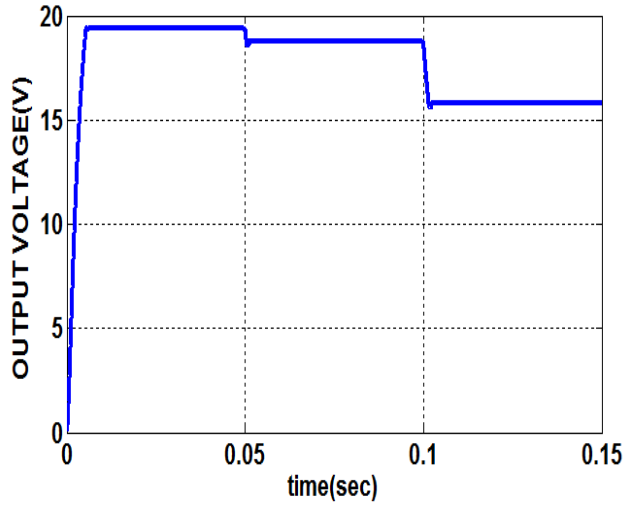

Figure 9. Simulation result of output voltage in dynamic conditions

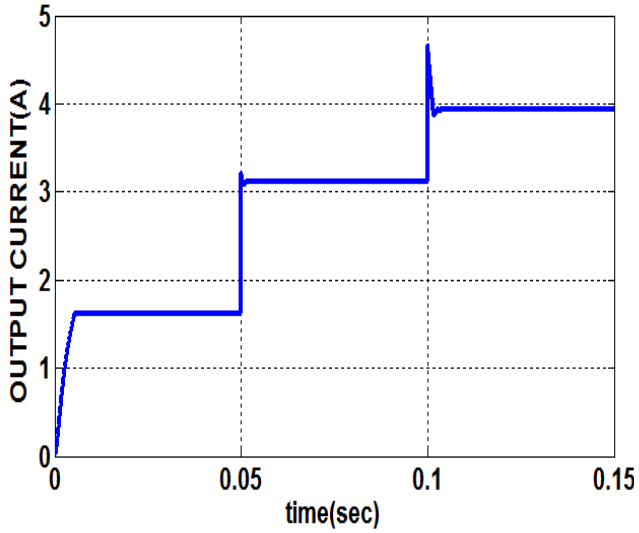

Figure 10. Simulation result of output current in dynamic conditions

V. Simulation Results and Discussion

Simulation is done in MATLAB® Simulink environment. The parameters used are listed in Table 2. We can achieve all the point of the characteristics by changing the value of the resistance. Fig. 9 and 10 shows simulation result+ of output voltage and current respectively, at starting load resistance of 10 ohm is connected, at t=50 ms load resistance have been changed from 10 ohm to 8 ohm and then at t=100 ms, load resistance has been changed to 6 ohm.Operating point corresponding to load resistance is shown in fig.8 At high load resistance, the operating point approaches the open circuit voltage. Similarly, at light load resistance, the operating point approaches the short circuit voltage. The fig.8 shows output voltage and output current at different value of resistance. Point A, B, C, D, E, and F corresponds to load resistance equal to 1.25, 2.5, 3.75,6,8 and 10 ohm respectively.

Output voltage and output current are shown in Fig. 9 and 10 respectively. Change in load happens at t= 50ms and t= 100ms. Transient condition are very good in the applied fuzzy logic control, settling time and voltage shoot is also very less as shown in fig. 8. Startup current is also within limit.

VI. Conclusions and Future Work

Fuzzy logic based control has been used to achieve full I-V characteristics. For getting good transient response inductance should be less as that will increase the ripple of the inductor current. So we have to optimize it. For getting good transient response capacitor should be large so that voltage across it will not decrease too much. Good transient response for the presented case is achieved, settling time and overshoot is within the limit. Hence the authors proposes that in future an optimization study for proper/optimal sizing of inductor and capacitance with good steady state and transient response need to be done.

Another area to investigate would be to expand upon the calculation of the I-V curve. Adding parameters such as time-of- the day or a location component to the emulator algorithm will make it to work more accurately and hence can emulate a solar panel under real world conditions. Thus, the PV emulator obtained would be able to emulate a real solar panel as the panel goes through an entire day in a user specified region. Shading could be another potential factor that could be included into the PV emulator. Since PV panels are composed of several solar cells connected in series and parallel, partial shading of the module will affect output characteristics of the solar panel. Developing a custom power supply would be another area of investigation. Developing the power supply would involve power electronic design of a DC-DC converter and some digital signal processing to control the output of the power supply. The custom power supply could bring down the cost of the PV emulator and depending on the output characteristics of the designed DC-DC converter, it can ease the emulation of more solar panels.

Acknowledgements

The authors are grateful for the support provided by the department of electrical engineering at IIT Kharagpur, India. Mr. Mohammad Tauquir Iqbal thanks Ministry of Human Resource Development, Govt. of India for providing him the GATE- Scholarship which enables him to pursue his studies at IIT Kharagpur. Mr. Mohammad Tauquir Iqbal also thanks Prof. (Dr.) Chandan Chakraborty, Professor and his supervisor for his M.Tech thesis dissertation at department of electrical engineering, IIT Kharagpur. Prof. (Dr.) Chandan Chakraborty always supported him with the ideas which were very helpful in understanding of the topic.

References

[1] M. Tariq, S. Bhardwaj and M. Rashid, “Effective battery charging system by solar energy using C programming and microcontroller”, American Journal of Electrical Power and Energy Systems, 2(2), 41-43. 2013.

[2] F. Robert, M. Ghassemi, and A. Cota. “Solar energy: renewable energy and the environment”. CRC Press, 2009.

[3] M. Tariq and K. Shamsi, “Application of RET to Develop educational infrastructure in Uttar Pradesh”. *International Journal of Recent Trend In engineering, ACEEE*, Vol. 4, pp 187-190, 2010.

[4] A. Tariq, M. Asim, and M. Tariq. "Simulink based modeling, simulation and Performance Evaluation of an MPPT for maximum power generation on resistive load." *2nd International Conference on Environmental Science and Technology IPCBEE*, Singapore, vol.6, Feb. 2011.

[5] D.C. Lu Dylan and Q. N. Nguyen, “A photovoltaic panel emulator using a buck-boost DC/DC converter and a low cost micro-controller”, *Solar Energy*, *Elsevier,* Volume 86, Issue 5, pp 1477-1484, May 2012.

[6] J. Chavarria, D. Biel, F. Guinjoan, A. Poveda, F. Masana and E. Alarcon, "FPGA-based design of a step-up photovoltaic array emulator for the test of PV grid-connected inverters," *in Industrial Electronics (ISIE), IEEE 23rd International Symposium on* , pp.485-490, 1-4 June 2014.

[7] C. Roncero-Clemente, E. Romero-Cadaval, V. M. Minambres, M. A. Guerrero-Martinez and J. Gallardo-Lozano, J. “PV Array Emulator for Testing Commercial PV Inverters”, *Elektronika ir Elektrotechnika*, 19(10), 71-75, 2013.

[8] S. Yuliang, "A Photo-voltaic array simulator", *Acta Energiae Solaris Sinica*, vol.18, pp.448-451, 1997.

[9] L. Hongliang, H. Mingzhi and Y. Xiaojie, "Investigation of photovoltaic array simulators based on different kinds of PWM rectifiers," *Communications, Circuits and Systems, ICCCAS. International Conference on* , pp.737-741, 23-25 July 2009

[10] K. Ahmed, T. LaBella and J. S. Lai. "High efficiency photovoltaic source simulator with fast response time for solar power conditioning systems evaluation." *Power Electronics, IEEE Transactions on* 29.(3) pp 1285-1297, 2014.

[11] J. Chavarria, D. Biel, F. Guinjoan, A. Poveda, F. Masana and E. Alarcon, "Low cost photovoltaic array emulator design for the test of PV grid-connected inverters," *Multi-Conference on Systems, Signals & Devices (SSD), 11th International* , pp.1-6, 11-14 Feb. 2014

[12] Duran, E.; Galán, J.; Sidrach-de-Cardona, M.; Andujar, J.M., "A New Application of the Buck-Boost-Derived Converters to Obtain the I-V Curve of Photovoltaic Modules," Power Electronics Specialists Conference, 2007. PESC 2007. IEEE, vol., no., pp.413-417, 17-21 June 2007.

[13] Cirrincione, M.; Di Piazza, M.C.; Marsala, G.; Pucci, M.; Vitale, G., "Real time simulation of renewable sources by model-based control of DC/DC converters," Industrial Electronics, 2008. ISIE 2008. IEEE International Symposium on , vol., no., pp.1548,1555, June 30 2008-July 2 2008.

[14] A. Al Nabulsi and R. Dhaouadi, "Efficiency Optimization of a DSP-Based Standalone PV System Using Fuzzy Logic and Dual-MPPT Control," *Industrial Informatics, IEEE Transactions on* , vol.8, no.3, pp.573,584, Aug. 2012

[15] Tsai-Fu Wu; Chien-Hsuan Chang; Yu-Kai Chen, "A fuzzy-logic-controlled single-stage converter for PV-powered lighting system applications," *Industrial Electronics, IEEE Transactions on* , vol.47, no.2, pp.287,296, Apr 2000

[16] Tanaka, Kazuo, and Michio Sugeno. "Stability analysis and design of fuzzy control systems." Fuzzy sets and systems 45(2), pp 135-156, 1992.

[17] Gupta, T.; Boudreaux, R.R.; Nelms, R.M.; Hung, J.Y., "Implementation of a fuzzy controller for DC-DC converters using an inexpensive 8-b microcontroller," *in Industrial Electronics, IEEE Transactions on* , vol.44, no.5, pp.661-669, Oct 1997.

Testing and Performance Analysis of 1KW Locally Made Grid-Tie Photovoltaic Inverter Using Thin Film Solar Panel

Khosru M Salim, Md. Jasim Uddin, Mohammad Rejwan Uddin, Saila Ishrat Annie and Zaima Tasneem

Department of Electrical and Electronic Engineering
Independent University, Bangladesh
Dhaka, Bangladesh

khosru@iub.edu.bd
jasimuddinjosh@gmail.com
rejwanuddin@yahoo.com
ishrat_annie@yahoo.com
zaimatasneem@gmail.com

***Abstract*— It is mandatory in Bangladesh to install solar panel on the rooftop of a newly build apartment or factory in order to get utility connection from the service provider. The most cost-effective and efficient way of producing energy using solar panel is to connect the panels to the utility grid through Grid Tie Inverter (GTI). GTI is one of the most important components of the grid tie solar system that basically converts dc power from the solar panel into ac power; synchronizing the phase, frequency and voltage of the utility grid. Presently almost all the GTI uses in Bangladesh are imported from other countries and it is very expensive. A low cost 1 kW grid tie inverter for solar PV module has been designed and implemented in the power electronic laboratory of the university. Physical demonstration was made by installing 1 kW Thin Film PV modules on the rooftop of the university building and setting up the inverter and others measuring equipments inside the lab. Based on the experimental data, the performance of the system is analyzed and presented in this paper.**

***Keywords*— Thin Film Photovoltaic Module, Grid-Tie Inverter, Performance Analysis**

I. INTRODUCTION

According to present government rules of Bangladesh, new building has to generate 3%-5% of total power consumed by them from solar [1]. Due to the frequent load shedding, most of the solar system installed in Dhaka or in the other major cities used as backup stand alone systems [2]. Stand alone solar system needs battery to store solar energy thus become expensive and also it needs frequent maintenances [3]. Recently, the power generation is increased and load shedding is reduced therefore the energy produced in the stand alone solar systems are not utilized properly. Now, utility service providers are encouraging their client to use grid tie solar system on the rooftop of their building which is less costly compared the stand alone systems and ensures effective use of their solar panels.

A Grid Tie Inverter can directly fed power to grid [4]. Power generated from PV (Photovoltaic) array is given to a GTI as input. By taking the reference from grid, the GTI creates output that is perfectly synchronized by phase and frequency with the grid. The block diagram of a grid connected PV system has been depicted in Fig.1.

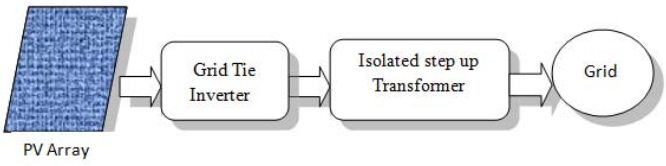

Fig. 1 Block diagram of a GTI system

Thin Film PV modules are used in this system because of its superior performances over crystalline PV modules considering shadow and temperature effects [5]. However, the thin film panels take larger roof space compared to its crystalline counterpart for generating same amount of power.

II. SYSTEM CONFIGURATION

The system configuration of a 1KW solar grid-tie PV system is made up of a 1KW thin film solar PV modules, a locally made GTI and an isolated step-up transformer. The specifications of these components are described in the later sections.

A. Solar PV Array

In our experiment thin film PV modules are used. 10 panels each of 95 Watt were installed in the roof top of the Lab. The thin film solar PV module specifications are described in Table 1.

Table 1
Specifications of Thin Film Module

Parameters	Specifications
Open Circuit Voltage (Voc)	71V
Short Circuit Current (Isc)	2.25A
Voltage at Maximum Power (Vpm)	53.5V
Current at Maximum Power (Ipm)	1.78A
Maximum Power (Pmax)	95W

For the experiment, 5 solar panels are connected in series and two such series combinations are connected in parallel. In

total, 10 solar panels are used to generate 950W which is approximately 1KW. The total voltage at maximum power produced by the PV array is = 53.5x5=267.5V. The total open circuit voltage of the PV array is = 71x5=355V. Panels are inclined from the ground at an angle of 15°. The solar thin film PV array which is installed for this experiment is shown in Fig. 2.

Fig. 2 Thin Film solar PV array

B. Grid-tie Inverter

The main function of a GTI is to convert the input DC power into AC power which will be aligned with the utility grid specifications [6]. H-Bridge inverter topology is used in the designed solar GTI PV system. The GTI used in this experiment consists of a power circuit, sensing circuit and control circuit. The power circuit consists of an intelligent IGBT module manufactured by MITSUBISHI. This module comprises of four IGBT and built-in gate drive circuits. The sensing circuit consists of a step-down transformer which steps down the grid voltage (312 V_{peak} or 220V) at the primary side of the transformer to 5V in the secondary side which is then rectified to obtain 5V DC voltage. A voltage divider circuit is then used to obtain 2V which is used as the reference in the PIC microcontroller (PIC 18f4431 used in the control circuit) to generate SPWM signals. The schematic diagram of the GTI is shown in Fig. 3.

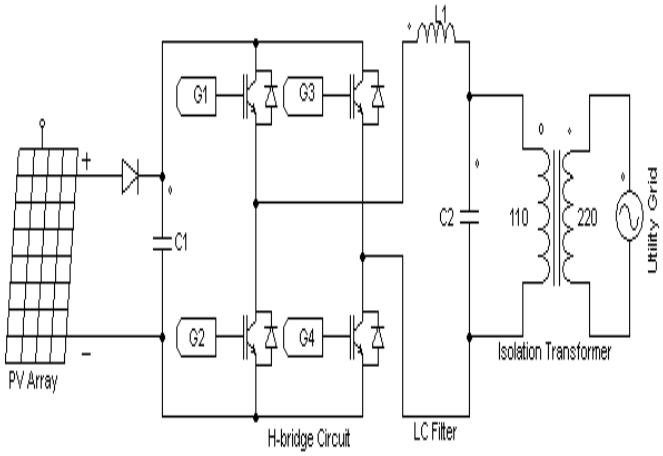

Fig. 3 Schematic diagram of the GTI

Fig. 4 represents the hardware prototype of the described GTI and its main components are highlighted with their objectives.

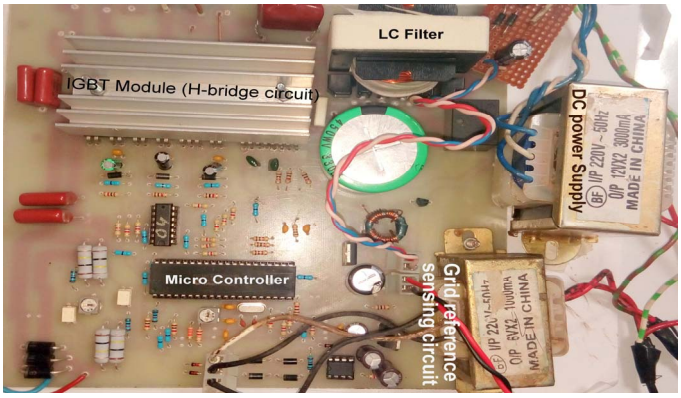

Fig. 4 Hardware prototype of Grid Tie Inverter

At the output of the GTI an LC filter is used to reduce the harmonics in which the values of L and C were obtained after many attempts of trial and error. Finally, the values are L=5mH and C=3uF.

C. Isolated Step Up Transformer

A 1 KVA 110/220 V isolated step up transformer is used in the solar GTI PV system to step up the inverter output voltage. Added to this, the transformer also serves to provide isolation between the grid and GTI.

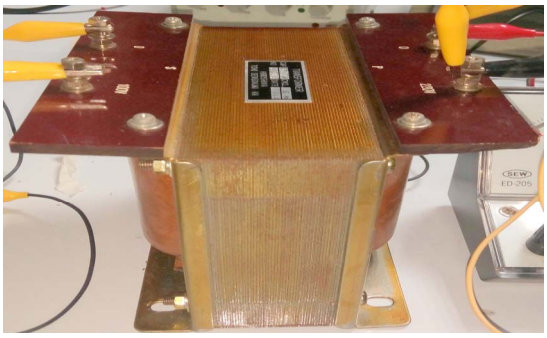

Fig. 5 Isolated step up transformer

III. EXPERIMENTAL SETUP

The input DC power is obtained from the readings of DC ammeter and DC voltmeter. This DC input is then fed into the GTI. The AC output of the GTI is fed into the 1KVA step-up transformer. The utility grid is then connected to the secondary side of the transformer through a wattmeter which is used to obtain the output power and an energy meter which is used to see that how much energy is given to the grid round the day. Total experimental setup is shown in Fig 6.

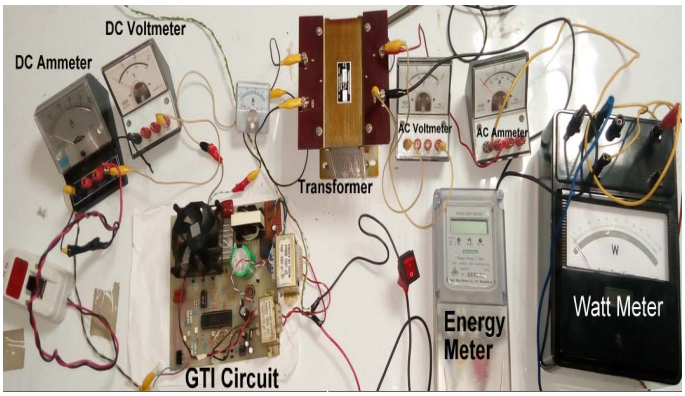

Fig. 6 Total Experimental setup

The output voltage of the GTI is shown in Fig. 7.

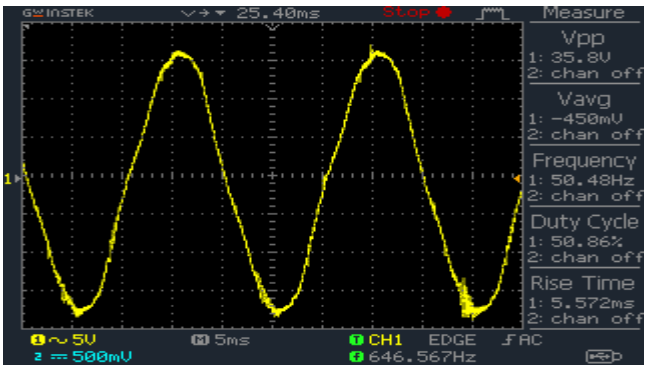

Fig. 7 GTI output voltage waveform

IV. PERFORMANCE ANALYSIS

The constructed 1kW PV system was connected to the grid and the performance of the GTI was tested round the day. During the day, the total energy that is being produced by the PV panels and the energy being fed to the grid are recorded at regular intervals from 7am to 5pm. It is observed that the energy production is higher during the morning but falls after noon. The maximum power generation occurs from 9.30am to 2.30pm and is above 400W. The system has an ESH (effective sun hours) of 5 hours. However, shadows or clouds will create sudden distortion in power generation. Fig. 8 represents the GTI input and output power performance round the day.

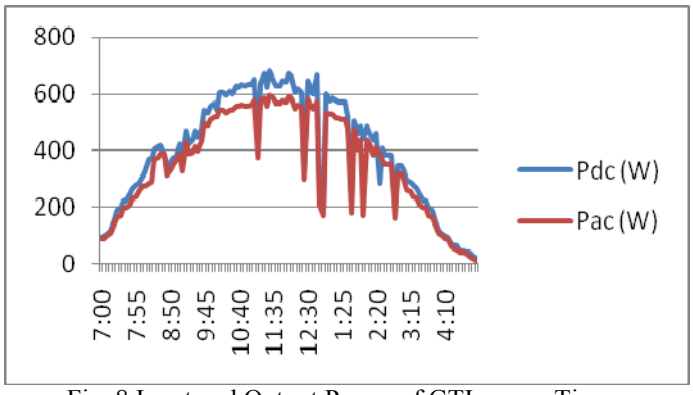

Fig. 8 Input and Output Power of GTI versus Time

The efficiency of the GTI is obtained using the formula as below:

$$\eta = \frac{P_{ac}}{P_{dc}} \times 100\% \qquad (1)$$

Taking the data from the experimental setup and using the formula, the value of efficiency is approximately 90%. Fig. 9 represents the efficiency curve.

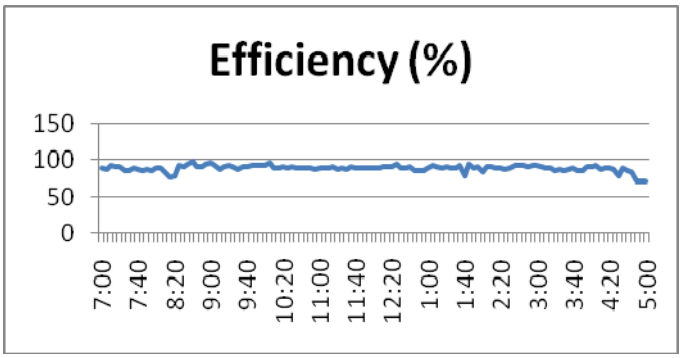

Fig. 9 Efficiency versus Time

Round the day, it has been observed from the energy meter readings that a total of 3.2 units (KWh) of energy have been given to the grid as shown in Fig. 10.

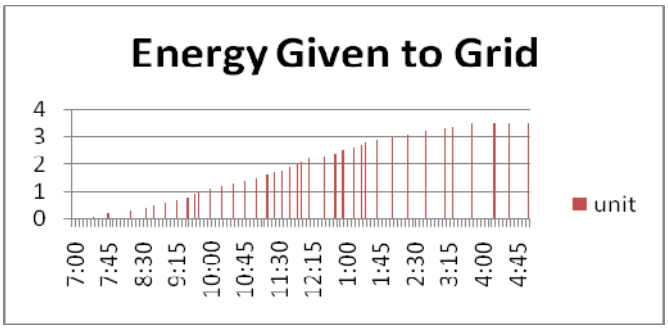

Fig. 10 Energy given to grid (KWH) versus Time

V. ECONOMIC ANALYSIS

The economic analysis of the 1KW grid-connected PV system is carried out to assess the cost and also to identify the breakeven point of the system. The cost of elements of grid-tied PV inverter installation is presented in Fig. 11 and the actual costs involved in PV pump installation are provided in Table 2.

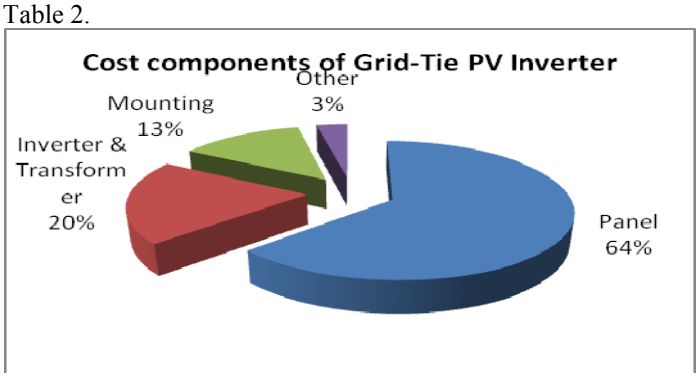

Fig. 11 Pie chart of cost components of solar GTI system

Table 2
1 KW Solar GTI system and its cost

Component	Cost
Panel (950W x 50Tk/W)	47,500
Inverter& Transformer	15,000
Mounting	10,000
Others	2,500
Total	**75,000**

The total installation cost for the system is BDT 75,000. The maximum cost is seen to be involved in the solar panels, which is 64% of the total cost.

It is already seen from the performance analysis section that a total of 3.2 units power is given to the grid per day. The average sunny days in Bangladesh is assumed to be 300 days in a year. Therefore the total power that will be exported to the grid is calculated to be 960 units/year.

According to Sustainable and Renewable Energy Development Authority (SREDA), the price of each unit that will be generated from renewable source and given to the grid will be BDT 15 per unit [7]. So, the price of the total power that will be produced in this system is BDT 14,400. The detailed calculation for the cost analysis is shown below:

Unit exported per day **=3.2 units/day**

Unit exported per year **= 960 units/year**
(3.5units/day x 300days/year)

Cost per unit **= 15 BDT/unit**

Cost per year **= 14,400 BDT/Year**
(Unit exported per year x cost per unit)

The breakeven point is calculated to identify the number of years by which the initial cost of the system will be recovered. The calculation for breakeven point is shown in Equation 1. It shows that the total initial cost of this Grid-tied PV inverter can be recovered within 5 years.

$$\text{Breakeven Point} = \frac{\text{Total installation cost}}{\text{Price of units exported to grid per year}} \quad (2)$$

$$= \frac{75{,}000}{14{,}400} = 5.2 \text{ years}$$

VI. CONCLUSION

The installed Grid-tie Inverter has been tested for a longer period of time successfully and the performances have been evaluated. During day time the panel always stays at its maximum power voltages which ensure its MPPT operations. The project has been tested in the lab for a month and the system stability is validated.

Thin film solar panel is considered because of its higher dc voltage and lower dc current that reduces dc transmission losses between panel and inverter. Again, thin film panels perform very well at higher temperature which is important for a country like Bangladesh where temperature is much higher during summer.

This locally made GTI can be used to provide power to the grid by a low cost solution. Over time, advancements in the manufacture of components will reduce the overall cost of the system and make the system economically more viable.

REFERENCES

[1] Official website of Bangladesh power development board; *http://www.bpdb.gov.bd*

[2] Bashar, S. A. (2009). "Solar power as a prime energy source in Bangladesh", The Daily Star (thedailystar.net), December 26, 2009. *(http://www.thedailystar.net/newDesign/print_news.php?nid=119244) (Accessed on 22/7/2015)*

[3] Fatima Binte Zia, Khosru M Salim, Rafid Haider, Nafisa Binte Yousuf, Rajin Alam, " Design and implementation of a single phase grid tie photovoltaic inverter". *2nd International Conference on the Developments in Renewable Energy Technology (ICDRET), 2012 . IEEE.*

[4] Saurav Das, Khosru M Salim, "Design and Implementation of One kilowatt Capacity Single Phase Grid Tie Photovoltaic Inverter". *International Conference on Electrical Engineering and Information & Communication Technology (ICEEICT), 2014. IEEE index.*

[5] The performance of thin film solar cells employing photovoltaic ZnSe/CdTe, CdS/CdTe and ZnTe/CdTe heterojunctions. *37th IEEE Photovoltaic Specialists Conference (PVSC), 2011*

[6] Md. Rejwanur Rashid Mojumdar, Arif Md. Waliullah Bhuiyan, Hamza Kadir, Md. Nizamul Haque Shakil and Ahmed-Ur-Rahman "Design & Analysis of an Optimized Grid-tied PV System: Perspective Bangladesh" *IACSIT International Journal of Engineering and Technology, Vol.3, No.4, August 2011*

[7] Official website of Sustainable and Renewable Energy Development Authority(SREDA), *http://www.sreda.gov.bd/index.php/documents/acts-policies-rules*

Performance of $CZTS_xSe_{1-x}$ Solar Cell with Various Mole Fractions of Sulfur for Different Buffer Layers

Sudipto Saha[#1], MD Zubair Ebne Rafique[#2], M. M. Shahidul Hassan[#3]
[#]*Department of EEE, Bangladesh University of Engineering and Technology*
Dhaka -1000, Bangladesh
[1]ssudiptosaha@yahoo.com
[2]zirshovon@gmail.com
[3]shassan@eee.buet.ac.bd

***Abstract*— Among the thin film solar cells, CZTSSe is the most promising one. In this article, the performance of CZTSSe solar cell with different potential buffer layers for different mole fractions of S of CZTSSe has been numerically investigated. It has been found that ZnSe buffer layer provides better performance in terms of efficiency than others within 0.7 mole fraction of S of CZTSSe. Above this value ZnO and ZnS both provide almost identical performance. The obtained results might be helpful in developing CZTSSe thin film solar cells by using proper mole fraction of sulfur in CZTSSe which has the potential to provide higher efficiency.**

***Keywords*— CZTS absorber layer, Thin film, solar cells, Buffer layers, SCAPS.**

I. Introduction

The future mass development of thin-film photovoltaic technologies calls for the development of cost-effective process based on earth-abundant, low-cost, and low-toxicity materials without significant reduction of the solar-cell efficiency. At industrial levels of production, thin film technologies based on $Cu(In,Ga)Se_2$ (CIGS) absorber layers have the highest cell efficiency (>20 %) [1]. A verified world-record efficiency of 17.4% for thin-film Cu(In,Ga)Se2-based photovoltaic submodules is also reported recently [2]. However, the scarcity of indium constitutes a potential limitation for future mass development, and consequently, its replacement has led to the investigation of materials with similar properties. In recent years, quaternary semiconductor $Cu_2ZnSn(S_xSe_{(1-x)})_4$ (CZTSSe) which is composed of earth-abundant and nontoxic elements, has attracted much attention due to its potential application in thin film solar cells as light absorber material. CZTSSe also offers promising characteristics for high performance and low cost absorber. One of the flexibilities that CZTSSe can offer is that its bandgap is readily tunable from 1.0 eV to 1.5 eV by adjusting the ratio of sulfur (S) and selenium (Se), thereby covering the range of the bandgaps predicted to yield the highest power conversion efficiencies [3]. So far, the best devices rely on Se-rich absorbers, with reported record efficiency of 12.6% [4]. Effects of different buffer layers for efficiency enhancement in CZTS and CZTSSe solar cells have already been investigated in literature [5]. But to the best of our knowledge, the effect of mole fraction or bandgap along with different buffer layers is still not reported in literature.

Here in this work, we have numerically investigated the performance of CZTS solar cell with different buffer layers along with the variation of mole fraction of S of CZTSSe. We have varied the mole fraction of S in $CZT(S_xSe_{1-x})$ from 0 to 1. As a result, bandgap varied from 1 eV to 1.46 eV [6]. Five different buffer layers were used in this investigation- Zinc Selenide (ZnSe), Zinc Oxide (ZnO), Indium (III) Sulphide (In_2S_3), Zinc Sulfide (ZnS), Cadmium Sulfide (CdS). While observing solar cell performance for different mole fractions of S of CZTSSe, we found, for all the buffer layers that CZTSe provides the best performance and CZTS provides the worst. For ZnSe and CdS buffer layers, simulation could be done for full span of bandgap.

II. Numerical Simulation

A. SCAPS-1D Numerical Simulation Program

For numerical analysis, we used SCAPS (a Solar Cell Capacitance Simulator) software (version 3.2.00), developed at the university of Ghent, Belgium under Professor Marc Burgelman in the Department of electronics and information system[7]. This tool is used for the analysis of both carrier related properties of hybrid semiconductor properties and non-carrier related properties such as dielectric constant, refractive index and the absorption constant. This simulation tool estimates the steady state band diagram, carrier transport and recombination profile based on Poisson equation and the electron and hole continuity equations. The Shockley-Read-Hall (SRH) model is used to calculate recombination currents for bulk defects and an extension of the SRH model for the interface defects.

B. Device Structure and Simulation

Fig. 1 shows the schematic of the vertical cross section of our simulated structure. The device consists of Molybdenum, CZTSSe, buffer layer, ZnO:Al and flat contact. Five different buffer layers- ZnO, ZnS, ZnSe, CdS and In_2S_3 have been used in this article. The test conditions such as temperature, bias voltage, illumination, etc. are set before simulation. The device has been illuminated with AM1.5 spectrum (1 kW/m^2). In this article the device and material parameters used in the simulation are based on literature values and theory. In some cases, reasonable estimations were also considered for

simulation. Device parameters used in the simulation are listed in table 1 [8].

Material parameters used for the simulation are listed in table 2 [8] [9]. Here Aα is the absorption constant for calculating α as a function of photon energy. In this study, α is defined as $\alpha\ (cm^{-1}) = A\alpha(h\nu - E_g)^{1/2}$, where h is the Planck's constant, ν is the photon frequency and E_g is the bandgap.

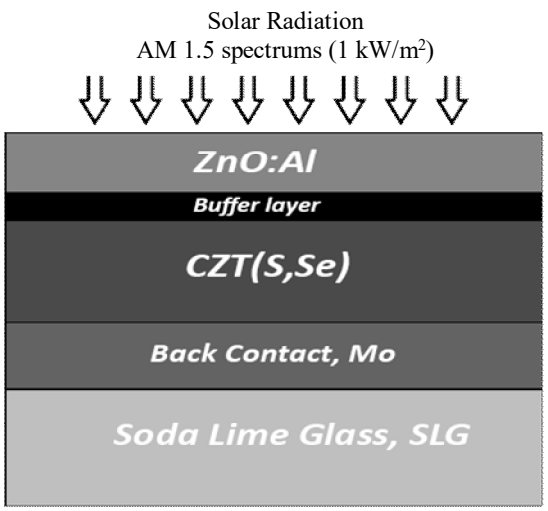

Fig. 1 CZTS solar cell structure for one dimensional simulation

TABLE I
DEVICE PARAMETERS USED IN THIS ARTICLE

Cell properties		**Back metal contact properties**		**Front metal contact properties**	
Cell temperature (K)	300.00	Electron work function of Mo (eV)	5.0	Electron work function (eV)	Flat band
Series resistance, R_s (Ω)	4.25	SRV* of electron (cm/s)	1.0E+5	SRV of electron (cm/s)	1.0E+7
Shunt resistance, R_{sh} (Ω)	400	SRV of hole (cm/s)	1.0E+7	SRV of hole (cm/s)	1.0E+5

* SRV stands for Surface Recombination Velocity

In this work the optical absorption constant of CZTSSe is in the range of 10^5 (1/cm $eV^{1/2}$). In this simulation, the effects of radiative recombination and Auger electron/hole capture have been considered in all the cases. Estimated value of radiative recombination coefficient is 5.0E-9 cm^3/s and for Auger hole/electron capture coefficient, it is about 1.0E-29 cm^6/s [5]. Furthermore, in the simulations, series resistance, (R_s) = 4.25 Ω and shunt resistance, (R_{sh}) = 400 Ω have been used to measure the device performances [8].

TABLE II
MATERIAL PROPERTIES OF DIFFERENT LAYERS

Material properties	**Absorber layer ($Cu_2Zn(Sn_xS_{1-x})_4$)**	**ZnO:Al**
Thickness (μm)	2.0	0.20
Bandgap (eV)	1 ~ 1.46	3.3
Electron affinity (eV)	4.5	4.6
Relative Dielectric permittivity	10.0	9.0
CB effective density of states (1/cm^3)	2.2E18	2.2E18
VB effective density of states (1/cm^3)	1.8E19	1.8E19
Electron thermal velocity (cm/s)	10^7	10^7
Hole thermal velocity (cm/s)	10^7	10^7
Electron mobility (cm^2/Vs)	100	100
Hole mobility (cm^2/Vs)	25	25
Shallow uniform donor density N_D (1/cm^3)	1.0E+1	1.0E+18
Shallow uniform acceptor density N_A (1/cm^3)	7.0E+16	0

III. RESULT AND DISCUSSION

In this work, effect of five different buffer layers has been studied, as stated earlier. For all the cases, thickness of the buffer layer is kept fixed at 500 nm. Donor density was also kept constant at 3×10^{19} cm^{-3}. Material properties of the buffer layer are presented in table 3 [9] [10].

TABLE III
BUFFER LAYER' S MATERIAL PROPERTIES

Material properties	**CdS**	**In_2S_3**	**ZnO**	**ZnS**	**ZnSe**
Bandgap (eV)	2.400	2.800	3.300	3.400	2.580
Electron affinity (eV)	4.5	4.7	4.6	4.4	4.1
Relative Dielectric permittivity	9.0	13.6	9.0	10	9.2
CB effective density of states ($1/cm^3$)	1.8E19	1.8E19	2.2E18	1.5E18	1.5E18
VB effective density of states ($1/cm^3$)	2.4E18	4E13	1.8E19	1.8E18	1.8E19
Electron mobility (cm^2/Vs)	3.5E+2	4.0E+2	1.0E+2	1.0E+2	5.4E+2
Hole mobility (cm^2/Vs)	5.0E+1	2.1E+2	2.5E+1	2.5E+1	2.8E+1

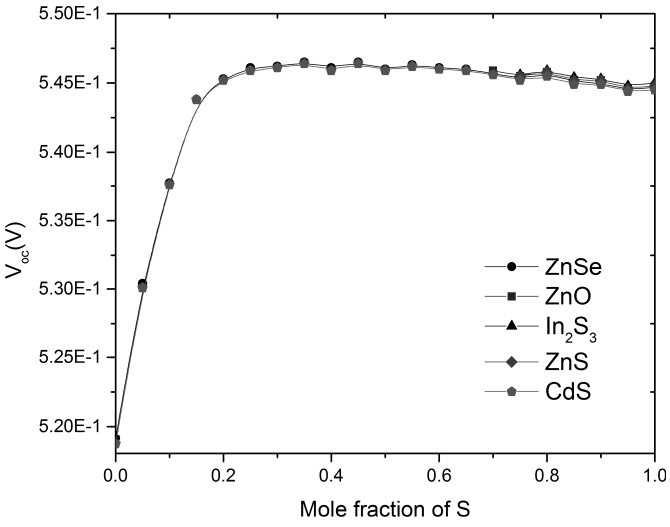

Fig. 2 Effects of mole fraction of S on open circuit voltage for different buffer layers

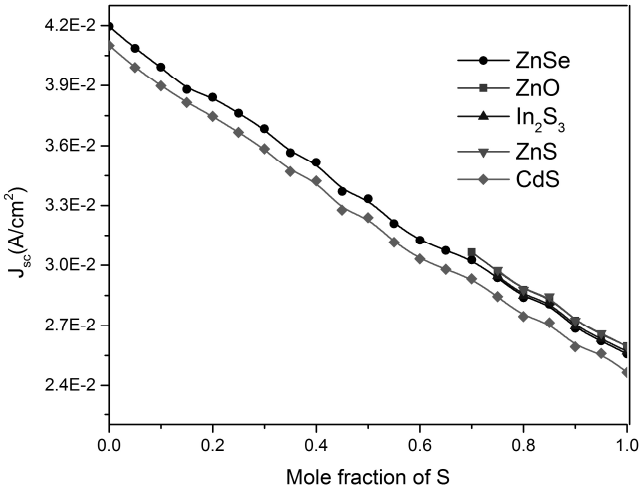

Fig. 3 Effects of mole fraction of S on short circuit current density for various buffer layers

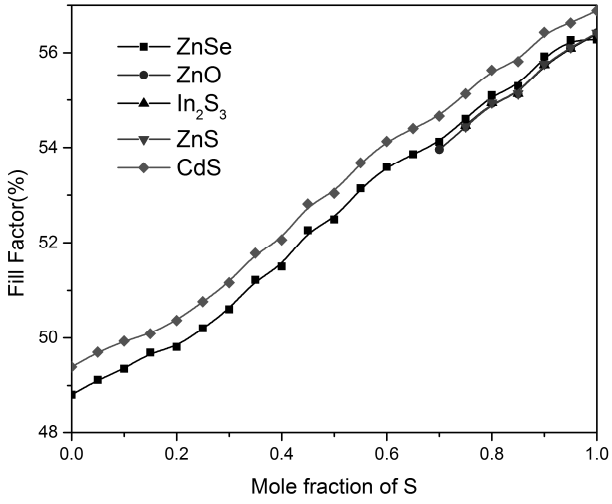

Fig. 4 Effects of mole fraction of S on Fill factor for different buffer layers

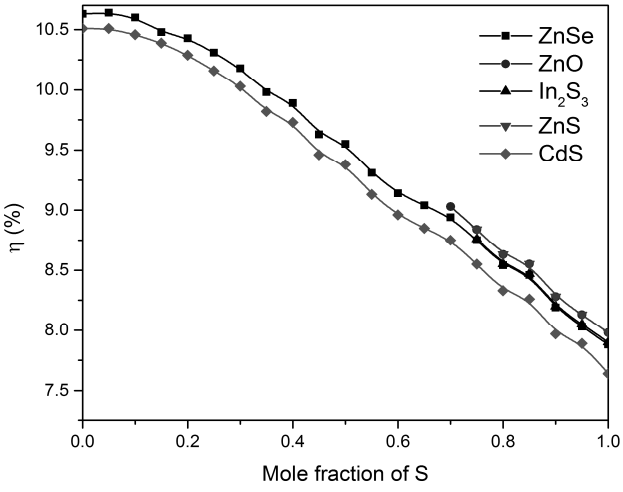

Fig. 5 Effects of mole fraction of S on efficiency for different buffer layers

For all buffer layers, maximum efficiency is found at minimum mole fraction of S of CZTSSe. For ZnSe, a highest efficiency of 10.63% (Fig. 5) is found for bandgap 1 eV with open circuit voltage of 0.5191 V (Fig. 2), short circuit current density of 41.96 mA/cm^2 (Fig. 3) and fill factor of 48.81% (Fig. 4). In this case, the value of S/(S+Se) in CZTSSe is zero. With this increase of S/(S+Se) ratio in CZTSSe, bandgap also increases.

High bandgap of CZTSSe results in less absorption of photon. For CZTS absorber, efficiency using ZnSe was found to be 7.88% (Fig. 5) with 0.5447 V (Fig. 2) open circuit voltage, 25.5736 mA/cm^2 (Fig. 3) short circuit current density and 56.28% (Fig. 4) fill factor.

For CdS buffer layer, simulation could be done for full span of mole fraction of S. Maximum value of efficiency is found 10.51% (Fig. 5) using this buffer layer at 0.5187 V (Fig. 2) open circuit voltage, 41.01 mA/cm^2 (Fig. 3) short circuit current density and 49.39% (Fig. 4) fill factor. For CdS layer, worst performance is observed when the ratio S/(S+Se) turns to 1 (Fig. 5). The minimum efficiency found using CdS layer is 7.64% (Fig. 5) with 0.5445 V (Fig. 2) open circuit voltage, 24.65 mA/cm^2 (Fig. 3) short circuit current density and 56.89% (Fig. 4) fill factor.

For ZnO, ZnS and In_2S_3 buffer layers, simulation results also indicate almost constant open circuit voltage, decreasing short circuit current density, increasing fill factor and decreasing efficiency for this particular environment.

IV. Conclusions

In this article, we have changed the mole fraction of Sulfur of $CZTS_xSe_{1-x}$ absorber layer and observed the change in open circuit voltage, short circuit current density, fill factor and efficiency for five different buffer layers. For a particular buffer layer, open circuit voltage changes linearly for mole fraction of S of CZTSSe upto 0.3 and beyond that, open circuit voltage is almost constant. With changing mole fraction of S upto 0.7, we found high short circuit current density for ZnSe buffer layer and minimum value is found for CdS buffer layer. For higher mole fraction of Sulfur of CZTSSe, ZnO and ZnS buffer layers provide higher short circuit current density than others. CdS buffer layer provides higher fill factor than others. For all the buffer layers, efficiency decreases with increasing mole fraction of Sulfur in CZTSSe. If the mole fraction of Sulfur is above 0.7, better performance is obtained from ZnO and ZnS buffer layers. Though ZnSe buffer layer has lower fill factor for mole fraction of S upto 0.7, it provides better performance in terms of efficiency than others. Above this mole fraction of S, ZnO and ZnS both provide almost identical performance. Further investigation can be done considering layer defects and interface defects.

Acknowledgment

The authors are very grateful to Dr Marc Burgelman at the University of Ghent for providing the software license of SCAPS-1D on request.

References

[1] P. Jackson, D. Hariskos, E. Lotter, S. Paetel, R. Wuerz, R. Menner, W. Wischmann, and M. Powalla, “New world record efficiency for cu (in, ga) se2 thin-film solar cells beyond 20%,” Progress in Photovoltaics: Research and Applications, vol. 19, no. 7, pp. 894–897, 2011.

[2] E. Wallin, U. Malm, T. Jarmar, O. L. Edoff, L. Stolt et al., “World-record cu (in, ga) se2-based thin-film sub-module with 17.4% efficiency,” Progress in Photovoltaics: Research and Applications, vol. 20, no. 7, pp. 851–854, 2012.

[3] W. Shockley and H. J. Queisser, “Detailed balance limit of efficiency of p-n junction solar cells,” Journal of applied physics, vol. 32, no. 3, pp. 510–519, 1961.

[4] W. Wang, M. T. Winkler, O. Gunawan, T. Gokmen, T. K. Todorov, Y. Zhu, and D. B. Mitzi, "Device Characteristics of CZTSSe Thin-Film Solar Cells with 12.6% Efficiency," Adv. Energy Mater., 2013.

[5] M. A. Olopade, O. O. Oyebola, and B. S. Adeleke, “Investigation of some materials as buffer layer in copper zinc tin sulphide (Cu2ZnSnS4) solar cells by SCAPS-1D,” Advances in Applied Science Research, pp. 3396-3400, 2012.

[6] A. Fairbrother, X. Fontan, V. Izquierdo-Roca, et al., "Single-Step Sulfo-Selenization Method to Synthesize $Cu_2ZnSn(S_ySe_{1-y})_4$ Absorbers from Metallic Stack Precursors," CHEMPHYSCHEM ARTICLES, DOI: 10.1002/cphc.201300157

[7] M. Burgelman, P. Nollet, and S. Degrave, “Modelling polycrystalline semiconductor solar cells,” Thin Solid Films, vol. 361362, p. 527–532, 2000.

[8] M. Patel and A. Ray, “Enhancement of output performance of Cu_2ZnSnS_4 thin film solar cells — A numerical simulation approach and comparison to experiments,” Elsevier Physica B, p. 4391–4397, 2012.

[9] F. Haque,1 N.A. Khan,1 K.S. Rahman, et al, "Prospects of Zinc Sulphide as an Alternative Buffer Layer for CZTS Solar Cells from Numerical Analysis", 8th International Conference on Electrical and Computer Engineering, p. 504-507, 20-22 December 2014.

[10] Nima Khoshsirat and Nurul Amziah Md Yunus, "Numerical Simulation of CIGS Thin Film Solar Cells Using SCAPS-1D," IEEE Conference on Sustainable Utilization and Development in Engineering and Technology, p. 63-67, 2013.

Design, Construction and Implementation of a Highly Efficient, Lightweight and Cost Effective Battery Charger for Electric Easy Bikes

Khosru M. Salim, Md. Jasim Uddin, M. Ishtiaque Rahman, Mohammad Rejwan Uddin

Department of Electrical and Electronic Engineering
Independent University, Bangladesh
Dhaka, Bangladesh

khosru@iub.edu.bd
jasimuddinjosh@gmail.com
ishtiaque_rahman@yahoo.com
rejwanuddin@yahoo.com

***Abstract*— Electric three-wheeler auto rickshaws known as easy bikes are becoming quite common in Bangladesh. Due to obvious advantages offered by these vehicles such as zero carbon emission and no requirement of gas encourages people to transition from traditional fuel-operated vehicle to electric vehicles. The battery charging stations for these vehicles employ bulky chargers containing iron core transformers with maximum efficiency around 80%. As a country which suffers from power shortages, it is highly desirable to have a charger that is more efficient. In this paper, a new type of charger is proposed which uses a ferrite core transformer. A prototype of this charger is built and compared with a conventional charger. It is found from the experiments that the proposed charger exhibits efficiency more than 90%. In addition, the proposed charger weighs only about 2 kilograms, whereas the conventional charger weighs about 10 kilograms.**

***Keywords*— Easy bikes, iron core transformer, ferrite core transformer, efficiency, charging current.**

I. INTRODUCTION

Global population increase has led to an exponential rise in the amount of transportation vehicles. Almost all of these vehicles are run on fossil fuels, which causes environmental problems. The rapid decrease of fossil fuel reserves is an equally alarming issue. As a green solution, electric vehicles are gradually becoming more and more popular. Electric vehicles have several advantages [1] over regular vehicle; they do not require any gas, they emit no harmful substances into the atmosphere, they are subsidized by the government, and they require less maintenance. However, there are a few disadvantages of these vehicles as well. For instance, electric vehicles are not suitable for countries facing major shortage of power. Electric vehicles contain a battery bank which needs to be charged at regular intervals. The chargers used to charge these vehicles contain iron core transformers, which gives rise to power losses, and hence, inefficient charging operation. If these chargers are replaced with more efficient ones, it will save a substantial amount of energy and in the process, encourage countries with power shortages to use more electric vehicles. In Bangladesh, the use of electric three wheeler auto rickshaws known as easy bikes are becoming more and more popular. The charging stations all employ the conventional iron core charger which is only about 80% efficient. Hence, there exists an excellent opportunity to save energy by improving the efficiency of easy bike battery chargers. Using the proposed charger, it is possible to achieve efficiencies of the order of 90%.

A considerable amount of research has been done over the years regarding the various aspects of electric vehicle charging. Pellitteri et al [2] proposed an efficient wireless charging scheme for electric pedal bikes. Bass and Zimmerman [3] explored the effects of electric vehicle charging on the power distribution system. Wang et al [4] highlighted the various design aspects related to inductive power transfer system necessary for constructing a contactless charger for electric vehicles. Zhou et al [5] proposed a multi function bi directional charger for plug-in hybrid electric vehicles, which can accomplish three functions namely, charging, vehicle to grid, and vehicle to home.

II. THE CONVENTIONAL EASY BIKE CHARGER

Electric easy bikes contain a 60V battery bank. The chargers used at present for charging these bikes typically consist of two major components, namely, an iron core toroidal transformer and a full bridge diode rectifier. The complete charging scheme of such a battery is represented in the form of a block diagram in the figure below. The iron core transformer of the charger primarily receives power from the grid, and steps down the voltage to an appropriate level that matches the battery bank voltage. This ac voltage is then fed to a full bridge rectifier, which provides a dc voltage that charges the battery bank. In order to identify the problems associated with this charging system, the practical aspects concerning the iron core transformer of the conventional charger have been explored. Keeping these points in mind, an actual charger has been examined in the lab with the aim of determining the system efficiency at a range of charging currents.

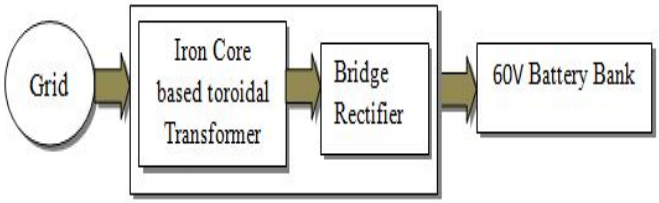

Fig. 1 Conventional easy bike charging scheme

A. The Iron Core Transformer and Its Associated Drawbacks

The main function of the iron core toroidal transformer in conventional easy bike charger is to step down the mains AC voltage to 60V, which matches the battery bank voltage. The typical charging power for a 60V battery bank is 600W. However, during the step-down operation, the transformer incurs power losses such as magnetizing loss in the core, eddy current loss, hysteresis loss, and resistive losses in the copper coil [6]. Depending on the efficiency of the transformer, these losses will vary. If an efficiency of 70% is assumed, a power loss of about 200W must be taken into account. Hence, the total input power of conventional charger should be about 800W to 900W. As a result, an iron core transformer with a high VA rating is required. This makes the charger quite bulky, which affects its portability significantly. The figure below shows a typical charger that weighs about 10 kilograms. About 95% of the total weight is attributed to the transformer.

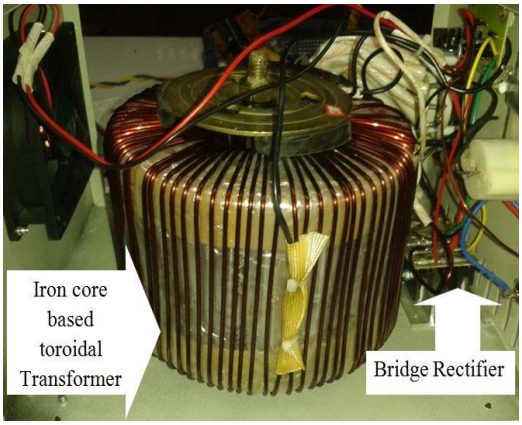

Fig. 2 Typical iron core easy bike charger

B. Experimentation with an Actual Charger

One of the primary activities of this research study was to examine an actual conventional electric easy bike charger. Parameters such as battery voltage, charging current and input power were monitored during the experiment. The following figure shows the experimental setup of conventional easy bike charger.

Fig. 3 Experimental setup of conventional charger

The setup consists of the following:

1. A variable transformer to control the charging current
2. A wattmeter to monitor the input power
3. A conventional 60V easy bike charger to convert the AC input into DC power
4. A 60V battery bank

The charging current was varied using the variac, and the corresponding input power was recorded using a wattmeter. The output power was measured by calculating the product of the charging current and the voltage that appeared across the battery bank. Finally, using the ratio of output to input power, the efficiency of the charging system was calculated. Table 1 below shows the experimental data obtained from the system.

TABLE I
EXPERIMENTAL DATA OF CONVENTIONAL CHARGER

$V_{battery\ (V)}$	$I_{char\ (A)}$	$P_{in\ (W)}$	η (%)
61	1	117	52.13
61.2	2	170	72
61.8	3	240	77.25
62.3	4	305	81.70
62.8	5	370	84.86
63.2	6	445	85.21
63.7	7	520	85.75
64.1	8	595	86.18
64.8	9	650	89.72
65.2	10	720	90.55
65.6	11	800	90.2
65.9	12	900	87.86
66.3	13	965	89.31

III. THE PROPOSED HIGH FREQUENCY CHARGER – OVERVIEW OF SYSTEM DESIGN AND CONSTRUCTION

A. Design Procedure in Brief

Creating a functional prototype of the proposed charger involved a few strategic steps. The abstract idea was implemented using PSIM software, where the preliminary

testing and parameter adjustments were made. Then, once a stable model was created in PSIM, the next step was to design the hardware and improve it through necessary adjustments of component values, until the desired outcome was obtained.

B. Working Principle of the Proposed Charger

The fundamental difference between a conventional charger and the proposed charger is that the proposed charger uses a high frequency ferrite core transformer. This drastically reduces the weight of the charger. The power from the grid is manipulated in several stages in order to achieve the desired charging condition for the battery bank. The figure below is a block representation of the system containing the proposed charger.

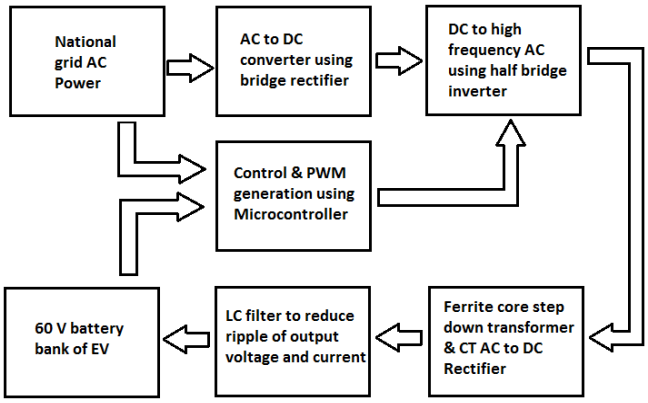

Fig. 4 Block diagram describing the charging system containing the proposed charger

The ac voltage from the grid is first converted to dc using a full wave diode rectifier. The rectified output is fed to a half bridge inverter constructed using MOSFETs. A microcontroller is used to provide the gate signals to the MOSFETs. The output of the inverter is high frequency ac voltage which is applied across the ferrite core transformer in order to step down the voltage as required for charging operation. However, voltage is ac and therefore must be converted to dc using a center tap rectifier. Finally, an LC filter is used to remove any ripple from the dc voltage before it is applied across the battery bank for charging. The figure below shows the entire arrangement of the proposed charger in PSIM.

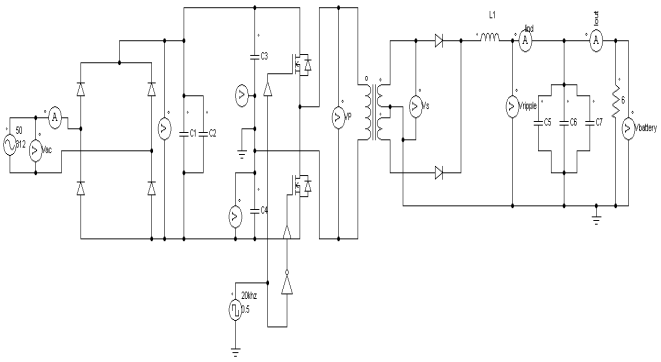

Fig. 5 PSIM schematic consisting of proposed charger

1) Design Issues Regarding Ferrite Core Transformer: A high frequency ferrite core transformer was used in the prototype. The transformer is designed to ensure that the flux density in the core of the transformer is maintained at a considerably high level which minimizes the eddy current loss of the transformer. To make the prototype more cost effective, the inductance of the transformer is also used by the LC filter circuit. Furthermore, ferrite shield has been used above the surface of the transformer to maximize the magnetic field strength and minimize eddy current loss. All these factors contribute in making the transformer very highly efficient (around 98%).

2) *LC Filter Design:* In order to prevent short circuits, a very small dead time between complementary PWM signals was provided. During this short period, both MOSFETs are turned off. For this reason, the output current and voltage contain some ripple. So, in order to reduce this ripple in current a small inductor must be used. Similarly, to reduce the ripple in voltage a small capacitor bank should be used in parallel with the load. The inductance and capacitance of the filter was determined using the equation [7] below. The higher the frequency of ripple, the smaller the size of the filter. In this study, since the switching frequency of half bridge inverter was 20kHz, a small filter worked quite well to reduce the ripple in the output.

$$f = \frac{1}{2\pi\sqrt{LC}} \tag{1}$$

The figure below shows the completed prototype of the proposed charger.

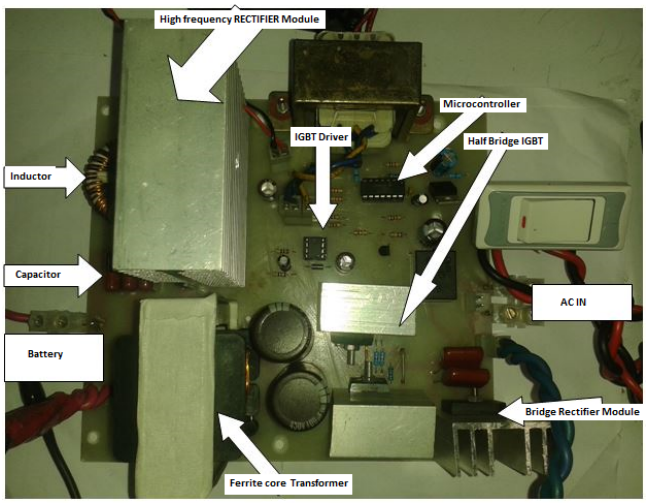

Fig. 6 Prototype of proposed charger

C. Experimental Setup of the Proposed Charger

A similar experiment to the conventional charger was conducted for the purpose of comparing the two charging systems. In the proposed system, the same parameters such as battery voltage, charging current and input power were monitored during the experiment. The following figure shows the experimental setup of the proposed easy bike charger.

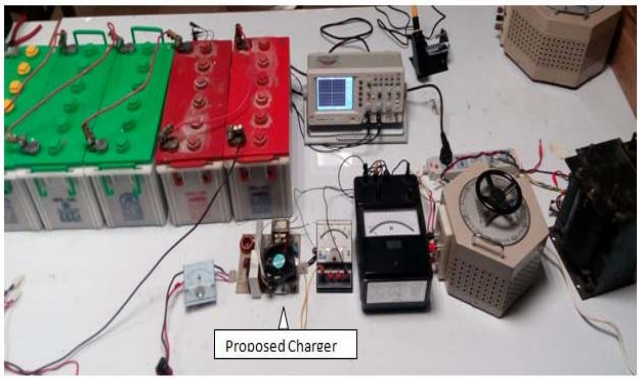

Fig. 7 Experimental setup of Conventional Charger

Just as with the conventional setup, in the proposed setup the charging current was varied using the variac, and the corresponding input power was recorded using a wattmeter. The output power was measured by calculating the product of the charging current and the voltage that appeared across the battery bank. Finally, using the ratio of output to input power, the efficiency of the charging system was calculated. Table 2 below shows the experimental data obtained from the charging system containing the proposed charger.

TABLE II
EXPERIMENTAL DATA OF PROPOSED CHARGER

$V_{battery\ (V)}$	$I_{char\ (A)}$	$P_{in\ (W)}$	η (%)
61	1	95	64.21
61.2	2	150	81.6
61.8	3	210	88.28
62.3	4	260	95.84
62.8	5	325	96.61
63.2	6	385	98.49
63.7	7	455	98
64.1	8	525	97.67
64.8	9	600	97.2
65.2	10	665	98.04
65.6	11	750	96.21
65.9	12	830	95.27
66.3	13	890	96.84

IV. RESULTS AND DISCUSSIONS

From the data obtained in Tables 1 and 2, a curve of efficiency, η, against charging current, I_{char}, can be plotted for both systems using the same axes. As a result, since the same charging current is applied in both cases, a direct comparison of efficiency can be made. The figure below shows the curves of the two systems.

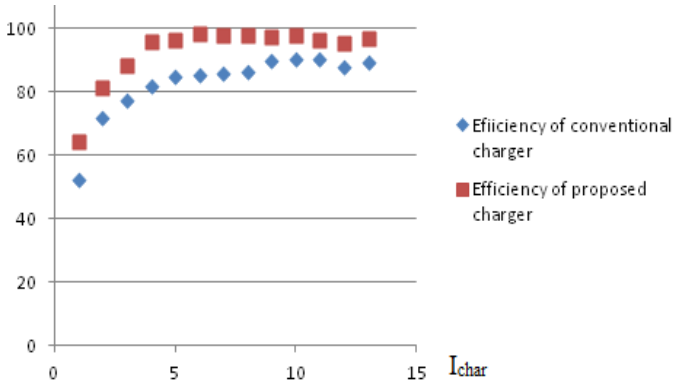

Fig. 8 Graph of efficiency against charging current for both systems

D. Comparison of Efficiencies

It is quite apparent from the figure above that the efficiency of the proposed charging system is significantly higher than that of the conventional system. The average efficiency of the conventional charging system is 82%, whereas that of the proposed system is 93%. Therefore, the proposed charger is roughly 11% more efficient than the conventional one.

E. Comparison of Size

The use of the ferrite core transformer in the proposed charging system has resulted in a much lighter charger than the conventional iron core charger, which weighs about five times as much as ferrite core charger. This makes the proposed charger much more compact, portable and easier to handle.

F. Comparison of Price

Although at present, the price of the proposed charger is not too less than the conventional charger, as time progresses the proposed charger is expected to become only cheaper. The reason is that it is mainly comprised of silicon, which exhibits a decline in price with the passage of time. On the other hand, the contrary is true for the iron core charger, since the price of iron is rising with time.

V. CONCLUSIONS

In this paper, a detailed description of the design and construction of a more efficient, lightweight and cost-effective charger for electric easy bikes has been presented. A direct comparison of the proposed charger has been made with a typical conventional charger by creating the same charging conditions in the lab. The use of the ferrite core transformer in the proposed charger not only makes it much lighter, but also more efficient. Furthermore, the cost of such a charger is expected to fall with time, whereas iron core chargers are likely to become more expensive. The experimental findings suggest that if the proposed charger is produced in a large scale, it has the potential to completely replace the conventional iron core chargers. Considering the fact that there are about one million easy bikes in Bangladesh at present, implementing the proposed charging scheme can boost energy savings by a huge amount.

REFERENCES

[1] Conserve Energy Future. [Online]. Available: http://www.conserve-energy-future.com/advantages-and-disadvantages-of-electric-cars.php, Accessed: Aug. 4, 2015.

[2] F.Pellitteri, V. Boscaino, A. O. Di Tommaso, F. Genduso, and R. Miceli, "E-bike battery charging: Methods and circuits," in *Proc. Int. Conf. Clean Elect. Power (ICCEP), 2013*, Alghero, 11-13 Jun. 2013, pp. 107-114.

[3] N. Zimmerman and R. Bass, "Impacts of electric vehicle charging on electric power distribution systems," Oregon Transportation Res. and Edu. Consortium, Portland, OR, USA, Sep. 2013. [Online]. Available: http://pdxscholar.library.pdx.edu/cgi/viewcontent.cgi?article=1165&context=ece_fac

[4] C. S. Wang, O. H. Stielau, and Grant A. Covic, "Design Considerations for a Contactless Electric Vehicle Battery Charger," *IEEE Trans. Ind. Electron.,vol. 52, no. 5, pp. 1308-1314, Oct. 2005.*[Online]. Available: https://researchspace.auckland.ac.nz/bitstream/handle/2292/243/243.pdf%3Fsequence%3D1, Accessed on: Aug. 6, 2015.

[5] X. Zhou, G. Wang, S.Lukic, S. Bhattacharya, and A. Huang, "Multi-function bi-directional battery charger for plug-in hybrid electric vehicle application," in *Proc. Energy Conversion Congr. and Exposition, 2009*, San Jose, CA, USA, 20-24 Sep. 2009, pp. 3930–3936.

[6] Electrical Engineering Portal. [Online]. Available: http://electrical-engineering-portal.com/transformer-heat-copper-and-iron-losses, Accessed on: Sep. 3, 2015.

[7] Radio-Electronics.com. [Online]. Available: http://www.radio-electronics.com/info/rf-technology-design/rf-filters/simple-lc-lowpass-filter-design.php, Accessed on: Sep. 7, 2015

Energy Usage Pattern of Off-grid Population in Bangladesh

Hasna J. Khan[1], Asma J. Huque[2]
Kaysar Ahmed[3], Rafiur Rahman[4], Tanvir Ahmed[5], and Rashedul Alam[6]
[1, 2, 3, 4, 5, 6]Prokaushali Sangsad Limited (PSL), Dhaka, Bangladesh
[1]hasnajkhan@gmail.com

Abstract— **This paper presents a study of the power and energy consumption patterns in off-grid rural areas as learned from the 100kWp Purobi Green Energy Ltd. solar minigrid that has been operating in the Enam Nahar Bazar, Sandwip, Bangladesh for about 5 years. The study reveals the critical applications of energy in the rural areas are for the lighting, fan, refrigeration, communication, and medical purposes. Major share of the energy is consumed by motor based appliances, especially in the commercial sector for businesses whereas lighting, which is the most critical use of energy in rural areas, accounts for the least**

***Keywords*— solar minigrid; Bangladesh, load management, energy consumption, load pattern**

I. INTRODUCTION

About 20% of the world's population does not have access to electricity. A major part of this population is living in the rural areas where national utility line has not yet reached or cannot reach in the near future due to the rural population being dispersed, having small incomes, low electric demand, remoteness of the location and the cost of erection and maintenance of transmission and distribution lines in comparison to low power consumption in such areas [1]. Compared to costs for establishing national grid connections to such remote places, cost of erecting a renewable energy based power plant which can generate power locally in contract to transmitting power from grid to locality is a much more feasible choice. With over 50% - 100% more solar irradiation than in the European countries, solar power is the best option for countries like Bangladesh [2, 3, 4, 5].

For renewable energy sources, management of load is of utmost importance due to the intermittent nature of the source [1, 6]. Study of load patterns can help motivate consumers to change their energy usage patterns or appliances for better usage of energy. It also helps detect any unwanted power consumption from such intermittent sources [7] and the factors responsible for the rise in consumption pattern of electricity and the sufferings face by the poor people without electricity in rural areas [8]. Finally, the key to any energy development project is to understand it current energy usage in the locality and identifying scopes of improvement [9].

II. ENERGY CONSUMPTION IN BY DIFFERENT SECTOR OF CONSUMERS IN ENAM NAHAR BAZAR, SANDWIP

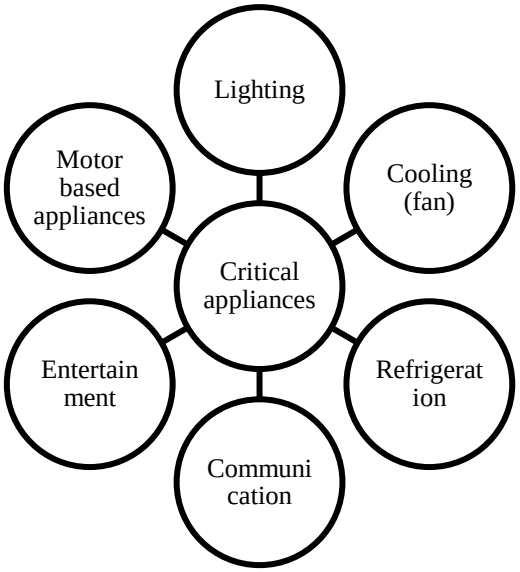

Fig 1. Appliances critical for low-income populations

Demand for energy in rural areas is limited, basically, to critical applications, for improving lives and livelihood, like lighting, cooling, refrigeration, communication, entertainment, medical, and agricultural uses for their basic purposes (fig 1). These few aspects have the most impact in alleviating poverty and illiteracy in the rural areas. In [10, 11] an analysis of a 100kWp Purobi Green Energy Ltd (PGEL) solar minigrid implemented in the Enam Nahar Bazar, Sandwip, Hatiya, Bangladesh has been presented.

Powering a total of nearly 300 clients, the PGEL solar minigrid has helped in the uplifting of the residential life style, educational quality, and commercial and industrial activities through reliable electricity supply. But with an increasing number of connections and aggregate energy consumption (fig. 2), it has become of utmost importance to study and find potential scopes for energy consumption and waste reduction through studying the load patterns as in the PGEL supplied region and the market condition for energy efficient products usable in rural areas for possible replacements. Fig 3 shows comparison of energy consumption between of residential and

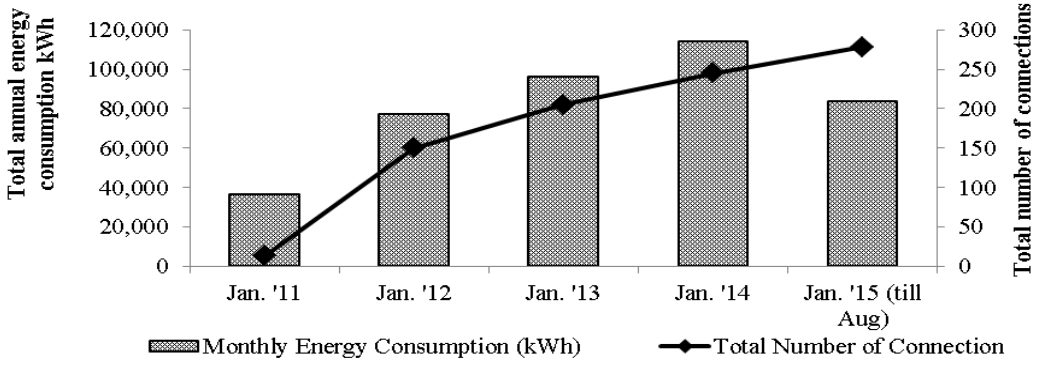

Fig 2. Annual energy consumption and number of connections of the PGEL solar minigrid

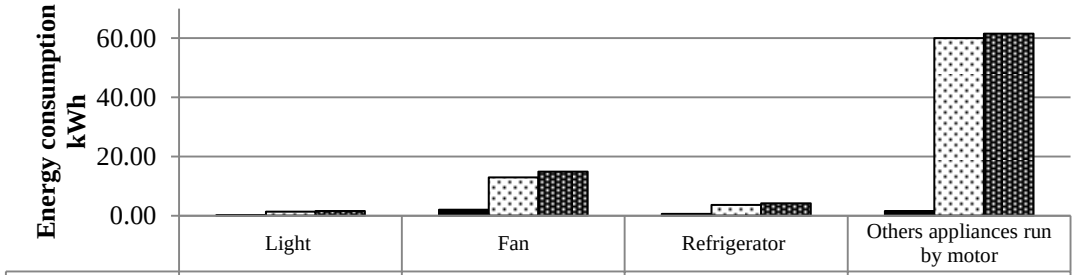

	Light	Fan	Refrigerator	Others appliances run by motor
Residential use	0.17	1.96	0.60	1.60
Commercial use	1.39	12.96	3.60	60.00
Total	1.56	14.92	4.20	61.60

Fig 3. Energy usage by different sectors for different

commercial user of Sandwip, and sub-categories of lights, fans, refrigerator and other appliances run by motors. It is seen that lighting consumes the least amount of energy while motor based appliances are the highest consumers of energy for both sectors. It can be deduced that for any kind of load management and energy efficiency improvement step, the obvious target will have to be the motor based appliances.

III. Energy Consumption by Different Appliances

Figure 4 shows the breakup of energy usage by the different appliance categories in different kinds of businesses. This analysis combined with the previous figure helps narrow down the domain where energy efficient products and load management can have maximum impact. Fans (AC induction motor based appliance) are the major energy consumer for the rural households, and the second largest for hospitals, diagnostics centres, schools, training centres, banks, offices, and residential hotels. Other motor based appliances are the major energy consumer for stationary shops, tailors, carpenter shops and small workshops.

Figure 5 shows a breakdown of the motor based appliances, their rated power and the type of motor used for both residential and commercial purposes. The shaded region shows the range of the rated power of the appliances used by different consumers.

The figure shows that a higher percentage of power consumption by motor based appliances is in the commercial sector which employs appliances of wide range power ratings. Machines like air compressors, water lifting pumps, wood-working tools, and vacuum cleaners have a wide range of available power, indicating very high potential for energy efficiency measures through proper choice of machinery of different rating.

The shaded area following figure shows the range of energy consumption per appliance for different applications. Depending on season and daily necessary usage, the energy consumption can vary greatly. For instance, during the winter season the fans are not used at all. Wood-working tools may not be used for more than 4 hours a day but may account for higher energy consumption due to high power consumption. Sewing machines are low power consuming machines but are operated for longer hours like 4 hours and above, which accounts for their high energy consumption. Refrigerator compressors are low power consuming units but are run for more than 8 hours each day which leads to a very high energy consumption. Overall it can be seen that machines like air compressors, wood-working tools, marble/wood-cutter, lathe machine, hand grinding machines and sewing machines account for huge amount of energy consumption as these machines are one of the primary sources of income for those shops.

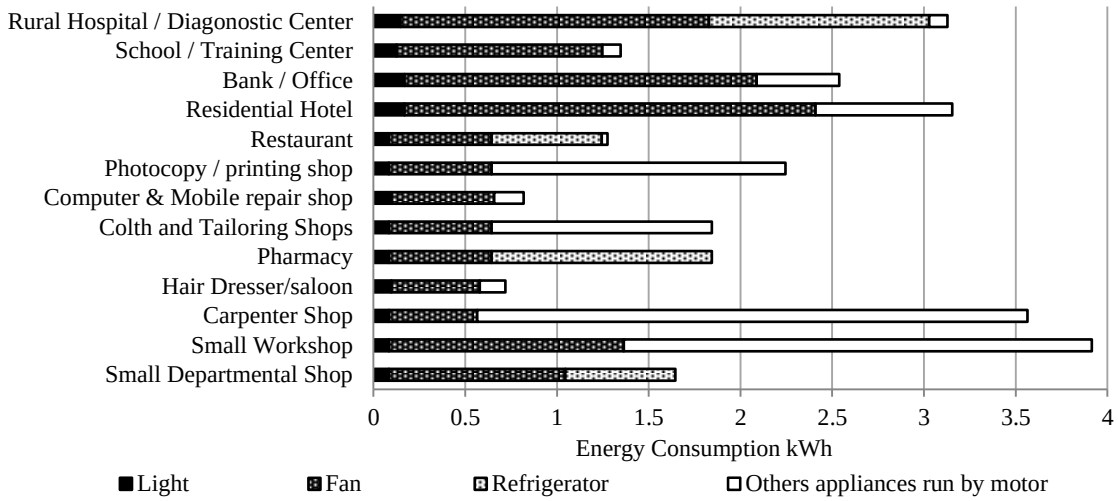

Fig 4. Daily energy consumption of different businesses in Sandwip

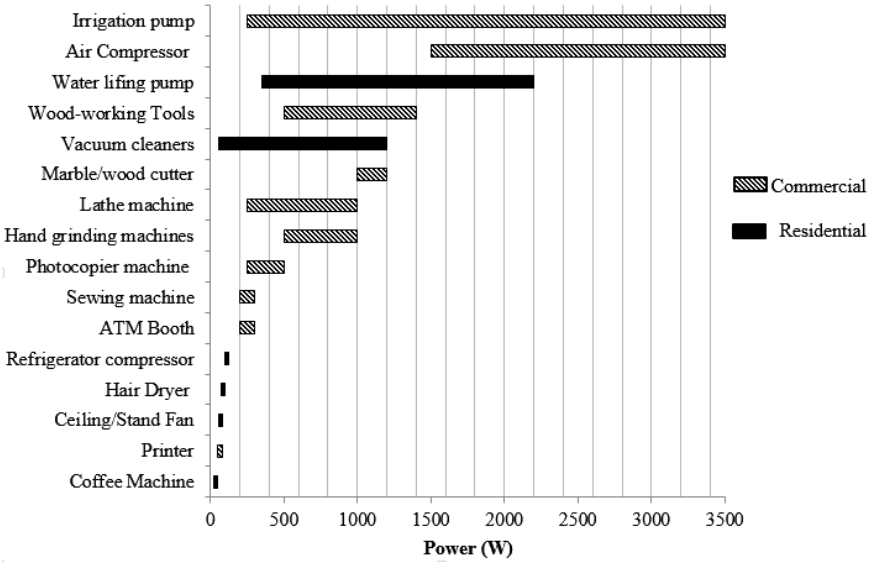

Fig 5. Power range of different motor based appliances used by different sectors in rural area

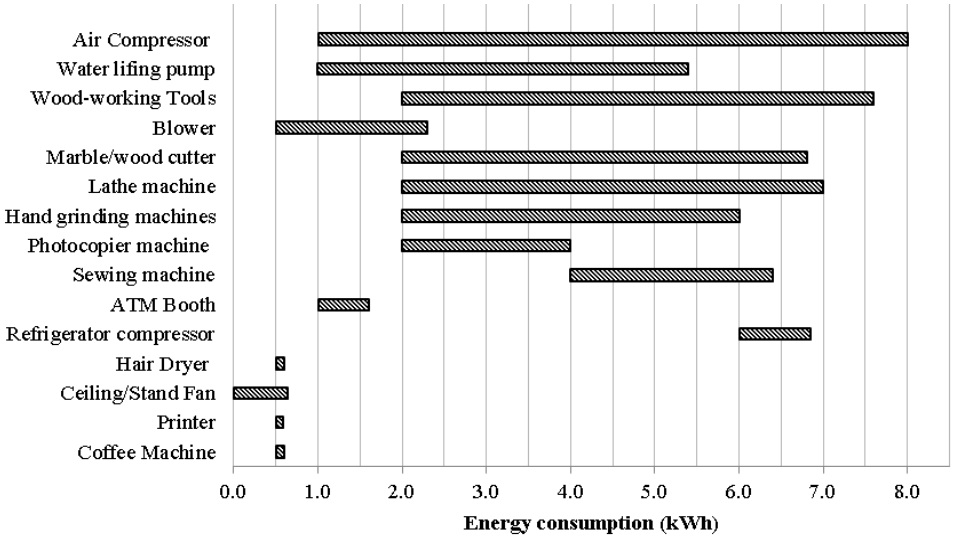

Fig 6. Energy usage range for different appliances

IV. Future Works

Determination of absolute energy consumption of such appliances is beyond the scope of this paper as it would require a thorough survey of the whole PGEL electrified area in both residential and commercial sector. The future study will focus on determining exact usage of energy by different appliances by a thorough survey of the Enam Nahar market. An exact load profile determination will be followed by energy consumption reduction and load management efforts, which is demand side management (DSM). Consumers will be provided access to information on the economic and environmental benefits of using energy efficient appliances. Such knowledge will become particularly important for household appliances like fan, refrigerators and TV, along with commercial appliances like pumps and motors. Energy saving will be determined for replacing AC induction motors in the motor based appliances by Brushless DC motors (BDCM), and LED lights can replace CFL lamps that may be used in the market already which are known for improved energy efficiency.

V. Conclusion

From the primary analysis it is revealed that a huge scope lies for load management and energy efficiency measures regarding the motor based appliances in Enam Nahar. However, since LED is mostly used for lighting, it may not amount to a significant change for PGEL in energy saving albeit being the most common use of energy in rural areas. The motor based appliances account for the highest individual energy consumption making them the anchor loads for feasible solar minigrids like PGEL. Although they are the highest consumers of energy and thus the highest source of income for the minigrids, energy consumption reduction and load management measures should be taken to expand the electrified region by such limited renewable energy generation.

References

[1] Sahu, A.K, Dr Shandilya, A.M, Dr. Bhardway, S.K, "Forecasting and management of load for rural areas," *International Journal of Scientific and Research Publications*, vol. 3, Issue 1, January 2013

[2] Khan, S.A.; Rahman, R.; Azad, A., "Solar Home System Components Qualification Testing Procedure and Its Effect in Bangladesh Perspective," in *Global Humanitarian Technology Conference (GHTC), 2012 IEEE* , vol., no., pp.381-386, 21-24 Oct. 2012

[3] A. Rajoriya & E. Fernandez, "Sustainable energy generation using hybrid energy system for remote hilly rural area in India", *International Journal of Sustainable Engineering*, Vol. 3, No. 3, pp. 219–227, Sept. 2010

[4] Dr. M. M. Qurashi & Engr. Tajammul Hussain, "Renewable Energy Technologies for Developing Countries Now and to 2023" *Islamic Educational, Scientific and Cultural Organization*

[5] Caisheng Wang & M. Hashem Nehrir, "Power Management of a Stand-Alone Wind / Photovoltaic / Fuel Cell Energy System", *IEEE Transactions on Energy Conversion*, vol. 23, No. 3, pp. 957-967, Sept. 2008

[6] J. Heinonen, S. Junnila, "Residential energy consumption patterns and the overall housing energy requirements of urban and rural households in Finland," *Energy and Buildings*, vol. 76, pp. 295-303, June 2014

[7] Roy, N., "Green building energy analytics: Challenges and opportunities," in *Pervasive Computing and Communication Workshops (PerCom Workshops), 2015 IEEE International Conference on* , vol., no., pp.292-292, 23-27 March 2015

[8] Dash, P, "Consumption pattern of electricity in rural and urban areas: a case study of Rourkela, Sundergarh district of Odisha," M. S. thesis dissertation, National Institute of Technology, Rourkela, India

[9] Van Acker, V.; Szablya, S.J.; Louie, H.; McLean Sloughter, J.; Pirbhai, A.S., "Survey of energy use and costs in rural kenya for community microgrid business model development," in *Global Humanitarian Technology Conference (GHTC), 2014 IEEE* , vol., no., pp.166-173, 10-13 Oct. 2014

[10] Khan, H.J.; Huque, A.J.; Kaysar Ahmed Sagor, Tanvir Ahmed, Rashedul Alam, M. Riazul Hamid, "Experience from First Solar Mini Grid Service in Bangladesh," in *Decentralized Solution for Developing Economies Springer Proceedings in Energy*, pp 43-52, March 2015

[11] Khan, H.J.; Huque, A.J., "Reliable power supply with solar mini grid in Sandwip Island of Bangladesh," in *Developments in Renewable Energy Technology (ICDRET), 2012 2nd International Conference on the* , vol., no., pp.1-4, 5-7 Jan. 2012

Prediction of Solar Irradiation in Bangladesh Using Artificial Neural Network (ANN) and Data Mapping Using GIS Technology

Khan Md. Rabbi[1], Indrajit Nandi[2], Abu Shoaib Saleh[3], Faiaz Faisal[4], Satyajit Mojumder[5]

Department of Mechanical Engineering, Bangladesh University of Engineering and Technology, Dhaka – 1000, Bangladesh

[1]khanrabbi92@gmail.com

[2]nandiindrajit11@gmail.com

[3]abushoaibsaleh@gmail.com

[4]protyayfaisal69@gmail.com

[5]sjit018@gmail.com

***Abstract*— In this paper, an artificial neural network (ANN) model is used to predict the monthly solar energy potential in Bangladesh. Used data are taken from NASA database for the past 22 years average from 1983 to 2005 and eight divisional cities are considered in this study. A multi-layered feed forward ANN model of four layers with eight independent input variables i.e. average temperature, sunshine duration, wind speed, precipitation, humidity, elevation, cloud coverage and atmospheric pressure to predict the monthly solar irradiation .Data from six cities are used for training and the remaining two cities were considered for testing and validation. A solar irradiation map is developed by data mapping using GIS technology. From the illustrations, the predicted data show good agreement with the observed data. This indicates that, this model can be used to predict solar irradiation of Bangladesh and to provide sufficient information about the feasibility of solar powered projects.**

***Keywords*— solar irradiation; ANN; MLFN; renewable energy; GIS; Bangladesh.**

I. INTRODUCTION

Bangladesh, lying east of India on the Bay of Bengal, is a South Asian country of lush greenery and many waterways. It is located between 20.87◦N & 26.48◦N latitude and 88.35◦E & 92.3◦E longitude [1]. The area of Bangladesh consists of about 147,570 square kilometres of total area accompanied by numerous rivers. Bangladesh is a tropical country experiencing dry weather from September to May and undergoing monsoon from June to August. It consists of eight divisions named Dhaka, Chittagong, Khulna, Rajshahi, Barisal, Sylhet, Rangpur and Mymensingh. Almost all regions are suffering from electricity crisis. Electricity supply in the rural areas is insufficient which barely meet the needs especially in some areas where electricity has not reached yet. Natural disasters often strike upon the country and badly damage the infrastructure. Instalments of new power plants are costly but the demand is increasing. To meet the increasing demand of electricity, uses of solar energy could be a big opportunity and the amount of solar energy incident over Bangladesh makes it convenient. With the help of solar power plant, this demand can be mitigated, especially the household demand to a great extent. While establishing solar power plant, cost effectiveness should be kept under consideration. So site selection, system design and Implementation are the key things for cost effective solar power plant and for that solar irradiation data is prerequisite to have efficient system design and better solar output. As our government has given greater consideration on several solar projects so the solar irradiation data is very much needed. But there is a limitation of meteorological device available for the direct measurement of solar irradiation data. Estimation of solar irradiation data using an alternative model will be a great solution for a developing country like Bangladesh. This paper studies the application of Artificial Neural Network model and gives a prediction about solar irradiation in two divisional cities of Bangladesh.

ANN model will be a very reliable and suitable model to predict solar irradiation as there is a limitation on the number of meteorological station to record solar irradiation availability. In Bangladesh, some meteorological stations only have relative humidity, temperature, wind speed and sunshine duration. Measurement of solar irradiation with reliable and calibrated pyrometers is not available in a sufficient location. Al-Alawi and Hinai [2] developed an ANN model to predict global solar radiation in several locations where necessary measurement instruments are not available and then used the model to estimate global solar radiation in Oman. Kalogirou et al. [3] predicted the amount of energy consumption of a passive solar building based on ANN model. Jiang [4] estimated monthly mean solar diffusion radiation in China using ANN model. Mohandes et al. [5] developed neural network model to predict daily global solar radiation in Saudi Arabia using latitude, longitude, and the sunshine duration as inputs. Rumbayan et al. [6] developed an ANN model to estimate solar irradiation in different regions of Indonesia based on input data i.e. average temperature, average relative humidity, average sunshine duration, average wind speed, average precipitation, longitude, latitude and month of the year. Koca et al. [7] used an ANN model to forecast solar radiation in Mediterranean region of Anatolia in Turkey. Ouammi et al. [8] estimated monthly and yearly solar irradiation in Morocco by using a three layered and back propagated ANN model. Wang et al. [9] forecasted a short time solar irradiance using statistical data based on neural network. Ozgoren et al. [10] developed neural network model

based on multi-nonlinear regression to estimate solar radiance in any place of Turkey. Izgi et al. [11] also estimated short time global radiation using ANN model. Dahmani et al. [12] developed an artificial neural network to give a prediction on tilted global solar radiation.

The main focus of this study is to establish an Artificial Neural Network model to give a prediction on solar irradiation in eight divisional cities of Bangladesh based on NASA earth data. As there is a lack of suitable measurement instrument, an ANN model will be a great measurement platform for the solar engineers for designing a solar power plant.

II. THEORETICAL BACKGROUND AND LITERATURE REVIEW

A. Artificial Neural Network Theory

ANN is mimicking of learning process of human brain and a strong machine learning tool. It is a widely accepted method used over decades for prediction model as an alternative of complex problems. Because of its learning capability, nonlinearity, input output mapping, adaptivity and fault tolerance rate makes it very useful for prediction [113]. ANN is a connection of small individual interconnected neural networks of multiinput nonlinear process with weighted interconnections. The weights of the interconnection between neurons and their learning rates are adjusted during training process to achieve desired output. Here we use multilayer feed forward neural network (MLFN) model for our paper.

B. Multi-layered Feed Forward Neural Network

MLFN trained with back propagation algorithm are mostly used ANN in scientific research. The basic structure of MLFN is input, hidden and output layer. Hidden layer can be of many layers with large units of interconnected neurons. Hidden layer operates like a blackbox model [13]. Its working mode is training and prediction mode. For training of MLFN and predictin using MLFN we need two data set. During the training process weights are adjusted to obtain desired output and prediction mode to assure the developed model.

C. Solar Energy Potential

As Bangladesh is located in 20’30’’and 26’45’’ north latitude and a tropical country, solar energy reaches at earth surface makes it very efficient for solar system implementation. Bangladesh is just few meters high above sea level, hydro power is not efficient. For the lack of available data wind energy, bio energy and ocean energy are not also very efficient. So solar energy is the ultimate suitable form of renewable energy for both urban and rural area of Bangladesh. That’s why solar irradiation measurement is necessary.

D. Review

Numerous studies on ANN model has been carried out in recent years. These studies have given a prediction on monthly solar irradiation. As ANN is of nonlinear behavior and no need for primary assumption to develop data relationships, it becomes a necessary tool for estimating solar irradiation.ANN models are developed to model various solar radiation variables in different locations. Yadav et al. [14] gave a review on artificial neural network models to identify best suitable method for solar radiation prediction.Yadav et al. [15] designed a neural network model to determine most relevant input parameters for prediction of solar radiation. Ozgur kisi [16] tried fuzzy genetic approach to estimate solar radiation and gave a compare with ANN approach. Egeonu et al. [17] developed a temperature based ANN model trained with the Levenberg Marquardt algorithm to provide a forecast on solar radiation in Nigeria. Şenkal [18] applied artificial neural network approach for giving a model and prediction of mean perceptible water and solar radiation in specific location in Turkey based on meteorological data.

III. DATA COLLECTION AND METHODOLOGY

This study was carried out for Bangladesh, which comprises eight divisions. Divisional cities were taken for study as these cities are highly populated and thus energy consumption rate is also high in these cities. Latitude & longitude of eight divisional cities has been given in Table -1 and monthly solar irradiation of eight divisional cities was enlisted in Table-2.

TABLE I. GEOGRAPHICAL CO-ORDINATES OF EIGHT DIVISIONAL CITIES

No.	City	Latitude	Longitude
1	Dhaka	23.70°	90.37°
2	Chittagong	22.37°	91.80°
3	Barisal	22.70°	90.37°
4	Khulna	22.82°	89.55°
5	Mymensingh	24.75°	90.40°
6	Rajshahi	24.37°	88.60°
7	Rangpur	25.73°	89.25°
8	Sylhet	24.90°	91.87°

The procedure implemented in this research is given in details as follows: in first step of building the artificial neural network the data are defined as input & output. Sunlight duration, temperature, wind speed, humidity, precipitation, cloud coverage, atmospheric pressure & elevation were input parameters and monthly solar irradiation was output. Then the data were divided into three purposes – training, testing & validation. Total 96 data are taken for the study among which 67 data are used as training data, 14 data are taken for testing & the rest as validation data.

IV. ARTIFICIAL NEURAL NETWORK MODELING

Paper demonstrates a feed forward back propagation neural network with one hidden layer to estimate the monthly solar radiation for eight divisional cities in Bangladesh. Here the input layer consists of eight units and hidden layer with 16 neurons and output layer with 1 neuron (Fig. 1) to estimate solar irradiation.70% of the total data was used for training, 15% for testing and 15% for validating the developed model. 14 combinations are tested & Mean Absolute Percentage Error (MAPE) is determined for each of them (Table 2). The combination with lowest MAPE is chosen for prediction.

TABLE II. MEAN ABSOLUTE PERCENTAGE ERROR FOR DIFFERENT LAYER COMBINATION

No.	Combination	MAPE
1.	8-10-1	18.27075834
2.	8-12-1	13.76045635
3.	8-14-1	13.12041298
4.	8-15-1	23.18527765
5.	8-16-1	6.956345501
6.	8-18-1	13.02736446
7.	8-20-1	15.65731949
8.	8-22-1	7.951355134
9.	8-24-1	13.21370951
10.	8-25-1	14.4509271
11.	8-9-18-1	17.13428176
12.	8-10-4-1	15.92907026
13.	8-9-14-1	9.641712081
14.	8-9-9-1	21.10584328
15.	8-9-10-1	10.85348962

For the simplicity and better performance of the model the input and output data were pre-processed within threshold range [0, 1] and then return to original value after prediction. For any data X

$$X_{max} = \max\{X\} \quad (1)$$

$$X_{min} = \min\{X\} \quad (2)$$

$$X' = (X - X_{min}) \ / \ (X_{max} - X_{min}) \quad (3)$$

Here X may be input or output. X' is 1 when $X = X_{max}$ and 0 when $X = X_{min}$. In this analysis back propagation algorithm was implemented in the neural network. The weights and biases were adjusted according to the Levenberg-Marquardt optimization. The network is instructed to learn using Gradient Decent algorithm with momentum.

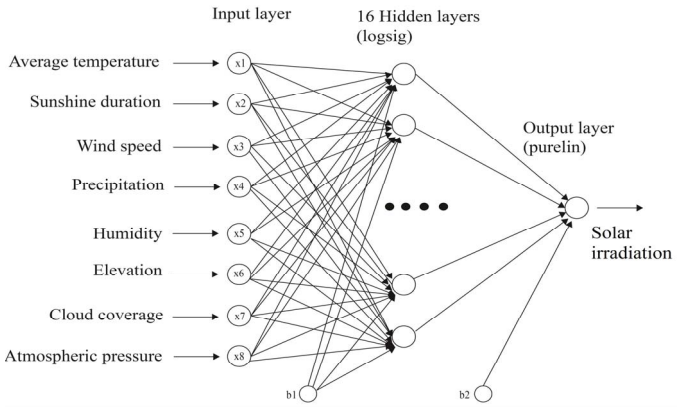

Fig. 1. Best predictive model architecture (8-16-1)

A logistic sigmoid transfer function (LOGSIG) [19] was used for the hidden layer which is

$$LOGSIG(X) = \frac{1}{1+e^{(-X)}} \quad (4)$$

For inputs X_j (j = 1, 2, 3, 4 . . . , n) each input is weighted by weight factor W_{kj} and a portion of the original signal is passed to the network .If the sum of total input is U_k then

$$U_k = \sum_j X_j W_{kj} + b_k \quad (5)$$

Where, W_{kj} is the weight means the connection strength from unit j to k. The bias b_k help to adjust the inputs. Based on learning rate weight is updated in each iteration by equation

$$W_{kj}^{new} = W_{kj}^{old} - \eta \frac{\delta E}{\delta W_{kj}} \quad (6)$$

Here, η is the learning rate and $\delta E/\delta W_{kj}$ is the gradient of error .The error calculation is very much important for back propagation cycle for the beter fitting of the model cause the training will end when the error will be minimum. The error can be defined as

$$E = \sum_p \sum_j (O_{pj} - D_{pj})^2 \quad (7)$$

Here, O_{pj} is the observation value and D_{pj} is the predicted value by ANN.

V. RESULT AND DISCUSSION

The monthly experimental value of solar radiation in eight different divisions has been shown in Table 3. From Fig. 5, it is shown that the highest value of solar radiation occurred in April and the lowest solar radiation happened in September. It is also found from the Fig. 5 is that the deviation between the predicted and experimental value were almost close.

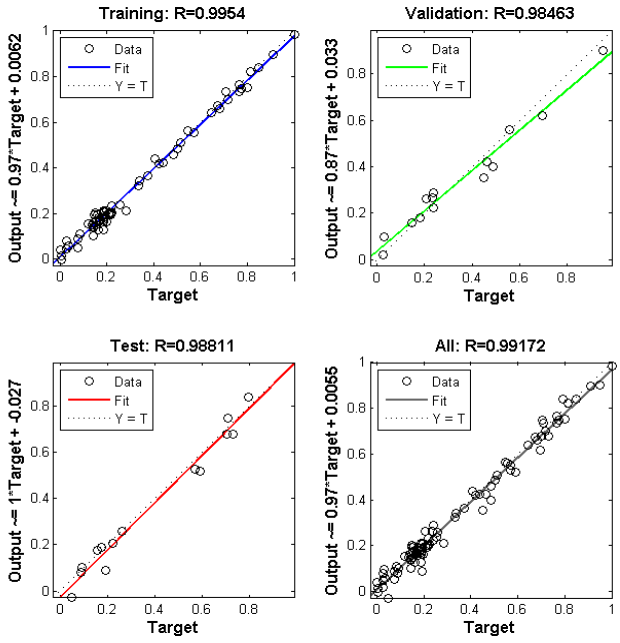

Fig. 2. Performance regression plot for predictive model

TABLE III. MONTHLY SOLAR IRRADIATION DATA

City	Jan	Feb	March	April	May	June	July	Aug	Sept	Oct	Nov	Dec
Dhaka	4.36	4.92	5.59	5.76	5.3	4.53	4.23	4.29	4.01	4.32	4.28	4.21
Chittagong	4.42	4.98	5.44	5.51	5.11	4.16	4.04	4.18	4.01	4.28	4.25	4.28
Barisal	4.34	4.95	5.57	5.65	5.25	4.05	3.89	3.91	3.83	4.29	4.23	4.24
Khulna	4.29	4.88	5.58	5.83	5.53	4.2	3.89	3.9	3.83	4.29	4.23	4.21
Mymensingh	4.37	5.08	5.81	5.86	5.19	4.47	4.12	4.18	3.82	4.3	4.38	4.19
Rajshahi	4.32	5.25	5.95	6.33	5.74	5.04	4.41	4.36	4.03	4.42	4.46	4.21
Rangpur	4.34	5.22	6.1	6.2	5.74	4.76	4.19	4.29	3.89	4.67	4.66	4.26
Sylhet	4.37	5.04	5.6	5.62	4.84	4.22	4.18	4.3	3.94	4.36	4.29	4.17

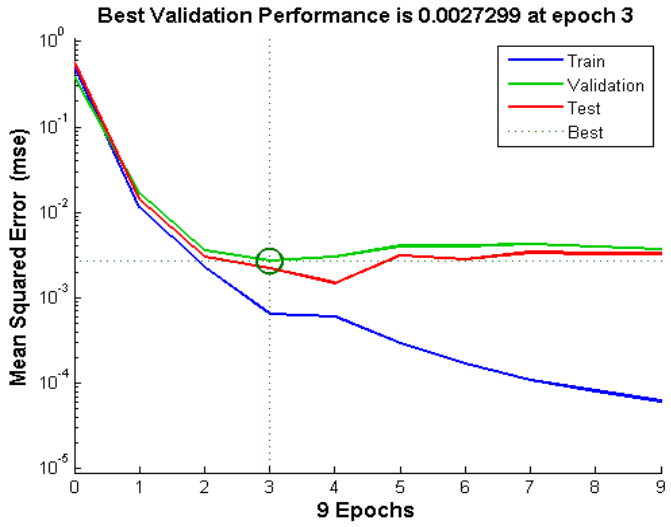

Fig. 3. Training, validation and test mean squared errors

The experimental & predicted values of solar irradiation are plotted using MATLAB GUI (Graphical User Interface) tool. The GUI is developed (Fig. 4) with unique call-back function. Data is loaded and plotted for two different cities Dhaka and Chittagong.

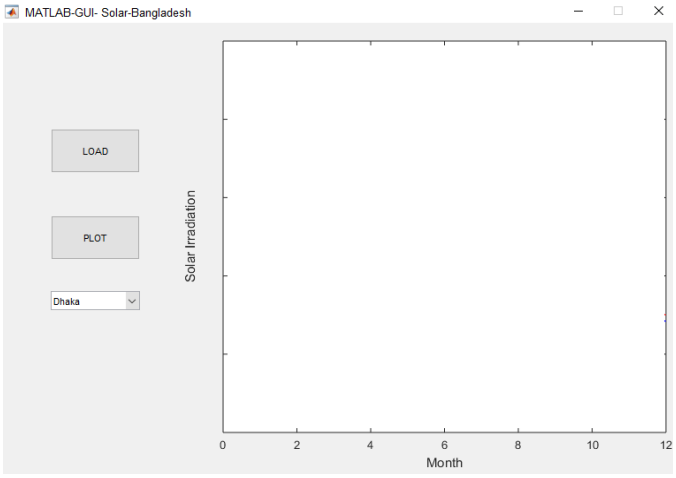

Fig. 4. MATLAB GUI model

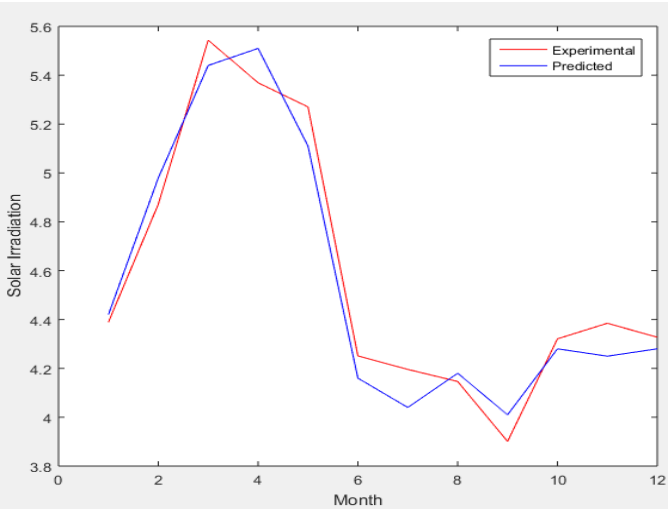

Fig. 5. Comparison of predicted and observed value for Dhaka city

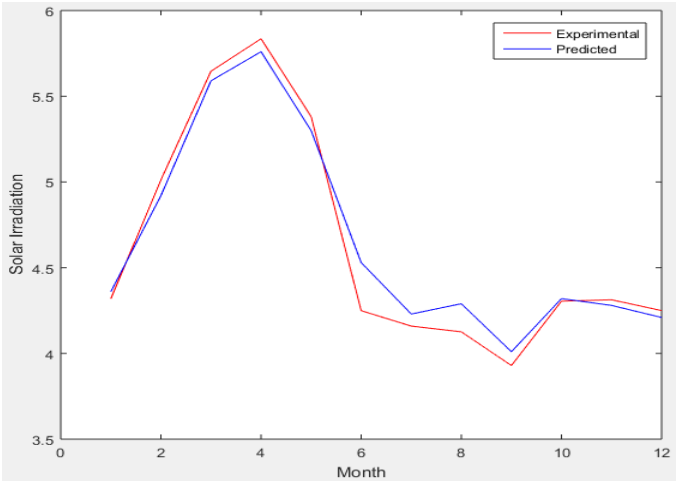

Fig. 6. Comparison of predicted and observed value for Chittagong city

The monthly solar radiation data for Chittagong city have been shown in Fig. 6 in similar manner as Fig. 5. The highest predicted value has been found in March and the lowest has been in September like Dhaka city.The predicted value and the experimental value were nearly equal.

The training of the input data was done by adjustment of the weights & biases of the whole network to reduce the Mean Squared Error (MSE) to a minimal range. At the time of training, each neuron takes the input signals, sums them up using weights and biases and then sends the result through suitable transformations as output. The training has been carried out till the point where the MSE attains a sufficiently small value. Here, MSE ≤ E, where the stopping criteria was taken E = 10^{-3}. In this study, the training was terminated after 19 epoachs. Fig. 2 illustrates the training, validation and test mean squared errors. At the time of training, the performance function MSE of the training data subset is nearly close to 10^{-3} where the MSE for validation & testing data was slightly greater than the stopping criteria.Thus it can be assumed that the training phase was completed successfully.

Error histogram is included to ensure the accuracy of training and validation test. As it can be seen from Fig. 7 that error between target and output values are in tolerable limit for different instances of the model.

The fineness-of-fit between the targeted output and the predicted output has been illustrated in Fig. 2. The linear regression of each curve was in range of 90% accuracy. So it can be said that the ANN model prediction was excellent to estimate solar radiation.

The comparison between measured value (H_{mi}) and estimated value (H_{pi}) were determined by mean average percentage error (MAPE) by equation

$$MAPE = \frac{1}{n}\sum_{i=1}^{n}\left|\frac{H_{mi} - H_{pi}}{H_{mi}}\right| \qquad (8)$$

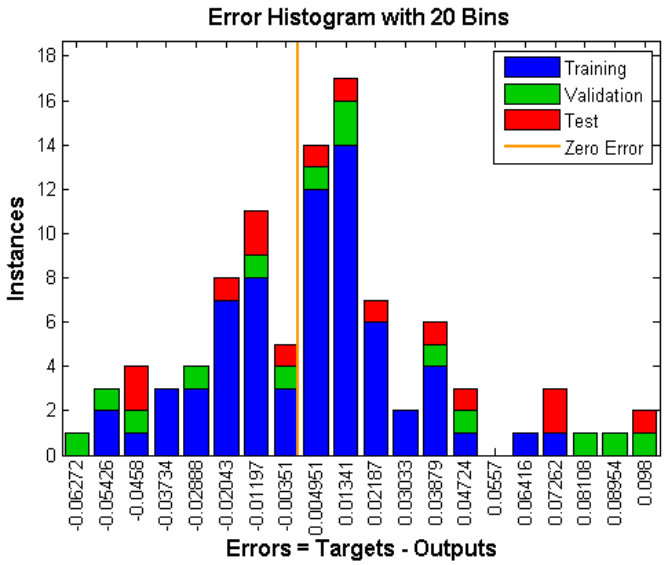

Fig. 7. Error histogram during training and validation

The annual solar irradiation map for divisional cities have been developed by Geographic Information System (GIS).GIS uses statistical analysis & database technology for mapping to shows where and how things move over a period of time.

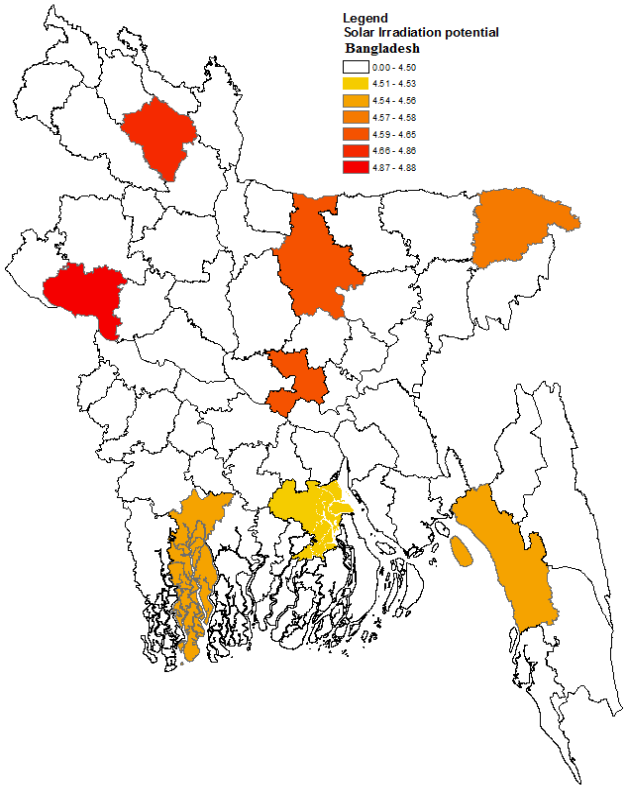

Fig. 8. Solar irradiation map for eight divisions of Bangladesh

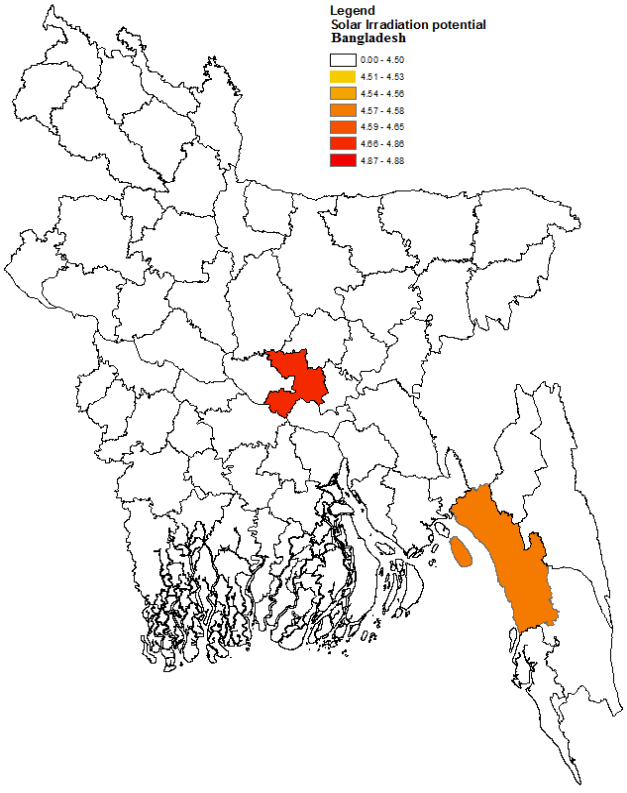

Fig. 9. Predicted solar irradiation map for Dhaka & Chittagong

GIS based solar irradiation maps were used by Gastli et al. [20] to show solar electricity prospects in Oman. Geographical co-ordinates of Bangladesh is WGS 1984 UTM ZONE 45N.By mapping it shows that solar irradiation potential is much than northern region of Bangladesh.

VI. CONCLUSION

This paper represents a predictive model of solar irradiation Using Artificial Neural Network (ANN). It is observed through the study that the ANN model developed can be implemented for prediction of solar irradiation over Bangladesh.

The model is developed for eight divisional cities in Bangladesh namely Dhaka, Chittagong, Barisal, Khulna, Mymensingh, Rajshahi, Rangpur and Sylhet. Model has been trained for 70% of the total dataset while 15% data has been used for testing and the remaining 15% has been for validating.

The trained model was used to predict the solar irradiation of Dhaka & Chittagong to determine its accuracy. It is found that, the predictive model holds good with the observed values. Thus, this predictive model can be useful to estimate solar irradiation potential in remote locations in Bangladesh where the solar potential is not much known.

This predictive model will be helpful for researchers and engineers around the country for selection of location, design and planning of solar plants. Thus, this model satisfies the predictive criterion in both economic and environmental point of view.

Future research investigations can be conducted on mapping of solar potential over Bangladesh along with this model.

ACKNOWLEDGMENT

Authors are thankful to Multiscale Mechanical Modeling and Research Network (MMMRN) for their advices and comments throughout the investigation. Authors gratefully acknowledge NASA website (http://eosweb.larc.nasa.gov) for data.

REFERENCES

[1] http://mynasadata.larc.nasa.gov/latitudelongitude-finder/?lat=&lng=

[2] S. M. Al-Alawi and H. A. Al-Hinai. “An ANN-based approach for predicting global radiation in locations with no direct measurement instrumentation,” Ren. Energy, vol. 14, pp. 199-204, 1998.

[3] A. S. Kalogirou and M. Bojic. “Artificial neural networks for the prediction of the energy consumption of a passive solar building,” Energy, vol. 25, pp. 479-491, 2000.

[4] Y. Jiang. “Prediction of monthly mean daily diffuse solar radiation using artificial neural networks and comparison with other empirical models,” En. Policy, vol. 36, pp. 3833-3837, Aug 2008.

[5] S. Rehman and M. Mohandes. “Artificial neural network estimation of global solar radiation using air temperature and relative humidity,” En. Policy, vol. 36, pp. 571-576, Nov 2007.

[6] M. Rumbayan and K. Nagasaka. “Estimation of Daily Global Solar Irradiation in Indonesia with Artificial Neural Network (ANN) Method,” Int. J. Adv. Sci. Engg. Info. Technology, vol. 1, pp. 190-193, 2011.

[7] A. Koca, F. O. Hakan, Y. Varol, and G. O. Koca. “Estimation of solar radiation using artificial neural networks with different input parameters for Mediterranean region of Anatolia in Turkey,” Expert Sys. Applications, vol. 38, pp. 8756-8762, 2011.

[8] A. Ouammi, D. Zejli, H. Dagdougui, and R. Benchrifa. “Artificial neural network analysis of Moroccan solar potential,” Ren. Sust. En. Reviews, vol. 16, pp. 4876-4889, Jun 2012.

[9] F. Wang, Z. Mi, S. Su, and H. Zhao. “Short-term solar irradiance forecasting model based on artificial neural network using statistical feature parameters,” Energies, vol. 5, pp. 1355-1370, 2012.

[10] M. Ozgoren, M. Bilgili, and B. Sahin. “Estimation of global solar radiation using ANN over Turkey,” Expert Sys. Applications, vol. 39, pp. 5043-5051, 2012.

[11] E.Izgi, A. Öztopal, B. Yerli, M. K. Kaymak, and A. D. Şahin. “Short–mid-term solar power prediction by using artificial neural networks,” Solar Energy, vol. 86, pp. 725-733, Dec 2012.

[12] K. Dahmani, R. Dizene, G. Notton, and C. Paoli, C. Voyant and M. L. Nivet. “Estimation of 5-min time-step data of tilted solar global irradiation using ANN (Artificial Neural Network) model,” Energy, vol. 70, pp. 374-381, 2014.

[13] S. A. Kalogirou. "Artificial neural networks in renewable energy systems applications: a review," Ren. Sust. En. Reviews, vol. 5, pp. 373-401, Mar 2001.

[14] A. K. Yadav and S. S. Chandel. “Solar radiation prediction using Artificial Neural Network techniques: A review,” Ren. Sust. En. Reviews, vol. 33, pp. 772-781, 2014.

[15] A. K. Yadav, H. Malik, and S. S. Chandel. “Selection of most relevant input parameters using WEKA for artificial neural network based solar radiation prediction models,” Ren. Sust. En. Reviews, vol. 31, pp. 509-519, Jan 2014.

[16] O. Kisi. “Modeling solar radiation of Mediterranean region in Turkey by using fuzzy genetic approach,” Energy, vol. 64, pp. 429-436, Oct 2013.

[17] D. I. Egeonu, H. O. Njoku, P. N. Okolo, and S. O. Enibe. “Comparative Assessment of Temperature Based ANN and Angstrom Type Models for Predicting Global Solar Radiation,” In Afro-European Conference for Industrial Advancement, vol. 334, pp. 109-122, 2015.

[18] O. Şenkal. “Solar radiation and precipitable water modeling for Turkey using artificial neural networks,” Meteoro. Atmos. Physics, vol. 127, pp 1-8, Aug 2015.

[19] M. Khayet, C. Cojocaru, and M. Essalhi. "Artificial neural network modeling and response surface methodology of desalination by reverse osmosis, "J. Memb. Science, vol. 368, pp. 202-214, Feb 2011.

[20] A. Gastli and Y. Charabi. “Solar electricity prospects in Oman using GIS-based solar radiation maps,” Ren. Sust. En. Reviews, vol.14, pp. 790-797, Feb 2010.

Control of Bidirectional DC/DC Converter for Back to Back NPC-based Wind Turbine System under Grid Faults

[1]Md Shafquat Ullah Khan, *Student Member*, *IEEE*, [2]Ali I. Maswood, *Senior Member*, *IEEE,*
[3]Hossein Dehghani Tafti, *Student Member*, *IEEE*
[4]Muhammad M. Roomi, *Student Member, IEEE and* [5]Mohd Tariq, *Student Member, IEEE.*

[1]Energy Research Institute @ NTU (ERI@N), School of Electrical and Electronic Engineering, Nanyang Technological University, Singapore.
[2,3,4,5]School of Electrical and Electronic Engineering, Nanyang Technological University, Singapore.
Email: [1]khan0015@e.ntu.edu.sg, [2]eamaswood@ntu.edu.sg

***Abstract*—Viability and reliability of the wind power has made Wind Turbine Systems (WTSs) a popular renewable energy resource. A bidirectional DC/DC converter is proposed in this study for the WTS. The proposed DC/DC converter controls the DC-link voltage by injecting the difference between the extracted power from permanent magnet synchronous generator (PMSG) and the output power of the grid-tied inverter, to the energy storage system. The proposed DC/DC converter controller compensates the shortage of extracted active power from PMSG under wind reduced speed condition in order to inject the constant power to the grid during normal operation. The back to back (BTB) neutral point clamped (NPC) converter is proposed to extract the maximum power from PMSG and inject the extracted power to the grid. The proposed WTS structure achieves fault ride through capability and it can inject reactive power to the grid in order to enhance the PCC voltages under voltage sags. The proportional resonant (PR) current controller is implemented for both rectifier and grid-tied inverter due to its fast response and low steady state error. The adaptive space vector modulation (ASVM) is used to generate the switching signal while balances the DC-link capacitor voltages. The performance of the proposed controller is investigates under grid faults as well as reduced wind speed condition and results have proven the applicability of the proposed controller.**

***Keywords*—Wind Turbine System, DC/DC Converter, Back to Back NPC Converter, Bidirectional Energy Storage System, Proportional Resonant Controller.**

I. INTRODUCTION

With the motto of "Clean Power Plan" USA is moving fast towards renewable energy. In fact, the whole world is moving towards greener and cleaner energy with target of achieving an environmentally better world. The driving force is not just the inspiration to make the world a better place but the alarming issue of reducing vault of limited fossil fuel available. Wind Power is one of the chief sources of renewable energy. Along with all other renewable sources, wind energy conversion is on a radical rise. In last two decades the increase of mainstream wind power has been remarkable as the exponential rise is seen from 6 MW in 1996 to 282.6 GW in 2012 [1]. And now the rise is not to settle down as investments in this sectors estimates the capacity to rise about 800 GW by 2020, if not more. The advancement in Wind Energy sector is marked by groundbreaking break through not only in mechanical features but also in electrical traits as well.

With high penetration of wind power in the previously stable power networks, numerous concerns regarding stability, efficiency and power quality have emerged. As a result of this issue many countries have already implemented grid codes for large scale wind power generations that are connected to the grid [2]. As a solution, power electronics has been playing a major role in improving the wind generated power.

Some companies are building larger wind turbines having generation capability as high as 10 MW [3]. This range is expected to double by 2020. In higher power conversion ranges, more complicated power conversion topologies are required. For low power applications, two-level is more efficient whereas for high power applications the converter capacity is limited due to the semiconductor current and voltage limitations. Consequently, multi-level converters are gaining much popularity for higher power applications [4]. Generally, Back to Back (BTB) power conversion is used in Wind Turbine System (WTS) to get full control of the active and reactive power [5]. BTB Neutral Point Clamped (NPC) has come up as a popular industrial solution for medium voltage converter applications [2], [6], [7].

Three-level NPC converter is used along with DC choppers for WTS in [8]. The DC choppers are considered to control the DC-link voltage under grid fault. The difference of power between the extracted power from the wind generator (P_{0_PMSG}) and the injected power to the grid (P_{0_Inv}) is converted to heat in DC chopper resistor [8]. However, the energy (P_{0_PMSG}- P_{0_Inv}) can be stored in a storage system. A bidirectional DC/DC converter along with an energy storage system (ESS) is proposed in this paper in order to store P_{0_PMSG}- P_{0_Inv} under grid faults. On top of that the stored energy can be used to regulate the output power of the inverter under wind speed variations.

Various topologies like Electric Double Layer Capacitor (EDLC) or supercapacitor are researched for the ESS in WTS. High energy density with fast dynamic response along with long life cycle of supercapacitors made them suitable for WTSs [9]. However, the supercapacitor cannot be deployed independently due to the issues of controllability and limited voltage range [10], [11].

In this paper a single unit Bidirectional Energy Storage System (BESS) is proposed in order to overcome the operational constrains of an independent supercapacitor. A BTB three-level NPC converter is proposed for the wind power

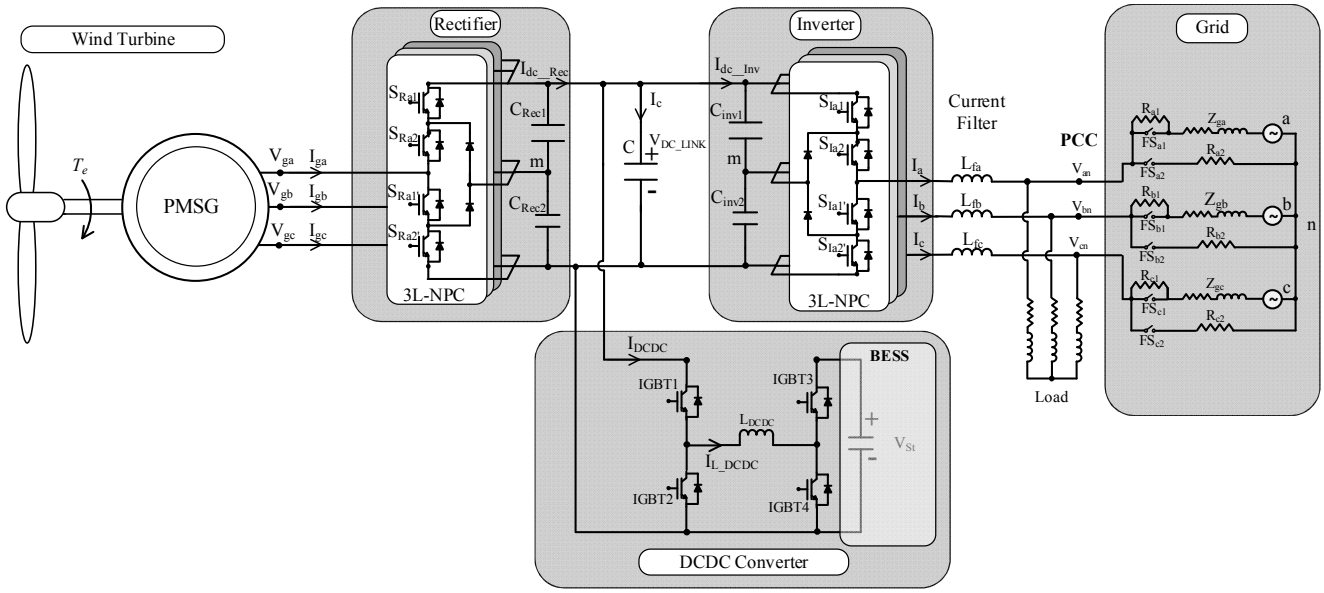

Fig. 1. Proposed PMSG WTS with BTB three-level NPC Converter and bidirectional DC/DC Converter with BESS

system due to its advantages compared to the two-level converters [4], [12]. Though, the implementation of the conventional PI current controller is simple, it suffers from multiple frame transformation and high computational complexity [13]. Consequently, a proportional resonant (PR) controller is applied for the control of the NPC converter. The performance of the proposed structure is investigated on a 50 kW wind power plant under various operational conditions and results have proven the validity.

II. Proposed System Structure

A comprehensive schematic of the proposed WTS is depicted in Fig. 1. The system is consisted of three parts: permanent magnet synchronous generator (PMSG), BTB NPC converter and bidirectional DC/DC converter. The PMSG converts the mechanical energy of the wind to electrical energy while BTB NPC converters extract the maximum power from PMSG and inject it to the grid. The bidirectional DC/DC converter is connected to the DC-link.

A. Permanent Magnet Synchronous Generator

WTS with PMSG requires BTB full scale energy conversion [4]. In direct drive, the wind turbine is directly connected to the generator. The mechanical power obtained from the wind is given by

$$P_m = \frac{1}{2}\rho\pi R^2 V^3 C_p(\lambda) \tag{1}$$

where ρ is the air density (kg/m^3), R is the radius of rotor (m), V is the wind speed (m/s), C_p is the coefficient of performance, λ is the tip speed ratio of the wind turbine blades ($\lambda = \frac{\omega_t R}{V}$).

The equations for the PMSG in the d-q coordinate are given by:

$$u_q = -R_s i_q - L_s\left(\frac{di_q}{dt}\right) - \omega_e L_s i_d + \omega_e \lambda_f \tag{2}$$

$$u_d = -R_s i_d - L_s\left(\frac{di_d}{dt}\right) + \omega_e L_s i_q \tag{3}$$

$$T_e = \frac{3}{2} P_n \lambda_f i_q \tag{4}$$

where, L_s is the Synchronous Inductance, R_s is the synchronous resistance, i_d and i_q are the d-q currents, u_d and u_q are the d-q voltages, ω_e is the rotor speed, λ_f is the flux of the permanent magnet and P_n refers to the PMSG pole pairs.

B. Back to Back Power Conversion Topology

In the proposed BTB NPC energy conversion topology, a three-level NPC rectifier is deployed to convert the output AC-power of the PMSG to the DC-power of the DC-link. Additionally, another three-level grid-tied NPC inverter is considered to convert the DC-power to AC- power and inject to the grid, as shown in Fig. 1. It can be seen that both rectifier and inverter circuits are consisted of two pairs of IGBT switches (S_{Ra1} and S_{Ra2} for the rectifier and S_{Ia1} and S_{Ia2} for the inverter) with their complementary switches. The rectifier controls the PMSG by controlling its output currents (I_{ga}, I_{gb}, I_{gc}) according to the MPPT controller. The NPC Rectifiers are connected to two series of capacitors (C_{Rec1} and C_{Rec2}) so are the NPC Inverters (C_{Inv1} and C_{Inv2}). The NPC operates with three different switching states to synthesize the three output pole voltage stepped levels at $V_{DC\_LINK}/2$, 0 and $-V_{DC\_LINK}/2$ with respect to the midpoint m of DC-link.

Despite the increasing demands of renewable energy resources, several regulations such as IEEE Std. 1547-2003 and IEEE Std. 929-2000 must be complied strictly to ensure the power quality of the renewable grid-connected system. Therefore, lower current harmonic distortion can be achieved with the aid of output filter inductors which are connected between the inverter and the grid. Due to the intelligent synthesis of three-level output voltage waveforms, the filter

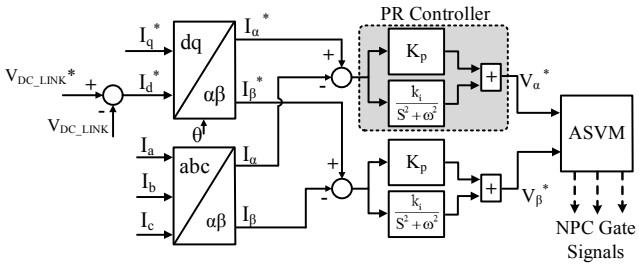

Fig. 2. VOC-PR controller for BTB NPC converter

size can be much smaller compared to the conventional two-level inverters [13].

C. Bidirectional DC/DC Converter with BESS

The proposed bidirectional DC/DC Converter consists of four IGBTs and an Inductor (L_{DCDC}), as shown in Fig. 1. Buck-boost capability can be achieved by controlling the IGBT switches in different modes. The DC/DC converter is connected to the BESS which is consisted of supercapacitor and battery storage system. Based on the voltage of the DC-link and BESS the controller performs the buck or boost operation either charging or discharging of the BESS.

III. Control Structure

The proposed WTS is consisted of three independent controllers: NPC rectifier controller, NPC inverter controller and the DC/DC converter controller. The NPC rectifier controller regulates the extracted power of the PMSG based on the MPPT [14]. The NPC inverter adjusts the injected power to the grid to the extracted power from the PMSG and synthesizes its currents to the grid voltages.

Due to the high penetration of distributed generation units in the power system, fault ride through (FRT) capability is one of the requirements of new standards and grid codes [15] which should be implemented in the control of the WTS. During normal grid operation, the grid-tied inverter adjusts the DC-link voltage to its nominal value by regulating the injected active power to the grid. However, under grid faults, the grid-tied NPC inverter should inject reactive power to the grid according to grid codes and hence it cannot control the DC-link voltage. Consequently, the proposed DC/DC converter controller is responsible to regulate the DC-link voltage by charging or discharging the BESS. The details of the proposed controllers are as follows.

A. Inverter and Rectifier Control

The control of the rectifier is done basing on the maximum power point obtained from the MPPT of the PMSG. As shown in Fig. 3, the controller of the inverter or rectifier has a phase locked loop (PLL), voltage oriented controller (VOC) and adaptive space vector modulation (ASVM) [16].

The measured DC-link voltage (V_{DC_LINK}) is compared to its reference value and the difference is fed into the PI controller which produces the reference d-axis current (I_d^*). The q-axis reference current (I_q^*) is set to zero for unity power

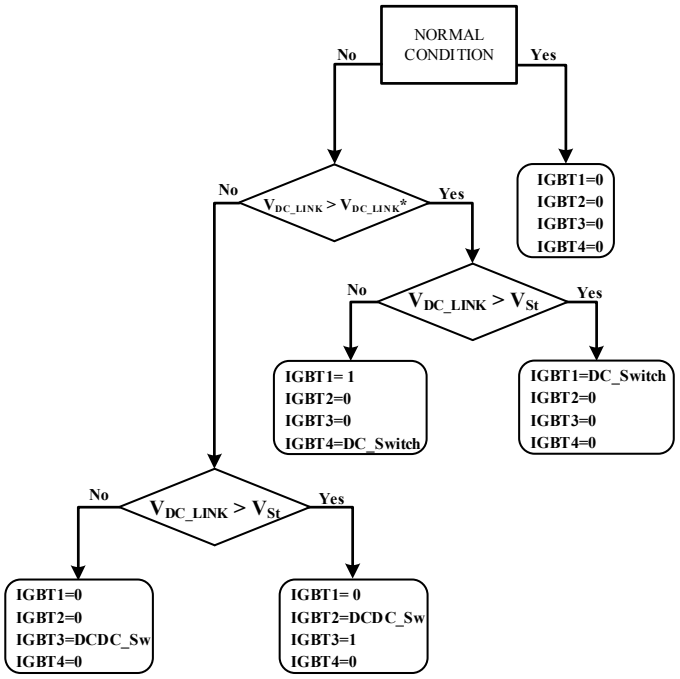

Fig. 3. Proposed DC/DC Converter Control Algorithm

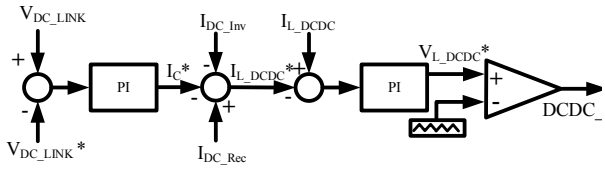

Fig. 4. Proposed DC/DC Controller

factor operation. Though the conventional PI controller has simple implementation, this paper proposes a PR controller for controlling the converter currents in stationary coordinate (αβ-coordinate). The measure three phase currents of the converter (I_{ga}, I_{gb} and I_{gc} for rectifier and I_a, I_b and I_c for grid-tied inverter) are transferred to stationary frame through the Clark transformation. The transfer function of the PR controller is given below:

$$G_{PR} = K_P + \frac{K_i}{(S^2 + \omega^2)} \quad (5)$$

where,

K_P : Proportional gain term

K_i : Integral gain term

ω : Resonant frequency

The reference voltages (V_α^* and V_β^*) are obtained from the PR controller and can be directly fed into the ASVM without the need of inverse Park or Clark transformation. The voltage balancing of the capacitors are found better in the ASVM than the classical SVM. This technique can balance the DC-link capacitor voltages by selecting the appropriate switching state. The detailed implementation of the ASVM is presented in [16].

B. Proposed DC/DC Converter Control:

During the normal condition of the grid, the DC/DC converter is dormant or inoperative and all the DC/DC converter IGBTs are switched off. Under the grid fault there are four operating conditions that can be visualised through the control algorithm as shown in Fig. 3.

If the DC-link voltage is greater than the reference DC-link voltage ($V_{DC\_LINK} > V_{DC\_LINK}^*$), indicates that the extracted power from the PMSG (P_{O_PMSG}) is larger than the injected power to the grid (P_{O_Inv}). Therefore the difference between these two values (P_{O_PMSG}-P_{O_Inv}) should be injected to the ESS. Accordingly, the direction of the power in the DC/DC converter is from DC-link to the ESS and IGBT4 will remain off. Based on the V_{DC_LINK} and voltage of ESS (V_{St}), the converter should perform boost or buck conversion and accordingly the switches will be controlled. Hence four different operation modes can be implemented as follows:

- If the $V_{DC\_LINK} > V_{DC\_LINK}^*$ and $V_{DC\_LINK} > V_{st}$, then the IGBT1 is controlled and all other IGBTs are set to 0.
- If $V_{DC\_LINK} > V_{DC\_LINK}^*$ and $V_{DC\_LINK} < V_{st}$, IGBT1 is set to 1, IGBT 2 and 3 are set to 0, IGBT 4 is controlled (DC_Switch).
- If $V_{DC\_LINK} < V_{DC\_LINK}^*$ and $V_{DC\_LINK} > V_{St}$, IGBT 4 and 1 are set to 0, IGBT 3=1 and IGBT 2 is controlled.
- If $V_{DC\_LINK} < V_{DC\_LINK}^*$ and $V_{DC\_LINK} < V_{St}$, only IGBT 3 is controlled and all other are set to 0.

The proposed controller of IGBTs is portrayed in Fig. 4. The instantaneous DC-link voltage is compared to its nominal value and the error is controlled through a PI controller while calculates the reference capacitor current (I_C^*). It can be seen from Fig. 1 that the DC/DC inductor reference current (I_{L_DCDC}) can be calculated as follows:

$$I_{L\_DCDC}{}^* = I_{DC\_Rec} - I_{DC\_Inv} - I_C{}^* \qquad (6)$$

where, I_{DC_Inv} : the instantaneous inverter input current
I_{DC_Rec} : the instantaneous rectifier output current

The current of the DC/DC inductor is controlled through the PI controller which results in the reference inductor voltage ($V_{L\_DCDC}^*$). Subsequently, the IGBT switching signal (DCDC_Sw) is generated through a PWM technique.

IV. Result Evaluation

The performance of the proposed WTS structure is investigated in simulations models that are developed in Matlab/Simulink© and PSIM Software. The PMSG is modelled according to a medium voltage PMSG for Wind Turbine specifications. The PMSG is connected to a back to back (AC/DC/AC) full scale converter. The considerations of grid voltage, grid frequency, line inductance, DC-link capacitance, DC-link voltage and the switching frequency of NPC converters are tabulated in Table I. The performance of the system in three different conditions are considered. *Case A* being normal performance, *Case B* is the performance of the proposed system under grid fault and *Case C* is the system response analysis for sudden drop in wind speed.

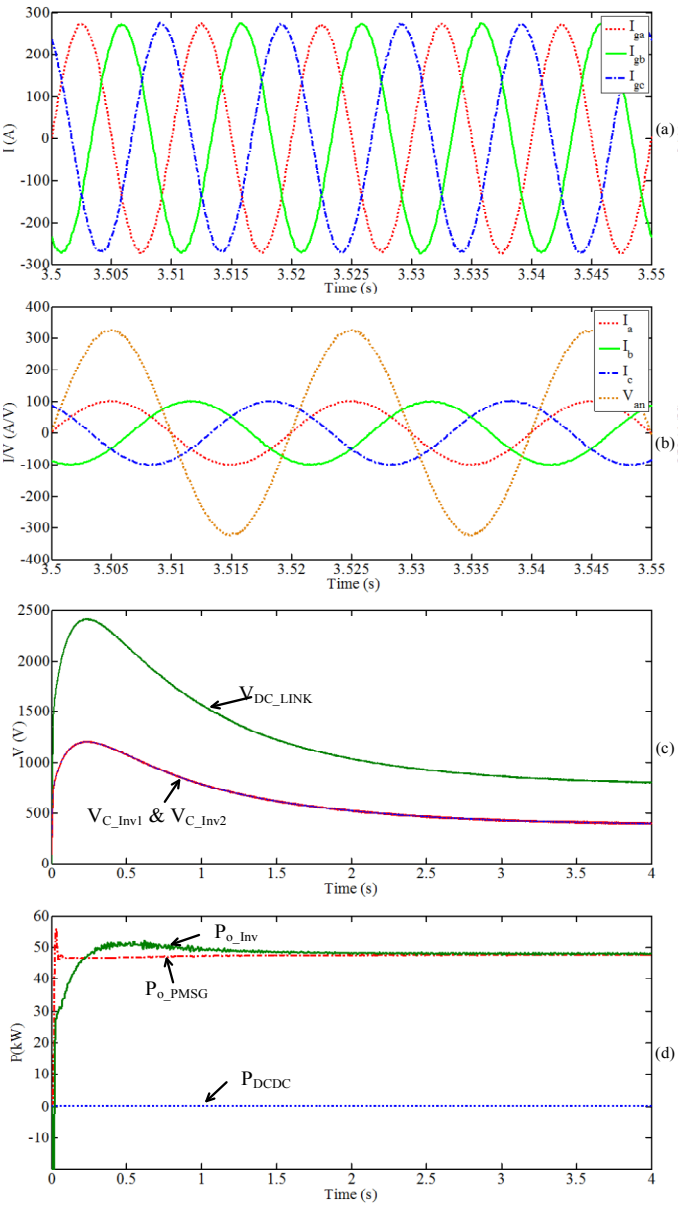

Fig. 5. *Case A*: Performance of the proposed Wind Energy Conversion System under steady state: (a) PMSG Three-Phase Currents, (b) NPC Inverter Three Phase Currents and Phase-A Voltage (c) DC-link Voltage (d) Extracted Power from PMSG injected to the Grid and Storage System

TABLE I. Simulation Parameters

Parameter	Symbol	Value
Grid Voltage	V_{PCC-ab}	400 $V_{l-l,rms}$
Grid Frequency	f	50 Hz
Line Inductor	L_f	5 mH
DC/DC Converter Inductor	L_{DCDC}	1 mH
DC-link Capacitor	C	2.2 mF
DC-link Voltage	V_{dc}	770 V_{dc}
NPC Switching Frequency	$f_{s,inv.}$	10 kHz

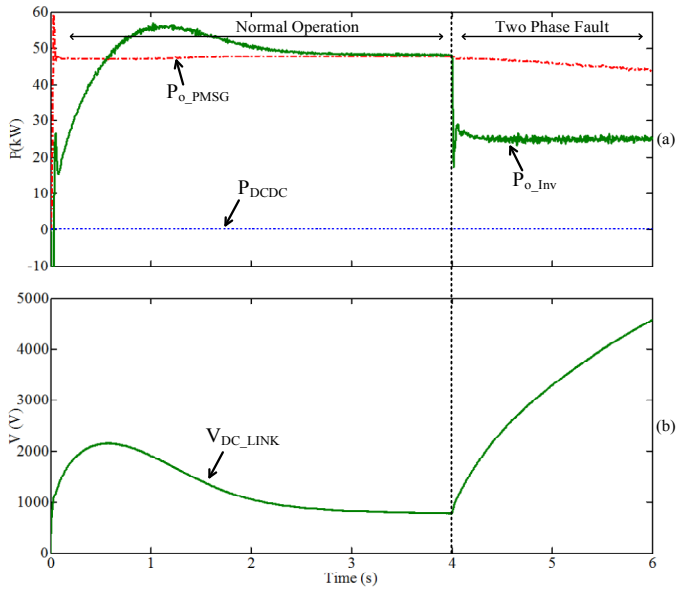

Fig. 6. *Case B*: Performance of the proposed WTS under two phase fault without DC/DC converter: a) Extracted power from PMSG, injected power to the Grid and storage system and (b) DC-link Capacitor Voltage

A. Case A:

The steady state performance of the proposed controller is shown in Fig. 5. The output phase currents of the PMSG are depicted in Fig. 5(a) which are sinusoidal with less harmonic contents due to the three level voltage operation of the NPC rectifier. The inverter output currents are depicted in the Fig. 5(b). It can be seen that there is no phase shift between Phase A current (I_a) and its voltage (V_{an}) which proves the unity power factor operation of the proposed controller. The capacitor voltage balancing performance of the ASVM is shown in Fig. 5(c). Additionally, It can be observed that the DC-link voltage which is at steady state value due to the controlled operation of the NPC inverter in adjusting the P_{o_inv} with the P_{o_PMSG} as depicted in Fig. 5(d). During this steady state operation all power from the PMSG is transferred to the grid and the DC-link voltage is constant.

B. Case B:

A two-phase fault is occurs in the grid which results a voltage sag at the PCC at t=4.0 s. The performance of the WTS without considering the proposed DC/DC converter controller is depicted in Fig. 6. Because of the voltage sag, the inverter injects reactive power to the grid and consequently its injected active power is reduced even though the PMSG is taking maximum active power from wind (Fig. 6(a)). Due to the difference of P_{0_PMSG} and the P_{0_Inv} the voltage at the DC-link capacitor exceeds its nominal value as shown in Fig. 6(b). This situation would trigger the DC-link capacitor protection devices and would disconnect the WTS from the grid.

Again the same scenario is analyzed but this time activating the DC/DC converter with the proposed controller. After the fault occurred, the resulting voltage sag is shown in Fig 7(a). During the steady state, there is no phase shift between the voltages and current because the inverter only injects active power and the injected reactive power is zero as shown in Fig. 7(b). However after t=4.0 s, the inverter starts to inject reactive power to the grid and consequently it's active power is reduced. The power difference is injected to the BESS through the DCDC converter which is around 30 kW. The DC-link capacitor voltage is fairly constant and the inverter capacitor voltages are also balanced due to the performance of the ASVM. As a result the WTS does not pose any threat to the grid and thus this operation provides the system fault ride through (FRT) capability.

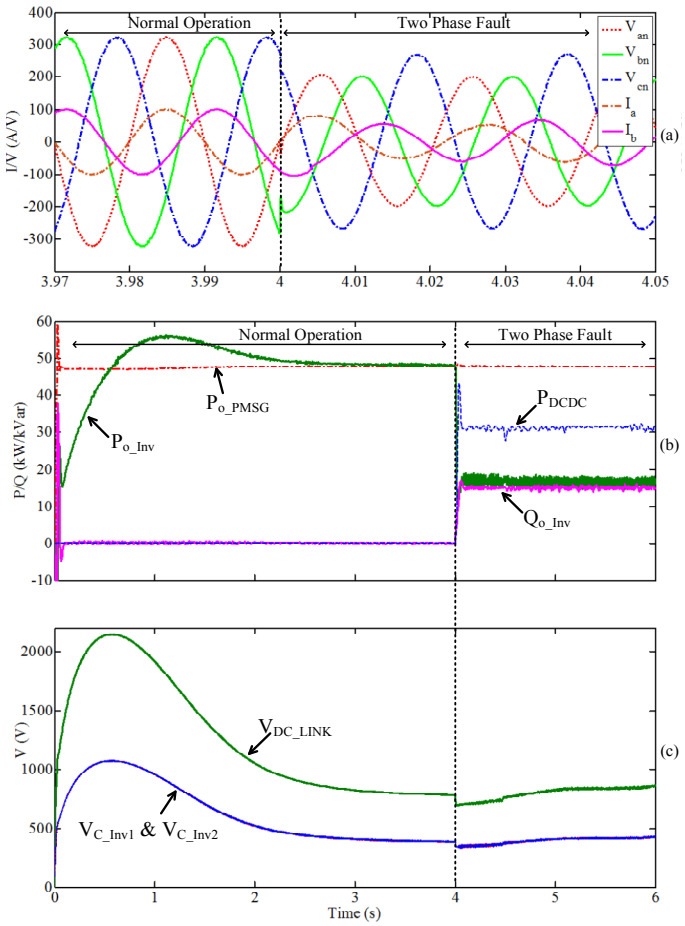

Fig. 7. *Case B*: Performance of the proposed WTS under grid two phase fault with DC/DC Converter: (a) Grid Phase Voltage and Inverter output current, (b) Extracted Power from PMSG, injected power to the grid and storage system, Injected Power to the Grid and (c) DC-link capacitor voltage

C. Case C:

The whole scenario is reassessed for the case of sudden drop of wind speed. The wind speed drops after t=4.0 s. The drop of wind speed causes the wind turbine to rotate less and thus the PMSG's input of mechanical power reduces. This eventually results in the decrease in the generated power. Fig. 8(a) shows the reduced frequency of the voltage and current due to the reduced wind speed at t=4.0 s. The target of any source is to operate undisrupted. The difference of the PMSG power and optimal active power is drawn from the storage system. As the P_{o_PMSG} reduces, the DC/DC converter is activated and provides the inverter with the required power for

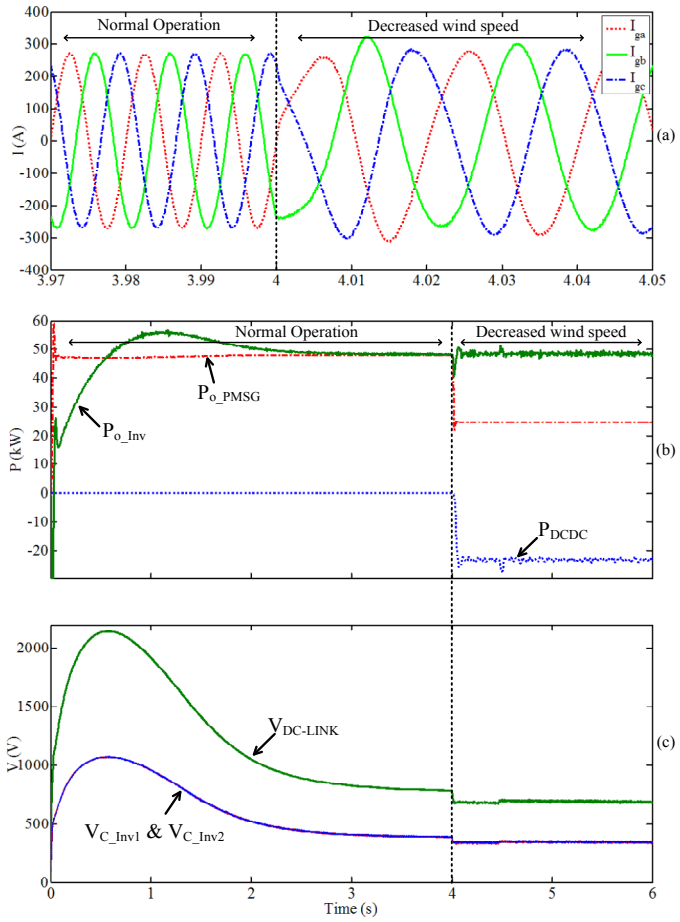

Fig. 8. *Case C*: Performance of the proposed WTS during decreased wind speed: (a) PMSG output currents, (b) Extracted power from PMSG, injected Power to the grid and the storage system and (c) DC-link Capacitor Voltage

continuous constant active power supply to the grid. As shown in the Fig 8(b), the difference in the PMSG power is compensated by the storage system. The inverter output power P_{0_Inv} goes though some glitches due to the reduction of input power from the generator but the compensation power P_{DCDC} ensures the output of the inverter to be fairly constant. During this operation the DC-link voltage remains near its nominal value though it decreases minimally. The NPC Inverter and the converter operates successfully. The V_{C_Inv1} and V_{C_Inv2} are balanced throughout the operation and varies with variations in the DC-link voltage.

V. CONCLUSION

This paper proposes the control of bidirectional DC/DC converter connected to the BESS. The DC-link voltage is remained at its nominal value due to performance of the proposed DC/DC converter controller while the reactive power is injected to the grid in order to enhance the PCC voltage. Besides the output power of the inverter remained constant due to the compensation of the power by the proposed DC/DC converter under reduced wind speed. The result evaluation proves the applicability of the proposed controller for the medium-power WTS.

ACKNOWLEDGEMENT

Authors would like to acknowledge gratefully the support provided by Energy Research Institute at NTU (ERI@N) for this work.

REFERENCES

[1] K. Ma, F. Blaabjerg, and D. Xu, "Power devices loading in multilevel converters for 10 MW wind turbines," in *Proc. - ISIE 2011 IEEE Int. Symp. Ind. Electron*, pp. 340–346.

[2] Ke Ma; Blaabjerg, F., "Modulation Methods for Neutral-Point-Clamped Wind Power Converter Achieving Loss and Thermal Redistribution Under Low-Voltage Ride-Through," in *Industrial Electronics, IEEE Transactions on* , vol. 61, no. 2, pp. 835-845.

[3] Faulstich, A.; Stinke, J.K.; Wittwer, F., "Medium voltage converter for permanent magnet wind power generators up to 5 MW," in *Power Electronics and Applications, 2005 European Conference on* , pp. 11-14.

[4] Yaramasu, V.; Bin Wu; Sen, P.C.; Kouro, S.; Narimani, M., "High-power wind energy conversion systems: State-of-the-art and emerging technologies," in *Proceedings of the IEEE*, vol. 103, no. 5, pp. 740-788, 2015.

[5] Blaabjerg, F.; Chen, Z.; Teodorescu, R.; Iov, F., "Power Electronics in Wind Turbine Systems," in *Power Electronics and Motion Control Conference, IPEMC 2006. CES/IEEE 5th International*, pp. 1-11.

[6] Alepuz, S.; Calle, A.; Busquets-Monge, S.; Kouro, S.; Bin Wu, "Use of Stored Energy in PMSG Rotor Inertia for Low-Voltage Ride-Through in Back-to-Back NPC Converter-Based Wind Power Systems," in *Industrial Electronics, IEEE Transactions on* , vol. 60, no. 5, pp. 1787-1796, 2013.

[7] Yazdani, A.; Iravani, R., "A neutral-point clamped converter system for direct-drive variable-speed wind power unit," in *Energy Conversion, IEEE Transactions on* , vol. 21, no. 2, pp. 596-607, 2006.

[8] Calle-Prado, A.; Alepuz, S.; Bordonau, J.; Nicolas-Apruzzese, J.; Cortes, P.; Rodriguez, J., "Model Predictive Current Control of Grid-Connected Neutral-Point-Clamped Converters to Meet Low-Voltage Ride-Through Requirements," in *Industrial Electronics, IEEE Transactions on* , vol. 62, no. 3, pp. 1503-1514, 2015.

[9] Abbey, C.; Joos, G., "Supercapacitor Energy Storage for Wind Energy Applications," in *Industry Applications, IEEE Transactions on* , vol.43, no.3, pp. 769-776, 2007.

[10] Allegre, A.L.; Bouscayrol, A.; Trigui, R., "Influence of control strategies on battery/supercapacitor hybrid Energy Storage Systems for traction applications," in *Vehicle Power and Propulsion Conference, 2009. VPPC '09. IEEE*, pp.213-220.

[11] Wei Li; Joos, G.; Abbey, C., "A Parallel Bidirectional DC/DC Converter Topology for Energy Storage Systems in Wind Applications," in *Industry Applications Conference, 2007. 42nd IAS Annual Meeting. Conference Record of the 2007 IEEE*, pp.179-185.

[12] Wu, B.; Lang, Y.; Zargari, N.; Kouro, S., "Wind Energy System Configurations," in *Power Conversion and Control of Wind Energy Systems*, 1, Wiley-IEEE Press, 2011, pp.153-171.

[13] Dehghani Tafti, Hossein; Maswood, Ali I.; Ukil, Abhisek; Gabriel, Ooi H.P.; Ziyou, Lim, "NPC photovoltaic grid-connected inverter using proportional-resonant controller," in *Power and Energy Engineering Conference (APPEEC), 2014 IEEE PES Asia-Pacific* , pp.1-6.

[14] Can Huang; Fangxing Li; Zhiqiang Jin, "Maximum Power Point Tracking Strategy for Large-Scale Wind Generation Systems Considering Wind Turbine Dynamics," in *Industrial Electronics, IEEE Transactions on* , vol. 62, no. 4, pp.2530-2539, 2015.

[15] Iov, F., Teodorescu, R., Blaabjerg, F., Andersen, B., Birk, J. and Miranda, J., "Grid Code Compliance of Grid-Side Converter in Wind Turbine Systems," in *Power Electronics Specialists Conference, 2006. PESC '06. 37th IEEE*, pp.1-7.

[16] Dehghani Tafti, H.; Maswood, A.I.; Ziyou Lim; Ooi, G.H.P.; Raj, P.H., "Proportional-resonant controlled NPC converter for more-electric-aircraft starter-generator," in *Power Electronics and Drive Systems (PEDS), 2015 IEEE 11th International Conference on*, pp. 41-46.

From Strain to Extraction: A Review to Produce Biodiesel from Microalgae in Bangladesh

Shitab Ishmam[*1], Wasel-Ur-Rahman[*2], Shabab Bin Karim[*3], Sayedus Salehin[*4], A.K.M. Sadrul Islam[*5]

[#]*Department of Mechanical and Chemical Engineering, Islamic University of Technology*
Board Bazar, Gazipur-1704, Bangladesh

[1]shitabishmam@gmail.com
[2]wasel13@hotmail.com
[3]shabab.2677@gmail.com
[4]sayedus@iut-dhaka.edu
[5]sadrul@iut-dhaka.edu

***Abstract* — Fossil fuel energy resources are unsustainable. World reserves are gradually depleting and the greenhouse gas emissions associated with their use are contributing to global warming. Therefore, there are vigorous research initiatives all aimed at developing alternative fuel resources that are both sustainable and carbon neutral. Based on contemporary research, third generation biofuels that are specifically derived from microalgae are considered to be a technically viable alternative energy resource that is free from the major problems associated with the use of fossil fuels.**

This paper provides an overview of the current status of microalgae use for biodiesel production, including their cultivation, harvesting, and processing keeping Bangladesh in perspective. The microalgae species most suitable for biodiesel production in Bangladesh are mentioned as well.

***Keywords*— Microalgae, Biofuel, Bangladesh, Biomass, Sustainable Energy**

I. INTRODUCTION

In recent years, energy crisis has turned into a major problem throughout the world. The deposits of conventional fossil fuel are reducing day by day. Moreover, increasing carbon emission is deteriorating the ozone layer rapidly and thus increasing global warming. At this rate, many low-laying islands like the Maldives will be engulfed very soon. So, necessity of finding clean and renewable source of energy has become an important issue. Among different sustainable, clean renewable energy sources, only solar energy and biogas have become prominent in Bangladesh. Other sources like tidal energy, wind energy are not efficiently utilized in our country [1]. Recently some high-lipid containing species of microalgae has been identified in different freshwater bodies in Bangladesh [2], which can be used to produce biofuels in commercial methods. Microalgal biofuel is an excellent replacement of conventional diesel as its properties are almost as same as that of the petroleum [3].Moreover, production of microalgae does not require arable land space, which can easily solve the food versus fuel dispute. Microalgae can also be successfully used in treatment of waste water from different industries.

II. SELECTION OF STRAIN

Till now, about 35000 species of microalgae have been discovered, although the available species in the world is assumed to be significantly higher. Almost all algal Phyla have microalgae representatives and microalgae can be found in most environments on earth. The first and most critical step in developing a reliable and commercially viable process for production of microalgae to obtain biofuel is selection of algal species and strain. For commercial scale production, a species must demonstrate high productivity in proposed culture system. The main target is to increase the productivity of lipid, but it itself is not sufficient for potential commercial production. The important properties considered during selection of strain are given below.

1) *Optimum Temperature and Temperature tolerance:* Geographical location and its climate is an important factor for production of microalgae. The average temperature of Bangladesh varies from 23.9°C to 31.1°C during summer and from 7.2°C to 12.8°C in winter [4]. It is to be kept in mind that, the lethal temperature for microalgae is generally slightly higher than optimum temperature. Strain with broad optimum range usually shows better growth [5-6]. Respiration during night time causes loss of biomass significantly [7]. So, length of day is also needed to be considered.
2) *CO_2 supply, pH and O_2 tolerance:* For high rates of photosynthesis, efficient uptake of inorganic Carbon by the cell is very important. All microalgae can take up CO_2 and some can take up carbon in the form of HCO_3^- [8-9] . Generally, inorganic carbon exists in 4 forms in water - CO_2, H_2CO_3, HCO_3^-, CO_3^{2-}. Uncontrolled pH can be fatal for microalgae, as CO_2 is converted into HCO_3^- with increasing pH. Most of the microalgae cannot uptake HCO_3^- as their nutrient. Moreover photosynthesis nearly ceases at pH 9.00.It should be noted that, CO_2 diffusion from air to the medium is greater at more alkaline pH [10-11].
3) *Respiration rate:* Respiration rate is usually dependent on conditions like temperature, nitrogen content, light etc.
4) *Salinity:* For production of lipid enriched microalgae, salinity of water is an important factor. Use of saline water reduces the pressure on fresh water requirement for cultivation [12]. It also reduces the possibility of

contamination by local freshwater strains in the medium.

5) *Competitive strain:* The selected strain must outlive other weaker strains for successful cultivation. Some selected species can outcompete contaminating organisms by surviving in high pH and producing DMSO (dimethyl-sulphoxide).This can act as an antibiotic and helps in successful long term outdoor production.

At present, viable strains which are available in Bangladesh are [14]:

Oedogonium: It is widely available in Bangladesh and can be collected from nearby ponds or other still water sources. Its growth rate is also good. It contains 29-49% lipids of its dry weight from which the biodiesel can be extracted.

Spirogyra: It is one of the most common and available algae found in Bangladesh. Its growth rate is very good in Bangladeshi atmosphere. But its lipid content is lower than the Oedogonium. It contains around 18-22% lipids of its dry weight.

Navicola: It is also a single cell alga. It is not readily available but found at some areas. Its Lipid content is around 25-40% of its dry weight.

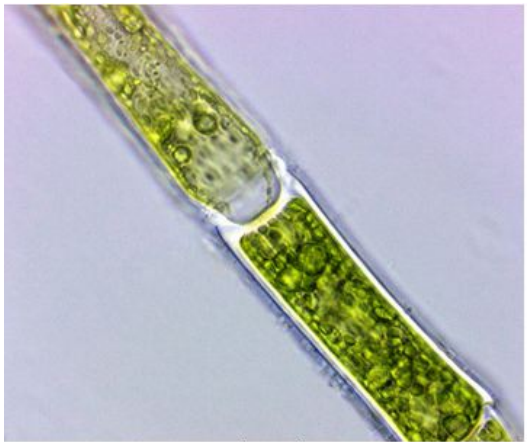

Fig.1 Photo-autotrophic microalgae under microscope (Oedogonium) [13]

III. CULTIVATION

Recent decades have seen tremendous advancement in the field of algal biotechnology. Different methods for greater algal biomass production have been developed including closed photo bioreactors and open pond systems. [15]

A. Method of Cultivation:

Considering the environmental issues of Bangladesh and economic aspects, raceway ponds have been identified as the most feasible option for commercial cultivation of microalgae. Raceway pond is the most widely used medium for microalgae cultivation because of its low production cost. The pond can be built above or below the ground level and a lining of plastic, such as HDPE geotextile liners is provided. The culture in the ponds should be circulated at about 20-30 cm/s, to keep the algae suspended and provide relatively even illumination to the algae and prevent thermal stratification. For circulation and mixing of microalgae in medium, Archimedes pump, air lift, propeller, pumps etc. are used. Generally an 8-blade paddle wheel is considered optimal. At least one of the blades is always immersed in the culture. [16]

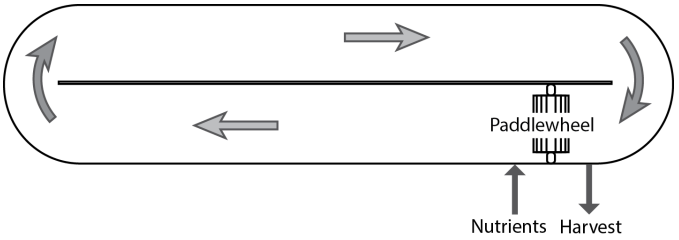

Fig. 2 A typical raceway pond used for cultivation. [17]

B. Management and control of contamination

Open pond systems are severely prone to natural contamination. Unlike laboratory culture, large volume of water used in open pond culture is very difficult to sterilize. Possible contaminating agents and processes are:

- Bacteria, protozoa, fungi and other algae which can blow in by wind or via the water source.
- Culture collapse due to phage-like activity has also been reported occasionally in Arthrospira (Spirulina) pond cultures [18]

Possible ways of reducing the contamination rate are as follows [16]:

1. Culture conditions can be optimized for the selected strain only, so that other strains can't grow well.
2. By controlled use of specific chemicals.
3. Expelling contaminating organisms by netting.

C. Productivity of outdoor open pond system

For economic and sustainable production of biofuels from algae high and reliable annual average biomass and lipid productivity is essential. Productivity of microalgae varies from species to species. Using approach based on available solar energy and a realistic microalgae photosynthetic efficiency, it has been calculated that the maximum achievable biomass productivity is no more than 10 g(C)/ m^2 /day.[19] Depending on average solar irradiation and other factors, average biomass productivity in open ponds may vary from 20-25 gm (dry weight)/m^2 /day. In winter (lower light, short days and lower temperatures) productivities can be up to five times or lower than summer productivities.

D. Limitations of growth

Extensive studies have revealed that, efficiency of using external nutrient sources for growth is limited for any specific species. It may depend on cell size, genetic factors like rRNA gene copy number [20] etc. generally, heterotrophic organisms have faster growth rate than photolithotrophic or chemolithotrophic organisms.

1) Metabolism products

For specific trophic mode, metabolism products will have important effect on growth rate. Generally, oil producing species have lower specific growth rate than similar sized other cells without intracellular oil. Even in case of extracellular oil producing species, production reduces as photosynthetic products are divided up rather than producing more catalysts.

2) Light attenuation

Mass algal culture requires optically dense medium. In outdoor culture, challenge of supra-optimal incident irradiation is faced. About 90% of radiation is generally absorbed by first 10mm of water with algae suffering severe light inhibition. The rest portion of algae uses the photon very efficiently, but lacks the required light. So, for higher growth rate, arrangements should be made to avoid self-shading. Efficiency of production can be increased by reducing the optical pathway [19]. By reducing the size of light harvesting antenna, the penetration of photon into deeper water can be increased. It has been found that, the production rate of *Chlamydomonous* can be increased significantly by reducing antenna size at high irradiance.[21]

3) Nitrogen content

Nitrogen content of culture medium affects the lipid content of microalgae. When there is nitrogen deficiency in the medium, protein production is reduced. As a result, the unused carbon from photosynthesis is stored as triglyceride. Study by Thomas et al shows that nitrogen deficient condition increases the lipid content of microalgae. But this is not verified for a great number of algal species.

IV. HARVESTING

In simple terms, harvesting is separating the algae from its supporting medium and/or concentrating the algal biomass. The harvesting technology that needs to be chosen, depends on the type of algae being cultivated. e.g. characteristics of the microalgae, size, density etc. [22] The most common harvesting methods are screening, coagulation, flocculation, flotation, sedimentation, filtration and centrifugation [23]. The choice of technology for algae harvesting should be energy efficient and inexpensive for feasible biofuel production.

In various algae-harvesting technologies such as sedimentation, flotation, filtration and centrifugation, coagulation & flocculation of algal cells is carried out as an upstream treatment. [24]

Coagulation and *flocculation* are two distinct processes. Coagulation is used to condition suspended, colloidal and dissolved matter to help in subsequent processing. It involves the addition of a chemical coagulant(s). The aggregation of the destabilised particles and the precipitation products that are formed by one or more coagulants, into larger particles is known as flocculation. Coagulation-flocculation causes algal cells to become aggregated into larger clumps, which are more easily filtered and/or settle more rapidly to facilitate harvesting. Coagulation and flocculation may be initiated through the use of inorganic coagulants, organic coagulants (often polymers) or by using autoflocculation, bioflocculation, ultrasound and electrocoagulation procedures.

Inorganic coagulants can include Alum ($Al_2(SO_4)_3 \cdot 18H_2O$), Ferrous Sulphate ($FeSO_4.7H_2O$) etc. each having a particular optimal pH range for proper functioning. Organic coagulants may include Chitosan, Praestol® etc.

Coagulation and flocculation improves the ease of solid-liquid separation processes involved later. However, all microalgae may not require flocculation to be removed effectively.

Solid-liquid separation techniques constrain either the liquid or the solid.

Liquid constrained systems include gravity thickening, centrifugation, sedimentation and flotation [25].

1) *Gravity Thickeners:* Gravity thickeners rely provide a final solids concentration of generally 2–3%. Most commonly used gravity thickeners are circular in shape. The influent is pumped up through the middle section of the thickener and is released. With time the particles settle, and several zones are created. The top zone consists of relatively clear media and the lower zones consist of particles. Gravity thickeners frequently have a sloped base and scrapers to collect the settled solids for removal [25].
2) *Centrifugation:* Centrifugal processes generate a centrifugal force which acts radially and accelerates the movement and separation of particles based on a density difference between the particle and the surrounding medium. If the particle is denser than the media the particle migrate outwards otherwise it migrates inwards. The maximum discharge concentration typically achieved in continuous centrifugation processes are 10–20% solids. The decanter centrifuge and the disk stacked centrifuge seem to be the most promising centrifugal devices for the recovery of microalgae. In Table I, the two centrifuges are compared [25].

TABLE I
COMPARISON OF TWO CENTRIFUGAL EQUIPMENTS (Adapted from [25])

Device	Energy Requirements (kWh/m^3)	Biomass concentration in solid discharge (%)	Reliability
Disc stacked and nozzle	0.7–1.3	2–15	Very good
Decanter	8	22	Very good

3) *Flotation:* Flotation is a separation process which uses air or gas bubbles. The bubbles adhere to the particles, which are then carried to the liquid surface where they can be separated, usually by skimming. The gas bubbles can be generated within the flotation cell or it can be introduced in to it. The most common gas used for flotation is air. Dispersed air flotation, dissolved air flotation (DAF), bio-flotation and electrolytic flotation are the most popular flotation mechanisms [25].

Particle constrained systems include cake filtration, screening, attachment etc.

1) *Filtration:* All filtration processes need a filter media. The processes generally operate under gravity, pressure or vacuum [25]. Algal suspension is forced to pass across the filter medium by a suction pump. The medium retains the algae biomass. Filtration process is able to harvest microalgae or algal cells of very low density. But the deposited cells often cause fouling/clogging of the medium [24].
2) *Attachment:* Sometimes the microalgae cells can be removed by physical, chemical or electrical attachment to other materials, which can be directly submerged into the culture medium. Magnetic particles can also be added to separate microalgae by magnetic separation techniques [25].

The harvested biomass slurry consists of 5–15% dry solid content and needs to be processed rapidly after harvest.

Dehydration or drying is commonly carried out after harvesting. Sun drying, low-pressure shelf drying, spray drying, drum drying, fluidised bed drying and freeze drying are some of the methods that have been used.

Sun drying is the cheapest dehydration method but brings certain disadvantages into the scenario, e.g. long drying times, loss of material etc. Spray drying is relatively expensive. Freeze drying is equally expensive but extraction of oils is easier from freeze-dried biomass [22].

V. EXTRACTION PROCESS

In simple terms, extraction is taking out the lipid oil from the harvested microalgae where oil is pressed in between the cell wall and the plasma membrane.

Extraction processes can be physical (screw press methods) or chemical (organic solvents) and where the latter has proved to be more workably approached.

A. *Types of lipids present:*

Lipids present in algae can be classified as:

(i) Neutral lipids (NLs) [triacylglicerols (TAGs), wax esters, hydrocarbons, fatty acids (FA)s, and sterols];
(ii) Phospholipids (PLs) (phosphatidylcholine, PC,phosphatidylethanolamine(PEA), phosphatidylserine(PS)
(iii) Phosphatidylglycerol(PG),and phosphatidylinositol(PI);glycolipids(GLs)(sulfoquinovosyldiacylglycerol(SQDG), monogalactosyldiacylglycerol(MGDG), and digalactosyldiacylglycerol (DGDG).

Autoxidation, the spontaneous free radical reaction of organic compound with oxygen, is the responsible for the degradation of lipids during processing and storage. It results in deteriorated lipid macromolecules which cannot be used as biodiesel [26].Algae which harvested in the increasing growth rate will contain more polar lipids (GLs and PLs) where as those harvested in a late steady phase contains more neutral lipids. (TAGs).

B. *Thermodynamics of solvent extraction:*

One endothermic and two exothermic processes are involved in dissolution process. Firstly, separation of lipid molecules into individual molecules is an endothermic process and its energy is small for nonpolar TAGs and slightly higher for polar lipids (i.e. PLs and GLs) [26].These are next dispersed into solvent and energy is required to dissociate the solvent molecules. Higher the intermolecular attraction; higher the energy required: non-polar solvent < polar solvent < hydrogen-bonded solvent. Thirdly, which is exothermic process, the lipid molecules interact with close-by solvent molecules. The following order represents shows the increasing of energy released: *both solvent and lipid molecules are non-polar < one is polar and the other is non-polar < both molecules are polar < lipid molecules are dissolved by solvent molecules*. The overall result whether exothermic or endothermic is determined by the difference in energy released in lipid-lipid, solvent-solvent interaction and energy gained lipid-solvent interaction. When solvent molecules are highly inter- associated, as with water, the dissolution is only possible if the resulting solution results in stronger lipid-solvent interaction. In short, it can described by the principle of '*like dissolve like'*,i.e. polar lipid dissolves in polar solvent. When solubility parameters (polarity index, solubility parameters and dipole moments) for solvent and lipid are similar, the solvent will be a good candidate for a given application. [26]

C. Ideal solvent characteristics:

Some of the factors that need to be consider when selecting an ideal solvent: they should be volatile (for easy removal later), free from toxic or reactive impurities (to avoid reaction with the lipids), form a two-phase system with water (to remove non-lipids), and be ineffective towards undesirable components (e.g., proteolipid protein, small molecules)[26]. A solvent with high solubility at elevated temperature and low solubility at ambient temperature may be desirable, because the oil can be separated from the solvent without evaporation.

D. Cell wall and plasma membrane:

The cell wall (CW) gives cells rigidity and strength, offering protection against stresses. The CW is an extracellular polymeric structure composed of polysaccharides, proteoglycans, peptides, proteins, and associated inorganic elements [26] Electron-microscopy studies have shown that the CW is made up of two major components: (1) an arranged fi biller structure (2) a continuous matrix [26]
Plasma membrane (PM) is a light membrane which surrounds the protoplasm directly beneath the CW and a layer of mucilage (a viscous secretion or bodily fluid). [26]

E. Biomass Pre-treatment:

In order for a rapid and smooth extraction of lipids from microalgae; it may often be extracted in the wet state directly after harvesting. The cells do not need to be deteriorated since they are broken by the extracting solvent. The breakage of the CW and PM may be necessary to: 1. Time for extraction can be reduced 2. Use of high temperatures and pressure is not necessary to make the lipid–solvent interaction occur 3.less solvent required 4. To permit the solvent to easily penetrate into the cell and release cell contents into the bulk for increasing the lipid yield. [26] This may be accomplished by using one of the well-established cell-disruption techniques such as sonication, homogenization in a tissue grinder, blender or in high-pressure flow device, freezing and grinding with a pestle and mortar, autoclaving microwaves and osmotic shock. Generally, bead mill may be the pre-treatment choice for microalgae cells with strong cell wall.

F. Extraction of lipid from microalgae:

All the linkages between the lipid and other nonpolar lipid cells must be diminished without causing any disruption on the lipid. There are three ways in which lipid bond between each other :(i) van der Waals or London forces can be found in neutral or non -polar lipids, such as triacylglycerol's are bound by relatively weak forces through their hydrocarbon chains. (ii) Hydrogen bonding and electrostatic association are the strongest of interaction and it is by which lipids are bound to proteins, and (iii) the less frequent covalent association. [26] For extracting lipid having ionic bonds as the mode of association the pH value should be shifted out of the neutral region [27]. In case of poor cell wall strength to solvents the recovery yield of lipid can be elevated by adding water because it causes swelling of the cellular structure [27]
A method explained in [28] uses a technique to quantitatively extract lipid using a combination of chloroform: methanol: water in a ratio 1:2:0.8 v/v/v. It has been the most commonly used technique for the extraction of lipids from microalgae at analytical level in the last 50 years (over 23,500 journal citations currently [29])

G. Fatty Acid extraction by direct saponification of dry microalgae biomass:

Direct saponification of microalgae biomass enables fatty acids to be obtained as potassium or sodium salts instead of as crude lipids (impure lipids) in a first step. This process of direct saponification is cost effective and less time consuming. Direct saponification of biomass could ideally be induced in two stages, first lipid extraction with a solvent, and second alkaline hydrolysis of the extracted lipids to get rid of fatty acid salts. Three major conclusions can be drawn lipid or fatty acid extraction when using dry microalgae biomass:
(1) Higher the polarity of the solvent; higher the extraction efficiency.
(2) For each solvent system the yield of lipid extraction is slightly higher than the yield of fatty acid extraction and
(3) Attention should be centred on selecting and optimum solvent mixture because saponification is an instantaneous process. [26]

In Bangladesh, documented extraction of lipids from microalgae has been few and far between although most of the processes are sustainable taking in the climate, environment available technology into account. In [14] extraction was done by mechanical process using ball mill as well as chemically using a soxhlet extractor.

VI. Conclusions

From selecting a suitable strain for cultivation, harvesting up to the extraction of lipid each processes need very calculated steps in order to achieve an ultimate goal. Like for cultivation the strains selected must be tested under outdoor conditions, preferably over a whole annual cycle to assess performance under the highly variable (diurnal and seasonal) conditions of irradiance and temperature before we are ensured to go for mass culture. For harvesting, a single best method, universal process, or a series of processes, is yet to be identified that will be suitable in all situations and for all microalgae species. Consequently, harvesting and dewatering processes must be tailored based on the species of microalgae and its growth conditions, whilst being adaptable to handle the natural variations in the output from the culture system. However, given that most species that are currently of interest as potential biodiesel feed stocks are cultivated as individual cells which are too small for a simple filtration and have a low density difference to the growth media, the first step in a biomass recovery system is likely to consist of a two stage harvesting module (e.g. flocculation followed by flotation or gravity sedimentation). In case of extraction processes involved we see that, extraction of lipids by mechanical methods from microalgae that do not involve any solvents (oil press), or with supercritical CO_2, which are workable

processes for oil seed extraction, their use for microalgae has proved to be unworkable. Finally, lipid extraction from biomass and its subsequent conversion into FAMEs by transesterification would be a very attractive method if there is no need for previous lipid refining, which is unlike, due to the unusual high content of fatty acids in the microalgae oil. Microalgae as a renewable energy source has a very high prospectus in Bangladesh and further investigation as well as collaborative research would lead potential aspects of development in this area.

REFERENCES

[1] Islam, AKM Sadrul, Mazharul Islam, and Tazmilur Rahman. "Effective renewable energy activities in Bangladesh." Renewable Energy 31, no. 5 (2006): 677-688.

[2] Naz, S., M. Zaman, U. Nahar, and S. M. G. G. Azam. "Reports on epiphytic species of Oedogonium from Bangladesh." *Plant Environ. Dev* 1, no. 1 (2007): 45-51.

[3] Kais, Md Imran, Farsad Imtiaz Chowdhury, and Kazy Fayeen Shahriar. "Biodiesel from Microalgae as a solution of third world energy crisis." In *World Renewable Energy Congress*, pp. 192-199. 2011.

[4] Shahid, Shamsuddin. "Recent trends in the climate of Bangladesh." Climate research (Open Access for articles 4 years old and older) 42, no. 3 (2010): 185.

[5] Goldman, Joel C. "Temperature effects on phytoplankton growth in continuous culture1." *Limnology and Oceanography* 22, no. 5 (1977): 932-936.

[6] Borowitzka, Michael A. "Limits to growth." In *Wastewater treatment with algae*, pp. 203-226. Springer Berlin Heidelberg, 1998.

[7] Grima, E. Molina, JA Sánchez Pérez, F. Garcia Camacho, JM Fernández Sevilla, and FG Acien Fernandez. "Productivity analysis of outdoor chemostat culture in tubular air-lift photobioreactors." *Journal of applied phycology* 8, no. 4-5 (1996): 369-380.

[8] Korb, Rebecca E., Peter J. Saville, Andrew M. Johnston, and John A. Raven. "SOURCES OF INORGANIC CARBON FOR PHOTOSYNTHESIS BY THREE SPECIES OF MARINE DIATOM1." *Journal of phycology* 33, no. 3 (1997): 433-440.

[9] Giordano, Mario, John Beardall, and John A. Raven. "CO 2 concentrating mechanisms in algae: mechanisms, environmental modulation, and evolution."*Annu. Rev. Plant Biol.* 56 (2005): 99-131.

[10] Hoover, Thomas E., and David C. Berkshire. "Effects of hydration on carbon dioxide exchange across an air-water interface." *Journal of Geophysical research* 74, no. 2 (1969): 456-464.

[11] Lee, Yuan-Kun, and S. John Pirt. "CO2 absorption rate in an algal culture: effect of pH." *Journal of Chemical Technology and Biotechnology. Biotechnology* 34, no. 1 (1984): 28-32.

[12] Borowitzka, Michael Armin, and Navid Reza Moheimani. "Sustainable biofuels from algae." *Mitigation and Adaptation Strategies for Global Change* 18, no. 1 (2013): 13-25.

[13] (2015) The Algae Information website. [Online]. Available: http://www.algae.info/Algaecomplete.aspx

[14] Dr. Noor Al Qudus, Syeda Zohra Halim, Md. Sarzid Hasan A Techno-Economic Assessment of Algae Bio-Fuel Production in Bangladesh, Technical Report, Bangladesh Climate Change Trust (BCCT), Ministry of Environment and Forest, Government of Bangladesh, September 2013.

[15] Mata, Teresa M., Antonio A. Martins, and Nidia S. Caetano. "Microalgae for biodiesel production and other applications: a review." *Renewable and sustainable energy reviews* 14, no. 1 (2010): 217-232.

[16] Borowitzka, Michael A., and Navid Reza Moheimani. "Open pond culture systems." In *Algae for Biofuels and Energy*, pp. 133-152. Springer Netherlands, 2013.

[17] (2015) Florida Home Energy [Online]. Available: http://www.myfloridahomeenergy.com/help/library/energy-services/algal-fuels/#sthash.4w6OEFm2.dpbs

[18] Shimamatsu, Hidenori. "Mass production of Spirulina, an edible microalga." In *Asian Pacific Phycology in the 21st Century: Prospects and Challenges*, pp. 39-44. Springer Netherlands, 2004.

[19] Ritchie, R. J. "Modelling photosynthetic photon flux density and maximum potential gross photosynthesis." *Photosynthetica* 48, no. 4 (2010): 596-609.

[20] Flynn, Kevin J., John A. Raven, T. Alwyn V. Rees, Zoe Finkel, Antonietta Quigg, and John Beardall. "IS THE GROWTH RATE HYPOTHESIS APPLICABLE TO MICROALGAE? 1." *Journal of Phycology* 46, no. 1 (2010): 1-12.

[21] Richmond, Amos, Zhang Cheng-Wu, and Yair Zarmi. "Efficient use of strong light for high photosynthetic productivity: interrelationships between the optical path, the optimal population density and cell-growth inhibition." *Biomolecular Engineering* 20, no. 4 (2003): 229-236.

[22] Brennan, Liam, and Philip Owende. "Biofuels from microalgae—a review of technologies for production, processing, and extractions of biofuels and co-products." *Renewable and sustainable energy reviews* 14, no. 2 (2010): 557-577.

[23] Chen, Chun-Yen, Kuei-Ling Yeh, Rifka Aisyah, Duu-Jong Lee, and Jo-Shu Chang. "Cultivation, photobioreactor design and harvesting of microalgae for biodiesel production: a critical review." *Bioresource technology* 102, no. 1 (2011): 71-81.

[24] Show, Kuan-Yeow, Duu-Jong Lee, and Jo-Shu Chang. "Algal biomass dehydration." *Bioresource technology* 135 (2013): 720-729.

[25] Pahl, Stephen L., Andrew K. Lee, Theo Kalaitzidis, Peter J. Ashman, Suraj Sathe, and David M. Lewis. "Harvesting, thickening and dewatering microalgae biomass." In *Algae for Biofuels and Energy*, pp. 165-185. Springer Netherlands, 2013.

[26] Grima, Emilio Molina, María José Ibáñez González, and Antonio Giménez Giménez. "Solvent extraction for microalgae lipids." In *Algae for biofuels and energy*, pp. 187-205. Springer Netherlands, 2013.

[27] Kates, M. "Separation of lipid mixtures." *Techniques of lipidology: Isolation, analysis and identification of lipids* (1986): 186-278.

[28] Bligh, E. Graham, and W. Justin Dyer. "A rapid method of total lipid extraction and purification." *Canadian journal of biochemistry and physiology* 37, no. 8 (1959): 911-917.

[29] Burja, Adam M., Roberto E. Armenta, Helia Radianingtyas, and Colin J. Barrow. "Evaluation of fatty acid extraction methods for Thraustochytrium sp. ONC-T18." *Journal of agricultural and food chemistry* 55, no. 12 (2007): 4795-4801.

Comparative Study of Matlab-Simulated and Conventional Si-based Solar Panel

M. F. Hossain, M. D. Hossain
Department of Electrical and Electronic Engineering, Rajshahi University of Engineering &Technology
Rajshahi-6204, Bangladesh
E-mail: dr.faruk_eee@ruet.ac.bd

***Abstract*—Solar cells are promising devices for clean electric energy and have attracted intensive research. Modeling and simulation of photovoltaic solar cells allows the prediction of cell behavior under different physical and environmental parameters. Mathematical model of photovoltaic system is made depending on Shockley diode equation. The aim of this paper is to describe the comparative study between the MATLAB-SIMULINK based modeling of solar panel and conventional Si-based solar panel. Finally nice agreements have been obtained between the simulation and experimental results.**

Keywords—Photovoltaic solar panel, Solar cell model, Fill factor, Maximum power point

I. INTRODUCTION

The conventional energy sources exhibit some problems such as pollution, less energy security and the most important is that these sources are limited. Renewable energy sources (such as PV system) are clean and almost have no impact on the environment. That's why the renewable energy sources are getting more popular all over the world. Thus, the renewable energy sources have become a more important contributor to the total energy consumed in the world. In fact, the demand for solar energy has increased by 20% to 25% over the past 20 years. The market for PV systems is growing worldwide. In fact, nowadays, solar PV provides around 4800 GW. Between 2004 and 2009, grid connected PV capacity reached 21 GW and was increasing at an annual average rate of 60% [1]. Solar cells are devices that convert sunlight into electrical energy. A PV cell is a basic unit that generates voltage in the range of 0.5 to 0.8 volts depending on cell technology used. This small generation is not of much commercial use if these cells are not integrated and connected together in a module to give the handsome voltage at least to charge a standard battery of 12 volts. Thus what we see physically in a PV system is the commercially available module; which are further connected in series and parallel to form a PV system as per the system requirement of voltage and the current [2].The operation of solar cells may be described from a PN junction where thereare diffusion currents and drift currents for the direct and reverse polarization, respectively. Usually, the cells operate in reverse direction so that the current drift is desirable. When the PN junction is exposed to light, photons with energy greater than the gap of energy are absorbed, causing the emergence of electron-hole pairs [4].These carriers are separated under the influence of electric fields within the junction, creating a current that is proportional to the incidence of solar irradiation and finds its path through an external electrical load.

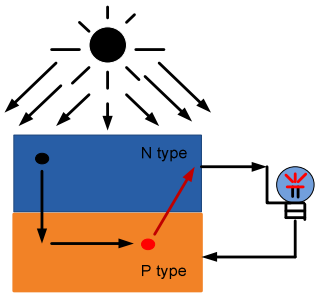

Fig. 1 Basic photovoltaic solar cell structure

II. MATHEMATICAL MODELING OF SOLAR CELL

The most important component that affects the accuracy of the simulation is the PV cell model. Modeling of PV cell involves the estimation of the I-V and P-V characteristics curves to emulate the real cell under various environmental conditions. The most popular approach is to utilize electrical equivalent circuit, which is primarily based ondiode [2, 5].

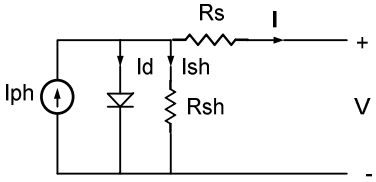

Fig. 2 Solar cell equivalent circuit

Fig. 2 represents a single solar cell as aparallel current source, I_{ph}, an exponential diode, D and a shunt resistance, R_{sh}that are connected in series with a resistance R_s [1,2,5,6]. In view of that current to the load can be given as:

$$I = I_{ph} - I_O \left(e^{\left(\frac{q\,(V+I\,R_S)}{KT}\right)} - 1 \right) - \frac{V + IR_S}{R_{sh}} \qquad (1)$$

In this equation, I_{ph} is the Photo current, Io is the reverse saturation current of the diode, K is the Boltzmann constant, T is junction temperature, q is the electron charge, V is the voltage across the diode, R_s & R_{sh} series and shunt resistance of the cell respectively [5].

Table1. Solar cell parameters

NAME	SYMBOL	VALUE	UNIT
Reverse saturation	Io	1×10^{-9}	A
Electronic charge	q	1.6×10^{-19}	C
Series resistance	R_s	.001	Ω
Boltzmann constant	K	1.3×10^{-23}	J/K
Photo current	I_{ph}	4	A
Shunt resistance	R_{sh}	1000	Ω
Temperature	T	300	K
Voltage	v	0:0.01:0.6	volt

Photocurrent mainly depends on the solar radiation and cell working temperature [1, 6, 7] Which can be expressed as:

$$I_{ph} = [I_{SC} + K_I(T - T_r)]\, G \qquad (2)$$

Where I_{SC} = Cell's short circuit current at 25^0c and 1 KW/m^2, K_I = Cell's short circuit current temperature coefficient, T_r= cell's reference temperature, G = solar insolation in KW/m^2. On the other hand the cell saturation current varies with the cell temperature [6] which is described as:

$$I_S = I_{RS}\left(\frac{T}{T_r}\right)^3 e^{\left[q\, E_G \frac{\left(\frac{1}{T_r} - \frac{1}{T}\right)}{AK}\right]} \qquad (3)$$

Where I_{RS} is the cell reverse saturation current at a reference temperature and solar radiation E_G is the band gap energy of the semiconductor used in the cell. The ideality factor A depends on the PV technology. The reverse saturation current at reference temperature can be approximately obtained as:

$$I_{RS} = \frac{I_{SC}}{e^{\left[\frac{q\, V_{OC}}{N_S\, AKT}\right]} - 1} \qquad (4)$$

Since a PV cell produces very low power, the cells should be arranged in series-parallel configuration on a module to produce enough power. As mentioned earlier, PV panel is a group of PV modules which are connected in series and parallel circuit configurations to generate the required voltage andcurrent [6, 7].The equivalent circuit for a PV module arranged in N_P parallel and N_S series cells is shown in Fig. 3.

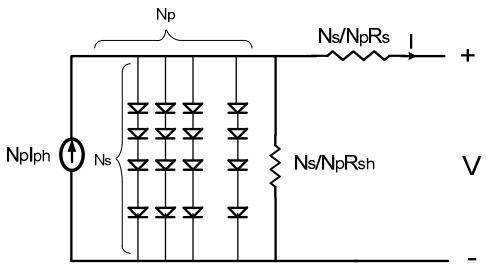

Fig.3 Equivalent circuit models of generalized PV array/panel.

The terminal equation for the current and voltage of the panel becomes as follows:

$$I = N_P\, I_{Ph} - N_P\, I_S\left(e^{\left[\frac{q\left(\frac{V}{N_S} + \frac{I_{RS}}{N_P}\right)}{AKT}\right]} - 1\right) - \frac{\left(\frac{N_P\, V}{N_S} + I_{RS}\right)}{R_{sh}} \qquad (5)$$

Where, N_S=N_P=1 for a PV cell and represent the number of series and parallel cells for the PV array respectively [6, 7].

III. SIMULINK Based Modeling Of PV Module

As shown in Fig. 5, a generalized PV module is made by SIMULINK based subsystem modeling. In this model 36 cells are connected in series and user friendly masking icon is also shown in Fig. 6

The subsystem is made based on the equations (2), (3), (4), (5) [6, 11].

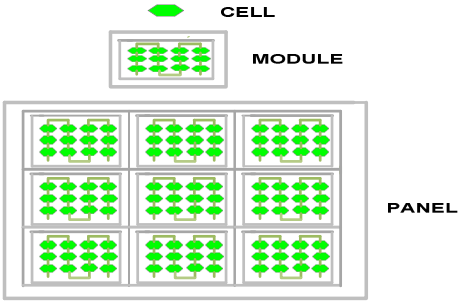

Fig. 4 Photovoltaic hierarchy

By varying the environmental and physical parameters, I~V and P~V curves are obtained from the SIMULINK based modeling(Fig. 7).

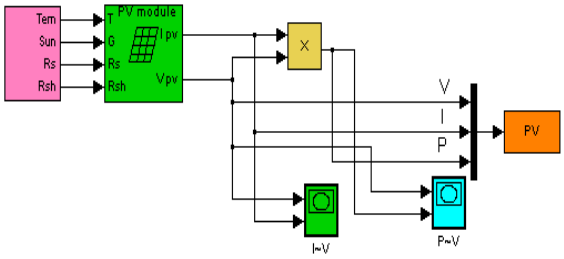

Fig.6 SIMULINK based modeling for PV module

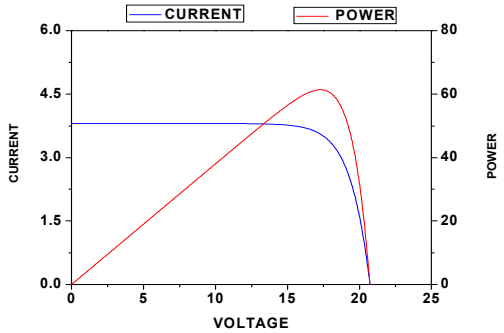

Fig. 7 I~V & P~V curves for PV module

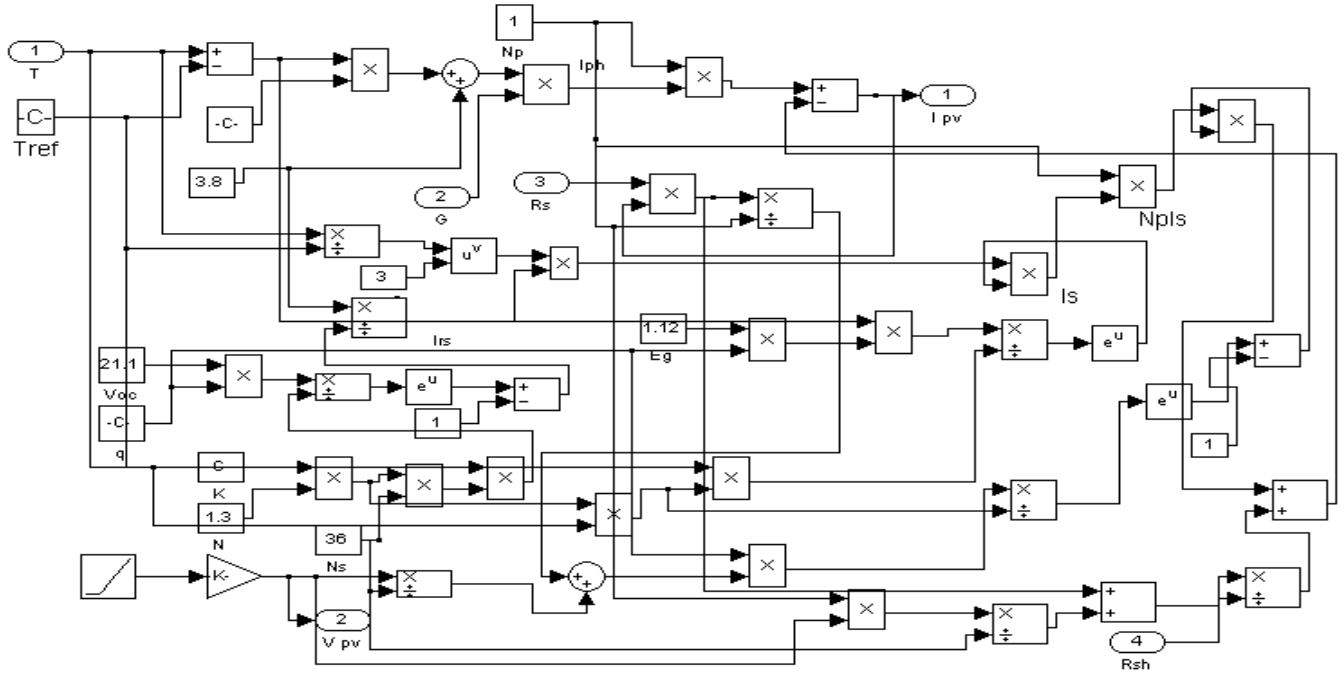

Fig. 5 SIMULINK based subsystem for PV module

IV. Basic Parameters of Solar Cells

A. Short Circuit Current

Short circuit current is the light generated current or the photo current, I_{Ph}. It is the current in the circuit when the load is zero in the circuit. It can be achieved by connecting the positive and negative terminals by copper wire.

B. Open Circuit Voltage

Open circuit voltage is obtained by setting I=0 in the equation (1) and by neglecting the series and shunt resistances we obtain as:

$$V_{oc} = \frac{AKT}{q} ln\left(\frac{I_{ph}}{I_o} + 1\right) \quad (6)$$

C. Fill Factor

Fill Factor is a key parameter in evaluating the performance of solar cells. It decreases when the series resistance is high and tends to be higher whenever the open circuit voltage is high [10]. So, for an efficient cell it is desired series resistance to be as small as possible. The maximum value of fill factor can be 1 but is not possible in practice and can be calculated as follows:

$$FF = \frac{P_{max}}{V_{oc} I_{sc}} \quad (7)$$

D. Maximum Power

No power is generated under short or open circuit. The power output is defined as:

$$P_{OUT} = V_{OUT}\, I_{OUT} \quad (8)$$

The maximum power is provided by the device is achieved at a point on the characteristics as:

$$P_{max} = V_{max}\ \ I_{max} \quad (9)$$

The maximum possible output can be given as:

$$P_{max} = V_{OC}\, I_{SC}\, FF \quad (10)$$

E. Solar Cell Efficiency

Solar cell power conversion efficiency can be given as:

$$\eta = \frac{P_{max}}{P_{in}} = \frac{V_{OC} I_{SC}\, FF}{P_{in}} \quad (11)$$

Solar PV module power conversion efficiency is directly related with the fill factor, so with the increasing of fill factor efficiency is increased and vice versa.

V. SIMULINK Based Modeling of PV Panel

Power produced by a single module is not enough for commercial use, so modules are connected to form a panel to supply the load [6]. The connection of modules in a panel may be in series for higher voltage or parallel for higher current. Figure 8 shows the SIMULINK based PV panel for 2 modules

and Fig. 9 showsI~V and P~V curves of the PV panel for 2 modules.

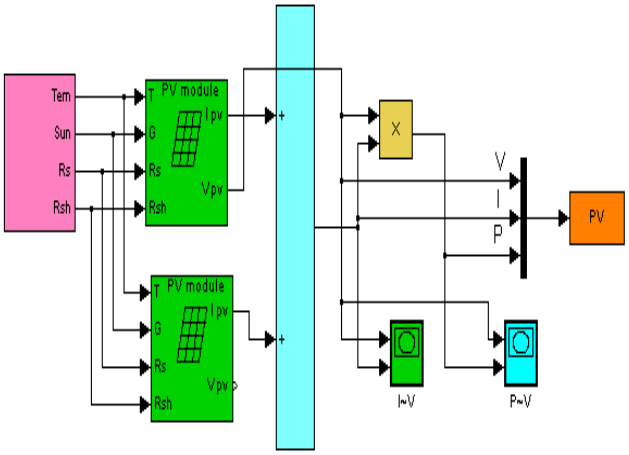

Fig. 8 SIMULINK based PV panel for 2 modules

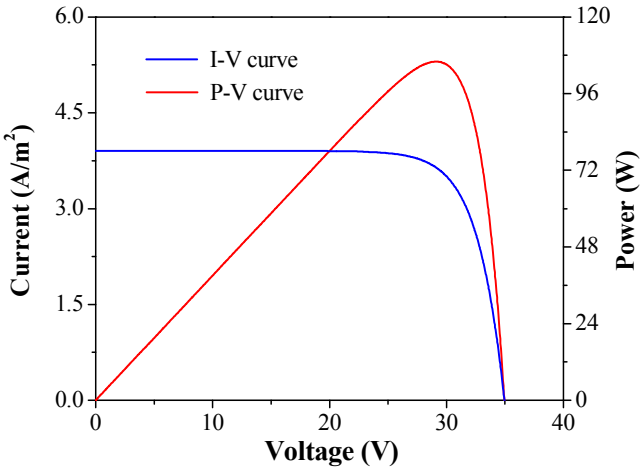

Fig. 9 I~V and P~V curves of PV panel for 2 modules

, Fig. 10 shows PV panel for more than 2 modules, I~V and P~V curves can be obtained from the SIMULINK modeling. These curves are shown in Fig. 11.

Table 2: Standard parameters of each of the Module of ET 250 Photovoltaic trainer

Number of cells	36 (monocrystalline)
Module area	0.63m²
Max. Power	85Wp
Short-circuit current	5.29A
Open-circuit voltage	21.94V
Slide resistor	0---10 Ohm
Measuring ranges Temperature	0---100°C
Voltage	0---20V
Current	0---20A
Illuminance	0---2000W/m²
LCD digital Displays	0---199.9mv DC

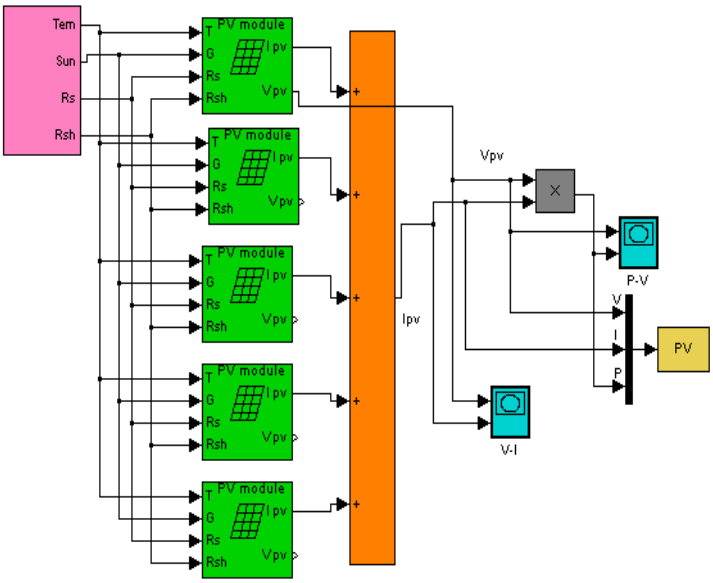

Fig. 10 SIMULINK based PV panel model for more than 2 modules

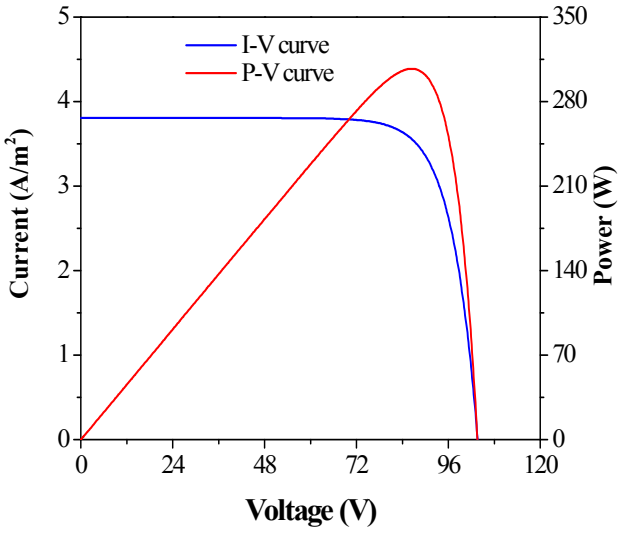

Fig. 11 I~V and P~V curves of PV panel for more than 2 modules

VI. Comparing Between The Experimental And Simulation Results

For series connected modules the simulation results are compared with the experimental results. For measuring experimental results ET 250 photovoltaic trainer is used in our lab. In our experiments two modules are connected in series for higher voltage. Tilt is set to$23^0$for the PV array, solar radiation is measured 0.75 KW/$m^2$and trainer is taken in south in the experiment (Fig. 12). Cables can be used to connect the two modules in series or parallel. A slide resistor simulates varying loads. Thus the slide resistor makes it possible to record current-voltage curves. The separate measuring unit provides display of all relevant variables. Sensors on the solar module detect radiation and temperature [3].

Fig. 12Solar panel setup for experimental results

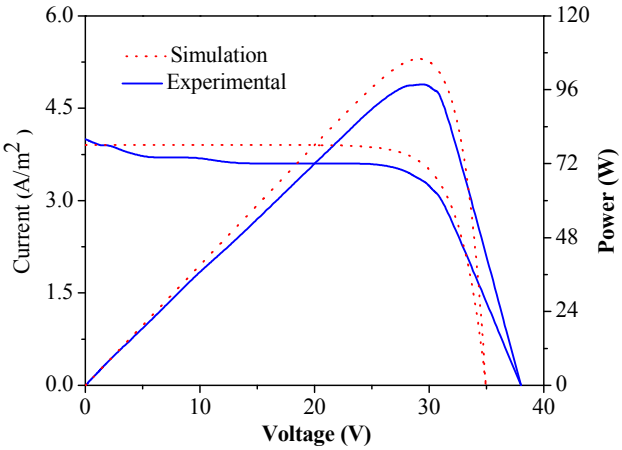

Fig. 13 I ~V and P~V curves for series connected modules

Table3:Performance observation

Parameters	Simulation results	Experimental results
I_{SC} (A/m^2)	3.8	3.8
V_{OC} (V)	35	38
Efficiency (%)	14.39	12.81
Fill Factor (%)	0.804	0.67

SIMULINK based model of photovoltaic panel is evaluated with the experimental results for two series connected modules. From Fig.13 it is shown that for irradiation 0.75 KW/m^{2}and temperature 27^{0}C, good agreement between the open circuit voltage and short circuit current, but fill factor collapses for the experimental results. Again it is shown that due to the collapsing of fill factor maximum power point is collapsed for the experimental results. Efficiency for experimental and simulation results are 12.81% and 14.39% respectively measured from equations (7) and (11).

VII. Conclusion

MATLAB-SIMULINK is a smart tool for predicting the physical and environmental parameter changes of PV cell, module and array. In this paper, Matlab-SIMULINK based and the conventional Si-based photovoltaic solar panel were successfully simulated and compared with conventional solar panel. Good agreement was achieved between the simulation and experimental results for series connected modules. This study can be extended by grid connected PV system for future research.

References

[1] T. Salmi, M. Bouzguenda, A. Gastli and A. Masmoudi, "MATLAB SIMULINK based modeling of photovoltaic cell", International J. Renew. Energy Res., vol. 2, no. 2, 2012.

[2] V.Khanna, B. K. Das and D. Bisht, "MATLAB/SIMELECTRONICS models based study of solar cells", International J. Renew. Energy Res. vol. 3, no. 1, pp. 30–34, January 2013.

[3] M. R. Sultana, and M.F. Hossain, "Investigation of the Photovoltaic of Si- based solar cells under different Light Illumintions", Proc. ICMIME Int. Conf. Commun., November 2013.

[4] S. S. Mohammed, "Modeling and Simulation of Photovoltaic module using MATLAB/Simulink", International Journal of Chemical and Environmental Engineering, vol. 2, no. 5, pp. 350–355, October 2011.

[5] R. Khan, and M.F. Hossain, "Effects of internal resistance on the photovoltaic parameters of solar cells," Proc. ICMIME Int. Conf. Commun., pp. 733–739, November 2013.

[6] S. Said, A. Massoud, M. Benammar, and S. Ahmed, "MATLAB-SIMULINK based photovoltaic array system employingsimpowersystems tool box," J. of Energy and Power Eng., pp.1965–1975, December 2012.

[7] H. L. Tsai, C.S. Tu and Y. J. Su, "Development of generalized photovoltaic model using MATLAB/SIMULINK," Proc. WCECS. Int. Conf. Commun. pp. 778-788, October 2008.

[8] J. R. Hernanz, J. Campayo, E. Zulueta, O. Barambones, P. Eguía I. Zamora, "Obtaining the characteristics curves of a photocell by differentmethods," Proc. ICREPQ Int. Conf. Commun., March 2013.

[9] D. Bonkoungou, Z. Koalaga and D. Njomo, "Modelling and Simulationof photovoltaic module considering single-diode equivalent circuitmodel MATLAB", Int. J. Emerg. Technol. and Adv. Eng. vol. 3, no. 3, pp. 493–502, March 2013.

[10] S. K. Ghosh, M.H. Shawon, A. Rahman and R. Abdullah, "Modeling of PV array and analysis of different parameters," Int. J. Emerg. Technol. and Adv. Eng. vol. 2, no. 5, pp. 358–363, May 2013.

[11] S. Panwar, and R. P. Saini, "Development and Simulation of Solar Photovoltaic model using Matlab/simulink and its parameter extraction", Proc. ICCCE Int. Conf. Commun. April 2012.

Modeling of J-V Characteristics of CZTS Based Thin Film Solar Cells Including Voltage and Space Dependent Electric Field in the Absorber Layer

[1]Ayesha, [2]Kulsum, [3]Shamara Kabir Silvi, [4]Md. Iqbal Bahar Chowdhury
United International University, Dhaka, Bangladesh
Email: [1]aysha969@gmail.com, [2]kulsum264@yahoo.com, [3]shamara.kabir@gmail.com, [5]ibchy@eee.uiu.ac.bd

Abstract— ***This work proposes an analytical model incorporating the effects of the series resistance to deduce the current-voltage characteristics for ZnO/CZTS based thin film solar cell. The evolving mathematical intractability for the inclusion of the series resistance has been resolved by using the concept of perturbation theory. The various effects utilizing the proposed model has been observed and analyzed. The model may be helpful to gain more physical insight of the CZTS based solar cells.***

Keywords— ZnO/CZTS based Solar Cell, J-V Characteristics, non-uniform electric field , Perturbation Theory.

I. INTRODUCTION

Thin film solar cell based on CZTS ($Cu_2ZnSnSe_4$) is a promising solar cell with appreciable efficiency compared to any other thin film solar cell. CZTS stands for copper, zinc, tin and selinide and is a quaternary semiconductor structure having elements which are structurally related compounds. The elements used here are available in the earth-crust that makes it a very inexpensive material. It has a direct band gap of about 1.4-1.5eV [1], for which it has good absorption quality. CZTS based solar cells reached an efficiency of 6.7% [2]. In the emitter side, CZTS has various options for selecting materials to increase its absorption efficiency such as ZnO, ZnS and CdS. Use of ZnS provides high efficiency but due to the presence of sulphur, these solar cells are not very environmental friendly. As a window material CdS is not preferable owing to the presence of cadmium, which causes environmental hazards when dumped. In this regard ZnO will be the best option. Moreover, ZnO is structurally compatible with CZTS and helps in the absorption of the photons due to its transparency and high absorption quality [3]. A familiar solar cell based on CIGS ($Cu_2InGaSe_4$) material also provide high efficiency, but due to the use of rare element like Indium and gallium makes it an expensive material. These solar cells also have to use CdS as the window material. Therefore, CZTS is more preferable than CIGS as in CZTS based solar cells more structurally compatible, more abundant and less harmful elements such as zinc and tin can be introduced and environmentally clean ZnO can be used instead of CdS as window material.

In CZTS based solar cells, higher percentage of incident light is absorbed in first few micrometers of lightly doped CZTS layer. The photo-generated carriers in this region are collected by the voltage-dependent electric field [4]–[6]. A few studies have been reported in the literature to model the current-voltage (J-V) characteristics of CZTS based solar cells. Chandrasekharan [7] developed a numerical model. However, voltage and space dependent electric field developed in the absorber region is not considered in the model. Following the approach of Anjan *et al*. [8], Ayesha *et al.* [9] developed an analytical model for CZTS based thin film solar cells. Similar to [8], the model in [9] utilizes voltage-dependency of the electric field in the absorber region; but the number of fitting parameters used are less than in [8] and the model is made fully analytical by using the concept of perturbation theory. However, the model of [9] assumes that the absorber layer is fully depleted, for which the electric field therein can be considered as spatially independent. Therefore, the model is applicable for very lightly doped absorber where the assumption of full-depletion is justified.

This work proposes a model, following the approach of Mannan *et al.* [10] for employing the nonuniform electric field in the absorber layer and the approach of [9] to make the model fully analytical to extend its application even to heavily doped absorber layer. The variations of J-V characteristics under different parameters, i.e., life time of holes and electrons, choice of window material and width of emitter region have also been analysed.

II. ANALYSIS

Fig. 1(a) shows the hetero-junction structure of ZnO/CZTS-based solar cell, where the emitter region is of heavily doped ZnO and the absorber region is of comparatively lightly doped CZTS. The transparent, conducting, thin ZnO layer acts as the window layer, absorbs highly energetic photons and contributes a minor portion of the photo-generated current. Major portion of the incident photons having lower energy are absorber in the thicker absorber layer and hence, contributes most to the photo-generation current. However, the electric field developed in the absorber layer has the role to separate the photo-generated electron-hole pairs and drives them away to the opposite contacts. The profile of this electric field is shown in Fig. 1(b, c) for fully depleted and partially depleted

absorber layers respectively. Clearly, uniform field approximation as considered in the conventional models is applicable for intrinsic or very lightly doped absorber; but in practical cases for a little increase in the absorber doping

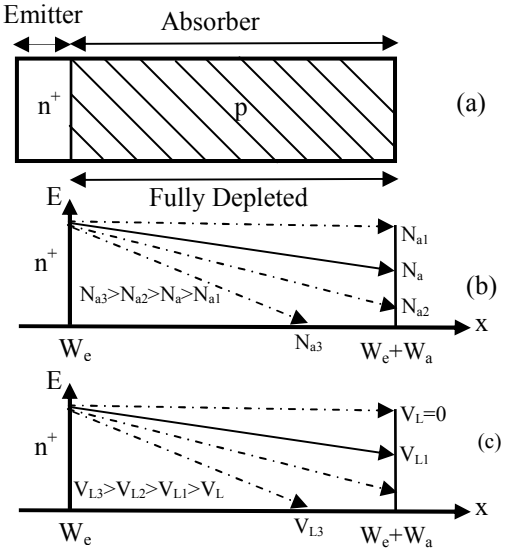

Fig. 1. Electric Field (E) Profile

results in a linearly-decreasing electric field. However, the electric field in the depletion region close to the emitter side is considered negligible due to its very narrow width. If the absorber layer is fully depleted under short circuit condition, then increase in the absorber doping level [Fig. 1(b)] or in the load voltage [Fig. 1(c)] decreases the field at the right of the absorber layer. Since the electric field is linear throughout the absorber layer and non-zero at the edge, solving Poisson's Equation this field can be calculated as [9]

$$E(x)=\frac{V_{bi}-(V_L-J_L R_S)}{W_a}+\frac{qN_a}{\varepsilon}\left(x-\frac{W_a}{2}\right) \quad (1a)$$

where, ε is the permittivity of absorber material (CZTS), W_a is the absorber width which is equal to the metallurgical base width, V_L and J_L are the load voltage and load current respectively, R_s is the series resistance and V_{bi} is the built-in voltage across the absorber layer. However, if the absorber doping level or the load voltage is further increased, the depletion edge moves towards the left. Hence, the depletion width is no longer equal to the base width and the electric field becomes zero before the base edge. Under this situation, the expression for the electric field can be expressed as found in the standard text books [11]:

$$E(x)=\frac{qN_a}{\varepsilon}(x-W_a) \quad (1b)$$

Using the expression of the electric field given by Eqn. 1(a) or 1(b) for fully or partially depleted absorber layer, the current and its continuity equations can be solved to determine the photo-generated current. These equations are as follows

$$J_n(x)=qn(x)\mu_n E(x) \quad (2)$$

$$J_p(x)=qp(x)\mu_p E(x) \quad (3)$$

$$\frac{dJ_n(x)}{dx}=\frac{qn(x)}{\tau_n}-q\alpha(\lambda)G_0(\lambda)e^{-\alpha(\lambda)x} \quad (4)$$

$$\frac{dJ_p(x)}{dx}=-\frac{qp(x)}{\tau_p}+q\alpha(\lambda)G_0(\lambda)e^{-\alpha(\lambda)x} \quad (5)$$

where, $J_n(x)$ and $J_p(x)$ stands for electron current density and hole current density respectively, n(x) and p(x) is electron and hole density, E(x) for electric field at any point x in Fig. (1), μ_n and μ_p represents electron and hole mobility, α for wavelength-dependent absorption coefficient of the material and G_0 for the optical generation rate given by

$$G_0(\lambda)=(1-R(\lambda))\frac{\lambda I_0(\lambda)}{hc} \quad (6)$$

Where, h is Planck's constant, c is the velocity of light, $I_0(\lambda)$ is the intensity of light, $R(\lambda)$ is the reflection coefficient and λ is the wavelength of the incident light.

Combining Eqns. (2) and (4) and Eqns. (3) and (5) gives the first order differential equations of n(x) and p(x) in the absorber layer as

$$\frac{dn}{dx}+\left[\frac{1}{E(x)}\frac{dE}{dx}-\frac{1}{\tau_n\mu_n E(x)}\right]n(x)=-\frac{\alpha(\lambda)G_0(\lambda)}{\mu_n E(x)}e^{-\alpha x} \quad (7)$$

$$\frac{dp}{dx}+\left[\frac{1}{E(x)}\frac{dE}{dx}+\frac{1}{\tau_p\mu_p E(x)}\right]p(x)=\frac{\alpha(\lambda)G_0(\lambda)}{\mu_p E(x)}e^{-\alpha x} \quad (8)$$

Since electrons and holes are swept out by the electric field from the absorber layer in the opposite direction, it can be assumed that $p(W_e) \approx 0$ and $n(W_e+W_a) \approx 0$. Using these boundary conditions, the solutions for the electron and hole concentration can be obtained as

$$n(x)=\frac{\alpha(\lambda)G_0(\lambda)}{\mu_n IF_n(x)}\int_{W_e+x}^{W_e+W_a}e^{-(\alpha+f_n(x))}dx \quad (9)$$

$$p(x)=\frac{\alpha(\lambda)G_0(\lambda)}{\mu_p IF_p(x)}\int_{W_e}^{W_e+x}e^{-(\alpha+f_p(x))}dx \quad (10)$$

and the electron and hole current densities can be evaluated as

$$J_n(x)=qG_0(\lambda)\alpha(\lambda)e^{f_n(x)}\int_{W_e+x}^{W_e+W_a}e^{-(\alpha+f_n(x))}dx \quad (11)$$

$$J_p(x)=qG_0(\lambda)\alpha(\lambda)e^{f_p(x)}\int_{W_e}^{W_e+x}e^{-(\alpha+f_p(x))}dx \quad (12)$$

where, $IF_n(x)=Ee^{-f_n(x)}$, $IF_p(x)=Ee^{-f_p(x)}$,

$$f_n(x)=\int\frac{dx}{\mu_n\tau_n E(x)},\ f_p(x)=\int\frac{dx}{\mu_p\tau_p E(x)}$$

The photogenerated current J_{ph} can be obtained by adding the average electron current density ($J_{n,avg}$) and average hole current density ($J_{p,avg}$) in the absorber layer and can be expressed as

$$J_{ph} = J_{n,avg} + J_{p,avg} \tag{13}$$

where, $J_{n,avg}$ and $J_{p,avg}$ can be calculated according to [9] as

$$J_{n,avg} = \frac{1}{W_a}\int_0^{W_a} J_n(x)dx \tag{14}$$

$$J_{p,avg} = \frac{1}{W_a}\int_0^{W_a} J_p(x)dx \tag{15}$$

The load current density (J_L) against the load voltage (V_L) of any solar cell including the effect of series resistance can be expressed as

$$J_L(V_L) = -J_{ph}(V_L) + J_0(V_L)(e^{\frac{V_L - J_L R_s}{nV_T}} - 1) \tag{16}$$

where, J_0 is the dark saturation current density, n is the ideality factor and V_T is the thermal voltage. Since the band-gap of ZnO (E_g = 3.35 eV) is comparatively higher than that of CZTS (E_g = 1.45 eV), the dark saturation current at the emitter region caused by diffusion is negligible and hence, is dominated by the recombination process in the absorber region. In [9], the expression for J_0 is given as

$$J_0(V_L) = \frac{qn_i W_a}{2\sqrt{\tau_n \tau_p}} \tag{17}$$

where, q is the electronic charge, n_i is the intrinsic carrier concentration and τ_n and τ_p are the lifetimes of electron and hole respectively for CdTe, and W_a is the width of the absorber layer. From (16) it is observed that the load current (J_L) at any load voltage (V_L) can only be determined using numerical methods due to the presence of unknown J_L on both sides. However, using the concept of the perturbation theory this J_L can be determined analytically.

According to the perturbation theory, if J_L at any V_L is known then, the same at $V_L+\delta V_L$ can be determined using this value, provided that $\delta V_L \rightarrow 0$. Proceeding in the same manner, currents at $V_L+2\delta V_L$, $V_L+3\delta V_L$ …….. can be determined from the current values at $V_L+\delta V_L$, $V_L+2\delta V_L$ …… respectively. Photo-generated current calculated without considering R_s can be used as the initial guess of this process.

III. Results and Discussions

Simulation results based on the proposed model are presented and discussed in this section. The incident photon flux is the air mass (AM) 1.5 global spectrum, which is obtained from the ASTM G-173-03 standard [12]. The absorption coefficients for ZnO and CZTS are obtained from the absorption curves in Ref. [7]. The thickness of ZnO and CZTS layers are 0.1 and 3.0 μm respectively.

Figs. (2) and (3) display the current-voltage (J_L-V_L) characteristics curves of CZTS based solar cells using ZnO and CdS as buffer layer respectively. Since ZnO (E_g = 3.35 eV) has higher bandgap than CdS (E_g = 2.42 eV), ZnO has absorption coefficient than CdS and shorter wavelength photons can pass through the ZnO layer i.e. more photons can be absorbed in the absorber layer if ZnO is used instead of CdS as a buffer layer. Therefore, the number of photo-generated carriers and hence, the photo-generated current is higher for ZnO buffer layer. This fact is observed in both Fig. (2) and Fig. (3). From Fig. (3), it is also seen that CdS buffer layer is more sensitive to the change of the buffer layer thickness. This is because of the fact that lower absorption coefficient of CdS than ZnO causes high-energy photons to be absorbed in the region further to the top contact i.e. if the buffer layer thickness is increased, the probability of absorption in CdS increases causing greater increase in the current than that for ZnO.

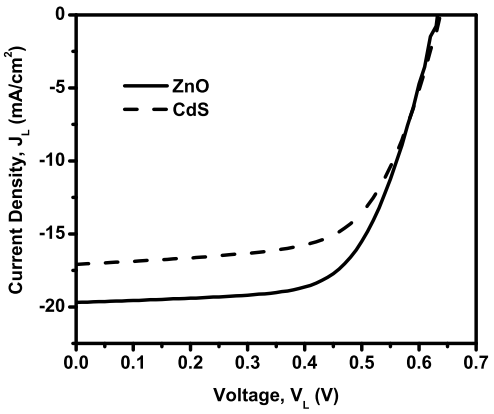

Fig. 2. J_L-V_L Characteristics of the proposed model for CZTS based solar cells using CdS and ZnO as buffer layer respectively.

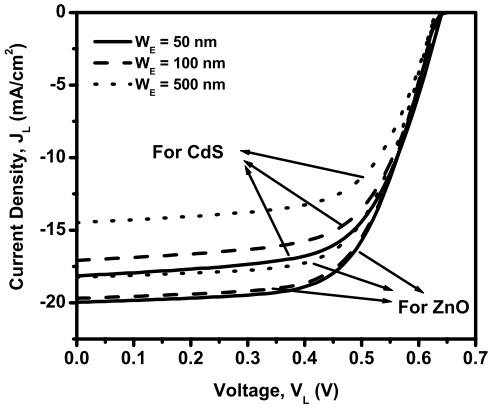

Fig. 3. J_L-V_L characteristics curve under the variation of buffer layer width (WE) for CZTS based solar cells using CdS and ZnO as buffer layer respectively.

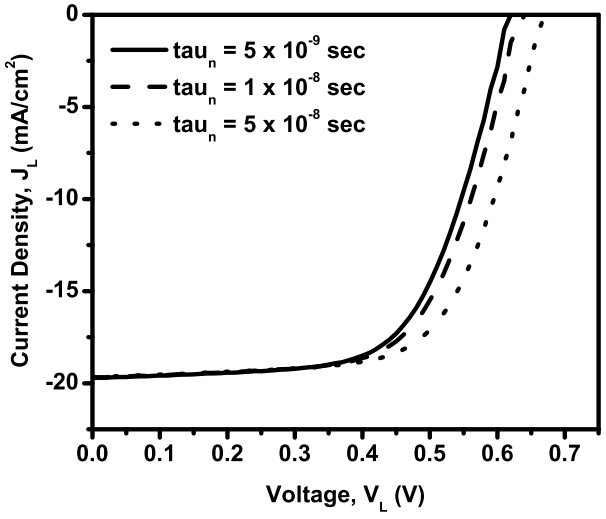

Fig. 4. J_L-V_L characteristics curve against the variation of electron lifetime (τ_n).

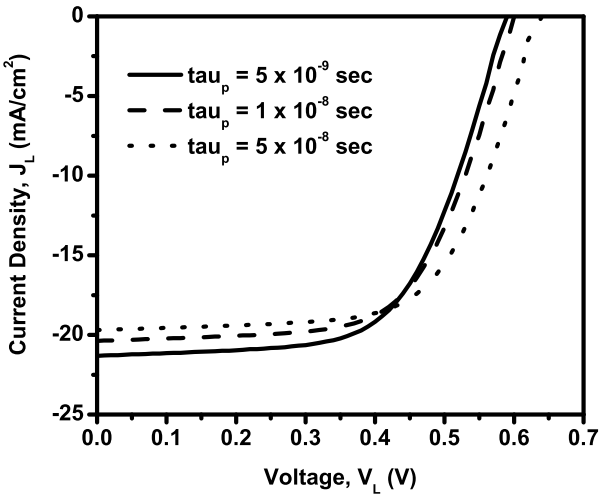

Figure. 5. J_L-V_L characteristics curve against the variation of hole lifetime (τ_p)

J_L-V_L curves have been shown for different lifetimes of electrons (τ_n) in [Fig. (4)] and of holes (τ_p) in [Fig. (5)]. It is found that J_L increases with the increase in any of τ_n or τ_p and effect of τ_p has a noticeably greater impact on current than that of τ_n. This phenomenon is quite logical. In fact, most of the photons are absorbed near the emitter side of the n-p junction. Since the fully depleted p-region is much longer than the n-region, it can be argued that the most of the absorption and hence the generation of electron-hole pairs is occurred in a region, which is more distant from bottom contact than from the top contact [Fig. (1)]. Therefore, the holes have to travel a longer distance than the electrons do before leaving the cell i.e. holes experience more recombination than the electrons. Hence, the impact of τ_p is greater than that of τ_n on J_L.

IV. Conclusion

An analytical model for the current-voltage characteristics including the series resistance of a ZnO/CZTS-based thin film solar cells has been developed in this work using perturbation theory. The proposed model incorporates both the voltage and the space dependency of the electric field in the absorber region. The model shows that ZnO is better than CdS as a window material and is less sensitive to the layer thickness than CdS does. The model also shows that the CZTS based solar cells are more sensitive to the hole transport than the electron transport. Therefore, the proposed model is more accurate and provides better insight of the physics of the thin-film solar cells.

V. References

[1] H. Katagiri, "Cu_2ZnSnS_4 thin film solar cells", *Thin Solid Films*, vol. 480, pp. 426- 432, 2005.

[2] H. Katagiri, K. Jimbo, S. Yamada, T. Kamimura, W.S. Maw, T. Fukano, T. Ito, andT. Motohiro, "Enhanced Conversion Efficiencies of Cu_2ZnSnS_4 -Based Thin Film Solar Cells by Using Preferential Etching Technique," *Applied Physics Express*, vol. 1, no. 4, pp. 041201, 2008.

[3] L. Schmidt-Mende and J. L. MacManus-Driscoll, "ZnO—nanostructures, defects, and devices," *Materials Today*, vol. 10, no. 5, pp. 40–48, 2007.

[4] J. Nelson, *The Physics of Solar Cells*, Imperial College Press, Chap. 8, 2003

[5] S. Hegedus, "Current-Voltage Analysis of a-Si and a-SiGe Solar Cells including Voltage-dependent Photocurrent Collection," *Prog. in Photovoltaics: Research and Applications*, vol. 5, pp. 151–168, 1997.

[6] C. Thompson, D. Desai, and S. Hegedus, "Voltage Dependent Photocurrent Collection in CdTe/CdS Solar Cells," *Prog. in Photovoltaics: Research and Applications*, vol. 15, pp. 587–602, 2007.

[7] R. Chandrasekharan, "Numerical modeling of tin-based absorber devices for cost-effective solar photovoltaics," *Ph. D. Thesis,* The Pennsylvania State University, May 2012.

[8] M. S. Anjan and M. Z. Kabir, "Modeling of Current-Volatge characteristics of CdS/CdTe Solar Cells," *Phys. Stat. Solidi A,* vol. 208, pp; 1813–1816, 2011.

[9] M. A. Mannan, M. S. Anjan and M. Z. Kabir, "Modeling of Current-Voltage Characteristics of Thin Film Solar Cells," *Solid-State Electron*, vol. 63, pp. 49–54, 2011.

[10] M. M. Haque, M. M. Rahman and M. I. B. Chowdhury, "Current-Voltage Characteristics of CdS/CdTe Thin Film Solar Cells: An Analytical Approach," *Proceedings of 2014 3rd International Conference on Non-Conventional Energy (ICDRET 2014)*, pp. 1-4, May 29-31, 2014, Dhaka, Bangladesh.

[11] J. Wilson and J.F.B. Hawkes, *Optoelectronics-An introduction,* 2nd ed., Englewood Cliffs, NJ, Prentice Hall, 1989, pp. 483

[12] NREL,http://rredc.nrel.gov/solarspectra/am1.5/ASTMG173/ASTMG173.html.

Design and Analysis on Biogas Producing from Wastes of Dhaka City

Md. Moniruzzaman, Md. Ashraful Islam, Md. Gius Uddin, Md. Syed Ali, M. Muhibbullah
Department of Electrical and Electronic Engineering
Bangladesh University
Mohammadpur, Dhaka-1207, Bangladesh
monir_005@yahoo.com, hassan.zehad@gmail.com, giusuddin1@gmail.com,
eeezpsayedali@gmail.com, m.muhibbullah@bu.edu.bd

***Abstract*—There are twenty million people live in Dhaka city, where daily a large amount of waste produced which can be utilized for better purposes. The project has been completed to create biogas which will be more cost effective, eco-friendly, cut down landfill, generate a high quality renewable fuel, and reduce carbon dioxide (CO_2) and methane (CH_4) emissions. A biogas reactor has been build up for producing biogas in electrical circuit lab of Bangladesh University. We collect wastes from our nearest dustbin and our residence. We made a mini biogas plant by three plastic bottles and other necessary materials. The operating principle of the plant is similar with anaerobic digesting system to produce biogas. Anaerobic digestion is a microbiological process for producing biogas, which consists of primarily methane (CH_4) and carbon dioxide (CO_2). The produced gas should be purified by deducting carbon dioxide (CO_2) and other gases. The biogas can be used for producing electricity and also for numerous purposes.**

Keywords—biogas; city waste; renewable energy; methane;

I. INTRODUCTION

Due to the lack of petroleum, coal and gas, it threatens supply of fuel throughout the world; another problem of their combustion, leads to research in different corners to access the new sources of energy; like renewable energy. The renewable energy resources are solar, wind, thermal, hydro, biomass and biogas etc. However biogas is distinct from others because of its utilization, control and collection simplicity. It has no any geographical limitations or it require advanced technology for producing energy. City waste contains about 70% of kitchen waste. Large amount of this waste produced per day. Kitchen waste is organic material having high calorific value and nutritive value to microbes, that's why efficiency of methane production can be increased. As a result, the size of reactor and cost of biogas production is reduced. In Dhaka city, kitchen waste dispose in landfill which causes public health hazards and diseases like malaria, cholera, typhoid and others. Uncontrolled removal of wastes, several undesirable situations is created. It does not only lead to polluting surface, groundwater and also promotes the reproduction of flies, mosquitoes and others. Further, it emits unpleasant smell and methane, which is a greenhouse gas; contributes to global warming. Using low calorific inputs like cattle dung, distillery effluent, municipal solid waste (MSW) or sewerage, in biogas plant, making methane generation highly inefficient. We can make this system extremely efficient by using kitchen or food wastes. Although all city wastes contain similar type of organic substances, however wastes should be different for different places. In 2003, Dr. Anand Karve [1] developed a compact biogas system that uses starchy or sugary feedstock material e.g. waste grain flour, spoilt grain, overripe or misshapen fruit, non edible seeds, fruits and rhizomes, green leaves, kitchen waste, leftover food etc. and the analysis shows that this new system is 800 times more efficient than conventional biogas plants. In compact biogas system, 2kg of feedstock produces approximately 500g of methane; the reaction is completed within 24 hours and the conventional system, 40kg of feedstock produce the same amount of methane, and required around 40 days for completing the reaction. Thus, from the point of view of conversion of feedstock into methane, the system developed by Dr. Anand Karve [2, 3] is more efficient as the conventional system. We have tried to design and analysis on biogas producing from wastes of Dhaka city using the conventional method. The proper disposal of our city waste will be done in eco-friendly and cost effectively.

II. WASTES IN DHAKA CITY

Bangladesh is the 9th most populous country and 12th most densely populated countries in the world. Currently, according to a United Nation Population Fund Association (UNFPA) report, Dhaka is one of the most polluted cities in the world and one of the issues concerned is the management of municipal waste [4]. The total waste collection rate in Dhaka city is 37% only. When waste is not properly collected, it will be illegally disposed of and this will cause serious environmental and health hazards [5]. Bangladesh has minimal waste collection coverage which forces majority of the waste to be dumped in open lands. These wastes are not disposed of properly, where general waste is often mixed with hazardous waste such as hospital waste. In a report on solid waste management in Asia, the data showed that, in Dhaka, only about 42% of generated waste is collected and dumped at landfill sites, and the rest are left uncollected. As much as 400 tons are dumped on the roadside and in open space [6]. The composition and resulting character of municipal solid waste are always dependent on the source of its generation. Each city has a unique blend of activities and resulting waste characteristics. Experience shows that approximately 60% of waste is generated by residential areas of Bangladesh. In urban areas of Bangladesh solid waste has a very high

organic content that varies from 70- 85%. The solid waste of Dhaka city has similar amount of organic matters. High moisture and organic content coupled with high prevailing temperatures make frequent removals necessary to avoid bad smell due to rapid decomposition of waste. This places additional burden on already over-strained system. Solid waste, at the point of collection, has a high density. Density will increase as the waste is handled, through loading, transport in carts and vehicles, and eventually by compaction with landfill equipment at a disposal site. Density of waste at the pick-up point ranges from 390 to 540 kg/cubic meter. For different reasons biogas plant should be encouragement in this region.

III. BIOGAS

Biogas is produced by bacteria through the bio-degradation of organic material under anaerobic conditions. Natural generation of biogas is an important part of bio-geochemical carbon cycle. It can be used both in rural and urban area.

TABLE I. COMPOSITION OF BIOGAS [7]

Types of gas	**Biogas 1 Household waste**	**Biogas 2 Agrifood industry**	**Natural gas**
Composition	60% CH_4 33 % CO_2 1% N_2 0% O_2 6% H_2O	68% CH_4 26 % CO_2 1% N_2 0% O_2 5 % H_2O	97% CH_4 2.2% C_2 0.3% C_3 0.1% C_4+ 0.4% N_2
PCS kWh/m3	6,6	7,5	11,3
PCI kWh/m3	6,0	6,8	10,3
Density (kg/m3)	1,21	1,11	0,73
Index of Wobbe	6,9	8,1	14,9

Composition of biogas depends upon feed material also. Biogas is about 20% lighter than air has an ignition temperature in range of 650 to 750 0C.An odorless & color less gas that burns with blue flame similar to LPG gas. Its caloric value is 20 Mega Joules (MJ) /m3 and it usually burns with 60 % efficiency in a conventional biogas stove. This gas is useful as fuel to substitute firewood, cow-dung, petrol, LPG, diesel, & electricity, depending on the nature of the task, and local supply conditions and constraints.

Many factors affecting the fermentation process of organic substances under anaerobic condition are

a. The quantity and nature of organic matter.
b. The temperature.
c. Acidity and alkanity (PH value) of substrate.
d. The flow and dilution of material.

Advantage of biogas technology:

1. Production of energy.
2. Transformation of organic wastes to very high quality fertilizer.
3. Improvement of hygienic conditions through reduction of pathogens.
4. Environmental advantages through protection of soil, water, air etc.
5. Micro-economical benefits by energy and fertilizer substitutes.
6. Macro-economical benefits through decentralizes energy generation and environmental protection.

Principles of biogas production:

Organic substances exist in wide variety from living beings to dead organisms. Organic matters are composed of carbon (C), combined with elements such as Hydrogen (H), Oxygen (O), Nitrogen (N), Sulphur (S) to form variety of organic compounds such as carbohydrates, proteins & lipids. In nature MOs (microorganisms), through digestion process breaks the complex carbon into smaller substances.

There are two types of digestion process:

1. Aerobic digestion.
2. Anaerobic digestion.

The digestion process taking place in the presence of oxygen (O_2) is called aerobic digestion and that of taking place without oxygen is called anaerobic digestion.

IV. EXPERIMENTAL DETAILS

The work conducts at our lab in small scale with plastic bottles.

Source of kitchen waste:

The used waste is collected from our residence i.e. cooked rice and vegetables which crushed by grinder; slurry prepared with water mixing.

Lab scale:

This experiment made with three 5.0 litters' bottles. Here different types of concentration & combination of wastes are used. Different parameters of input are measured e.g. total solid, volatile solid, volatile fatty acid, pH, temperature, nitrogen, carbon, and phosphorous.

Precautions while collecting sample kitchen waste:

1. A separate container for kitchen waste e.g. egg shells, peels and chicken mutton bones whose are crushed separately by grinder.
2. Another container collects the wet waste, stale cooked food, waste milk products. The vegetables refuse like peels, rotten potatoes, coriander leaves collected in bags.
3. A separate container for hen meaner collects from near market.
4. Cow dugs collect near a dairy farm.

Installations:

By avoiding the choking of the plant is important aspect in smoother running of plant. This occurs due to thick biological waste that not reaches to the microorganisms to digest. The easy answer to this problem is to convert solid wastes into liquid slurry. Mixer can be used to convert solid into slurry.

Analysis of gas produced in our reactor;

Syringe method:

Syringe method was used for the measurement of amount of methane and carbon dioxide in gas produced. A syringe fitted with flexible tube and dilute sodium hydroxide (NaOH) solution was used for carbon dioxide percentage estimation, since NaOH absorbs CO_2 but does not absorbs methane.

Procedure followed:

1. Prepare 100 ml of dilute sodium hydroxide solution by dissolving granules of NaOH in about 100 ml of water.
2. Take 20-30 ml sample of biogas produced during experiment into the syringe (initially fill syringe with H_2O to reduce air contamination) and put end of the tube into the NaOH solution, then push out excess gas to get a 10 ml gas sample.
3. Now take approximately 20 ml of solution and keep the end of the tube submerged in the NaOH solution while shaking syringe for 30 seconds.
4. Point it downwards and push the excess liquid out, so that syringe plunger level reaches 10 ml. Now read the volume of liquid, which should be 3-4 ml indicating about 30-40% of gas absorbed so we can say the balance of 65-60% is methane.
5. If the flame does not burn properly and you get over 50% methane (a reading of less than 5 ml of liquid) you must have nitrogen or some other gas present.

Analytical methods and calculations [8]

Total solids (TS%)–It is the amount of solid present in the sample after the water present in it is evaporated. The sample, approximately 10 gm is taken and poured in foil plate and dried to a constant weight at about 105 °C in furnace.

$$TS\% = \frac{Final\ weight}{Initial\ weight} \times 100$$

Volatile solids (VS%)–Dried residue from Total Solid analysis weighed and heated in crucible for 2hrs at 500 0C in furnace. After cooling crucible residue weighed.

$$VS\% = \left(100 - \frac{V_3 - V_1}{V_2 - V_1}\right) \times 100$$

V_1= Weight of crucible
V_2= Weight of dry residue & crucible
V_3= Weight of ash & crucible (after cooling)

Volatile fatty acids (VFA)–are fatty acids with carbon chain of six carbons or fewer. They can be created through fermentation in the intestine. Examples include: acetate, propionate, and butyrate. There are many titration methods for VFA measurement. I had used two methods for VFA measurement.

Method 1:

a. Take 100 ml sample in beaker
b. Filter the sample
c. Check pH of filtrate
d. Take 20 ml of filtrate and add 0.1M HCl until pH reaches 4
e. Heat in the hot plate for 3 minutes
f. After cooling titrate with 0.01M NaOH to take pH from 4 to 7. 7. Amount of HCl & NaOH recorded

Total VFA contents in mg/l acetic acid = (Volume of NaOH titrated) * 87.5

Method 2:

Titration procedure for measurements of VFA and alkalinity according to Kapp:

1. Before analysis, the sample needs to be filtered through a 0.45µm membrane filter.
2. Filtered sample (20-50ml) is put into a titration vessel, the size of which is determined by the basic requirement to guarantee that the tip of the pH electrode is always below the liquid surface.
3. Initial pH is recorded
4. The sample is titrated slowly with 0.1N sulphuric acid until pH 5.0 is reached. The added volume A1 [ml] of the titrant is recorded.
5. More acid is slowly added until pH 4.3 is reached. The volume A_2 [ml] of the added titrant is again recorded.
6. The latter step is repeated until pH 4. 0 is reached, and the volume A_3 [ml] of added titrant recorded once more.
7. A constant mixing of sample and added titrant is required right from the start to minimize exchange with the atmosphere during titration.

Calculation scheme according to Kapp:

$$Alk = \frac{A \times N \times 1000}{SV}$$

Alk = Alkalinity [mmol/l], also referred to as TIC (Total Inorganic Carbon).

A = Consumption of Sulphuric acid (H_2SO_4, 0.1N) to titrate from initial pH to pH 4.3 [ml]. A= $A_1 + A_2$ [ml].

N = Normality [mmol/l].

SV = Initial sample volume [ml].

VFA = Volatile fatty acids [mg/l acetic acid equivalents].

N = Normality [mmol/l]

B = Consumption of sulphuric acid (H_2SO_4, 0.1N) to titrate sample from pH 5.0 to pH 4.0 [ml], due to HCO_3/CO_2 buffer.

B = $A_2 + A_3$ [ml]

SV = Initial sample volume [ml]

Alk = Alkalinity [mmol/l]

A/TIC-ratio:

The A/TIC-method was developed at the Federal Research Institute for Agriculture (FAL) in Braunschweig, Germany. Used as an indicator of the process stability inside the digester, it expresses the ratio between Volatile Fatty

Acids and buffer capacity (alkalinity), or in other words the amount of Acids (A) compared to Total Inorganic Carbon (TIC).

A [mg/ l] = VFA [mg/ l]

TIC [mg/l] = Alkalinity [mg/ l]

Organic Content – Organic dry matter weigh the sample and weigh remaining ashes Organic content = {Mass of TS - Mass of ashes}/Mass of TS

Gas cleaning system [9]:

The various impurities e.g. water vapor, CO_2 and H_2S are present in raw biogas. Gas cleaning systems offered include H_2S scrubber and CO_2 removal. The modern gas cleaning and up gradation systems, convert biogas into a regular vehicle grade fuel having methane content, and qualities comparable to compressed natural gas (CNG).

Hydrogen sulfide (H_2S) scrubber system:

Innovative Environmental Technologies Pvt. Ltd. (IETL)'s bio scrubber H_2S scrubber system (used for H2S removal from all type of gases viz. biogas, natural gas, acid gas, tail gas, vent gas streams, shale gas, syn gas, etc.) plays a pivotal role in pollution control function in the bio renewable energy sector as well as the oil and gas sector. Our gas desulphurization system/H_2S scrubber system known as bio scrubber is a leading gas cleaning system that is vital because H_2S gas is corrosive; water vapor may cause corrosion when combined with H_2S on metal surfaces, reducing the heating value.

Gas desulphurization system:

In IETL's Gas desulphurization system, clean bio-technology is used. No expensive catalyst and chemical is required in gas cleaning system. H_2S scrubber operates at ambient temperature and pressure. Low cost to clean biogas, as up to 92% caustic recycled. In H_2S Scrubber, partial co-absorption of CO_2 takes place. Very high H_2S removal efficiency over 99% is gained. H_2S reduction to less than 200 ppm guaranteed with a bio scrubber system. Elemental sulphur as by-product of gas cleaning system with 80-90% purity is achieved. IETL's Gas desulphurization system has been working successfully in many industries for the last 12 years.

Description of the plant:

This experiment help to understand that biogas generation is possible from kitchen waste. We installed three different digesters where three different wastes used. Different mixtures produce different amount of gas. We used three types of mixture as follows

1. Only kitchen waste
2. Kitchen waste and cow dung
3. Kitchen waste and hen manure

Plan of digester:

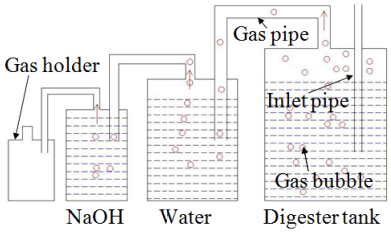

Fig. 1. Biogas plan

Necessary Apparatus:

Digester tank, plastic pipe, NaOH, water, bottle, gum, plastic pipe.

Process:

First take a 5 litter water bottle for digester tank. A PVC (inlet) pipe is adjusted with the digester tank as fig 1. Digester tank, water bottle, NaOH bottle and gas holder are inter linked with similar plastic pipe.

Working Process:

Biogas technology has mainly concentrated on "wet fermentation" of agricultural waste. So biogas produces mainly by fermentation process which converts waste into Methane (CH_4) gas. The methane gas contains some water vapors and extra gases which send through the plastic pipe into water bottle for absorbing water vapors. Again, the gas is sent through the plastic pipe into NaOH bottle for absorbing CO_2 gas. As a result fresh Methane gas is sent into the gas holder. A valve is provided for using the gas. Factors affecting biogas yield [10] are

a. Carbon/Nitrogen (C/N) ratio
b. Temperature
c. pH value
d. Loading rate

Carbon/Nitrogen (C/N) Ratio:

The relationship between the amount of carbon and nitrogen present in organic materials is expressed by the carbon/nitrogen (C/N) ratio. A suitable C/N ratio plays an important role for the proper proliferation of the bacteria for the degradation process. Depending upon the relative richness in carbon and nitrogen content, feed material can be classified as nitrogen or carbon-rich. It is generally found that during digestion, micro-organisms utilize carbon 25 to 30 times faster than nitrogen, i.e. carbon content in feedstock should be 25 to 30 times of the nitrogen content. To meet this requirement, constituents of feedstock are chosen in such a way to ensure a C/N ratio of 25:1 to 30:1.

Temperature:

Most digesters installed in the field lack mechanisms for temperature control and removal of dissolved oxygen. Hence, efficiency of these digesters is reported to be low, particularly during the winter months. In general, mesophilic bacteria are most active in the temperature range of 35-40°C and thermophilic bacteria in the range of 50-

60°C. Choosing one fermentation process in according to the natural climatic conditions in which the plant is located. The methanogens are inactive in extreme high and low temperatures, while the optimum temperature is 35°C.

pH Value:

It is essentially a measure of the acidity and alkalinity of a solution before feeding to a digester. The pH value of 7 is regarded as neutral, less than 7 as acidic and more than 7 as alkaline. Augenstein et al. suggested that during anaerobic fermentation, micro-organisms require a natural or mildly alkaline environment for efficient gas production. An optimum biogas production is achieved when the pH value of input mixture in the digester is between 6.25 and 7.50 [11]. The pH value in a biogas digester is also a function of the retention time. In the initial period of fermentation, as large amounts of organic acids are produced by acid forming bacteria, the pH value inside the digester can decrease below 5. This inhibits or even stops the digestion or fermentation process. Methanogenic bacteria are very sensitive to pH value and do not rise the value of 6.5. Later, as the digestion process continues, concentration of NH_4 increases due to the digestion of N_2, which can increase the pH value to above 8. When the CH_4 production level is stabilized, the pH range remains between 7.2 and 8.2. According to studies in China, during the period when ambient temperature varies between 22 and 26°C, it takes approximately 6 days for pH value to acquire a stable value. Similarly, during the period when ambient temperature ranges between 18 and 20°C, it takes approximately 14-18 days for pH value to attain a stable value [12]. Recent experiments performed at IIT Guwahati [13] showed that normally pH value stabilizes as fermentation proceeds following figure.

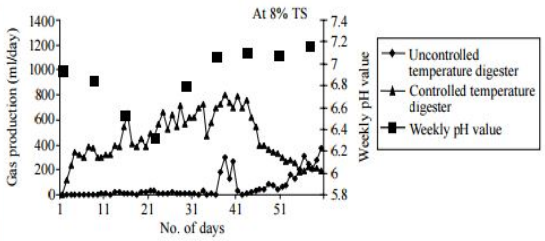

Fig. 2. pH vs. gas production

Loading Rate:

Loading rate is defined as the amount of raw materials fed per day per unit volume of digester capacity. It is an important parameter that affects gas yield. If the plant is overfed, acids will accumulate and methane production will be inhibited since micro-bacteria cannot survive in acidic situation. Similarly, if the plant is underfed, the gas production will also be low because of alkaline solution, which is also not a favorable condition for anaerobic bacteria.

V. RESULTS AND DISCUSSIONS

Experiment 1:

This experiment accomplished with 2 kg kitchen waste e.g. vegetable, food, meat etc. are crushed with blender; then mixed with 2 liter water to make slurry in a biogas digester. After 4 or 5 days, it produced gas bubble i.e. biogas. The production of biogas depends on the following factors

a. Temperature (35-40^{0}C for bacteria)
b. pH (Suitable Range 6.25-7.20)
c. C/N ratio (Carbon and Nitrogen ratio 25:1 to 30:1)

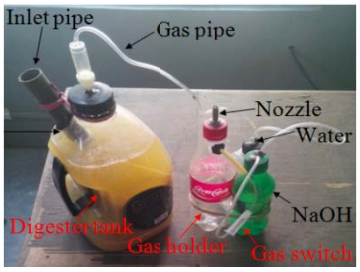

Fig. 3. Biogas Digester

Observation:

1. Water level of inlet pipe increased
2. Smell like as rotten egg

Results: Gas produced and burnt with blue flame.

Fig. 4. Biogas Burn

Experiment 2:

This experiment done by 2.5 kg cow dung and kitchen waste and 2 liter water is mixed in biogas digester. The kitchen waste must be crushed with a blender machine. After 3 or 4 days gas produced. For biogas production, similar factors maintained as experiment 1.

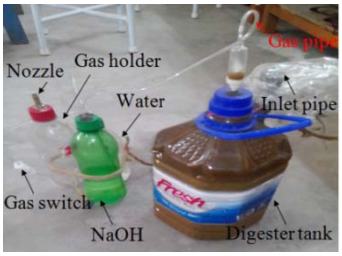

Fig. 5. Biogas Digester

Observation:

1. Water level of inlet pipe is increased
2. Smell like as rotten egg

Results: Gas produced and burnt with blue flame.

Fig. 6. Biogas Burn

Experiment 3:

This experiment done 2.5 kg hen meaner, cow dung, kitchen waste and 2.5 liter water is properly mixed in a digester. After 4 or 5 days gas produced. For biogas production, similar factors maintained as experiment 1.

Observation:

1. Water level of inlet pipe is increased
2. Smell like as rotten egg

City waste is increasing day by day not only in Dhaka city but also in the world. Though the waste is fall down in dustbin it pollute environment seriously. If the waste may be used to produce biogas it gives two facilities, one is safe the environment from pollution and second is achieve biogas which is the easiest form of renewable energy.

These three experiments have not produced same amount of gas that is given bellow-

- Experiment No.-1: Start producing biogas after 4 or 5 days and capable to burn after 15 days.
- Experiment No.-2: Start producing biogas after 3 or 4 days and capable to burn after 12 days and the amount of produced gas more than that of the first experiment.
- Experiment No.-3: Start producing biogas after 2 or 3 days and the amount of produced gas more than that of the above two experiments.

Finally we decided that the experiment No.-3 is more effective for biogas production and produce more amount of gas among them and less time required.

VI. CONCLUSION

The amount of waste is rising gradually with alarming rate and 70% of those are foods and vegetables which are may become a renewable energy source. The proper disposal of our city waste will be done in eco-friendly and cost effective way. While calculating the cost effectiveness of waste disposal we have to think more than monitory prospects. The dumping of food in places and making the places unhygienic can be taken good care of. It adds to the value of such biogas plants. Using the natural processes like micro organism's kitchen waste and biodegradable waste viz. paper, pulp can be utilized. Anaerobic digestion is controlled biological degradation process which allows efficient capturing and utilization of biogas (approx. 60% methane and 40% carbon dioxide) for energy generation. Anaerobic digestion of food waste is achievable but different types, composition of food waste results in varying degrees of methane yields, and thus the effects of mixing various types of food waste and their proportions should be determined on case by case basis.

Acknowledgement

The authors are really showing gratitude to the Lecturer Md. Moniruzzman, Department of Electrical & Electronic Engineering of Bangladesh University who gives us encouragement always. We are also grateful to the authority of Bangladesh University for providing their logistic support and guiding us in a different aspects.

References

[1] Karve .A.D. (2007), Compact biogas plant, a low cost digester for biogas from waste starch, http://www.arti-india.org.

[2] REN21,wikipedia, September 2015, http://en.wikipedia.org/ wiki/ REN21

[3] Renewable 2014 Global Status Report, http://www.ren21.net/ Portals/ 0/documents/Resources/GSR/2014/GSR2014_full%20report_low%2 0res.pdf

[4] Waste management in Bangladesh, April, 2015, http://en.wikipedia .org/wiki/Waste_management_in_Bangladesh#cite_note-2

[5] Waste management in Bangladesh, http://en.wikipedia.org/wiki/ Waste_management_in_Bangladesh#cite_note-5

[6] Waste management in Bangladesh, http://en.wikipedia.org/wiki/ Waste_management_in_Bangladesh#cite_note-7

[7] Biogas,http://www.biogas-renewable-energy.info/biogas_ composition.html

[8] Theses Report, http://ethesis.nitrkl.ac.in/2547/1/THESIS_ FINAL_ REPORT.pdf, Chapter 7

[9] Biogas Cleaning System, http://www.ietl.in/index.php/biogas-cleaning-desulphurization-system-H2S-scrubber, http://en.wikipedia .org/wiki/Waste_management_in_Bangladesh#cite_note-1

[10] A Discussion on Factors Affecting Biogas Production and Field Investigation of a Novel Duplex Digester, http://web.iitd.ac.in /~ adewan/Dewan_2005_SESI_Duplex_Digester.pdf

[11] Report No. ETSU B 1118, 1986, Research into the development of Prototype Units for the Production of Biogas Methane from Farm Wastes and Energy Crops, Department of Microbiology, University College, Cardiff.

[12] Wise, D.L., 1987, Global Bioconversions, CRC Press, Florida, Vol. IV, pp. 178-189.

[13] Mahanta, P., Dewan, A., Saha, U.K. and Kalita, P., 2004, Influence of Temperature and Total Solid Concentration on the Gas Production Rate of Biogas Digester, Journal of Energy in Southern Africa, Vol. 15 (4), pp. 112-117.

A Techno-economic Assessment for Charging Easy Bikes Using Solar Energy in Bangladesh

Md. Mustafizur Rahman[#1], Md. Abdullah Hil Baky[#2], A.K.M. Sadrul Islam[#3], Md. Abdullah Al-Matin[*4]

[#]*Department of Mechanical and Chemical Engineering, Islamic University of Technology, Board Bazar, Gazipur-1704, Bangladesh*

[1]rahman23@iut-dhaka.edu

[2]ahilbaky@yahoo.com

[3]sadrul@iut-dhaka.edu

[*]*Infrastructure Development Company Limited, UTC Building, Level-17, 8 Panthapath, Dhaka-1215, Bangladesh*

[4]matin@idcol.org

***Abstract*— In Bangladesh easy bikes are charged using electricity from the national grid. There are about 200,000 easy bikes over the country. It has been a debate to run these bikes using electricity from grid as Bangladesh is facing severe electricity crisis. Only about 55% of the population have access to electricity from the national grid. Easy bike charging by renewables offers good solution from economic and environmental point of view. Electricity production from solar energy is free from fossil fuel use and thus greenhouse gases (GHGs) are not emitted. This study aims at developing a spared-sheet-based techno-economic model to estimate the cost of charging of easy bikes using solar energy. The model also calculates the mitigation of GHG emissions. The cost of charging is found to be Tk. 14.08/km for a charging time of 6 hours. If the bikes are charged using grid electricity, the cost of charging is found to be Tk. 7.44/km at an electricity cost of Tk. 7.6/kWh. If the electricity cost passes Tk. 17/kWh, easy bike charging from solar energy is cost competitive compared to charging from conventional grid electricity. The results show that 1860.5 kg-CO_2/year/easy bike can be mitigated if the bikes are charged using solar electricity instead of conventional grid electricity. A sensitivity analysis is conducted to see the impact of various parameters on the unit cost (Tk./km) of charging.**

***Keywords*— Solar energy; techno-economic; GHG emissions; charging time; renewable resource**

I. INTRODUCTION

Bangladesh, a south Asian country, is a small country with 147,570 square km and a population of almost 160 million which leads to a population density of about 1015/km. Its geological position is 20°34" to 26°38" north latitude and 88°01" to 92°41" east longitude. Among 160 million people only 55% is under the electrification facility but rest of them uses mainly kerosene and diesel as source of light at night. As of September 2015, the total installed capacity of electricity generation in Bangladesh was 11,877 MW which constitutes mainly with 7474 MW from gas, 230 MW from hydro and 2507 MW from HFO (Heavy Fuel Oil), etc. [1]. Renewable energy sectors are not yet well developed in Bangladesh. There are 15 MW solar energy capacities through rural households and 1.9 MW wind power in Kutubdia and Feni. Bangladesh has planned to produce 10% by 2020 from renewable energy sources like wind, waste, and solar energy [2].

Using gas and oil as source of power generation leads to produce harmful greenhouse gases. Another biggest greenhouse gas emission source is the fuel consumption in transportation sector which mainly uses oil and gas. Different developed countries set limit of greenhouse gas emissions since around 33.7% of the world's total greenhouse gas emission is caused by the transportation sector [3]. In the US, transportation sector causes greenhouse gas emissions of about 28% [4]. NHTSA (National Highway Traffic Safety Administration) of USA issued rules to reduce emissions of greenhouse gases to 163 g/mile within 2025 [5]. Mitigation of greenhouse gases and limited reservation of oil and gas corresponds to search for alternate source of energy for cars. This can be accomplished by alternative fuel vehicles such as EV (electric vehicles), PHEV (Plug in Hybrid Electric Vehicle) and FCV (Fuel Cell Vehicles) [5]. Using these alternate fuel vehicles helps in both minimizing the pressure on natural resources and reducing the emission of greenhouse gases. Renewable energy sources such as solar, wind and hydro can be used to charge electric vehicles since using grid electricity again imposes pressure on the natural resources of the country as well as increases greenhouse gas emissions. Although the advantage of the use of EVs is known but there is not sufficient study related to the economic aspects of these renewable energy systems.

The influence of large scale implementation of PHEVs and EVs on the power systems of five northern European countries (Denmark, Finland, Germany, Norway and Sweden) were analysed by Hedegaard et al. [6]. They decided that if economic support is not available for renewable energy technologies, coal based electricity can be used for EV charging. Goransson et al. [7] investigated the integration of PHEVs with wind energy which resulted a 4.7% reduction in CO_2 emissions as compared to CVs (conventional vehicles). Current literature on EVs and renewable energy integration were reviewed by Richardson and indicated significant reduction in GHG emissions in the transportation and power industries [8]. Wind energy capacity can be increased by large scale integration of wind energy with PHEVs upon conversion

of a vehicle fleet to 50% PHEVs [9]. The effect of different EV charging strategies were investigated by Ekman [10] and it was found that electrification of transportation sector will reduce the excess wind power. A mixed integer linear programming model is constructed by Weis et al. [11] for capacity expansion, plant dispatch, and plug-in hybrid electric vehicle (PHEV) charging and it was found that cost of integrating PHEVs reduce to half by controlled charging. This save is about 5-10% higher with almost 20% penetration of wind compared to no wind power. According to Liu et al. [12] electric vehicles can balance between electricity supply and demand and can increase wind energy integration by 8% in Mongolia, China and integration of wind energy both saves energy service cost and fuel cost. Electric vehicles penetration by hydro was investigated in a case study by Camus et al. [13] where it shows that for the year 2020 the cost of charging EVs could be reduced from 20 cents/kWh at pick hours to 5.6 cents/kWh at off pick hours. The study shows 3%, 14%, and 10% reduction in energy consumption, fossil fuel use and CO_2 emissions, respectively for the condition when electric vehicles are used.

There is scarcity of assessments of renewable energy technologies for charging electric vehicles in Bangladesh. There is very limited study on independent techno-economic assessment for charging electric vehicles from renewable technologies. Very few studies worked on wind and hydro for charging electric vehicles. The objective of this paper is to develop a spread-sheet-based model to estimate the cost of charging easy bikes using solar energy. Considering the lack of sites for hydro and wind power plants in Bangladesh the suitable source is considered to be solar energy. In this paper, an insight of load calculation and cost determination for charging an electric vehicle (three wheeler easy bike) using solar power is discussed. A sensitivity analysis is done to observe the impact of different input parameters on the unit cost of charging. Greenhouse gas (GHG) mitigation is discussed if the easy bikes are charged using electricity from solar energy. GHG emissions are calculated based on the national grid electricity mix for Bangladesh.

II. METHOD

A. *Goal and Scope*

The purpose of this study is to conduct a techno-economic assessment of charging easy bike three wheeler with electricity obtained from solar energy in Bangladesh. An excel-based bottom-up model is developed to estimate the cost of charging an easy bike. The model is developed using the fundamental engineering principles. All the components (e.g. solar panel, batteries, charge regulators, etc.) are designed to satisfy the load demand. The functional unit used in this research is Tk./km. Bangladesh has a great potential for solar energy. The country receives about 4.67 kWh/m^2 solar radiation daily. This study only assesses the solar energy for charging easy bikes. The other renewable resources (e.g. wind, hydro, etc.) are out of the scope of this study due to lack of potential of these resources.

B. *Techno-economic Assessment*

The easy bike considered in this study has five batteries of 120 Ah, 12 volts (1.44 kWh) each to travel a distance of approximately 110 km. Fig. 1 shows a typical easy bike for five passengers. Scale of operation is indicated by number of charging points. Usually, a home would have a single charging point. But in Bangladesh easy bikes are operated by business companies that require more charging points. In this study ten charging points are considered. The assessment is done for six hours of charging. Charging time varies from four to eight hours. For the base case six hours is considered. The effect of charging time is shown in the sensitivity analysis later in the paper. The load requirement (kWh) for the charging station is calculated by multiplying load requirement per easy bike per day with number of charging points. 90% of the charge is assumed to be consumed as the bike is driven [14]. The power requirement (kW) is found from the load requirement and charging hours. This load will be satisfied by electricity produced by solar energy. Solar energy is not continuous around the clock. Therefore solar energy systems require energy storage device such as battery. Batteries will store the energy to fulfil the energy demand of the charging system. Solar panel sizing is done using the load requirement, solar hours a day, and efficiency factor. Solar hours and the efficiency factor are taken as 6 hours and 75%, respectively. For reliability, batteries have been designed to store energy for 3 days without electricity production from solar energy.

The system consists of solar panel, batteries, and charge controllers. The charging station is assumed to be situated very close to the energy production system. The interest rate and inflation rate are taken as 10% and 7.33%, respectively [15], [16]. The costs are in Bangladeshi Taka (Tk.) where the base year is 2014. All present cost numbers are amortized over the life time of the components. The conversion rate is used as 1 USD to 77 Tk.

Life time of components, efficiencies of charging and discharging of batteries, interest rate, inflation rate and various cost numbers used in this research are presented in Table 1.

Fig. 1. A typical easy bike for five passengers in Bangladesh

TABLE I. KEY ASSUMPTIONS AND INPUT PARAMETERS USED FOR MODELLING

Parameter	Unit	Value	Source/comment
Interest rate	%	10	[15]
Inflation rate	%	7.33	Based on annual average inflation rate for the year of 2014 found in Bangladesh Bank website [16]
Charging time of one EV per day	hours	6	[17]
Solar panel			
Life time of solar panel	years	25	[18]
Solar panel price	Tk./W_p	57	Based on personal communication with an expert from IDCOL [19]
Lead-acid battery			
Charging efficiency	%	90	[20]
Discharging efficiency	%	95	[20]
Depth of discharge	%	80	[20]
Battery storage cost	Tk./kWh	2500	Based on personal communication with an expert from IDCOL [19]
Life time of batteries	years	5	Based on personal communication with an expert from IDCOL [19]
Charge regulator			
Life time of charge controller	years	10	Based on personal communication with an expert from IDCOL [19]
Charge regulator cost	Tk./unit	20,833	Based on personal communication with an expert from IDCOL [19]
Charging station			
Charging station material cost	Tk./kW	29,630	[14]
Life time of charging station	years	10	[17]
Yearly maintenance cost for the components	%	2	[14]

III. RESULTS AND DISCUSSION

Solar energy is used as the electricity source for charging easy bikes. The techno-economic model developed in this study provides capital cost, annual cost, and unit cost of charging. The model also finds the sensitive parameters that have an impact on unit cost (Tk./km) of charging.

A. Economics of Solar-powered Charging

Total load for ten charging points is found to be 80 kWh for charging five 120 Ah (12 volt) batteries for each easy bike. To satisfy the load demand, total capacity for solar panel is calculated as about 18 kW_p. Considering Tk. 57/W_p for panel, capital cost for solar panel is estimated as Tk.1,012,978. The capital cost for all the items are furnished in Table 2. Due to data unavailability, the cost of civil works is assumed to be 0.5% of the capital cost [14]. The civil works cost is found to be Tk. 13,534. Similarly no data are available for maintenance cost for the components of the system. A 2% of capital cost is assumed as the yearly maintenance cost. The yearly maintenance cost is estimated to be Tk. 87,737. Fig. 2 depicts the yearly cost components of the solar-powered charging system. All the cost numbers in Fig. 2 is in Tk. 1000. The capital cost of the components are amortized over the life time of the components with an interest rate of 10%. The annual cost of batteries is the highest due to high storage cost of batteries and lower life time than solar panels. The cost of solar panels, batteries, charge controllers, charging station material, civil works, and maintenance are found to be Tk. 111,598, Tk. 231,416, Tk. 65,098, Tk. 67,802, Tk. 1,589, and Tk. 87,737, respectively.

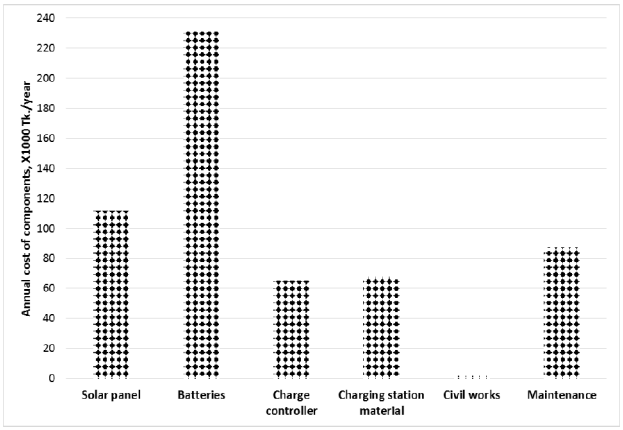

Fig. 2. Annual cost of components calculated in this study

The cost of charging an easy bike is estimated to be Tk. 14.08 per km driven. To estimate the cost of charging, average distance driven by an easy bike driver is assumed to be 110 km daily [19]. This value is cross-matched by discussing with easy bike drivers. If the total annual cost is divided by the annual average load of easy bikes, the unit cost of electricity would be Tk. 19.36/kWh. This number fairly matches with the result obtained in [22]. The small variation in results is due to difference in assumptions and cost numbers used in the studies.

TABLE II. CAPITAL COST FOR ALL THE ITEMS OF CHARGING STATION

Parameter	Unit	Value	Source/comment
Solar panel (each)	W_p	250	Based on personal communication with an expert from IDCOL [19]
Number of units		72	Calculated from the total size (kW) of solar panel and each solar panel capacity
Charge controller (each)	kW	2.4	Based on personal communication with an expert from IDCOL [19]
Number of units		8	Calculated from the total size (kW) of solar panel and each controller capacity
Capital cost			
Solar panel	Tk.	1,012,978	
Batteries (lead-acid)	Tk.	877,260	
Charge controller	Tk.	400,000	
Charging station material	Tk.	416,614	
Civil works	Tk.	13534	Civil works cost is assumed to be 0.5% of the total capital cost [14]

The model also estimates the charging cost when the easy bikes are charged with conventional grid electricity. The cost of charging is found to be Tk. 7.44/km considering electricity cost of Tk. 7.6/kWh. The cost of charging with solar energy is higher than using conventional charging which is obvious due to the reason that extracting energy from sun using solar panels is much more expensive that producing electricity in fossil fuel power plants. But if the cost of grid electricity crosses Tk. 17/kWh, charging with electricity from solar is more cost competitive.

B. Environmental Impact

The grid electricity emission factor for Bangladesh is taken as 0.637 kg-CO_2eq/kWh [23]. Based on the average distance travelled by an easy bike, the GHG mitigation potential is found to be 1860.5 kg-CO_2eq/easy bike in year. For the environmental impact analysis only operational emissions are considered. Due to lack of data in public domain, emissions from equipment production are not considered and usually these emissions are less than 1% of the total. Hence the findings will not change much.

C. Sensitivity Analysis

A sensitivity analysis is done to see the impact of various input parameters on cost of charging. All the parameters are varied by ±20%. The base case values for interest rate, charging time, battery storage cost, solar panel cost, and life time of solar panel, battery and charge controller are taken as 10%, 6 hrs., Tk. 2500/kWh, Tk. 57/W_p, and 25 yrs., 5 yrs. and 10 yrs., respectively. Fig. 3 shows the sensitivity analysis for charging cost, Tk./km. Cost of charging is increased as the interest rate, battery storage cost, and solar panel cost are increased. Battery storage cost has a big impact on result. A 20% increase in battery cost increases the cost of charging by 8.82%. On the other hand cost of charging shows a decreasing trend when charging time and life time of the components (e.g. solar panel, batteries, and charge controller) are increased. As the charging time is increased, charging cost reduces. A 20% increase in charging time from 6 hrs. to 7.2 hrs. reduces the cost of charging from Tk.14.08/km to Tk.13.62/km. This is because infrastructure for fast charging is much expensive than that of slow charging. Life time of solar panel and charge controller have minor impact on cost of charging.

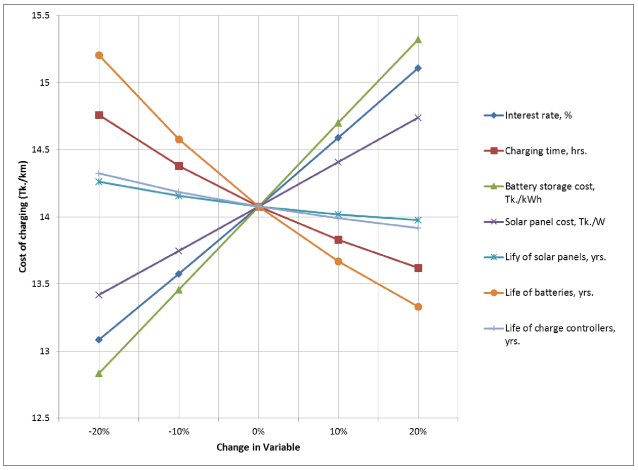

Fig 3. Sensitivity analysis for cost of charging

IV. CONCLUSIONS

This paper provides an estimation of cost of charging easy bikes with solar energy and conventional grid electricity through the development of a data-intensive spread-sheet-based model based on fundamental scientific principles. The accuracy of the model is checked by the numbers published in literature and sharing the numbers with renewable energy experts. Charging with grid electricity is cost competitive but has environmental impacts. Charging with solar energy can reduce 1860.5 kg-CO_2eq/vehicle in a year. The cost of charging is found to be Tk. 14.08/km for a charging time of 6 hours. The cost of charging using grid electricity is Tk. 7.44/km. When conventional electricity cost is increased from Tk. 7.6/kWh to Tk. 17/kWh, charging with solar energy is more cost effective. Sensitivity analysis shows that battery storage

cost has a big impact on cost of charging. The results of this paper will help the industry to consider solar energy to charge easy bikes which is more environmentally friendly.

ACKNOWLEDGMENT

The authors would like to thank the renewable energy experts of Infrastructure Development Company Limited (IDCOL) for supporting this research with various data sources.

REFERENCES

[1] Bangladesh Power Development Board. Available from: www.bpdb.gov.bd. [Accessed: September 2015].

[2] M.A.H. Mondal and M. Denich, "Assessment of renewable energy resources potential for electricity generation in Bangladesh," *Renewable and Sustainable Energy Reviews*, vol. 14(8), pp. 2401-2413, 2010.

[3] S.F. Tie and C.W. Tan, "A review of energy sources and energy management system in electric vehicles," *Renewable and Sustainable Energy* Reviews, vol. 20 (0), pp. 82-102, 2013.

[4] United States Environmental Protection Agency (EPA). National Greenhouse Gas Emissions Data. Available from: http://www.epa.gov/climatechange/ ghg emissions/usinventoryreport.html.

[5] US Environmental Protection Agency and the US National Highway Traffic Safety Administration. 2017 and later model year light-duty vehicle greenhouse gas emissions and corporate average fuel economy standards. Available from: http://www.nhtsa.gov/staticfiles/rulemaking/pdf/cafe/2017-25_CAFE_Final_Rule.pdf.

[6] K. Hedegaard, H. Ravn, N. Juul, and P. Meibom, "Effects of electric vehicles on power systems in Northern Europe," *Energy*, vol. 48 (1), pp. 356-68, 2012.

[7] L. Goransson, S. Karlsson, and F. Johnsson, "Integration of plug-in hybrid electric vehicles in a regional wind-thermal power system," *Energy Policy,* vol. 38(10), pp. 5482-92, 2010.

[8] D.B. Richardson, "Electric vehicles and the electric grid: a review of modeling approaches, impacts, and renewable energy integration," *Renewable and Sustainable Energy Reviews*, vol. 19(0), pp. 247-54, 2013.

[9] W. Short and P. Denholm, "A preliminary assessment of plug-in hybrid electric vehicles on wind energy markets," NREL/TP-620-39729, April 2006.

[10] C.K. Ekman, "On the synergy between large electric vehicle fleet and high wind penetration -an analysis of the Danish case," *Renewable Energy*, vol. 36(2), pp. 546-53, 2011.

[11] A. Weis, P. Jaramillo, and J. Michalek, "Estimating the potential of controlled plug-in hybrid electric vehicle charging to reduce operational and capacity expansion costs for electric power systems with high wind penetration," *Applied Energy,* vol. 115(0), pp. 190-204, 2014.

[12] W. Liu, W. Hu, H. Lund, and Z. Chen, "Electric vehicles and large-scale integration of wind power -the case of Inner Mongolia in China," *Applied Energy*, vol. 104(0), pp. 445-56, 2013.

[13] C. Camus, T. Farias, and J. Esteves, "Potential impacts assessment of plug-in electric vehicles on the Portuguese energy market," *Energy Policy,* vol. 39(10), pp. 5883-97, 2011.

[14] A. Verma, R. Raj, M. Kumar, S. Ghandehariun, and A. Kumar, "Assessment of renewable energy technologies for charging electric vehicles in Canada," *Energy*, vol. 86(0), pp. 548-559, 2015.

[15] A. Zubair, A.A. Tanvir, and M.M. Hasan, "Optimal Planning of Standalone Solar-Wind-Diesel Hybrid Energy System for a Coastal Area of Bangladesh," *International Journal of Electrical and Computer Engineering*, vol. 2(6), pp. 731-38, 2012.

[16] Banladesh Bank, Available from; https://www.bb.org.bd/econdata/inflation.php. [Accessed: October 2015].

[17] A. Schroeder and T. Traber, "The economics of fast charging infrastructure for electric vehicles," *Energy Policy*, vol. 43(0), pp. 136-44, 2012.

[18] R. Kannan, K. Leong, R. Osman, H. Ho, and C. Tso, "Life cycle assessment study of solar PV systems: an example of a 2.7 kWp distributed solar PV system in Singapore," *Solar Energy*, vol. 80 (5), pp. 555–563, 2006.

[19] Infrastructure Development Company Limited (IDCOL), Available from: http://www.idcol.org/.

[20] S. Shokrzadeh and E. Bibeau, "Repurposing batteries of plug-in electric vehicles to support renewable energy penetration in the electric grid," *SAE Int*. SAE Technical Paper 2012-01-0348, 2012.

[21] B. Fleck andM. Huot, "Comparative life-cycle assessment of a small wind turbine for residential off-grid use," *Renewable Energy*, vol. 34(12), pp. 2688-96, 2009.

[22] Solar E.Technology Australia, ABN 40699540462. Available from: www.solar-e-technology-bd.com.

[23] M. Brander, A. Sood, C. Wylie, A. Haughton, and J. Lovell, Technical Paper, "Electricity-specific emission factors for grid electricity," 2011, Available from: http://ecometrica.com/assets//Electricity-specific-emission-factors-for-grid-electricity.pdf.

Reduction of Cooking Energy and CO_2 emission using Heat Retention Cooker for Rice Cooking

Sayedus Salehin[*1], A.K.M. Sadrul Islam[*2], A.N.M. Zobayer[#3]

[*]*Department of Mechanical and Chemical Engineering, Islamic University of Technology*
Board Bazar, Gazipur-1704, Bangladesh

[#]*Sustainable Energy for Development (SED)*
Deutsche Gesellschaft für Internationale Zusammenarbeit (GIZ) GmbH,
Road 90, House 10/A, Gulshan-, Dhaka 1212, Bangladesh

[1]sayedus@iut-dhaka.edu

[2]sadrul@iut-dhaka.edu

[3]anm.zobayer@giz.de

***Abstract*—Heat retention cooker such as Hot Bag is a promising solution for reducing cooking energy which employs the retained heat for cooking in an urban kitchen or elsewhere. Different kinds of food items may be cooked using Hot Bag including rice, potato, chicken, beef, and vegetables etc. which require water for their cooking. When the food is heated to its boiling temperature on the cooking stove, the food can be continued to be cooked using this cooker by retaining the heat. This option offers several benefits including reduction of fuel usage, greenhouse gas emission, energy savings for cooking leading to monetary savings, indoor air pollution reduction etc. This paper presents a significant energy savings while cooking rice with Hot Bag as compared to cooking using traditional method. The tests showed energy savings of 42% for cooking rice. Also, the CO_2 reduction is 123 grams per kg of rice. Heat retention tests have been carried out to understand the thermal behavior of the system. The thermal analysis of the heat transfer from the Hot Bag is also presented.**

Keywords—heat retention cooker; cooking; energy efficiency; energy saving; rice cooking; green house gas emission

I. INTRODUCTION

Household energy use has 10% share in world's primary energy consumption in developing countries, a total of 1,090 Mtoe. Cooking is the main consumer of energy in the households in developing countries followed by lighting and heating. And household use of biomass in these countries accounts for almost 7% of world primary energy demand [1].

Food item cooking involves heating at specific temperature range for certain duration. Heating required for cooking can be obtained by burning fuel, electricity etc. Since significant amount of energy is consumed during the heating process, even a small percentage of reduction in energy in cooking will contribute to an enormous energy savings. Moreover, cooking is carried out in almost every single house every day, at least once if not for every meal. The temperature range and heating duration varies for each food item. In order for the food to be properly cooked, the food item has to be kept at the certain temperature range for a certain time period.

Many of the food items in Bangladesh contain starch. This starch has highly organized structures, known as starch granules. When starch is heated with water, it undergoes a transition process in which the starch granules break down the inter-molecular bond in presence of water and heat, this phenomenon is called gelatinization. Gelatinization temperature is regarded as the temperature at which the phase transition of starch granules from an ordered state to a disordered state occurs [2]. The gelatinization temperature for rice and potato are 66°C-82°C and 55°C-66°C, respectively [3].

Insulating boxes have been used to reduce the energy consumption during cooking in many countries as a tradition. Sometimes they are used to keep the cooked food item hot for several hours. In 2006, a social entrepreneur, Sarah Collins from South Africa has started an enterprise on WonderBag after the serious power cut problem in her country [4]. This bag makes use of insulation to retain the heat for slow cooking. The Hot Bag used for the study is similar to the WonderBag and is imported from South Africa. The Hot Bag must retain this temperature for slow cooking for a longer duration for slow cooking.

There have been several reports which suggest that using the Hot Bag will lead to a significant amount of energy savings. This paper has quantified the amount of energy that can be saved by using such bags. Also, the energy savings will be varied for different food items as well as the cooking methods used. In this study, the energy consumption, possible energy savings and CO_2 emission reduction potential by using this cooker have been quantified and analyzed.

II. Hot Bag: An overview

Hot Bag may be considered as a kind of Heat Retention Cooker (HRC). Using thermal insulation, this cooker may be used for slow cooking by retaining the heat within the enclosed space. It has the potential to minimize the fuel consumption by reducing the energy consumption in conventional cooking. This is especially essential in areas with fuel shortage. In many areas, in Bangladesh or elsewhere in underdeveloped or developing countries, women have to travel a long distance for collecting fuel for cooking. For many, this journey is often dangerous due to various reasons.

The specifications of the cooker in Fig. 1 which has been used for the tests are as follows:
Weight = 0.472 kg
Height = 22 cm
Outer Dia (full open) = 95 cm
Outer Dia (full closed with a pan having capacity of 3 liter) = 45 cm
Base Dia = 38 cm
Insulation Thickness = 12 cm
Holding capacity = 6 liter pan

Fig.1 Hot Bag used for the tests

Fig. 2 Hot Bag in full open position

Fig. 3 Hot Bag in full closed position

Heat is retained within the cooker using insulating materials. Polystyrene micro beads have been used as thermal insulating material having a thermal conductivity of 0.03 W/m-K. These micro beads are placed within compartments and then sewed with the bag. The micro beads having diameters of 2-3 mm used in the cooker can be seen in Fig. 4.

Fig. 4 Polystyrene micro beads used as insulating material in the cooker

III. Methodology

Induction cooking stove has been used to provide heat for cooking and the energy consumption has been measured. This section elaborates the description of the methods and materials employed during the experiments.

A. Induction Cooker

Induction cooker makes use of induction heating for cooking. When electricity is supplied, the high frequency electromagnet induction element within the cooker generates a magnetic field. The cooking vessel has to be of ferromagnetic material e.g. Stainless Steel, cast iron etc. The magnetic field generated a loop current flow through the metal of the cooking vessel and this current flow through the resistance of the metal generates heat.

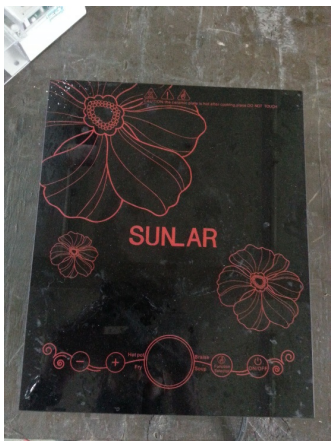

Fig. 5 Induction cooker used for experiments

For cooking rice, SUNLAR-SL-STR Induction cooker has been used with a rated voltage of 220 V at 50 Hz frequency and maximum current flow of 9A. The manual shows that Induction cooker has a maximum power output of 2000W. However, the experiment suggests that the maximum power obtained from the Induction cooker is 1400 W. The thermal efficiency of the Induction cooker has been experimentally found to be ~82%. For controlling the power output from the Induction cooker, GGG- TDGC Variac has been used with a capacity of 5KVA and Frequency of 50 Hz.

B. Measuring Methods

For measuring the energy consumed during cooking, an energy meter has been used whose display shows the power output of the induction cooker, energy being consumed, voltage, and current at regular interval. The energy meter used in the experiments is a single phase static kWh meter manufactured by Modern Energy Co. Ltd. '*300'* Thermometer has been used to measure the temperature during cooking. A variac has been used to control the power output for cooking. Fig. 6 shows the experimental setup for cooking using Induction cooker.

Fig. 6 Experimental set up for cooking using Induction cooker

C. Energy Savings

The energy saving by using Hot Bag can be obtained by conducting tests. Firstly, the rice has been cooked using conventional method i.e. heating on the induction cooker for duration as needed. Later on a different test, the same rice of same quantity has been heated up to the boiling point, kept at that temperature for a certain time and then placed in the Hot Bag for slow cooking. For both the cases, the energy consumption has been measured and the difference in the energy consumption gives the energy savings.

D. CO_2 Emission Reduction

The cooking makes use of thermal energy which is originated from fossil fuel sources in most of the cases. Burning fossil fuel releases CO_2 in the atmosphere which is harmful for the environment. Also it is one of the main causes of greenhouse emissions and one of the main reasons for global warming is the greenhouse gas emission. The electricity is supplied from the national grid which originates from power plants e.g. gas power plants, coal power plants, nuclear power plants etc. and have different CO_2 emission amounts depending on their share in the national grid. For Bangladeshi context, CO_2 emission from Induction Cooker which runs on electricity is 0.1425 gm/kJ. [5]

IV. Thermal Analysis

The heat transfer is often in transient state in cooking of food materials, where the temperature changes over time. While the food material is kept inside Hot Bag, the heat transfer phenomena can be explained by Lumped Heat Capacity method. In this analysis, it is assumed that the internal thermal resistance can be neglected as compared to the external thermal resistance. The convective heat transfer from the heat retention cooker can be expressed as

$$q = hA\,(T - T_\infty) = c\rho V \frac{dT}{dt} \qquad (1)$$

Where,
q = Heat transfer rate, W
h = Convective heat transfer coefficient, W/m^2K
A = Surface area for convection, m^2
T = Temperature of the Hot Bag, ^0C
T_∞ = Room temperature, ^0C
V = Volume, m^3
c = Specific heat, kJ/kg-K
ρ = Density, kg/m^3
t = time.

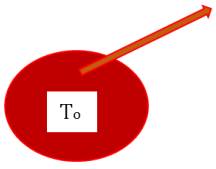

Fig. 7 Heat transfer phenomena from Hot Bag

When $T=T_0$ at t=0, the solution to Eq. 1 can be expressed as,

$$\frac{T-T_\infty}{T_0-T_\infty} = e^{-\left[\frac{hA}{\rho cV}\right]t} \quad (2)$$

$$\theta = e^{-mt} \quad (3)$$

Here m is defined as, $m = \frac{hA}{\rho cV} = \frac{1}{\frac{1}{hA}\rho cV}$, Where, $\frac{1}{hA}$ is the thermal resistance and ρcV is the thermal capacitance.

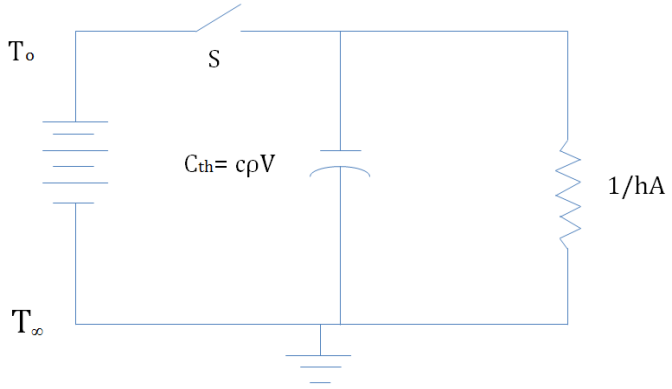

Fig.8 Analogous electric circuit for heat transfer

Fig.8 shows an analogous electrical circuit for the phenomena. It is noticed that the thermal capacity of the system is charged initially at potential T_0 by closing the switch S. When S is opened, the energy stored in the thermal capacitance is dissipated through the resistance *1/hA*.

A graph of the dimensionless temperature as a function of time can be seen in Fig.9.With time, the temperature decays exponentially. The time constant *m* determines the shape of the curve. Here m has the dimension of $(\text{time})^{-1}$. As the value of m increases, the curves become steeper which indicates that the value of m will cause the solid to respond faster to a change in ambient temperature. The definition of *m* reveals that increasing the surface area for a given volume and the heat transfer coefficient increases *m*.

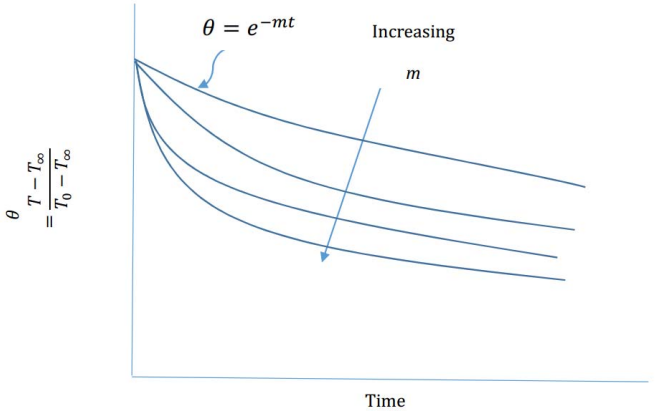

Fig. 9 Dimensionless temperature as a function of time

V. Heat Retention Test

Heat retention test was carried out to evaluate the heat retention potential of the Hot Bag. 4 liters of water in a pan is placed in the bag after heating it to 100℃ and the Hot Bag is closed. The temperature readings are taken at equal intervals to evaluate the heat retention capacity. On a different experiment, the same amount of water in the same pan is kept without the Bag after heating it to the same temperature and the temperature readings are taken. Two results are then compared.

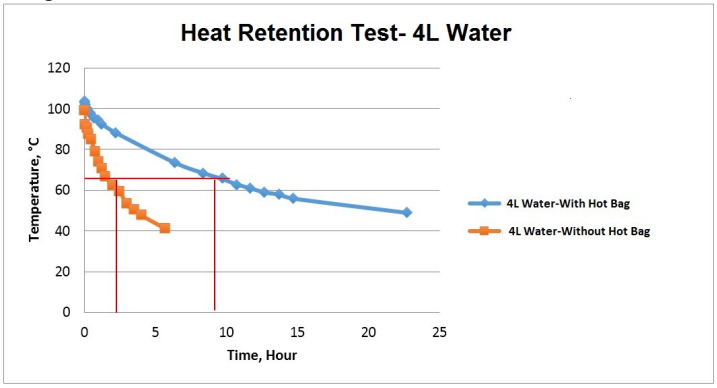

Fig. 10 Heat retention test for 4 liter water with and without Hot Bag

Fig.10 shows the heat retention test for 4 liter water with and without Hot Bag. The graphs shows that the heat loss rate is higher when the bag is not used. Considering a temperature of 65℃, a temperature many food items are cooked, water reaches to this temperature in around 2.5 hours without Hot Bag where it takes for water to reach the same temperature for around 9 hours with Hot Bag from the same temperature of 100℃.

VI. Cooking Tests

For evaluating the performance of the Hot Bag, rice cooking has been undertaken in controlled environment using Induction Cooker with and without bag. Bangladesh produces 33889632 Metric tons of rice, being the 6th ranked country in the world [6]. Almost in every household, rice is cooked at least twice daily, for lunch and dinner. Hence, it is of great interest to assess the possible energy savings and CO2 emission reduction. Minicate rice has been chosen for the experiments since this type of rice is widely used. 1 kg of rice and 2.5 liters water were put on the cooking pan and cooked using conventional method.

Fig.11 Cooked rice by conventional method

Fig.12 Cooked rice using Hot Bag

A. Cooking rice with Hot Bag

The room temperature and the water temperature were 34.6^{0}C and 29.5^{0}C respectively during the test. 1 kg rice was mixed with 2.5 liters of water and put on the pan. The induction cooker was switched on with full power controlled by Variac. A thermocouple has been inserted into the rice-water mixture to measure the temperature throughout the process. The temperature reached the boiling temperature 100^{0}C after 13 minutes. Soon after that, the power input was decreased to 75% (1.06 kW) at 15 minutes. The cooking is completed at 29 minutes, and the induction cooker is switched off. Total energy consumption corresponds to 0.57 kWh. Fig.13 shows the temperature profile during the cooking.

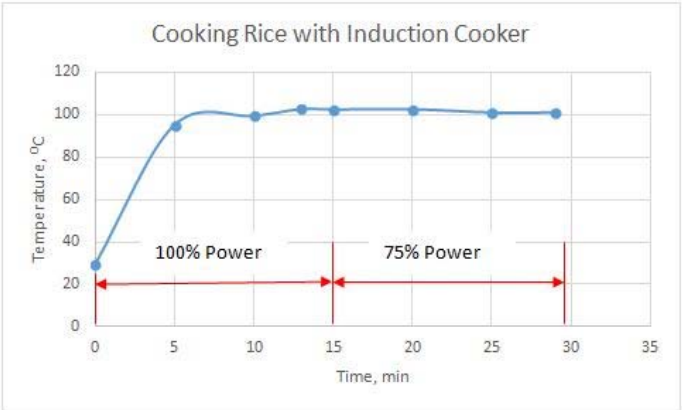

Fig. 13 Temperature profile for cooking rice with Induction cooker

B. Cooking rice without Hot Bag

The room temperature and the water temperature were 34.6^{0}C and 32^{0}C respectively during the test. 1 kg rice was mixed with 2.5 liters of water and put on the pan. The induction cooker was switched on with 100% power (1.39 kW) controlled by Variac. A thermocouple has been inserted into the rice-water mixture to measure the temperature throughout the process. The temperature reached the boiling temperature 100^{0}C at 14.5 minutes. Instantly after that the pan was put inside the Hot Bag and sealed off. The pan was kept inside the Hot Bag for 35 minutes. The temperature was 94.7^{0}C when the Hot Bag was opened after 35 minutes. The rice was cooked perfectly. Fig. 14 shows the temperature profile during the cooking.

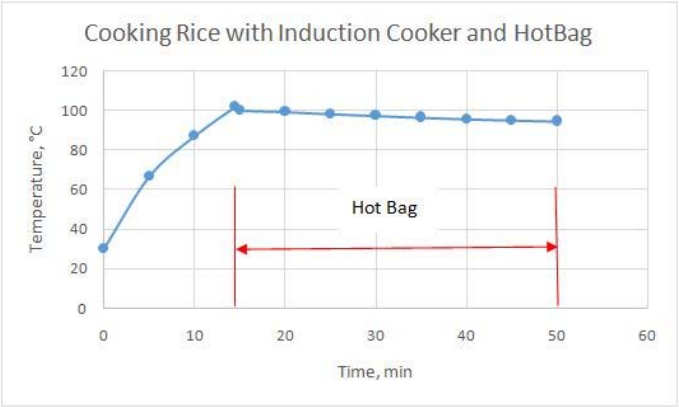

Fig. 14 Temperature profile for cooking rice with Induction cooker and Hot Bag

VII. Results and Discussions

The energy consumption has been calculated for cooking rice with and without the heat retention cooker. For Induction cooker, energy meter reading shows the energy in kWh which is then converted to kJ (1 kWh = 3600kJ). Plain rice has been cooked using Induction cooker both with Hot Bag and without Hot Bag and then the energy consumption has been compared.

For cooking rice with Induction cooker alone, 0.57 kWh, equivalent to 2052 kJ, has been consumed. The cumulative energy consumption profile can be seen in Fig.15.

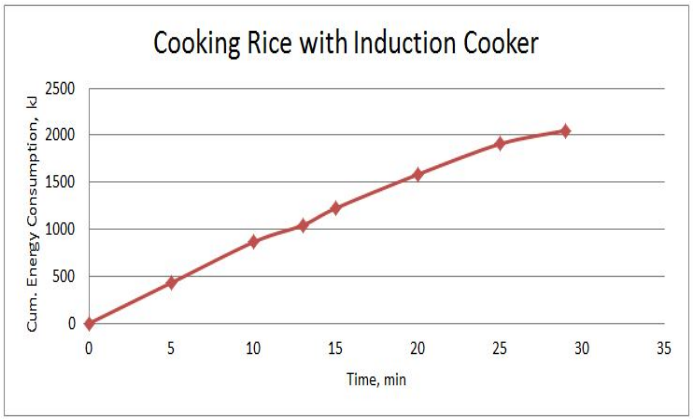

Fig. 15 Energy consumption profile for cooking rice with Induction Cooker

Same amount of rice was cooked with Induction cooker and Hot Bag. The pot was put instantly in the cooker after reaching the boiling temperature and kept there for 35 minutes. The total energy consumption was 1188 kJ yielding 42% energy savings. The cumulative energy consumption profile is shown in Fig.16 The savings of 864 kJ leads to 123 grams of CO_2 emission. The cooking with heat retention cooker required additional 20 minutes as compared to cooking Induction cooker alone.

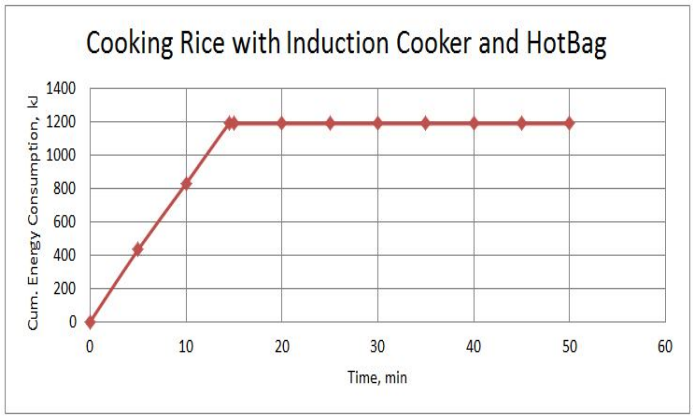

Fig. 16 Energy consumption profile for cooking rice with Induction Cooker and Hot Bag

Cooking rice with and without Hot Bag needs energy consumption of 2052 kJ and 1188 kJ of energy, respectively, thus saving 864 kJ of energy (42%) while using the Hot Bag. The CO2 emission reduction is 123 gm per kg of rice for using the heat retention cooker.

VIII. Conclusions

This paper analyzed the performance of the Hot Bag for energy savings and CO_2 savings. Induction cooker has been used for cooking rice and energy consumed was measured. The study reveals that the Hot Bag reduces a significant amount of energy consumption. The tests showed energy savings of 42% for cooking rice. The Hot Bag will also help reducing the impact on Carbon footprint. The CO_2 emission can be reduced 123 grams per kg of rice. The thermal analysis of the heat transfer from the Hot Bag have been analyzed. The food cooked during the tests have been tasted and it has been found that the texture of the food items cooked using Hot Bag was better.

Acknowledgment

The authors expresses its gratitude to Gesellschaft für Internationale Zusammenarbeit (GIZ) Bangladesh for funding the project and assistance throughout the project. The authors thanks the colleagues at the department of mechanical and chemical engineering for their kind cooperation, especially Mr. Abu Hossain and Mr. Mokhtar from MCE department and Mr. Baten Khan for assisting in the experiments.

References

[1] https://www.iea.org/publications/freepublications/publication/cooking.pdf.

[2] Ubwa, S. T., J. Abah, K. Asemave, and T. Shambe. "Studies on the Gelatinization Temperature of Some Cereal Starches." International Journal of Chemistry 4, no. 6 (2012): p22

[3] Morales-Sanchez, E., J. D. C. Figueroa, and M. Gaytan-Martínez. "Wet method for measuring starch gelatinization temperature using electrical conductivity." Journal of food science 74, no. 7 (2009): E382-E385.

[4] http://www.climateactionprogramme.org/climate-leader-interviews/sarah_collins_wonderbags_founder_explains_how_her_invention_is_changing_liv, accessed 20 September 2014

[5] Technical Report, Solar Bottle Light 'BotolBati': Energy Efficiency Improvement of Baonea-badh Slum, http://www.change.org.bd/Solar%20Bottle%20Light_CHANGE_GIZ.pdf, Accessed 27 July, 2014

[6] Food And Agriculture Organization Of The United Nations Website, http://faostat.fao.org/site/339/default.aspx., Accessed 13 June 2014

Design and implementation of a Micro Controller Based Portable Solar Charge Controller Tester

Mahmud Ibrahim[1], Shahriar Ahmed Chowdhury[2], M. Fayyaz Khan[3]

Centre for Energy Research, Department of EEE
United International University, Bangladesh
[1]mahmud.ibrahim021@gmail.com
[2]shahriar.ac@gmail.com
[3]fyk@eee.uiu.ac.bd

***Abstract*—** As a sustainable and alternative source of renewable energy, utilization of solar power has become immensely popular nowadays. In Bangladesh, there are more than 4 million SHSs which have been installed till January, 2015 [1]. Under this Solar Home System (SHS) program of IDCOL, there are a number of partner organizations (PO), providing their supports for establishing remote rural area electrification program under SHS. Solar charge controller plays crucial role and ensures reliability, better performance and durability of the installed systems. By complying with the standards of the solar charge controller (CC), one can make SHS program durable and feasible for rural electrification program. Therefore, Centre for Energy Research (CER) of United International University (UIU) designed a portable charge controller tester which can measure the parameters according to the set standards of the solar charge controller of IDCOL. By this solar charge controller tester (SCT), LVD, HVD, LVR, HVR, charging & discharging efficiencies can be measured with testing of reverse polarity protection, reverse current leakage protection etc. The main focus of this paper is to highlight the salient features of the designed solar charge controller tester. A number of charge controllers were tested with the implemented SCT and the test results found to be highly satisfactory and the accuracy of measurement was within one percent.

Keywords— SHS, solar charge controller, Solar Charge Controller Tester (SCT), IDCOL, DC- DC converter.

I. INTRODUCTION

An efficient and smart design of a solar charge controller ensures SHS as an economically feasible and technically sustainable system. The specifications of a solar charge controller are determined by the type of load and storage device used in the systems. In a developing country like Bangladesh, it is reported that the charge controller which are used in the field are not complying the standard of the IDCOL SHS program [2]. So, it is imperative to test the SHS equipment in the field. In this paper, the prime aim is to develop a microcontroller based portable SCT to test solar charge controllers which are already installed in the off grid areas. The development and detailed operation of the SCT has been explained in this paper.

According to IDCOL SHS program standards [3] for a solar charge controller, LVD stands for low voltage disconnect. Whenever the battery voltage drops below 11.6±0.1V, it is recommended that the solar charge controller must disconnect the load to prevent deep discharge and ensure depth of discharge (DOD) to maintain at 70% [3]. If the LVD of a charge controller is set below this level, then the battery will be affected by sulfation [4] which reduces the lifetime and the overall capacity of that battery. HVD represents the High voltage disconnect point. In charging mode, 14.3±0.2V is the optimum high voltage threshold for a lead acid battery. After this threshold voltage level, lead acid battery starts emitting hydrogen and oxygen gas by hydrolysis process which reduces the water level [5, 6]. LVR means the load reconnect voltage of a battery terminal once disconnected by a solar charge controller. It should be 12.6±0.2V as per IDCOL SHS program's standard of Bangladesh. However, in solar home system applications, protection of the solar charge controller is mandatory. Short circuit, Over-load, Reverse polarity and Reverse Current leakage protection are basic protection schemes of a solar charge controller which should be strictly maintained. If a solar charge controller doesn't have for example, a basic protection criteria like reverse current leakage protection, then at night, solar panel will behave like a load. A short circuit may cause serious dangers including explosions which may be a threat to the human lives. So, considering all of these facts, a portable SCT can be a good solution for measuring LVD, LVR, HVD, HVR, Reverse polarity protection, Reverse current leakage protection, charging and discharging efficiency of a solar charge controller at the site installation.

II. RESEARCH OBJECTIVE

The objective of the work is to develop a solar charge controller tester (SCT), which can measure the set points as well as check the basic protection components that have to be present according to IDCOL SHS standard.

III. METHODOLOGY

Solar charge controller tester (SCT) is basically a micro-controller based smart circuit or gadget with two DC-DC converters [7] for battery and panel voltage simulation used as a virtual hardware. After connecting to a target device, it will initially measure the terminal voltage of the target system's battery. After that, it will measure the self-current consumption of the charge controller. It takes power from the target SHS system's field battery on operational mode. Therefore no extra power supply is required. Two ammeters and two voltmeters are integrated in this gadget to measure the charging and discharging efficiency of the target solar charge controller. At the same time, the reverse polarity and reverse current leakage protection operation can be indicated through

LED. It has four built-in user input buttons to investigate the LVD, HVD. LVR, HVR and three extra input buttons for master reset option, efficiency measurement option and test data save option. The logical circuit diagram of this gadget has been shown in figure-1. It has a 20 character LCD display for value display and settings.

IV. Logical Block Diagram

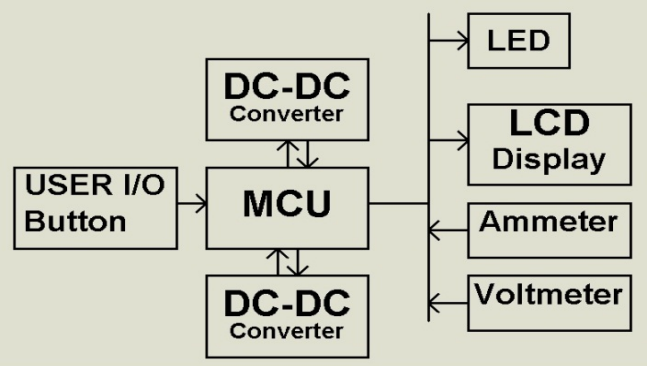

Fig 1.a) Overall logical block diagram of SCT

Figure1 (a) represents the over-all logical SCT block diagram. There are two DC-DC boost converters which act as two variable power supplies. One of these power supply acts as virtual battery and the other as a virtual panel. In this system, targetted solar home system battery will supply power to the SCT. The input voltage of the DC-DC boost converter is 9V. For this purpose, a voltage regulator has been used in between battery and converter (figure 1.b). So device will start raising voltage from a voltage level (9V; below LVD set value) of a target solar charge controller. The set value of LVD is 11.6V as per IDCOL TSC standard. Voltmeter and ammeter have also been implanted for voltage and current measurements simultaneously. A set of LED and LCD display are used for indication and data display purposes. There are some user input push buttons used for device settings, calibration, measurement and data storage. For example, if a user of SCT wants to calibrate it, the user button can be used to do that. If a user of SCT wants to measure set points of a target system and save the values; then he has to only press the save button of SCT device.

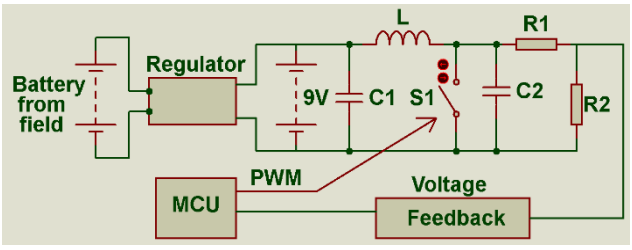

Fig 1. b) DC-DC boost converter circuit diagram.

In the figure 1.b) two batteries have been placed. One of them is a target system's battery and the other one is a virtual battery for boosting up the voltage level from 9V to 18V and acting as a virtual power supply according to the Pulse width modulated (PWM) signal from micro-controller. Each boost converter has two capacitor (C1 & C2), one inductor (L), one switch (S1) and two resistors for voltage feedback to the micro-controller (MCU). There are two boost converters in the SCT gadget, one for varying the battery voltage level and the other one is for solar panel voltage variation to act as a variable power supply. MCU will sense the output voltage of the boost converter and show it to the LCD display. If input button mentioned as "boost" is pressed, then the PWM signal will change its duty cycle from 0% to 50% maximum with a variation of 5% step size. Whenever, the duty cycle of the PWM signal is crossing more than 50%, then the MCU will automatically reset the duty cycle to 0%.

V. Test Procedure of a Target Charge Controller Using SCT Device

A. Initial Normal operation mode

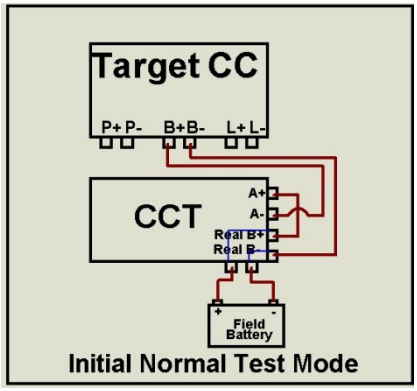

Fig 2: Normal Test mode: battery voltage and self-current consumption measurement.

In figure 2, the SCT device is connected to the target charge controller's battery terminal via an in-built ammeter on tester. In the initial test mode, a target charge controller's battery terminal is connected to the SCT device labeled as "CCT" in the diagram via a mili-ampere (mA) meter (A+ & A-). And the target system's lead acid battery (as field battery) is also connected with the CCT power terminal (Real B+ & Real B-). There is an in-built voltmeter in the CCT device (parallel with real B+ and real B- terminal), which will initially measure the terminal voltage of the connected target system's battery. The mili-ampere (mA) meter is used to measure the accurate self-current consumption of the target charge controller. After getting the voltage and current data, the tester will automatically show the result on the LCD display.

B. LVD Test Mode

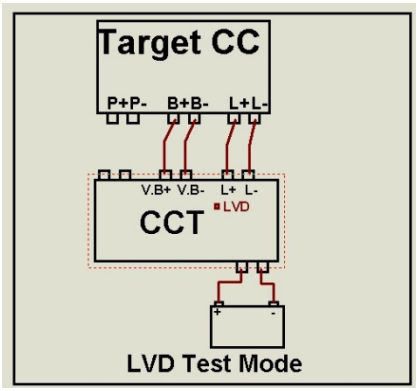

Fig 3: LVD test mode connection diagram.

In figure 3, the connection diagram between the target solar charge controller (target CC) and SCT has been represented as CCT. The battery terminal of the target CC is connected with the CCT virtual battery (V.B+ and V.B- terminal) and load terminal is also connected with the L+ and L- terminal of CCT. After pressing and holding the LVD button of the SCT device, then LVD operation will start progressing. In this operation mode, the in-built DC-DC boost converter start decreasing the virtual battery terminal voltage via decreasing PWM signal and micro-controller will wait till the target charge controller stops providing load support. Whenever the load becomes off, the micro-controller will get that voltage level of the virtual battery terminal and display as LVD = ”voltage” on LCD display.

C. LVR Test mode

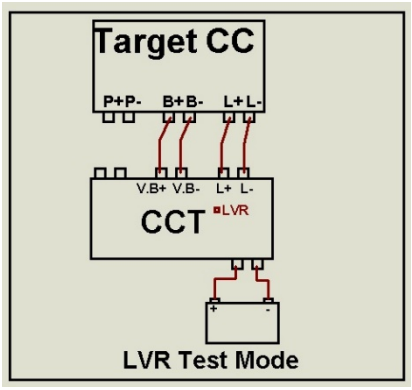

Fig 4: LVR test mode connection diagram.

As mentioned above, the connection diagram is exactly same as LVD test mode. But a button option is created to measure the LVR of the target solar charge controller. While this button is pressed and hold for few seconds, the internal DC-DC boost converter starts pumping the virtual battery terminal voltage until the target solar charge controller reconnects the load. Whenever the target charger controller connects the load again, then the micro-controller will get informed and get the virtual battery terminal voltage and display it on the LCD display such as LVR= ”voltage”.

D. HVD Test Mode

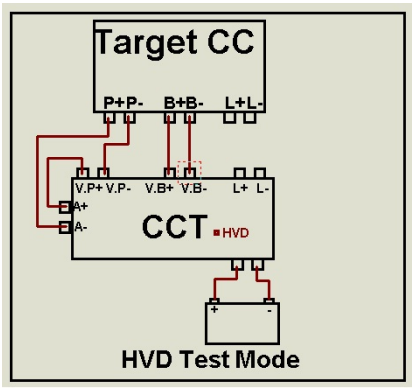

Fig 5: HVD test mode connection diagram.

Figure 5 shows the connection diagram that describes the High voltage Disconnect (HVD) testing procedure. In this case, SCT (CCT) in-built virtual panel voltage terminal (V.P+ & V.P-) is connected with target charge controller’s panel terminal (P+ & P-) via an ammeter. The virtual battery terminal (V.B+ & V.B-) of the tester is also connected to the target charge controller’s battery input terminal (B+ & B-). After pressing and holding the HVD button of the tester, the virtual battery voltage level starts boosting voltage level via DC-DC boost converter up to 18V. Whenever, the charging current become zero (as charging off) done by the target, then the tester will automatically display the HVD voltage for the target charge controller in the LCD display. In this whole testing process, the virtual panel voltage terminal should remain in maximum 18V voltage level which is ensured by voltage the feedback path of SCT device.

E. HVR Test Mode

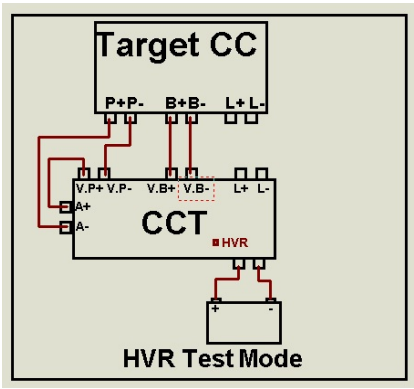

Fig 6: HVR test mode connection diagram.

High voltage battery charging reconnect mode testing procedure is shown in the figure 6. In this mode, the connection between target charge controller and SCT is same as HVD test mode. In this test mode, after pressing the button named “HVR” the virtual battery terminal of the CCT circuit starts decreasing the voltage level until the charging mode started and current start to flow by the target charge controller. While internal micro-controller ensures the charging current, it

will automatically display the HVR voltage set point of target charge controller in to the LCD display of SCT such as HVR=”voltage”.

F. Reverse polarity protection test Mode

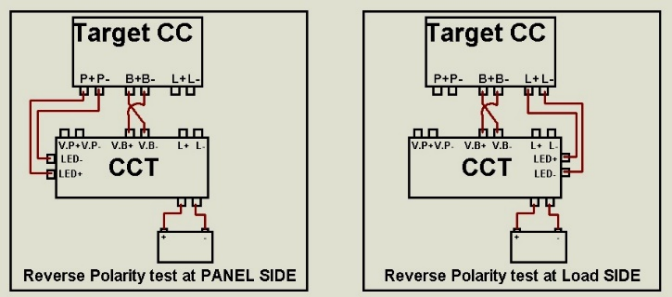

Figure 7: Reverse polarity protection test mode block diagram a) on panel side (left) and b) on load side (right).

Reverse polarity protection is the basic protection type of a solar charge controller. The existence of this protection scheme on the target charge controller should be done when the battery terminal is connected reversely to the battery input terminal of a charge controller. Figure 7.(a) represents the reverse polarity protection testing procedure from the panel side. Target CC battery terminal (B+& B-) reversely connected with the CCT device virtual battery terminal (V.B- & V.B+). Panel terminal (P+ & P-) of the target CC connected with the LED terminal (LED+ & LED-) of the CCT. If reverse current protection is provided in the target charge controller, then there will be no current flow and the LED light of tester will not glow, if no then the LED light will glow and ensure no reverse polarity protection is provided. On the other hand, in figure 7.(b) the connection diagram for testing the reverse polarity existence at the load side has been shown. Here LED terminal of the CCT is connected with the Load terminal (L+& L-) of the target CC. As mentioned above the tester LED light will not glow for protection existence, if not then it will glow.

G. Reverse current leakage protection Test Mode

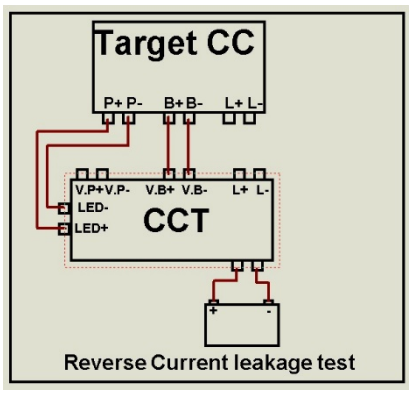

Fig 8: Reverse current leakage test mode connection diagram.

Reverse current leakage protection is the most important protection criteria for a solar charge controller. During night the panel voltage becomes negligible compared to the battery terminal voltage. This means a panel can be considered acting as a load if no reverse current flow protection provided inside the solar charge controller. A single diode can provide this protection. Figure 8, demonstrates the testing procedure for reverse current leakage protection situation. Battery terminal of the target CC (B+ & B-) is connected with virtual battery terminal of CCT (V.B+ & V.B-). Panel terminal of the target CC (P+ & P-) is connected with LED light terminal of the CCT (LED+ & LED-). If current flows on the reverse side from battery to panel, and then the LED light glows and confirms that no reverse current leakage protection has been provided in the target charge controller.

H. Charging and Discharging efficiency measurement Tests

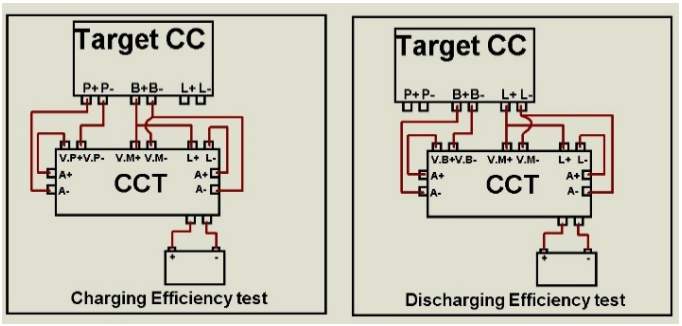

Fig 9: a) Charging efficiency and b) Discharging efficiency test mode connection diagram.

Figure 9.a shows the charging efficiency of the target charge controller. For this purpose, virtual panel voltage terminal (V.P+&V.P-) is connected to the target charge controller panel input terminal (P+& P-) via an ammeter (A+ &A-). Battery terminal of target CC (B+& B-) is connected to the in-built load simulator of the CCT via second ammeter of the CCT. Two in-built voltmeters are connected in parallel with virtual panel and virtual battery terminal for voltage measurement. After connecting this configuration, and pressing the eff button of the CCT, tester will calculate the input and output power and show them as a ratio called charging efficiency of the target charge controller.

The discharging efficiency of the target charge controller is also measured like above shown diagram figure 9.b). In the discharging mode, load terminal of the target CC (L+ & L-) is connected with the load simulator terminal (L+ & L-) of the CCT device via an ammeter. But this time the virtual battery voltage level terminal (V.B) is directly connected to the target charge controller battery input terminal (B+ & B-) as shown in figure 9.b. Same as above two voltmeters are also parallel with both battery and load terminal to measure voltage. After pressing the “eff” button of the CCT, it will calculate the

discharging efficiency. This efficiency will automatically be displayed through the LCD as discharge efficiency= "…%".

VI. DESIGN SPECIFICATION

In this proposed SCT, a 12-bit Analog to digital converter (ADC) with 1.25Msps has been used for more accurate result. An Atmel AVR micro-controller [8] has been used for faster data processing and calculation. The operating frequency of the micro-controller is 16 MHz. It has a manual option for choosing its power supply. Therefore, the same device can work as a portable device as well as can perform with target system's battery. The self-consumption of the whole device is around 25mA without LCD display and 55mA with one LCD display and one LED light. 50 target solar charge controller have been tested with this SCT to confirm its performance as well as accuracy of measurement.

VII. DISCUSSION AND CONCLUSION

In Bangladesh, SHS program of IDCOL has been a great success. Such success story is being obscured due to some partner organizations and local market business people who are producing solar charge controllers not conforming to the IDCOL technical specifications [2]. Also, in most of the cases, no required protections are embedded in the system affecting not only the performance of the system, but also endangering the people staying around the system during times of severe faults. Therefore, it is very important to strictly maintain the standards of the SHS systems. The difficult part of SCC is to test the device at site as in that case, two separate dc sources are required. In this paper, the proposed testing device can effectively and reliably be tested at site due to availability of an inbuilt power source. So SCC can be randomly selected at site and tests can be carried out quite comfortably without sending the SCC to the testing labs. This proposed solar charge controller tester (SCT) can help the testing of solar charge controller in the field.

REFERENCES

[1] http://idcol.org/home/solar.

[2] Journal on :Technical apprasial of solar home systems in Bangladesh: A field investigation, Shahriar Ahmed Chowdhury, Renewavle energy,vol. 36,issue 2, feb,2011. pp-77

[3] Technical specification of Solar Home System Program, TSC standards, IDCOL.(http://idcol.org/download/76fb8aca65b1ce10d291b5cb4c2f99fd.pdf)

[4] Battery university: sulfation of led acid battery & how to prevent it, Oct,2015 (http://batteryuniversity.com/learn/article/sulfation_and_how_to_prevent_it)

[5] Battery University: Charging lead acid battery and charging profile, Oct,2015 (http://batteryuniversity.com/learn/article/charging_the_lead_acid_battery)

[6] Gassing of lead acid battery, Lauderdale Alternator & Battery , Oct,2015 http://www.sonnenschein.org/Gassing.htm

[7] Application report by Texas Instrument on boost converter, Oct,2015 (www.ti.com/lit/an/slva372c/slva372c.pdf)

[8] Atmel AVR micro-controller technical specification and features. http://www.atmel.com/products/microcontrollers/avr/

Meshed PV Systems

Walter Commerell[#1], Rudy Müller[*2], V. Shanmuganandam[*3], Sattya Bhattacharjee[*4]

[#1]*Institute for Energy- and Drive Technology, University of Applied Sciences Ulm*
Prittwitzstrasse 10, 89075 Ulm, Germany
[1]commerell@hs-ulm.de

[*2]*Phocos AG*
Magirus-Deutz-Strasse, 12, 89077 Ulm, Germany
[2]rudy.mueller@phocos.com

[*3]*Phocos Ltd. India*
270A/270B Burma Colony, Chennai-600096, Tamil Nadu, India
[3]shanmugam@phocos.com

[*4]*Rentec Solar Ltd., Bangladesh,*
6/11Humayun Road, Mohammadpur, Dhaka 1207, Bangladesh
[4]rentecsolarltd@gmail.com

Abstract

Manufacturers involved in development and production of control electronics for renewable off-grid energy systems generally offer various types and charge controllers, in the range comprising 2 A to 300A with a system voltage of 12/24/32/36/48VDC (Phocos) and also other products like off-grid inverters, solar refrigerator/freezer, Solar TV, micro turbine, etc. All these products are used in off grid system. For off grid inverter requires a charge controller that controls the charging of the batteries and an inverter that converts the DC power from the solar panels and the batteries into AC power. These systems normally provide a small amount of power due to the cost of larger systems. Plans are to introduce solar micro-inverter which converts direct current generated by single module to renewable power. The output from several micro-inverters is combined and fed to electrical grid. The main advantage of micro-inverters is small amounts of shading, debris or snow lines on solar module do not disproportionately reduce the output of the entire array. Each micro inverter of harvests optimum power by performing MPPT system for its connected module. The design of the system is simple, safe and simplified management.
Key Words: Phocos, charge controller, inverter, micro-inverter, adaptive control.

I. Introduction

Meshed networks means a topology with nodes connected to each other who form a network. Each node relays data and /or energy to the network.

II. Situation of Grids Worldwide

The currently not accessible market of energy is huge, the possibility to further develop that exists but there is limited capacity of developing that unless new forms of renewable energy sources are integrated into that.

Considering the worldwide use of energy, 30% of the population make use of a grid that is becoming older; 40% have an unreliable grid and another 30% of the population have no access to energy.

New forms of energy sources have to supplement, to be integrated into these power systems if that is to be further expanded, to be made more reliable. Wind, solar, small hydro, still do not contribute with more than 2 percent into that.

Localized/distributed energy generation is becoming more feasible, more reliable, long lasting and used as well as due to its inherent flexibility (size, flexible placement, ease of installation and developing of advanced electronics) that allows that extra amount of power to be conveniently integrated into existing networks.

Installing an integrating these small, customized power generation plants (e.g. wind, PV-solar) in the point of consumption also saves costs that normally would be associated to the infrastructure and power lines of a regular power distribution network.

Integrating more “distributed power generation plants” will also inherently make the whole power network/system become far more reliable.

III. State of the Art and Future Development

Mini and Micro Grids work well as long as those are kept integrated.

Very required is a flexible adaptive method that can also keep the grid stability also when the systems become islanded from a larger “power distribution ring” for example, maintaining stable voltage and frequency/phase parameters.

Current solution is made possible by means of larger and stable energy sources (like hydro and nuclear power plants).

Power quality must also be handled by the smaller power contribution sources (distributed generators).

Reactive power, harmonic power/currents must be equated/solved by smaller contributors; currently that is being realized by sharing these needs/duties among the larger power contributors.

Finding ways to have smaller power contributors to also deal larger amounts of power becomes a requirement; that must also become possible under "weak" grid conditions.

Any transient phenomena must also be dealt with in a distributed way, locally; Transients happen and occur far too fast to be corrected by "usual network control systems"; The handling of this phenomena must be equated locally.

Use of payment forms and formulas for the distributed energy generation, contributed in this way must be handled through a customer friendly and accepted payment policy.

Long analysis and simulation of systems parameters and algorithms have to be prepared and optimized in order to respond to people's expectations; Adaptive control must be extensively implemented.

IV. Problem Solution: A General View

Self-forming grid (SFG) concept, basic requirements:

1. An adaptive, expandable self-forming AC grid;
2. Capable of using various renewable energy sources;
3. Must be prepared to do effective load-sharing, deal with energy storage, load-scheduling also shedding;
4. Capable to operate full distributed adaptive generation, do power factor correction, harmonic compensation;
5. To operate both, under grid-tied and islanded conditions;
6. To be capable of further organic development from a small AC island up to a "large" grid-tied mesh;
7. Modularly expandable to fulfil individual requirements;
8. To be fault proven and continue to be operational even under partial fallout.
9. Adaptive to user/demand requirements;
10. System must be capable of operating stable under very demanding conditions and providing prioritizing vital systems and loads;

Figure 1 shows a possible starting point with two-isolated PV off grid systems.

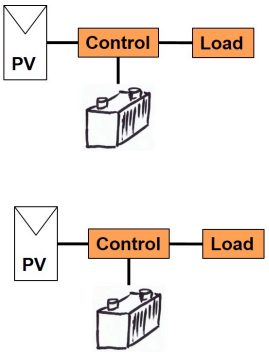

Fig. 1 Starting point PV off grid systems

Sometimes you find PV mini grid systems as shown in figure 2.

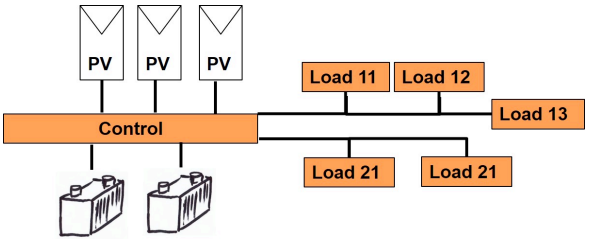

Fig. 2 PV mini grid system

If the system is growing it can form a first mesh shown in figure 2

V. PV Systems Topologies

In meshed networks nodes are connected to other nodes for exchange of information and energy. These offers the possibility to generate self-healing networks where a problem in the net is identified and the net reacts in a way the information of energy uses another way to the demand. These kind of nets are very reliable.

A. Fully connected network

In a fully connected network each node is connected to each other node. This offers the maximum flexibility in energy flow.

B. Partly connected network

In a partly connected network not every node is connected to others. The system can lose contact to other parts of the system and is not fully capable of self-healing.

VI. Preferred Solutions

To present a modular "plug and play", self-forming, self-adjusting grid, using standard AC wiring techniques, with incorporated DC/AC storage;

The fully adaptive mesh with total automatic / adaptive control

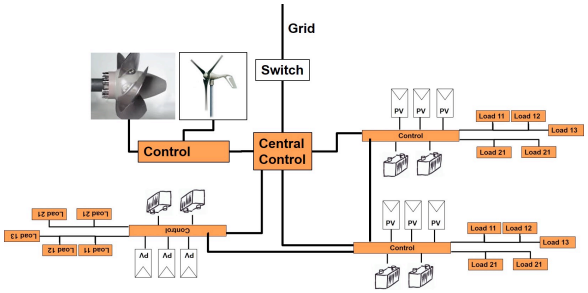

Fig. 3 Meshed off grid system with possible grid connection

Figure 3 show the growing meshed net with several decentralized power and load system with integrated different energy sources as wind, hydro, and PV.

PV panels with integrated MPPT controllers / optimizers;
Immediate conversion from sunlight in to AC power;
Full support to AC power quality; to supply reactive power also at night hours;
Adaptive and automated operation:

1. Start the grid any time, join the grid if already up;
2. To monitor the power sources maximum power point, and capable of continuous constant power delivery to stabilize the grid;
3. Support grid voltage regulation: to stabilize grid at under and overvoltage conditions;
4. To safely run the grid; to actively monitor grid real operating conditions at
5. Over/under voltage, current limiting, fault ride-through, soft-start, surges, harmonics
6. Capable of distributed, adaptive and, proportional load-sharing

VII. CONCLUSIONS

It becomes apparent that through the use of advanced electronic systems, selecting convenient and adequate, high speed switching control electronics, that more efficient and even more distributed power networks can be realized offering a high flexibility in the integration of various power systems, of all sizes, even very small ones. Developing dedicated electronics with a high degree of adaptability (adaptive control) is key for the success of Meshed power systems, especially when PV of all sorts and capacities, also other types of energy sources are considered.

REFERENCES

[1] Amirnaser Yazdani; Rajat Majumder; Balarko Chaudhuri; Nilanjan Chaudhuri, “Multi-terminal Direct-Current Grids: Modeling, Analysis, and Control”, Wiley-IEEE Press; September, 2014.

[2] Mark Hankins; Stand-Alone Solar Electric Systems, Earthscan Expert Series, 2010.

Modeling of Graphene/SiO_2/Si(n) Based Metal-Insulator-Semiconductor Solar Cells

[1]Muhammad Johirul Islam, [2]Md. Mahmudul Hasan, [3]Rifat Sami and [4]Md.Iqbal Bahar chowdhury
United International University, Dhaka, Bangladesh.
Email: [1]johir021@yahoo.com, [2]m_hasan9071@yahoo.com, [3]samirifat@yahoo.com, [4]ibchy@eee.uiu.ac.bd

***Abstract*—In this work a graphene based MIS structure for solar energy conversion has been modeled and analyzed. The MIS structure is formed by inserting an oxide layer in the conventional graphene/n-Si Schottky structure to obtain improved performance. Simulation of the model for this MIS structure shows this performance improvement. Using the simulation results this work also analyzes the effects of semiconductor layer width and semiconductor doping level on the current-voltage characteristics.**

***Index Terms*—Graphene, MIS solar cell, Schottky junction solar cell, Interface states, Tunneling current.**

I. Introduction

Graphene is a monolayer of carbon atoms packed into a two-dimensional (2D) honeycomb lattice shows excellent thermal conductivity, high mobility and high carrier velocity, possesses optimum electrostatic scaling owing to its monolayer thin body [1]. Therefore, graphene attracts huge interest in various electronic and optoelectronic applications, which include its use as a transistor, as a photodetector and as a saturable absorber of light. In silicon photovoltaics this interesting material can be exploited and as antireflection coating [2] and as a semitransparent electrode. As an antireflection coating material, a single-layer graphene shows high transparency with 97.7% transmittance [3]. As an electrode, graphene-based anodes are widely-reported [4], [5], whereas, stable graphene-based cathodes with low work function and excellent conductivity are generally more difficult to achieve, as n-type graphene devices have very limited thermal and chemical stabilities and are usually sensitive to the influence of the ambient environment [6]. Recently, significant progress has been made in p-graphene/n-Si Schottky junction solar cells. Graphene on silicon solar cell in [7] shows an efficiency of ∼1.0-1.7 %, open circuit voltage of ∼0.42-0.48 V, short circuit current density of $\sim 4-6.5\ mAcm^{-2}$ and fill factor of ∼45-56% measured on air mass 1.5 global illumination condition. Kuang *et al.* reported [8] a graphene/GaAs Schottky junction based solar cell with an efficiency of ∼2.218%, open circuit voltage of ∼0.389 V and short circuit current density of ∼8.191 mA and fill factor of 0.548 under AM1.5 illumination. However, till to date, few works related to MIS solar cells are reported in the literature [9]–[13], but none of these works explores the use of graphene.

in this work a model is presented for a graphene-SiO_2-Si(N) based MIS solar cell. Using this model the superiority of this MIS solar cell over Schottky junction solar cell has been investigated. The effects of semiconductor doping level and the width of the semiconductor region have also been analyzed in this work.

II. Theory

The graphene-SiO_2-Si(N) based metal-insulator-semiconductor (MIS) solar cell analyzed in this work is shown in Fig. (1). In this structure, the monolayer graphene replaces the metal electrode, the SiO_2 layer is very thin (typically $< 10\ nm$) to increase the efficiency of Schottky junction and n-type doped silicon acts as the absorber layer.

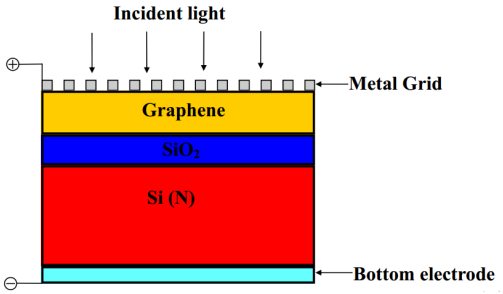

Fig. 1. Schematic diagram of graphene-SiO_2-Si(N) based MIS solar cell.

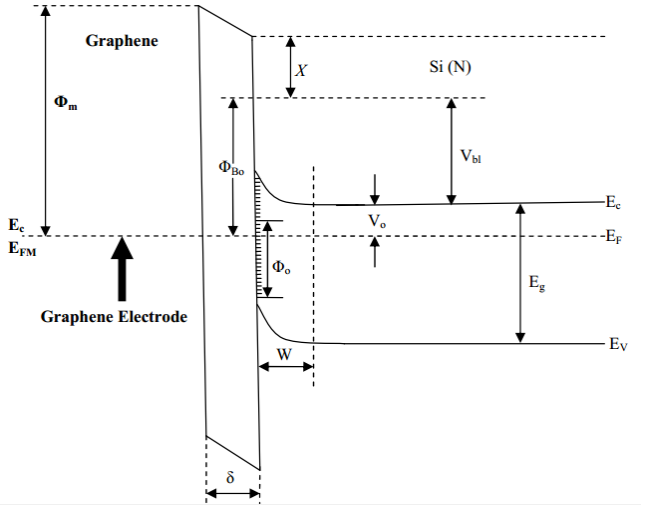

Fig. 2. Energy Band Diagram for graphene-SiO_2-Si(N) based MIs solar cell under equilibrium condition.

The energy band diagram under equilibrium condition for the MIS structure of Fig. (1) is shown in Fig. (2). In this

figure, φ_m is the graphene work function, χ and E_g are the electron affinity and the band gap of silicon respectively, δ is the interfacial oxide layer thickness, w is the depletion layer width in the semiconductor, φ_0 is the energy level above the valance band to which surface states are filled in an isolated semiconductor, V_{bi} is the built-in voltage and φ_{bo} is the Schottky barrier height without considering interface states. However, in the MIS type solar cells the interfacial oxide layer thickness (δ) and the density of the interface states (D_{ss}) can strongly affect the magnitude of barrier height [11]. Incorporating these effects, the modified Schottky barrier height, φ_{bn} for n-type silicon type can be expressed as [11]

$$\begin{aligned} \varphi_{bn} &= \gamma\varphi_{bo} + (1-\gamma)(E_g - \varphi_0) \\ \varphi_{bo} &= \varphi_m - \chi, \quad \gamma = \frac{1}{1+\alpha}, \quad \alpha = \frac{qD_{ss}\delta}{\xi_i} \end{aligned} \tag{1}$$

where, ξ_i is the permittivity of the interfacial oxide layer. The electric field developed across the depletion region due to the difference in the work functions between graphene and semiconductor separates the photo-generated electron-hole pairs. The photo-generated current under illumination condition results a voltage V across the MIS cell, which partly appears across the oxide layer as V_i and the rest V_s appears across the semiconductor depletion region such that $V = V_i + V_s$. The voltage V_i causes the Schottky barrier height to increase, resulting an effective barrier height φ^*_{bn} as

$$\varphi^*_{bn} = \varphi_{bn} + qV_i \tag{2}$$

The effective Schottky barrier height φ^*_{bn} controls the tunneling current and hence, affects the current-voltage characteristics of MIS solar cells. Under illuminated condition, the energy band diagram for the MIS structure is shown in Fig. (3).

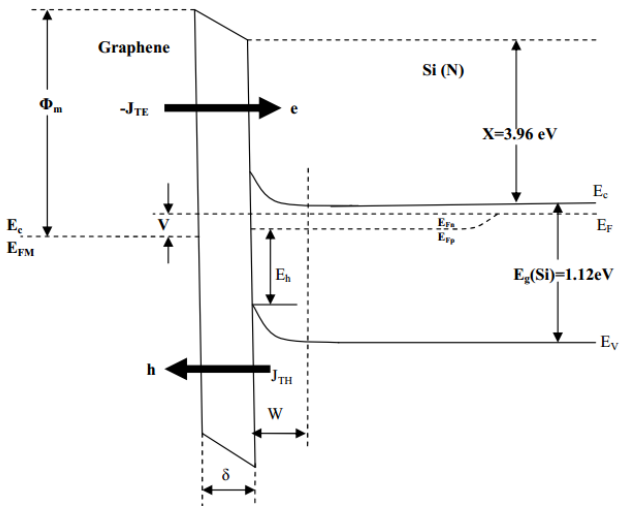

Fig. 3. Energy Band Diagram for graphene-SiO_2-Si(N) based MIS solar cell under illumination condition.

The total current under under illumination condition for a solar cell is [13].

$$J_{total} = J_{Light} - J_{Dark} \tag{3}$$

For MIS solar cell, J_{Light} is the photocurrent generated in the bulk and in the transition region and can be given by:

$$J_{Light} = \int_{\lambda_{min}}^{\lambda_g} \left[J_{dl}(\lambda) + J_{pw}(\lambda)\right] d\lambda \tag{4}$$

where $J_{dl}(\lambda)$ is the contribution of carriers generated in the depletion layer and $J_{pw}(\lambda)$ is the contribution of the diffusion of holes at the depletion layer boundary and λ_{min}, λ_g are the minimum wavelength of the solar spectrum and the wavelength corresponding to the silicon energy gap respectively. For monochromatic illumination J_{dl} can be written as:

$$J_{dl}(\lambda) = \int_0^w G(x,\lambda)dx \tag{5}$$

where, $G(x,\lambda)$ is the optical electron-hole pair generation rate and can be expressed as [13]:

$$G(x,\lambda) = \left[\frac{\alpha(\lambda)N(\lambda)}{1 - r_f r_b e^{-2\alpha d}}\right]\left(e^{-\alpha x} + r_b e^{-\alpha(2d-x)}\right) \tag{6}$$

where $\alpha(\lambda)$ is the absorption coefficient of silicon, $N(\lambda)$ is the photon flux density of the solar spectrum, r_f and r_b are the reflection coefficient at the front and back surfaces respectively. Therefore, the expression for J_{dl} can be deduced as

$$J_{dl}(\lambda) = \left[\frac{\alpha(\lambda)N(\lambda)}{1 - r_f r_b e^{(-2\alpha d)}}\right]\left\{1 - e^{(-\alpha w)} + r_b e^{(-\alpha(2d-w))} - r_b e^{(-2\alpha d)}\right\} \tag{7}$$

The expression of $J_{pw}(\lambda)$ can be obtained by solving the hole continuity equation as

$$J_{pw}(\lambda) = \frac{qL_p}{\alpha^2 {L_p}^2 - 1}\left\{ - L_p G'(w,\lambda) + \left[\frac{S_P{}' G(d,\lambda) + L_p G'(d,\lambda)}{S_p{}' \sinh(v_p) + \cosh(v_p)}\right] - \left[\frac{G(w,\lambda)(S_p{}' \cosh(v_p) + \sinh(v_p))}{S_p{}' \sinh(v_p) + \cosh(v_p)}\right]\right\} \tag{8}$$

where

$$G'(x,\lambda) = \frac{\partial G(\chi,\lambda)}{\partial \chi}, S_p{}' = \frac{S_p L_p}{D_p}, v_p = \frac{d-w}{L_p}$$

J_{Dark} in Eqn. (3) is called dark current and in a MIS solar cell is due to field emission (tunneling), minority carrier diffusion and carrier recombination. In [11], [12] these currents are expressed as

$$J_{Dark} = J_{eto}\left[e^{\frac{qv_s}{nkT}} - 1\right] + J_{do}\left[e^{\frac{qv_s + \Delta}{kT}} - 1\right] + J_{ro}\left[e^{\frac{E_{Fn} - E_{Fp}}{2kT}} - 1\right] \tag{9}$$

where I_{eto}, I_{do} and I_{ro} are the reverse saturation currents associated with electron tunneling, hole diffusion and recombination mechanisms respectively, E_{Fn} and E_{Fp} are the electron and quasi-Fermi levels, k is the Boltzmann constant and T is the temperature,

$$\Delta = E_g - \varphi^*_{bn} - E_h \tag{10}$$

where E_g is the band gap of Si, E_h is the minorrity carrier quasi-Fermi level, n is the ideality factor and is related with

the oxide thickness and interface state density as given by Card *et al.* [12]

$$n = 1 + \left[\frac{\xi_s}{w} + qD_{ss}\right]\frac{\delta}{\xi_i} \tag{11}$$

where ξ is the permittivity of Silicon. The reverse saturation currents are given by [11], [12] as

$$J_{eto} = A * T^2 e^{-\sqrt{\chi}\delta} e^{\left(\frac{-q\varphi^*_{bn}}{kT}\right)} \tag{12}$$

$$J_{do} = \frac{qn_i^2}{N_d}\left\{\frac{\left[S_p coth(\frac{d-w}{Lp} + \frac{D_p}{L_p})\right]}{\left[\frac{d-w}{Lp} + \frac{S_p L_p}{D_p}\right]}\right\} \tag{13}$$

$$J_{ro} = \frac{qn_i w}{2\tau_p} \tag{14}$$

where A* is the effective Richardson's constant, ni is the intrinsic carrier concentration, N_d is the doping concentration, S_p is the surface recombination velocity of holes at the back surface, D_p, L_p and τ_p are the minority carrier diffusion constant, diffusion length and life time respectively and d is the cell thickness. The depletion layer width (w) is given as [14]

$$\mathrm{w} = \left[\frac{2\xi_s}{qN_d}\left(v_{bi} - v_s - \frac{kT}{q}\right)\right]^{\frac{1}{2}} \tag{15}$$

where v_{bi} is the built in voltage. Finally, the performance parameters of a MIS solar cell which include the open circuit voltage, V_{oc} [12], the fill factor, FF and the conversion efficiency, η can be defined as

$$V_{oc} = n\left[\varphi_{Bn} + \frac{kT}{q}\sqrt{\chi}\delta + \frac{kT}{q} log\left(\frac{J_{sc}}{A * T^2}\right)\right] \tag{16}$$

$$FF = \frac{V_m I_m}{V_{oc} J_{sc}} \tag{17}$$

$$\eta = \frac{V_m I_m}{P_{inc}} \tag{18}$$

where, J_{sc} is the short circuit current density, P_{inc} is the incident optical power and V_m , I_m correspond the cell voltage and current respectively under maximum cell power condition.

III. Result and Discussion

This section presents and analyzes the simulation results based on the model deduced in this work. The device width, the oxide layer thickness and the Si-doping level are chosen as 0.5 μm, 1 nm and 3×10^{18} cm^{-3} respectively. For a given $\varphi_0 = 0.3$ eV the interface state density is assumed as 5×10^{12} cm^{-2}. The incident photon flux is the air mass (AM) 1.5 global spectrum, which is obtained from the ASTM G-173-03 standard [15]. The absorption coefficients for silicon are obtained from [16]. $E_h \geq 0.085$ V [10] for N_d of 3×10^{18} cm^{-3} and oxide thickness is 1 nm.

Fig. (4) compares the current-voltage characteristics (J_L vs. V_L) curves for a graphene/n-Si based Schottky junction solar cell and graphene-SiO_2-n-Si based MIS solar cell. From this figure, it is evident that the open circuit voltage significantly increases in the MIS solar cell with only a 1 nm thick oxide layer compared to Schottky junction solar cell. This is expected since the insertion of a thin oxide layer increases the barrier height and results in an increase in the open circuit voltage [Eqn. (16)]. The fact of the increase in open circuit voltage due to insertion of a thin oxide layer in the Schottky junction solar cell is also consistent with the results found in the literature [17], [18]. The Fig. (4) also provides a comparative picture of graphene based MIS solar cell with three other MIS solar cells which uses three different commonly used transparent conducting oxides (TCO) such as Indium Tin Oxide (ITO), Zinc Oxide (ZnO) and Tin Oxide (SnO_2) as metal electrode. Owing to the higher transmittance (which results in higher J_{SC}) and higher electron affinity (which causes higher V_{OC} except ITO), graphene shows the better J-V characteristics than others. The performance improvement of graphene MIS solar cell over all the four solar cells mentioned in Fig. (4) is also reflected in the performance parameters listed in Table 1. This table shows that graphene MIS solar cells have the highest value in all performance parameters (except the V_{OC} and the FF for ITO).

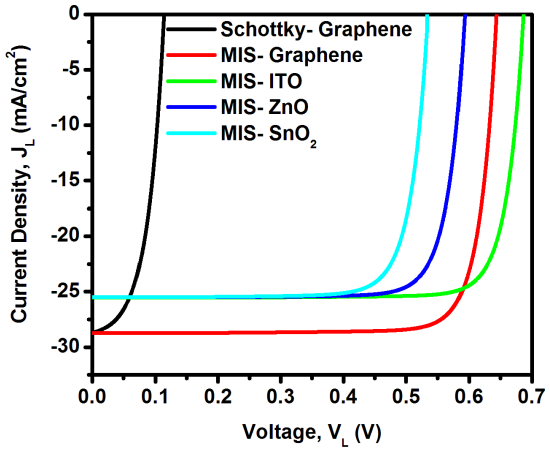

Fig. 4. Current-Voltage characteristics curves graphene/n-Si based Schottky junction solar cell and graphene/ITO/ZnO/SnO_2-SiO_2-n-Si based MIS solar cells.

Cell Type	J_{SC} (mA/cm^2)	V_{oc} (V)	FF (%)	η (%)
Graphene-Schottky	28.37	0.114	51.90	1.697
Graphene-MIS	28.37	0.705	82.78	15.297
ITO-MIS	25.24	0.771	83.59	14.658
ZnO-MIS	25.21	0.624	70.59	12.358
SnO_2-MIS	25.18	0.533	62.32	10.899

TABLE I
Performance comparison of graphene/n-Si based Schottky junction solar cell and graphene/ITO/ZnO/SnO_2-SiO_2-n-Si based MIS solar cells.

Fig. (5) shows that increase in the device width increases both the short circuit current density (J_{sc}) and the open circuit voltage (V_{oc}) with a greater increase for the short circuit current density. Increase in the device width causes increased photon absorption resulting in an increased photo-generated current. Since open circuit voltage increases logarithmically with the short circuit current [Eqn. (16)] the increase in V_{oc} with the increase in the device width is lower than that in J_{sc}.

Fig. (6) shows that the increase in the doping level in the

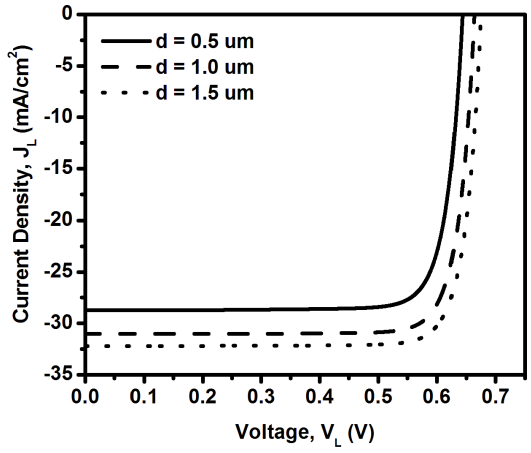

Fig. 5. Current-Voltage characteristics curves of graphene-SiO_2-n-Si based MIS solar cell for different device width.

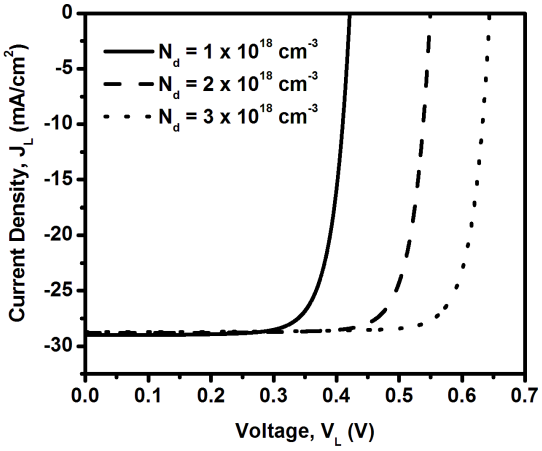

Fig. 6. Current-Voltage characteristics curves of graphene-SiO_2-n-Si based MIS solar cell for different semiconductor doping level.

semiconductor increases the open circuit voltage significantly with a small decrease change in the short circuit density. This can be explained as follows. When doping level is low, the depletion region is wide Eqn. (15)], which is effective to drift the photo-generated carrier to the terminals; as doping level increases, the depletion region shrinks causing the the collection rate of the photo-generated carriers to reduce i.e. causing the short-circuit density to reduce. However, increase in the doping level increases the band shift against the Fermi levels as explained in [19] for which open circuit voltage increases.

IV. Conclusion

This work presents a simple analytical model for a graphene/SiO_2/n-Si based MIS solar cell. Simulation of the model results show that the MIS structure has higher open circuit voltage, fill factor and conversion efficiency than the graphene/n-Si based Schottky junction solar cell. Moreover, comparison with three commonly used transparent conducting oxides as metal electrode shows the superior performance parameters of graphene-electrode based MIS solar cells. Model results also show that increasing the Si layer width has greater impact on the short circuit density than the open circuit voltage. From the model it is also evident that increased Si-doping level increases the open circuit voltage while decreases the short circuit. All these results are expected and also, consistent with the results obtained in the literature.

References

[1] K. Mohanram and X. Yang, "Graphene Transistors and circuits," *Nanoelectronic Circuit Design*, Edited by N. K. Jha and D. Chen, pp. 349-376, Springer Science & Business Media, 2010.

[2] R. Won, "Photovoltaics: Graphene-silicon solar cells", *Nature Photonics*, vol. 4, no. 7, pp. 411–411, July 2010.

[3] F. Bonaccorso, Z. Sun, T. Hassan and A. C. Ferrari, "Graphene photonics and optoelectronics", *Nature Photonics*, vol. 4, no. 9, pp. 611–622, Aug. 2010.

[4] H. Park, S. Chang, M. Smith, S. Gradečak, J. Kong, "Interface engineering of graphene for universal applications as both anode and cathode in organic photovoltaics", *Scientific reports*, vol. 3, April 2013.

[5] D. Zhang, F. Xie, P. Lin and W. C. H. Choy, "Al-TiO2 composite-modified single-layer graphene as an efficient transparent cathode for organic solar cells", *ACS nano*, vol. 7, no. 2, pp. 1740-1747, Jan. 2013.

[6] F. Schedin, A. K. Geim, S. V. Morozov, E. W. Hill, P. Blake, M. I. Katsnelson, K. S. Novoselov, "Detection of individual gas molecules adsorbed on graphene", *Nature materials*, vol. 6, no. 9, pp. 652-655, July 2007.

[7] L. Xinming, H. Zhu, K. Wang, A. Cao, J. Wei, C. Li, Y. Jia, J. Li, X. Li and D. Wu, "Graphene-on-silicon Schottky junction solar cells", *Advanced Materials*, vol. 22, no. 25, pp. 2743-2748, April 2010.

[8] Y. Kuang, Y. Liu, Y. Ma, J. Xu, X. Yang, X. Hong and J. Feng, "Modeling and Design of Graphene GaAs Junction Solar Cell", *Advances in Condensed Matter Physics.*, 2015.

[9] F. Bouzid, S. B. Machich, "The effect of solar spectral irradiance and temperature on the electrical characteristics of a ZnO-Sio2-Si (N) photovoltaic structure", *Revue des énergies Renouvelables.*, vol. 13, no. 2, pp. 283-294, 2010.

[10] D. Hocine, M. S. Belkaïd and K. Lagha, "Influence of interfacial oxide layer thickness on conversion efficiency of SnO2/SiO2/Si (N) Solar Cells", *Revue des Energies Renouvelables.*, vol. 11, no. 3, pp. 379-384, 2008.

[11] J. P. Singh and R. S. Srivastava, "Efficiency of SnO2/Si solar cells", *Indian Journal of Pure and Applied Physics.*, vol. 20, pp. 104-110, February 1982.

[12] H. C. Card and E. S. Yang, "MIS Schottky Theory under Conditions of Optical Carrier Generation in Solar Cells", *Applied Physics Letters.*, vol. 29, no. 1, pp. 51-53, 1976.

[13] A. H. M. Shousha, "Performance characteristics of thin film MIS solar cells", *Solar & wind technology.*, vol. 6, no. 6, pp. 705-712, 1989.

[14] S. M. Sze and K. K. Ng, "Physics of semiconductor Devices", *John Wiley, Interscience.*, pp. 832, 2006.

[15] NREL,http://rredc.nrel.gov/solarspectra/am1.5/ASTMG173/ASTMG173.html.

[16] M. A. Green and M. J. Keevers, "Optical properties of intrinsic silicon at 300 K," *P*rog. Photovoltaics Res. Appl., vol. 3, pp. 189-192, 1995.

[17] J. P. Ponpon and P. Siffert, "Open-circuit of MIS silicon solar cells," *J.* of Appl. Phys., vol. 47, no.7, pp 3248-3251, July 1976.

[18] G. P. Srivastava and P. K. Bhabtnagar, "Theory of Metal-Oxide-Semiconductor Solar Cells," *S*olid-State Electronics, vol. 22, pp. 581-587,1979.

[19] L. Zhu, G. Shao and J. K. Luo, "Numerical Study of Metal Oxide Heterojunction Solar Cells," *S*emicond. Sci. Technol., vol. 26, pp. 085026, 2011.

A Wave-to-Wire Model of Ocean Wave Energy Conversion System Using MATLAB/Simulink Platform

Jakir Hossain
BS in EEE
Khulna University of Engineering and Technology,
Khulna-9203, Bangladesh
jakirhossain471@gmail.com

Sarder Shazali Sikander
MS in EE
National Université of Science and Technologie Islamabad,
Pakistan
shazali.ali67@gmail.com

Eklas Hossain
PhD Candidate
Center for Sustainable Electrical Energy Systems,
University of Wisconsin Milwaukee,USA
shossain@uwm.edu

***Abstract* -- Renewable energy sources, unlike the conventional combustible fuels, are naturally distributed and extensively available in a boundless manner all over the world in different forms. Here, in this paper, authors elucidate the scopes and opportunities of the ocean wave to develop a low-cost, environmental friendly, and sustainable electrical power generation system. At the present time most technological modernizations aimed at exploiting such resources are at early stage of development, with only a handful of devices close to be at the commercial demonstration stage. None of them, though, operates converting the wave energy contents at its very origin: the orbital motion of water particles right below the ocean surface. The Sea spoon device catches the kinetic energy of ocean waves with favorable conversion proficiency, according to specific "wave-motion climate". In this letter, authors illustrate a possible methodology of converting this naturally exorbitant energy with efficient conversion methodology and simulating the conversion environment with MATLAB/Simulink platform.**

Index Terms – Converter, Inverter, Microgrid, OWSC, PMSG, Renewable Energy, Simulink-Model, Wave-Energy, Wave-to-Wire model.

NOMENCLATURE

PMSG – Permanent Magnet Synchronous Generator
OWSC – Oscillating Wave Surge Converter
WEC – Wave Energy Converter

I. INTRODUCTION

Energy provision is the biggest issue to face for the world's economy at any latitude. Nowadays the energy demand of developing Countries as well as that one of developed economies is huge and increasing at an unbearable pace. Considering the limited stocks of such an energy source, and the drawbacks related to the emissions associated to its utilization, the problem to find alternative energy sources and suitable conversion technologies must be solved in order to guarantee the growth and preserve the planet environment. Considering the present scarcity of electrical power generation in all over the world, it is an urgent requirement to find new sources of energy for electricity generation. Besides to reduce the carbon emission and minimize the global warming effects modern energy technologies are moving on to the renewable energy sources. Considering the availability, cost, location and reliability, there is a huge possibility of utilizing the ocean wave power. Among renewable energies sources, ocean wave's power, around the coasts worldwide, has been estimated to be in the order of 1TW (1 TW/h 1012W) [1].

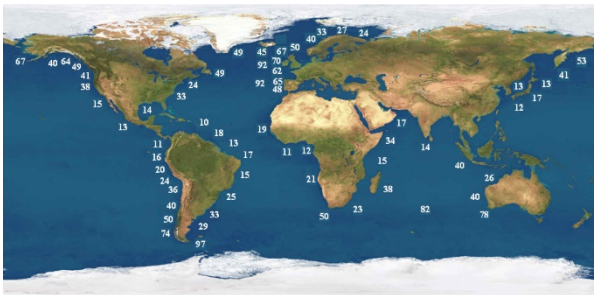

Fig. 1. Global distribution of approximate yearly average wave power in kW/m crest length.

The availability harness able ocean wave power per meter crest length of the world wide cost lines have been represented in fig. 1. From the figure it can be seen that sea waves offers the uppermost energy density among renewable sources. Waves are created by winds, which in turn are generated by solar energy. Solar energy intensity of typically 0.1-0.3 kW/m2 of horizontal surface is converted to an average power flow intensity of 2-3 kW/m2 of a vertical plane perpendicular to the direction of wave propagation just below the water surface. A comparison of Wave Energy among the other popular

available renewable energy sources have been represented in table 1.

In this paper section I discussed the necessity of wave energy and the future possibility of harness able energy. Section II describes the overall floor plan of the Wave-to-Wire model. Section III discuss about the simulation platform and possible methodology to harness wave power and finally section IV deals with the simulation outcome. Section V conclude the overall output of this work.

TABLE 1
COMPARISONS OF WAVE ENERGY WITH OTHER RENEWABLE ENERGIES [2]

	Photovoltaic	Wind	Wave
Status	Early commercial	Commercial	Pre-commercial
Energy Source	Sun	Sun	Sun-Wind
Power Density	1 kW/m2 at peak solar insolation	1 kW/m2 at 12 m/s [General Electric (GE) 1.5 MW machine]	25 kW/m at Sun Francisco, average annual power flux
Variability	Daily cycles-clouds	When it blows	24×7 and highly variable
Predictability	Poor	Hours	Daily
Availability	20-30%	30-40%	80-90%
Potential Sites	Limited	Limited	Extensive but limited
Average Power Output per Plant	Scalable to 5 MW	Scalable to 30 MW	Scalable to 100+ MW [Provides Highest energy density]
Environmental issues	Visual Pollution	Noise and Visual Pollution	None [Virtually no environmental impacts]

II. SYSTEM DESCRIPTION

The wave to wire model of a WECs device have been presented in this paper in complete methodology. The system under simulation consist of a series of oscillating paddle like body which are emerged in the nearshore location. Those oscillating bodies moves back and forth with the oscillation of the sea wave. This back and forth motion is converted into the mechanical rotation using gear mechanisms and further converted into the oscillating electrical energy. The output from the PMSG is highly oscillating.

To remove the unnecessary oscillation from output power an AC to DC converter block is integrated with the system and further this DC output is converted to the suitable frequency using an inverter block to the microgrid system. Fig. 2. Representing the overall block diagram of the system under consideration.

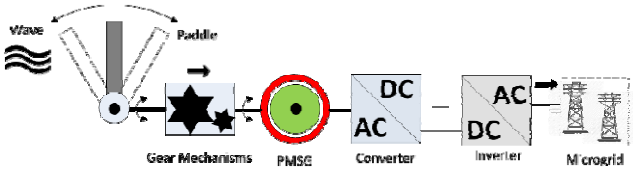

Fig. 2. Block diagram of a Wave-to-Wire model of Wave Energy Conversion System [4]

III. MODELING THE RESOURCES

The wave field in water of depth **h** may be characterized by an amplitude **a**, a wave number k (λ= 2π/k) and the radian frequency **ω**. These are related by a radiation function G(a, k, ω) = 0. For the incident wave the surface elevation is

$$\eta(x, y, t) = a\cos(kx\cos\beta + ky\sin\beta - \omega t) \quad (1)$$

The capture width is the device ability to capture the power

$$\delta(\omega, \beta) = 2P/\rho g a^2 C_g \quad (2)$$

Where P stands for the mean power absorbed by the device and c_g is the wave group velocity. For a single thight-moored semi-submerged axisymmetric device following equation holds

$$m_m\ddot{X} = F_f(t) + F_{ext}(X, \dot{X}, t) \quad (3)$$

$$F_f(t) = F_s(t) + F_r(t) + F_h(t) \quad (4)$$

Where F_f (t) are the wave induced forces and $F_{ext}(X,\dot{X},t)$ are the external forces. The velocity of the motion of the device $p=m_b\dot{\eta}$ can be expressed as

$$\dot{p}(t) = \dot{-}A(\infty)\ddot{\eta}(t) - \int_0^\infty k(\tau)\eta(t-\tau)d\tau - C\eta(t) + F_m(t) + F_e(t) \quad (5)$$

Where the convolution term represents the radiated wave force, in case of time domain model the convolution is approximated by a state space model.

IV. SIMULATION OF A WAVE-TO-WIRE MODEL

To harness the wave power we need proper and economically efficient wave energy converters (WECs). There are various wave energy converter concepts available, despite this large variation in conversion

terminologies oscillating wave surge converters (OWSCs) like aquamarine power Oyster are promising technology. In our simulation we have used OWSC type converter technology in which a hinged deflector is positioned perpendicular to the wave direction (a terminator), that moves back and forth exploiting the horizontal particle velocity of the wave. A prototype graphical representation of OWSC device have been represented in fig. 3. The wave energy conversion technology available all over the world is summarized in fig. 4.

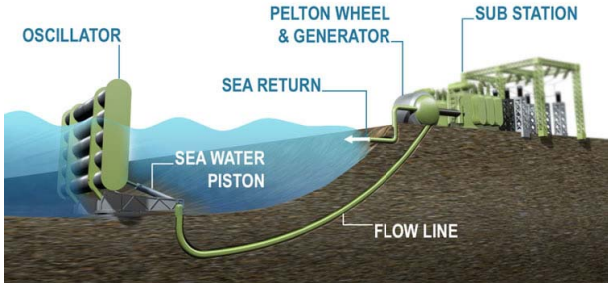

Fig. 3. Oscillating wave surge converter (OWSC)

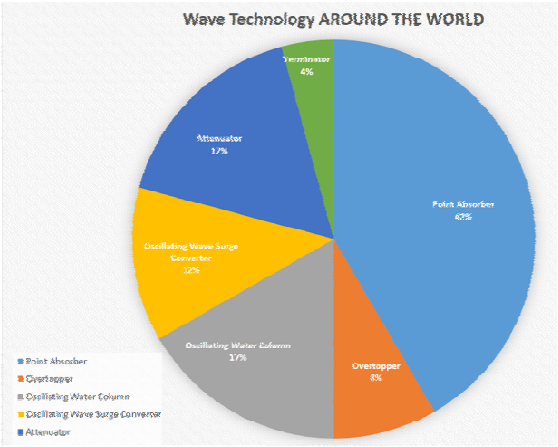

Fig. 4. Global percentage of Wave Energy Conversion technology available globally

A. *Location of Devices and Power Availability*

The power density of the wave is dependent on the water depth and the sea bed slope. Power density of the ocean wave is decreases with the decrease of the water depth the highest energy density is available at 100 to 90 meter water depth is about 41 kW/m crest length. The variation in wave power density and distribution accordance with bed slope and water depth have been represented in fig. 5.

Based on the power available and water depth, WECs can be classified into three basic categories such as Onshore, Nearshore and Offshore WECs. The availability of gross wave power and exploitable wave power is represented in fig. 6.

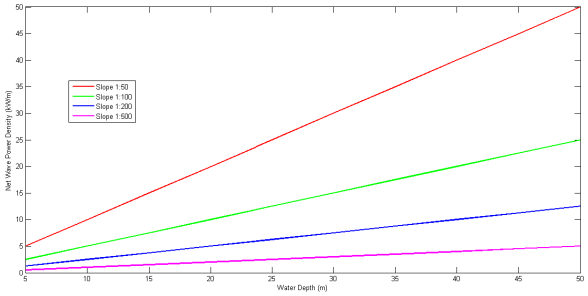

Fig. 5. Decrease in total wave power with water depth over various bed slopes

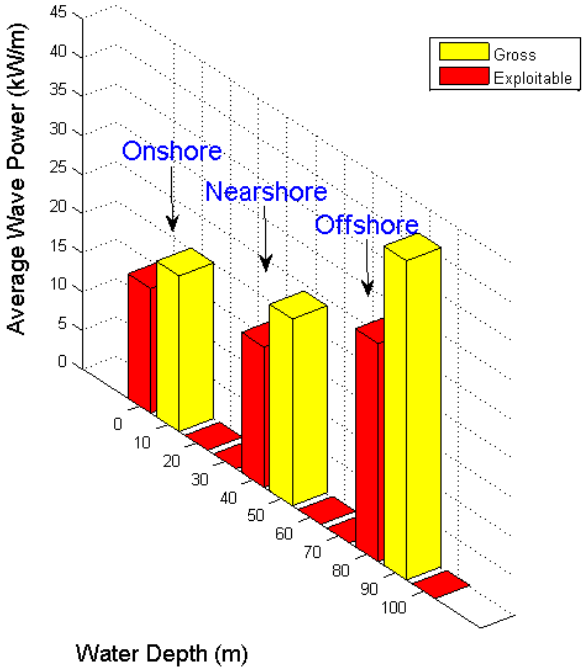

Fig. 6. Average gross wave power and exploitable wave power at the three different location of WECs

B. *Incident Wave Profile*

The simulation time of the Simulink model can be adjusted manually. For having more realistic results a proper wave profile is necessary, which is considered representative of a sea state. For simulating the Wave Energy Conversion system an incident wave profile with suitable wave height and frequency from the statistical data of sea state analysis of Bangladeshi coastal areas have been considered. The incident wave height is chosen as 0 to 5 meter and wave period is 8 second.

The mechanical power stored in the sea wave can be expressed by the equation

$$P = \frac{\rho g^2}{64\pi} H_{m0}^2 T_e \approx \left(\frac{kw}{m^3 S}\right) H_{m0}^2 T_e \qquad (6)$$

From equation (6) it is clear that the Incident mechanical power of the sea wave is the function of wave height and wave period. From equation (6) the corresponding mechanical power of the incident wave profile can be calculated which is shown in fig. 7. From which the input average mechanical average power is found to be 20 kW/m crest length.

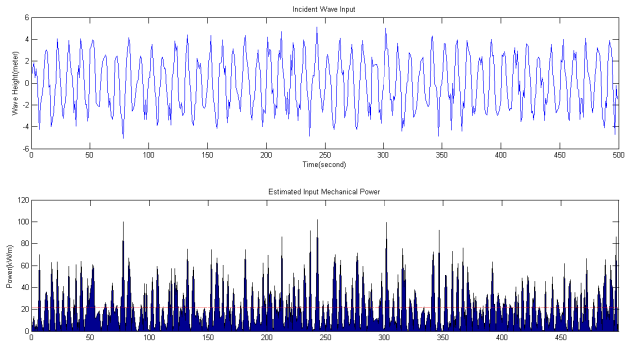

Fig. 7. Incident Wave Profile and Input Mechanical Power in kW/m crest length

C. *Hydrodynamic Model in MATLAB/ Simulink*

A program in Matlab is written and a Simulink model is implemented which is composed by a hydrodynamic model, a block for the passive loading control and the bidirectional/unidirectional case and visualization part with a lot of scope blocks. The most important components of this model are the PTO block for the WEC (control) and the block of the State-Space Radiation Force. With an appropriate setting of the switches the different cases can be implemented: this model is very flexible and the mechanic power is calculated as product of PTO force and velocity of the buoy. Fig. 8. shows the Hydrodynamic Model of the proposed system, which will convert input oscillating mechanical energy to rotary motion of flywheel.

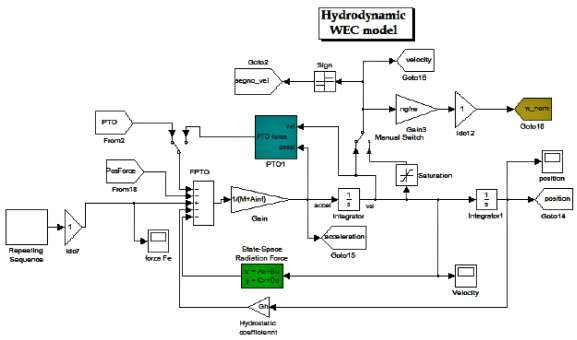

Fig. 8. Hydrodynamic Model of Dynamic WEC

D. *DC to AC Inverter Simulink Model*

To reduce the oscillating and multiple frequency harmonics effect from PMSG output parameters. First PMSG output voltage is converted into 300 V DC using and rectifier circuit and then this 300V DC output voltage is converted into 480 V (RMS) AC at 60 Hz frequency using a six pulse inverter block as shown in fig. 9. to integrate with the national grid.

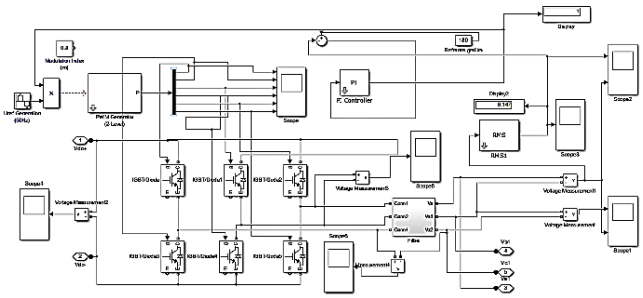

Fig. 9. 300 V DC to 480 V AC inverter model using Simulink

This 480 V AC 60 Hz system is than connected with a grid. To simulate the national grid environment various resistive load and RLC load have been integrated with the system which will creates the practical environment of a functional grid connection. Integrated load model using Simulink is represented in fig. 10.

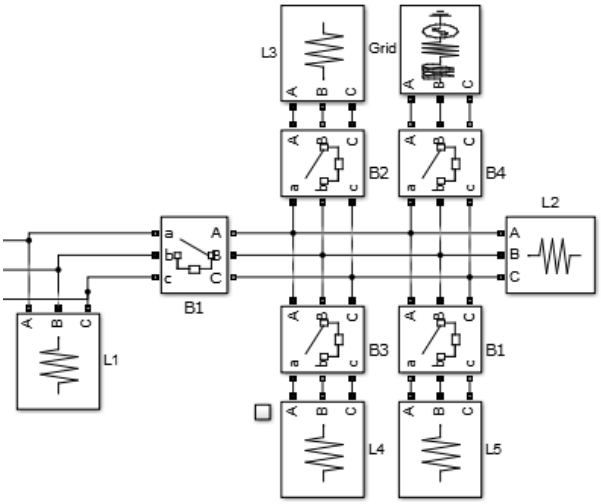

Fig. 10. Integrated 3 phase loads and Switch-gears

E. *Simulink model of Entire "Wave to Wire Model"*

The entire Simulink model of Wave Energy Converter to the grid connection named “Wave to Wire Model”[6,7] which includes Mechanical wave energy conversion from harnessing wave power to electrical power generation, power smoothing and harmonics reduction and grid integration have been represented in fig. 11.

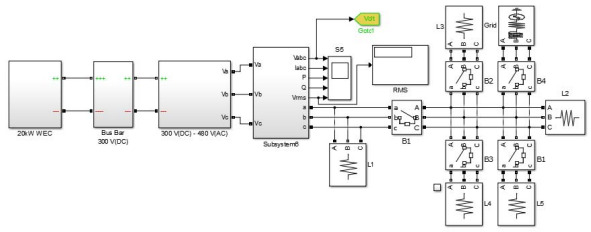

Fig. 11. Wave to Wire model of Wave Energy Conversion System

V. SIMULATION RESULTS

Electrical output from the PMSG of a single unit WEC after rectification and before integrated to bus bar is represented in fig.12. Where the average output voltage is around 300 V DC with a very high level of harmonics present

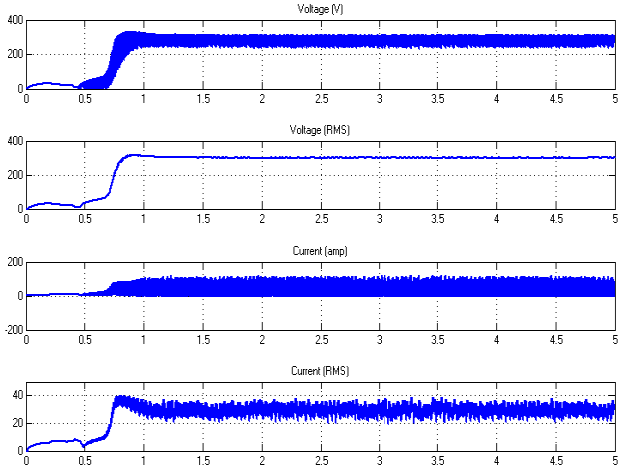

Fig. 12. DC Voltage (1) and RMS Voltage (2), Rectified Current (3), RMS Current (4) in Amp from the PMSG

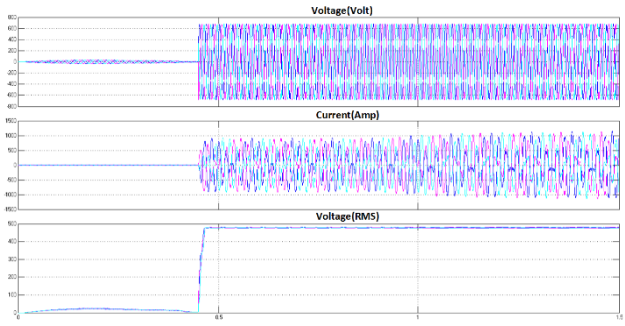

Fig. 13. Output Voltage (1) in Volt, Current (2) in Ampere and RMS Output Voltage (3) in Volt from the Simulation

Using a 300 V DC to 480 V AC inverter and after elimination of harmonics from the output, The electrical parameters have been represented in fig. 13. from the figure the output voltage is found to be 678.925 V (Peak) at 60 Hz and the RMS output voltage is exactly 480 V (RMS) as specified in inverter unit. From the initial condition the system will become fully functional and stable within first 0.5 second (due to the high inertia of WEC devices and mechanical friction of other rotational components) and ran smoothly for the rest of the time.

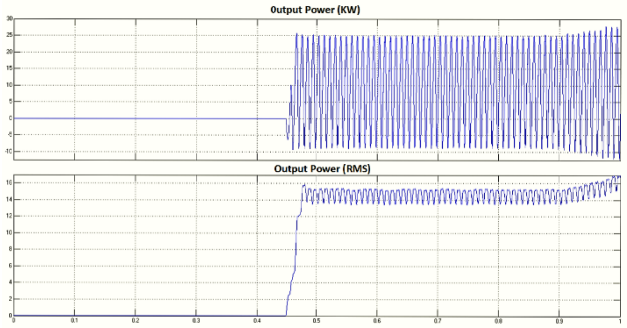

Fig. 14. Output Electrical Power (1) and RMS Power Output (2) in kW from the simulation

Fig. 14. Shows the actual output power and the RMS output electrical power of the system and it is found to be around 14 kW with a very small amount of oscillation that determines the overall system efficiency to 70%, as the input equivalent mechanical power is 20 kW and the output electrical power is 14 kW. The small amount of oscillation can be reduced using super capacitor of storage unit with the system.

VI. CONCLUSION

In this letter, a comprehensive mathematical wave-to-wire model [5] of the wave energy hyperbaric converter has been demonstrated. The basic subsystems of the converter have been neatly explained, and the dynamic models have been integrated to evaluate the energy conversion system. In this arrangement, when the generator is connected to the grid, the initial conditions are chosen such that the generated voltage has the same magnitude, phase angle, and frequency of the grid, to provide synchronism between the generator and the grid. In a real situation, a synchronism relay should be adopted to have the desired consistency. The average value of the generated power is about 14 kW, and the electric power oscillations are close to 7.1428%. Here, the terminal voltage is 480 V. In future, the grid integration of renewable energy sources

will be focused with advanced methodology to stable distributed generation based power system, where ocean wave energy will contribute an important role in case of islanded microgrid system [9-17]

APPENDIX

PMSG DESIGN

The dynamic model of the surface-mounted permanent magnet generator in the magnet flux reference system is [3]

$$u_{sd} = -R_s i_{sd} - L_s \frac{di_{sd}}{dt} + L_s \omega i_{sq}$$

$$u_{sq} = -R_s i_{sq} - L_s \frac{di_{sq}}{dt} - L_s \omega i_{sd} + \omega \psi$$

and the electromagnetic torque is represented by

$$T_e = \frac{3}{2} p \psi i_{sq}$$

TABLE II
PMSG DESIGN PARAMETERS [3]

Nominal power	P = 20 kW
Number of pole	p = 2
Nominal frequency	f = 60 Hz
Nominal voltage	V = 300 V
Power factor	Cos θ = 0.95
Nominal speed	$\omega = \frac{2\pi f}{p} = 188.4\ rad/s$ $n = \frac{60\omega}{2\pi} = 1500\ rpm$
Nominal torque	$T = \frac{P}{\omega} = 106.15711\ Nm$
Nominal Magnetic flux	$\varphi = \frac{V}{2\pi f} = 0.8$
Permanent magnet flux	$\varphi_{pm} = 0.9 * \varphi = 0.72$
Nominal efficiency	$\eta = 0.95$
Stator resistance	$R_s = 2.030625 \times 10^{-4} \Omega$
Stator inductance	$L_s = 0.003441\ H$

TABLE III
TABLE OF PARAMETERS [3]

η	Surface elevation
K	Wave number
C_g	Wave group velocity
P	Mean power absorbed
F_f	Wave induced force
F_{ext}	External forces
F_S	Exciting force
F_r	Radiation force
F_h	Hydrostatic buoyancy force
δ	Capture width
a	Wave amplitude
ρ	Water density

REFERENCES

1. Falnes, J.."A review of wave-energy extraction", Marine Structures, 200710.
2. Czech, B.; Bauer, P., "Wave Energy Converter Concepts: Design Challenges and Classification," in Industrial Electronics Magazine, IEEE , vol.6, no.2, pp.4-16, June 2012 doi: 10.1109/MIE.2012.2193290.
3. R. Monajemy e R. K. Fellow, «Control and Dynamics of Constant-Power-Loss-Based Operation of Permanent-Magnet Synchronous Motor Drive System,» IEEE TRANSACTIONS ON INDUSTRIAL ELECTRONICS, vol. 48, n. 4, pp. 839-843, AUGUST 2001.
4. Hazra, S.; Bhattacharya, S.; Uppalapati, K.K.; Bird, J., "Ocean energy power take-off using oscillating paddle," in Energy Conversion Congress and Exposition (ECCE), 2012 IEEE , vol., no., pp.407-413, 15-20 Sept. 2012 doi: 10.1109/ECCE.2012.6342793.
5. Garcia-Rosa, P.B.; Vilela Soares Cunha, J.P.; Lizarralde, F.; Estefen, S.F.; Machado, I.R.; Watanabe, E.H., "Wave-to-Wire Model and Energy Storage Analysis of an Ocean Wave Energy Hyperbaric Converter," in Oceanic Engineering, IEEE Journal of , vol.39, no.2, pp.386-397, April 2014 doi: 10.1109/JOE.2013.2260916.
6. Forehand, D.I.M.; Kiprakis, A.E.; Nambiar, A.J.; Wallace, A.R., "A Fully Coupled Wave-to-Wire Model of an Array of Wave Energy Converters," in Sustainable Energy, IEEE Transactions on , vol.PP, no.99, pp.1-11 doi: 10.1109/TSTE.2015.2476960
7. Jasinski, M., "Vector Control of AC/DC/AC Converter - Generator Subset in Wave-to-Wire Power Train for Wave Dragon MW," in EUROCON, 2007. The International Conference on "Computer as a Tool" , vol., no., pp.1324-1327, 9-12 Sept. 2007 doi: 10.1109/EURCON.2007.4400613
8. Amon, E.A.; Brekken, T.K.A.; Schacher, A.A., "Maximum Power Point Tracking for Ocean Wave Energy Conversion," in Industry Applications, IEEE Transactions on , vol.48, no.3, pp.1079-1086, May-June 2012 doi: 10.1109/TIA.2012.2190255
9. Eklas Hossain, Ersan Kabalci, Ramazan Bayindir and Ronald Perez "Microgrid testbeds around the world: State of art", Energy Conversion and Management 86 (2014) 132–153.
10. Eklas Hossain, Ersan Kabalci, Ramazan Bayindir and Ronald Perez "A Comprehensive Study on Microgrid Technology", International Journal of Renewable Energy Research, Vol.4, No.4, 2014 1094–1107.
11. Eklas Hossain, Sheroz Khan and Ahad Ali "Low voltage power line characterization as a data transfer method in public electricity distribution networks and indoor distribution networks", Electric Power Conference in Canada, 2008. (EPEC) 2008, Pg. No. 1-7.
12. Eklas Hossain, Sheroz Khan and Ahad Ali "Modeling Low Voltage Power Line as a Data Communication Channel", World Academy of Science, Engineering and Technology) 2008, Vol. 45, Pg. No. 148-152.
13. Eklas Hossain, Riza Muhida, Ahmad Faris Dzulkipli and Khairul Azizi Abdul Rahman "Solar cell efficiency improvement using compound parabolic concentrator and an implementation of sun tracking system", International Conference on Computer and Information Technology (ICCIT) 2008, Pg. No. 723-728.
14. Eklas Hossain, Riza Muhida, and Ahad Ali "Efficiency improvement of solar cell using compound parabolic concentrator and sun tracking system", Electric Power Conference in Canada, 2008. (EPEC) 2008, Pg. No. 1-8.
15. Ersan Kabalci, Ramazan Bayindir and Eklas Hossain "Hybrid microgrid testbed involving wind/solar/fuel cell plants: A desing and analysis testbed", International Conference on Energy Research and Application (ICRERA), 2014, Pg. No. 880-885.
16. Ersan Kabalci, Eklas Hossain and Ramazan Bayindir "Microgrid test-bed design with renewable energy sources", International Conference on Power Electronics and Motion Control Conference and Exposition (PEMC), 2014, Pg. No. 907-911.
17. Eklas Hossain, Ramazan Bayindir, Ersan Kabalci and Erdal Bekiroglu "Microgrid facility at European union", International Conference on Energy Research and Application (ICRERA), 2014, Pg. No. 873-879.

Dye-Sensitized Solar Cells: Sensitized with Triple Dyes in Ultraviolet to Near Infrared

Ashraful Islam[1], Liyuan Han[2]
Photovoltaic Materials Unit
National Institute for Materials Science
1-2-1 Sengen, Tsukuba, Ibaraki 305-0047, Japan
[1]ISLAM.Ashraful@nims.go.jp

Idriss M. Bedja[5]
CRC, Optometry Department, CAMS
King Saud University
Riyadh 11433, Saudi Arabia

Md. Akhtaruzzaman[3] Towhid H. Chowdhury[4]
Solar Energy Research Institute (SERI)
Universiti Kebangsaan Malaysia (UKM)
Bangi 43600; Selangor Darul Ehsan, Malaysia

Antoine Mirloup[6], and Raymond Ziessel[7]
ICPEES-LCOSA, UMR 7515 CNRS
Université de Strasbourg, ECPM
25 rue Becquerel , 67087, Strasbourg Cedex 02, France

Co-sensitization of triple dyes for panchromatic absorption is rare in literature, here we present a dye sensitized solar cell co-sensitized with molecular engineered organic butyloxyl chain induced Y1 dye, bodipy dye TP2A, and squaraine based dye SQ1. The co-sensitized TP2A+SQ1 showed efficiency of 5.60%. The co-sensitized triple dies employed in a dye sensitized solar cell shows a wide coverage in the visible spectrum of 300nm-800nm region. By controlling the volumetric ratio a high photocurrent density (JSC) of 14.59 mAcm^{-2} and 0.703 fill factor were achieved. This yielded to an impressive efficiency of 6.21% for Y1+TP2A+SQ1 co-sensitized dyes, which is higher than that of each individual dyes. It was also observed that the efficiency of co-sensitized triple dyes is higher than co-sensitized of TP2A+SQ1 in solar cells.

Keywords— dye sensitized solar cell, co-sensitization, bodipy dye, squaraine dye.

I. INTRODUCTION

Dye sensitized solar cells (DSSCs) has been considered as a frontier in third generation solar cells. It has successfully attracted the attention of materials scientists due to their extraordinary potential of light weight, easy material synthesis process, flexible physical structure and independent vacuum condition processing. DSSCs are comprised with an electrode, dye sensitizer, electrolytes, counter electrode and a transparent conducting substrate. Generally in DSSCs, the dye dictates the performance [1-3]. The main function of an efficient dye is to capture the maximum incident light over the visible spectrum and inject the photo-generated electron into the semiconductor oxide with matched energy level. Ruthenium based dyes N719 dye has shown impressive absorption in the visible spectra but it lacks of absorption in the infrared (IR) region [4]. Besides, Ruthenium based dyes are quite unattractive in large scale production due to their complex synthesis method, purifications techniques and limited availability. Thus metal free organic dyes have attracted interest in pursuit to design efficient DSSCs [5-7]. To achieve panchromatic absorption by a single organic dye is difficult, as there have been only a few dyes showing this rare potential [8-13]. But co-sensitization of multiple organic dyes which contain maximum absorption in sensitive smaller parts of the visible region of 300-800 nm is possible. Co-sensitization of multiple organic dyes in different wavelengths has been adopted by numerous scientists due to its potential ease of synthesis process [14-19]. Nonetheless, careful molecular engineering is necessary to obtain such organic dyes of different wavelengths and tailor them together to obtain panchromatic absorption. Recently, the co-sensitization of three dyes was reported by Chen et.al. where they comprised of merocyanine dye, hemicyanine dye and squarylium cyanine dye in a solar cells system to enhance a panchromatic absorption between 400-700 nm [20]. Cheng et al. also reported similar triple dyes co-sensitized DSSCs and achieved panchromatic absorption in 400-700 nm regions [21]. To our knowledge, these are the only instances of panchromatic absorption by triple dyes. On our pursuit to achieve panchromatic absorption, we have successfully demonstrated with multi-dyes system from ultraviolet to near infrared regions. For this attempt we selected our three dyes of Y1, TP2A and SQ1 (Fig. 1) in different absorption region. Our previously reported dye Y1 has shown with intense absorption maxima between 350-400nm [22]. The butyloxyl-substitued phenyl as an electron donating unit, thiophene as a π-spacer and a cyanoacetic acid group as an acceptor and anchor resulted in Y1 molecule. Y1 shows a strong absorption around 400 nm and successfully overcame the short wavelength dip in the incident photon to conversion efficiency (IPCE) spectrum. Boron dipyrromethene (Bodipy) dye TP2A was successfully investigated and the peak absorption maxima of 581nm was reported [23]. Upon deposition on a transparent TiO_2 electrode, TP2A dye showed broadened adsorption spectra in 500-650 nm region. We have also designed and verified near infrared (NIR) absorbing squaraine dye SQ1 which has broad absorption spectra in 600-700 nm region [24]. From our observation it is evident that, if co-sensitized together these dyes must achieve panchromatic absorption from 350-800 nm region. Here in this report we adopted the co-sensitization of these three different ranges of light absorbing dyes

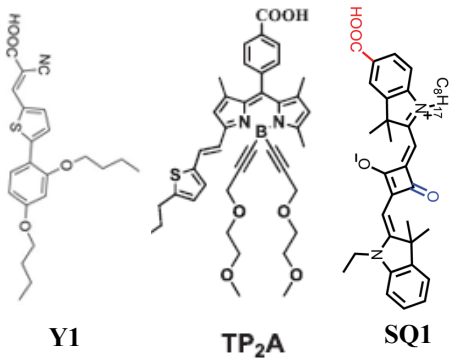

Fig. 1. Chemical structures of Y1, TP_2A and SQ1

(Y1+TP2A+SQ1) for the first time and by controlling the volumetric ratio achieved an overall efficiency (η) of 6.21%. The large panchromatic absorption occupancy from UV to NIR region yields with photocurrent density (J_{SC}) of 14.59 $mAcm^{-2}$ and fill factor (FF) of 0.703.

II. EXPERIMENTAL SECTION

The synthesis and characterization of Y1, TP2A and SQ1 has been reported previously [22-24]. UV-Vis and fluorescence spectra were recorded in a 1 cm path length quartz cell on a Shimadzu UV-Vis to near IR 3100 spectrometer. The current–voltage characteristics were measured using a black metal mask with an area of 0.25 cm^2 under AM 1.5 sunlight (100$mWcm^{-2}$). IPCE spectra were measured with a monochromatic incident light of 1 x 10^{16} photons cm^{-2} in direct current mode (CEP-2000BX).

III. RESULT AND DISCUSSION

Fig. 2 shows the absorption spectra of triiodide (I_3^-), Y1, TP2A and SQ1 dyes in ethanol solution. The absorption spectrum of triiodide is in the range of 320-450 nm with molar extinction coefficient of 2.73x10^4 $M^{-1}cm^{-1}$. The dip in the triiodide effects greatly at the IPCE spectrum in DSSCs operation [25]. Y1 dye shows intense absorption between 350-450 nm with peak absorption at 390 nm. The bodipy TP2A dye's absorption is between 320-600 nm. As reported earlier, the vinyl-thienyl side arms contributes to the absorption peak in 350 nm region and another peak of 581 nm of the TP2A corresponds to the lowest energy transition of the bodipy core. The absorption peak at 350 nm suggests that it can overcome the dip of triiodide in this region. The absorption maxima of squaraine based IR dye SQ1 occurs at 647 nm and show broad absorption intensity in 550-700 nm region. Interestingly, the peak absorption band of TP2A dye is marked between the gaps of two absorption peaks of SQ1 which seem to be an ideal match for co-sensitized DSSCs to harvest light in the entire region. The highest molar extinction coefficients of dyes at maximum peaks for Y1, TP_2A and SQ1 are recorded at 3.0x10^4 $M^{-1}cm^{-1}$, 1.1x10^5 $M^{-1}cm^{-1}$ and 30.0x10^5 $M^{-1}cm^{-1}$ respectively. In comparison to the triiodide, all the dyes have higher molar extinction coefficient, which suggests that, if co-

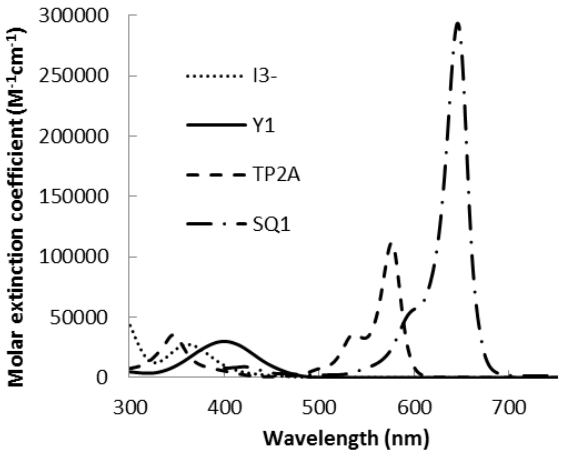

Fig. 2. UV-visible Spectra of Y1, TP2A and SQ1, and the hole transporter triiodide in ethanol solutions.

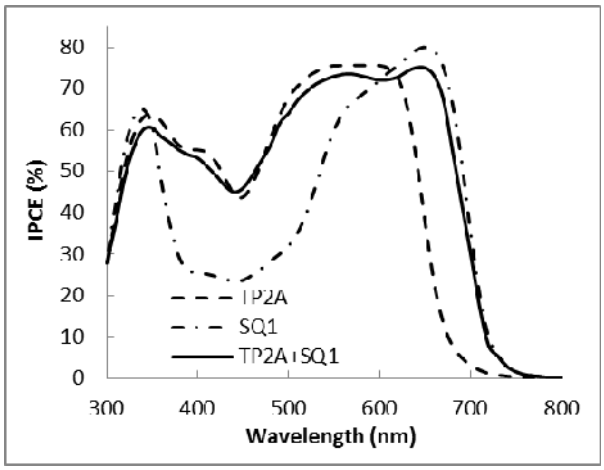

Fig. 3. IPCE spectra of DSSCs sensitized with TP2A, SQ1 and TP2A+SQ1.

sensitized together these dyes should overcome the dip of triiodide and harvest light efficiently in 300-800 nm region.

Considering the impressive absorption of bodipy TP2A dye and squaraine SQ1 dye, we have co-sensitized these two dyes and fabricated DSSCs. The fabricated DSSCs were measured under standard AM 1.5 irradiation (100 $mWcm^{-2}$). Fig. 3 shows the IPCE spectra as a function of the wavelength of bodipy dye TP2A, squaraine dye SQ1 and co-sensitized TP2A+ SQ1 dyes. TP2A shows broad IPCE spectra within 300-670 nm region. The maximum IPCE peak of 75% is observed between 535-600 nm regions, whilst another peak of 63% is recorded at 345 nm. The perceived big dip of IPCE spectra at 370-445 nm suggests inefficient light harvesting in the region. The maximum absorption peak of SQ1 dye is 80% at 675 nm and 65% at 350 nm. The onset wavelength was recorded up to 800nm which is in the NIR region. The huge dip in 360-550 nm suggests poor absorption in this region. Whereas in the same region, TP2A dye shows steady absorption. The IPCE spectrum of TP2A + SQ1 leads to an

improved J_{SC} = 13.60 mAcm^{-2}. The improved short circuit current attributes to an impressive efficiency of 5.60%. The short-circuit current (J_{SC}), open circuit voltage (V_{OC}), fill factor (FF) and overall power conversion efficiency (PCE) data are presented in Table 1.

Fig. 4 shows the IPCE spectra of butyloxyl chain induced dye Y1, TP2A, SQ1 and Y1 dye co-sensitized with best efficient TP2A+SQ1. The Y1 dye has good IPCE absorption at 315-480 nm wavelength region. A steady IPCE over 80% is observed at 400-480 nm region. In comparison with a big dip containing TP2A dye in the same region, it's obvious that co-sensitization of these dyes should lead to increased IPCE at the entire wavelength from 300-800 nm. We successfully co-sensitized Y1+TP2A+SQ1 at 1:2:1 molar ratio and achieved panchromatic absorption from 300-750 nm. The highest onset wavelength was recorded as high as 800 nm. By addition of Y1 dye to the TP2A+SQ1 successfully increases absorption at UV region which leads to an IPCE band over 70%. The broad absorption at UV region contributes to higher J_{SC} of 14.59 mAcm^{-2}, V_{oc} of 0.605 V and η of 6.21% for co-sensitized Y1+TP2A+SQ1 DSSC as seen in Table 1.

TABLE 1

The current–voltage performance data of DSSCs sensitized by single dye and mix-dye system.				
Compound	***J_{sc} (mAcm^{-2})***	***V_{oc} (V)***	***F.F.***	***Effi. (%)***
Y1	6.56	0.698	0.750	3.44
TP_2A	11.40	0.526	0.710	4.26
SQ1	9.51	0.541	0.652	3.35
TP_2A+SQ1	13.60	0.580	0.709	5.60
Y1+TP_2A+SQ1	14.59	0.605	0.703	6.21

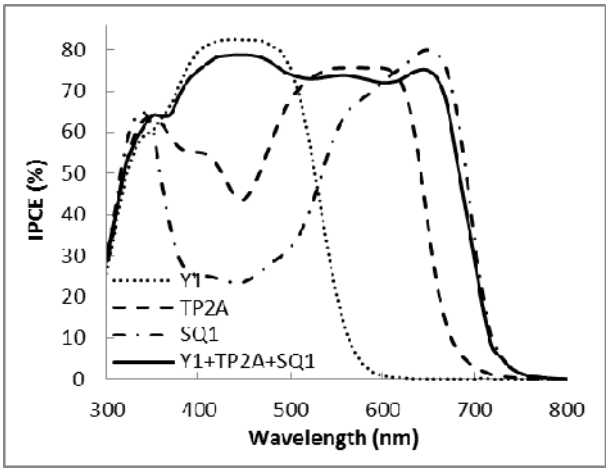

Fig. 4. IPCE spectra of DSSCs sensitized with dyes Y1, TP2A, SQ1 and multi-dyes of Y1+TP2A+SQ1.

Fig. 5 shows the I-V curves for DSSCs composed of Y1, TP2A, SQ1, co-sensitized TP2A+SQ1 and Y1+TP2A+SQ1 dyes under standard AM 1.5 illumination. The J_{SC} and V_{OC} parameters have been shown in Table 1. It is evident that Y1,

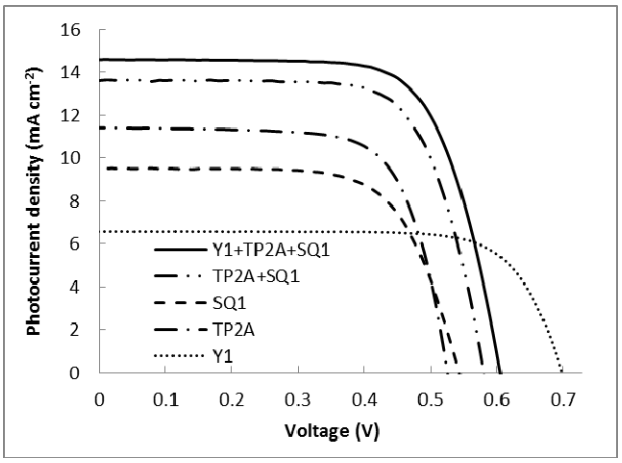

Fig. 5. I-V curves of DSSCs sensitized with Y1, TP2A, SQ1, TP2A+SQ1 and Y1+TP2A+SQ1.

TP2A and SQ1 individually have lower efficiency than that of the co-sensitized ones. The increased J_{SC} contributes to the improved efficiency, whereas the V_{OC} had minimal or no effect for DSSCs based on co-sensitized TP2A+SQ1 dye. The DSSC consisting of co-sensitized Y1+TP2A+SQ1 dyes showed V_{OC} of 0.605V which is 0.025V higher than TP2A+SQ1 based DSSC.

IV. CONCLUSIONS

We have fabricated DSSCs by co-sensitization of organic butyloxyl chain induced Y1 dye, bodipy dye TP2A, squaraine based dye SQ1 and achieved panchromatic absorption in 300-800 nm wavelength region. The panchromatic absorption range of this work is highest to be recorded for triple dye based DSSCs till date. The Y1+TP2A+SQ1 dye based DSSCs show J_{SC} of 14.59 mAcm^{-2}, V_{OC} of 0.605V and efficiency (η) of 6.21%. This is higher than that of individual dyes and TP2A+SQ1 based DSSCs. IPCE spectrum of Y1+TP2A+SQ1 dye based DSSCs show better injection efficiency than each of individual dyes and TP2A+SQ1 dyes. In conclusion, butyloxyl chain induced Y1 dye to TP2A+SQ1 dye significantly improves the IPCE spectrum in 300-400 nm region which leads to enhance the J_{SC} for Y1+TP2A+SQ1 dye based DSSCs. The J_{SC} enhancement is attributed to the combined light harvesting ability of Y1, TP2A and SQ1 dyes. These triple dye co-sensitized solar cells showed panchromatic response with >70% over the entire visible spectra extending to NIR region. The PCE of 6.21% proves the usefulness of these co-sensitized DSSCs in practical electronic appliances.

ACKNOWLEDGMENT

This work was partly supported by the JSPS KAKENHI grant No. 26288113 (AI). MA acknowledges the support of the Solar Energy Research Institute (SERI) of the University Kebangsaan Malaysia (UKM) through the Science Fund research grant with code 03-01-02-SF1149 of the Ministry of Science, Technology and Innovation (MOSTI), Malaysia.

REFERENCES

[1] A. Mishra, M. K. Fischer and P. Bäuerle, Angewandte Chemie International Edition, 2009, 48, 2474-2499.

[2] M. Akhtaruzzaman, A. Islam, A. El-Shafei, N. Asao, T. Jin, L. Han, K. A. Alamry, S. A. Kosa, A. M. Asiri and Y. Yamamoto, Tetrahedron, 2013, 69, 3444-3450..

[3] M. Akhtaruzzaman, H. E. Mahmud, A. Islam, A. E. Shafei, M. R. Karim, K. Sopian, L. Han and Y. Yamamoto, Materials Chemistry and Physics, 2013, 142, 82-86.

[4] M. Grätzel, Journal of Photochemistry and Photobiology A: Chemistry, 2004, 168, 235.

[5] A. Hagfeldt, G. Boschloo, L. Sun, L. Kloo and H. Pettersson, Chemical reviews, 2010, 110, 6595-6663.

[6] Y. Wu and W. Zhu, Chemical Society Reviews, 2013, 42, 2039-2058.

[7] S. Zhang, X. Yang, Y. Numata and L. Han, Energy & Environmental Science, 2013, 6, 1443-1464.

[8] Y. Chiba, A. Islam, Y. Watanabe, R. Komiya, N. Koide and L. Han, Japanese Journal of Applied Physics, 2006, 45, L638.

[9] H. Tian, X. Yang, R. Chen, A. Hagfeldt and L. Sun, Energy & Environmental Science, 2009, 2, 674-677.

[10] J.-H. Yum, E. Baranoff, S. Wenger, M. K. Nazeeruddin and M. Gratzel, Energy & Environmental Science, 2011, 4, 842-857.

[11] N. Koumura, Z.-S. Wang, S. Mori, M. Miyashita, E. Suzuki and K. Hara, Journal of the American Chemical Society, 2006, 128, 14256-14257.

[12] C. Qin, A. Islam and L. Han, Dyes and Pigments, 2012, 94, 553-560.

[13] S. Qu, C. Qin, A. Islam, J. Hua, H. Chen, H. Tian and L. Han, Chemistry – An Asian Journal, 2012, 7, 2895-2903.

[14] A. Ehret, L. Stuhl and M. Spitler, The Journal of Physical Chemistry B, 2001, 105, 9960-9965.

[15] R. Y. Ogura, S. Nakane, M. Morooka, M. Orihashi, Y. Suzuki and K. Noda, Applied Physics Letters, 2009, 94, 073308.

[16] A. Islam, T. Swetha, M. R. Karim, M. Akhtaruzzaman, L. Han and S. P. Singh, physica status solidi (a), 2015, 212, 651-656.

[17] C.-M. Lan, H.-P. Wu, T.-Y. Pan, C.-W. Chang, W.-S. Chao, C.-T. Chen, C.-L. Wang, C.-Y. Lin and E. W.-G. Diau, Energy & Environmental Science, 2012, 5, 6460-6464.

[18] J. Chang, C.-P. Lee, D. Kumar, P.-W. Chen, L.-Y. Lin, K. J. Thomas and K.-C. Ho, Journal of Power Sources, 2013, 240, 779-785.

[19] S. Zhang, A. Islam, X. Yang, C. Qin, K. Zhang, Y. Numata, H. Chen and L. Han, Journal of Materials Chemistry A, 2013, 1, 4812-4819.

[20] Y. Chen, Z. Zeng, C. Li, W. Wang, X. Wang and B. Zhang, New journal of chemistry, 2005, 29, 773-776.

[21] M. Cheng, X. Yang, J. Li, F. Zhang and L. Sun, ChemSusChem, 2013, 6, 70-77.

[22] L. Han, A. Islam, H. Chen, C. Malapaka, B. Chiranjeevi, S. Zhang, X. Yang and M. Yanagida, Energy & Environmental Science, 2012, 5, 6057-6060.

[23] C. Qin, A. Mirloup, N. Leclerc, A. Islam, A. El-Shafei, L. Han and R. Ziessel, Advanced Energy Materials, 2014, 4.

[24] C. Qin, Y. Numata, S. Zhang, X. Yang, A. Islam, K. Zhang, H. Chen and L. Han, Advanced Functional Materials, 2014, 24, 3059-3066.

[25] M. Grätzel, Inorganic chemistry, 2005, 44, 6841-6851.

Impacts of Renewable Energy Integration into the High Voltage (HV) Networks

GM Shafiullah
School of Engineering and Information Technology, Murdoch University, Australia
Email: g.shafiullah@murdoch.edu.au

Abstract— **Current power systems creates environmental impacts as well as global warming due to utilisation of fossil fuels, especially coal, as carbon dioxide is emitted into the atmosphere. It is therefore a fundamental concern today to be able to bring higher percentages of renewable electricity into the energy mix as these sources are climate-frindly and unlimited. However, intermittent nature of power output from renewable energy sources, in particular wind and solar, introduces potential technical impacts that affect quality of power observed including voltage fluctuations, power fluctuations, overloading of distribution transformers and voltage and current harmonics injection into the network. This study developed a simulation model with power system simulation software PSS Sincal to investigate the potential adverse impact of large-scale renewable energy (RE) penetration into the Rockhampton power networks, Queensland, Australia. From the model analyses, it has been clearly evident that large-scale RE integration not only influence in the low voltage distribution network but it also influence in the transmission, subtransmission and high voltage (HV) distribution network in terms of power quality issues such as voltage fluctuations, overloading of tranformers and injection of harmonics.**

Index Terms— **High voltage (HV) networks; Renewable energy; voltage fluctuations; harmonics.**

I. INTRODUCTION

The intermittent nature of renewable energy (RE) sources, in particular solar and wind energy, has an impact on system operations including voltage and frequency, overloading of substation transformers, current and voltage harmonics and PQ in general, that influences the overall performance of the power systems. The asymmetrical solar irradiation due to weather conditions, seasonal variation and geographic location produces voltage fluctuations in the output power of RE systems at the point of coupling (PCC) of the network. This voltage fluctuation is exacerbated in single phase PV systems as voltage increases both in phase and neutral, hence causing phase imbalance in the network. For wind energy generation, potential technical difficulties not only occur due to the design of wind turbine types but also due to the intermittent nature of the wind source, electrical equipment and the grid connection characteristics, and also grid quality issues [1 – 2].

In general, power flows from the upstream network (the transmission network) to the downstream network (the distribution or low voltage network). However, with integration of RE systems feeding back into the grid, if the power generation from these systems is greater than the load in the local network, this causes reverse power flows as RE's are mostly connected in the distribution network, i.e., near the customer loads [1 - 4]. Intermittent nature of RE also causes uneven generation and hence might exceed the capacity of the connected transformer. Integration of RE introduces phase unbalanced conditions in the network due to uneven connection of RE source input to the different phases. RE also cause's bi-directional power flow at the point of connection and increases network voltage which also influences transformer utilisation of the power network. The operation of the power network involves reactive power due to customer loads, line impedances and RE sources, in particular induction generators used in wind turbines which are unsafe for the smooth operation of the network. The control of reactive power improves the power factor and voltage regulation [5 – 6]. Inverters connected with RE sources, non-linear customer loads and power electronics devices introduce harmonics in the low voltage (LV) networks as well as HV networks that causes overheating of transformers, tripping of circuit breakers, and reduces the life of connected equipment [7]. Therefore, RE integration not only influences the distribution network but also creates impacts in the transmission, subtransmission and high voltage (HV) distribution networks.

Therefore, a simulation model has been developed to investigate the level of potential impacts resulting from the large-scale RE integration into the power networks. By increasing PV/wind integration into the network, the points at which distributed generation starts to have an impact on utility grid operations will be investigated with regards to network performance standards and finally, worst-case scenarios are identified through targeted simulation. Several case scenarios were considered based on varying levels of RE

integration to explore the in-depth characteristics of transmission, sub transmission and HV distribution network of the Rockhampton power systems. Load flow, load curve and harmonic analyses were carried out for each of the case scenarios to investigate voltage regulation, transformer loading, power distribution in the network, voltage and current harmonics with the integration of RE into the grid. Load flow study only measures the maximum feeder and line voltages and maximum power generation at a particular time. However, load curve analysis defines the voltage regulation and power distribution over time. Therefore, this study has conducted both load flow and load curve analysis to know the precise scenario of the Rockhampton power network with large-scale RE integration.

II. MODEL EVALUATION

A model was developed for the Rockhampton power network, Queensland, Australia to investigate the adverse impacts of large-scale RE integration into the grid. In previous studies [8 - 9], impacts of RE integration into the low voltage (LV) distribution network was investigated and it was observed that RE integration causes voltage fluctuations, harmonic distortion and as well as transformer overloading and reactive power compensation in the LV distribution network. Therefore, this study is aiming to develop a model to investigate the RE integration issues in the Rockhampton HV network in particular, transmission, subtransmission and high voltage distribution network. Powerlink [10] (a State Government Owned Corporation) is responsible for transmitting electricity from generating stations to Glenmore and Egans Hill Bulk Supply Station's (BSSs) through 132 kV transmission lines. Electricity is transmitted to Frenchville (FRN), Purkhurst (PKH), Pandoin (PAN) and Rockhampton Glenmore (RGL) substations from Glenmore BSS through a 132/66 kV step-down transformer as shown in Figure 1. Similarly, a 132/66 kV step-down transformer at Egans Hill BSS allows transmission of electricity to Berserker (BER), Canning St (CST), Lakes Creek (LCR) and Rockhampton South (RSH) substation in Rockhampton City through 66 kV transmission lines. A 66/11 kV step-down transformer is used in each substation to transmit electricity to the forty four feeders available in the considered eight substations through 11 kV transmission lines. The Rockhampton power network is shown in Figure 1, in which red lines represent 132 kV transmission lines, blue lines represent 66 kV subtransmission lines and all other lines are 11 kV distribution lines.

In this study, two feeders were selected from each substation considering the maximum length of the feeders and maximum connected loads. In each feeder, three observation points were selected, one at the start of the feeder, one in the middle of the feeder and one at the end of the feeder. Therefore, six observation points were considered for each substation, and a total of forty eight observation points were considered in the Rockhampton power network to investigate voltage fluctuations, power regulation and current and voltage harmonic distortion in the transmission, subtransmission and HV distribution network. The six observation nodes for the PAN substation are shown in Figure 2.

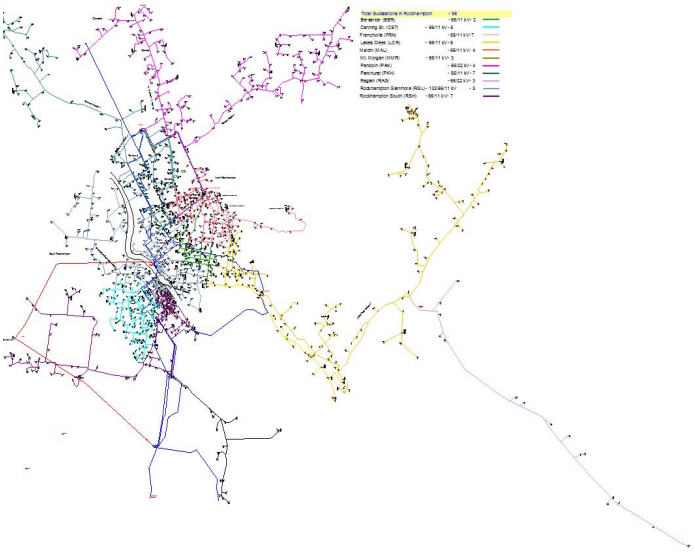

Figure 1: Rockhampton power Network

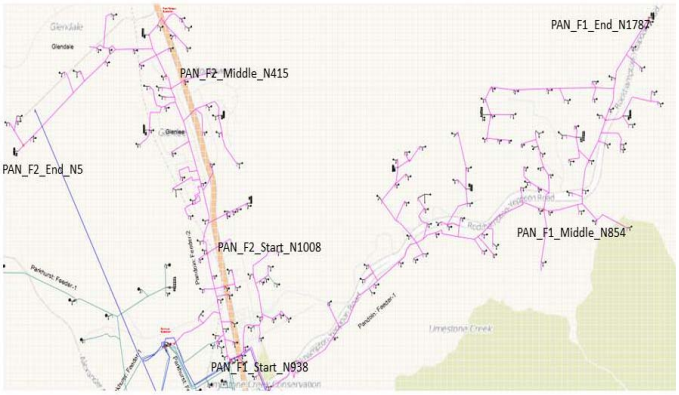

Figure 2: Observation nodes in the two feeders of PAN Substation

Distribution transformer's (DTs) (11kV/415V) were connected with each load of the feeders and solar PV and wind turbine were connected with the LV side of the DT and, hence, line to line and line to neutral voltages are 415V and 240V respectively. Based on the availability of solar radiation and wind speed, it can be stated that, to meet customer load demand, solar or wind energy generation capacity should be 2.0 times or 1.7 times respectively of the load demand [11 - 12]. Therefore, this study, considered with RE integration equal or more than 100% of total loading. Moreover, this study considered both decentralised RE connection approach such as at the same node with the load connection, and also centralised connections such as at the observation points stated above with a large amount of RE. Levels of generation from RE sources were varied based on the percentage of contribution with respect to load demand. Daily load profiles for PV and wind were used based on solar radiation and wind speed collected from Bureau of Meteorology (BOM), Australia [13]. PV, wind and load harmonics considered for the study are based on regulatory standards AS4777 [14], IEEE 519 [15] and AS/NZS 61000.3.2 [16].

Modelling Case Scenarios

As stated earlier, to know the precise scenario of Rockhampton power systems in particular transmission, sub transmission and HV distribution network in this case study several case scenarios were considered based on the PV/wind integration levels and load demands as given below:

- *Case 1: Grid with only loads:* This case study only considers connected loads for different substations without any RE integration.
- *Case 2: Grid with 100% PV integration*: In addition to the grid supplies, 100% PV of total loading was connected with a decentralised connection approach, i.e., with individual LV DTs to match the load demand.
- *Case 3: Grid with 100% decentralised plus 25% centralised RE integration:* In addition to 100% PV of total loading with a decentralised connection approach, this case also considered 25% RE of total loading with a centralised connection approach. Solar PV was connected at the start and middle observation points of the feeder, and a wind turbine was connected at the end observation point of the feeder. 1000 kW RE was connected centrally at each observation point, giving 3000kW in each feeder and 6000kW in each substation.

III. RESULTS ANALYSIS

This study investigated voltage regulation, power flow characteristics, transformer utilisation and total harmonic distortion of Rockhampton power network.

Voltage Regulation

A load flow study was conducted to explore the voltage regulation in the transmission, subtransmission and HV distribution network of the Rockhampton power network to investigate whether the system can control the voltages to within the allowable limits of ±6% of the nominal voltage as per Australian standard AS4777 [14] with the introduction of large-scale RE integration into the network. Figure 3 shows the voltages of different studied case scenarios across the Power Link transmission network (132kV_Trans_PowerLink) and the bulk supply power points at Glenmore (132kV_Trans_1) and Egans Hill (132kV_Trans_2). Figure 3 shows that voltage across the HV 132kV side of the Glenmore BSS is always higher than the rated voltage, and Egans Hill BSS is always lower than the rated voltage. On the other hand, voltage regulation is equal to the rated voltage in the Power Link transmission system for the studied cases. System voltage increases in both the BSSs with the integration of RE as shown in Case 2 and Case 3 compared to Case 1. Case 3 is simply Case 2 with an additional 25% RE of total loading added via centralised RE connections, and the percentages of rated voltage at Glenmore BSS for Case 2 and Case 3 in Phase 1 are 101.25% and 101.30% respectively.

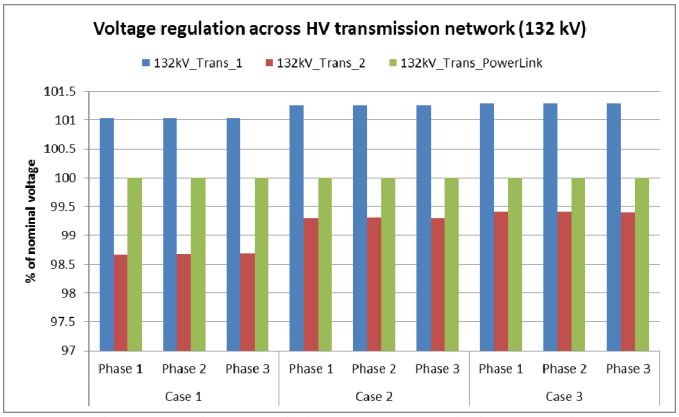

Figure 3: Voltage regulation across transmission network

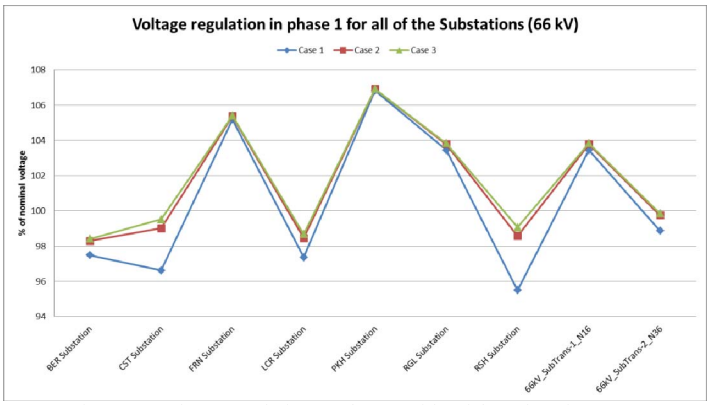

Figure 4: Voltage regulation on the HV side of the substations

Figure 4 shows the network voltages on the HV side of all the substations including the LV side of the BSSs. The figure shows that voltages are always higher than the rated voltage in the Glenmore BSS while lower than the rated voltage in the Egans Hill BSS. From Figure 4 it can be seen that the voltage in Case 1 was the highest in the PHK substation which is 106.81% of the rated voltage, while the lowest 95.49% of the rated voltage is in the RSH substation. On the other hand, voltage of the Frenchville substation itself almost touches the upper regulatory threshold limit, and the percentages of rated voltage in Case 1, Case 2 and Case 3 are 105.18%, 105.37% and 105.39% respectively. RGL substations also exceeded the rated voltage, while the system voltage of the remaining four substations is lower than the rated voltage. The increased integration of RE into the Rockhampton power network increases voltage regulation in different substations as shown in Figure 4 for Case 2 and Case 3. The percentages of rated voltage of RSH substation for Case 1, Case 2 and Case 3 are 95.49%, 98.57% and 99.07% respectively.

Voltage regulation on the LV side of the substation (66kV/11kV), i.e., in the 11kV DN, is shown in Figure 5. Without any RE integration in Case 1, it was shown that voltage across RSH is the lowest and across FRN is the highest and percentages of rated voltage in RSH and FRN are 94.99% and 100% respectively. In Case 2, voltage was increased with the integration of 100% decentralised PV of

the total loading in all of the substations. In this case, percentage of rated voltage of RSH substation increased to 98.74%. Voltage further increases with the addition of 25% RE of total loading with a centralised connection approach as reverse power flows occur in several locations due to higher generation of RE and hence, increased surplus electricity is fed back to the grid. In this case, the line to ground voltage of RGL was higher than the rated voltage, and both FRN and PKH just touch the rated voltage while the remaining other four substations have lower than the rated voltage. It is to be noted that phase to ground rated voltage of the feeders are 6.35 kV. The percentages of rated voltage in RGL substation for Phase 2 are 99.15%, 100.50% and 100.63% for Case 1, Case 2 and Case 3 respectively. Therefore, it can be concluded that centralised RE integration with decentralised PV further increases the voltage regulation of the substation. Voltage regulation of FRN and PKH substations was almost equal to the rated voltage for all of the studied case scenarios as a turbo generator was connected in these two substations.

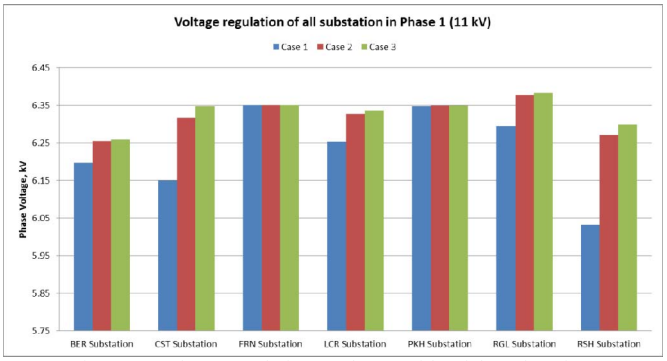

Figure 5: Voltage regulation on the LV side of the substations

Voltage regulation over time for feeder 2, BER substation is shown in Figure 6 (a) and Figure 6 (b) for Case 1 and Case 3 respectively. From Figure 6 (a) it is clearly evident that voltage reduces from the source end to the receiving end. Voltage drops in cables or conductors, bus impedances and transformers throughout the feeders are responsible for this voltage reduction along the feeders. Figure 6 (a) shows that voltage dropped significantly in the middle of the day as load demand is at its maximum during this period and, at 2:00 pm, voltage at BER_F2_End observation node dropped to 94.98% of the rated voltage. However, with the integration of RE in Case 3, voltage rises significantly during the middle of the day as PV generation is at its maximum during this period and RE generation was more than the load demand. At 12:00pm (midday), voltages at BER_F2_Start, BER_F2_Middle and BER_F2_End were 99.74%, 101.48% and 101.97% respectively of the rated voltage, and it was shown that voltage is lowest at the start of feeder and highest at the end of the feeder due to increased RE generation. Therefore, voltage regulation exceeded the allowable limit of 1% at the point of RE connection defined by the local DNSP.

Power Distribution

Power distribution in the Rockhampton power network with different case scenarios were investigated from load flow and load curve analyses. From Figure 7 (a) it can be seen that, without any RE integration in Case 1, maximum power required from the grid is 4724 kW at 2:00pm as customer load demand is at its maximum during this period. With the integration of 100% PV of total loading for Case 2, power requirement from the grid is a minimum of 702 kW at 12:00pm as PV generation was at its maximum in this period and only 1125 kW power is required from the grid at 2:00pm while the load demand is at its maximum as shown in Figure 7. However, the power requirement from the grid was the same at 8:00pm as PV couln't generate any energy during this period.

Transformer Utilisation

To maintain smooth power supply up to the receiving end, i.e., to the customers, substation transformers should always operate within their safe operating limits defined by the local DNSP. Currently all of the substation transformers' capacities in Rockhampton are within their allowable safety limits. Figure 8 shows transformer loading of RSH substation for Case 1 and Case 2. For Case 1, maximum transformer loading is 90.99% at 2:00pm as shown in Figure 8 (a) as load demand is the highest and there was no PV generation in this case study. Minimum transformer loading in Case 1 is 36.43% at 5:30am due to minimum load demand. For Case 2, transformer loading was reduced to 43% at 2:00pm as shown in Figure 8 (b) as PV fulfilled most of the required customer load demands; however, transformer loading is the same at 8:00pm as there was no generation from PV.

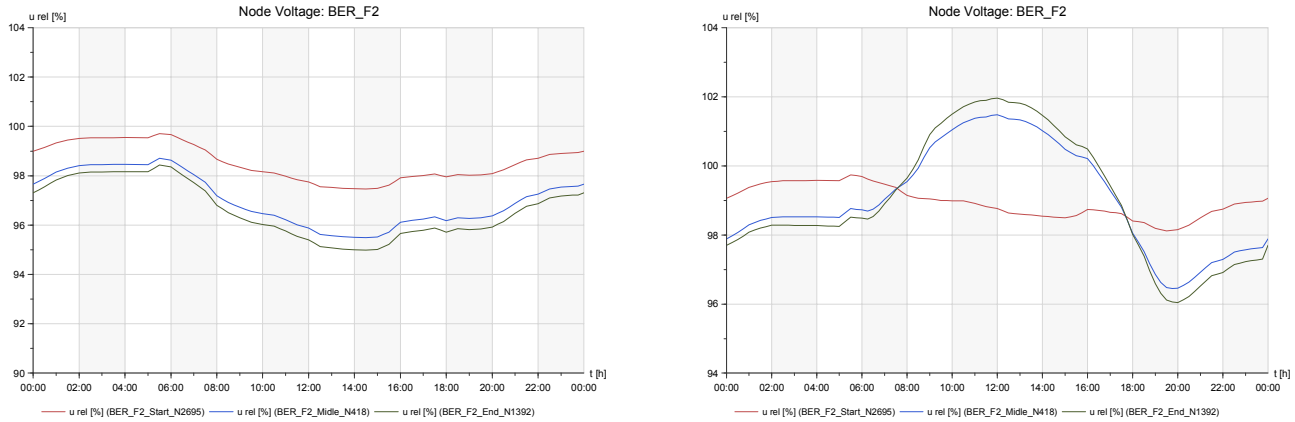

(a) (b)

Figure 6: Voltage regulation of Feeder 2, BER Substation for (a) Case 1 and (b) Case 3

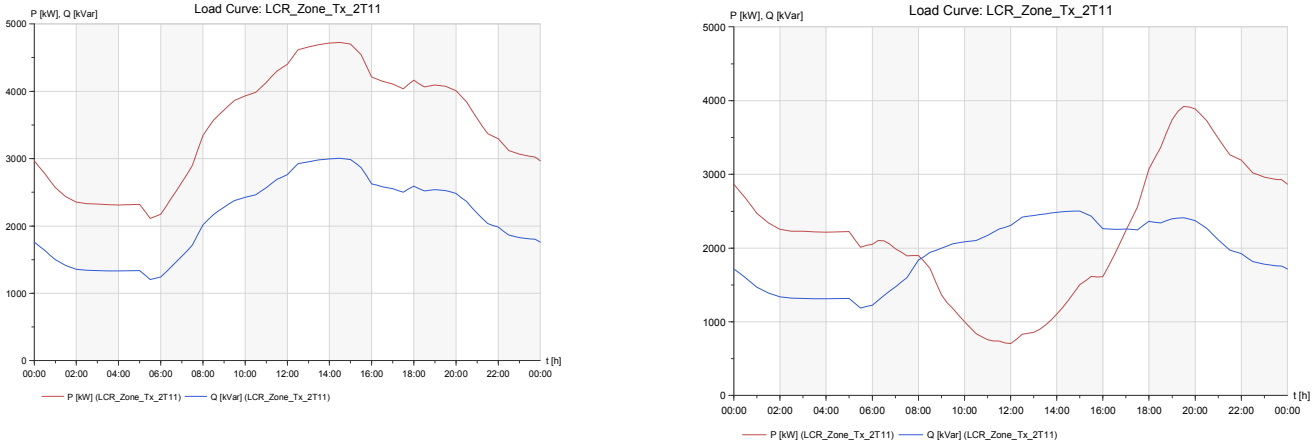

(a) (b)

Figure 7: Power distribution across LCR Substation for (a) Case 1, and (b) Case 2

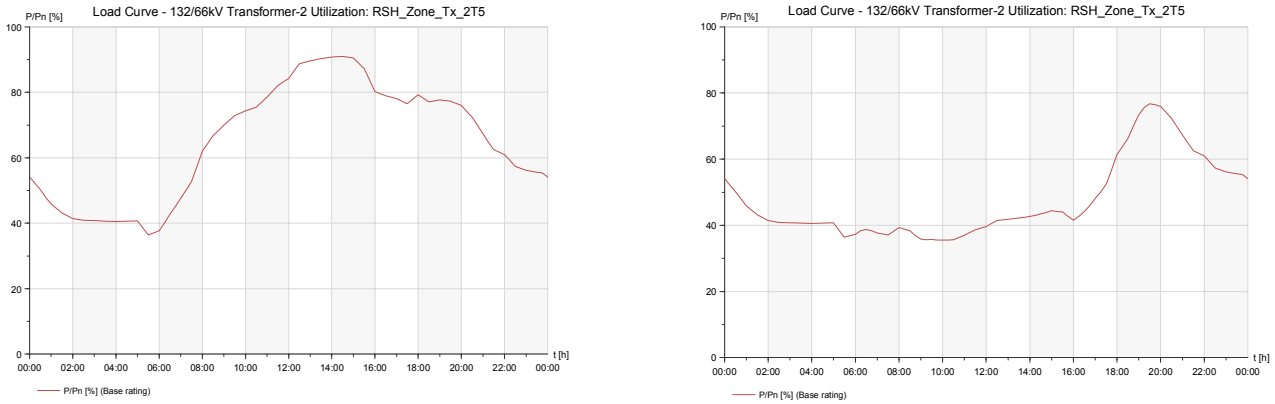

(a) (b)

Figure 8: Substation transformer utilisation of RSH Substation for (a) Case 1 and (b) Case 2

Harmonic Distortion

Harmonic current is of the most concern as most of the adverse effects that occur in the power network are due to these currents. This study investigated both current and voltage harmonic distortion in the Rockhampton power network resulting from the integration of RE. From Figure 9 it is clearly evident that harmonic current distortion increases with the increase of RE integration as PV inverter, wind turbine and power electronics devices are connected in the network. Total current harmonic distortion is increased in both the BSSs with the increasing integration of RE, and the THD exceeded the regulatory standard for both Case 2 and Case 3 as stated in AS 4777 [14], though the THD is higher in the Egans Hill BSS

(132kV_Trans_2) compared to the Glenmore BSS (132kV_Trans_1) as shown in Figure 9.

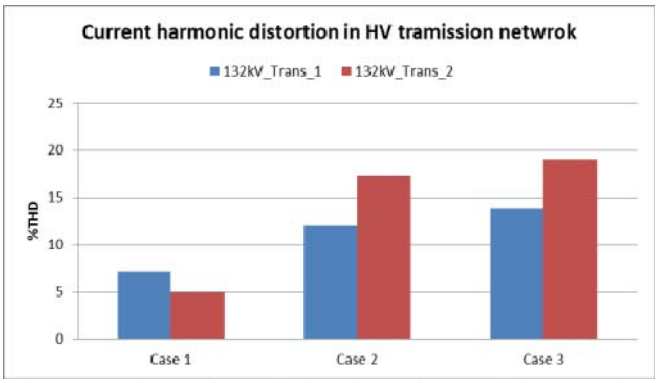

Figure 9: Total current harmonic distortion on the transmission network

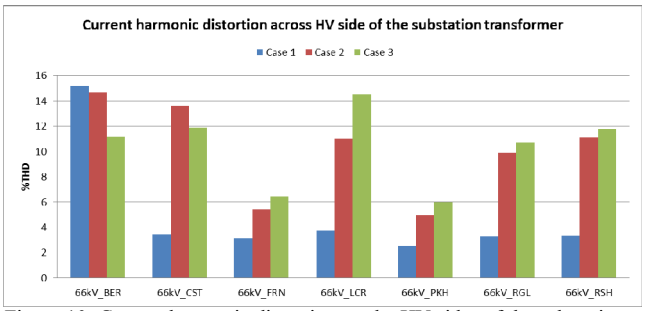

Figure 10: Current harmonic distortion on the HV sides of the substations

Current harmonic distrotion across the HV side of the substations in the Rckhampton power network is shown in Figure 10, from which it can be seen that current harmonic distortion increases with the increase of RE integration into the network for all of the substations except the BER and CST substations which is an interesting findings. Without any RE integration (Case 1), current harmonic distortion of BER substation exceeded the regulatory standard while other substations are within the safety limits. However, for Case 2 and Case 3, i.e., with RE integration, current harmonic distrotion of all the substations in the Rockhampton power network exceeded the regulatory standard except the FRN and PKH substations which have turbo generators connected with it. However, from the results, it was seen that current harmonic distortion is comparatvely lower in the case of centralised RE connections compared to decentralised RE connections.

As current harmonic distortion on the HV side of the BER, CST, LCR, RGL and RSH substations exceeded the regulatory standard, this study further explored the current harmonic distortion on the LV side of these substations. From Figure 11, it can be seen that, for Case 1, current harmonic distortion of only the RSH substation exceeded the regulatory standard of 8%, while for Case 2, CST, LCR and RSH substations exceeded the regulatory standard. It can also be seen that, for Case 2 with the integration of 100% PV of total loading in decentralised connections, increased harmonics occur in all of the studied substations. However, with the added integration of centralised RE connections in Case 3, total current harmonic distortion decreases in all of the substations as the load current increases due to the centralised RE connections. In Case 3, only LCR and RSH exceeded the regulatory limit. Current harmonic distortions of Case 1, Case 2 and Case 3 for the LCR substation are 4.01%, 10.84% and 10.42% respectively, while the comparative results for the RSH substation are 8.81%, 31.35% and 25.34% respectively. Therefore, it can be stated that total current harmonic distortion of the RSH substation is the highest among all the substations and significantly beyond the Australian regulatory limit of 8%; this outcome needs to be mitigated.

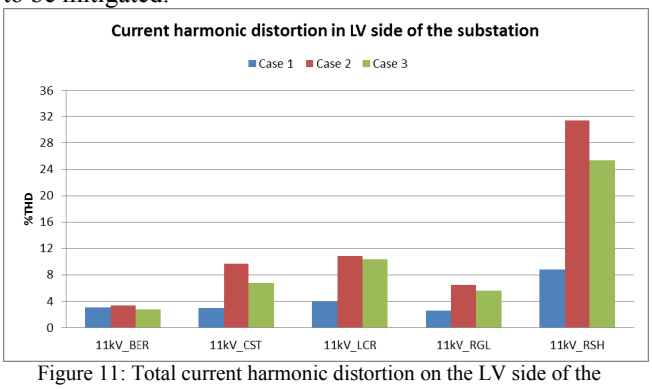

Figure 11: Total current harmonic distortion on the LV side of the substations

Total voltage harmonic distortion in transmission and subtransmission network is shown in Figure 12 in which it can be seen that voltage harmonic distortion is significantly high in all of the observation nodes. Voltage harmonic distortion increases with the increase of RE integration as shown for Case 2 and Case 3 compared to Case 1. Voltage harmonic distortion for studied cases on the HV side of all of the substations are shown in Figure 13 in which it can be seen that voltage harmonic distortion is still high for all of the case studies, and significantly increases with the increase of RE generation as shown in Case 2 and Case 3.

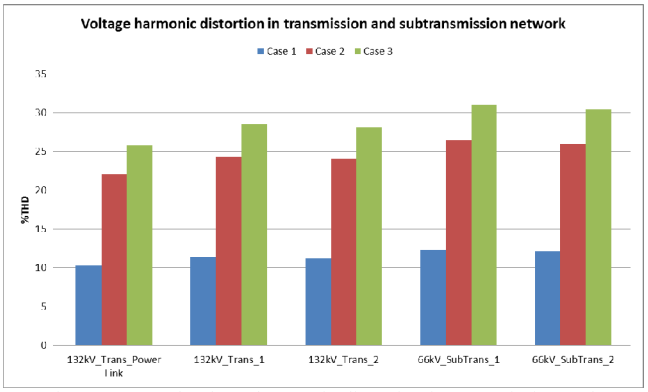

Figure 12: Total voltage harmonic distortion in transmission and subtransmission networks

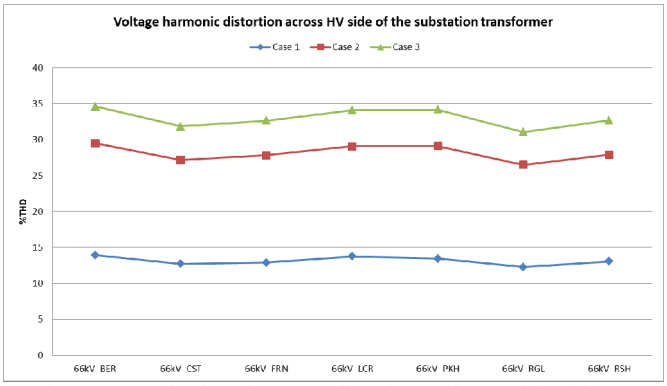

Figure 13: Total voltage harmonic distortion on the HV side of the substations

IV. CONCLUSIONS

Uncontrolled and intermittent nature of generation of power by RE sources causes voltage fluctuations, overloading of transformers and harmonics injection into the network. This study developed a simulation model to explore the potential adverse impacts on the HV networks with large-scale RE integration. The major findings from this study are:

- Integration of solar PV using a decentralised connection approach increases voltage regulation of the power network during the middle of the day as solar PV generation was at its maximum during this period.
- Integration of RE influences transformer loading throughout the day, however, transformer capacity of the network is within the safety limits for the present integration levels.
- Integration of RE introduces significant harmonics in the Rockhampton power network, and current harmonic distortion exceeded the regulatory limits assigned by the local DNSP for few substations. However, current harmonic distortion is comparatively less for centralised RE connections.
- It was shown that a centralised connection approach is a suitable solution, particularly for large-scale RE integration, as influences of voltage regulation and harmonic distortion were comparatively less. Moreover, despite the traditional decentralised connection of roof-top solar PV systems, it is suitable for these and other RE systems to be connected centrally instead of connecting with the individual loads (except for heavy commercial loads).

REFERENCES

[1] GM Shafiullah, Amanullah M. T. Oo, S. Ali, and P. Wolfs, "Potential challenges of integrating large-scale wind energy into the power grid – A review", Journal of Renewable & Sustainable Energy Reviews, ELSEVIER.

[2] Y. Guo, D. J. Hill, Y. Wang, "Global Transient Stability and Voltage Regulation for Power Systems", IEEE Transactions on Power Systems, vol. 16, pp. 678-688, 2001.

[3] J. D. Glover, M.S. Sarma, and T. J. Overbye, Power System Analysis and Design, 5th edn, Cengage Learning, Stamford, Connecticut, 2012.

[4] M. Arif, Amanullah M. T. Oo, S. Ali, and GM Shafiullah, "Impacts of Storage and Solar Photovoltaic in the distribution network", Proceedings of the Australian Universities Power Engineering Conference (AUPEC 2012), 26-29 September, 2012, Bali, Indonesia.

[5] M. A. Eltawil and Z. Zhao, "Grid-connected photovoltaic power systems: Technical and potential problems – A review", Journal of Renewable and Sustainable Energy Review, ELSEVIER, vol. 14, pp. 112-129, 2010.

[6] R. Albarracin, and H. Amaris, "Power Quality in distribution power networks with photovoltaic energy sources", Proceedings of the 8th International Conference on Environment and Electrical Engineering, IEEE, Karpacz, Poland, 10-13 May, 2009.

[7] A. A. Latheef, D. A. Robinson, V. I. Gosbell, V. Smith, "Harmonic impact of photovoltaic inverters On low voltage distribution systems", Proceedings of the 12th International Conference on Harmonics and Quality of Power, Lisbon, Portugal, 1 – 5 October, 2006.

[8] GM Shafiullah, Amanullah M. T. Oo, and Alex Stojcevski, "Voltage regulation in renewable energy integration into the distribution network", Proceedings of the Australian Universities Power Engineering Conference (AUPEC 2013), 29 Sep. - 03 Oct. 2013, University of Tasmania, Tasmania, Australia.

[9] GM Shafiullah and Amanullah M. T. Oo, "Analysis of harmonics with renewable energy integration into the distribution netwrok", Proceedings of the IEEE ISGT 2015 Conference, 3 – 6 Nov. 2015, Bangkok, Thailand.

[10] Powerlink Queensland, [Online Available]: https://www.powerlink.com.au/.

[11] Ergon Energy, Network Management Plan 2012/13 to 2016/17, Part A: Electricity supply for Regional Queensland, [Online Available]: http://www.ergon.com.au/.

[12] Origin Energy, Household peak demand, [Online Available]: http://www.originenergy.com.au/3404/MtStuart-Power-Station.

[13] Bureau of Meteorology, Weather Data, Australian Government, Melbourne, [Online Available]: http://www.bom.gov.au/.

[14] Standards Australia, AS 4777, "Grid connection of energy systems via inverter", 2005, [Online Available]: http://www.saiglobal.com.

[15] IEEE Std. 519- 1992 - IEEE Recommended Practices and Requirements for Harmonic Control in Electrical Power Systems, IEEE, 1993, [Online Available]: http://ieeexplore.ieee.org/xpls/abs_all.jsp?arnumber=210894&tag=1

[16] AS/NZS 61000.3.2: Electromagnetic compatibility (EMC), 2009, Part 3.2: Limits - Limits for harmonic current emissions (equipment input current less than or equal to 16 A per phase), [Online Available]: http://infostore.saiglobal.com/store/details.aspx?ProductID=1129989

High Performance and Stable Molybdenum Telluride PV Cells with Indium Telluride BSF

Mrinmoy Dey[1, 2*] and Maitry Dey[3]

[1]Department of Electrical and Electronic Engineering, Chittagong University of Engineering and Technology, Chittagong-4349, Bangladesh

[2]Renewable Energy Laboratory (REL), Chittagong University of Engineering and Technology, Chittagong-4349, Bangladesh

[3]Department of Electrical and Electronic Engineering, Premier University, Chittagong-4203, Bangladesh

[*]mrinmoycuet@yahoo.com

***Abstract*—Molybdenum telluride ($MoTe_2$) is a very promising candidate for photovoltaic (PV) cell for its higher efficiency and better cell stability. In this research work, the cell performances (*Jsc*, *Voc*, FF and conversion efficiency) of ultra-thin $MoTe_2$ PV cell was investigated by numerical analysis utilizing AMPS (Analysis of Microelectronic and Photonic Structures) simulator. During the study, it was found that 1µm thickness of $MoTe_2$ absorber layer is adequate for acceptable range of cell conversion efficiency. The hidden potentiality of $MoTe_2$ PV cell was examined by adding Indium Telluride (In_2Te_3) back surface field (BSF) between absorber layer and back contact metal. The conversion efficiency of 17.06% (FF = 0.730, *Voc* = 0.98 V and *Jsc* = 23.74 mA/cm^2) has been achieved for 1 µm absorber layer of $MoTe_2$ PV cell without BSF, whereas higher conversion efficiency is 25.29% (FF = 0.847, *Voc* = 1.08 V and *Jsc* = 27.60 mA/cm^2) achieved at room temperature with only 0.7 µm of $MoTe_2$ absorber layer along with 100 nm In_2Te_3 BSF. This research work also analysis the thermal stability of the cell structure for both baseline case and proposed cell. The normalized efficiency of the baseline case cell structure is linearly decreased with the increased of operating temperature at the gradient of -0.0275%/°C which indicates better stability without BSF. In addition, the normalized efficiency of the proposed $MoTe_2$ PV cell with In_2Te_3 BSF is almost unchanged in higher operating temperature.**

***Keywords*—$MoTe_2$, Photovoltaic cell, AMPS, In_2Te_3 BSF, Thermal Stability.**

I. INTRODUCTION

Molybdenum Telluride ($MoTe_2$) is a binary compound material also called Molybdenum Ditelluride recognised as potential candidate for high efficient, cost-effective and stable PV cells for thin film technology. The $MoTe_2$ is a semiconductor material has a direct band gap of 1.1 eV and a high work function of 4.7 eV [1]. It is corresponding to a mass percentage of 27.32% molybdenum (Mo) and 72.68% tellurium (Te). The transition metal dichalcogenides have been extensively investigated considering the electronic, optical, magnetic and catalytic properties of those materials. The challenges of the improvement of cell conversion efficiency are the material usages and the thermal stability which are numerically analyzed to explore the hidden potentiality of the $MoTe_2$ PV cell for higher cell performance parameters. $MoTe_2$ can be formed by electro-deposition from a solution of molybdic acid (H_2MoO_4) and tellurium dioxide (TeO_2). Moreover, Tellurium pressure or vapor is often play vital role for the preparation of the $MoTe_2$ thin films [2,3].

In this research work, n-CdS (2.42 eV) window layer is chosen with p-$MoTe_2$ absorber layer. This research work motivates ultra-thin CdS/$MoTe_2$ PV cells with the insertion of BSF layer for higher conversion efficiency along with better stability also. As a back contact metal, Cu is used below absorber layer material but it creates efficiency degradation with time. It was found from this research work that the insertion of suitable BSF was more effective when numerically applied to the baseline case $MoTe_2$ PV cells with thinner absorber layer showed high cell performance parameters. Consequently, BSF was inserted between the absorber layer and back contact of the modified proposed cell and initiated very much promising results to implement of this ultra-thin $MoTe_2$ PV cell.

During the research work, AMPS simulator is used for numerical analysis [4] to explore the possibility of ultra-thin CdS/$MoTe_2$ cell structure with In_2Te_3 BSF layer to improve cell performances of the $MoTe_2$ PV cells. It was observed from the numerical analysis that less than 1 µm $MoTe_2$ absorber layer with SnO_2/Zn_2SnO_4 front contact, CdS as window layer and In_2Te_3 as BSF material are suitable materials for high efficient (25.29%) and stable CdS/$MoTe_2$ PV cell.

II. MODELING AND SIMULATION

Solar cell models are widely used in research methodology to simplify the complicated system by ignoring the non essential features in a very convenient way. The prerequisite condition of a good model, all the significant parameters are taken into account and the non important ones are neglected. Worldwide more than 200 groups are used AMPS-1D program to design solar cell structure [5]. The baseline case structure of $MoTe_2$ PV cell was utilized to estimate the highest efficiency of CdS/ $MoTe_2$ PV cell and it was modified to investigate the possibility of efficient ultra-thin solar cells with suitable BSF insertion. In this study, the numerical modeling and simulation were done by using AMPS-1D simulator to explore the effect of insertion In_2Te_3 BSF on ultra-thin $MoTe_2$ PV cell.

In this research work, the first modification in the CdS/$MoTe_2$ PV cell was to reduce CdS layer to 70 nm with Zn_2SnO_4 buffer layer. The second modification was to

change the $MoTe_2$ doping concentration to ~10^{17} cm^{-3} which is now achievable for p-$MoTe_2$ absorber layer material. The second last modification is to reduce the $MoTe_2$ absorber layer thickness to the extreme limit for achieving ultra-thin CdS/$MoTe_2$ PV cell. The last modification was the placing of In_2Te_3 BSF to reduce the barrier height in the valence band and to minimize the minority carrier recombination losses at the back contact of the ultra-thin CdS/$MoTe_2$ PV cell.

The baseline case structure of $MoTe_2$ PV cell is depicted in Fig.1 and the modified proposed ultra thin $MoTe_2$ PV cell (Glass/SnO_2/Zn_2SnO_4/CdS/$MoTe_2$/In_2Te_3/Ni) structure for higher cell performance is shown in Fig. 2.

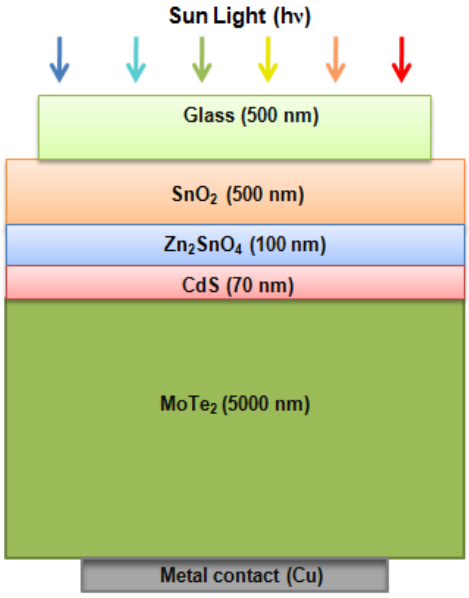

Fig.1 The baseline case $MoTe_2$ PV cell structure

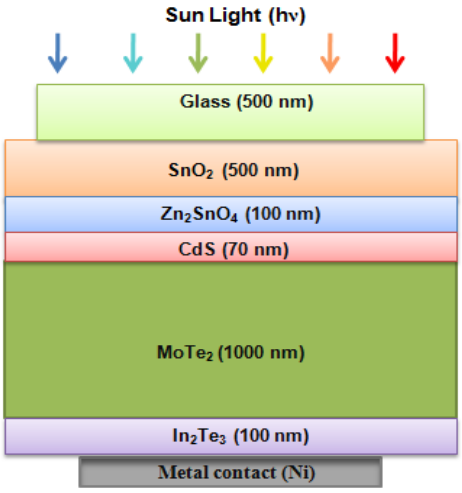

Fig.2 The modified proposed $MoTe_2$ PV cell structure

In this research work, the numerical analysis was done for all layers in the proposed cell were n-SnO_2 TCO (Transparent conducting oxide) layer, n-Zn_2SnO_4 buffer layer, n-CdS window layer, p-$MoTe_2$ absorber layer and p-In_2Te_3 BSF layer. This modified proposed cell structure showed the hidden potentially of attaining a high efficient (around 25%) CdS/$MoTe_2$ PV cell consists of 500 nm SnO_2, 100 nm of Zn_2SnO_4, 70 nm of CdS, 1 µm of $MoTe_2$ and 100 nm of In_2Te_3 BSF layer. For a particular solar cell model, the number of parameters that can be varied is larger than 50 [6]. Therefore, it is necessary to minimize the number of variable parameters with the help of computer specifically through simulator at reasonable values by fixing many of them though it is really dispute to select the practically achievable parameters for different layers of the proposed cells. In this work, Table I shows the used material parameters, which were selected based on experimental data, literature values or in some cases reasonable estimations [7, 8].

TABLE I
THE MATERIAL PARAMETERS USED FOR THE NUMERICAL ANALYSIS OF THE PROPOSED CELLS

Parameters	**n-SnO_2**	**n-Zn_2SnO_4**	**n-CdS**	**p-$MoTe_2$**	**p-In_2Te_3**
Thickness, W (µm)	0.5	0.1	0.07	0.1-5.0	0.1
Dielectric constant, $\varepsilon/\varepsilon_0$	9	9	9	13	12
Electron mobility, µe (cm^2/Vs)	100	32	350	110	1000
Hole mobility, µp (cm^2/Vs)	25	3	50	426	200
Electron and hole concentration n, p (cm^{-3})	1×10^{20}	1×10^{19}	1×10^{17}	1×10^{17}	7.5×10^{19}
Band gap, Eg (eV)	3.3	3.35	2.42	1.1	2.10
Density of states at conduction band, Nc (cm^{-3})	2.2×10^{18}	1.8×10^{19}	1.8×10^{19}	1×10^{15}	1×10^{16}
Density of states at valence band, Nv (cm^{-3})	1.8×10^{19}	2.4×10^{18}	2.4×10^{18}	1×10^{17}	1×10^{17}
Electron affinity, χ (eV)	4.20	4.50	4.50	4.20	3.47

III. Results and Discussion

A. Optimization of Absorber Layer

In this research work, considering the initial point was a four layers device model ($SnO_2/Zn_2SnO_4/CdS/MoTe_2$) of the $MoTe_2$ baseline case structure. The increasing value of *Jsc*, FF and *Voc* causes the improvement of cell conversion efficiency for both baseline and proposed modified cell. Researchers kept the absorber layer around 5 µm or above in most highly performance baseline case solar cells structure. Consequently, numerical analysis was done with the proposed cell to reduce the thickness of $MoTe_2$ absorber layer in order to preserve the usages of $MoTe_2$ materials and the cost of the fabricated cells in the end.

In a typical $MoTe_2$ PV cell structure, the thickness of absorber layer is usually keep over 5µm. 80% of the $MoTe_2$ material could be saved if the thickness of $MoTe_2$ material reduction from 5 µm to less than 1 µm and the film deposition rate can be kept unchanged. Then the deposition time and energy could be at least four times lower. Therefore, thinner solar cells are produced without compromising much with their performance and it leads to manufacture of lower cost solar cell devices since they require less materials, less fabrication time and energy. Thus, a new configuration with In_2Te_3 BSF could be implemented in the $CdS/MoTe_2$ PV cell structure to restrain the possible recombination losses at the back contact of such ultra-thin $MoTe_2$ absorber layer.

B. Insertion of In_2Te_3 BSF

In order to reduce the barrier height in the valence band and to minimize the possible recombination loss at the back contact of ultra-thin $MoTe_2$ PV cell, a high band gap (*Eg*) material In_2Te_3 (*Eg* = 2.10 eV) was placing at the back contact caused reduction of back surface recombination rate in between the absorber and BSF layer. This high band gap material would act as a BSF to bounce back the carriers (electrons) from the $MoTe_2/In_2Te_3$ junction and thus would contribute in the enhancement of carriers.

From the numerical analysis, all the layers of the PV cell structure are similar to the previous optimized cell except an additional 100 nm In_2Te_3 BSF layer just before the final back contact metal of the proposed modified cell. Now the modified cell with the entire cell parameters of Table I were simulated utilizing AMPS simulator. Table II shows that the AMPS simulated results to compare the cell performances together with thermal stability with and without BSF layer.

It is apparent from Table II that the proposed cell without In_2Te_3 BSF shows conversion efficiency of 17.06% only whereas the conversion efficiency increased to 25.17% rapidly with the placing of 100 nm In_2Te_3 BSF layer in between the absorber layer and back contact for 1 µm of $MoTe_2$ PV cell.

TABLE II THE OUTPUT PARAMETERS OF PROPOSED CELLS WITHOUT BSF LAYER AND WITH BSF LAYER

Structure/ parameters	V_{oc} (V)	Jsc (mA/cm^2)	FF	Eff. (%)
Base case	0.98	23.740	0.730	17.06
In_2Te_3 BSF	1.07	27.90	0.842	25.17

Table II shows that the proposed modified cell structure with In_2Te_3 BSF have higher *Voc*, *Jsc* and FF compare with the same cell structure without BSF because of reduced back surface recombination and improved back contact formation with p-$MoTe_2$.

Calculations have been carried out for the $CdS/MoTe_2/In_2Te_3$ PV cell configuration to find the effect of reduction in thickness of $MoTe_2$ absorber layer with BSF insertion. In Fig. 3, the simulation results for variation of $MoTe_2$ absorber layer thickness from 0.1 µm to 5 µm with and without 100 nm In_2Te_3 BSF layer are shown together for comparison on the cell performance parameters of $MoTe_2$ PV cell.

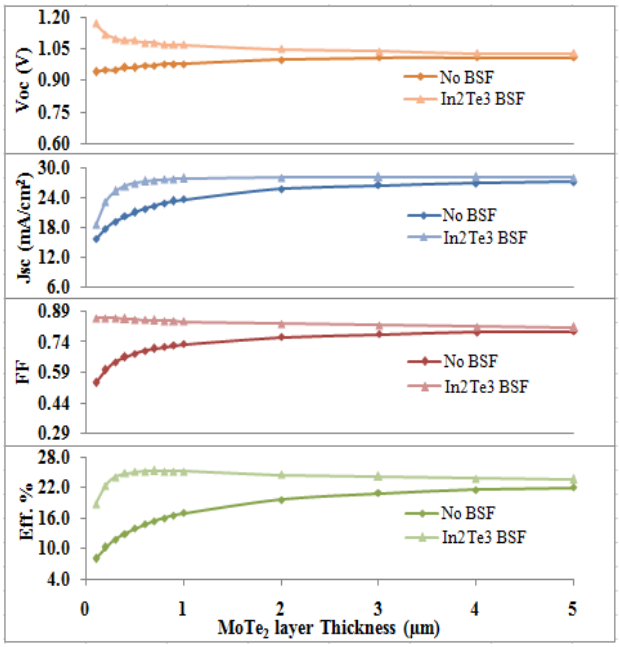

Fig.3 Effect of the $MoTe_2$ thickness variation on cell performance of the proposed cells with and without In_2Te_3 BSF

From Fig. 3, it is observed that the cell performance parameters are fill factor, open circuit voltage and current density illustrate declining trend for the cell structure without BSF whereas with the decrease of the absorber layer thickness in the 1µm range along with highly doped In_2Te_3 BSF the fill factor, open circuit voltage and current density show rising trend. Indeed, the improvement of the cell conversion efficiency in ultra-thin $MoTe_2$ PV cell depends mainly on the rise of *Voc* and FF. In this numerical analysis, conversion efficiency of $MoTe_2$ PV cell showed highest value of 25.29% (FF = 0.847, *Voc* = 1.08 V and *Jsc* = 27.60 mA/cm^2) at 0.7 µm of $MoTe_2$ absorber layer with 100 nm of In_2Te_3 BSF layer which was 8% greater than the baseline case structure (17.06%).

Investigation of cell performance parameters for both baseline case and proposed modified cell are performed by varying of p-type doping of $MoTe_2$ from 1×10^{13} cm^{-3} to 1×10^{17} cm^{-3}. The simulation has been carried out to examine the performance of cell parameters with higher doping concentration. It is evident from Fig. 4 that the cell conversion efficiency is increased with the increase of doping concentration of absorber layer for without BSF and with In_2Te_3 BSF in the proposed cell structure. It is also seen

that with the increase of absorber layer doping concentration, the *Voc* and FF are increased in both case but *Jsc* is decreasing after a certain stage for without BSF layer and it is remain unchanged for with In_2Te_3 BSF modified cell structure.

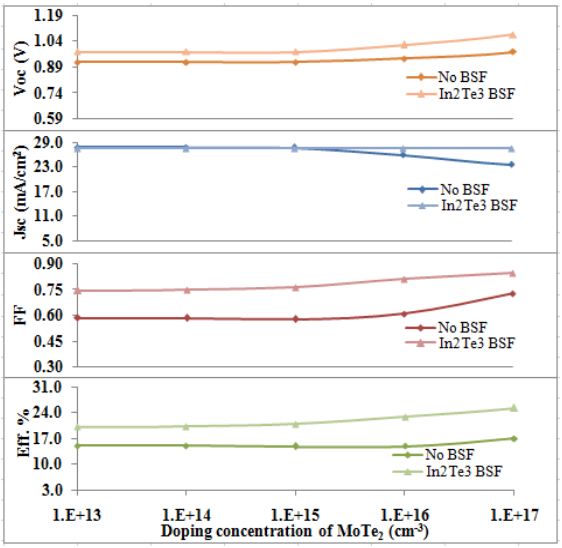

Fig.4 Effect of the doping concentration of $MoTe_2$ on cell performance of the proposed cells with and without In_2Te_3 BSF

C. *Effect of Operating Temperature*

The cell performance parameters of PV cell structure depend on the operating temperature as it is playing a very important role in practical case. The stability of the proposed cells at higher operating temperatures can be investigated for both without BSF and with In_2Te_3 BSF layer. Electron and hole mobility, carrier concentration, density of states and band gap of the material parameters are affected at higher operating temperature. In order to explore the hidden potentially of In_2Te_3 BSF layer in the proposed $MoTe_2$ PV cell is investigated to observe the effects of higher operating temperature on the cell performance parameters. Numerical analysis was done by simulations and carried out with cell operating temperature ranging from 20°C to 180°C. It is clear from Fig. 5 that the cell conversion efficiency is decreased with the increased of operating temperature.

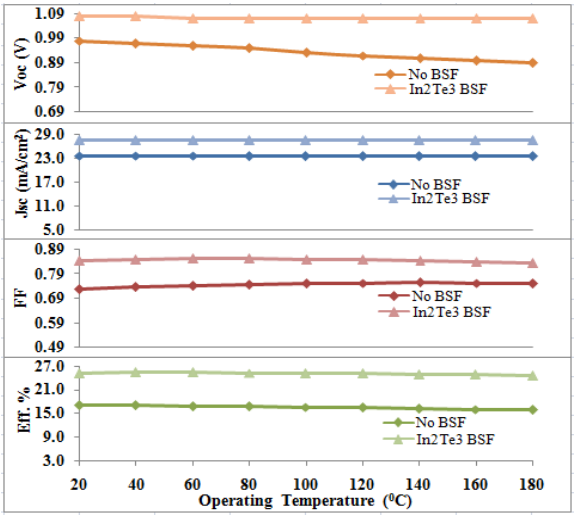

Fig.5 Effect of temperature on cell performances of the proposed cells with and without In_2Te_3 BSF

It is clear from Fig. 6 that without BSF layer, the normalized efficiency of the cells decreased with the increase of operating temperature. The normalized efficiency of the proposed cell structure without BSF layer is linearly decreased with the increased of operating temperature at a temperature coefficient (TC) of -0.0275%/°C whereas the normalized efficiency of the modified cell with In_2Te_3 BSF is increased up 55°C and then operating temperature from 60°C the normalized efficiency is linearly decreased at a temperature co-efficient of -0.016%/°C which shows better stability than without BSF layer in proposed modified cell with In_2Te_3 layer .

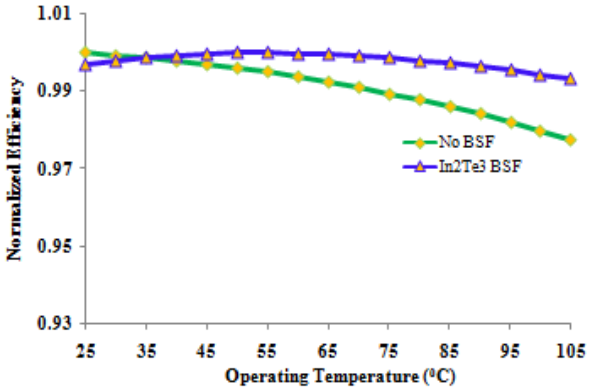

Fig.6 Effect of operating temperature on normalized efficiency

IV. CONCLUSION

The proposed modified ultra-thin $MoTe_2$ PV cell with In_2Te_3 potential BSF was investigated for the possible BSF effect and found the highest efficiency with only 0.7 µm $MoTe_2$ absorber layer along with 100 nm of In_2Te_3 BSF showed the best conversion efficiency of 25.29% (FF = 0.847, *Voc* = 1.08 V and *Jsc* = 27.60 mA/cm^2). It was also found from the $MoTe_2$ baseline case PV cell (SnO_2/Zn_2SnO_4/CdS/$MoTe_2$) structure that 1 µm thickness $MoTe_2$ absorber layer is possible with acceptable range of efficiency of 17.06% (FF = 0.730, *Voc* = 0.98 V and *Jsc* = 23.74 mA/cm^2) without BSF layer. The thermal stability of the proposed cell without BSF at higher operating temperatures with a linear TC of -0.0275%/°C whereas the normalized efficiency is increased from operating temperature range from 25°C to 55°C and a linear TC of -0.016%/°C from temperature ranging from 60°C to 105°C in the proposed cell with In_2Te_3 BSF. The conversion efficiency is increased to 8.23% in the proposed cell with In_2Te_3 layer (25.29%) compared with modified cell without BSF layer (17.06%).

ACKNOWLEDGMENT

This work has been supported by the department of Electrical and Electronic Engineering (EEE) and Renewable Energy Laboratory (REL), Chittagong University of Engineering and Technology (CUET), Bangladesh.

REFERENCES

[1] T. Löher, Y. Tomm, C. Pettenkofer, A. Klein and W. Jaegermann, "Structural dipoles at interfaces between polar II-VI semiconductors CdS and CdTe and non-polar layered transition metal dichalcogenide semiconductors $MoTe_2$ and WSe_2," Semiconductor Science and Technology, vol.15, no. 6, pp. 514–522, 6 March, 2000.

[2] J. C. Bernede, J. Pouzet, N. Manai and A. Ben Mouais, "Structural characterization of synthesized molybdenum ditelluride thin films," *Materials Research Bulletin*, vol. 25, no. 1, pp. 31–42, January 1990.

[3] A. Ouadah, J. C. Bernede, J. Pouzet and M. Morsli, "$MoTe_2$ thin films synthesized by solid state reactions between Mo and Te Thin Films," Physica Status Solidi (a), vol. 134, no. 2, pp. 455–466, 1992.

[4] S. J. Fonash, "A Manual for AMPS-ID," *The Centre for Nanotechnology Education and Utilization*, Pennsylvania State University, PA 16802, 2008.

[5] H. Zhu, A. K. Kalkan, J. Hou, and S. J. Fonash, "Applications of AMPS-1D for solar cell simulation," *AIP Conference Proceedings*, vol. 462, pp. 309–314, March 1999.

[6] M. Burgelman, J. Verschraegen, S. Degrave, and P. Nollet, "Modeling thin film PV devices," *Progress in Photovolaic: Research and Applications*, vol. 12. No. 2-3, pp. 143-153, March 2004.

[7] M. A. Matin, M. M. Aliyu, A. H. Quadery and N. Amin, "Prospects of novel front and back contacts for high efficiency cadmium telluride thin film solar cells from numerical analysis," *Solar Energy Materials and Solar Cells*, vol. 94, no. 9, pp. 1496–1500, September 2010.

[8] N. Dhar, P. Chelvanathan, K. S. Rahman, M. A. M. Bhuiyan, M. M. Alam, K, Sopian and N. Amin, "Effect of p-type transition metal dichalcogenide molybdenum ditelluride (p-MoTe2) layer formation in Cadmium Telluride solar cells from numerical analysis," in *Proceedings of the 39th Photovoltaic Specialists Conference*, pp. 3487 - 3492, 16-21 June 2013.

Antimony Telluride as a Novel BSF for Highly Stable Ultra-Thin CdTe Solar Cells

Mrinmoy Dey[1, 2*], Maitry Dey[3], M. A. Matin[1, 2] and Nowshad Amin[4, 5]

[1]Department of Electrical and Electronic Engineering, Chittagong University of Engineering and Technology, Chittagong-4349, Bangladesh

[2]Renewable Energy Laboratory (REL), Chittagong University of Engineering and Technology, Chittagong-4349, Bangladesh

[3]Department of Electrical and Electronic Engineering, Premier University, Chittagong-4203, Bangladesh

[4]Solar Energy Research Institute (SERI), The National University of Malaysia, 43600 Bangi, Selangor, Malaysia

[5]Department of Electrical, Electronic and Systems Engineering, The National University of Malaysia, 43600 Bangi, Selangor, Malaysia

[*]mrinmoycuet@gmail.com

***Abstract*— For cost-effective, high efficiency, better cell stability and clean generation of solar electricity polycrystalline ultra-thin cadmium telluride (CdTe) is the leading solar cell material in the world. AMPS (Analysis of Microelectronic and Photonic Structures) simulator is used to investigate the cell performance parameters (*Voc, Jsc*, FF and conversion efficiency) of ultra-thin CdTe solar cell along with its thermal stability. In this research work, it was found in the proposed cell that 1µm absorber layer ultra thin CdTe solar cell generated cell conversion efficiency at satisfactory level. This ultra-thin CdTe absorber layer was investigated along with 100 nm Sb_2Te_3 back surface field (BSF) layer to explore the hidden potentiality of BSF layer which minimize the recombination losses at the back contact and to reduce the barrier height in the valence band of the proposed modified cell. During the research work, higher conversion efficiency of 20.26% (*Jsc* = 24.12 mA/cm^2, FF = 0.839, *Voc* = 1.00 V) has been achieved with only 0.8 µm of CdTe absorber layer along with 100 nm Sb_2Te_3 BSF whereas conversion efficiency is 18.68% (*Jsc* = 21.47 mA/cm^2, FF = 0.85, *Voc* = 1.02 V) without BSF layer. Moreover, the proposed CdTe solar cell without BSF layer showed better stability at the temperature co-efficient (TC) of -0.18%/°C. Consequently, the normalized efficiency of the proposed cell with Sb_2Te_3 BSF is increased up to 50°C and then it is decreased linearly for the operating temperature ranging from 55°C to 105°C at the TC of -0.14%/°C.**

Keywords—Cell stability, Ultra-thin, AMPS, Solar cell, Sb_2Te_3 BSF.

I. INTRODUCTION

Polycrystalline Cadmium Telluride (CdTe) is the leading potential candidate for cost-effective, efficient and better stability second generation solar cells. The CdTe is a II-VI binary compound semiconductor material having high absorption co-efficient over 5×10^5/cm and a direct band gap of 1.45 eV which is very close to the optimum band gap for solar cells capable for generating high conversion efficiency. In this research work, improvement of cell efficiency, material usages and the thermal stability of the solar cell are the major challenges that can be examined by numerical analysis to investigate the cell performance parameters of CdTe solar cell.

In thin film technology, approximately 100% of the incident solar radiation is absorbed with the absorber layer thickness of 2µm in CdTe solar cell [1]. CdTe technology has a variety of low cost techniques to manufacture CdS/CdTe cell which are close-spaced-sublimation (CSS), physical vapour deposition (PVD), chemical bath deposition (CBD) and magnetron sputtering method. In 1972 Bonnet et al. reported CdTe thin film solar cell with an efficiency of 6% [2] and Xuanzhi Wu published a paper reporting record efficiency of 16.5% for CdS/CdTe solar cell in 2001 [3]. The highest theoretical efficiency for CdTe is about 29% at standard solar spectrum whereas first solar achieved 21.5% efficiency for CdTe solar cell.

As hetero-junction partner, polycrystalline n-CdS window layer is chosen with p-CdTe absorber layer. This research work motivates ultra-thin CdS/CdTe solar cells with the insertion of BSF layer for higher conversion efficiency. It was found that the insertion of suitable BSF was more effective when numerically applied to the champion and baseline case CdTe solar cells with thinner absorber layer. As a result, BSF was inserted to the modified cell and found very much promising results to implement the ultra-thin CdTe solar cell.

Many researchers are trying to increase the conversion efficiency of CdS/CdTe solar cells with a variety of BSF in the interface of absorber layer and back contact. These BSF are As_2Te_3 as discussed by Romeo et al. [4], PbTe as discussed by Matin and Dey [5] and GeTe as discussed by Dey et al. [6]. The specific BSF material preferred in this work is Antimony Telluride (Sb_2Te_3) to explore the hidden potentiality of CdTe solar cell.

In this research work, numerical analysis was done by utilizing AMPS simulator [7] to investigate the possibility of ultra-thin CdS/CdTe cell with Sb_2Te_3 BSF layer to improve cell performances of the CdTe solar cells. It was showed from numerical analysis that less than 1 µm CdTe absorber layer along with Sb_2Te_3 as BSF material are suitable materials for high efficient (20.26%) ultra-thin and stable CdS/CdTe cell.

II. MODELING AND SIMULATION

AMPS-1D program is used in worldwide to design solar cell structure by more than 200 groups [8]. The baseline structure of CdTe cell was utilized to estimate the highest efficiency of CdS/CdTe solar cell and it was modified to investigate the possibility of efficient ultra-thin solar cells with addition of suitable BSF. In this work, numerical modeling and simulation were done by using AMPS-1D simulator to explore the effects of Sb_2Te_3 BSF insertion on ultra-thin CdTe solar cell.

In this research work, the first modification in the typical CdS/CdTe cell was to reduce CdS layer to 80 nm with Zn_2SnO_4 buffer layer. The second modification was to change the CdTe doping concentration to ~10^{17} cm^{-3} which is now achievable for p-CdTe absorber layer material. The third modification is to reduce the CdTe absorber layer thickness to the extreme limit for achieving ultra-thin CdS/CdTe solar cell. The final modification was the placing the Sb_2Te_3 BSF to reduce the minority carrier recombination loss at the back contact of the ultra-thin CdS/CdTe solar cell.

The conventional structure of CdTe solar cell is illustrated in Fig.1 and the modified proposed ultra thin CdTe solar cell (Glass/SnO_2/Zn_2SnO_4/CdS/CdTe/Sb_2Te_3/Mo) structure for higher cell performance is shown in Fig. 2.

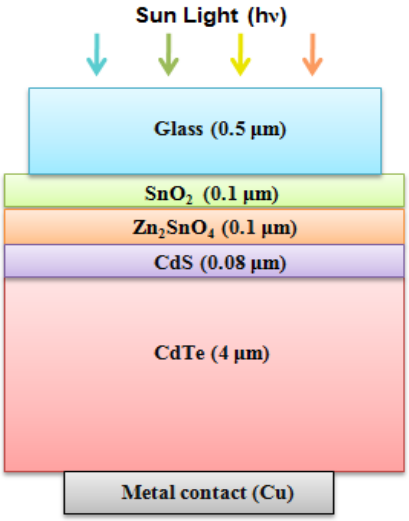

Fig.1 The conventional CdTe solar cell structure

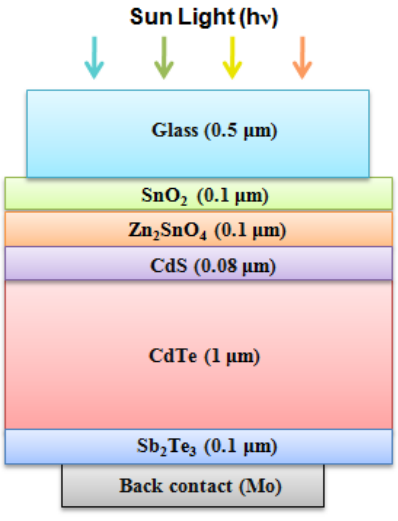

Fig.2 The proposed modified CdTe solar cell structure with Sb_2Te_3 BSF

In this analysis, the four layers of the proposed cell are n-Zn_2SnO_4 buffer layer, n-CdS window layer, p-CdTe absorber layer and p-Sb_2Te_3 BSF layer. This proposed modeling showed the possibility of getting a higher performance (around 20%) CdS/CdTe solar cell consists of 100 nm of Zn_2SnO_4, 80 nm of CdS, 1 µm of CdTe and 100 nm of Sb_2Te_3 BSF layer. In case of numerical analysis, the number of parameters that can be varied is larger than 50 of a particular solar cell model [9]. As a result, it is compulsory the aid of computer to design a problem with 50 variables. At the same time, it is necessary to minimize the number of variable parameters at reasonable values by fixing many of them though it is really dispute to select the practically achievable parameters for different layers of the proposed cells. Many of the parameters depend on fabrication techniques and deposition methods and can thus vary even between devices fabricated in the same batch from the same technology.

In this study, Table I shows the used material parameters, which were selected based on experimental data, literature values or in some cases reasonable estimations [10].

TABLE I THE MATERIAL PARAMETERS USED FOR THE NUMERICAL ANALYSIS OF THE PROPOSED CELLS

Parameters	n-CdS	p-CdTe	Sb_2Te_3
W (µm)	0.08	0.1-2.9	0.1
$\varepsilon/\varepsilon_0$	9	9.4	55
µc (cm^2/Vs)	350	500	1094
µp (cm^2/Vs)	50	60	320
n, p (cm^{-3})	1×10^{17}	1×10^{17}	7.5×10^{19}
Eg (eV)	2.42	1.45	0.3
Nc (cm^{-3})	1.8×10^{19}	7.5×10^{17}	1×10^{16}
Nv (cm^{-3})	2.4×10^{18}	1.8×10^{18}	1×10^{17}
χ (eV)	4.50	4.28	4.15

III. RESULTS AND DISCUSSION

A. *Absorber Layer Optimization*

Optimization of absorber layer preserves the CdTe material usages. In this work, the starting point was a three layer device model (SnO_2/CdS/CdTe) structure of the CdTe baseline case [10]. The increasing value of *Jsc,* FF and *Voc* causes the improvement of cell conversion efficiency of the proposed cell. Researchers kept the CdTe absorber layer is around 5 µm or above in most highly performance CdS/CdTe solar cells. As a result, further numerical analysis was done with the proposed cell to reduce the thickness of absorber layer in order to cost effective CdTe solar cells.

Several research groups all over the world are interested much to manufacture CdS/CdTe cells with thinner CdTe absorber layer as its lower production cost and consequently time and energy. 75% of CdTe material could be saved if the thickness of CdTe material reduction from 4 µm to less than 1 µm. Then the deposition time and energy could be at least three times lower. Therefore, thinner solar cells are produced without compromising much with their performance and it leads to manufacture of lower cost solar cell devices since they require less materials, less fabrication time and energy. Thus, a new configuration with Sb_2Te_3 BSF could be implemented in the CdS/CdTe solar cell structure to restrain the possible recombination losses at the back contact of such ultra-thin CdTe absorber layer.

B. Exploring the Effects of Sb_2Te_3 BSF

In order to reduce the possible recombination loss and the barrier height at the back contact of ultra-thin CdTe solar cell, Sb_2Te_3 (*Eg* = 0.3 eV) is placing at the back contact as a low band gap material which causes reduction of back surface recombination rate at the CdTe/Sb_2Te_3 interface. This low band gap material would act as a BSF to bounce back the carriers (electrons) from the CdTe/Sb_2Te_3 junction and consequently contributes in the enhancement of electrons.

In this numerical analysis, the formation of different layers of the solar cell structure are similar to the previous optimized cell except an additional 100 nm Sb_2Te_3 BSF layer is inserted just before the final back contact metal in the proposed modified cell. The modified cell with the entire cell parameters of Table I were simulated along with 100 nm Zn_2SnO_4, 80 nm CdS, 1 µm CdTe and 100 nm Sb_2Te_3 BSF layers. The AMPS simulated results are shown in Table II to compare the cell performances with and without Sb_2Te_3 BSF layer.

It is clear from Table II that the proposed CdTe solar cell with 1 µm absorber layer along with placing of 100 nm Sb_2Te_3 BSF layer in between the absorber layer and final back contact metal shows the conversion efficiency of 20.19% whereas without the insertion of BSF the conversion efficiency is just 18.68% .

TABLE II THE OUTPUT PARAMETERS OF PROPOSED CELLS WITHOUT BSF LAYER AND WITH BSF LAYER

Parameters/ Structures	Base Case	Sb_2Te_3 BSF
Open circuit voltage, *Voc* (V)	1.02	1.00
Current density, *Jsc* (mA/cm^2)	21.470	24.174
Fill factor, FF	0.850	0.834
Efficiency (%)	18.68	20.19

Table II shows that the proposed modified cell structure with Sb_2Te_3 BSF have higher *Jsc* and FF compare with the same cell structure without BSF because of reduced back surface recombination and improved back contact formation with p-CdTe. Simulated J-V characteristics of both the cells are shown in Fig. 3 to analysis the cause of superior CdS/CdTe solar cell performance.

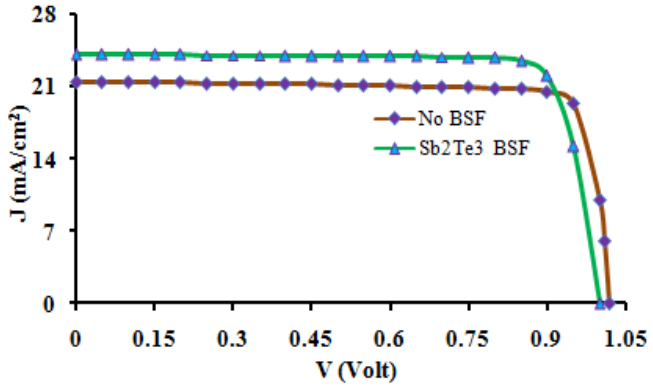

Fig.3 J-V characteristics of the proposed cells

Calculations have been carried out for the CdS/CdTe/Sb_2Te_3 configuration to find the effects of reduction in thickness of CdTe absorber layer with BSF insertion. In Fig. 4, the simulation results for variation of CdTe absorber layer thickness from 0.1 µm to 4 µm with and without 100 nm Sb_2Te_3 BSF layer are shown together to compare the performance of cell parameters.

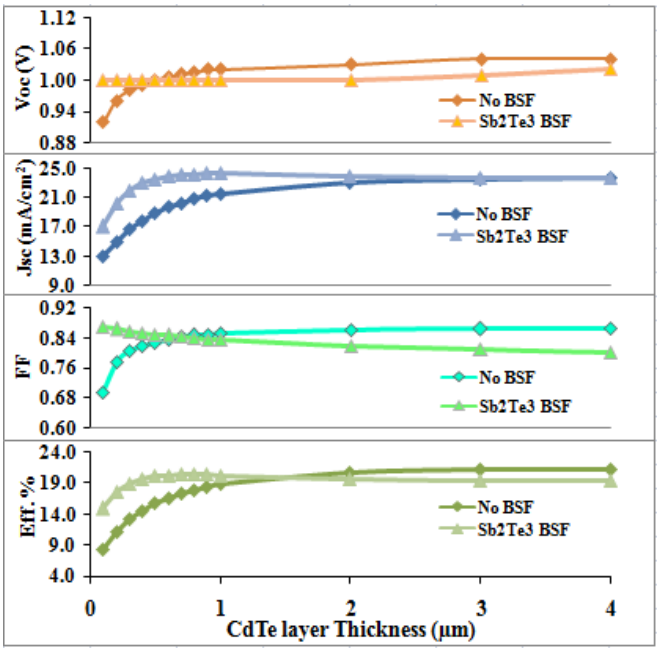

Fig.4 Effect of the CdTe thickness variation for the proposed cells with and without Sb_2Te_3 BSF

It is seen from the Fig. 4, both *Voc* and FF show decreasing trend for the cell without BSF whereas the *Voc* and FF show increasing trend with the decrease of the thickness of absorber layer in the presence of highly doped Sb_2Te_3 BSF. In fact, the increase of *Voc* and FF both has the largest contribution to improve the efficiency of ultra-thin CdTe solar cell in this numerical analysis. These results of cell performances with the insertion of Sb_2Te_3 BSF layer are agreeable to the related published works [5, 6, 10]. In this research work, the CdTe solar cell conversion efficiency showed highest value of 20.26% (*Jsc* = 24.12 mA/cm^2, FF = 0.839, *Voc* = 1.00 V) at 0.8 µm of CdTe absorber layer with Sb_2Te_3 BSF layer.

It is evident from the Fig. 5 that the long wavelength spectral response (SR) is achieved with only 0.8 µm thickness of CdTe absorber layer along with Sb_2Te_3 BSF.

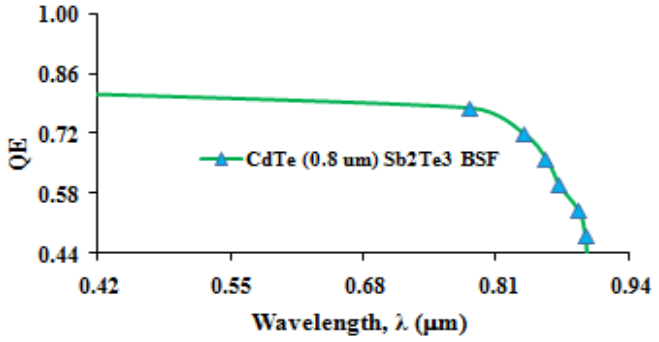

Fig.5 Spectral response on CdS/CdTe (0.8 µm)/ Sb_2Te_3 cell structure

C. *Investigation of Thermal Stability*

The operating temperature plays a very significant role in realistic case and it affects the cell performances of the solar cell. At higher operating temperature, parameters such as the electron and hole mobility, carrier concentration, density of states and band gap of the materials are affected. In order to investigate the effects of higher operating temperature on the performances of the solar cells with Sb_2Te_3 BSF, simulations were carried out with cell operating temperature ranging from 20°C to 120°C and the simulated results are shown in Fig. 6. It is clear from Fig. 6 that the cell performance parameters of CdTe solar cell with Sb_2Te_3 BSF show higher value than that of without BSFat higher operating temperature.

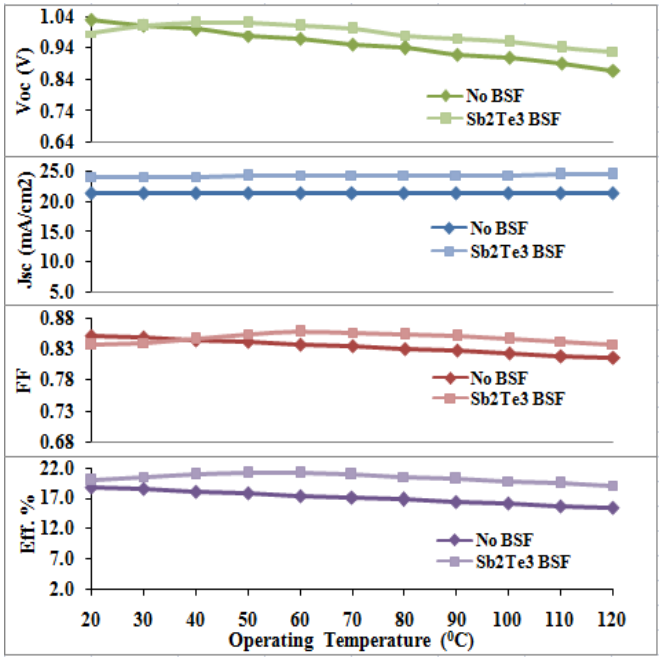

Fig.6 Effect of temperature on cell performances of the proposed cells with and without Sb_2Te_3 BSF

From Fig. 7, it is obvious that without BSF layer the normalized efficiency of the cells linearly decreased with the increase of operating temperature ranging from 25°C to 105°C at a temperature coefficient (TC) of -0.18%/°C. But in case of 100 nm Sb_2Te_3 BSF layer insertion in the proposed CdTe solar cell the normalized efficiency is increased up to 50°C and then it is decreased linearly for the operating temperature ranging from 55°C to 105°C at the TC of -0.14%/°C that indicates better cell stability which is good agreement with related published work [5, 6, 10].

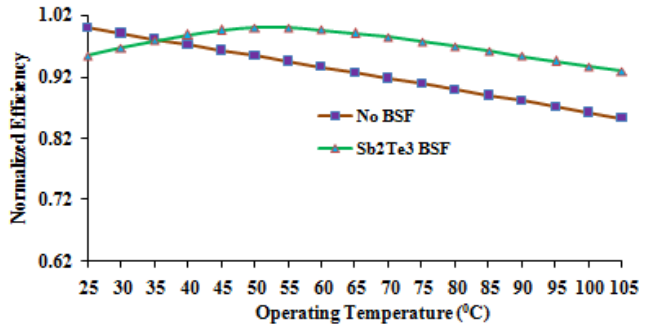

Fig.7 Effect of operating temperature on normalized efficiency

IV. CONCLUSION

The potential BSF material Sb_2Te_3 was investigated for the possible BSF effect in ultra-thin CdTe cell with an insertion of 100 nm BSF layer, the highest efficiency was found where the Sb_2Te_3 BSF with 0.8 µm CdTe absorber layer showed the best conversion efficiency of 20.26% (*Jsc* = 24.12 mA/cm^2, FF = 0.839, *Voc* = 1.00 V). It was found from the CdTe baseline case cell (SnO_2/CdS/CdTe) structure that 1 µm thick CdTe absorber layer is possible with acceptable range of efficiency of 18.68% (*Jsc* = 21.47 mA/cm^2, FF = 0.85, *Voc* = 1.02 V) without BSF layer. The thermal stability analysis of the proposed cells with Sb_2Te_3 BSF layer showed better stability at higher operating temperatures ranging from 55°C to 105°C with a linear TC of -0.14%/°C whereas proposed cell without BSF having TC of -0.18%/°C.

ACKNOWLEDGMENT

This work has been supported by the department of Electrical and Electronic Engineering (EEE) and Renewable Energy Laboratory (REL), Chittagong University of Engineering and Technology (CUET), Bangladesh.

REFERENCES

[1] C. S. Ferekides, U. Balasubramanian, R. Mamazza, V. Viswanathan, H. Zhao and D.L. Morel, "CdTe thin film solar cells: device and technology issues", *Solar Energy*, vol. 77, no. 6, pp. 823–830, December 2004.

[2] D. Bonnet, and H. Rabenhorst, "New results on the development of a thin film p-CdTe-n-CdS heterojunction solar cell," in *Proceedings of the 9th IEEE Photovoltaic Specialists Conference*, p. 129, 1972.

[3] X. Wu, "High-efficiency polycrystalline CdTe thin-film solar cells," *Solar Energy*, vol. 77, no. 6, pp. 803-814, December 2004.

[4] N. Romeo, A. Bosio, S. Mazzamuto, A. Romeo, and L. Vaillant-Roca, "High efficiency CdTe/CdS thin film solar cells with a novel back contact," in *Proceedings of the 22nd European Photovoltaic Solar Energy Conference*, pp. 1919–1927, Milan, Italy, 2007.

[5] M. A. Matin and Mrinmoy Dey, "High Performance Ultra-Thin CdTe Solar Cell with Lead Telluride BSF," in *Proceedings of the 3rd International Conference on Informatics, Electronics & Vision,* pp. 1-5, Dhaka, Bangladesh, May 2014.

[6] Mrinmoy Dey, M. A. Matin, Nipu Kumar Das and Maitry Dey, "Germanium Telluride as a BSF material for high efficiency ultra-thin CdTe solar cell," in *Proceedings of the 9th International Forum on Strategic Technology,* pp. 334-338, Cox's Bazar, Bangladesh, October 2014.

[7] S. J. Fonash, "A Manual for AMPS-ID," *The Centre for Nanotechnology Education and Utilization*, Pennsylvania State University, PA 16802, 2008.

[8] H. Zhu, A. K. Kalkan, J. Hou, and S. J. Fonash, "Applications of AMPS-1D for solar cell simulation," *AIP Conference Proceedings*, vol. 462, pp. 309–314, March 1999.

[9] M. Burgelman, J. Verschraegen, S. Degrave, and P. Nollet, "Modeling thin film PV devices," *Progress in Photovolaic: Research and Applications,* vol. 12. No. 2-3, pp. 143-153, March 2004.

[10] M. A. Matin, M. M. Aliyu, A. H. Quadery, and N. Amin, "Prospects of novel front and back contacts for high efficiency cadmium telluride thin film solar cells from numerical analysis," *Solar Energy Materials and Solar Cells*, vol. 94, no. 9, pp. 1496–1500, 2010.

Techno-Economic Analysis of a Hybrid PV-Wind-Diesel Energy System for Sustainable development at Coastal Areas in Bangladesh

SK. A. Shezan[1]
[1]Department of Mechanical Engineering, University of Malaya, Kuala Lumpur-50603
Email: shezan.ict@gmail.com

A.Z. M. Salahuddin[3]
[2]Faculty of Nuclear Science & Bio-medical Engineering, Military Institute of Science and Technology, Mirpur, Dhaka, Bangladesh.
Email:opu_bka@yahoo.com

M. Farzana[2]
[2]Department of Electrical & Electronics Engineering, American International University- Bangladesh.
Email:rimin20@yahoo.com

A. Hossain[4]
[2]Department of Nuclear Science & Engineering, Military Institute of Science and Technology, Mirpur, Dhaka, Bangladesh.
Email:altab76@gmail.com

Abstract:

Power generation capacity of Bangladesh needs to be enhanced to support the rising electricity demand. Bangladesh has predominantly used fossil fuel generators for the past decades. Saint Martin's Island and Kuakata are two significant areas that lie at or near the coast of Bangladesh with an average annual solar radiation of 4.81 and 4.65 kWh/m^2/d respectively. The monthly average wind speeds at a height of 25 meters are 4.79 and 4.54 m/s, respectively. Considering this data and the benefits of the Optimized hybrid systems, HOMER (Hybrid Optimization Model for Electric Renewable) is used to optimize a system for each of these areas. The costs of energy found from the proposed optimized PV-wind-diesel hybrid Energy system for Saint Martin's island and Kuakata are 30.768 and 30.759 Tk/kWh, respectively, the net present cost (NPC) also has been evaluated as 13219616 Tk. which are quite reasonable with respect to the present situation in Bangladesh. The major objective of this proposed optimized design is to supply the maximum load demand using renewable sources with the minimum cost of energy (COE) and reduce the burning of fuel and also reduce the emission of CO_2. The proposed energy system is able to meet 67.3% and 62.3% load demand using renewable sources, which helps to reduce the GHG (Green Houses Gas) emission by 67% and 64% for Saint Martin's island and Kuakata, respectively when compared to a diesel system. Total load served throughout the year is 33,611kWh, which is 16% higher than the previously designed system with approximately equivalent COE.

Keywords: Hybrid system, PV-Wind-Diesel, Renewable and sustainable energy, Optimization, Feasibility.

Nomenclature:	
PV	Photovoltaic
COE	Cost of Energy
NPC	Net Present Cost
SRE	Sustainable Rural Energy
BPDB	Bangladesh Power development board.
HOMER	Hybrid optimization Model for Electric Renewable.
NREL	National Renewable Energy Laboratory.

I. INTRODUCTION

In recent years, due to rapid technological development, declining cost of equipment needed for renewable energy systems, government economic incentives and pollution free characteristic of resources, significant worldwide attention has been directed towards power production from the renewable sources, such as PV, wind, biomass, geothermal, ocean wave, tides, etc. Many countries have set up or demonstrated large, small and micro

power generation systems using exploitable renewable resources [1, 2]. In Bangladesh, to establish the use of alternative and sustainable energy sources, several NGOs and government organizations are working continuously to develop the solar and wind power sector. In 2004, a survey carried out by

the Local Government Engineering Department (LGED) under the Sustainable Rural Energy (SRE) program recorded that, Saint Martin's island (situated just south off the coast of Cox's Bazar) houses 778 families with an annual energy demand of 359 MWh. In order to meet this demand, the Bangladesh Power Development Board (BPDB) installed a 30 kW diesel generator, which is currently out of service [3]. Therefore, it is evident that a more suitable solution is needed to fulfill the demands of these areas.

The annual average solar radiation is similar throughout the coastal region of Bangladesh. Average annual global solar radiations at Saint Martin and Kuakata are 4.81 and 4.65 kWh/m^2/d, respectively, and monthly average wind speed at 25m height are 4.79 and 4.54 m/s, respectively. This is known as a hybrid system. Since the hybrid system contains various costly components needed for renewable energy systems, perfectly optimized system designs are needed to lower net system cost and the cost of energy (COE) [4].

Several hybrid system optimization techniques and simulation programs have been developed so far. Due to the incorporation of non-linear components with many optimization parameters and failure of classical methods, genetic algorithms based design and operation control techniques are used for solving complex problems [5]. Computer aided simulating programs, such as HYBRID2 developed by the National Renewable Energy Laboratory (NREL) from USA and TRNSYS by the University of Wisconsin from USA were developed to simulate the hybrid system [6]. Though HYBRID-2 is unable to optimize the system, a very accurate simulation of a hybrid model is possible with this tool. Initially, TRNSYS was developed for thermal system simulation and later, PV system was included with TRNSYS to simulate the hybrid system. However, this tool is also unable to optimize the system [7].The operation and control of PV-diesel, hybrid system is achieved through an artificial neural network. For optimization purposes, a dispatch strategy has been applied by setting a starting and stopping point of the diesel generator [8]. In order to optimize a solar-wind hybrid system, iterative and probabilistic calculation techniques considering the loss of power supply probability (LPSP) were proposed. Using these techniques, the optimized system with minimized system cost was designed [9]. HOMER (Hybrid Optimization Model for Electric Renewable) simulation program was developed by NREL, USA to optimize the micro-power hybrid system using a kinetic battery model [10]. This model is widely used as a hybrid system optimization program and continuously updated with the new features. Technically, HOMER always finds the most energy efficient combination of hybrid system based on the energy source models, load profile, data of solar radiation, wind speed, fuel price and component details [11]. In 2012, for Saint Martin Island, an optimized design has been carried out using HOMER, while this author's efforts were concentrated to reduce the COE. They were able to extract only 31% load demand (31% renewable fraction) using renewable energy and the rest of the energy demands were met by diesel [12].As the fuel price was low (56Tk./L), the proposed model was feasible for that time. Considering a significant increase in the price of diesel and the demand of a more environmentally friendly system, the model become obsolete at present and the need for an alternate optimized system has become obvious [13].

The main objective of the present work is to design a sustainable optimized hybrid system design by focusing the maximum power production using renewable sources with minimum COE. The excess energy generation for Saint Martin's island and Kuakata has been considered. Then a hybrid system is designed and components optimization of the designed system with energy balance calculation is carried out using HOMER micro-power optimization model to minimize the COE. In order to estimate the system cost and production cost of energy, cost calculations studies are done. This includes costs, such as capital, operation, maintenance, replacement, fuel and interest. This economic analysis is carried out to determine the feasibility of the proposed system. Finally, a comparative study is shown with other hybrid energy systems for confirming the practicability of the proposed optimized system.

I. SELECTION OF ENERGY SOURCE

Fig.1 shows the relation between the solar radiation and the wind speed over the course of a year. It also shows a complementary relationship between the wind and solar systems. So, for implementation of a renewable energy system at Saint Martin's island and Kuakata, a combined wind and photovoltaic system along with diesel system would be the most feasible option [11].

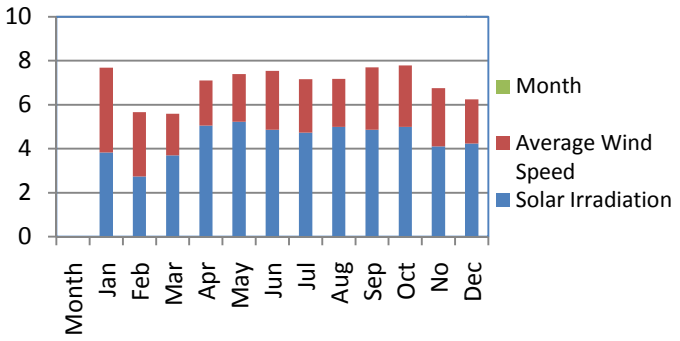

a) Saint Martin's Island

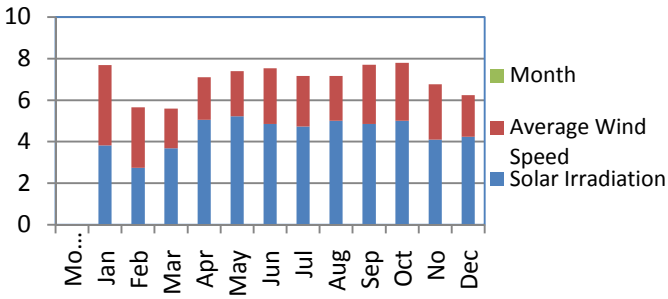

b) Kuakata

Fig.1. The average wind speed and solar irradiation curve for a) Saint Martin's Island and b) Kuakata

II. OPTIMIZED DESIGN OF A HYBRID MODEL

Before starting the computer aided simulation, mathematical models of each component of hybrid systems are described below. Fig. 2 shows the schematic visual diagram of a complete solar wind hybrid energy system. The hybrid energy system consist of Wind turbine, Solar (PV) module, Load demand, diesel generator as power back-up, Battery back-up and converter to convert the power dc to ac.

Fig.3 shows the proposed structure of hybrid system for Saint Martin's Island and Kuakata. In the structure, we have included diesel generators with renewable power generators (wind and solar). During design the system, we concentrate to maximize the output power from the renewable sources for minimizing per unit COE. Diesel generator, battery bank and converter (inverter and rectifier) are added as part of back-up and storage systems during adverse weather conditions. This proposed optimized system structure with the concept of the hybrid system is shown in Fig.3.

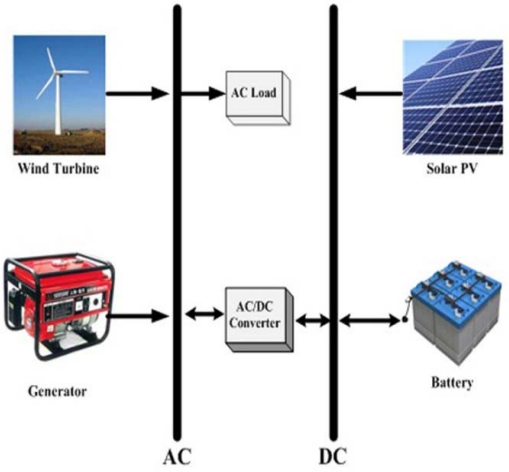

Fig. 2: Schematic Block diagram of a Hybrid Solar Wind Hybrid Energy System.

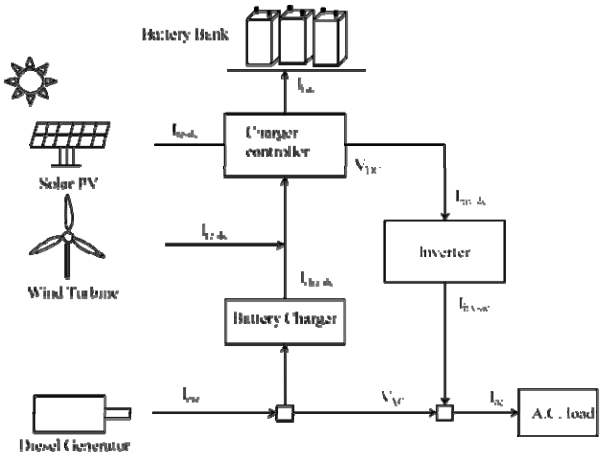

Fig.3. Solar PV-wind-diesel hybrid system

III. RESULTS AND DISCUSSION

(a) Optimized Results And Analysis

Using HOMER simulation tool, performance analysis of the proposed hybrid system is carried out. HOMER configured hybrid system is shown in Fig.4. HOMER represents the optimized results categorically and detailed results are shown using sensitivity parameters, like wind speed, solar radiation, fuel cost, maximum annual capacity shortage and renewable fraction. To design the optimized hybrid system, HOMER performs thousands of simulations using sensitivity parameters. Simulations are conducted considering different values for wind speed, solar radiation, diesel price and minimum renewable fraction; providing experimental flexibility.

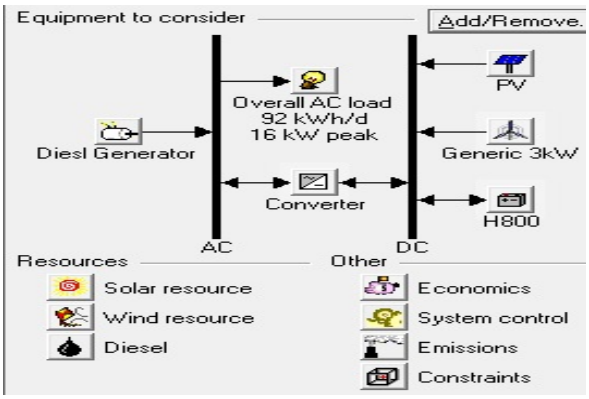

Fig. 4: Proposed hybrid system in HOMER.

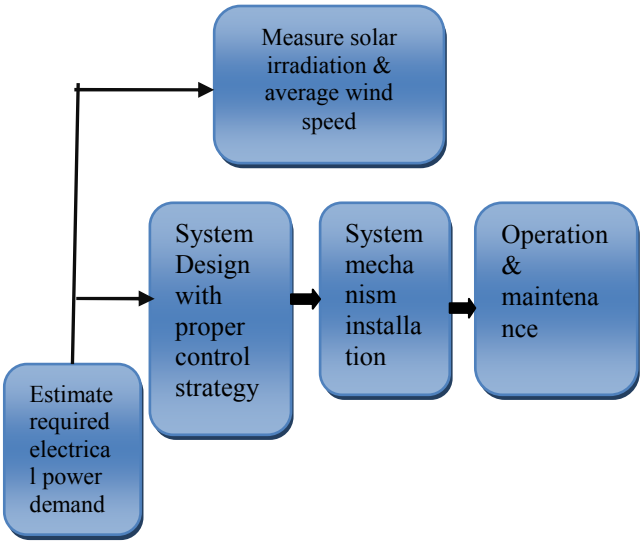

Fig. 5: complete flow chart of the hybrid energy system.

Figure 5 shows the general process of the simulation process of a complete hybrid solar-wind energy system. This diagram shows the sequential and active mechanism of solar-wind hybrid energy system in HOMER platform.

The most feasible optimized system found by HOMER for specific load demand includes solar irradiation 4.81 kWh/m^2/d, wind speed 4.79 m/s, fuel price 68 Tk./L and hub height 30m, as pictorially shown in Fig. 6. From Fig.4, it can be observed that after performing a lengthy optimization process, HOMER arranged the most feasible optimized system at the top of the window and showed the contribution of renewable sources (renewable fraction) to the total power production.

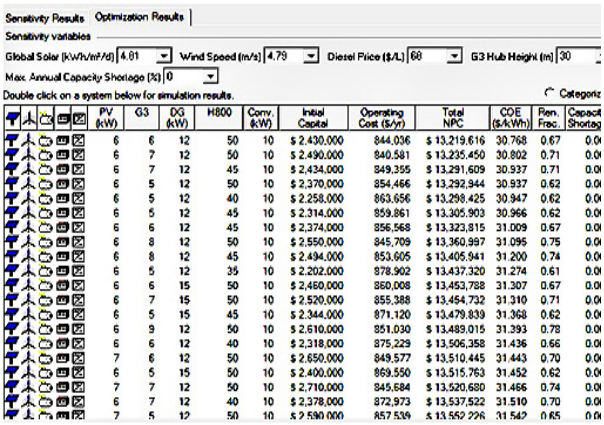

a) Saint Martin

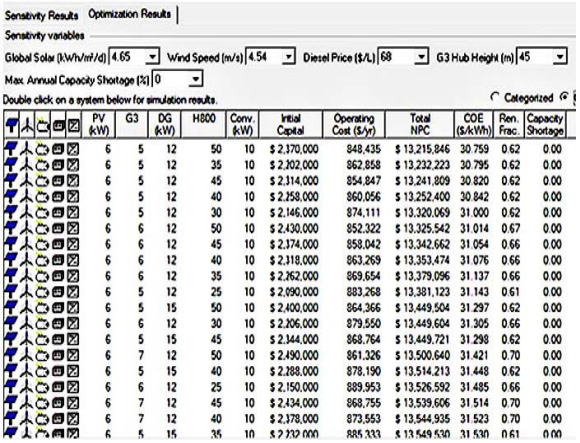

b) Kuakata

Fig.6. Simulated results of PV-wind-diesel system for wind speed 4.79 m/s, solar irradiation 4.81kWh/m2/d, fuel price 68 Tk./L, and maximum annual capacity shortage of 0%

Table 1: Optimized system architecture of solar-wind-diesel hybrid system.

System Component	Saint martin's island	Kuakata
	Size	size
PV Array	6 kW	6 kW
Wind turbine	6 Generic 3kW	5 Generic 3kW
Diesel Generator	12 kW	12 kW
Battery	50 Hoppecke 8 OPzS 800, 12 V and 800 Ah	50 Hoppecke 8 OPzS 800
Converter	10 kW	10 kW
DOD of Battery	20-80	20-80

At a cost of 30.768tk/kWh and an initial cost of 13,219,616tk/kWh, the optimized hybrid wind-pv-

diesel system designed for Saint Martin's island provides a much more feasible approach to meeting the energy demand there.

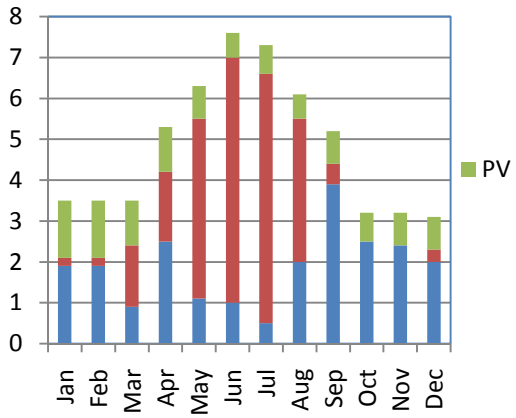

a) Saint Martin's Island

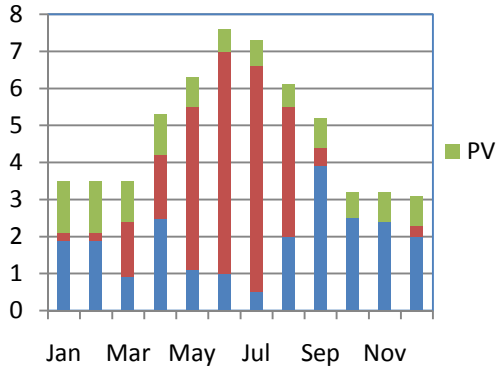

b) Kuakata

Fig.7. Power generated from the optimized hybrid PV-wind-diesel system across a year.

Fig.7 shows the monthly average electric power production from the HOMER optimized hybrid system. From Fig.6, it can be seen that the power produced by a diesel generator is almost same, while the power produced from wind and photovoltaic show their full complementary behavior across the year.

(b) Economic Feasibility Analysis

HOMER analyses the system according to the minimization of COE and maximizing the power output of the system. Other factors, which influence the analysis are capital cost, operating cost, renewable energy factor, total NPC (net present cost) and diesel consumption rate. Table 2 shows the capital cost, replacement cost, operation and maintenance cost and fuel cost of different system components.

(c) Environmental Effects

The proposed solar-wind-diesel hybrid system reduces gas emission by a significant amount due to the reduced fuel consumption. This reduction in gas emission is determined using HOMER software. The emission of this optimized system has been decreased by 67 and 64% from the existing diesel based energy system for Saint Martin's island and Kuakata, respectively. Emissions from various pollutants of this optimized system are shown in Table 2.

Table 2: Emission of various gasses from the optimized system

Pollutant	Saint Martin Emission kg/yr.	Kuakata Emission kg/yr.
Carbon dioxide	15,613	17,063
Carbon monoxide	38.5	42.1
Unburned hydrocarbons	4.27	4.67
Particulate matter	2.91	3.18
Sulfur dioxide	31.4	34.3
Nitrogen oxides	344	376
% reduction	67	64

DESIGNENHANCEMENTANALYSIS

a) *Comparative Study*

Table 4 shows a comparison study of the proposed hybrid system with other energy systems for Saint Martin's Island. The simulation results and comparative results clearly reveal that solar-wind-diesel hybrid system is the most feasible and cost effective off-grid power system at the present situation of Bangladesh.

Table 4: Cost comparisons with other energy systems.

Energy System	Net Present Cost (Tk.)	Fuel Cost (Tk.)	Cost of Energy (Tk./kWh)
Solar-Wind-Diesel	13219616	5153862	30.768
Solar-Diesel	15497075	9904494	36.064
Diesel	19879434	15520376	46.621

b) *Improvement Summary of Proposed Optimized System*

HOMER simulates the system configuration numerous times using given parameters to obtain the

optimization results and ranks the most optimized system based on the COE production and NPC. In the simulation, parameters are set up in such a manner that HOMER can find an optimized system that can deliver the maximum power using renewable sources while burning less fuel. The proposed optimized system is able to serve about 33,611 kWh/yr AC load, which is 16% higher compared to the previous optimized system with approximately equivalent COE, though the current diesel price is about 68Tk./L, which is 21% higher than the previous price (previous price was 56Tk./L). This improvement in designing an optimized system will certainly help to attract the investors to set up the commercial plants.

Table 5: Proposed optimized system compared to the previously optimized system.

Criterion	Proposed Optimized System	Previously Optimized System
PV array	6 kW	8 kW
Wind turbine	18 kW	3 kW
Diesel generator	12 kW	15 kW
Fuel price	68 Tk./L (present)	56 Tk./L (2012)
Renewable fraction	67.3%	31%
% GHGs reduction	67%	39%
Cost of Energy (COE)	30.768 tk/kWh	26.539 Tk./kWh
Accolade served	33,611 kWh/yr.	28,394 kWh/yr.

I. CONCLUSION

Pollution, emissions of greenhouse gases, and the rise of energy demands are increasing the dependence on importing energy from neighboring countries. Among the numerous renewable sources, solar and wind represent the most viable option for use in a power generation system fueled by sustainable energy. In the coastal areas where grid connection is not available or grid extension is not feasible, renewable sources, like wind and solar PV based hybrid system scan be potential solutions. In these areas, a solar-wind-diesel hybrid energy system can be a cost effective solution since the renewable energy sources are abundant. It will also reduce the pressure on the national grid. Moreover, the proposed hybrid system reduces the emission of gases and helps to trim down the environmental pollution. The hybrid model proposed in the present work will be able to meet the load demand with a reasonable COE. The most significant findings from this analysis is the reduction of CO_2 emissions in comparison with the other conventional power plants.

Acknowledgements

The authors are thankful for the support provided by University of Malaya (UM), American International University of Bangladesh (AIUB) and Military Institute of Science & Technology (MIST).

References

[1] Li, X., D. Hui, and X. Lai, *Battery energy storage station (BESS)-based smoothing control of photovoltaic (PV) and wind power generation fluctuations.* Sustainable Energy, IEEE Transactions on, 2013. **4**(2): p. 464-473.

[2] Nehrir, M.H., C. Wang, K. Strunz, H. Aki, R. Ramakumar, J. Bing, Z. Miao, and Z. Salameh, *A review of hybrid renewable/alternative energy systems for electric power generation: configurations, control, and applications.* Sustainable Energy, IEEE Transactions on, 2011. **2**(4): p. 392-403.

[3] Hossain, A. and O. Badr, *Prospects of renewable energy utilisation for electricity generation in Bangladesh.* Renewable and Sustainable Energy Reviews, 2007. **11**(8): p. 1617-1649.

[4] Shezan, S.K.A., R. Saidur, A. Hossain, W.T. Chong, and M.A. Kibria, *Performance Analysis of Solar-Wind-Diesel-Battery Hybrid Energy System for KLIA Sepang Station of Malaysia.* IOP Conference Series: Materials Science and Engineering, 2015. **88**(1): p. 012074.

[5] Goldberg, D.E., *Genetic Algorithm in Search, Optimization and Machine Learning, Addison.* W esley Publishing Company, R eading, MA, 1989. **1**(98): p. 9.

[6] Green, H.J. and J.F. Manwell, *HYBRID2: A Versatile Model of the Performance of Hybrid Power Systems*1995: National Renewable Energy Laboratory.

[7] Dufo-Lopez, R. and J.L. Bernal-Agustín, *Design and control strategies of PV-Diesel systems using genetic algorithms.* Solar Energy, 2005. **79**(1): p. 33-46.

[8] Ohsawa, Y., S.-i. Emura, and K. Arai. *Optimal operation of photovoltaic/diesel power generation system by neural network.* in *Neural Networks to Power Systems, 1993. ANNPS'93., Proceedings of the Second International Forum on Applications of*. 1993. IEEE.

[9] Diaf, S., G. Notton, M. Belhamel, M. Haddadi, and A. Louche, *Design and techno-economical optimization for hybrid PV/wind system under various meteorological conditions.* Applied Energy, 2008. **85**(10): p. 968-987.

[10] Manwell, J.F. and J.G. McGowan, *Lead acid battery storage model for hybrid energy systems.* Solar Energy, 1993. **50**(5): p. 399-405.

[11] Shaahid, S. and I. El-Amin, *Techno-economic evaluation of off-grid hybrid photovoltaic–diesel–battery power systems for rural electrification in Saudi Arabia—a way forward for sustainable development.* Renewable and Sustainable Energy Reviews, 2009. **13**(3): p. 625-633.

[12] Shafiullah, G., M. Amanullah, A. Ali, D. Jarvis, and P. Wolfs, *Economic analysis of hybrid renewable model for subtropical climate.* Int. J of Thermal and Environmental Engineering, 2010. **1**: p. 57-65.

[13] Shezan, S.A., R. Saidur, K. Ullah, A. Hossain, W. Chong, and S. Julai, *Feasibility analysis of a hybrid off-grid wind–DG-battery energy system for the eco-tourism remote areas.* Clean Technologies and Environmental Policy: p. 1-14.

A Multi Criteria Decision Making Methodology for Selecting a Renewable Energy Option

Samantha Islam[*1], S G Ponnambalam[1]

[1] *Advanced Engineering Platform and School of Engineering*
Monash University Malaysia
47500 Bandar Sunway, Malaysia
[*1]samantha.islam@monash.edu,
[1]sgponnambalam@monash.edu

Hon Loong Lam[2]

[2]*Faculty of Engineering*
The University of Nottingham Malaysia,
43500 Selangor, Malaysia
[2]HonLoong.Lam@nottingham.edu.my

***Abstract*—Multi Criteria Decision Making (MCDM) methods have become increasingly popular in decision-making for sustainable energy because it includes multiple sustainability indicators and various alternatives. The conventional methods like the technical feasibility or cost benefit analysis are not adequate to integrate all the elements of an environmentally sound energy plan. A sustainable selection of the energy alternatives considers social and environmental criteria along with technical and economic. Therefore, the sustainable selection provides a different result than the conventional one. Multi criteria decision making methods assemble and handle a wide range of sustainability indicators and provides a valid decision support for choosing among alternatives based on the goal and scope of the study. In this study, a Waste to Energy option is selected for a cement industry located in Dhaka, Bangladesh. The sustainability indicators are identified and ranked based on the interview taken from three decision makers. Fuzzy Analytical Hierarchy Process (FAHP) method has been adopted which allows the decision-makers to assign the relative importance values for the sustainability indicators. Finally Fuzzy TOPSIS method is applied in order to compare a set of energy alternatives against these indicators.**

***Keywords*— Multi Criteria Decision Making (MCDM), sustainability, Waste to Energy, Fuzzy Analytical Hierarchy Process, TOPSIS**

I. INTRODUCTION

Energy is a basic need for different purposes in industrial facilities around the world. Energy incurs the highest cost in a production system. However, global population and energy needs are increasing hand-in-hand. As a result, conventional energy sources are being decreased and the energy prices are getting high day by day. In addition to the diminishing nature, the conventional energy source also causes severe contamination to the environment. Therefore, a rising awareness of environmental issues has forced industries to use Renewable energy (RE) sources.

Sustainable energy planning endeavor involves selecting among a set of energy sources and conversion devices that can meet all sustainability dimension. Various Studies evaluated social, economic and environmental impacts of renewable energy systems [7]. However in case of selecting among various energy sources, technical indicators also become utterly important as the selected technology has to be feasible for the study under consideration [1, 2]. Analysis among these sustainability indicators is important as different indicator involve different weightage value depending upon the study. Again, for different indicator, different energy option's strength is different. Therefore, these kinds of problems are solved using Multiple criteria decision-making (MCDM).

Multiple criteria decision-making (MCDM) is an operational evaluation and decision support approach suitable for addressingcomplex problems featuring high uncertainty, conflicting objectives, multi interests and perspectives [3].Different groups of decision makers become involved in this process, each group bringing along different criteria and points of view, which must be resolved within a framework of understanding and mutual compromise [4]. Due to the availability and uncertainty of information as well as the vagueness of human feeling and recognition, it is relatively difficult to provide exact numerical values for the criteria. Therefore, the subjective judgments of decision makers are converted to fuzzy number to provide quantifiable indices for decision making as the fuzzy linguistic approach can take the optimism/pessimism rating attitude of decision-makers into account. Therefore, to assess preference ratings, Fuzzy MCDM becomes more suitable instead of conventional numerical equivalence method.

Numerous studies are performed on Fuzzy MCDM for energy option selection [3, 5-7]. For evaluation of criteria, Analytical Hierarchy Process (AHP) is the most popular [8]. Ansari & Ashraf [8] apply Fuzzy MCDM method for selection of best energy source for electricity generation in India. Ahmad and Tahar [8] compare various renewable resources potential and utilize them for prioritizing renewable options. Kaya and Kahraman [3] utilize fuzzy TOPSIS methodology for the selection of the best energy technology alternative.

Cement manufacturing is highly energy intensive because of the extreme heat required for its production process. Producing of cement requires high amount of electricity and heat for kilns. The common wastes produced in a cement industry are: rejected

limestone, scrap waste, packaging waste, used and unused refractories, food waste etc. Besides, some industries collect other industries waste to burn it in incineration to produce huge heat for kilns. However, these wastes can be also a great source for electricity production in the industry.

In this study, an integrated fuzzy AHP and TOPSIS methodology is proposed to make a multi-criteria selection among various Waste to Energy (WtE) options for a backup energy source in a cement industry located in Dhaka, Bangladesh. The three decision makers selected for this study are: Officer (environment, health and safety), Management Trainee(technical) and Officer(finance).

The indicators are decided based on the literature and discussion with decision makers. The criteria considered for this selection are given in table I :

TABLE I

THE CRITERIA CONSIDERED FOR THE FOUR CATEGORIES.

Criteria	Sub criteria
Technical	Resource availability Efficiency feasibility Training opportunity
Environmental	Emission Waste handling Land requirement noise
Economic	Establishment cost Operating cost Payback period Service life
Social	Compatible to national energy policy Job creation Safety

The available WtE technology are given below

Alternative 1: Waste co-combustion

Co-combustion of waste together with a base fuel in a boiler is a simple and economically suitable way to replace fossil fuels by biomass and to utilize waste. There are several options: Co-combustion with coal in pulverized or fluidized bed boilers, combustion on added grates inserted in pulverized coal boilers, combustors for added fuel coupled in parallel to the steam circuit of a power plant, external gas producers delivering its gas to replace an oil, gas or pulverized fuel burner.

Alternative 2: Waste gasification

Gasification is a process that converts waste into carbon monoxide, hydrogen and carbon dioxide. This is achieved by reacting the material at high temperatures, without combustion, with a controlled amount of oxygen and/or steam. The power derived from gasification of the resultant gas is considered to be a source of renewable energy.

Alternative 3: Waste incineration

Incineration with energy recovery is one of several waste-to-energy (WtE) technologies. While incineration and gasification technologies are similar in principle, the energy product from incineration is high-temperature heat whereas combustible gas is often the main energy product from gasification.

Alternative 4: Waste pyrolysis

Pyrolysis is the basis of several methods that are being developed for producing fuel from waste of industries. This is the most environments friendly among these four.

II. METHODOLOGY

A common approach for handling fuzzy AHP is using Triangular Fuzzy Numbers (TFNs) for the pairwise comparison scale of fuzzy AHP, and using the extent analysis method for the synthetic extent values of the pairwise comparisons. A TFN denoted as $L= (l, m, u)$ where $l < m < u$, has the following triangular type membership function:

$$L(x) = \begin{cases} 0 & x < 1 \\ \dfrac{(\mathrm{x} - \mathrm{l})}{(\mathrm{m} - \mathrm{l})} & l \le x \le m \\ \dfrac{(u - x)}{(u - m)} & m \le x \le u \\ 0 & x > u \end{cases}$$

In this methodology, decision makers are asked to indicate the relative importance of two evaluation criteria in the same level. The scores of pairwise comparison are treated as linguistic variables, which are represented by positive TFNs (Table II).

TABLE II

THE SCORES OF PAIR-WISE COMPARISONS

Linguistic terms	Fuzzy scale
Absolutely strong (AS)	(2, 5/2, 3)
Very strong (VS)	(3/2, 2, 5/2)
Fairly strong (FS)	(1, 3/2, 2)
Slightly strong (SS)	(1, 1, 3/2)
Equal (E)	(1, 1, 1)
Slightly weak (SW)	(2/3, 1, 1)
Fairly weak (FW)	(1/2, 2/3, 1)
Very weak (VW)	(2/5, ½, 2/3)

Absolutely weak (AW)	(1/3, 2/5, 1/2)

After obtaining the fuzzy judgment matrices, extent analysis method and the principle of TFNs comparison are used to derive the importance weights of criteria from pairwise comparisons. If the number of decision maker is more than 1, the decision matrices are aggregated by geometric mean of the fuzzy numbers.

After comparison is made, it is necessary to check the consistency ratio of the comparison. To do so, the graded mean integration approach is utilized for defuzzifying the matrix. According to the graded mean integration approach, a fuzzy number $L = (l, m, u)$can be transformed into a crisp number by employing the below equation:

$$P(L) = L = \frac{l + 4m + u}{6} \quad (1)$$

After the defuzzification of each value in the matrix, 'consistency ratio' [4, 9] of the matrix can easily be calculated by finding the eigen value $\lambda_{max}$of the matrix and RI values (Table III) for each matrix size.

$$CI = \frac{\lambda_{max} - n}{n - 1} \quad (2)$$

$$CR = \frac{CI}{RI} \quad (3)$$

TABLE III

RI VALUES USED IN CR CALCULATION

Matrix size	RI values
(1x1)	0
(2x2)	0
(3x3)	0.58
(4x4)	0.90
(5x5)	1.12
(6x6)	1.24
(7x7)	1.32
(8x8)	1.41
(9x9)	1.45
(10x10)	1.49

If CR is smaller than .10 then the following actions are performed to compute the normalized weight vector of the decision matrix.

Let *W* be the normalized weight vector of triangular fuzzy comparison matrix *A*, which includes the importance weights of criteria in the crisp form. The steps for calculating this vector are as follows.

The first step is to calculate the fuzzy synthetic extent value of each pair wise comparison. Linguistic pair wise comparisons are transformed to corresponding TFNs illustrated in Table 1. Denote C_{xy}as the TFN related to the pair wise comparison of criterion *x* over criterion *y*, which is represented as (l_{xy}, m_{xy}, u_{xy}). According to Chang [10]the value of fuzzy synthetic extent with respect to the criterion *x*, denoted as $S_x = (l_x, m_x, u_x)$can be obtained via Eq. (4):

$$S_x = \sum_{y=1}^{n} C_{xy} \left[\sum_{k=1}^{n} \sum_{y=1}^{n} C_{xy} \right]^{-1} \quad (4)$$

Where *n* is the size of the fuzzy judgment matrix *A*. To obtain$\sum_{y=1}^{n} C_{xy}$ perform the fuzzy addition operation such that,

$$\sum_{y=1}^{n} C_{xy} = \left(\sum_{y=1}^{n} l_{xy}, \sum_{y=1}^{n} m_{xy}, \sum_{y=1}^{n} u_{xy} \right); x = 1,2, \ldots, n \quad (5)$$

and to obtain $\left[\sum_{k=1}^{n} \sum_{y=1}^{n} C_{xy}\right]^{-1}$. The operation is as follows

$$\left[\sum_{k=1}^{n} \sum_{y=1}^{n} C_{xy} \right] = \left(\sum_{k=1}^{n} \sum_{y=1}^{n} l_{ky}, \sum_{k=1}^{n} \sum_{y=1}^{n} m_{ky}, \sum_{k=1}^{n} \sum_{y=1}^{n} u_{ky} \right) \quad (6)$$

and to obtain inverse of eqn(3) by using eqn(7) as follows

$$\left[\sum_{k=1}^{n} \sum_{y=1}^{n} C_{xy} \right]^{-1} = \left(\frac{1}{\sum_{k=1}^{n} \sum_{y=1}^{n} u_{ky}}, \frac{1}{\sum_{k=1}^{n} \sum_{y=1}^{n} m_{ky}}, \frac{1}{\sum_{k=1}^{n} \sum_{y=1}^{n} l_{ky}} \right) \quad (7)$$

The second step is to find the total integral value with index of optimism with eqn (8)

$$I_T^{\alpha}(S_x) = \frac{1}{2}[\alpha u_x + m_x + (1-\alpha) l_x] \quad (8)$$

Where α is index of optimism which represents degree of optimism for decision makers. If α approaches 0 in [0, 1], the decision makers are more pessimistic and otherwise they are more optimistic.

Finally, define the normalized importance weight vector $W = (w1, w2, ...,wn)$ of the fuzzy judgment matrix A by using eqn (9)

$$w_x = \frac{I_T^{\alpha} S_x}{\sum_{k=1}^{n} I_T^{\alpha} S_x} \quad (9)$$

Where w_x is a non fuzzy number.

After getting the weights of the criteria, TOPSIS method is used to evaluate the electricity alternatives and rank the priority for them accordingly. Here, the linguistic variables obtained are converted based on the verbal evaluating scale given in table IV.

TABLE IV

LINGUISTIC SCALES FOR THE IMPORTANCE OF EACH ALTERNATIVE

Linguistic term	Fuzzy number
Very poor (VP)	(0,1,3)
Poor (P)	(1,3,5)
Fair (F)	(3,5,7)
Good (G)	(5,7,9)
Very good (VG)	(7,9,10)

Then the step by step calculation is used to find the rank of the alternative energy source as follows[3]:

The first step is to construct normalized decision matrix. This step transforms various attribute dimensions into non-dimensional attributes, which allows comparisons across criteria. Normalize scores or data as follows:

$$r_{ij} = \frac{x_{ij}}{\sqrt{\sum_{i=1}^{m} x_{ij}^2}}, \quad i = 1,2,\ldots.,m; \quad j = 1,2,\ldots.,n \quad (10)$$

The next step is to construct the weighted normalized decision matrix. Let us assume a set of weights for each criteria is w_j for j = 1,…, n. Multiply each column of the normalized decision matrix by its associated weight. An element of the new matrix is:

$v_{ij} = w_j r_{ij}$, for i = 1, …, m; j = 1, …, n (11)

Then the positive ideal and negative ideal solutions are determined by following eqn (12) and (13) .The positive ideal solution is:

$A^* = \{ v_1^*, \ldots, v_n^* \}$, where $v_j^* = \{ max\ (v_{ij})\ if\ j \in J;\ min\ (v_{ij})\ if\ j \in J' \}$ (12)

And the negative ideal solution is:

$A' = \{ v_1', \ldots, v_n' \}$, where $v' = \{ min\ (v_{ij})\ if\ j \in J;\ max\ (v_{ij})\ if\ j \in J' \}$ (13)

Finally, the separation measures for each alternative are determined using the n-dimensional Euclidean distance. Separation from positive ideal solution is:

$$d_i^+ = \left\{ \sum_{j=1}^{n} \left(v_{ij} - v_j^+\right)^2 \right\}^{\frac{1}{2}}, i = 1,2,\ldots.,m \quad (14)$$

Similarly, the separation from the negative ideal solution is:

$$d_i^- = \left\{ \sum_{j=1}^{n} \left(v_{ij} - v_j^-\right)^2 \right\}^{\frac{1}{2}}, i = 1,2,\ldots.,m \quad (15)$$

Finally the relative closeness to the ideal solution C_i^* are determined. The relative looseness of the alternative A_i with respect to A^* is defined as

$$C_i^* = \frac{d_i^-}{(d_i^+ + d_i^-)}, i = 1,2,\ldots.,m \quad (16)$$

By comparing C_i^* values, the ranking of alternatives are determined. For ranking alternatives using this index, alternatives can be ranked in decreasing order. Therefore, the higher the relative closeness to ideal solution, the more preferable is the alternative. The basic principle of the TOPSIS method is that the chosen alternative should have the "shortest distance" from the positive ideal solution and the "farthest distance" from the negative ideal solution.

III. RESULTS AND DISCUSSION

The values taken from the linguistic scale shown in table II are assigned for different criteria by three decision makers. After applying eqn (1 to 9) discussed in previous section the weights and their normalized values are determined. The result of Fuzzy AHP is shown below in table V.

TABLE V

THE WEIGHTS OF THE CRITERIA AND SUB-CRITERIA

Criteria and Sub-criteria	Priority	Final priority
Technical	**0.285**	-
Resource availability	0.193	0.055
Efficiency	0.311	0.088
feasibility	0.361	0.103
Training opportunity	0.133	0.038
Environmental	**0.257**	-
Emission	0.360	0.092
Waste handling	0.288	0.074
Land requirement	0.212	0.054
Noise	0.138	0.035
Economic	**0.276**	-
Establishment cost	0.254	0.070
Operating cost	0.234	0.064
Payback period	0.304	0.084
Service life	0.205	0.056
Social	**0.180**	-
Compatible to national energy policy	0.414	0.074
Job creation	0.220	0.039
Safety	0.365	0.066

For TOPSIS method , the importance of each alternative for each criteria category is assigned by the scale shown in table 4. The scale assignment for positive and negative criteria is performed differently. For example, emission is a negative criteria. So, the WtE alternative with highest emission is assigned 'Very Poor(VP)'. On the other hand, for efficiency the alternative with highest efficiency is assigned 'Very Good(VG)'. By applying eqn (10 to 16) for TOPSIS method, the positive ideal solution(di+), negative ideal solution (di-), closeness (CCi) and rank are shown in Table VI.

TABLE VI

RANKING OF THE ALTERNATIVE OPTIONS

Option	di+	di-	CCi	Rank
ALT1	0.5074	0.3244	0.3900	2
ALT2	0.4373	0.4105	0.4842	1
ALT3	0.5777	0.2419	0.2951	4
ALT4	0.5460	0.3146	0.3655	3

From the above table, it is seen that the preference order of WtE technologies are Gasification>Co-combustion> Pyrolysis >Incineration. Incineration is a common practice in cement industries for waste management. The heat required to elevate the kiln temperature is usually attained from burning waste in incinerators. In spite of having higher efficiency, incineration is a highly emission intensive technique for waste to energy conversion. On the other hand, waste gasification in a gasifier and then energy conversion is the safest option among this four. Waste gasification also entails high energy efficiency. On the other hand, waste co-combustion is also a highly efficient process. However, requirement of other basic fuel i.e.: coal makes the process expensive and less environment friendly. Pyrolysis is the most environment friendly option, but its lower efficiency and higher cost makes the process less favorable for large scale production. Furthermore, pyrolysis process is still not so conventional, so not much training facilities are available.

If only technical feasibility would be considered then waste incineration or co combustion would be the best option for higher waste to energy conversion rate. However, considering sustainability as a selection criterion, the priority becomes different.

IV. CONCLUSION

This paper presents an idea of replacing the conventional selection of energy option with sustainable one. In conventional selection process, only cost and technical feasibility is considered while choosing an energy option. However, considering environmental and social factors along with these former two, makes the choice different. In this paper, the hierarchical order of the factors affecting a sustainable option for waste to energy technology is assessed with Fuzzy AHP method. The weightage value found is then applied for alternative WtE technology selection via TOPSIS method. The applied method shows that waste gasification is the most favorable option considering the technical feasibility and sustainability. In contrast, in spite of having better technical feasibility, waste incineration is found to be the worst selection as sustainability is also considered.

A sustainable choice of energy option is not only environment and tech friendly but also cost effective. This selection can also be useful for improving the overall sustainability of the industry.

REFERENCES

1. Kaya, T. and C. Kahraman, *Multicriteria renewable energy planning using an integrated fuzzy VIKOR & AHP methodology: The case of Istanbul.* Energy, 2010. **35**(6): p. 2517-2527.
2. Ahmad, S. and R.M. Tahar, *Selection of renewable energy sources for sustainable development of electricity generation system using analytic hierarchy process: A case of Malaysia.* Renewable energy, 2014. **63**: p. 458-466.
3. Kaya, T. and C. Kahraman, *Multicriteria decision making in energy planning using a modified fuzzy TOPSIS methodology.* Expert Systems with Applications, 2011. **38**(6): p. 6577-6585.
4. San Cristóbal, J., *Multi-criteria decision-making in the selection of a renewable energy project in spain: The Vikor method.* Renewable energy, 2011. **36**(2): p. 498-502.
5. Arce, M.E., et al., *The use of grey-based methods in multi-criteria decision analysis for the evaluation of sustainable energy systems: A review.* Renewable and Sustainable Energy Reviews, 2015. **47**: p. 924-932.
6. Mourmouris, J. and C. Potolias, *A multi-criteria methodology for energy planning and developing renewable energy sources at a regional level: A case study Thassos, Greece.* Energy Policy, 2013. **52**: p. 522-530.
7. Beccali, M., M. Cellura, and M. Mistretta, *Decision-making in energy planning. Application of the Electre method at regional level for the diffusion of renewable energy technology.* Renewable energy, 2003. **28**(13): p. 2063-2087.
8. Ansari, A.J. and I. Ashraf, *Best energy option selection using fuzzy multi-criteria decision making approach.* International Journal of Advanced Renewable Energy Researches (IJARER), 2012. **1**(5).
9. Kibria, A.S.M.G., M. Inoue, and T.K. Nath, *Analysing the land uses of forest-dwelling indigenous people in the Chittagong Hill Tracts, Bangladesh.* Agroforestry Systems: p. 1-14.
10. Heo, E., J. Kim, and K.-J. Boo, *Analysis of the assessment factors for renewable energy dissemination program evaluation using fuzzy AHP.* Renewable and Sustainable Energy Reviews, 2010. **14**(8): p. 2214-2220.